Optimisation des systèmes photovoltaïques : vers une meilleure efficacité et une performance sans défaut

Khaled Alosmani

THESE DE DOCTORAT DE

L'UNIVERSITE D'ANGERS

ECOLE DOCTORALE N° 602
Sciences pour l'Ingénieur
Spécialité : Energétique-Thermique

Par

Khaled ALOSMANI

Optimisation des systèmes photovoltaïques : vers une meilleure efficacité et une performance sans défaut

Optimizing PV systems : towards better efficiency and faultless performance

Thèse présentée et soutenue à Polytech Angers, le 11/12/2023
Unité de recherche : LARIS EA 7315
Thèse N° :

Rapporteurs avant soutenance :

Mme Frédérique DUCROQUET	CR CNRS HDR	IMEP-LaHC, Grenoble
M. Detlef SCHULZ	Pr	Helmut Schmidt University, Hambourg (Allemagne)

Composition du Jury :

Examinateur :	M. Cherif LAROUCI	Pr	ESTACA Saclay
Directeur de thèse :	M. Thierry LEMENAND	MCF HDR	Polytech Angers / LARIS
Co-encadrant :	M. Mohamad RAMADAN	MCF	Lebanese International University (Liban)
Co-encadrant :	M. Bruno CASTANIER	Pr	Polytech Angers / LARIS
Invité :	M. Ahmad HADDAD	Pr	Lebanese International University (Liban)

Table des Matières

Introduction

Au cours des dernières années, la demande mondiale d'énergie électrique a connu une augmentation notable, principalement due à la croissance industrielle, aux progrès technologiques et à l'urbanisation. Il est constaté que la consommation mondiale d'électricité augmente régulièrement, soulignant ainsi le rôle essentiel que joue l'électricité dans les sociétés modernes [1]. Outre les secteurs traditionnels (c'est-à-dire les domaines résidentiel et commercial), l'augmentation de la demande d'énergie est également liée aux tendances modernes, telles que l'internet dans sa forme actuelle améliorée avec ses dérivés correspondants (numérisation des services, cloud, etc.) et au secteur des véhicules électriques [2]. L'énergie électrique représente donc l'élément essentiel sur lequel les progrès économiques et la mise en œuvre de projets de collaboration à l'échelle internationale se basent, intimement liés au développement sociétal global et aux objectifs de durabilité. En conséquence, une telle augmentation de la demande d'énergie électrique pose différents défis, tels que la nécessité d'une production d'énergie efficace et de la modernisation des réseaux électriques.

Par conséquent, et afin de répondre à la demande croissante d'énergie, les combustibles fossiles sont de plus en plus surexploités, ce qui implique une combustion excessive qui libère davantage de gaz à effet de serre, exacerbe l'effet de serre et contribue potentiellement au réchauffement de la planète [3], provoquant ainsi de graves conséquences pour l'environnement et la santé humaine. En dégradant la qualité de l'air, par exemple, les émissions toxiques issues de la combustion des combustibles fossiles amplifient le taux d'occurrence des maladies respiratoires. D'autre part, il existe un lien de cause à effet entre l'augmentation de la consommation de combustibles fossiles

et la perturbation de l'équilibre de la Terre : la température moyenne mondiale augmente en raison des émissions de gaz à effet de serre, le mécanisme d'évaporation des océans s'intensifie, ce qui se traduit éventuellement par des événements météorologiques plus extrêmes, avec une perturbation des cycles de précipitations naturelles. Au-delà de ces instabilités environnementales nouvellement générées [4], les taux de mortalité des insectes et des animaux sont à leur tour bouleversés, exacerbant ainsi l'effet domino écologique.

Il n'est donc pas étonnant que la recherche moderne (dans les domaines d'intérêt concernés) mette l'accent sur la protection du climat et les émissions de gaz plus propres. En conséquence, l'adoption de systèmes photovoltaïques (PV) en tant que ressources énergétiques plus écologiques a suscité un intérêt considérable au niveau international, principalement en raison de leur potentiel à répondre aux demandes intensives d'énergie électrique, tout en atténuant les impacts sur l'environnement [5]. Essentiellement, les systèmes photovoltaïques produisent de l'électricité (courant continu) en exploitant l'énergie solaire, offrant ainsi une solution durable pour répondre aux besoins énergétiques croissants. Ceci étant dit, et en raison de l'abondance de l'irradiation solaire [6], les systèmes photovoltaïques offrent une ressource alternative prometteuse en matière d'énergie électrique, principalement caractérisée par leur méthodologie de travail non destructif, statique, et silencieuse. Néanmoins, la mise en œuvre généralisée des systèmes photovoltaïques, en plus de constituer une base respectueuse de l'environnement pour la demande d'énergie, réduit les effets néfastes du changement climatique en nécessitant moins de combustibles fossiles et de gaz.

Loin des évaluations théoriques, les systèmes photovoltaïques (comme tous les systèmes physiques) ne fonctionnent pas sans certains inconvénients, en particulier ceux induits par les fluctuations de l'irradiation et l'instabilité des performances due à l'apparition de différents types

de défauts [7]. En raison de leur dépendance à l'égard de l'intensité et de la disponibilité de la lumière solaire, l'énergie générée par les systèmes photovoltaïques est irrégulière et sensible aux variations des conditions environnementales (par exemple, les fluctuations de l'irradiation, les conditions d'ombrage partiel, etc.) À titre d'illustration, les conditions d'irradiation fluctuantes provoquées par le passage de nuages peuvent créer des points chauds (hotspots) sur les panneaux photovoltaïques, ce qui réduit la capacité d'extraction d'énergie du système photovoltaïque et sollicite ses composants électroniques, ce qui réduit la durée de vie des modules photovoltaïques et accroît les besoins de maintenance [8]. D'un autre point de vue, l'intermittence de la lumière solaire nécessite l'utilisation de systèmes de stockage d'énergie (par exemple, des batteries) pour compenser les conditions de faible irradiation et éviter les coupures de charge, ce qui ajoute à la complexité et à la charge financière de l'adaptation des systèmes photovoltaïques. En outre, une production d'énergie aussi conditionnelle et instable par les systèmes photovoltaïques réduit leur potentiel en tant que ressources énergétiques alternatives à long cycle de vie [9].

Cette étude vise à mieux optimiser le comportement opérationnel des systèmes photovoltaïques, en réduisant autant que possible les impacts négatifs des conditions environnementales indésirables (principalement liées à l'irradiation), ainsi que les conditions opérationnelles défectueuses. Cela se fait d'abord par une revue approfondie de la littérature sur différents défauts liés au photovoltaïque et différentes méthodes de compensation pour les irradiations fluctuantes. D'autre part, cette étude prend également en considération la création de modèles innovants qui servent à augmenter l'efficacité de la production d'énergie des systèmes photovoltaïques. Les objectifs ont été définis comme suit :

- La conception d'un système d'optimisation de l'angle d'inclinaison, qui prend en compte la zone d'installation du système PV (c'est-à-dire la latitude, la longitude), ainsi que les

dimensions de chaque panneau PV, puis génère le meilleur angle d'inclinaison en fonction des différentes saisons, ce qui produit la plus grande puissance électrique au coût actualisé de l'énergie le plus bas. Le modèle produit également le nombre maximum de panneaux photovoltaïques pouvant être installés dans une zone d'installation de forme carrée, sans aucun ombrage mutuel.

- Une configuration complète d'un nouveau chargeur solaire basé sur le suivi du point de puissance maximale (MPPT) pour les applications photovoltaïques hors réseau, capable de charger efficacement une banque de batteries dédié dans des conditions d'irradiation changeant rapidement.

- Une modification innovante de l'algorithme Particle Swarm Optimization (PSO), qui peut tracer instantanément toute la courbe caractéristique PV, dans des conditions d'ombrage partiel sévères (jusqu'à cinq points de puissance maximale locale).

- Une étude numérique examinant la faisabilité des applications de traqueurs solaires par rapport à la zone d'installation.

Pour atteindre les objectifs énoncés, une revue détaillée et approfondie de la littérature sur différents sujets liés aux défauts photovoltaïques et aux méthodes de compensation des fluctuations d'irradiance est présentée dans le **chapitre 1**. Cette revue globale est composée de sept sous-revues, prenant en compte les stratégies de maintenance photovoltaïque, y compris la maintenance prédictive utilisant les matériaux à changement de phase (PCM), les types de défauts PV et leurs méthodes de détection pertinentes. D'un autre côté, la revue de la littérature contient également des méthodes compensatoires liées à l'irradiance telles que le MPPT, la reconfiguration des panneaux photovoltaïques et les trackers solaires photovoltaïques. La

proposition de thèse est justifiée encore dans le **chapitre 1**, dans lequel il est ainsi précisé pourquoi le choix des différentes méthodes d'optimisation est entièrement lié à l'irradiation solaire. En d'autres termes, ce chapitre présente clairement d'abord la raison derrière la caractérisation des méthodes d'optimisation, et comment chacune améliore les performances des systèmes photovoltaïques en prenant principalement en considération l'irradiance comme entrée clé.

Le **chapitre 2** présente un modèle mathématique qui prend en compte la géométrie des panneaux photovoltaïques (longueur, largeur, etc.), puis calcule le nombre maximum de panneaux photovoltaïques pouvant être installés dans une zone d'installation de forme carrée sans qu'il y ait d'ombrage de la part des panneaux photovoltaïques voisins. En outre, le système conçu fournit l'angle d'inclinaison optimal qui, lorsqu'il est appliqué de manière saisonnière aux panneaux photovoltaïques, garantit un coût de l'énergie le plus bas possible**.**

Le **chapitre 3** présente un prototype complet de chargeur solaire simulé dans Matlab, mis au point après une étude et une analyse approfondie de différents modèles d'irradiation solaire fluctuante. La conception prend en compte le chemin complet d'un panneau photovoltaïque jusqu'à un banc de batteries lithium-ion dédié. En impliquant la conception de différents circuits électroniques de puissance, le système garantit toujours un processus de charge de batterie maximal mais sûr avec d'autres mécanismes de protection des batteries.

Le **chapitre 4** présente une nouvelle modification de l'algorithme original d'optimisation par essaimage de particules (PSO) basée sur les mécanismes pathologiques de l'évolution de la maladie du diabète de type 1 (T1D). En termes de précision de convergence et de vitesse d'exécution, l'algorithme PSO modifié permet d'obtenir une convergence meilleure et plus rapide dans la courbe caractéristique du PV. Dans des conditions d'ombrage partiel, présentant jusqu'à cinq points de puissance maximale locale dans la courbe caractéristique du PV, l'algorithme modifié, après avoir

configuré ses ensembles d'essaims imitant le comportement des immunocytes au cours de l'évolution du T1D, permet un traçage complet de la courbe caractéristique. En conséquence, cette nouvelle modification permet une extraction maximale de la puissance du réseau photovoltaïque.

Le **chapitre 5** présente une étude numérique sur la faisabilité des applications de suivi solaire pour les systèmes PV. Contrairement à l'idée reçue selon laquelle les suiveurs solaires augmentent en fait la quantité d'irradiation solaire absorbée par les panneaux PV, ce qui permet d'obtenir une plus grande puissance de sortie, cette étude étudie particulièrement l'effet de l'augmentation de la température due à l'application des suiveurs solaires. Après cette étude, on constate que les suiveurs solaires ne sont pas nécessairement bénéfiques pour les systèmes photovoltaïques en termes d'augmentation de la puissance de sortie. Au contraire, les suiveurs solaires, en raison de la chaleur accumulée due à l'intensification de l'absorption du rayonnement, peuvent réduire le cycle de vie des systèmes photovoltaïques et, par conséquent, la puissance de sortie globale pendant toute la durée de vie de ces systèmes.

Le **chapitre 6** résume les résultats globaux de cette étude et examine comment elle peut optimiser les performances des systèmes photovoltaïques. En outre, un tableau de données est réalisé pour rassembler toutes les conclusions, à la suite duquel un travail futur, en termes d'applications expérimentales, est recommandé pour exécuter le PSO modifié dans un prototype MPPT, ainsi que le chargeur solaire. D'autre part, le modèle de faisabilité des suiveurs solaires pourrait être codé dans une application pour smartphone, où l'étude de l'angle d'inclinaison peut être rapportée en tant que résultats physiques de systèmes PV réels**.**

Chapitre 1

Revue bibliographique et état de l’art

Les systèmes photovoltaïques peuvent apporter une contribution forte à la transition mondiale vers des sources d'énergie alternatives et renouvelables. Grâce à une source d'énergie propre et théoriquement illimitée (c'est-à-dire l'irradiation solaire sans exigences d'espace pour l'installation des systèmes photovoltaïques), les systèmes photovoltaïques réduisent de manière significative la dépendance aux combustibles fossiles limités, contribuant ainsi à atténuer le changement climatique. De plus, en décentralisant la production d'énergie (c'est-à-dire en l'appliquant partout), les processus de production d'électricité gagneraient en flexibilité et le réseau électrique qui en résulterait offrirait une meilleure répartition de la charge et de la demande. D'autre part, les facteurs d'évolutivité et de polyvalence qui caractérisent les systèmes photovoltaïques font que ces derniers conviennent mieux à la demande dynamique (c'est-à-dire des petits secteurs résidentiels aux grandes installations), tout en réduisant la pollution de l'air et de l'eau. On peut donc affirmer que les installations photovoltaïques soulignent la transition vers un paysage énergétique durable et respectueux de l'environnement.

Afin d'extraire et d'utiliser pleinement la capacité latente du PV, ce chapitre vise dans un premier temps à présenter un examen détaillé et approfondi des différents aspects clés des systèmes PV, généralement décomposés en différents défauts PV avec leurs techniques de maintenance respectives, et les critères de performance liés à l'irradiation. Ce chapitre présente ainsi huit résumés d'études bibliographiques que nous avons réalisées durant cette thèse, visant à mieux

exploiter les tendances actuelles des systèmes photovoltaïques, puis à atteindre les objectifs initiaux de cette thèse, à savoir l'optimisation des performances des systèmes photovoltaïques. Pour chaque étude que nous avons menée, par souci de concision, nous présenterons dans ce manuscrit leur objectif et un résumé des différentes conclusions. Les contributions sont consultables en ligne. La philosophie que nous avons adoptée est, dans un premier temps (les travaux de 1 à 4), de réaliser un état de l'art lié aux pertes de performance des PVs notamment à cause de leurs défaillances et les moyens de limiter ces pertes. Dans un second temps, les travaux 5 à 8, nous nous sommes intéressés à la maximisation du rendement énergétique d'un PV, aussi en fonction de ces contextes d'usage.

1.1 Revue des stratégies de maintenance pour les systèmes photovoltaïques. L'objectif de cette étude est de fournir un examen approfondi des différents types de techniques et de stratégies maintenance des systèmes photovoltaïques. Basée sur une analyse de 159 références bibliographiques, une évaluation critique de chaque méthode globale est menée pour trouver un lien entre chaque type et la probabilité d'utilisation, avec une analyse économique en termes de coûts de maintenance et d'augmentation de la production d'énergie. Cette étude a été publiée sous le titre “A review on maintenance strategies for PV systems” dans la revue “*Science of the Total Environment*” (2020), doi.org/10.1016/j.scitotenv.2020.141753.

Résumé : « Un des constats majeurs pouvant limiter le déploiement systématique des systèmes photovoltaïques est la perte d'efficacité voire les déficits de production liés à des défauts ou défaillances des PVs. Il devient important de recenser et de caractériser l'ensemble des événements pouvant affecter la performance fonctionnelle d'un PV en phase d'exploitation. Nous proposons ici un état de l'art des défaillances possibles, de leur criticité en termes de fréquence d'apparition et de conséquence pour un meilleur

diagnostic. Une bonne connaissance de ces défauts et de leur chronologie d'apparition peut permettre l'identification de signes précurseurs à une défaillance totale et ainsi une mise en place d'opérations de maintenance généralement moins chères et anticipatives au changement total du PV. D'une meilleure planification, il en résulte des gains sur les coûts directs de maintenance et sur la réduction de pertes financières liées à une diminution durable de l'efficacité des PVs. Cet article vise à présenter différents schémas utilisés pour l'intervention en cas de défaut, classés en fonction des méthodes de maintenance préventive, corrective, prédictive et en cas d'urgence, avec les effets correspondants sur l'environnement. Une comparaison critique entre les différentes stratégies est présentée, ainsi qu'une évaluation économique des coûts de maintenance et de l'augmentation de la production d'énergie. Chaque type de stratégie est expliqué individuellement afin de dévoiler quelles catégories de défaillances PV elle peut traiter. En recommandant le choix de la stratégie de maintenance, ce travail de revue scientifique est établi à l'intention des chercheurs dans le domaine pour maintenir de manière optimale un système PV durable. »

Conclusion : « Les méthodes correctives se concentrent sur la qualité de l'énergie, en particulier dans le cadre des techniques d'intelligence artificielle, où les méthodes s’appuient sur la forme de la production d'énergie, comme le maintien de la forme d'onde sinusoïdale pour la sortie de tension à l'onduleur avec un minimum de perturbations et de malformations de l'onde. Ces méthodes permettent également d'assurer une qualité d'énergie efficace. D'autres méthodes comme le nettoyage (avec ou sans eau), le déneigement et les techniques d'atténuation de l'ombrage mettent l'accent sur l'extraction de la plus grande puissance possible du système PV, soit en supprimant les obstacles (barrières physiques), soit en compensant les scénarios de faible irradiation au moyen d'unités de traitement de l'énergie (convertisseurs DC-DC). Enfin, les approches

manuelles directes (comme la réparation, le remplacement et les interventions au niveau du logiciel) permettent d'atténuer les pannes d'électricité, d'améliorer les performances du système et de retarder les opérations. Par conséquent, un système photovoltaïque corrigé en permanence (élimination de la poussière et de la neige) peut atteindre des taux de production d'énergie plus élevés.

La maintenance prédictive diffère des deux précédentes par sa propriété d'anticipation, c'est-à-dire que l'exécution de routines de maintenance programmées, collectées à partir de données informatives et d'enregistrements historiques des performances du système, réduit les risques de défaillance plus importants qui se produiront à l'avenir, en fonction des données connues. Elle est basée sur des modèles mathématiques avec des sorties discrètes qui analysent les événements défectueux possibles. Cela ne peut pas, par exemple, résoudre le problème des équipements déjà endommagés ou, en d'autres termes, remplacer les programmes de maintenance corrective.

La maintenance préventive, enfin, est l'ensemble des méthodes qui permettraient d'éviter les trois méthodes précédentes, en intervenant sur le système sans qu'aucune défaillance ne se produise (par exemple, refroidir les panneaux avant qu'ils ne surchauffent pour éliminer le problème de la chute de tension...). Chacune des techniques de maintenance étudiées contribue de manière unique à l'optimisation du comportement des systèmes photovoltaïques. En commençant par les méthodes préventives, le choix initial de l'architecture des cellules se portera sur des cellules fiables, flexibles en termes de température et d'humidité. L'onduleur, quant à lui, est conçu pour être une architecture sans transformateur. De cette manière, tous les problèmes liés au comportement non linéaire des cellules et les problèmes électriques liés aux transformateurs (courant de fuite, pertes par effet de Foucault...) seront limités. Un processus de refroidissement

programmé du système photovoltaïque est également conseillé pour garantir une production d'énergie optimale. En ce qui concerne les stratégies de maintenance prédictive, une combinaison de PEMCS (Predictive Energy Management and Control System) et de FMEA (Failure Mode and Effect Analysis) garantirait une distribution d'énergie décente avec un indicateur de défaut futur pour tous les équipements. Une inspection visuelle programmée est conseillée pour suivre toute dégradation de l'équipement. Du point de vue de la maintenance corrective, un système photovoltaïque compatible MPPT, avec des diodes de dérivation couplées en interne dans les panneaux photovoltaïques et avec un nettoyage continu et programmé des panneaux photovoltaïques, permettrait d'atteindre une productivité énergétique maximale avec moins de risques de brûlure des panneaux en raison de points chauds. » (Veuillez-vous référer à **l'annexe 1.1** pour une lecture complète du document).

1.2 Revue des défauts des systèmes photovoltaïques et de leurs méthodes de détection correspondantes. Cette étude basée sur une analyse de 295 références bibliographiques, vise à classer les différents types de défauts photovoltaïques en fonction de leur cause initiale de formation: interne (par exemple, à l'intérieur des modules photovoltaïques), externe (par exemple, environnementale) et électrique (par exemple, circuit). Ensuite, différentes méthodes de détection des défauts sont étudiées en fonction de leur localisation dans le système PV (c'est-à-dire du côté du courant continu ou du courant alternatif). Cet article intitulé “A critical review of PV systems’ faults with the relevant detection methods” est soumis à la revue “*Energy Nexus*”.

Résumé : « Les systèmes photovoltaïques (PV) sont souvent sujets à des défauts opérationnels qui affectent négativement leurs performances. En fonction de différents

types et natures, de tels défauts empêchent les systèmes PV d'atteindre leur puissance nominale et d'atteindre le niveau requis de la production d'énergie. En ce qui concerne l'optimisation opérationnelle des systèmes PV, cet article vise principalement à recenser et à classer les différents types de défauts PV, classés comme étant électriques, internes et externes, chacun étant examiné en détail : les défauts internes se produisent au niveau des cellules PV et peuvent être des courts-circuits, des circuits ouverts, des pontages ou des défauts de diodes de dérivation. Les causes d'anomalies externes, en revanche, sont principalement classifiés comme temporaires (dus par exemple aux ombrages de nuages, des tempêtes de neige, etc.) ou permanents (par exemple, bris de verre, défauts de cadre, etc.) défauts de non-concordance. Enfin, les défauts électriques impliquent des problèmes de circuit communs, tels que des courts-circuits (par exemple, court-circuit entre ligne et terre, ligne et ligne, etc.), des défauts d'unités de traitement de puissance (par exemple, défauts d'onduleurs) et des défauts d'arc (étincelles). En ce qui concerne les méthodes de détection, six méthodes majeures de détection de défauts sont étudiées pour la zone de courant alternative du système PV avec un total de vingt-neuf sous-méthodes. D'autre part, onze méthodes majeures de détection de défauts sont étudiées pour la zone de courant continu des systèmes PV avec un total de soixante-treize sous-méthodes. Les méthodes étudiées sont analysées d'une manière critique et comparées d'une manière pertinente les unes par rapport aux autres, au sein des sous-ensembles mutuels. Les données comparatives tabulées résultantes pour les défauts PV (c'est-à-dire les relations de cause à effet, l'impact sur les performances du système PV), ainsi que pour les méthodes de détection de défauts (mécanisme, zone et priorité d'application, etc.), composent un contexte riche pour les domaines de la sécurité des performances des systèmes PV. »

Conclusion : « La caractérisation des défauts photovoltaïques présentée améliore l'étude

de l'applicabilité d'un système de détection de défauts correspondant des deux côtés d'un système photovoltaïque. Les méthodes de détection de défauts côté DC, d'une part, reposent majoritairement sur l'acquisition de données sensorielles - les méthodes de surveillance statistique pour par exemple, collecter les données de performance PV qui, lorsqu'elles sont comparées à une référence, peuvent détecter un défaut. Les méthodes électriques sont les plus abondantes dans la littérature, car ces méthodes peuvent détecter chacun des trois principaux types de défauts. Les techniques basées sur le traitement du signal et le ML (« Machine Learning ») sont les plus complexes, car elles impliquent respectivement l'interprétation des formes d'onde et l'exploration de données. Les méthodes de détection DC les plus simples correspondent à IMR (« Insulation Monitoring Relay »), HET (« Heat Exchange and Temperature »), CDIT (« Climatic Data Independent Technique »), In/ThI (« Infrared/Thermal Imaging »), EI (« Electroluminescence Imaging »), UIM (« Ultrasonic Inspection Method »), LIT (« Lock In Thermography »), car elles reposent uniquement sur l'installation de matériel facilement disponible. Pour cela, de telles techniques, lorsqu'elles sont intégrées à un SCADA (« Supervisory Control And Data Acquisition »), présenteraient la méthode de détection de défauts PV la plus efficace et la plus fiable du côté DC d'un système PV.

En ce qui concerne les méthodes de détection de défauts PV du côté AC du système PV, contrairement aux méthodes basées sur AIT (« Artificial Intelligence Techniques ») et RDM (« Real-time Difference Measurement ») qui sont complexes à mettre en œuvre et nécessitent respectivement de lourdes installations de calcul, l'IDT (« Islanding Detection Techniques »), le RCD (« Residual Current Device ») et le GFDI (« Ground Fault Detection and Interruption fuse ») ont plus de priorité pour l'installation dans un système PV, tout en étant en même temps plus simples à adapter. L'essentiel est que les nouveaux RCD et GFDI ainsi que d'autres équipements pertinents sont fabriqués avec un petit

système intégré dans chacun, où ils peuvent être assignés à une adresse et contrôlés à distance (c'est-à-dire mis en réseau). Cela étant dit, de tels dispositifs peuvent être attribués graphiquement au SCADA, de telle sorte que lorsqu'un RCD se déclenche par exemple, un opérateur de site peut visualiser graphiquement ce problème, localiser directement la source de l'erreur et être en mesure d'envoyer des alarmes à distance pour un nouvel acquittement du défaut. Par conséquent, à travers cet article, nous concluons qu'un double système de détection de défauts AC-DC peut être facilement appliqué à un système PV, simplement en utilisant des dispositifs indicateurs de défauts (par exemple, RCD, RCBO « Residual Current Breaker with Over-current », MCB « Mechanical Circuit Breaker », LIT, etc.) qui possèdent la fonctionnalité d'adressage à distance (par exemple, via un réseau local, une communication peer-to-peer, etc.). De tels dispositifs, servant ainsi des deux côtés du système photovoltaïque, peuvent ainsi être reflétés dans un SCADA visuel qui dispose également de son propre ensemble de blocs de données avec lesquels il peut être mis en réseau. Les mécanismes de déclenchement peuvent ainsi être inspectés à distance, tout en localisant directement la source d'erreur, pour une mise en service ultérieure sur site.

La fiabilité, la durabilité et la durabilité des systèmes photovoltaïques sont grandement améliorées par une surveillance continue et des processus d'identification des défauts. Lorsqu'ils sont équipés d'outils de détection de pannes, comme celui suggéré dans cet article, les systèmes photovoltaïques garantissent une production d'énergie robuste et des performances plus sûres. » (Veuillez-vous référer à **l'annexe 1.2** pour une lecture complète du document).

1.3 Méthodes de détection des défauts basées sur les matériaux pour les systèmes photovoltaïques. Cette étude, basée sur une analyse de 17 références bibliographiques,

présente tout d'abord les différents types de matériaux intrinsèques du PV, à partir desquels les cellules PV sont créées. En outre, un lien est établi entre les matériaux étudiés et les méthodes de détection des défauts correspondantes. Sous le titre de "Material Based Fault Detection Methods for PV Systems", cette étude est publiée dans "*Key Engineering Materials*" (2020), doi: https://doi.org/10.4028/www.scientific.net/KEM.865.111.

Résumé : « L'efficacité globale d'un système photovoltaïque est fortement affectée par les matières premières de fabrication des cellules photovoltaïques. Pour qu'une source d'énergie renouvelable soit fiable et censée produire une puissance maximale avec une durée de vie plus longue avec un minimum d'erreurs, il faut faire attention aux défauts opérationnels des systèmes photovoltaïques liés aux différents types de matières de fabrication premières. Les différents scénarios de défaillance survenant dans un système photovoltaïque en effet, diminuent sa puissance de sortie, réduisent son espérance de vie et interdisent au système de répondre aux demandes de charge, entraînant de graves pannes de courant consécutives. Cet étude vise d'abord à présenter les différents types des matériaux de fabrication des panneaux photovoltaïques, les défauts liés à ces matériaux, qui se produisent au niveau de la cellule photovoltaïque, et par conséquent, les techniques de détection de défauts correspondant à chaque type de défaut. »

Conclusion : « Nous constatons que les substances radicales utilisées dans la fabrication des cellules photovoltaïques jouent un rôle crucial dans la détermination de l'efficacité globale du système photovoltaïque. Il existe différents défauts pour chaque matériau qui dépendent principalement de la structure interne de la cellule. Les défauts étudiés vont du court-circuit ouvert aux erreurs des diodes de dérivation. Cet article présente les différents principes physiques utilisés dans la fabrication des cellules et répertorie les

défauts susceptibles de se produire. En conséquence, des techniques de détection des défauts ont été présentées. En outre, nous montrons comment sélectionner une technique de détection des défauts en fonction de la nature du défaut. » (Veuillez-vous référer à **l'annexe 1.3** pour une lecture complète du document).

1.4 Brève revue des algorithmes mathématiques pour les techniques de maintenance prédictive et la détection d'anomalies dans les systèmes Photovoltaïques. Cette étude, basée sur une analyse de 25 références bibliographiques, présente une vue d'ensemble des modèles mathématiques utilisés dans les systèmes de prédiction et de diagnostic des pannes photovoltaïques. Les méthodes étudiées sont à base de l'intelligence artificielle (IA) et des techniques de prise de décision basées sur des algorithmes. Le niveau de détection et la précision de chacune des méthodes évaluées sont clairement expliqués. Intitulé "A short review on mathematical algorithms for predictive maintenance techniques and anomaly detection in PV systems", ce document est publié dans "*Proceedings of the 31th European Safety and Reliability Conference*" (2021), 10.3850/978-981-18-2016-8_368-cd.

Résumé : « L'applicabilité des systèmes photovoltaïques (PV) en tant qu'approvisionnement efficace en énergie renouvelable pour une durée de vie moyenne de vingt-cinq ans est compromise après que de tels systèmes seront confrontées à des événements défectueux. Comme tous les systèmes extérieurs, les PV sont souvent soumis à divers types de pannes et à des conditions de fonctionnement indésirables. À chaque instant, les modules PV peuvent interagir avec différents défauts électriques. D'autre part, des conditions extérieures difficiles peuvent également affecter le bon fonctionnement du

système PV. La réduction de l'efficacité et les déficits de production sont les résultats les plus courants de l'interaction du système PV avec des événements défectueux, reflétés comme un comportement inapproprié du système. À partir de ce point, naît le besoin d'un système de diagnostic et de prédiction, qui estime la possibilité d'un potentiel futur réalisable et d'un défaut partiellement observable parmi un large ensemble de modes de défaillance possibles, avant même qu'ils ne se produisent, indépendamment des matériaux bruts des cellules PV utilisés. Dans l'intérêt d'une conception de système PV durable et fiable, cet étude vise à explorer différents modèles mathématiques de techniques de prédiction de défauts. Fondés sur l'intelligence artificielle et la prise de décision basée sur des algorithmes, divers algorithmes prédictifs sont passés en revue et comparés en ce qui concerne l'exactitude du risque d'événement. Par exemple, un modèle probabiliste basé sur les chaînes de Markov calcule les taux de défaillance, tandis que les réseaux neuronaux convolutifs indiquent un panneau défectueux et que les algorithmes de détection de code-barres automatisés basés sur l'apprentissage supervisé détectent les défauts des modules PV. L'évaluation critique entre différents modèles servira comme une base d’information lors du choix d'une technique prédictive de défaut PV. »

Conclusion : « Un système photovoltaïque peut être considéré comme un ensemble d'interconnexions entre différents sous-réseaux. Le côté DC, qui comprend le générateur photovoltaïque, le régulateur de charge et le parc de batteries, est relié à l'onduleur pour fournir de l'énergie consommable au côté AC. Le risque de défaillance est plus élevé du côté DC, étant donné que des défaillances internes, externes et électriques peuvent se produire au niveau du champ photovoltaïque, plutôt que des défaillances purement électriques, qui peuvent se produire du côté du courant alternatif. Les systèmes photovoltaïques étant installés à l'extérieur, le réseau peut être confronté à de nombreuses défaillances, en particulier celles dues à l'instabilité de l'environnement. Comme un

système PV peut très bien fonctionner sans un programme de maintenance prédictive, il est recommandé d'adapter un prédicteur de défaillance principalement pour les grandes fermes PV, en mettant l'accent sur la détection des défaillances liées à la zone DC, étant donné qu'elles sont les plus difficiles à reconnaître. Lorsque la puissance générée est exprimée en mégawatts, une interruption plus précoce de la défaillance pourrait permettre d'économiser l'immense rentabilité résultant de la perte d'énergie ou de l'intermittence. Le choix entre l'historique du processus ou l'architecture de la technique quantitative se réfère à la disponibilité de l'ensemble des données relatives à l'irradiation solaire, à la température et à d'autres critères liés à l'efficacité. Enfin, l'un des défis que nous proposons de relever à l'avenir est la définition et la mise en œuvre d'un schéma décisionnel allant de la collecte et du traitement des données à la décision de maintenance dans un contexte global de gestion des centrales photovoltaïques. » (Veuillez-vous référer à **l'annexe 1.4** pour une lecture complète du document).

1.5 Étude des algorithmes d'extraction de la puissance maximale d'un système photovoltaïque avec les convertisseurs DC-DC correspondants. La procédure de cette étude qui est basée sur une analyse de 128 références bibliographiques est décomposée en deux grandes parties : les algorithmes MPPT (« Maximum Power Point Tracker ») d'une part, et le matériel physique des convertisseurs DC-DC d'autre part. Les algorithmes sont principalement classés en deux catégories : les algorithmes locaux et les algorithmes globaux basés sur le point de puissance maximale exploitée (MPP). Les convertisseurs DC-DC, quant à eux, ont été perçus comme isolés ou non isolés. Intitulée “An investigation on maximum power extraction algorithms from PV system with corresponding DC-DC converters”, cette étude est publiée dans “*Energy*” (2020), doi.org/10.1016/j.energy.2021.120092.

Résumé : « Cet étude vise à explorer les différentes approches utilisées pour suivre le point de puissance maximale de fonctionnement (MPP) des modules PV (photovoltaïques), en réalisant la plus grande quantité d'extraction d'énergie disponible, ce qui permet de réaliser un comportement économique et productif efficace dans les systèmes PV. Cette procédure se déroule en deux parties : la mise en œuvre de l'algorithme et la conception des unités de traitement d'alimentation DC-DC . Avant tout, tous les algorithmes MPP relèvent de deux grandes catégories : MPP local (se produit lors de rayonnements solaires homogènes) et MPP global (se produit dans des conditions d'ombrage partiel). Chacun des deux groupes possède différentes méthodologies de génération d'algorithmes. Deuxièmement, les PPU sont généralement classés comme des convertisseurs DC-DC isolés ou non isolés. Chaque collection règne sur des convertisseurs buck, boost et buck-boost avec diverses configurations de circuits. Une évaluation critique et une comparaison ont été menées pour les algorithmes et les convertisseurs en termes d'efficacité, de fiabilité et de complexité. Après analyse et comparaison de différents schémas de suivi du point de puissance maximale, il s'avère que le meilleur algorithme à adapter est issu de l'ensemble global de suivi du point de puissance maximale, sous exploitation des topologies de courbes caractéristiques. Pour l'architecture PPU, il est conclu qu'un convertisseur buck-boost non isolé est le meilleur à choisir lors de la conception d'un tracker MPP. »

Conclusion : « Les algorithmes de suivi sont conçus pour détecter un seul maximum (local, sous irradiation homogène) ou plusieurs (lorsque de nombreux pics locaux existent dans la courbe P-V d'un réseau PV en raison de conditions d'ombrage partiel). Pour les trackers de pics locaux, différents algorithmes ont montré une efficacité comprise entre 93,5 % et 99 % dans la détection des pics, mais tous ont eu un comportement oscillant autour du MPP (Maximum Power Point), ce qui a parfois donné lieu à un faux pic. Ces

algorithmes n'ont pas été en mesure de se stabiliser face à des conditions météorologiques changeant rapidement (fluctuation de la température et de l'irradiation), ce qui a entraîné des pertes de puissance cumulées.

En outre, les algorithmes GMPP (Global Maximum Power Point) se sont avérés adaptés à la détection des pics locaux et globaux, car ils réduisent les oscillations et diminuent le temps de fonctionnement du contrôleur lors de la détection du pic dans des conditions climatiques qui changent rapidement. Ces algorithmes ont également permis d'accélérer la vitesse de convergence en négligeant tout balayage inutile. Leur efficacité de détection augmente de 97,36 % à 99,99 % pour certains algorithmes. La construction des convertisseurs isolés est plus complexe que celle des convertisseurs non isolés, car la mise en œuvre d'un transformateur augmente les pertes par hystérésis et par courants de Foucault, ce qui réduit le rendement de conversion global (91,2 %) par rapport aux convertisseurs non isolés (> 95 %).

Enfin, il est recommandé de mettre en œuvre un convertisseur DC-DC buck-boost non isolé avec un algorithme de suivi GMPP comme solution finale pour détecter la puissance de crête pour différents systèmes PV, en raison de la capacité d'augmenter/diminuer la tension de sortie dans des conditions d'irradiation non uniformes. » (Veuillez-vous référer à **l'annexe 1.5** pour une lecture complète du document).

1.6 Atténuation des effets de l'ombrage partiel sur la performance du système PV grâce à la reconfiguration du réseau PV. Une étude, basée sur une analyse de 176 références bibliographiques a été menée pour réduire les impacts négatifs des conditions d'ombrage partiel (PSC) sur les systèmes photovoltaïques par la reconfiguration des réseaux photovoltaïques. Trois catégories principales ont été identifiées pour reconfigurer

les réseaux photovoltaïques : les techniques physiques, électriques et physiques-électriques combinées. Chacune des méthodes étudiées est comparée de manière critique aux autres selon un modèle mathématique standardisé. Intitulée “Mitigating the effects of partial shading on PV system’s performance through PV array reconfiguration: A review”, cette étude est publiée dans “*Thermal Science and Engineering Progress*” (2022), doi.org/10.1016/j.tsep.2022.101280.

Résumé : « Cet étude vise à explorer les différentes méthodes de reconfiguration (PVR « PV array Reconfiguration ») de réseau photovoltaïque (PV), utilisées pour réduire les impacts négatifs des conditions d'ombrage partiel (PSC « Partial Shading Conditions »), qui affectent les performances d'un système PV (c'est-à-dire les hotspots, le déséquilibre électrique, etc.). La classification des différentes techniques PVR est formée en trois catégories principales : combinaison physique, électrique et physique-électrique. Le PVR physique modifie les emplacements réels des panneaux dans le réseau. Appelés méthodes de reconfiguration statique, cet ensemble comprend des méthodes basées sur les puzzles, les nombres, la symétrie, la maximisation de la distance et inspirées de la nature. D'autre part, le PVR électrique réorganise les interconnexions électriques entre les panneaux photovoltaïques et est composé de configurations électriques basées sur des algorithmes, basées sur l'intelligence artificielle, hybrides et de configurations électriques améliorées de base. Une méthode PVR combinée (physique-électrique) réunit les deux catégories précédentes. Chaque méthode des trois principaux ensembles est comparée de manière critique aux autres pertinentes, selon un modèle mathématique, qui comprend de nombreux indices de performance : facteur de remplissage (FF), perte de puissance de discordance (P_{ML}), perte de puissance en pourcentage ($\%P_{LOSS}$), ratio de performance (PR), ratio d'exécution (ER), efficacité (η), pourcentage d'amélioration de la puissance ($\%PE$) et puissance de sortie DC (P_{DC}). L'enquête approfondie sur les différentes

techniques PVR a montré qu'un panneau PV configuré comme Total Cross Tied (TCT), déplacé physiquement au moyen de l'algorithme Static Shade Dispersion Physical Array Relocation (SD-PAR), tout en interférant avec une matrice de commutation contrôlée par l'algorithme Modified Harris Hawks Optimizer (MHHO) pourrait être une solution optimale et efficace pour atténuer passivement les effets des PSC. »

Conclusion : « Dans le présent document, les méthodes de PVR ont été caractérisées comme étant soit physiques, soit électriques, soit combinées physique-électrique. Les techniques physiques de PVR sont basées sur les ajustements de positionnement des modules PV dans le réseau. Ce grand ensemble contient des techniques basées sur des puzzles (difficiles à construire), des méthodes basées sur des nombres et des méthodes basées sur la symétrie (nécessitant des circuits complexes). En outre, les techniques basées sur la maximisation de la distance nécessitent des espaces supplémentaires pour être mises en œuvre, tandis que la méthode basée sur Lo Shu impose des compétences informatiques complexes. Parmi les différents PVR physiques, l'algorithme SD-PAR résiste à tous les modèles d'ombrage possibles, avec une efficacité de près de 100 % et une amélioration de la puissance de 70 % (tableau 7). Dans le cadre d'un futur PVR, il est d'abord recommandé de configurer les panneaux photovoltaïques en TCT, afin de trouver un compromis entre la complexité et l'efficacité par rapport à d'autres interconnexions électriques (RSP-TCT (« Rearranged Series Parallel – Total Cross Tied »), RBL-TCT (« Rearranged Bridge Linked – Total Cross Tied »), R-TCT (« Random – Total Cross Tied »), etc.). Successivement, l'algorithme SD-PAR, après différentes itérations, relocalise (une seule fois) les modules configurés TCT. À ce niveau, le processus de reconfiguration statique est effectué. Ensuite, les modules PV configurés doivent être

interférés avec un SM (« Switching Matrix ») qui, à son tour, est contrôlé par l'algorithme MHHO. Théoriquement, cette planification de configuration croisée devrait permettre d'obtenir un rendement proche de 100 %, une augmentation de la puissance de plus de 75 %, une réduction des pertes de désadaptation et de puissance à environ 10 % et 3 % respectivement, ainsi qu'un facteur de remplissage élevé de l'ordre de 80 %. Ce schéma PVR est encouragé à être étudié expérimentalement dans des systèmes PV réels, afin d'obtenir des résultats discrets et quantitatifs, qui évaluent son efficacité par rapport à l'atténuation des PSC, et une meilleure productivité de l'énergie PV. » (Veuillez-vous référer à **l'annexe 1.6** pour une lecture complète du document).

1.7 Aperçu de l'utilisation des matériaux à changement de phase (PCM) pour le refroidissement des systèmes photovoltaïques. Cette étude, basée sur une analyse de 24 références bibliographiques analyse l'utilisation des matériaux à changement de phase (PCM) dans l'optimisation thermique des systèmes photovoltaïques. Elle révèle tout d'abord les différents types de PCM utilisés à cette fin, par rapport à d'autres technologies de refroidissement. Une méthode de sélection optimale des PCM est présentée sur la base de différents aspects thermiques. Intitulée “An overview on the Use of Phase Change Material (PCM) for PV Cooling”, cette étude est publiée dans “*Key Engineering Materials*” (2022), 10.4028/p-t2m41c.

Résumé : « Les processus de gestion thermique pour les applications de refroidissement de panneaux photovoltaïques (PV) augmentent l'efficacité globale des systèmes PV et permettent de maximiser la production d'énergie. En conséquence, cet étude recense les méthodes récentes de gestion thermique des systèmes photovoltaïques, qui impliquent l'utilisation de matériaux à changement de phase (PCM) à l'arrière des modules photovoltaïques. Comparées à d'autres méthodes de refroidissement (telles que les

méthodes basées sur l'air et l'eau), les techniques basées sur le PCM nécessitent moins d'entretien, sont respectueuses de l'environnement et ont un cycle de vie plus long. Étant donné que les PCM sont de nature diverse et qu'il existe de nombreuses méthodes pour guider leur procédure de sélection, cet étude commence par exposer les différents types de PCM, qui se peuvent être des PCM organiques, inorganiques, eutectiques et commerciaux, avec les caractéristiques de chacun. Après avoir reconnu différentes natures de PCM, un processus de sélection est établi en fonction de la température de fusion, de la chaleur latente ou de la conductivité thermique du PCM. Les résultats ont montré que le PCM commercial est la meilleure option suivie par le PCM organique, en raison de leurs aspects chimiques améliorés par rapport au PCM inorganique et eutectique. Concernant les critères de sélection PCM, le procédé le plus simple mais suffisant est basé sur la méthode de la température de fusion, en raison des calculs simplifiés par rapport aux autres grandeurs thermiques. À la fin, des recommandations de travaux futurs sont formulées, liées à l'évaluation du cycle de vie du PCM et aux effets des cycles de refroidissement/chauffage sur l'entropie PV. »

Conclusion : « Dans ce travail, quatre classifications principales ont été établies pour les PCM, les PCM commerciaux offrant la plus grande gamme de T_{melt} (température de fusion), ce qui leur permet de convenir à différentes zones climatiques. En l'absence de contraintes économiques, les PCM commerciaux constituent la meilleure option, suivis par les PCM organiques, principalement les composés de paraffine, pour leur non-toxicité et leurs meilleurs aspects chimiques par rapport aux PCM inorganiques et eutectiques. En d'autres termes, la cire de paraffine et les PCM commerciaux sont meilleurs et plus largement utilisés que les autres dans les zones tropicales et subtropicales. Dans les zones climatiques sèches et tempérées, un seul PCM n'est pas suffisant pour refroidir les modules PV en raison des températures ambiantes élevées, ce qui nécessite une

structuration en cascade de plusieurs PCM. Le processus de sélection du PCM par approche directe, en revanche, est grandement facilité par le choix basé sur T_{melt}, car les calculs de la température ambiante sont plus simples que le traitement d'autres quantités thermiques telles que la chaleur latente et la conductivité thermique. La température de fusion d'un PCM doit être aussi proche que possible de T_{PV} dans le cadre du STC (« Standard Test Conditions »). En général, les PCM utilisés sont respectueux de l'environnement et considérés comme des matériaux de stockage d'énergie non dangereux. Les recommandations pour les travaux futurs commencent par l'évaluation du cycle de vie des différents types de PCM par rapport à la rentabilité, et par des études sur la relation entre les cycles de refroidissement/chauffage continus et l'entropie des modules photovoltaïques. » (Veuillez-vous référer à **l'annexe 1.7** pour une lecture complète du document).

1.8 Évaluation comparative de différents suiveurs solaires : Vers une conception rentable, facile à mettre en œuvre et à haut rendement. Les différents types de suiveurs solaires sont classés, en se basant sur une analyse de 218 références bibliographiques, en fonction de leurs systèmes de contrôle, de leurs mécanismes d'entraînement, du nombre d'axes mobiles et de leurs stratégies de suivi. Les différents suiveurs (traqueurs) examinés sont comparés les uns aux autres de manière critique, ce qui permet de sélectionner de manière optimale un suiveur solaire pour une application photovoltaïque. Intitulée “Comparative assessment of different solar trackers: Towards a cost effective, easily implemented and high efficiency design” cette étude est destinée à être soumise à “*Renewable Energy*”.

Résumé : « Pour un fonctionnement efficace des systèmes photovoltaïques avec une

extraction maximale d'énergie, réalisée en minimisant les pertes de capture des radiations, et en s'assurant que les panneaux photovoltaïques sont exposés de manière perpendiculaire aux rayons du soleil, cet article vise d'abord à explorer les différentes normes de classification pour les suiveurs solaires (ST). Les systèmes de contrôle sont d'abord fondés sur une structure en boucle ouverte ou fermée. Les mécanismes d'entraînement, actifs ou passifs, constituent la deuxième étiquette de la classification des suiveurs solaires. En outre, le nombre d'axes mobiles est la troisième caractérisation des suiveurs, basée sur des plates-formes à axe unique ou à double axe. La destination finale de la classification d'un suiveur solaire est sa stratégie de suivi, qui peut être basée sur le processeur, sur la date et l'heure ou sur un schéma combinant la date et l'heure et les capteurs. Une comparaison critique entre les différentes méthodologies pour chaque critère est établie afin de conclure à une conception efficace du traqueur solaire basée sur les avantages et les inconvénients des différents modèles. Une étude économique est également menée pour déterminer dans quelle mesure il est intéressant d'installer un ST dans un système photovoltaïque. Ce travail servira de base d'information pour les chercheurs dans ce domaine afin de les aider à concevoir un traqueur solaire précis et adapté à chaque cas. Un modèle futur de traqueur solaire est proposé à la fin, basé sur la classification la plus avantageuse de chaque terme. »

Conclusion : « La diversité des types de trackers solaires constitue un choix difficile pour adapter un tracker spécifique à un système. Afin de concevoir un tracker précis, il faut bien identifier leurs différentes caractérisations. Dans cet article, les trackers solaires ont été classés en fonction des stratégies de contrôle, des mécanismes d'entraînement, du nombre d'axes mobiles et des stratégies de suivi.

Dans le cadre des stratégies de contrôle, le contrôle en boucle fermée se révèle plus

compétitif que celui en boucle ouverte. Les signaux de rétroaction aident à réduire les erreurs différentielles (le cas échéant), obtenant ainsi des sorties plus précises. Le mélange de contrôles en boucle ouverte et fermée, appelés stratégies hybrides, tire parti des deux natures des schémas de contrôle, mais consomme en revanche plus de temps opérationnel.

Contrairement aux méthodes de conduite passive, basées sur des alliages à mémoire de forme et des mousses à mémoire de forme, qui dépendent des implications thermiques de l'environnement environnant des ST, les trackers actifs s'avèrent plus efficaces, plus fiables et approuvés par les utilisateurs. En contrôlant directement les actionneurs mécaniques (moteurs), la précision est meilleure, plutôt que déviée par la dissipation thermique dans les techniques passives. Le choix de moteurs pas à pas pour faire pivoter l'orientation des panneaux photovoltaïques est recommandé par rapport à l'utilisation de moteurs à courant continu à aimant permanent, de moteurs à induction à courant alternatif ou de toute autre forme d'actionneurs mécaniques. En effet, les moteurs pas à pas consomment moins d'énergie lorsqu'ils se déplacent dans des positions angulaires spécifiées, plutôt que dans d'autres types de moteurs, ce qui augmente l'efficacité énergétique du système. Les suiveurs à deux axes minimisent les pertes de rayonnement (dues à la rotation de la terre autour du soleil, à l'absence d'espace disponible pour installer les modules PV à différents angles solaires, etc.) que les suiveurs à axe unique. Par conséquent, plus de faisceaux de radiations sont captés grâce à un degré de liberté plus élevé dans le positionnement, ce qui permet de récolter plus d'énergie. Les méthodes de programmation basées sur l'intelligence artificielle pour que le suiveur solaire s'auto-apprenne et s'appuie sur les expériences de suivi précédentes renvoient aux compétences du concepteur dans ce domaine et à la manière de les utiliser dans la conception d'un système de suivi solaire. De telles routines de programmation nécessitent un algorithme

de codage complexe, qui peut être considéré comme consommateur de temps et d'argent. Un compromis entre la programmation complexe de l'IA (Intelligence Artificielle) et les langages de programmation de bas niveau (Assemblage, etc.) pourrait offrir une solution intermédiaire, comme la programmation d'un algorithme contrôlé en boucle fermée, en utilisant un langage de haut niveau (tel que C++) avec une plateforme Arduino. » (Veuillez-vous référer à **l'annexe 1.8** pour une lecture complète du document).

Les résultats les plus importants de l'analyse documentaire peuvent être classés en deux catégories principales : la première correspond à la recherche sur les pannes et la maintenance des systèmes photovoltaïques (études 1.1 à 1.4), tandis que la seconde prend en compte les différentes méthodes d'optimisation des performances des systèmes photovoltaïques (études 1.5 à 1.8), telles que la reconfiguration des panneaux photovoltaïques, l'application de MPPT et les applications des suiveurs solaires :

1- Les cellules photovoltaïques monocristallines et polycristallines sont les plus dominantes dans le marché photovoltaïque. Les cellules monocristallines ont un rendement plus élevé que les cellules polycristallines, mais elles sont plus sensibles (d'un point de vue performanciel) aux variations de température.

2- La possibilité d'un défaut PV est plus susceptible de se produire du côté DC d'un système PV, où les défauts dans cette zone des systèmes PV sont plus difficiles à reconnaître.

3- Les pannes photovoltaïques les plus probables sont celles qui sont liées aux conditions extérieures (par conditions externes, on entend tous les facteurs qui affectent les performances des systèmes photovoltaïques depuis l'extérieur des modules photovoltaïques, tels que les conditions environnementales) : elles sont principalement

dues à l'irradiation.

4- Lorsque les systèmes photovoltaïques sont soumis à un type de maintenance approprié, la production globale d'électricité peut être augmentée de 8,7 %, avec un affaissement de la tension atténué de 81 % et des distorsions réduites à 2 %.

5- Les suiveurs de point de puissance maximale globale possèdent la plus grande efficacité dans la détection du pic maximal parmi de nombreuses localisations dans une courbe caractéristique PV avec une efficacité comprise entre 97,36% et 99,99%. Lorsqu'ils fonctionnent en synergie avec un convertisseur DC-DC buck-boost non isolé, la courbe caractéristique peut être tracée de manière optimale, ce qui permet d'extraire une puissance maximale du système PV.

6- Un réseau photovoltaïque configuré en croix, relocalisé par l'algorithme SD-PAR, interféré avec une matrice de commutation qui est à son tour contrôlée par un algorithme d'optimisation harris hawk modifié, résulterait en une reconfiguration photovoltaïque avec un rendement élevé, une amélioration de la puissance de plus de 75%, une réduction du déséquilibre, et des pertes de puissance à environ 10% et 3% respectivement, avec un facteur de remplissage élevé d'environ 80%.

7- Les suiveurs solaires basés sur un processeur ont des performances supérieures aux autres techniques de suivi solaire.

Ces conclusions vont permettre de guider la définition et l'orientation des travaux de thèse présentées.

1.9 Positionnement de l'étude

En ce qui concerne les résultats des études présentées dans ce chapitre, et parmi les différentes conditions environnementales qui affectent les performances des systèmes PV, on peut conclure que

l'irradiation est considérée comme le facteur environnemental le plus crucial qui influence le comportement opérationnel et la production d'électricité de ces systèmes.

D'une part, l'irradiation est le principal moteur de la production d'électricité par les panneaux photovoltaïques. En effet et contrairement à la température par exemple, l'irradiation solaire influence directement la quantité d'énergie disponible pour la conversion, ce qui la rend fondamentale dans la détermination de la production globale du système.

D'autre part, et toujours en comparaison à la température, l'irradiation solaire est un facteur moins contrôlable. Alors que la température peut être maîtrisée et régulée par divers moyens, comme le démontrent les différentes analyses documentaires de ce chapitre concernant l'optimisation thermique des systèmes PV, grâce à des techniques telles que l'utilisation de matériaux à changement de phase (PCM) et d'autres méthodes de refroidissement (air, eau, etc.), il est plus complexe de réguler l'irradiation incidente sur les panneaux PV. En d'autres termes, l'irradiation dépend intrinsèquement des conditions environnementales et ne peut être augmentée artificiellement. Cette incapacité à contrôler ou à augmenter l'irradiation à la surface des panneaux photovoltaïques souligne son importance primordiale pour l'efficacité et le fonctionnement du système photovoltaïque.

Par conséquent, l'efficacité globale des systèmes photovoltaïques est fortement liée aux niveaux d'irradiation. Par exemple, lorsque les niveaux d'irradiation sont élevés, davantage de photons du soleil frappent les cellules photovoltaïques, ce qui entraîne une plus grande excitation des électrons et une production d'énergie plus importante. Inversement, pendant les périodes de faible irradiation, comme les jours nuageux ou couverts, le système PV reçoit moins de photons, ce qui entraîne une réduction de la production d'énergie. Cette relation directe et proportionnelle entre l'irradiation et la production photovoltaïque signifie que toute fluctuation ou variation de l'irradiation aura un impact direct sur les performances du système. Malgré les différents types de défauts photovoltaïques, comme indiqué dans ce chapitre, et l'impact négatif que certains peuvent avoir sur les performances

des systèmes photovoltaïques, les fluctuations de l'irradiation se répercutent immédiatement sur la production d'énergie de ces systèmes.

Outre les conditions environnementales, et en tenant compte du PV déclaré, les « hotspots » constituent particulièrement un défi majeur pour le bon fonctionnement des systèmes PV, où de tels défauts peuvent induire des scènes de brûlures importantes. Les « hotspots » sont directement et principalement liés à des conditions d'irradiation inhomogènes. Plus précisément, lorsqu'une zone localisée d'un module solaire reçoit un rayonnement inférieur ou supérieur à celui d'autres zones du même module, il se produit une distribution inhomogène de la température dans le module photovoltaïque. En conséquence, certaines parties du module se comportent comme une charge, qui dissipe le courant des autres cellules photovoltaïques fonctionnant normalement dans le module. À ce stade, les cellules ombragées deviennent polarisées à l'inverse, agissant ainsi comme des résistances plutôt que comme des conducteurs, ce qui conduit finalement à une augmentation des résistances et de la production de chaleur. En substance, l'irradiation influence directement les conditions dans lesquelles les « hotspots » peuvent se produire en affectant le déséquilibre du courant et de la température à travers le module PV, développant finalement une perte de désadaptation, dans laquelle certains panneaux fonctionnent à des niveaux de sortie de puissance différents des autres, réduisant ainsi la récolte globale d'énergie.

1.10 Travail de recherche développé

Pour les raisons mentionnées, et après l'examen approfondi des résultats de la vaste revue de la littérature qui compose une grande partie de cette thèse (représentant la source d'information et le contexte pour la prise de décision et l'orientation de cette recherche), ce travail de thèse propose d'optimiser la performance PV principalement en se concentrant sur le facteur d'irradiation. Sachant qu'il n'est pas possible d'augmenter la quantité d'irradiation projetée par le soleil, cette thèse vise donc à développer un comportement opérationnel spécifique du système PV selon quatre études

proposées basées sur l'irradiation, qui garantit le maximum de puissance disponible quelles que soient les conditions d'irradiation :

- L'optimisation dynamique de l'angle d'inclinaison β selon le modèle simulé proposé augmente l'irradiation normale directe captée par les panneaux PV, en raison de l'orientation/inclinaison optimisée, ce qui permet de générer plus d'énergie à partir du système PV.
- Le chargeur solaire basé sur le MPPT stocke la quantité d'énergie excédentaire générée dans des systèmes de stockage d'énergie en vue d'une utilisation ultérieure. Ainsi, le modèle simulé peut ajouter plus de flexibilité avec une grande précision dans la charge des batteries pour les systèmes photovoltaïques hors réseau, optimisant ainsi leur performance.
- L'algorithme MPPT modifié basé sur PSO et conforme de manière innovante aux mécanismes pathogènes du diabète de type 1 (T1D) réduit considérablement les effets des conditions d'ombrage partiel. Par conséquent, l'application de ce nouvel algorithme permettrait d'extraire la puissance maximale d'un réseau photovoltaïque sous cinq maximums locaux distincts, ce qui augmenterait et optimiserait les performances du PV.
- L'étude de faisabilité des suiveurs solaires, après avoir pris en compte les différents facteurs environnementaux relatifs à la zone d'installation du système photovoltaïque, permet de réduire l'entropie du système et d'augmenter son cycle de vie. Avec la recommandation d'appliquer ou non un suiveur solaire pour une zone d'installation particulière du système PV, sa performance est optimisée de manière préventive sur le long terme.

.

Chapitre 2

Optimisation de l’angle d’inclinaison des panneaux photovoltaïques pour minimiser le coût d’énergie

D'après le **chapitre 1**, et en ce qui concerne l'impact de l'irradiation sur la productivité de l'énergie photovoltaïque parmi de nombreux autres facteurs environnementaux, on peut affirmer que tout contrôle supplémentaire sur la quantité d'irradiation captée par les panneaux photovoltaïques conduirait finalement à une performance photovoltaïque optimisée. Cette étude vise donc à maximiser la quantité d'irradiation solaire absorbée par les panneaux photovoltaïques de deux manières :

- S'assurer qu'il n'y a pas d'ombrage mutuel entre les panneaux PV adjacents. L'absence d'ombrage se traduit par de plus grandes quantités d'absorption de l'irradiation. Un nouveau modèle mathématique est donc établi, qui prend en considération la géométrie d'un panneau PV, puis fournit l'espacement requis entre le nombre maximum de panneaux PV autorisés (de même géométrie) dans une zone de forme carrée.
- Modification mensuelle de l'angle d'inclinaison β en fonction de la zone géographique d'installation du système PV. Sur la base des données d'irradiation de trois zones géographiques distinctes, un angle d'inclinaison optimal est calculé pour différents mois de l'année pour chaque région.

Dans cette étude, la **section 1** correspond à une introduction aux effets de l'irradiation sur la productivité de l'énergie photovoltaïque et aux différentes méthodes utilisées dans la littérature

pour compenser ces effets. La **section 2** montre comment se déroule la procédure d'optimisation basée sur l'irradiation suggérée et tous les attributs (c'est-à-dire les coordonnées de la zone géographique, la période de l'année, la superficie totale de la zone de l'installation photovoltaïque, etc.). La **section 3** décrit le schéma de calcul du coût levé de l'énergie (LCOE). La **section 4** présente la procédure de calcul du rayonnement solaire absorbé en fonction de l'angle d'inclinaison. La **section 5** présente la formulation mathématique de l'espace minimum requis entre les panneaux PV adjacents, afin d'éviter tout ombrage mutuel. La **section 6** indique la taille du système PV, en termes de nombre de panneaux PV maximum autorisés à être installés dans une zone d'installation définie. La **section 7** présente la procédure de calcul de l'énergie produite mensuellement et de la puissance moyenne. La **section 8** présente la méthode de calcul du coût actualisé de l'énergie et du coût de la puissance. Les résultats de la simulation pour chacune des zones géographiques étudiées sont présentés dans la **section 9**, où ces résultats sont discutés dans la **section 10**. Enfin, des conclusions sont tirées à la **section 11**.

Les résultats de cette étude indiquent clairement qu'avec le schéma d'installation proposé pour les systèmes PV (c'est-à-dire basé sur l'évitement de l'ombrage mutuel des panneaux PV adjacents), et la modification mensuelle de l'angle d'inclinaison, le coût de l'électricité et la production moyenne d'électricité pour chacune des zones régionales étudiées seraient respectivement diminués et augmentés. Pour Belfort (France), le coût moyen mensuel de l'électricité a diminué de 11,72 $/W (β fixe) à 11,19 $/W (β optimisé), tandis que la production moyenne mensuelle d'électricité a augmenté de 23,3 kW (β fixe) à 47 kW (β optimisé). De même, à Tantan (Maroc), le coût moyen mensuel de l'électricité a également diminué de 4,94 $/W (β fixe) à 4,72 $/W (β optimisé), alors que la production moyenne mensuelle d'électricité a augmenté de 455 kW (β fixe) à 622 kW (β optimisé). A Tripoli (Liban), avec les mêmes conséquences de l'application d'une modification dynamique de l'angle d'inclinaison en fonction de la période de l'année, le coût moyen mensuel de l'électricité a diminué de 5,19 $/W (β fixe) à 4,96 $/W (β optimisé), avec la production moyenne

mensuelle d'électricité, augmentée de 215 kW (β fixe) à 473 kW (β optimisé).

Les résultats de cette étude servent bien l'objectif de cette thèse, qui est d'optimiser le comportement fonctionnel des systèmes PV : avec l'augmentation de la production d'énergie moyenne mensuelle qui en résulte par rapport au comportement opérationnel d'un système PV basé sur un β-fixe, cette étude améliore la performance d'un système PV, en prenant en considération le facteur d'irradiation (maximiser la quantité de radiations solaires sur la surface des panneaux PV), ce qui permet d'obtenir des résultats plus importants en termes d'énergie.

Optimisation de l'angle d'inclinaison des panneaux photovoltaïques pour minimiser le coût d'énergie

Cet article est publié dans « **Computers and Electrical Engineering** »

doi.org/10.1016/j.compeleceng.2021.107474

Résumé – Cet article étudie les effets de la variation de l'angle d'inclinaison du panneau photovoltaïque (PV) sur la rentabilité des réseaux PV. La modification mensuelle de l'angle d'inclinaison β effectuée dans le cadre de cette étude permet de réduire le coût actualisé de l'énergie (LCOE), améliorant ainsi la situation économique du système en réduisant la période de récupération de l'investissement en capital. Le résultat escompté de ce travail est double : il correspond à un nouveau modèle mathématique généralisé qui permet d'intégrer un nombre maximum de panneaux photovoltaïques dans une zone de forme carrée sans ombrage mutuel, et il étudie les valeurs mensuelles de l'angle d'inclinaison sur la base d'une sélection spécifique, ainsi que leurs effets sur le coût actualisé de l'énergie. L'application des résultats obtenus (c'est-à-dire les valeurs numériques de β) diminue à la fois le LCOE et le coût de l'électricité, tout en augmentant la production d'électricité pour un système PV situé à Tripoli-Liban (latitude : 34.38°), Belfort-France (latitude : 47.63°) et Tantan-Maroc (latitude : 28.38°).

Computers and Electrical Engineering 96 (2021) 107474

Contents lists available at ScienceDirect

Computers and Electrical Engineering

journal homepage: www.elsevier.com/locate/compeleceng

Optimization of PV array tilt angle for minimum levelized cost of energy

Khaled Osmani [a], Mohamad Ramadan [b,c,*], Thierry Lemenand [a], Bruno Castanier [a], Ahmad Haddad [b,c]

[a] LARIS EA 7315, Polytech Angers, UNIV Angers, France
[b] School of Engineering, International University of Beirut BIU, Beirut, Lebanon
[c] School of Engineering, Lebanese International University LIU, Bekaa, Lebanon

ARTICLE INFO

Editor: Dr. M. Malek

Keywords:
Optimum tilt angle
Levelized cost of energy
Average power
Power cost

ABSTRACT

This paper studies the effects of PhotoVoltaic (PV) tilt angle variation over the cost efficiency of PV networks. The monthly modification of the tilt angle β conducted by this study, decreased the levelized cost of energy (LCOE), thus enhancing the system's economical status, by reducing its capital investment's payback period. The intended outcome of this work is twofold: it corresponds to a generalized novel mathematical model which enables the maximum number of PV panels to be fit into a square shaped area without any mutual shading, plus it investigates the monthly tilt angle values based on a specific selection, and their effects on the LCOE. The application of the obtained results (i.e., numerical values of β) has diminished both the LCOE as well as the power cost, while increasing power production for a PV system located in Tripoli-Lebanon (latitude: 34.38°), Belfort-France (latitude: 47.63°) and Tantan-Morocco (latitude: 28.38°).

1. Introduction

The worldwide increasing energy demand can be well compensated by usage of solar photovoltaics as an alternative supply based on renewable energy [1]. In comparison with other renewable forms (i.e., wind, hydro, etc.), PhotoVoltaic (PV) systems represent reliable energy supplies, due to the abundancy of solar radiations, where a $1.2 \bullet 10^5$TW of energy hit the surface of the earth continuously [2]. Such large amount of energy can be partially granted from, upon installation of PV systems [3]. Furthermore, these systems are of non-detrimental nature, and able to produce power with a zero-noise and emission-less performance [4].

The omnipresent characteristics of solar radiations, low maintenance costs for PV systems, and their long lifetime (around 25 years), made them a popular energy option to be adapted [5]. Such systems reduce greenhouse gas emissions, decrease environmental damages, and contribute to stabilizing climate change and global warming, by reducing global emissions [6].

However, the main drawback of PVs is their low efficiency, where a single PV module is incapable of producing a significant power quantity, to meet load demands [7]. Additionally, PV's output is mainly dependent on radiation, environmental conditions, and ambient temperature [8]. The irregularity of sunrays availability, weather unpredictability, and presence of physical obstacles (i.e., trees, overhead cables, etc.) confront PV systems with Partial Shading Conditions (PSCs) scenarios [9]. Under non-homogeneous

This paper is for special section VSI-reg. Reviews processed and recommended for publication by Guest Editor H. S. Ramadan.

* Corresponding author at: School of Engineering, International University of Beirut BIU, Beirut, Lebanon.
E-mail address: mohamad.ramadan@liu.edu.lb (M. Ramadan).

https://doi.org/10.1016/j.compeleceng.2021.107474
Received 30 December 2020; Received in revised form 26 August 2021; Accepted 20 September 2021
Available online 12 October 2021

Nomenclature

Abbreviations

LCOE	levelized cost of energy
PV	photo voltaic
DNI	direct normal insulation
PSCs	partial shading conditions
MPPT	maximum power point tracker
GMPPT	global maximum power point tracker
PVGIS	photovoltaic geographical information system

Greek letters

β	tilt angle,
I_β	selected tilt angle,
α	altitude angle, °
δ	daily declination angle,
S_β	minimum spacing between PV modules
ψ	Azimuth angle, °

Units

kW	kilo watt
TW	terra watt
$kWh/m^2/day$	radiation
\$/W	power cost
c/kWh	levelized cost of energy
m^2	land area

Symbols

A	area
E	energy
N_{PV}	number of photovoltaic modules
P_{AV}	average power
C_{Power}	power cost
$A_{Spacing}$	spacing area
$A_{PV-Module}$	projected area on land
N_{S_β}	number of spacing areas

irradiance conditions, hotspots get created, yielding in permanent damages to PV modules, with a notable voltage drop on the shaded panel's terminals [10]. With the presence of multiple peaks in the power-voltage (P-V) characteristic curve of a PV module, it becomes difficult to extract maximum available power [11]. Besides, due to space limitation and mutual shadowing between adjacent PV modules, the PSCs become unavoidable [12].

The low efficiency of a PV module condemns the necessity of different interconnections between many modules (such as in series, parallel, etc.), in order to produce a consumable amount of power. However, inaccurate interconnections between modules in the PV system, decrease the life expectancy of the system, while diminishing both its performance and cost efficiencies, and increasing the system installation cost due to the need of extra wires [13].

Alternatively, Maximum Power Point Trackers (MPPTs) can elevate the PV array's efficiency in converting light into voltage, but only under uniform shading conditions [14]. In the case of many local peaks existence in the P-V curve, MPPTs fail to extract maximum available power. This can be solved by usage of Global Maximum Power Point Trackers (GMPPTs), where such systems locate the highest maximum among different locals in the P-V curve, ensuring a maximum array's performance [15–18]. Although GMPPTs reduce the problem of PV modules low efficiency, still, they are considered as an expensive solution which requires extra circuitry and complex algorithms implementations [19].

Another research track intended to elevate the efficiency and mitigating PSCs effects, proposes the implementation of single axis or double axis sun tracking as a solution [20]. Despite of the gain of these techniques, they also add an extra financial burden, especially for large scale PV farms, and they require complex control techniques and optimization algorithms to interact with weather change.

The PSCs combined with the poor efficiency of the modules, imply the need of larger areas for higher power production. This sheds the lights to the need of careful designs of a PV system's installation area, aiming to produce the maximum possible energy with the minimum cost.

The main factor playing the role in this optimization is the PV modules' tilt angle. While ample research focused on the improvement of the module's material to enhance its efficiency [21], large amount of energy could be lost if the modules are not correctly oriented and tilted. Current tilt angle optimization studies are missing important factors, disapproving their results [22]. In

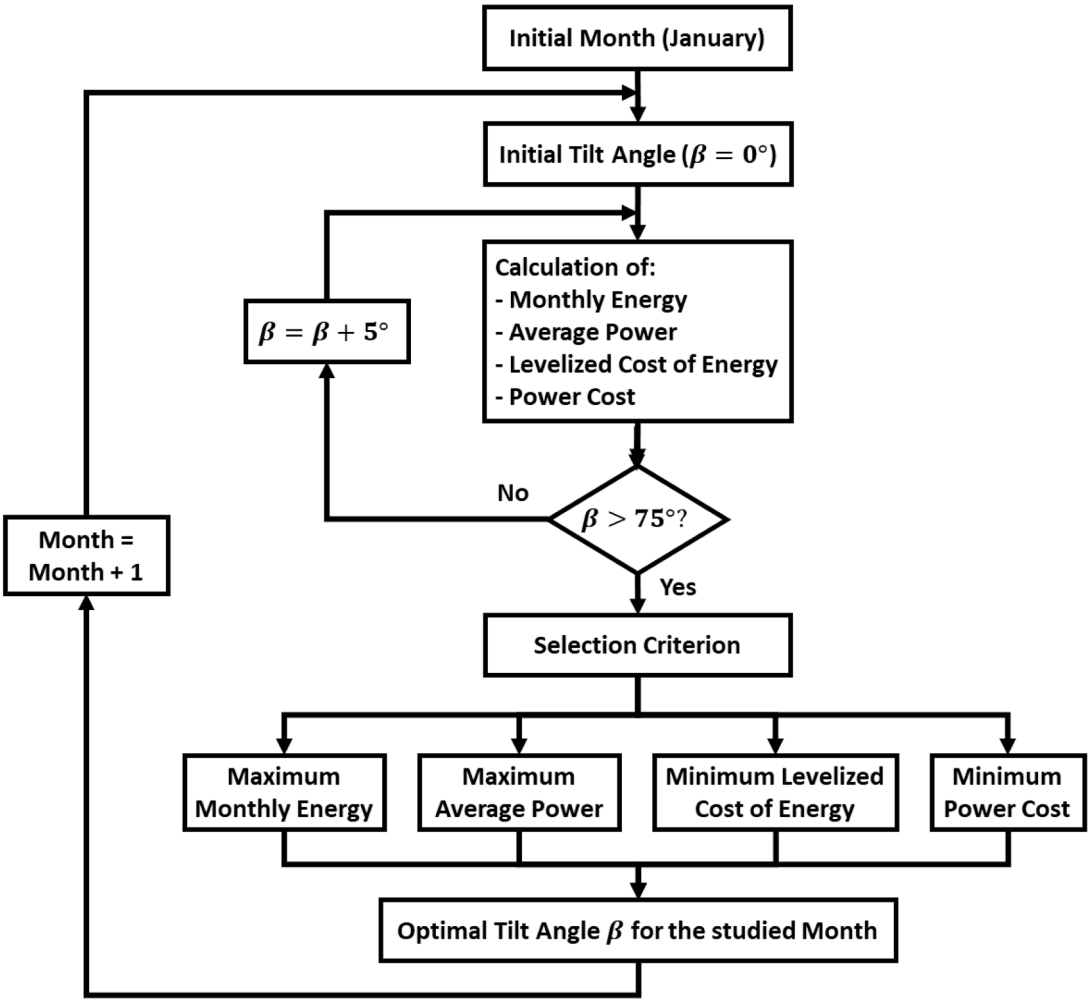

Fig. 1. Optimization procedure.

fact, most of such working methodologies focus on maximizing the energy absorption without taking into consideration the spacing between modules (to avoid mutual shading) and the energy cost [23]. This latter composes a great obstacle in front of PV systems, restricting their maximum efficiencies achievements. Furthermore, some of the PV tilt angle optimization methods are season specified, as they do not cover the tilt angle optimization process during the entire year, where others show that the adjustment of PV modules tilt angle is nearly irrelevant [24].

The current work deals with monthly optimization of the PV panels' tilt angle for minimum levelized cost of energy (LCOE): the net cost of power produced from PV systems over their lifetime. The optimization takes into consideration all variables affecting the produced power/energy and their costs: location coordinates, tilt angle, azimuth angle, altitude angle, monthly declination angle, direct normal insulation, average monthly daytime, land area, PV module efficiency, cost, and spacing between modules. The study considers the variation of these parameters over the entire year.

A new formula relating the number of PV modules to the number of spacing areas is established. Three distanced locations are studied to show the effect of latitude on the optimization process. This paper is organized as follows: Section 2 starts with the optimization procedure and Section 3 presents the calculation scheme. The calculation of solar radiation for different tilt angles is elaborated in Section 4. The spacing between PV modules is determined in Section 5. The PV array is sized in Section 6. Section 7 deals with the calculation of monthly produced energy and average power. Section 8 evaluates the LCOE and power cost, where results are shown in Section 9, and discussed in Section 10. Finally, conclusions are derived in Section 11.

2. Optimization procedure

The optimization procedure suggested in this paper is presented in Fig. 1. For each month, the PV array tilt angle β is varied from 0° to 75° with a step of 5° The boundary limits of β (between 0° and 75°) are chosen according to the PV system's site installation reliability. The outside of this interval corresponds to north/south poles, at which the usage of PV systems is precarious. For each tilt

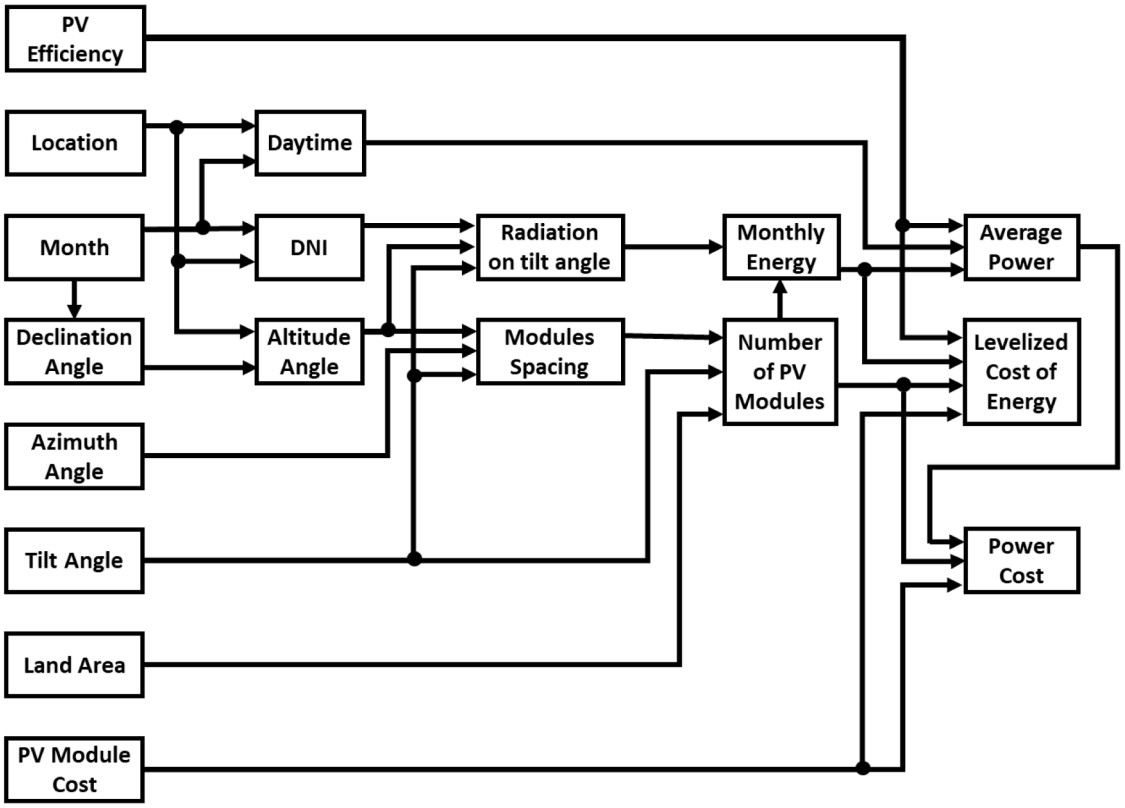

Fig. 2. Calculation procedure.

angle the monthly energy, the average power, the levelized cost of energy and the power cost are calculated. The optimal tilt angle is determined based on the previous calculations and a selection criterion, based on the minimum LCOE, minimum power cost and maximum produced average power.

This procedure is repeated for each month over the year to determine the monthly optimal tilt angle in the studied location. It is important here to mention that the optimization also considers the area of the installation site in addition to the location coordinates and geographical information.

The selection criterion task shown in Fig. 1, produces an optimal choice of $\boldsymbol{\beta}$, based on simple numerical comparisons: the maximum monthly energy once derived from the maximum number of PV modules ($\boldsymbol{N_{PV}}$), results in a maximum average power (proportionally related). Contrarily, this obtained energy corresponds to a minimum LCOE, which in turn refers to a minimum power cost (inversely proportional). The bottom line of $\boldsymbol{\beta}$ selection is hence based on the minimum obtained numerical value of LCOE.

3. Calculation scheme

The calculation procedure of monthly energy, average power, levelized cost of energy and power cost, is described in Fig. 2. The main factors that affect the optimization results are the studied location, the month, and the available land area.

In fact, the coordinates of the location and the month determine the daytime, the Direct Normal Insulation (DNI), the declination angle, the azimuth angle as well as the altitude angle of the sun. The radiation on the selected tilt angle is calculated from the DNI, the altitude angle of the sun and the tilt angle of the PV modules. The minimum spacing between modules to avoid shading and power loss is estimated from the altitude, azimuth, and tilt angles. The radiation on the selected tilt angle is used to calculate the monthly energy.

The maximum number of PV modules that can fit in the installation area without mutual shading, is computed from the available land area, the tilt angle and the minimum spacing between modules. Furthermore, the average power is established from the monthly energy, the daytime and the PV module's efficiency. The average power with the number of PV modules and their cost are used to determine the power cost (cost of produced kW). Finally, the LCOE is calculated from the monthly energy, the PV efficiency as well as the number and cost of PV modules.

4. Calculation of solar radiation for different tilt angles

The tilted PV modules, according to $\boldsymbol{\beta}$, absorb solar radiations, reaching their surface as $\boldsymbol{I_\beta}$. This radiation depends on the DNI and the altitude angle$\boldsymbol{\alpha}$of the sun (at noon) in the studied location, as well as the PV modules' tilt angle$\boldsymbol{\beta}$. The relationship between these

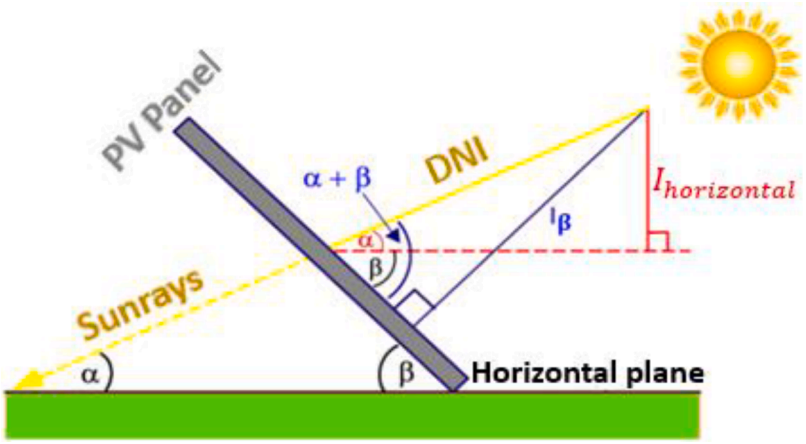

Fig. 3. Radiation on the selected tilt angle.

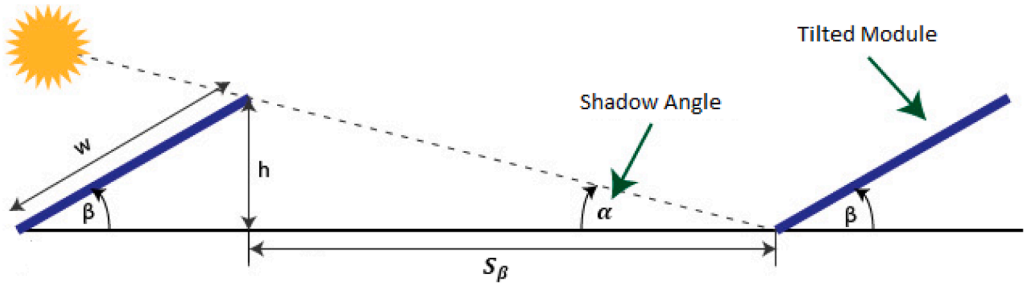

Fig. 4. Minimum spacing between PV modules.

variables can be elaborated from Fig. 3 as follows:

$$I_\beta = DNI \times sin(\alpha + \beta) \tag{1}$$

The altitude angle α of the sun at noon is calculated from the latitude L of the studied location and the daily declination angle δ of the sun, as expressed by the following equation:

$$\alpha = 90^\circ - L + \delta \tag{2}$$

The daily declination angle δ of the sun is calculated as follows:

$$\delta = 23.45^\circ \times sin\left[\frac{360}{365}(d - 81)\right] \tag{3}$$

where d is the number of day starting from $d = 1$ on the first of January.

5. Determination of spacing between PV modules

The quantity of solar radiation for different tilt angles is constrained by the PV system's installation area: the focus on obtaining as maximum as possible of solar irradiance, with the correspondent β, can cause mutual shading between adjacent PV modules, due to area limitation.

This scenario in turn, prohibits the destined aim behind optimizing the PV array's tilt angle. Therefore, the minimum spacing between PV modules, denoted as S_β, must be satisfied in order to reduce further complications.

This spacing depends on the PV module's width w, the tilt angle β, the altitude angle α of the sun at noon and the azimuth angle ψ of the sun with respect to south direction for northern hemisphere locations or north direction for southern hemisphere locations. The relationship between these variables can be determined using trigonometry from Fig. 4 as follows:

$$S_\beta = \frac{w \times sin(\beta) \times cos(\psi - 180^\circ)}{tan(\alpha)} \tag{4}$$

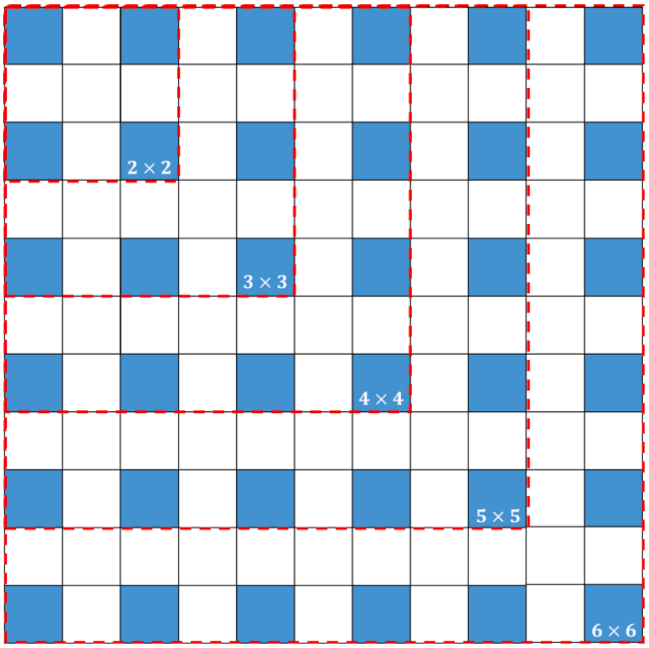

Fig. 5. PV modules distribution scheme.

Table 1
Correlation between the number of PV modules and spacing areas.

n	$N_{PV} = n^2$	N_{S_β}	Correlation
2	4	5	$N_{S_\beta} = n \times (n-1) + (2n-1) \times (n-1) = (2 \times 1) + (3 \times 1) = 5$
3	9	16	$N_{S_\beta} = n \times (n-1) + (2n-1) \times (n-1) = (3 \times 2) + (5 \times 2) = 16$
4	16	33	$N_{S_\beta} = n \times (n-1) + (2n-1) \times (n-1) = (4 \times 3) + (7 \times 3) = 33$
5	25	56	$N_{S_\beta} = n \times (n-1) + (2n-1) \times (n-1) = (5 \times 4) + (9 \times 4) = 56$
6	36	85	$N_{S_\beta} = n \times (n-1) + (2n-1) \times (n-1) = (6 \times 5) + (11 \times 5) = 85$
⋮⋮⋮n	⋮⋮⋮n^2	⋮⋮⋮	$N_{S_\beta} = (3n-1) \times (n-1) = 3n^2 - 4n + 1$

6. PV array sizing

The PV array sizing procedure, reflects the total number of PV modules, composing the array itself. The acknowledgment of $\boldsymbol{\beta}$, $\boldsymbol{S_\beta}$, the installation site area $\boldsymbol{A}$ and the PV module's parameters such as length $\boldsymbol{l}$ and width $\boldsymbol{w}$, allows the calculation of the total number of PV modules, denoted as $\boldsymbol{N_{PV}}$, that could fit in the area $\boldsymbol{A}$ without causing any mutual shading.

The PV array is considered to be square shaped: the number of PV modules in rows and columns are equal. Therefore, we define the total number of PV modules $\boldsymbol{N_{PV}}$ as follows:

$$N_{PV} = n \times n \tag{5}$$

with $\boldsymbol{n}$ as the number of PV modules in one row or column.

To determine $\boldsymbol{N_{PV}}$ for a given land area, first we need to know the correlation between the number of PV modules in one row or column $\boldsymbol{n}$ and the number of spacing areas N_{S_β}. For this aim, we consider a square distribution scheme as shown in Fig. 5. The results for a square array PV modules distribution are presented in Table 1.

The correlation between $\boldsymbol{n}$ and N_{S_β} is determined from the results of Table 1 as follows:

$$N_{S_\beta} = 3n^2 - 4n + 1 \tag{6}$$

In order to have enough spacing between PV rows and columns for different sun directions, we consider a square spacing area (white zones in Fig. 7). This means that the spacing distance $\boldsymbol{S_\beta}$ between rows and columns is the same. Therefore, each spacing area $\boldsymbol{A_{Spacing}}$ is defined by:

$$A_{Spacing} = S_\beta{}^2 \tag{7}$$

Since the PV modules are tilted with an angle $\boldsymbol{\beta}$, for each module the projected area $\boldsymbol{A_{PV\ -\ Module}}$ on land is:

$$\boldsymbol{A_{PV-Module}} = \boldsymbol{l} \times \boldsymbol{w} \times \boldsymbol{cos}(\boldsymbol{\beta}) \tag{8}$$

Hence, the PV system installation's area $\boldsymbol{A}$ is:

$$\boldsymbol{A} = \boldsymbol{N_{PV}}\ [\boldsymbol{l} \times \boldsymbol{w} \times \boldsymbol{cos}(\boldsymbol{\beta})] + \boldsymbol{N_{S_\beta}} \boldsymbol{S_\beta}^2 = \boldsymbol{n}^2\ [\boldsymbol{l} \times \boldsymbol{w} \times \boldsymbol{cos}(\boldsymbol{\beta})] + \left(3\ \boldsymbol{n}^2 - 4\ \boldsymbol{n} + 1\right)\ \boldsymbol{S_\beta}^2 \tag{9}$$

It follows that:

$$\boldsymbol{A} = \left[3\ \boldsymbol{S_\beta}^2 + \boldsymbol{l} \times \boldsymbol{w} \times \boldsymbol{cos}(\boldsymbol{\beta})\right]\ \boldsymbol{n}^2 - 4\ \boldsymbol{S_\beta}^2\ \boldsymbol{n} + \boldsymbol{S_\beta}^2 \tag{10}$$

It can be noted that Eq. (10) is a second order polynomial in terms of $\boldsymbol{n}$, of the generic form seen in Eq. (11):

$$\boldsymbol{a}\ \boldsymbol{n}^2 + \boldsymbol{b}\ \boldsymbol{n} + \boldsymbol{c} = 0 \tag{11}$$

By identifying both Eqs. (10) and (11), $\boldsymbol{a} = [3\boldsymbol{S_\beta}^2 + \boldsymbol{l} \times \boldsymbol{w} \times \boldsymbol{cos}(\boldsymbol{\beta})]$, $\boldsymbol{b} = -4\boldsymbol{S_\beta}^2$ and $\boldsymbol{c} = \boldsymbol{S_\beta}^2 - \boldsymbol{A}$. Since $\boldsymbol{n}$ is positive, the accepted solution of Eq. (11) is:

$$\boldsymbol{n} = \frac{-\boldsymbol{b} + \sqrt{\boldsymbol{b}^2 - 4\ \boldsymbol{a}\ \boldsymbol{c}}}{2\ \boldsymbol{a}} \tag{12}$$

Finally, the total number of PV modules $\boldsymbol{N_{PV}}$ in a square land area $\boldsymbol{A}$ for a given tilt angle $\boldsymbol{\beta}$ can be expressed as follows:

$$\boldsymbol{N_{PV}} = \left[\frac{-\boldsymbol{b} + \sqrt{\boldsymbol{b}^2 - 4\ \boldsymbol{a}\ \boldsymbol{c}}}{2\ \boldsymbol{a}}\right]^2 = \left[\frac{4\ \boldsymbol{S_\beta}^2 + \sqrt{16\ \boldsymbol{S_\beta}^4 - 4\ \left[3\ \boldsymbol{S_\beta}^2 + \boldsymbol{l} \times \boldsymbol{w} \times \boldsymbol{cos}(\boldsymbol{\beta})\right] \times \left(\boldsymbol{S_\beta}^2 - \boldsymbol{A}\right)}}{2\ \left[3\ \boldsymbol{S_\beta}^2 + \boldsymbol{l} \times \boldsymbol{w} \times \boldsymbol{cos}(\boldsymbol{\beta})\right]}\right]^2 \tag{13}$$

7. Calculation of monthly produced energy and average power

After finalizing the sizing procedure of the PV system, with known number of PV modules and their relative tilt angle, the monthly produced energy and average power can both be calculated. The monthly energy is determined by the radiation $\boldsymbol{I_\beta}$ reaching the array on the selected tilt angle, the PV modules' length $\boldsymbol{l}$ and width $\boldsymbol{w}$, as well as the number of PV modules $\boldsymbol{N_{PV}}$ as follows:

$$\boldsymbol{E} = \boldsymbol{I_\beta} \times \boldsymbol{l} \times \boldsymbol{w} \times \boldsymbol{N_{PV}} \times \boldsymbol{N_{Days}} \tag{14}$$

where $\boldsymbol{N_{Days}}$ is the number of days in the selected month.

The average power produced by the PV array is calculated from the monthly energy $\boldsymbol{E}$, the number of days in the selected month $\boldsymbol{N_{Days}}$, the PV modules' efficiency $\eta_{\boldsymbol{PV}}$, and the average daytime $\boldsymbol{T_{Day}}$ in the selected month as follows:

$$\boldsymbol{P_{AV}} = \frac{\boldsymbol{E} \times \eta_{PV}}{\boldsymbol{N_{Days}} \times\ \boldsymbol{T_{Day}}} \tag{15}$$

8. Evaluation of the levelized cost of energy and power cost

The most deciding parameter in the optimization of the PV tilt angle is the LCOE that represents the price in dollar cents of a unit of energy. It is given in cents per kilowatt hour (c/kWh), and evaluated from the cost of PV module $\boldsymbol{C_{PV}}$ in cents, the number of modules $\boldsymbol{N_{PV}}$, the monthly energy $\boldsymbol{E}$ in kW, the modules' efficiency $\eta_{\boldsymbol{PV}}$, and the array's lifetime in months $\boldsymbol{T_{PV\ -\ Lifetime}}$ as follows:

$$\boldsymbol{LCOE} = \frac{\boldsymbol{N_{PV}} \times \boldsymbol{C_{PV}}}{\boldsymbol{E} \times \eta_{PV} \times \boldsymbol{T_{PV-Lifetime}}} \tag{16}$$

The second parameter that determines the investment cost is the power cost $\boldsymbol{C_{Power}}$. It represents the cost of a unit of power in dollars per kilowatt ($/kW) and it is calculated from $\boldsymbol{C_{PV}}$, $\boldsymbol{N_{PV}}$ and $\boldsymbol{P_{AV}}$ as follows:

$$\boldsymbol{C_{Power}} = \frac{\boldsymbol{N_{PV}} \times \boldsymbol{C_{PV}}}{\boldsymbol{P_{AV}}} \tag{17}$$

9. Simulation results

In order to have graphical representations of pre-calculated quantities (such as LCOE, power cost, etc.) for the different locations (i.e., Tripoli, Belfort, Tantan) a tabulated model must be achieved: first and foremost, the model is originated by recognition of the location related DNI from the Photovoltaic Geographical Information System (PVGIS) [25]. Once the DNI is grasped, successively $\boldsymbol{I_\beta}$ can be calculated, according to Eq. (1) for the twelve months span during a year, for the given location.

From the same reference [25], the azimuth angle ψ can be obtained, as well as the daytime in hours, and duration of solar

Table 2
Levelized cost of energy (in c/kWh) for Tripoli under varying tilt angle from 0° to 75°.

LCOE ($\beta = 75°$)	10.29	9.40	8.22	9.23	9.00	8.74	8.46	7.44	7.07	7.29	8.05	10.04	8.60
LCOE ($\beta = 70°$)	10.02	9.02	7.71	8.38	7.86	7.43	7.26	6.63	6.53	6.94	7.79	9.80	7.95
LCOE ($\beta = 65°$)	9.83	8.74	7.31	7.72	7.02	6.50	6.41	6.02	6.12	6.66	7.61	9.65	7.47
LCOE ($\beta = 60°$)	9.72	8.54	7.01	7.22	6.38	5.82	5.77	5.55	5.79	6.45	7.49	9.57	7.11
LCOE ($\beta = 55°$)	9.69	8.41	6.78	6.82	5.89	5.30	5.28	5.18	5.54	6.30	7.43	9.56	6.85
LCOE ($\beta = 50°$)	9.73	8.35	6.61	6.51	5.52	4.90	4.91	4.90	5.35	6.20	7.43	9.63	6.67
LCOE ($\beta = 45°$)	9.85	8.35	6.50	6.28	5.22	4.59	4.61	4.68	5.21	6.16	7.48	9.77	6.56
LCOE ($\beta = 40°$)	10.04	8.42	6.44	6.10	4.99	4.35	4.39	4.51	5.12	6.16	7.59	10.00	6.51
LCOE ($\beta = 35°$)	10.33	8.55	6.42	5.98	4.81	4.16	4.21	4.38	5.06	6.20	7.77	10.31	6.52
LCOE ($\beta = 30°$)	10.71	8.75	6.46	5.91	4.68	4.02	4.08	4.29	5.05	6.30	8.01	10.74	6.58
LCOE ($\beta = 25°$)	11.22	9.04	6.55	5.88	4.60	3.92	3.98	4.24	5.07	6.45	8.34	11.28	6.71
LCOE ($\beta = 20°$)	11.87	9.42	6.70	5.90	4.55	3.85	3.92	4.22	5.13	6.66	8.77	11.98	6.91
LCOE ($\beta = 15°$)	12.70	9.91	6.90	5.96	4.53	3.81	3.89	4.24	5.24	6.93	9.31	12.88	7.19
LCOE ($\beta = 10°$)	13.77	10.53	7.17	6.08	4.55	3.80	3.89	4.28	5.39	7.29	10.01	14.04	7.57
LCOE ($\beta = 5°$)	15.16	11.34	7.53	6.24	4.60	3.81	3.92	4.36	5.60	7.75	10.92	15.56	8.07
LCOE (c/kWh) ($\beta = 0°$)	17.00	12.38	7.98	6.47	4.69	3.86	3.98	4.48	5.86	8.34	12.10	17.60	8.73
Month	Jan	Feb	Mar	Apr	May	Jun	Jul	Aug	Sep	Oct	Nov	Dec	Average

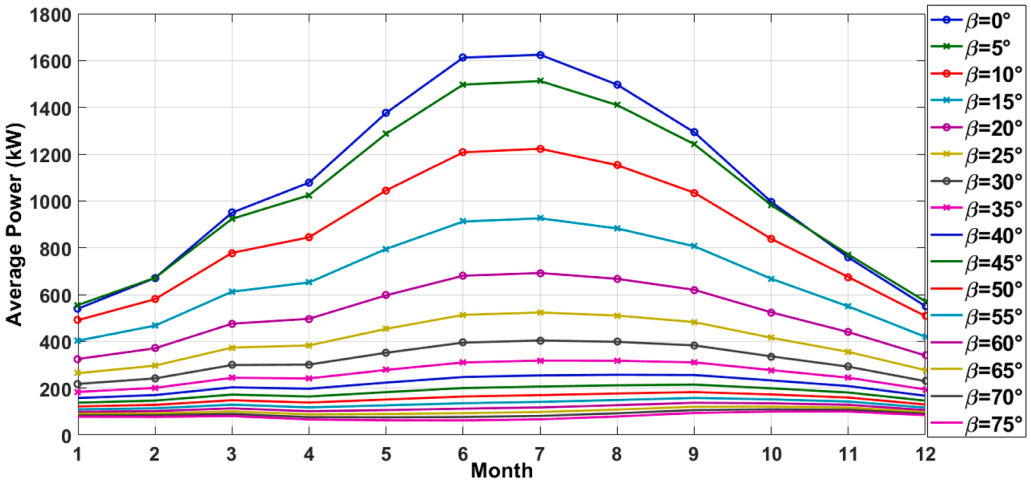

Fig. 6. Yearly average power for different tilt angles in Tripoli.

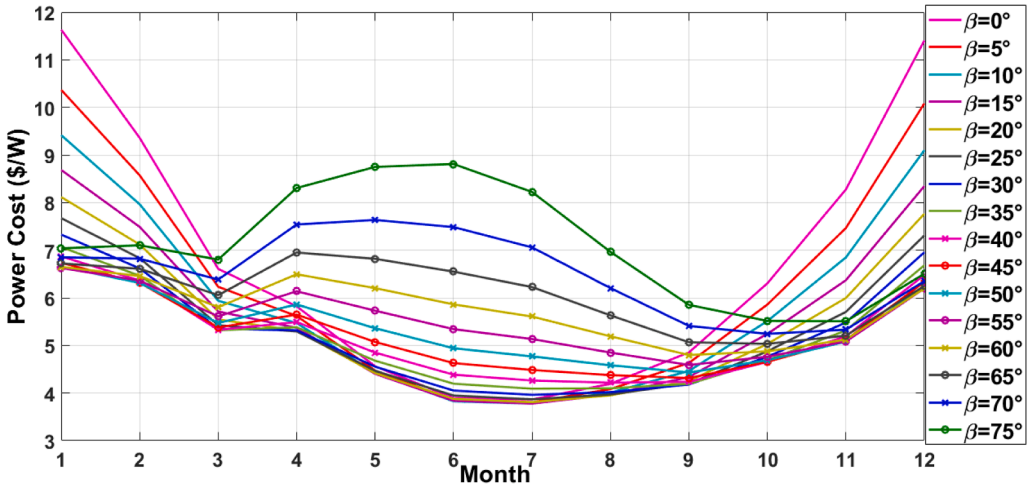

Fig. 7. Yearly power cost for different tilt angles in Tripoli.

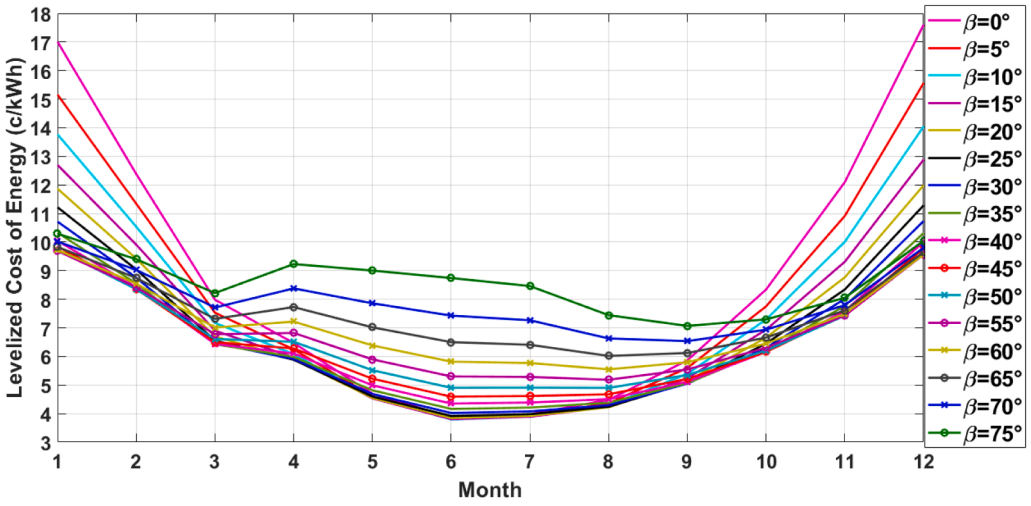

Fig. 8. Yearly LCOE for different tilt angles in Tripoli.

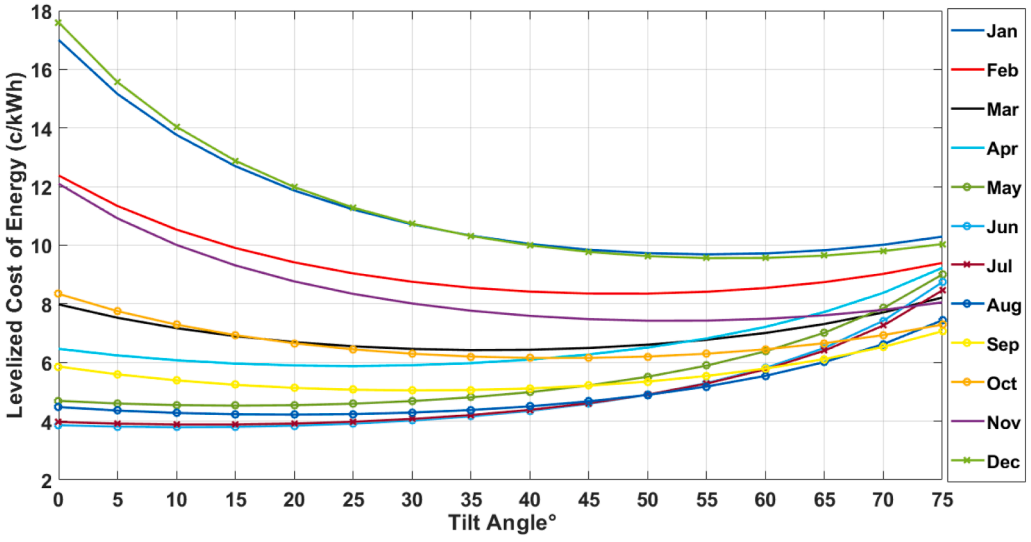

Fig. 9. Monthly LCOE for different tilt angles in Tripoli.

irradiation availability. This would result in obtaining S_β as presented in Eq. (4), and successively acquisitioning the $A_{Spacing}$ as mentioned in Eq. (7). While having the installation area land A in this work taken as 10, 000m^2, the number of PV modules N_{PV} can be calculated according to the dimensions of each PV module: in this work, the length and width of each module are $l = 1.675m$, $w = 0.951m$, respectively.

At this stage (i.e., obtainment of PV modules number), each of energy, average power, levelized cost of energy and energy cost can be calculated according to Eq. (14) to Eq. (17), respectively, for each of the three locations under investigation.

Three summarizing tables, concerning the monthly LCOE for different tilt angles ranging from 0° to 75° are to be shown for different locations.

9.1. Case study: Tripoli (Lebanon)

After applying the previously mentioned procedure, starting from Eq. (1) to (17), Table 2 covers different LCOE for each month and each β.

Fig. 6 represents the yearly average power for different tilt angles in Tripoli, where Figs. 7 and 8 present the yearly power cost and LCOE for the same location.

In order to compare the effect of adapting monthly varied tilt angles, to a fixed one over the entire year, a monthly LCOE for different tilt angle in Tripoli is shown in Fig. 9. It must be analyzed in a way corresponding to the lowest LCOE, to reveal the monthly optimal tilt angle.

Table 3
Levelized cost of energy (in c/kWh) for Belfort under varying tilt angle from 0° to 75°.

LCOE ($\beta = 75°$)	32.82	18.56	12.72	10.68	12.55	11.89	10.78	9.84	10.75	15.81	26.61	34.66	17.31
LCOE ($\beta = 70°$)	32.61	18.22	12.25	10.05	11.52	10.76	9.81	9.15	10.25	15.40	26.32	34.53	16.74
LCOE ($\beta = 65°$)	32.65	18.03	11.91	9.56	10.73	9.89	9.06	8.61	9.86	15.11	26.22	34.67	16.36
LCOE ($\beta = 60°$)	32.94	17.98	11.67	9.18	10.11	9.22	8.48	8.19	9.57	14.95	26.33	35.08	16.14
LCOE ($\beta = 55°$)	33.49	18.06	11.53	8.89	9.62	8.70	8.03	7.86	9.36	14.90	26.64	35.77	16.07
LCOE ($\beta = 50°$)	34.33	18.29	11.47	8.69	9.25	8.29	7.68	7.62	9.24	14.97	27.17	36.78	16.15
LCOE ($\beta = 45°$)	35.48	18.67	11.51	8.56	8.97	7.98	7.41	7.44	9.18	15.16	27.94	38.14	16.37
LCOE ($\beta = 40°$)	37.01	19.21	11.63	8.49	8.78	7.75	7.21	7.33	9.20	15.47	28.97	39.92	16.75
LCOE ($\beta = 35°$)	38.98	19.94	11.85	8.49	8.65	7.58	7.08	7.27	9.28	15.91	30.33	42.22	17.30
LCOE ($\beta = 30°$)	41.52	20.89	12.16	8.56	8.59	7.48	7.00	7.27	9.44	16.51	32.08	45.16	18.06
LCOE ($\beta = 25°$)	44.76	22.12	12.60	8.69	8.60	7.44	6.98	7.33	9.68	17.29	34.32	48.94	19.06
LCOE ($\beta = 20°$)	48.97	23.68	13.17	8.90	8.68	7.45	7.01	7.44	10.01	18.30	37.20	53.86	20.39
LCOE ($\beta = 15°$)	54.50	25.70	13.91	9.19	8.82	7.52	7.09	7.62	10.45	19.60	40.94	60.38	22.14
LCOE ($\beta = 10°$)	61.98	28.34	14.85	9.57	9.04	7.66	7.23	7.87	11.02	21.26	45.91	69.31	24.50
LCOE ($\beta = 5°$)	72.47	31.84	16.06	10.07	9.35	7.85	7.44	8.20	11.74	23.42	52.72	82.08	27.77
LCOE (c/kWh) ($\beta = 0°$)	88.04	36.64	17.64	10.71	9.75	8.12	7.72	8.62	12.67	26.30	62.45	101.55	32.52
Month	Jan	Feb	Mar	Apr	May	Jun	Jul	Aug	Sep	Oct	Nov	Dec	Average

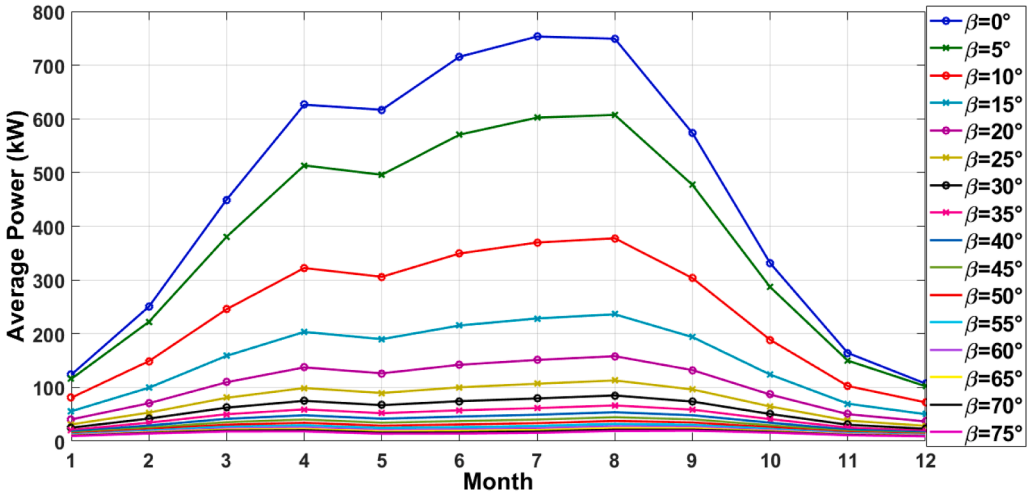

Fig. 10. Yearly average power for different tilt angles in Belfort.

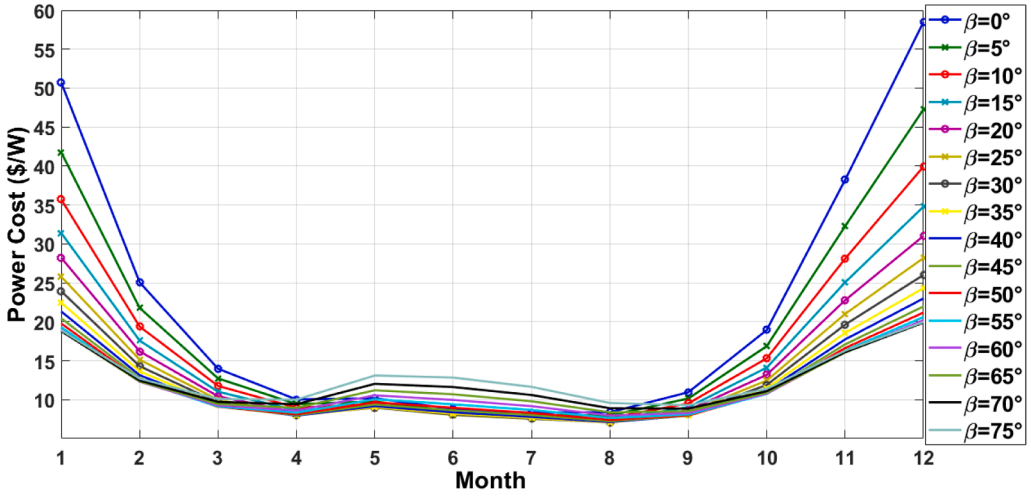

Fig. 11. Yearly power cost for different tilt angles in Belfort.

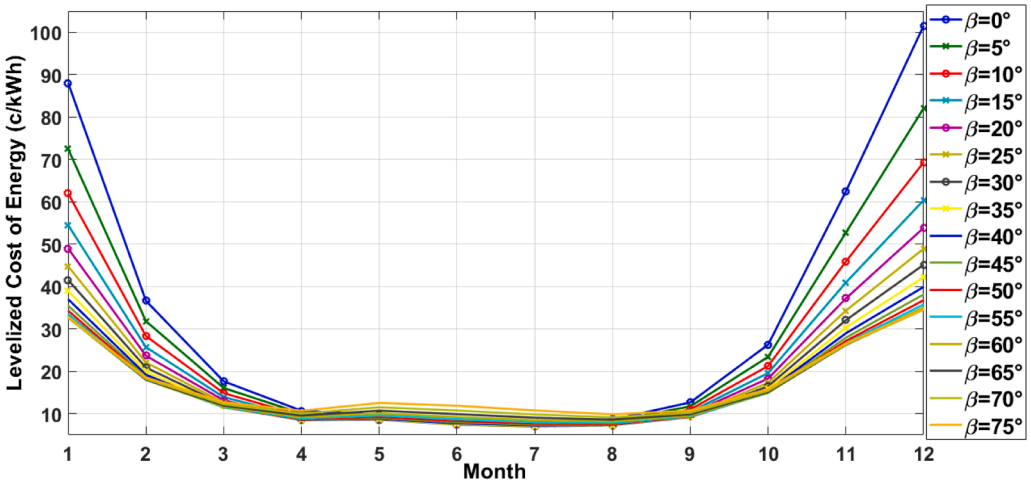

Fig. 12. Yearly LCOE for different tilt angles in Belfort.

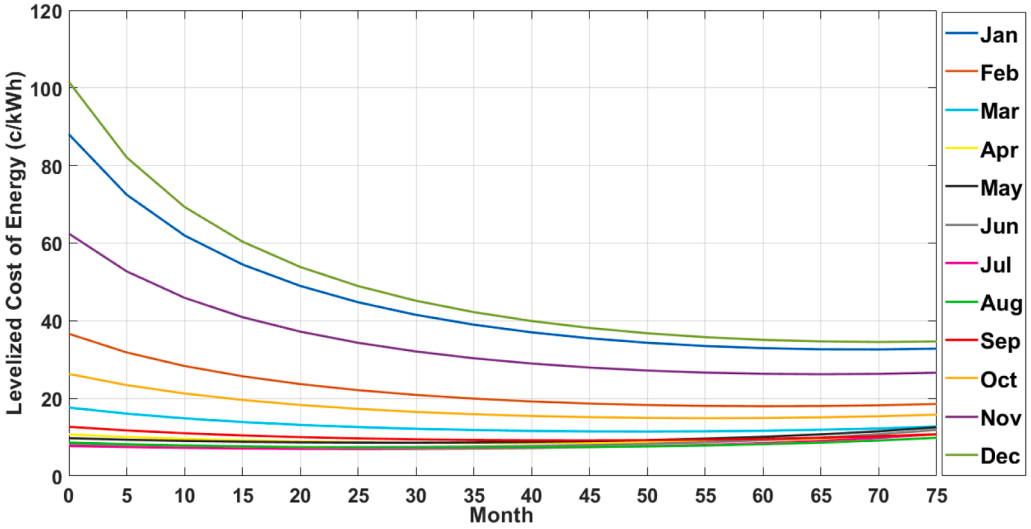

Fig. 13. Monthly LCOE for different tilt angles in Belfort.

Table 4
Levelized cost of energy (in c/kWh) for Tantan under varying tilt angle from 0° to 75°.

LCOE ($\beta = 75°$)	6.72	7.00	7.49	9.20	12.45	17.72	16.39	12.01	8.69	7.22	6.61	7.05	9.88
LCOE ($\beta = 70°$)	6.47	6.64	6.92	8.16	10.46	14.30	13.44	10.39	7.89	6.78	6.33	6.81	8.72
LCOE ($\beta = 65°$)	6.29	6.36	6.48	7.39	9.08	12.06	11.47	9.22	7.27	6.43	6.12	6.64	7.90
LCOE ($\beta = 60°$)	6.16	6.16	6.13	6.79	8.08	10.50	10.06	8.34	6.79	6.16	5.97	6.52	7.31
LCOE ($\beta = 55°$)	6.09	6.00	5.86	6.33	7.32	9.36	9.03	7.66	6.42	5.96	5.86	6.46	6.86
LCOE ($\beta = 50°$)	6.06	5.90	5.66	5.97	6.74	8.50	8.24	7.14	6.13	5.81	5.81	6.45	6.53
LCOE ($\beta = 45°$)	6.07	5.85	5.51	5.68	6.30	7.84	7.64	6.73	5.91	5.72	5.79	6.48	6.29
LCOE ($\beta = 40°$)	6.14	5.84	5.41	5.47	5.94	7.33	7.16	6.42	5.74	5.66	5.83	6.57	6.13
LCOE ($\beta = 35°$)	6.25	5.88	5.35	5.31	5.67	6.93	6.80	6.17	5.63	5.65	5.91	6.71	6.02
LCOE ($\beta = 30°$)	6.41	5.96	5.33	5.19	5.46	6.62	6.51	5.99	5.56	5.69	6.03	6.91	5.97
LCOE ($\beta = 25°$)	6.64	6.10	5.36	5.12	5.31	6.38	6.29	5.86	5.54	5.77	6.21	7.18	5.98
LCOE ($\beta = 20°$)	6.94	6.28	5.42	5.09	5.20	6.20	6.14	5.78	5.55	5.89	6.46	7.53	6.04
LCOE ($\beta = 15°$)	7.33	6.53	5.53	5.10	5.13	6.08	6.03	5.75	5.61	6.07	6.77	7.98	6.16
LCOE ($\beta = 10°$)	7.82	6.86	5.69	5.15	5.11	6.01	5.97	5.76	5.72	6.32	7.18	8.56	6.34
LCOE ($\beta = 5°$)	8.46	7.28	5.90	5.24	5.12	5.98	5.96	5.81	5.88	6.63	7.70	9.30	6.60
LCOE (c/kWh) ($\beta = 0°$)	9.28	7.81	6.18	5.37	5.17	6.00	6.00	5.91	6.09	7.03	8.37	10.27	6.95
Month	Jan	Feb	Mar	Apr	May	Jun	Jul	Aug	Sep	Oct	Nov	Dec	Average

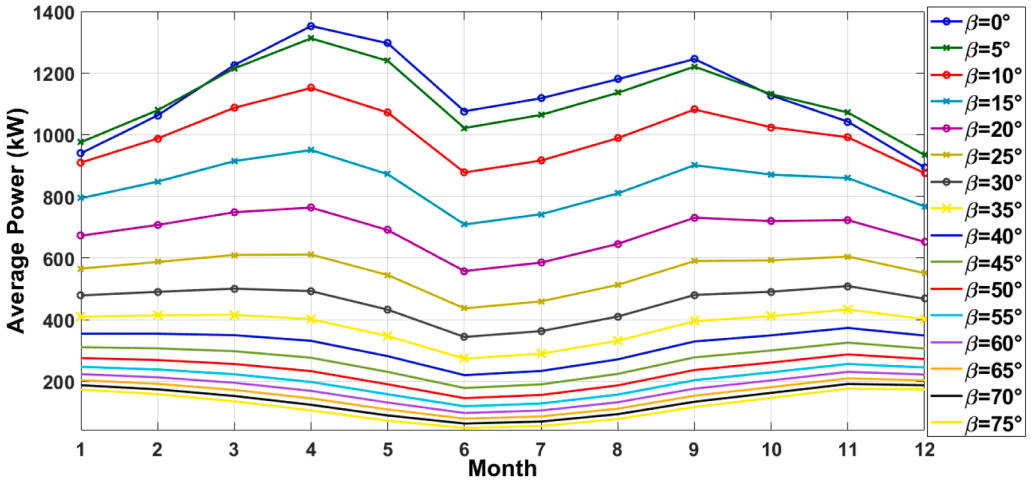

Fig. 14. Yearly average power for different tilt angles in Tantan.

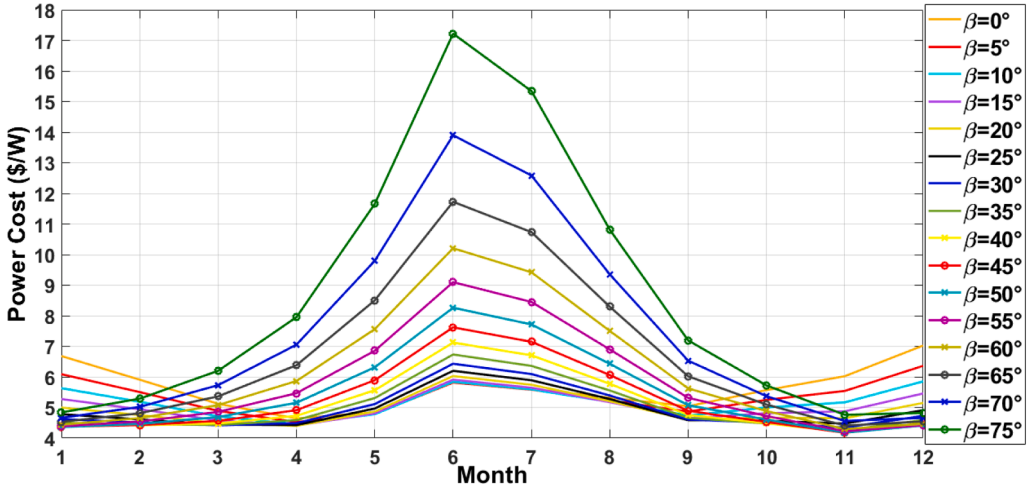

Fig. 15. Yearly power cost for different tilt angles in Tantan.

9.2. Case study: Belfort (France)

By applying the same previous procedures, Table 3 encapsulates different LCOE for each month and each β.

Fig. 10 represents the yearly average power for different tilt angles in Belfort, where Figs. 11 and 12 present the yearly power cost and LCOE, respectively for the same location. The monthly LCOE for different tilt angle in Belfort is shown in Fig. 13.

9.3. Case study: Tantan (Morocco)

Following the same procedure carried for Tripoli and Belfort zones, Table 4 lists different LCOE for each month and each β, for Tantan location. Figs. 14 and 15 represent the yearly average power and yearly power cost, respectively for different tilt angles in Tantan, whereas Fig. 16 presents the yearly LCOE for the same location. The monthly LCOE for different tilt angles in Tantan is shown in Fig. 17.

10. Discussion

The effects of applying a monthly adjusted β versus a fixed one, over a PV system located in either of Tripoli, Belfort or Tantan can all be described positively in terms of minimizing the LCOE, with a reduced power cost and an increased power production.

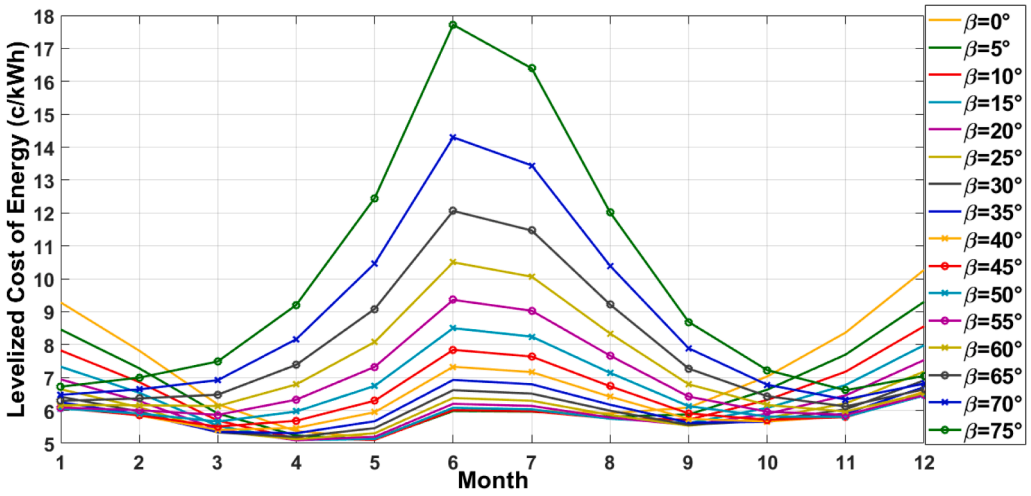

Fig. 16. Yearly LCOE for different tilt angles in Tantan.

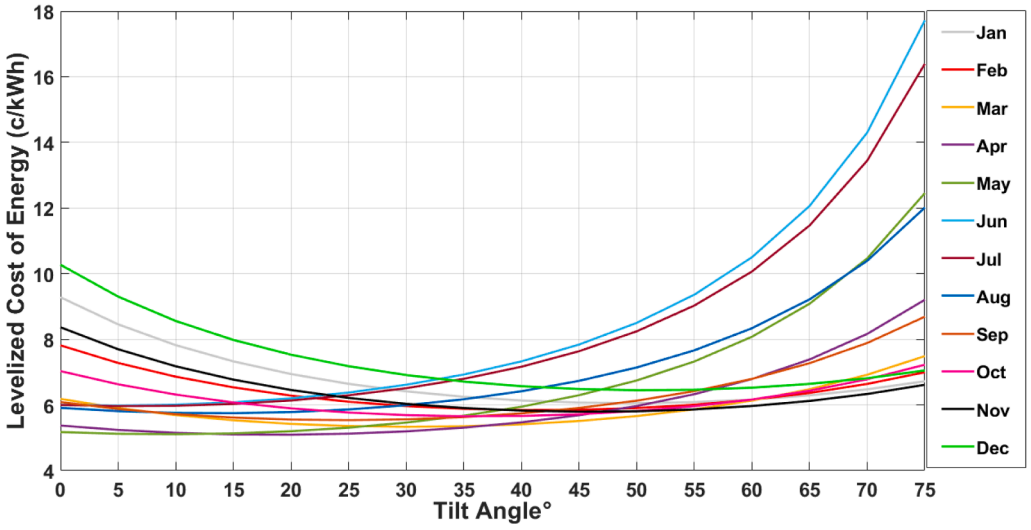

Fig. 17. Monthly LCOE for different tilt angles in Tantan.

10.1. Case of Tripoli

The monthly average LCOE for Tripoli, when β is optimized is 6.24 c/kWh and 6.51 c/kWh for a fixed β. The monthly average power cost for an optimized β scores 4.96 $/W with 5.19 $/W for a fixed β. Finally, the monthly average power produced, under optimized β, is 473 kW and 215 kW when β is fixed .

10.2. Case of Belfort

The monthly average LCOE for Belfort scored 15.47 c/kWh for a monthly adjusted β, and 16.07 c/kWh for a fixed one, whereas the monthly average power cost when β is optimized is 11.19 $/W, compared to 11.72 $/W when β is fixed. The monthly average power produced under optimized β is 47.0 kW for 23.3 kW for a fixed β.

10.3. Case of Tantan

The monthly average LCOE, for an optimized β registered 5.71 c/kWh as a monthly average LCOE, compared to 5.97 c/kWh when β is fixed. The monthly average power cost is 4.94 $/W and 4.72 $/W when β is fixed and optimized, respectively. For the monthly average power produced, the scores were of 622 kW and 455 kW for an optimized and fixed β, respectively.

As a graphical interpretation, Figs. 18, and 19 show pie charts of the monthly average power cost as well as monthly produced

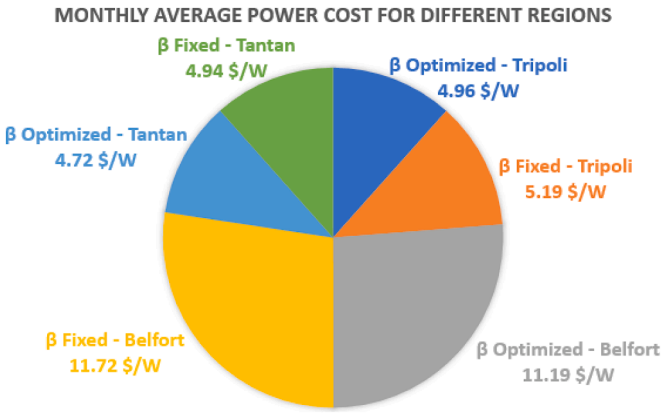

Fig. 18. Pie chart of monthly average power cost for different regions.

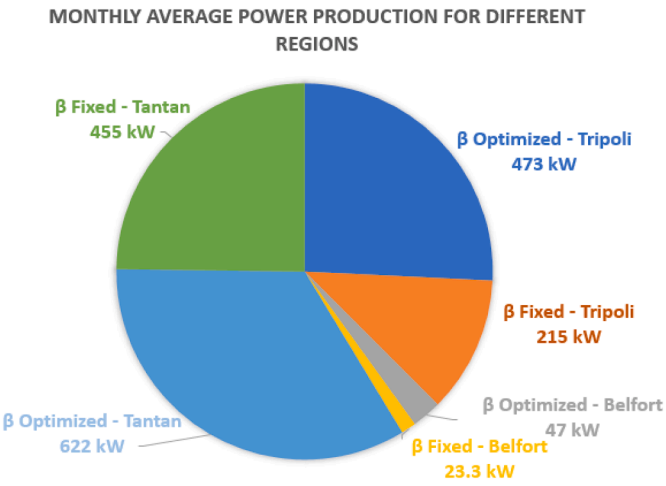

Fig. 19. Pie chart of monthly average power production quantities in different regions.

power, in the three designated regions under optimized and fixed β. Fig. 20 is a histogram representation for monthly LCOE for the three regions, also for optimized and fixed β.

11. Conclusion

A monthly tilt angle optimization procedure is selected in this study, based on the fact that the direct normal insulation reaching the earth's surface, negligibly variates during the span of a half month or a week (regarding earth's motion around the sun). Therefore, if adapted, a bimonthly or a weekly tilt angle optimization would have unnoticeable effects, on the PhotoVoltaic power generation. The realization of the tilt angle adjustments can be done through labour services since they already require frequent site visits for monitoring and maintenance purposes. Alternatively, automated facilities, such as robotic actuators, can be initialized through algorithms and other control schemes, to precisely modify the tilt angle. Unfortunately, such facilities would add more financial costs on the system, due to machinery requirement and corresponding maintenance fees.

The applicability of this model, over all regions around the globe (except for north/south poles) is based on the selection of latitude and longitude attributes, characterizing the desired location. Using the PhotoVoltaic geographical information system, the user can locate his designated location by graphically clicking it on the map, hence updating all variables required for the optimization process.

For all studied geographical locations, this work has decreased the levelized cost of energy by 4.32, 3.73, 4.35 and increased the produced power by 49.67, 50.36, 26.83%, while decreasing the power cost by 4.43, 4.48, 4.47% for Tripoli, Belfort and Tantan, respectively.

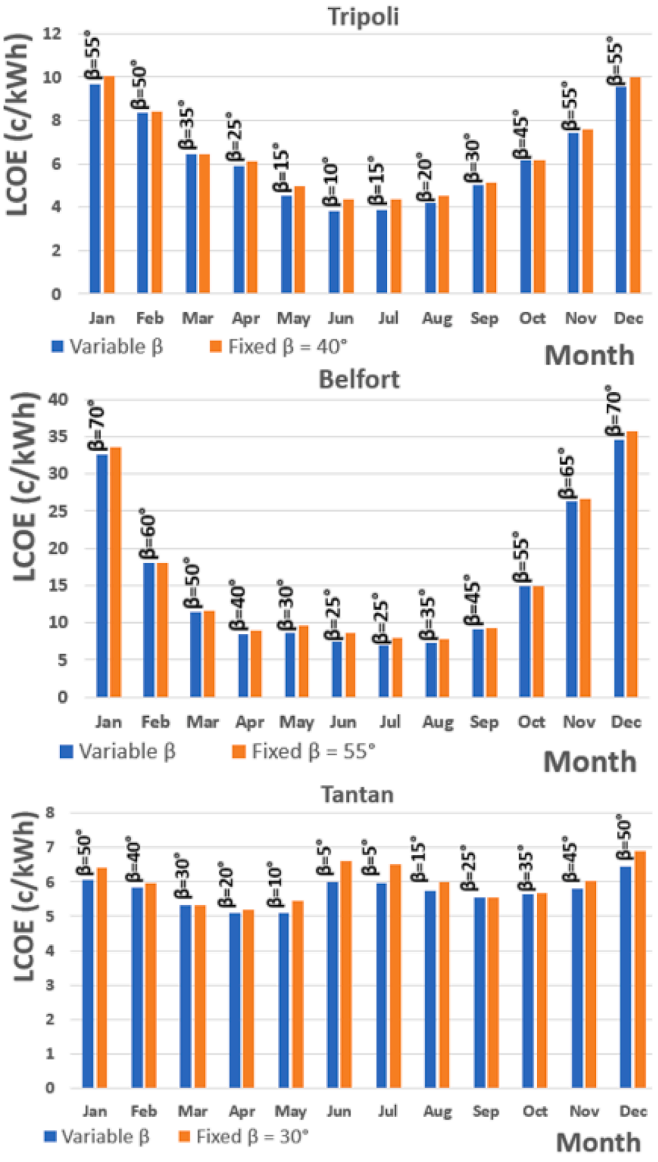

Fig. 20. Histogram representation of monthly average LCOE for the three regions under fixed and optimized β.

CRediT authorship contribution statement

Khaled Osmani: Writing – original draft, Investigation, Writing – review & editing, Visualization. **Mohamad Ramadan:** Writing – review & editing, Visualization, Supervision. **Thierry Lemenand:** Writing – review & editing, Visualization, Supervision. **Bruno Castanier:** Writing – review & editing, Visualization, Supervision. **Ahmad Haddad:** Conceptualization, Writing – review & editing, Visualization, Supervision, Project administration.

Declaration of Competing Interest

The authors declare that they have no known competing financial interests or personal relationships that could have appeared to influence the work reported in this paper.

References

[1] Prons-Seres de Brauwer C, Cohen JJ. Analyzing the potential of citizen-financed community renewable energy to drive Europe's low-carbon energy transition. Renew Sustain Energy Rev 2020;133. Article ID: 110300.
[2] Li G, Shittu S, Diallo TMO, Yu M, Zhao X, Ji J. A review of solar photovoltaic-thermoelectric hybrid system for electricity generation. Energy 2018;158:41–58.
[3] Nwaigwe KN, Mutabilwa P, Dintwa E. An overview of solar power (PV systems) integration into electricity grids. Mater Sci Energy Technol 2019;2(3):629–33.
[4] Jahangir MH, Shahsavari A, Rad MAV. Feasibility study of a zero emission PV/Wind turbine/wave energy converter hybrid system for stand-alone power supply: a case study. J Clean Prod 2020;262. Article ID: 121250.
[5] Osmani K, Haddad A, Lemenand T, Castanier B, Ramadan M. A review on maintenance strategies for PV systems. Sci Total Environ 2020;746. Article ID: 141753.
[6] S.Manju NSagar. Progressing towards the development of sustainable energy: a critical review on the current status, applications, developmental barriers and prospects of solar photovoltaic systems in India. Renew Sustain Energy Rev 2017;70:298–313.
[7] Shen L, Li Z, Ma T. Analysis of the power loss and quantification of the energy distribution in PV module. Appl Energy 2020;260. Article ID: 114333.
[8] Seapan M, Hishikawa Y, Yoshita M, Okajima K. Temperature and irradiance dependences of the current and voltage at maximum power of crystalline silicon PV devices. Sol Energy 2020;204:459–65.
[9] Chintapalli N, Sharma MK, Bhattacharya J. Linking spectral, thermal and weather effects to predict location-specific deviation from the rater power of a PV panel. Sol Energy 2020;208:115–23.
[10] Clement CE, Singh JP, Birgersson E, Wang Y, Khoo YS. Hotspot development and shading response of shingled PV modules. Sol Energy 2020;207:729–35.
[11] Lappalainen K, Valkealahti S. Number of maximum power points in photovoltaic arrays during partial shading events by clouds. Renew Energy 2020;152: 812–22.
[12] Tubniyom C, Jaideaw W, Chatthaworn R, Suksri A, Wongwuttanasatian T. Effect of partial shading patterns and degrees of shading on Total-Cross-Tied (TCT) photovoltaic array configuration. Energy Procedia 2018;153:35–41.
[13] P.R. Satpathy, R. Sharma. 2020. Parametric indicators for partial shading and fault prediction in photovoltaic arrays with various interconnection topologies. Energy Convers Manag 219, Article ID: 113018.
[14] da Rocha MV, Sampaio LP, da Silva SAO. Comparative analysis of MPPT algorithms based on bat algorithm for PV systems under partial shading conditions. Sustain Energy Technol Assess 2020;40. Article ID: 100761.
[15] Sridhar R, Subramani C, Pathy S. A grasshopper optimization algorithm aided maximum power point tracking for partially shaded photovoltaic systems. Comput Electr Eng 2021;92. Article ID: 107124.
[16] Mohamed-Kazim HA, Abdel-Qader I, Harb AM. Efficient maximum power point tracking based on reweighted zero-attracting variable stepsize for grid interfaced photovoltaic systems. Comp Electr Eng 2020;85. Article ID: 106672.
[17] Smadi IA, AL-Qudah R. Explicit one-step model and adaptive maximum power point tracking algorithm for a photovoltaic module. Comp Electr Eng 2020;85. Article ID: 106659.
[18] Srinivasarao P, Peddakapu K, Mohamed MR, Deepika KK, Sudhakar K. Simulation and experimental design of adaptive-based maximum power point tracking methods for photovoltaic systems. Comp Electr Eng 2021;89. Article ID: 106910.
[19] Osmani K, Haddad A, Lemenand T, Castanier B, Ramadan M. An investigation on maximum power extraction algorithms from PV systems with corresponding DC-DC converters. Energy 2021;224. Article ID: 120092.
[20] Zhu Y, Liu J, Yang X. Design and performance analysis of a solar tracking system with a novel single-axis tracking structure to maximize energy collection. Appl Energy 2020;264. Article ID: 114647.
[21] Osmani K, Haddad A, Lemenand T, Castanier B, Ramadan M. Material based fault detection methods for PV systems. Key Eng Mater 2020;856:111–5.
[22] Ullah A, Imran H, Maqsood Z, Butt NZ. Investigation of optimal tilt angles and effects of soiling on PV energy production in Pakistan. Renew Energy 2019;139: 830–43.
[23] Yassir A, Zamzami U, Fauzan K, Hasannuddin T, Subhan. Optimization of tilt angle for photovoltaic: case study Sabang-Indonesia. IOP Conf Ser Mater Sci and Eng 2019;536. Article ID: 012055.
[24] Beringer S, Schilke H, Lohse I, Seckmeyer G. Case study showing that the tilt angle of photovoltaic plants is nearly irrelevant. Sol Energy 2011;85(3):470–6.
[25] Website: https://re.jrc.ec.europa.eu/pvg_tools/en/#MR.

Khaled Osmani is currently a PhD student at Université d'Angers – France. His main research activities focus on renewable energy, photovoltaic systems, thermal management, and power electronics.

Mohamad Ramadan is an associate professor at the International University of Beirut. He is an editor in the International Journal of Thermofluids and guest editor in many international journals. He is editor in the Elsevier encyclopedia of smart materials He serves as reviewer in more than 40 international journals. He is in the organizing committee of several international conferences.

Thierry LEMENAND is Associate Professor in the Engineering School Polytech Angers (France), he is the head of the BEMS Department (Building Efficiency Maintenance and Safety) and is currently researcher at LARIS laboratory. He has been involved in fundamental and applied research in mixing and heat transfer intensification, and energy efficiency. He has published more than 60 papers in peer-reviewed journals"

Bruno Castanier is a full-professor at Université d'Angers and head of the "Reliability Engineering and Decision-Making tools" research team of the LARIS lab. His main research activities focus on Maintenance Modeling and Optimization for complex systems. He is the general chairman of the European Safety and Reliability Conference – ESREL 2021 – which is held in Angers.

Ahmad Haddad obtained his Ph.D. degree in Control Systems Engineering from the UTBM University (France - 2009). He is awarded by "The Marquis Who's Who Publications Board" and by the "International Biographical Center of Cambridge". In 2015 he was assigned the position of Assistant Dean at LIU University. He is promoted to Associate Professor in 2017.

Chapitre 3

Conception d’un chargeur solaire innovant de batterie Lithium-Ion basé sur le MPPT pour un fonctionnement sous des conditions d’irradiations fluctuantes

Les résultats du **chapitre 2** indiquent une meilleure productivité de puissance des systèmes PV après l'application de l'étude correspondante (c'est-à-dire l'application de la modification de l'angle d'inclinaison dynamique suggérée). Cette puissance supplémentaire produite peut toutefois être stockée en vue d'une utilisation ultérieure. Après les différentes études sur les différents types de systèmes PV dans le **chapitre 1** (par exemple, sur-réseau PV, hors-réseau PV, etc.), et en se concentrant sur les impacts importants des conditions d'irradiation fluctuantes sur la production d'énergie PV comme présenté dans le **chapitre 1**, cette étude vise à stocker l'énergie excédentaire produite par les systèmes PV dans des batteries au Lithium-Ion (Li-I). Ce processus peut être considéré comme complémentaire de l'étude présentée au **chapitre 2** : il prend en compte l'irradiation solaire et tous les blocs d'électronique de puissance nécessaires pour assurer une charge sûre et efficace des batteries au Lithium-Ion.

La **section 1** de cette étude correspond à une introduction générale sur les effets des fluctuations de l'irradiation sur les performances des systèmes photovoltaïques. La **section 2** présente la méthodologie de travail, qui constitue l'épine dorsale de la conduite de cette étude. La **section 3** présente l'installation du générateur photovoltaïque et la manière dont les modèles d'irradiation ont été conçus. La **section 4** présente la technique de conception du convertisseur DC-DC. La **section 5** prend en compte la modification de l'algorithme "P&O" et sa technique de mise en œuvre dans la conception, afin de garantir qu'une

puissance maximale est toujours extraite du champ photovoltaïque en fonction de chaque état d'irradiation. La **section 6** modélise le convertisseur bidirectionnel conçu, qui est principalement utilisé pour brancher/débrancher en toute sécurité la batterie Li-I conformément à certaines normes de sécurité prédéfinies. La **section 7** présente le modèle utilisé pour supprimer le courant de charge en fonction d'un modèle mathématique. La **section 8** présente l'ensemble du modèle, ainsi que les résultats de la simulation pour tous les modèles d'ombrage. La **section 9** propose une discussion et des travaux futurs, et la **section 10** présente les conclusions.

Trois modèles majeurs ont été établis dans cette étude:

- Convertisseur DC-DC synchrone entrelacé : présente une capacité de traitement de puissance accrue par rapport à d'autres conceptions d'électronique de puissance, tout en possédant également une meilleure réponse transitoire.
- Un algorithme "P&O" modifié : contrairement à l'algorithme "P&O" conventionnel, cette version améliorée permet de mieux identifier un "vrai zéro" dans la courbe caractéristique PV. Par conséquent, cette version modifiée ne reste pas bloquée sous le point de puissance maximale locale, et peut donc produire des « Duty Ratios » plus précis pour le convertisseur-abaisseur suivant.
- Chargement sûr de la batterie Li-I : grâce au système de suppression du courant et à la lecture de la profondeur de décharge (DoD) de la batterie Li-I, le processus de chargement de la batterie est le plus rapide et le plus sûr.

Les modèles d'irradiation solaire ont été conçus pour être extrêmement fluctuants (par un laps de temps de 0,5 seconde). Malgré ces conditions d'irradiation difficiles, le modèle a montré une efficacité moyenne allant de 87 % à 100 % en fournissant le courant de charge le plus rapide et le plus sûr, ainsi qu'une tension d'alimentation stable pour la batterie Li-I. On peut affirmer que ce modèle peut être appliqué à n'importe quel système photovoltaïque hors-réseau, avec ou sans l'étude présentée au **chapitre 2**. Dans tous les cas, ce modèle accélère en toute sécurité le processus de charge des systèmes de stockage d'énergie utilisés dans les systèmes photovoltaïques hors-réseau.

Conception d'un chargeur solaire innovant de batterie Lithium-Ion basé sur le MPPT pour un fonctionnement sous des conditions d'irradiation fluctuantes

Cet article est publié dans « **sustainability** »

https://doi.org/10.3390/su15129839

Résumé – Les conditions d'irradiation fluctuante constituent un défi face à un processus de charge de batterie approprié, lorsqu'il provient d'un réseau photovoltaïque (PVA). Le comportement du PVA dans de telles conditions (c'est-à-dire reflété par une courbe caractéristique PV perturbée) augmente la complexité du processus d'extraction de la puissance totale disponible. Ce fait gênant finit par entraîner une diminution de l'efficacité globale des systèmes PV, en particulier avec la présence de circuits impliqués dans l'électronique de puissance imprécis. En conséquence, le but de cet article est de concevoir un chargeur solaire de batterie complet, avec une capacité de suivi du point de puissance maximale, issu d'un PVA de 1,918 kWp, disposé en topologie série-parallèle.

La batterie visée est de type Lithium-Ion (Li-I), avec une tension de fonctionnement de 24 VDC et un courant nominal de 150 Ah. La conception a commencé par la configuration d'un convertisseur DC-CC synchrone entrelacé pour produire un niveau de tension souhaité, avec un faible courant d'ondulation d'inductance et une faible tension d'ondulation de sortie. Le convertisseur DC-DC est à son tour controllé par un algorithme Perturb and Observe (P&O) modifié, pour assurer un suivi efficace de la puissance maximale. Progressivement, la conception a utilisé une disposition du convertisseur DC-DC bidirectionnel pour assurer des valeurs de charge de courant sûres pour la batterie. De la même manière, le rôle du convertisseur bidirectionnel est de débrancher la batterie du système, au cas où la profondeur de décharge (DoD) serait inférieure à 25 %, maintenant ainsi la durée de vie de la batterie. L'ensemble de la configuration des sous-systèmes proposés conduit alors au processus de charge de batterie relativement le plus rapide, le plus sûr et le plus fiable. Les résultats montrent une efficacité (en termes de suivi de puissance PV) allant de 87 % à 100 % dans quatre conditions d'éclairement changeant rapidement. De plus, cet article suggère

un le futur processus d'industrialisation de la conception, conduisant à un prototype de chargeur solaire PV efficace.

sustainability

MDPI

Article

A Novel MPPT-Based Lithium-Ion Battery Solar Charger for Operation under Fluctuating Irradiance Conditions

Khaled Osmani [1], Ahmad Haddad [2,3], Mohammad Alkhedher [4], Thierry Lemenand [1], Bruno Castanier [1] and Mohamad Ramadan [2,3,*]

1 LARIS EA 7315, Polytech Angers, University of Angers, 49000 Angers, France; khaled.alosmani@etud.univ-angers.fr (K.O.); thierry.lemenand@univ-angers.fr (T.L.); bruno.castanier@univ-angers.fr (B.C.)
2 School of Engineering, International University of Beirut BIU, Beirut P.O. Box 146404, Lebanon; ahmad.haddad@liu.edu.lb
3 School of Engineering, Lebanese International University LIU, Bekaa P.O. Box 1803, Lebanon
4 Mechanical and Industrial Engineering Department, Abu Dhabi University, Abu Dhabi P.O. Box 59911, United Arab Emirates
* Correspondence: mohamad.ramadan@liu.edu.lb

Abstract: Fluctuant irradiance conditions constitute a challenge in front of a proper battery charging process, when originated from a PhotoVoltaic Array (PVA). The behavior of the PVA under such conditions (i.e., reflected by a disturbed PV characteristic curve) increases the complexity of the total available power's extraction process. This inconvenient fact yields eventually to a decreased overall efficiency of PV systems, especially with the presence of imprecise power-electronics involved circuits. Accordingly, the purpose of this paper is to design a complete battery solar charger, with Maximum Power Point Tracking ability, emerged from a PVA of 1.918 kWp, arranged in Series-Parallel topology. The targeted battery is of Lithium-Ion (Li-I) type, with 24 VDC operating voltage and 150 Ah rated current. The design began by configuring an interleaved synchronous DC-DC converter to produce a desired voltage level, with low inductor ripple current and low output ripple voltage. The DC-DC converter is in turns condemned by a modified Perturb and Observe (P&O) algorithm, to ensure efficient maximum power tracking. Progressively, the design encountered a layout of the bi-directional DC-DC converter to ensure safe current charging values for the battery. Under the same manner, the role of the bi-directional converter was to plug the battery out of the system, in case when the Depth of Discharge (DoD) is below 25%, thus sustaining the life span of the battery. The entire setup of the proposed sub-systems then leads to the relatively fastest, safest, and most reliable battery charging process. Results show an effectiveness (in terms of PV power tracking) ranging from 87% to 100% under four swiftly changing irradiance conditions. Moreover, this paper suggested the design's future industrialization process, leading to an effective PV solar charger prototype.

Keywords: MPPT; DC-DC converter; perturb and observe algorithm; shading; irradiance; control

Citation: Osmani, K.; Haddad, A.; Alkhedher, M.; Lemenand, T.; Castanier, B.; Ramadan, M. A Novel MPPT-Based Lithium-Ion Battery Solar Charger for Operation under Fluctuating Irradiance Conditions. *Sustainability* **2023**, *15*, 9839. https://doi.org/10.3390/su15129839

Received: 11 April 2023
Revised: 12 June 2023
Accepted: 12 June 2023
Published: 20 June 2023

1. Introduction

The massive growth of PhotoVoltaic (PV) systems' installations is globally witnessed, where their utilization is evident across various applications [1–3]. Among different forms of renewable energy supplies, the PV systems are mainly popularized to be adapted as resilient electrical power provisions, due to their silent performance, static architecture, non-detrimental nature, and for the abundancy of solar irradiance [4,5]. The improved maintenance techniques for PV systems [6–19], and the amelioration of the PV cells' raw materials [20–27], have yielded in an elevated overall efficiency, hence approbated their approval to be considered as next-generation electrical power providers. For example, in order to remove the toxic air pollutants (CO_2, greenhouse gas emissions, etc.) resulting from

the excessive burning of oil, gas and diesel for energy generation purposes, PV systems can well contribute, heading relatively towards a carbonless future [28–36].

Having various forms and structural designs, off-grid PV systems are receiving the highest interest [37–41], as they present an elevated flexibility in front of low solar irradiance scenarios, as well as possessing the ability to supply loads during nights. In terms of reliability, off-grid PV systems can fit in commercial, industrial, and residential power systems [42,43], hence having a greater applicability in different fields of application. Nevertheless, such systems lower electricity bills and consist of a backup power supply for grid failures/blackouts by:

- Reducing the need for diesel and fuel to generate electricity
- Decreasing the urge for the continuous generators' maintenance and monitoring routines
- Making less technical labor routines

However, these systems rely mainly on Energy Storage Systems (ESS) [44–51]. The excess energy generated by the PV panels (i.e., during peak sunlight) is stored by a battery bank, for example. The continuous power supply demanded by critical loads can be hence ensured by the utilization of that stored energy. In terms of energy usage optimization, the ESS also contribute to load balancing and equity. Moreover, since grid outages/malfunction generally occur in electrical systems, the ESS feature in off-grid PV systems provide accordingly a backup supply, thus relatively smoothing out the fluctuations between the energy supply and demand. This reliance on ESS on the other hand, provokes consecutive problems, thus arising the need for:

- Maximum solar power extractor to benefit from the total available power
- Power conditioning units for a safe voltage/current equalization
- Monitoring systems to continuously check the charging states, battery's feeding voltage, charging current, etc.

Accordingly, DC-DC converters (i.e., solid-state switch-controlled electronic hardware that are used to either boost or buck the desired output voltage, according to the feeding input levels) are designed to be controlled by Maximum Power Point Tracking (MPPT) algorithms [52–57] to compensate the highly non-linear behavior of the PV cells [58–62], thus extracting the maximum available power from the PV arrays. Classified as isolated and non-isolated layouts [63–72], the overall efficiency of such converters and performance are related to their designs' complexity. For instance, non-isolated DC-DC converters showed better efficiency versus isolated ones, but still exhibit erroneous behaviors such as power loss and rippled currents. Generally, and according to the work conducted in [63–72], it can be concluded that isolated DC-DC converters offer higher efficiency when compared to non-isolated converters due to the reduced power losses, while ensuring galvanic isolation, thus offering an improved electrical safety (i.e., against ground loops, etc.). Due to their isolation barrier, isolated DC-DC converters exhibit low ripple current, hence reducing the electromagnetic interference noise. On the other hand, however, isolated DC-DC converters are more complex in their designs, with larger sizes and heavier weights due to the presence of the isolation transformers. From another side, and after an investigation of the work in [63–72], it can be deducted that non-isolated DC-DC converters require fewer components for their realization and are more suitable for space-constrained applications when compared to isolated converters. Despite these advantages, the non-isolated DC-DC converters are less efficient when compared to the isolated converters and are prone to exhibit high-frequency harmonic oscillations. With that being said, the choice of a DC-DC converter for off-grid PV systems is a challenging task, which needs consideration according to many operational factors.

The MPPT algorithms on the other hand (i.e., composing the software which produces case-dedicated duty values, that in turn control the behavior of the solid-state switches in the DC-DC converters), are characterized for operation under uniform irradiance [73–82] or under partial shading conditions [83–99]. Such algorithms fluctuate in their complexity

levels and accuracy, ranging from simple (i.e., Perturb and Observe (P&O)) to complex (i.e., artificial-intelligence-based algorithms). The relation between the MPPT algorithm's complexity and its level of accuracy is reversal, where the simpler the algorithm is, the worser its efficiency becomes when compared with higher-leveled algorithms As for the MPPT algorithm used under homogeneous irradiance conditions in [73–82], they can be perceived as simple in application, have low computational requirements, and possess a fast response criterion. On the opposite side, such algorithms perform poorly under partial shading conditions, where they may exhibit an oscillatory behavior around the maximum power point, leading thus to a "false" peak in the PV's characteristic curve, and are generally vulnerable to local power maximums traps. On the other hand, the other MPPT algorithms that are used under partial shading conditions in [83–99], have a better improved efficiency than the ones in [73–82], where they can accurately identify the global power peak under complex and non-linear shading conditions. Still, such algorithms are way more complex to implement, where the artificial-intelligence-based [86] need training with a representative dataset, thus relying on accurate models and training data. Accordingly, and as it is the case with the choice of the DC-DC converters, the choice of the MPPT algorithm to be implemented in a PV-based solar charger, is also not a straightforward approach.

Charge controllers from another side, regulate the power flow from/into the ESS, by means of DC-DC converters (e.g., bi-directional, uni-directional, etc.) [100–103]. Such converters can be controlled using a Proportional Gain (PG) controller, reference voltage/current control scheme, closed-loop control, and others [104,105]. The uni-directional charge controllers in [100–103] have a simple design and are generally more cost-effective than the bi-directional converters, and offer a standard protection for the PV panels, since they allow the power flow in one direction (i.e., the route from the ESS to the PV panels is opened, hence the panels would never be subjected to any current from the ESS). On the other hand, uni-directional charge controllers have more limited functionality when compared to bi-directional converters, where they do not support the power flow from multiple PV sources. The bi-directional charge controllers, on the other hand, are more flexible in usage, enable more energy management than uni-directional controllers, and better facilitate the grid-integration with the PV systems. Despite their advantages, the bi-directional charge controllers are more complex in design, thus yielding to a reduced cost efficiency when compared to the uni-directional controllers and require advanced algorithms to ensure a stable operation. The controlling scheme in [104,105] is by itself another area of study, where for example the PG controller offers a good stability with appropriately tuned gains but can unfortunately show poor performance such as presence of overshoot, instability, current leakage, and others, [106] under improper gain tuning. Under the same approach of the DC-DC converter choice, as well as the MPPT algorithm, the charge controllers, on the other hand, require a careful selection process, when intended to be employed in off-grid PV systems.

Based on what has been precedent, and by taking into consideration the challenges for choosing a DC-DC converter to be controlled by an appropriate MPPT algorithm which dictates the operation of the charge controller, the aim of this paper is to design a novel solar battery charger, beginning by the design of an interleaved synchronous non-isolated DC-DC converter. According to the surveyed DC-DC converters, and after analysis of the pros and cons of each, in order to mitigate ripple current and minimize the equipment need and size of the converter, the interleaved synchronous non-isolated converter is chosen. The modification of the P&O algorithm presented in this work rearranged the proportionality between the algorithm's complexity and accuracy level, where a simple algorithm (far from artificial intelligence and machine-language-based methods) showed better accuracy than conventional P&O, and hence offered an intermediate trade-off.

- The bi-directional DC-DC converter used to control the charging/discharging processes of the battery is designed and controlled via PV array specifications (voltage, current, power, etc.)-based algorithm. At the final destination, the reference current (I_{ref}) is developed and interfered with a Proportional Integral (PI) controller to safely

charge the 24 V, 150 Ah Lithium-Ion (Li-I) battery with the maximum available current, resulting from different shading patterns. Accordingly, this paper's contribution can be summed up in the following points: improved design of a DC-DC converter: interleaved synchronous non-isolated converter, providing good efficiency, at the same time presenting low ripple currents.

- Modified MPPT algorithm: simply by adding an operational timer on the workflow process of a conventional P&O algorithm, the "real" power peak is more precisely identified, hence achieving a more power extractability option from the PVA.
- Enhanced bi-directional charge controller: not only does it ensures maximum safe charging current values for the ESS, but also plugs the battery out of the system according to a threshold SoC, yielding eventually in prolonging its lifecycle (when applied as a prototype).

The overall systematic design is a combination of multiple sub-systems, beginning with the PV Array (PVA) that is arranged in a 3×3 Series Parallel (SP) topology, with a maximum power of 1.918 kWp. The designed PVA is then succeeded with an interleaved DC-DC converter (controlled by modified P&O algorithm) which in turn is interfered with a bi-directional DC-DC converter (controlled by a reference current generator). The output target is to maximally charge the Li-I battery in the safest, fastest, and most accurate form.

The rest of this paper is composed as follows: Section 2 presents the overall working methodology behind the work in this paper, Section 3 reveals the PVA arrangement and different shading patterns used during the Matlab simulation of this design, Section 4 shows the designing steps for the interleaved DC-DC converter, Section 5 explains how the P&O was modified. Section 6 interprets the design structure of the bi-directional converter, which is controlled by current suppression scheme shown in Section 7, where in Section 8 the entire design, grouping physical structures (converters) with control and measurement modules (algorithm, scoping, etc.) is shown, and being subjected to four distinct irradiation patterns, Section 9 discusses the obtained results and offers future work plans for the design, and finally in Section 10 global conclusions are derived.

2. Working Methodology

In order to completely realize the work suggested in this paper, that is to design a complete solar charger, originated from the PVA, the design of each sub-component (e.g., DC-DC converter, bi-directional converter, etc.) is thoroughly investigated. Each of the electronic components are designed according to a mathematical model, yielding for the calculation of the required elements, such as resistors, capacitors, inductors, and others. The modification of the P&O algorithm, on the other hand, was based on a computational assessment in which the conventional P&O cannot dedicate accurate duty ratios in order to maximumly extract the available power from the PVA under different shading scenarios. The working methodology behind this work can be summarized according to the following points:

1. While attempting to mimic some extremely fluctuating solar irradiance conditions, the designed solar irradiance patterns in the Simulink environment varied from 100 W/m^2 to 1000 W/m^2 with different time lapses. For example, one of the solar irradiance patterns can have its irradiance step-wise of 100 W/m^2 decreased from 1000 W/m^2 to 100 W/m^2 during non-static time frames: a condition of 1000 W/m^2 irradiance can last, for example, x seconds, then 900 W/m^2 for y seconds and so on, until the minimum of 100 W/m^2 for example is reached. Different irradiance cycles exist for each of the designed irradiance patterns. This shall serve to emulate extreme solar irradiance fluctuating conditions (i.e., in real applications, such scenarios will be due to extreme cloud passage, swiftly moving physical obstacles, etc.)
2. According to the surveyed DC-DC converters from the work in the references [63–72], the mathematical model of the suggested interleaved synchronous DC-DC converter is justified after responding to the following questions:
    a. Based on what must the converter's switching frequency be?
    b. How to calculate the duty ratio?

c. What are the values of the capacitance/inductance for the converter's capacitor/inductor, respectively?

3. Concerning the MPPT algorithm (i.e., P&O) modification, and in order to stay away from further programming complexities, the work in this paper simply suggests analyzing the PV power curve using discretized samples by means of a code-based on-delay timer. The modified P&O can hence better "acknowledge" the power status of the PVA, thus more accurately assign duty ratios.
4. For an efficient implementation of the suggested bi-directional converter, its electrical parameters must be also modelled mathematically, for an optimum selectivity of inductance, capacitance, and resistance that are to be employed in its circuit architecture. Moreover, the bi-directional converter must take also into consideration the maximum allowed charging current, as well as the minimum permissible depth of discharge.

By taking all of the previous steps into consideration, a complete version of the solar charger is hence produced, in a cascaded topology, beginning by the PVA as main input, then successively toward the DC-DC converter (controlled by the modified P&O algorithm), then the bi-directional converter (controlled by a current control scheme), then eventually to the battery's terminals.

3. Set Up of PVA and Creation of Irradiation Patterns

The PVA with the power rating of 1.918 kWp, consisting of the input of this design, is sub-composed of multiple PV modules, each of a smaller power rating. Using the Series-Parallel (SP) interconnection scheme, the PVA is accordingly built. This type of PV Reconfiguration (PVR) is adapted among many others, such as parallel, series, Total Cross Tied (TCT), Honey Comb (HC), skyscraper puzzle, Sudoku, etc. [107–116] due to its superiority in terms of elevated efficiency and less need of extra interconnecting wires. The SP scheme is hence found optimum and would present an advantageous point for the future industrialization of the design, in regards to the system's cost efficiency. The electrical characteristics for each PV module composing the PVA are shown in Table 1. According to the parameters shown in Table 1, the PVA characteristic curves, such as Current-Voltage (I-V) and Power-Voltage (P-V) are plotted in Figure 1.

Table 1. Electrical characteristics of each PV module.

Module Data	Value	Model Parameters	Value
Maximum power	213.15 [W]	Light generated current	7.8654 [A]
Open circuit voltage	36.3 [V]	Diode saturation current	2.9273×10^{-10} [A]
Short circuit current	7.84 [A]	Diode ideality factor	0.98119
Voltage at maximum power V_{mpp}	29 [V]	Shunt resistance	313.0553 [Ω]
Current at maximum p(	7.35 [A]	Series resistance	0.39381 [Ω]

It can be noticed from Figure 1 that the maximum power affordable by the PVA at the Standard Test Conditions (STC) under an irradiance of 1000 W/m^2 and temperature of 25 °C is 1.918 kWp. The PVA, however, can encounter different shading scenarios, inhibiting it thus from achieving its maximum power capacity. This is mainly due to non-static shadow reflectors, such as moving clouds, birds, and other obstacles as shown in Figure 2.

In order to study the negative impacts of the probable rapidly fluctuating irradiance inducers as in Figure 2, a time-based irradiance signal generator is derived in this work, within a time frame of 10 s. The sensitivity of irradiance is set for 100 W/m^2 with a maximum time lapse of 1 s, as shown in Table 2, for different Solar Irradiation Patterns (SIPs). The logic behind the four shading patterns creation in Table 2 is derived after several assumptions, stating that at a defined time t, the incident irradiation hitting the PVA surface

is of a constant value x, resulting from clouds/birds' passage. For each irradiance value from 100 W/m^2 to 1000 W/m^2, as well as for each SIP, indicated is the time of irradiance-subjection. For example, in Table 2, the SIP2 has no time window during which the PVA is subjected to an irradiance of 100 W/m^2 where this same condition also applies for SIP3. For SIP4 from another side, the PVA is subjected to an irradiance of 1000 W/m^2, for example, only at t = 5 s and t = 10 s. This corresponds to the logic for all SIPs in Table 2. According to the values driven in Table 2, the graphical representation for different shading patterns, SIP1, SIP2, SIP3, and SIP4 is presented in Figure 3.

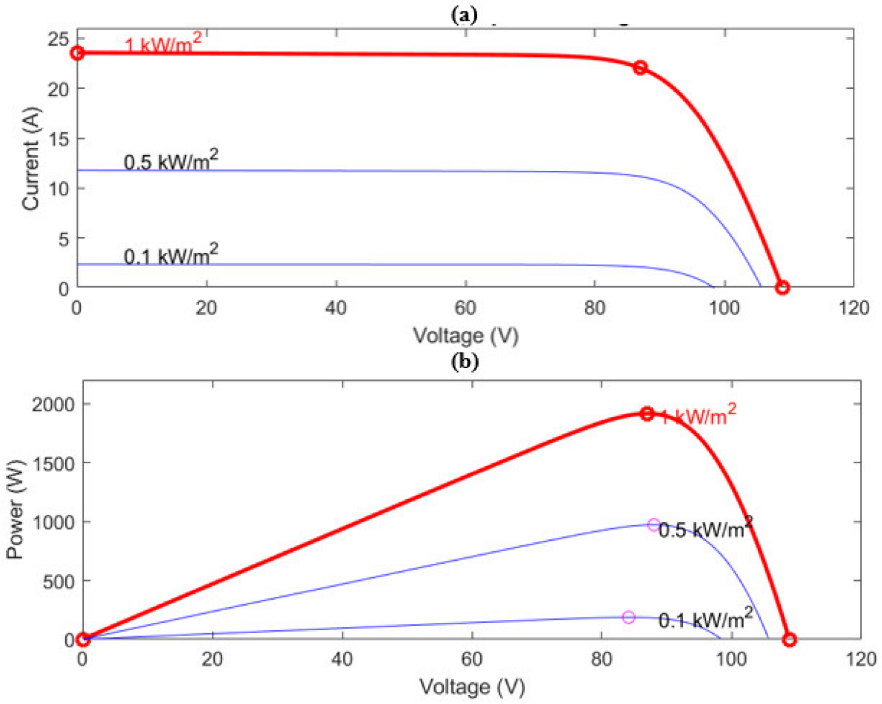

Figure 1. Characteristic curves for the SP PV array, (**a**) I–V curve, (**b**) P–V curve.

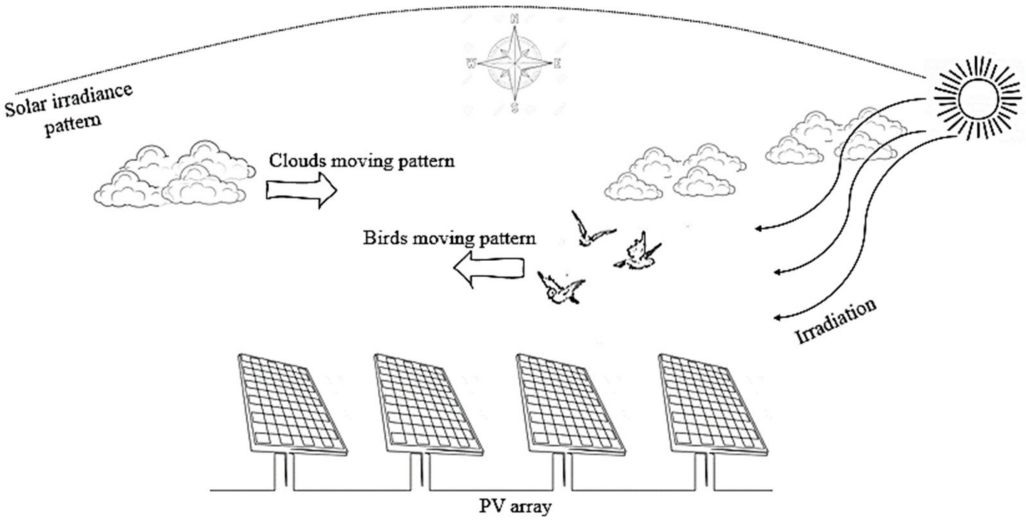

Figure 2. Causes of timely fluctuating shading scenarios.

Table 2. The data used for the irradiance curves generation.

Irradiance [W/m^2]	1000	t = 0 s t = 6.5 s	t = 1 s t = 2 s t = 4 s t = 7.7 s	t = 2 s t = 7.2 s t = 9 s	t = 5 s t = 10 s
	900	t = 0.7 s t = 2.7 s t = 6 s t = 8.2 s	t = 0.7 s t = 2.7 s t = 3.7 s t = 8 s	t = 1.7 s t = 2.2 s t = 7.2 s	t = 9 s
	800	t = 2 s t = 5 s t = 8.2 s t = 10 s	t = 1 s t = 2 s t = 6 s t = 8 s	t = 1.5 s t = 2.4 s t = 7 s t = 9.4 s	t = 8 s
	700	t = 1 s t = 2 s t = 3 s t = 7 s	t = 0.5 s t = 2.7 s t = 3.4 s t = 8.7 s	t = 1.2 s t = 2.7 s t = 5.2 s t = 6.7 s	t = 3 s
	600	t = 1.2 s t = 4.4 s t = 9.4 s	t = 1.2 s t = 5.4 s t = 8.4 s t = 9.4 s	t = 1 s t = 1.2 s t = 3 s t = 5 s t = 9.7 s	t = 1 s
	500	t = 1 s t = 3 s t = 5 s t = 7 s t = 8.7 s	t = 0 s t = 3 s t = 4.2 s t = 5.2 s	t = 0.75 s t = 1 s t = 3.26 s t = 3.49 s t = 4.74 s	t = 0 s
	400	t = 3.7 s t = 4.4 s t = 9.4 s	t = 8.7 s t = 9.4 s	t = 0.5 s t = 0.75 s t = 3.49 s t = 3.73 s t = 4.46 s	t = 2 s
	300	t = 3.6 s t = 9 s	t = 9 s t = 5.21 s	t = 0.29 s t = 0.5 s t = 3.73 s t = 4 s	t = 4 s
	200	t = 4.3 s t = 5.4 s	-	t = 0 s t = 0.29 s t = 4 s t = 4.24 s	t = 6 s
	100	t = 4 s t = 9 s	-	-	t = 7 s
Solar Irradiation Patterns		SIP1	SIP2	SIP3	SIP4

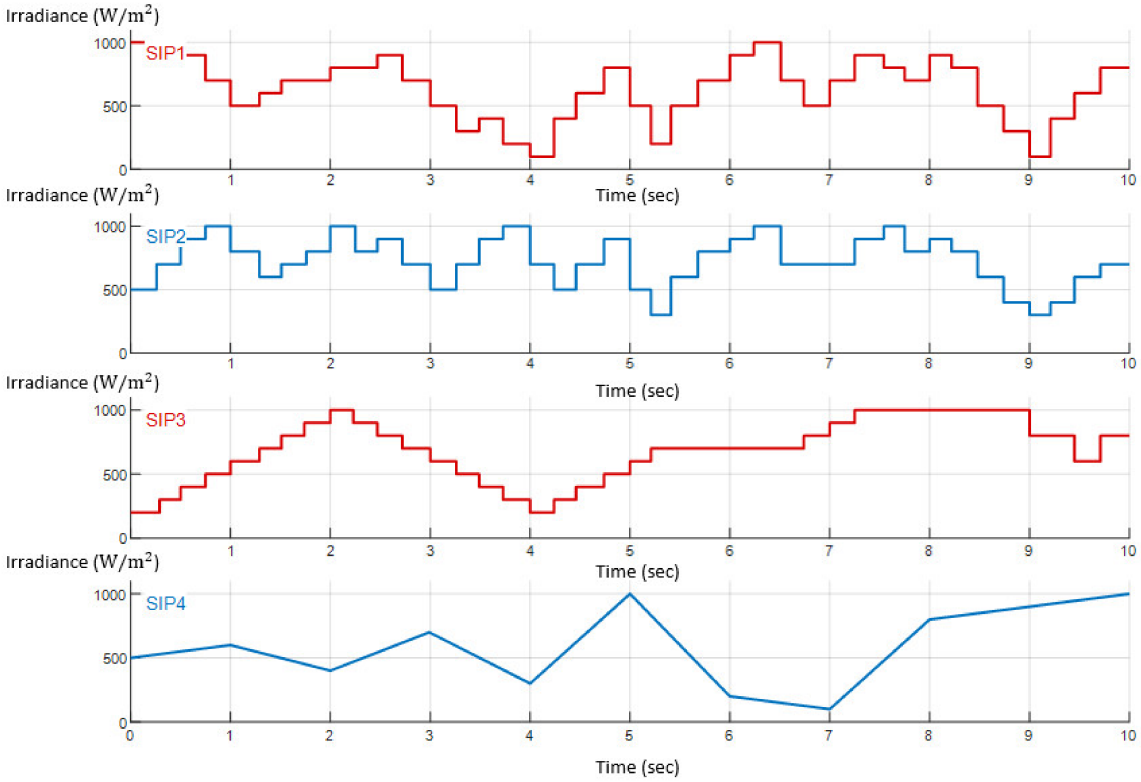

Figure 3. The four rapidly fluctuating distinct irradiation patterns.

4. Design of the DC-DC Converter

As intended to pull down the PVA output voltage, near the ESS voltage whilst maintaining the conservation of input/output power equalities, an interleaved synchronous buck converter is adapted in this work. First and foremost, the synchronous circuit form for the converter is an improved modification referring to the conventional buck converter [117]: the replacement of the diode with another solid-state switch (e.g., Metal Oxide Semi-conductor Field Effect Transistor (MOSFET), Insulated Gate Bipolar Transistor (IGBT), etc.) will negate any voltage drops across the diode, hence lowering losses and elevating the converter's efficiency. The synchronous buck converter is shown in Figure 4.

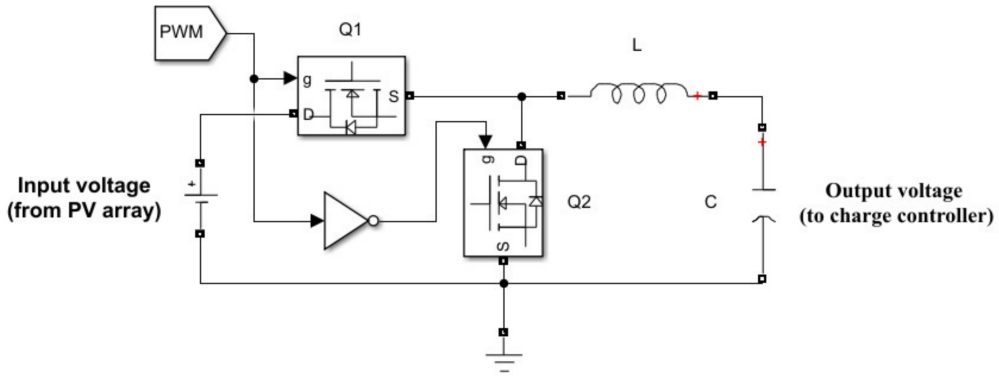

Figure 4. Synchronous DC-DC buck converter.

The Pulse Width Modulation (PWM) label shown in Figure 4 is obtained from the MPPT algorithm. The logic "NOT" gate, which is used in generating the gate signal to Q2, is there to ensure that both Q1 and Q2 are never conducting at the same time, thus eliminating any possibility of a bolted electrical short-circuit. Concerning its working routines, the circuit in Figure 4 operates under two modes:

1. Q1 is closed, Q2 is open: in this phase, the current flows in a clockwise direction, charging both inductor L and capacitor C.
2. Q1 is open, Q2 is closed: the energy stored in L is released, where current flows from the inductor itself. Under a certain threshold of inductor discharging, the capacitor becomes the main source of the current, until the next cycle begins.

The interleaved design used in this work takes two circuits of Figure 4 and connects them in parallel. The input and output capacitors are shared for the doubled circuit, as shown in Figure 5. The ripple current for the interleaved circuit is halved since each interleaved phase shares the total current.

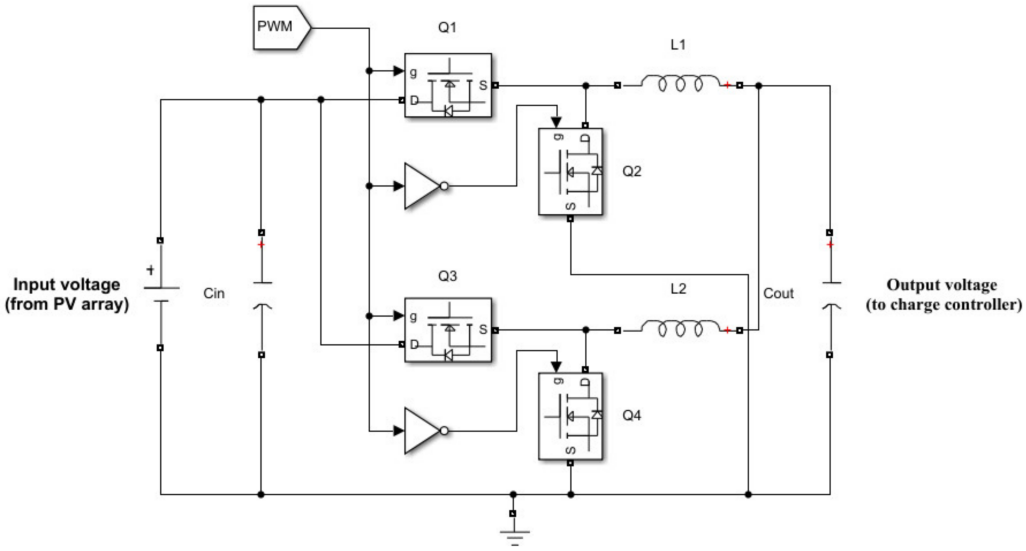

Figure 5. Interleaved Synchronous DC-DC buck converter.

The DC-DC converter circuit topology is to be based on an interleaved synchronous design, presenting an increased power handling capability (current and power are divided between the multiple converter phases). From the same perspective, the interleaved design provides also presents an improved efficiency by reducing the solid-state switches conduction losses (by distributing the load across multiple phases), as well as adapting a better transient response (the presence of multiple phases in the circuit architecture allows a better load sharing). The following parameters must be calculated in order to complete the design:

- Switching frequency f_s
- Duty ratio D
- Inductance L
- Capacitance C

The choice of f_s, for it to be followed by the PWM generation is solely based on the switching losses of the MOSFETs, where a higher f_s yields to smaller inductor and capacitor sizes, but in turn increases the switching losses as shown in Equations (1)–(3) for the high side MOSFETs [118–120].

$$P_{Loss[H]} = P_{Conduction[H]} + P_{Switching[H]} \quad (1)$$

$$P_{Conduction[H]} = I_{OUT}^2 \times R_{DS} \times D \quad (2)$$

$$P_{Switching[H]} = \left(\frac{t_{RH} + t_{FH}}{2}\right) \times V_{in} \times I_{OUT} \times f_s \quad (3)$$

Such that $P_{Loss[H]}$ denotes the total power losses on the high side MOSFETs, as a sum of conduction losses $P_{Conduction[H]}$ and switching losses $P_{Switching[H]}$. The term D represents the duty ratio generated by the MPPT algorithm, t_{RH}, t_{FH} the turn on/off (rise/fall) times, respectively, R_{DS} the drain to source MOSFET's resistance, V_{in} the input voltage to the converter originated from the PVA, I_{OUT} the output current, and f_s the switching frequency. Similarly, for the low side MOSFETs, the switching frequency related power losses are shown in Equations (4)–(6) [118–120].

$$\mathrm{P_{Loss[L]}} = \mathrm{P_{Conduction[L]}} + \mathrm{P_{Switching[L]}} \tag{4}$$

$$\mathrm{P_{Conduction[L]}} = \mathrm{I_{OUT}^2} \times \mathrm{R_{DS}} \times (1 - \mathrm{D}) \tag{5}$$

$$\mathrm{P_{Switching[L]}} = \left(\frac{\mathrm{t_{RL}} + \mathrm{t_{FL}}}{2}\right) \times \mathrm{V_{bodyDiode}} \times \mathrm{I_{OUT}} \times \mathrm{f_s} \tag{6}$$

where $V_{bodyDiode}$ represents the internal body diode forward drop voltage. As seen from Equations (1)–(6) the switching frequency is directly proportional to the MOSFETs' switching losses. Accordingly, a trade-off between L, C sizes and elevated losses, yields to an f_s choice of 15 kHz, for this design. The duty ratio D on the other hand, presented in Equation (7) must take into consideration that the output voltage is always equal to 26 V, as an effective and a safe feeding voltage level to the ESS of 24 VDC operating voltage.

$$\mathrm{D} = \frac{\mathrm{V_{out}} \times \mathrm{eff}}{\mathrm{V_{in}}} \tag{7}$$

where V_{out}, V_{in} represent the required output voltage and PV input voltage, respectively, with eff representing the converter's efficiency. Assuming a 100% efficiency (for simulation purposes only), and a V_{in} of 87 V (according to Figure 1), the duty ratio must be for instance equal to 0.298. This value is continuously increased/decreased according to the MPPT algorithm variations. Both L and C values can be calculated according to Equations (8) and (9) [121,122].

$$\mathrm{L} = \frac{\mathrm{V_{out}} \times (\mathrm{V_{in}} - \mathrm{V_{out}})}{\Delta \mathrm{I_L} \times \mathrm{f_s} \times \mathrm{V_{in}}} \tag{8}$$

$$\mathrm{C} = \frac{\Delta \mathrm{I_L}}{8 \times \mathrm{f_s} \times \Delta \mathrm{V_{out}}} \tag{9}$$

Such that ΔV_{out} represents the ripple voltage, and ΔI_L the inductor ripple current expressed in Equation (10) [122].

$$\Delta \mathrm{I_L} = (20\% \text{ to } 40\%) \times \mathrm{I_{out(max)}} \tag{10}$$

According to Equations (7)–(10), and by taking into consideration the chosen value of f_s with a desired ripple voltage of 10 mV, the required parameters for the converter design are shown in Table 3.

Table 3. DC-DC converter parameters values.

Parameter	Value
f_s	15 kHz
D	29.8%
L	14.97×10^{-4} H
C	2.3641×10^{-4} F

5. Configuration of the MPPT Algorithm

A conventional P&O algorithm could lead to an erroneous behavior under swiftly varying irradiance conditions [117]. Specifically, for the shading patterns created in Figure 3, the shading intensity varies within a 0.1 s to 0.5 s time lapses. Accordingly, the power difference between ideal and actual power curves (dP), as well as the voltage difference between PV and input voltage curves (dV), could possibly lead to a "false" zero as shown in Figure 6. Therefore, an inaccurate duty ratio D is generated by the MPPT algorithm, provoking a decrease in the system's efficiency, since the total available power from the PVA cannot be then extracted. The small valued power differences in the time frame $(4s; 6s)$ for example, are not taken into consideration in the conventional P&O algorithm.

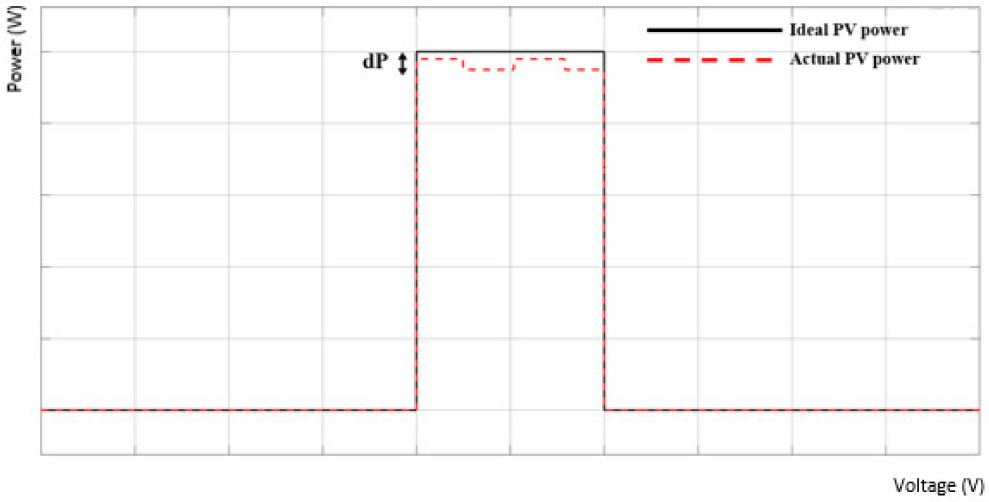

Figure 6. Misleading power differences in a conventional P&O algorithm.

The modification of P&O algorithm intended in this design is to achieve a "true" zero difference between dP quantities, hence attending a real maximum within the P-V characteristic curve. This process is achieved by setting a timer during the flow of the MPPT algorithm, which estimates the power differences using discrete samples and returning averaged values of dP to be investigated. Below are the process' steps:

1. Continuously check whether dP is equal or not to zero, by establishing a timer at each time interval: if the sampled values of dP within the interval have a mean value of zero, then the entire power difference is equal to zero in that timing frame as shown in Figure 7.
2. Set the above sampling method at each new time interval.
3. All mean values resulting from all intervals must be equal to zero.
4. If the condition in the previous step is not satisfied, then modify the duty ratio respectively.

This sampling method could decrease the performance efficiency of the algorithm by requiring more time for execution. This in turn can be compensated by a conditional statement at each checkpoint of dP. According to the I-V and P-V curves shown in Figure 1, the power difference can be checked after the voltage is equal to 80 V, since the maximum peak lies to its right. The complete modified P&O flowchart is expanded in Figure 8.

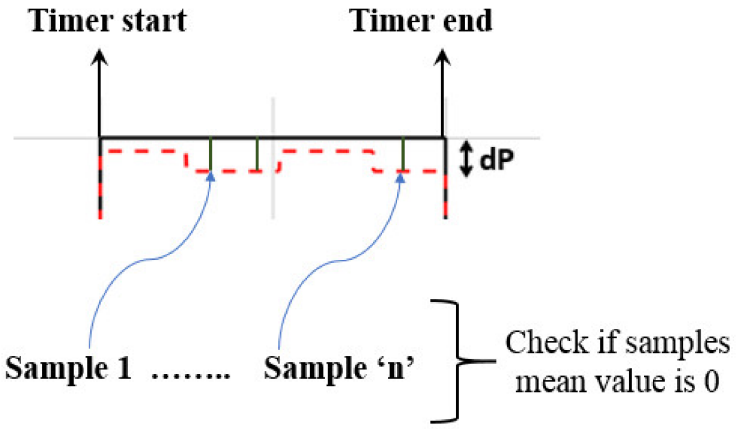

Figure 7. Sampling of power differences in a time frame.

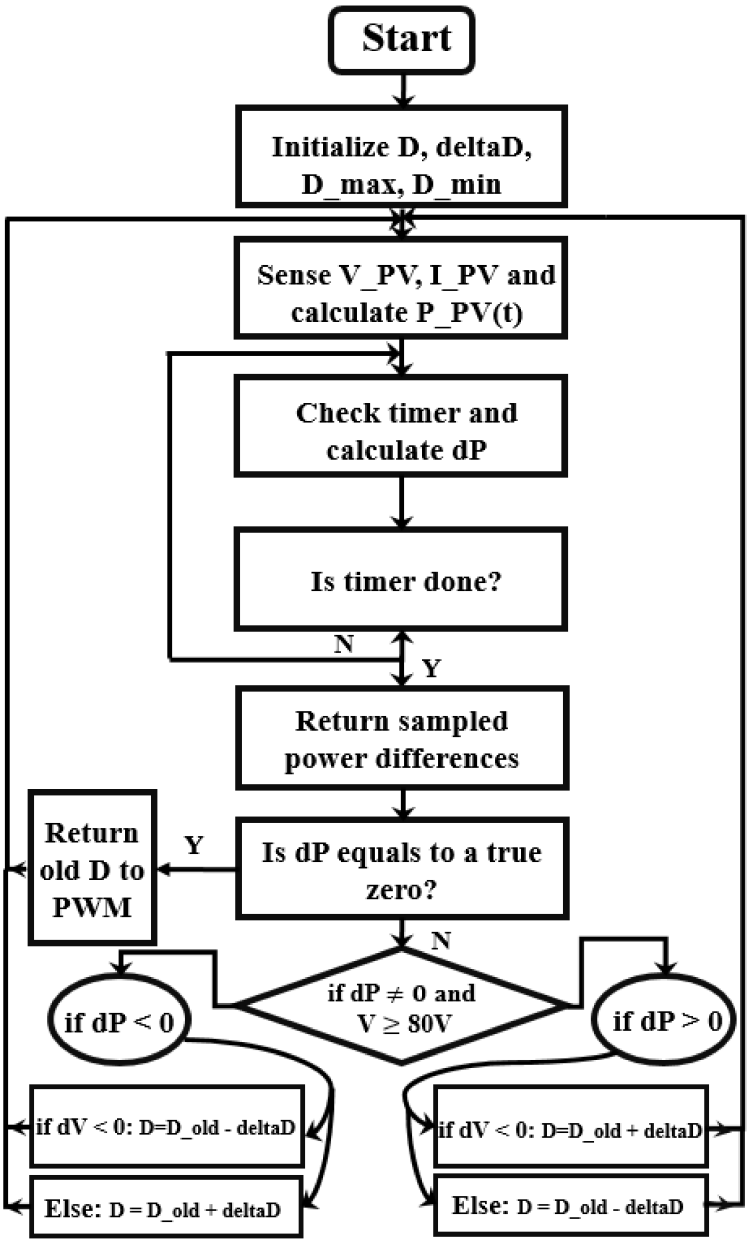

Figure 8. Modified P&O flowchart.

6. Modeling of the Bi-Directional Converter

So far, the design compromising the DC-DC converter, accompanied by the modified MPPT algorithm, offers a maximum power extraction from the PVA under different fluctuating SIPs. Regardless of the solar irradiance's intensity, the modified P&O algorithm ensures accurate as well as dynamic duty ratios generations in order to equivalently set the action of the DC-DC converter (i.e., the conducting/non-conducting states of the solid-state switches). However, it still cannot be confronted with the ESS, due to the following reasons:

- Inability to maintain safe current charging levels for the ESS under high irradiance conditions. The charging current delivered by the PVA might exceed the nominal current charging rate, related to the ESS as indicated in Table 4.
- When the charging currents are not balanced, the ESS gets overcharged, hence, its lifecycle would be reduced consecutively.
- Under discharging states (i.e., at nights or during low irradiance conditions) the battery can exceed the recommended Depth of Discharge (DoD), also causing an increase in its aging rate, and quicker deterioration.

Table 4. Characteristics of the Li-I battery.

Battery Parameter	Value
Rated voltage	24 V
Rated capacity	150 Ah
Cut-off voltage	18 V
Fully charged voltage	27.9357 V
Nominal charging current	58 A

According to Table 4, when the charging current provided by the PVA exceeds 58 A, the battery's internal electrodes become flooded, thus risking deterioration and posing hazards to the surrounding environment (i.e., risk of burnouts, explosions, etc.). Consequently, the designed bi-directional DC-DC converter offers current charging safety for the battery, with respect to the data in Table 4. From a first point of view, the battery's charging current should never exceed 58 A, where the DoD must never be below 25%. This converter is designed using two MOSFET switches, one for the charging process, the other for the discharge, with an LC circuit, where a dummy resistive load is added to interpret the DoD, as shown in Figure 9. Additionally, a controlled switch to plug in/out the battery in case of with respect to DoD is added.

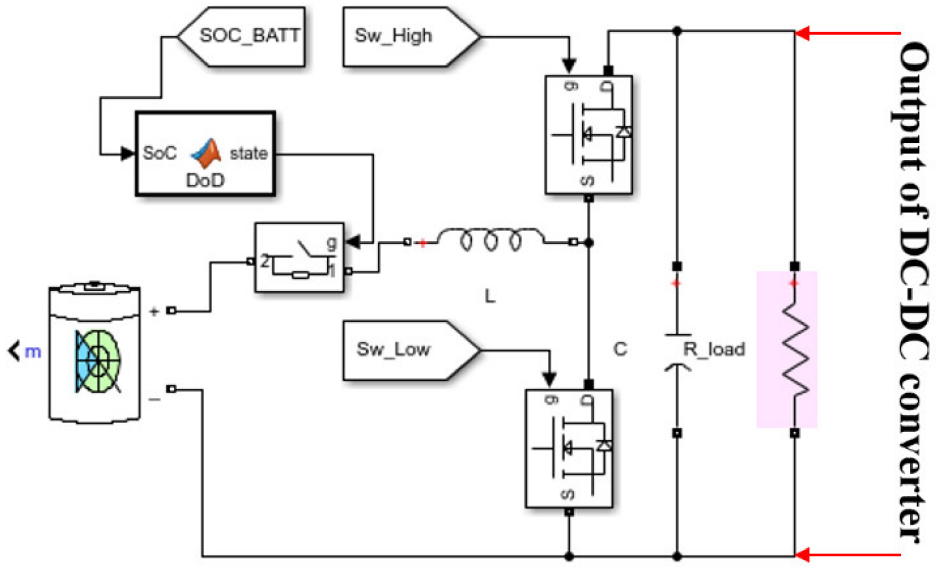

Figure 9. The bi-directional DC-DC converter design.

Regardless of the tactic used to control the circuit in Figure 9, which will be presented in-depth in Section 7, the inductor L and the capacitor C are selected based on Equations (11)–(12), respectively [123].

$$L = \frac{D \times \left(V_{int\_synch\_conv} - V_{batt\_charge}\right)}{f_S \times \Delta I_L} \tag{11}$$

$$C = \frac{(1 - D) \times V_{batt\_charge}}{f_S^2 \times 8 \times L \times \Delta V_{out}} \tag{12}$$

Such that D represents the duty ratio of PWM generation for the MOSFETs, f_S the switching frequency, ΔI_L the desired inductor ripple current, $V_{int\_synch\_conv}$ the actual voltage outputted from the interleaved synchronous DC-DC converter designed in Section 3, V_{batt_charge} the needed voltage level to feed the battery. On the other hand, ΔV_{out} denotes the output ripple voltage. Subsequently, the items composing this bi-directional converter are revealed in Table 5.

Table 5. Parametric values for the bi-directional converter design.

Item	Value
L	2.5 mH
C	3300 µF
R	200 Ω

7. Current Suppression and DoD Control Schemes

The circuit of Figure 9 possesses two switches controlled via PWM generation. The rule is to always keep the two switches phase sequenced as both should never be mutually on or off, as indicated in Figure 10. The high side MOSFET conducts as long as there is sufficient power to charge the battery (i.e., presence of solar irradiance). The inductor L in Figure 9 acts as a current suppressor, while continuously changing its impedance, according to the different PWM states, with respect to Equation (13).

$$Z = \sqrt{R^2 + X_L^2} \tag{13}$$

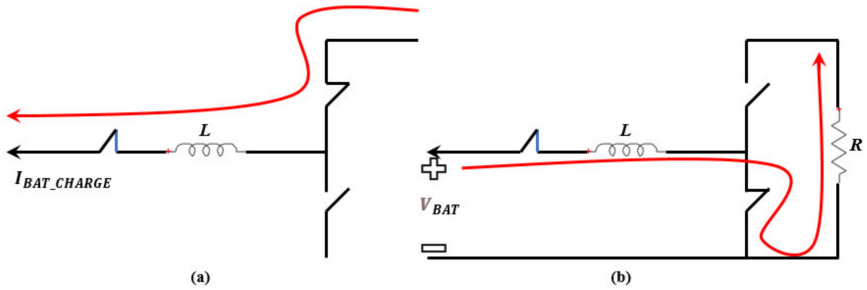

Figure 10. Power flow in/out the battery, (**a**) charging case (**b**) discharging case.

With Z denoting the impedance of the inductor, R its Equivalent Series Resistance (ESR) and X_L its reactive inductance. Assuming a perfect inductor (i.e., ESR = 0), the current passing through is shown in Equation (14).

$$I_L = \frac{V_L}{X_L} = \frac{V_L}{2\pi f L} \tag{14}$$

With V_L representing the voltage across the inductor, f the switching frequency and L the inductance. Accordingly, the continuous change of X_L with respect to f acts as a current limiter, while extracting its maximum safe quantity.

The battery charging current I_{BAT_CHARGE} must never exceed 58 A as a maximum value according to Table 4. For instance, at 1000 W/m^2 the maximum value of the current that is extractable from the PVA is valued at 58 A, where at 500 W/m^2, its value becomes 33 A. With that being said, a reference current I_{ref}, which is mainly dependent on the solar irradiance levels, must be considered as a reference for high/low sides MOSFETs PWM generation. To ensure that I_{BAT_CHARGE} is as closest as possible to I_{ref}, these two quantities are differentiated, where the resulting error signal (if any) will later be fed into a Proportional Integral (PI) controller as shown in Figure 11.

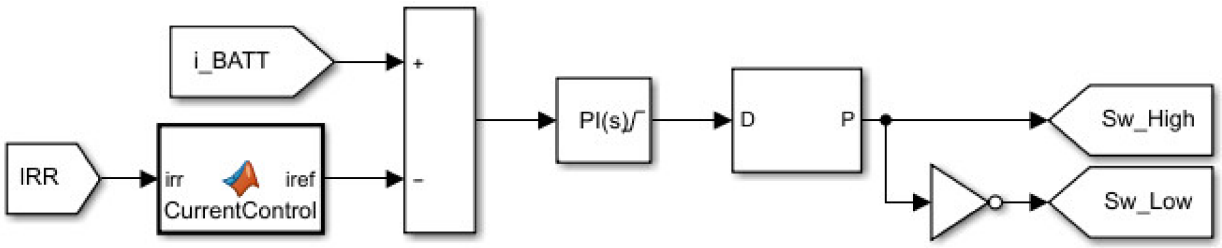

Figure 11. Battery charging current control.

The PWM signals for the MOSFETs in Figure 9 are hence directly controlled by the PI output, with the latent aiming to have the lowest error between I_{BAT_CHARGE} and I_{ref}. On the other hand, in order to monitor the DoD and make sure that the battery would be automatically plugged out of the entire circuit when $DoD \leq 25\%$, a controlled switch is added, as seen in Figure 9 that works as follows:

- As long as DoD >25%, a high logic is set on its gate signal, hence forcing it to be closed (i.e., in a conduction state)
- The above process workflow is halted when the DoD that is acknowledged from battery SoC, drops below 25%.

Both current suppression and DoD control schemes will eventually charge the battery with maximum safe current level, while not permitting the battery to discharge below 25% under low irradiance scenarios and during nights.

8. Overall Layout with Results

The overall circuit, which is composed of multiple designs investigated from Section 2 to Section 6, is shown in Figure 12. In this circuit, the SIPs are to be manually chosen, from the irradiance signal builder. For each SIP, exist different simulation results in terms of the battery charging current, SoC, the feeding voltage, and the overall efficiency. The PVA is set under 25 °C for all SIPs, having its ideal voltage and current referred to as V_PV and I_PV, respectively, where V_IN represents its actual output voltage. The entire circuit of Figure 12 is subsequently arranged with respect to each of its sub-components: the signal builder with the PVA representing the input, to the DC-DC converter, the bi-directional converter, all the way along the battery's terminals. As for the control schemes, the MPPT algorithm is written within a Matlab script, having V_PV, I_PV, V_IN, and P_IDEAL as inputs, such that after the modified P&O flowchart execution, a "duty" is outputted, where it controls the solid-state switches of the interleaved DC-DC converter. The bi-directional converter, on the other hand, is operated with the current control scheme, by means of the final output of the PI controller.

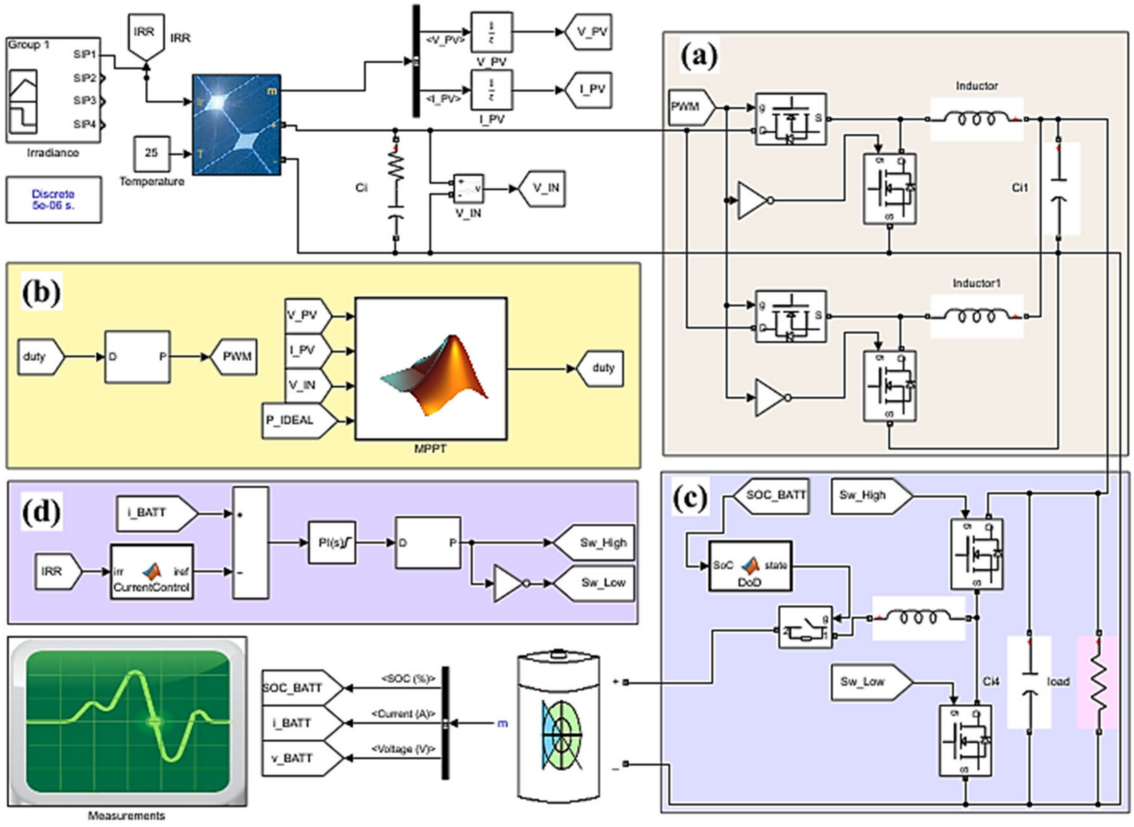

Figure 12. The solar charger overall design, (**a**) interleaved synchronous DC-DC converter, (**b**) MPPT algorithm, (**c**) bi-directional DC-DC converter, (**d**) current suppression and DoD control schemes.

The "Measurements" subsystem block, included in Figure 12, involves scopes circuitry, mean efficiency calculations, and power conversion as revealed in Figure 13: for example, the P_PV is calculated based on a scalar multiplication of I_PV and V_PV. The efficiency is scoped from another part, based on the numerical assessment between P_IDEAL and P_PV. For each of the SIPs, the measurements subsystem block of Figure 13 outputs different graphs covering the alignment between the P_IDEAL as well as P_PV and other battery related electrical characteristics/processes.

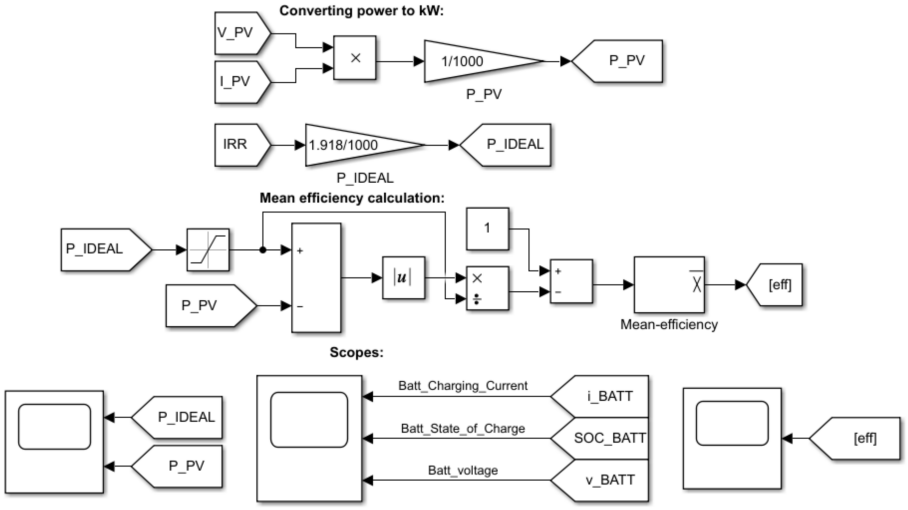

Figure 13. Measurements block subsystem.

8.1. Results for SIP1

The design shown in Figure 12 will be successively exposed to all different irradiance patterns. For this case, the application of SIP1 as designed in Figure 3 would reflect the response of the entire circuit, by showing the closeness between the actual and the ideal power curves as shown in Figure 14. On the other hand, the battery charging process, including the charging current, state of charge, and battery voltage are shown in Figure 15. Lastly, Figure 16 reveals the mean efficiency for the design. The analysis of these results for all SIPs is to be investigated in Section 8.

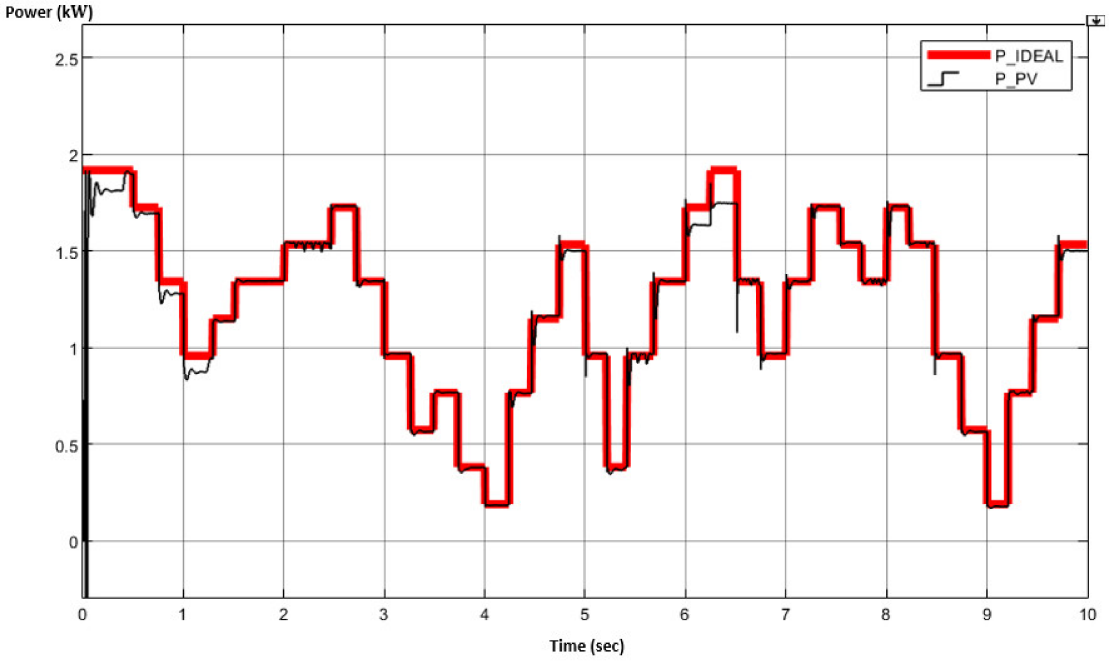

Figure 14. The alignment between the ideal and actual PV power curves (kWp) for SIP1.

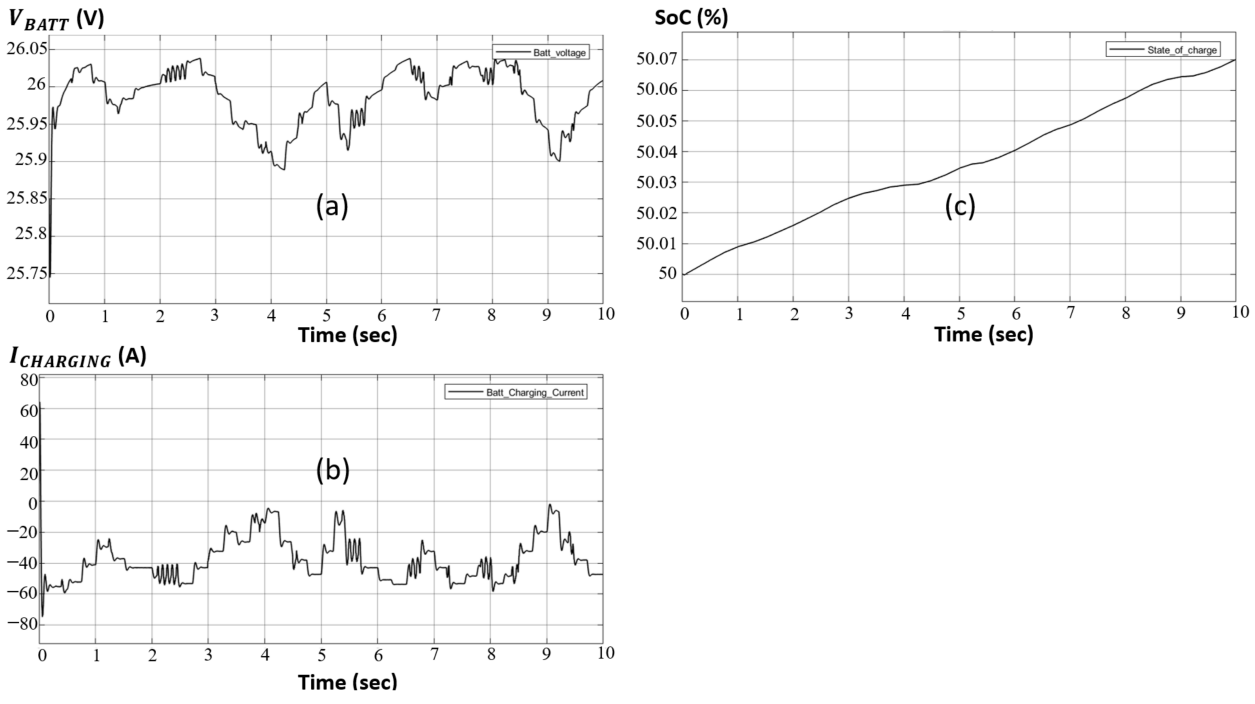

Figure 15. Battery's related curves under SIP1: (**a**) the battery voltage, (**b**) the battery charging current, and (**c**) the battery state of charge.

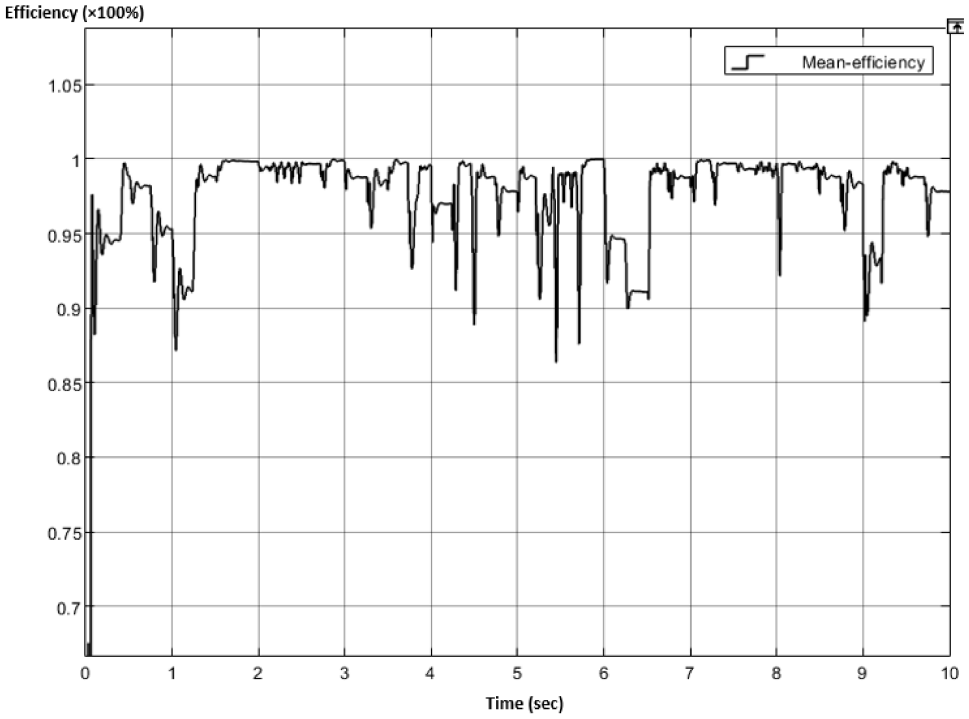

Figure 16. Mean efficiency (%) of the design under SIP1.

8.2. Results for SIP2

While switching the irradiance patterns to SIP2, the same circuit as in Figure 12, reflects different performance reactions, where the closeness between the actual and the ideal power curves is shown in Figure 17. The battery charging process, including the state of charge, the charging current, and the battery voltage, are expanded in Figure 18. The design mean efficiency particularly under SIP2 is shown in Figure 19.

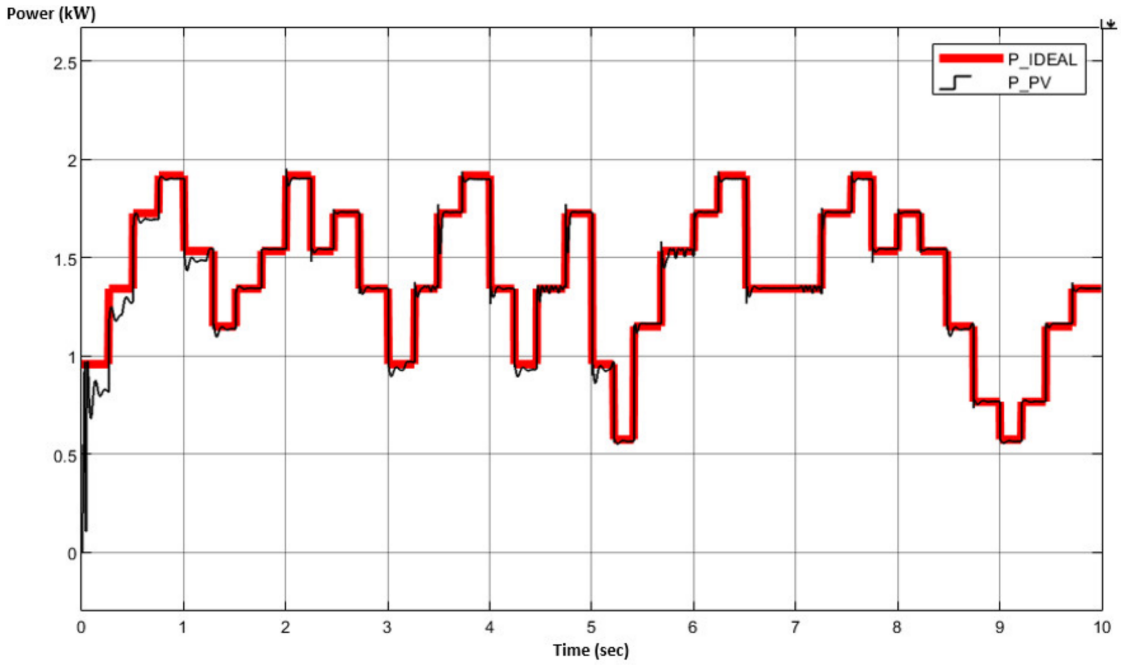

Figure 17. The alignment between the ideal and actual PV power curves (kWp) for SIP2.

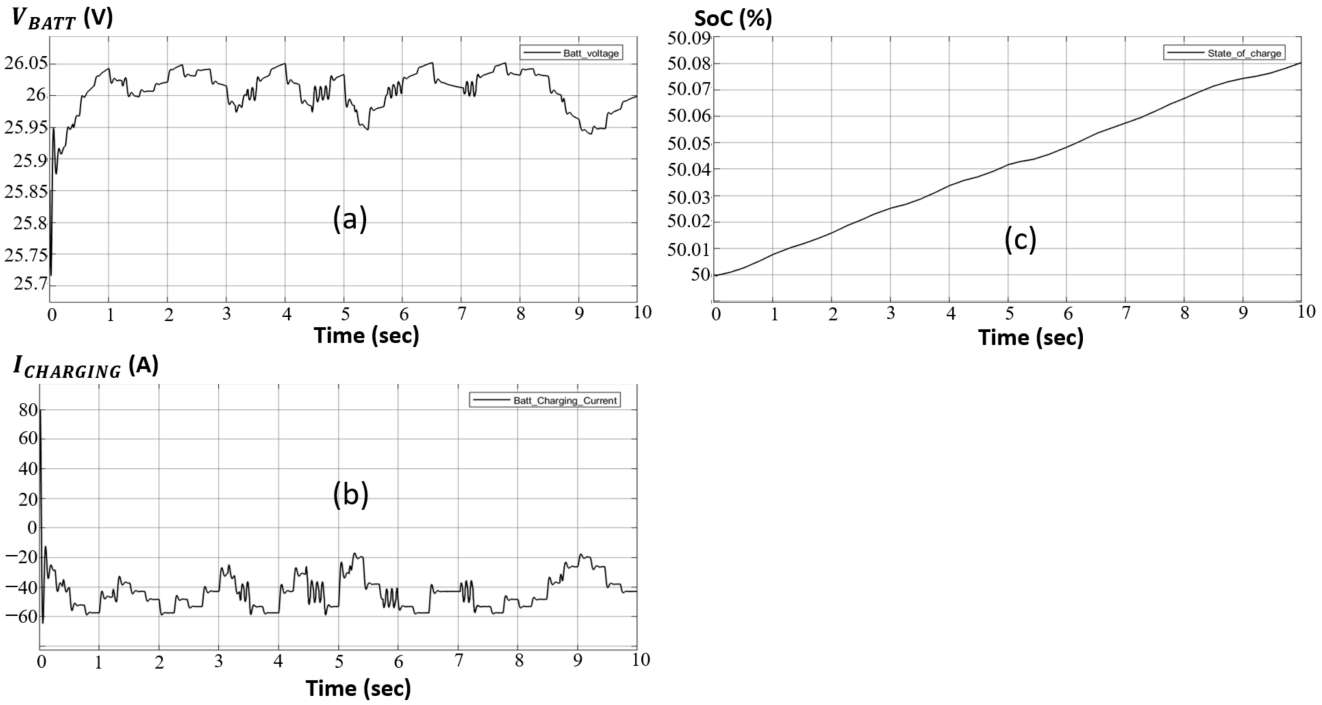

Figure 18. Battery's related curves under SIP2: (**a**) the battery voltage, (**b**) the battery charging current, and (**c**) the battery state of charge.

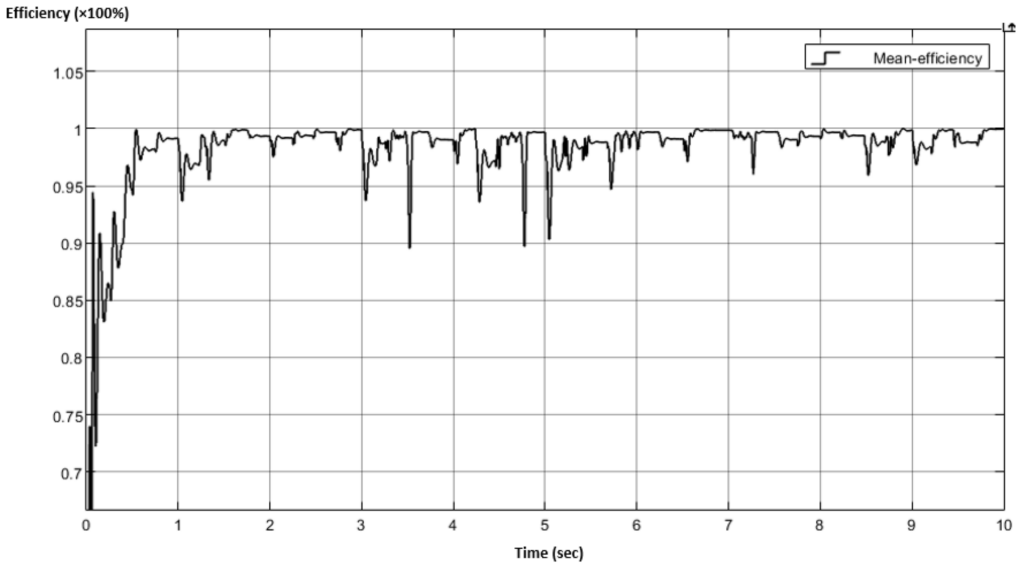

Figure 19. Mean efficiency (%) of the design under SIP2.

8.3. Results for SIP3

After switching the irradiance patterns to SIP3, Figure 20 shows the relevant closeness between the new actual and the ideal power curves. The battery charging process, including the state of charge, the charging current, and the battery voltage, are revealed in Figure 21. The design mean efficiency for SIP3 is shown in Figure 22.

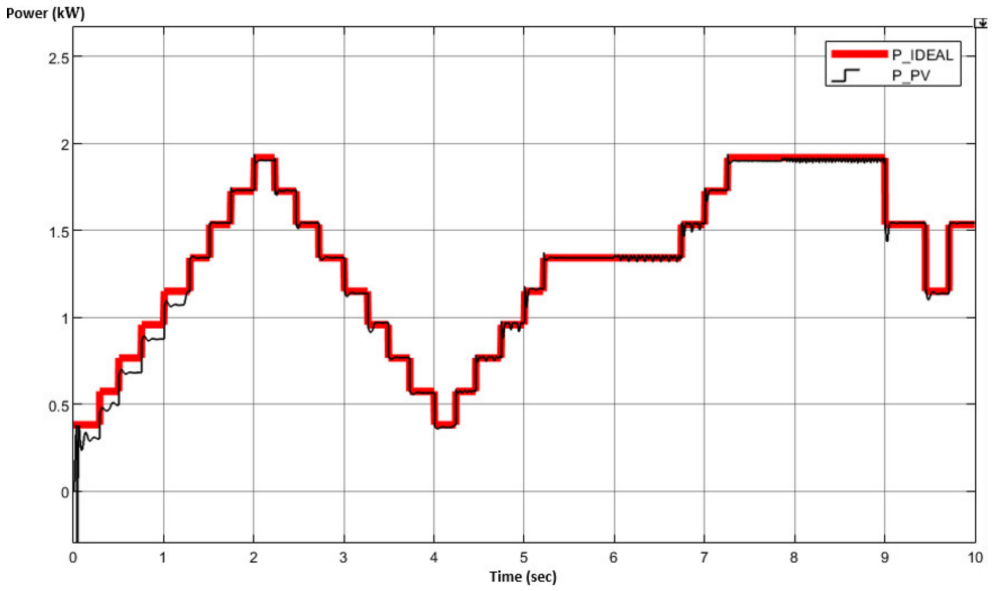

Figure 20. The alignment between the ideal and actual PV power curves (kWp) for SIP3.

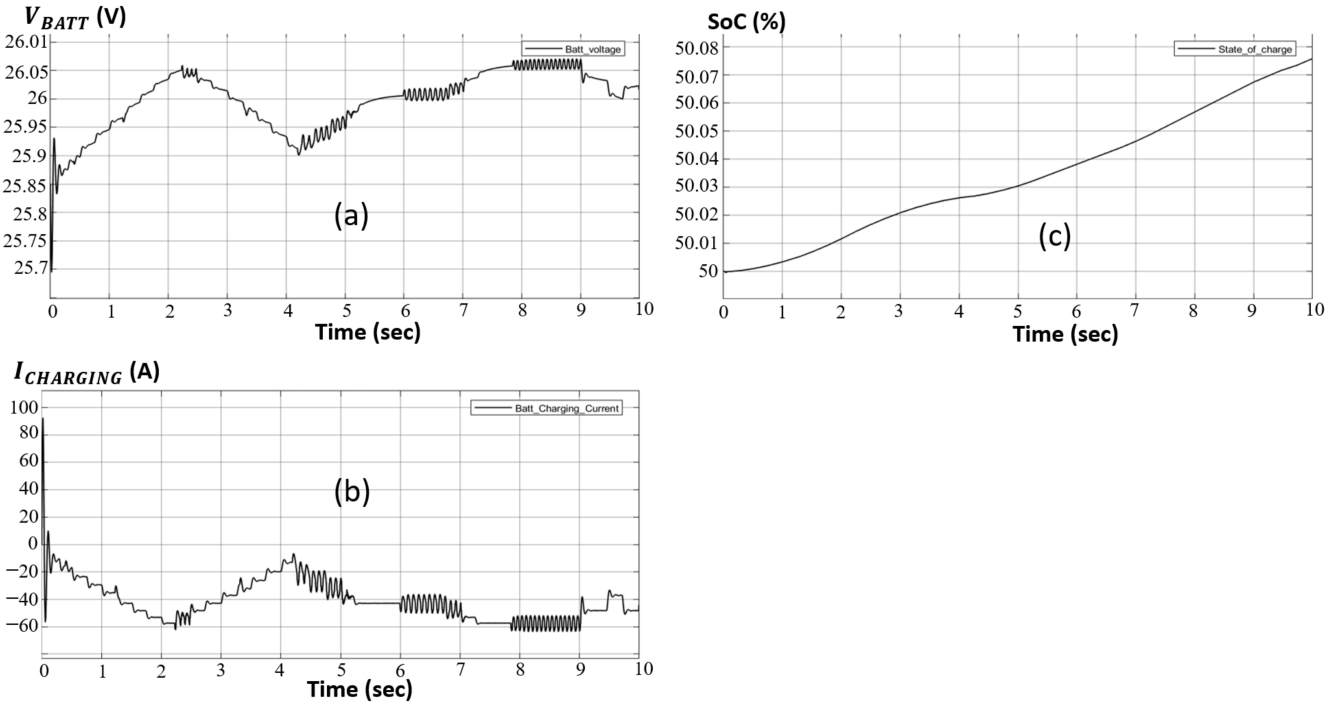

Figure 21. Battery's related curves under SIP3: (**a**) the battery voltage, (**b**) the battery charging current, and (**c**) the battery state of charge.

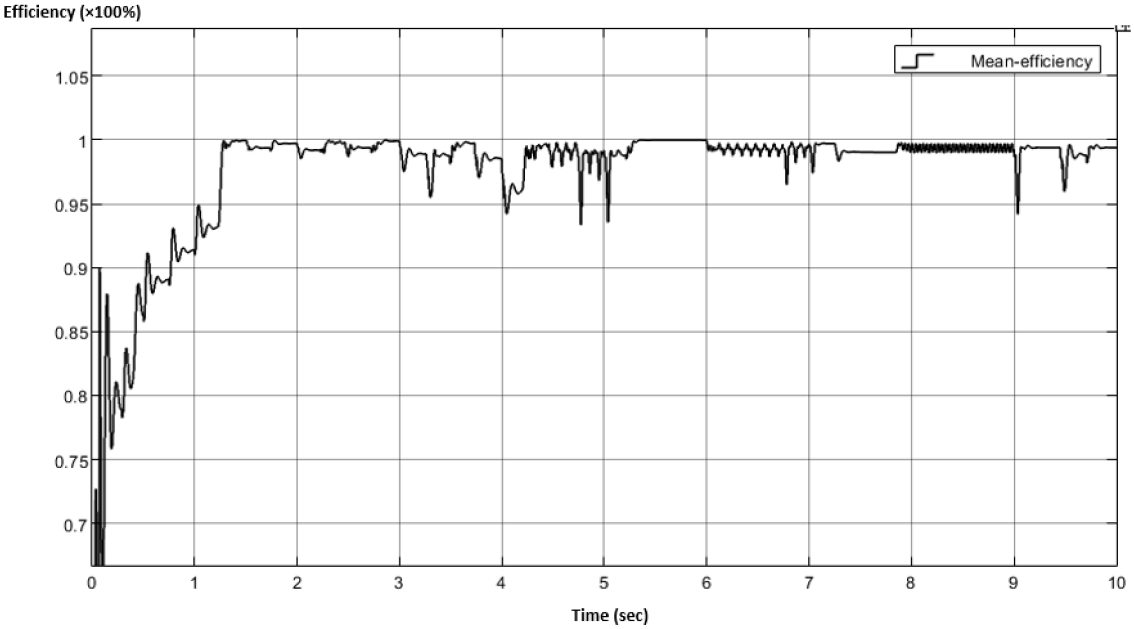

Figure 22. Mean efficiency (%) of the design under SIP3.

8.4. Results for SIP4

The SIP4 is applied to the same circuit design, where Figure 23 shows the alignment between the actual and the ideal power curves. Under the same conditions, Figure 24 encapsulates everything concerning the battery charging process, where finally in Figure 25, revealed is the mean efficiency for the design under SIP4 conditions.

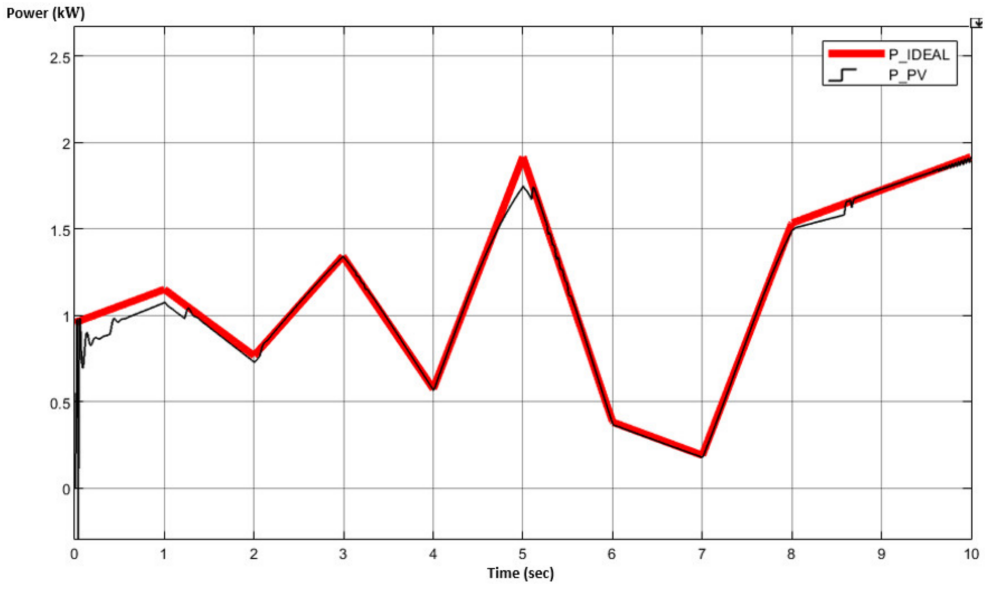

Figure 23. The alignment between the ideal and actual PV power curves (kWp) for SIP4.

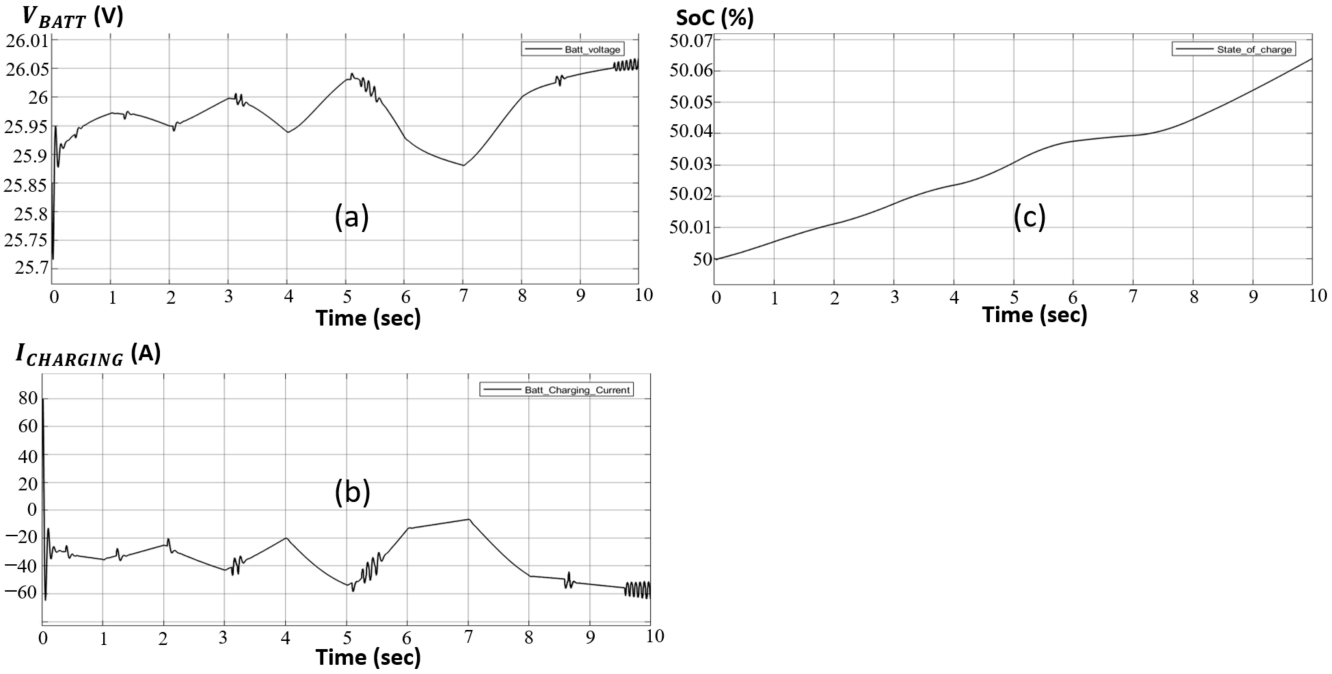

Figure 24. Battery's related curves under SIP4: (**a**) the battery voltage, (**b**) the battery charging current, and (**c**) the battery state of charge.

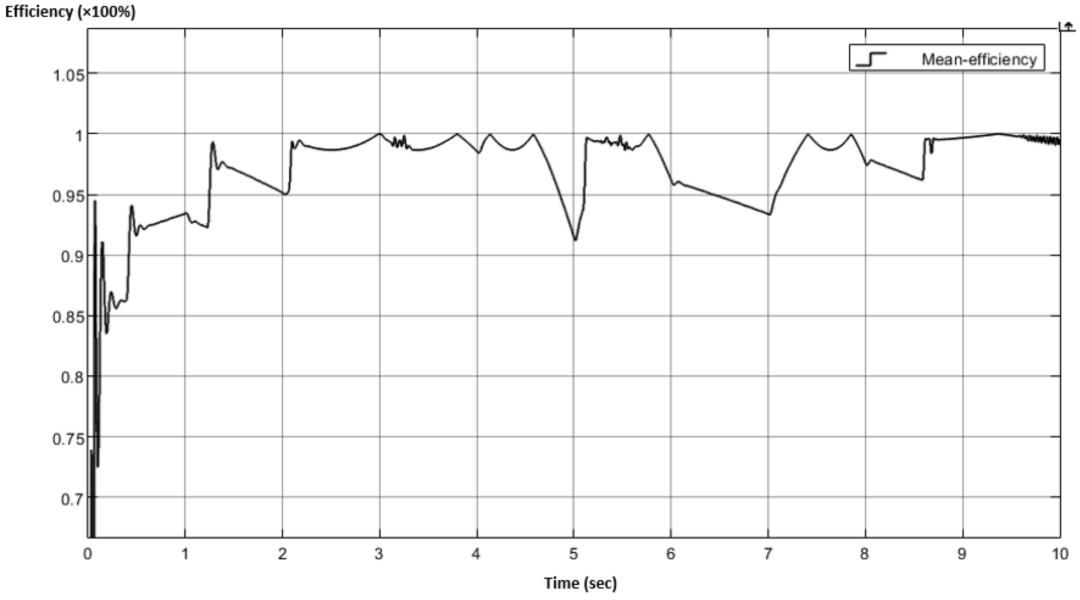

Figure 25. Mean efficiency (%) of the design under SIP4.

8.5. Results for Zero Irradiance (during Nights, etc.)

Instead of applying an actual time varying SIP, the design in this case is encountered with a zero irradiance, reflecting hence as null power output. The objective behind this exposure is to investigate the battery's charging process shown in Figure 26 and to detect whether the battery would be plugged off the circuit in case of a marginal state of discharge (i.e., $DoD \leq 25\%$).

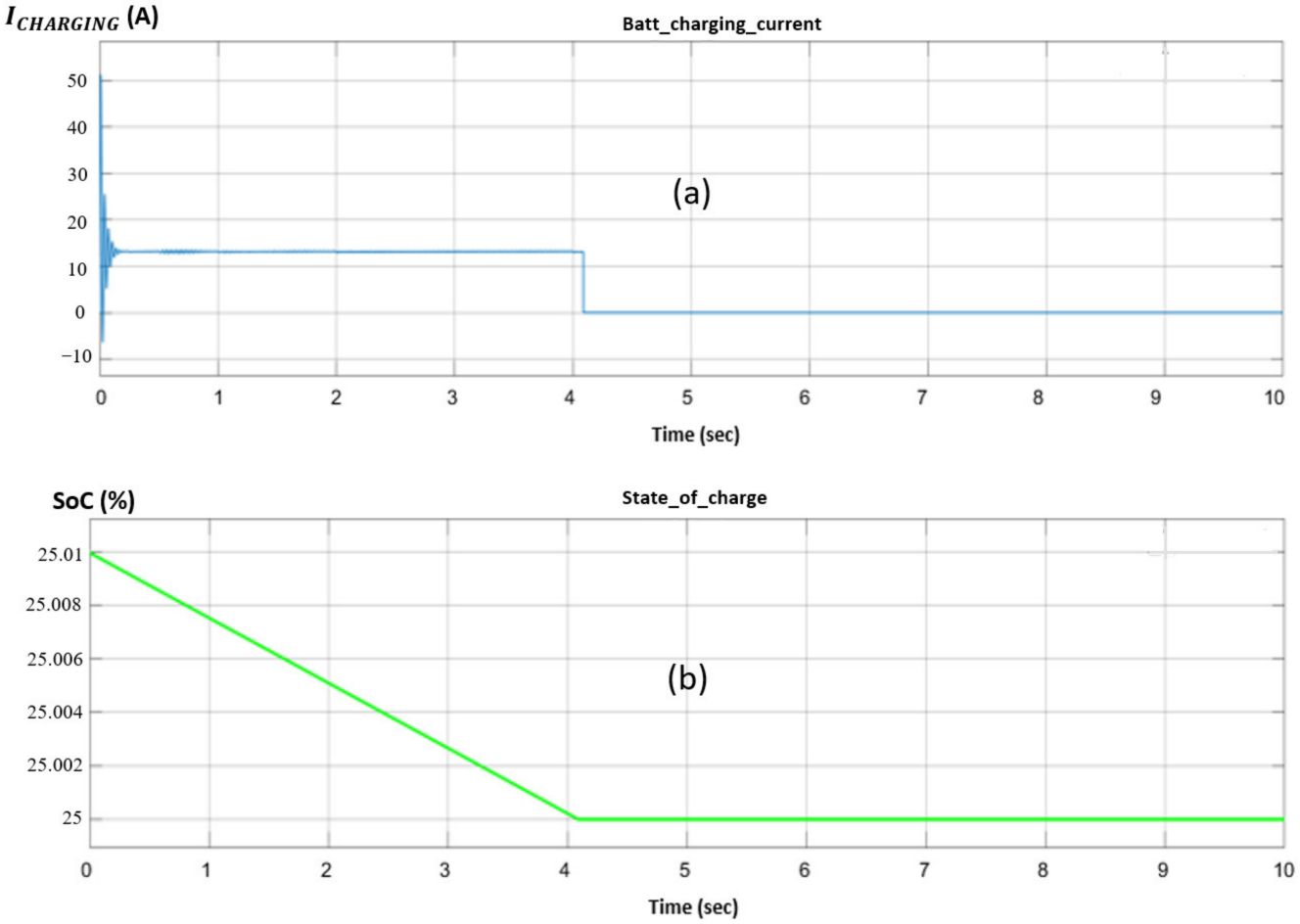

Figure 26. The battery's discharge current (**a**) and state of charge (**b**) under zero irradiance.

9. Discussion and Future Work

The overview of the different results for the investigated SIPs were satisfactory in general. Despite that the design has followed a regulation loop control, its response, however, did not constantly show an efficiency of 100%: this can be justified by the fact that the irradiance patterns are extremely fast (i.e., in order of 0.5 s), where the modified P&O algorithm cannot momentarily cope with. In other words, the obtained ideality factor was less than one, due to the computational speed of the proposed MPPT algorithm with respect to the SIP fluctuating speed. Beginning with SIP1, the mean efficiency ranged from 87% to 99.9%. This pattern in particular was the most complex, having the most rapidly fluctuating irradiance conditions with a time lapse of 0.5 s per variation. For SIP2, the mean efficiency ranged between 90% to 99.9%, where this pattern was less complex than the previous. In the case of SIP3, an increase in the mean efficiency is witnessed, where it ranged from 92% to 100%, such that the maximum efficiency scored from 93% to 100% for SIP4.

For each of the irradiance patterns, the SoC was continuously increasing, with modified slopes according to Figure 15, Figure 18, and Figure 21. The curve defining piece-wise slopes were directly based on the irradiance levels, where an increase in irradiance is reflected by a sharper upward directed line segment. As for the charging current, from the same figures, it can be noticed that its largest possible amount, supported by the PVA under specific irradiance values, is safely injected to the battery. The battery feeding voltage, also for all irradiance patterns, fluctuated between 25.9 V and 26.05 V, just as it was initially designed to be an output from the DC-DC interleaved synchronous buck converter. Accordingly, the battery under all irradiance circumstances would have the optimum safest feeding voltage (i.e., around 26 V) to be fed from.

For the case where there is not any irradiance (Figure 26, zero irradiance), the bi-directional DC-DC converter plugs out the battery when its SoC reaches 25%. The current value seen in Figure 26 is positive (according to the passive sign convention), meaning that no charging to the battery is occurring, but instead, current is being drawn from the battery. Within the same figure, where at T = 4.2 s, the SoC is equal to 25%. Successively to the right of this point, the SoC stabilizes at 0%, since the battery gets plugged out of the system for protective purposes (e.g., decelerate its aging process, saving its internal electrodes from excessive discharge, etc.). By taking into consideration what has been precedent, the contribution of this paper can be pointed out as follows:

1. The design has considered extreme irradiance fluctuations, with a time variance of 0.5 s, and irradiance intensity random variations from 100 W/m^2 to 1000 W/m^2. Such irradiance fluctuations generally do not take place under real environmental conditions, regardless of the location of the PV systems' installation. Since the design has shown a good overall efficiency under such unrealistic irradiance conditions, it can be said that it should work as good or even better under actual irradiance conditions, when prototyped.
2. The synergistic cooperation between the modified P&O algorithm as well as the improved DC-DC converter resulted in minimal current/voltage ripples, thus, the voltage feeding/current injection to the battery are greatly smoothed.
3. The implemented low-threshold detection ability of the battery's SoC, and hence its conditional removal out of the system, protects its electrode from the effects of over-discharging, thus sustaining its expected lifecycle.

Moreover, the full set of sub-designs shown in Figure 12, can be industrialized into a real prototype, serving arrays of 1.918 kWp. The simplicity of algorithm implementation and power electronic converters, such as the DC-DC interleaved synchronous converter, and the bi-directional DC-DC converter offers the following advantages:

- Weight reduction of the gadgets: the smaller sizes of capacitors, inductors, etc. decreases the size of the entire system, making it more flexible for size-constraint applications.
- Financial reliability: the decreased complexities in the algorithms' establishments for different control sections of the design (i.e., MPPT control, current suppression, etc.), as well as the minimized components size, makes the overall design cost effective, and able to be manufactured without the need of special machinery and big industrial plants.
- Flexibility for improvement: while only modifying the power electronics items, the system could fit for larger PVA applications.
- Ability of hybridization: a set of this system could fit into multiple 3×3 PVA composing a PV farm, where the output of each is mutually injected to a DC grid as shown in Figure 27.

The industrialization of this design can be obtained and arranged in a Polyvinyl Chloride (PVC) enclosure, to improve its Ingress Protection (IP) rating, thus making it resilient in front of severe weather fluctuations as presented in Figure 28. The following list of items comprises its main backbone:

- Arduino: as a central processing unit, used to execute arithmetical procedures (calculation of power, etc.) as well as for the implementation of the modified MPPT algorithm.
- Liquid Crystal Display (LCD): this shall replace the scopes used during the simulation in Matlab/Simulink, thus offering a vivid physical display.
- Voltage/current sensors: used to captivate the real current/voltage quantities from the PVA. These sensors' data are then to be subjected to Analog to Digital Converters (ADC) to be inputted as discrete samples into the processor.
- Power electronic converters: implemented in Printed Circuit Boards (PCBs) in order to reduce space and facilitate connections.

- PVC enclosure: to cover the electronic boards of the design, making it waterproof and shock absorbent.

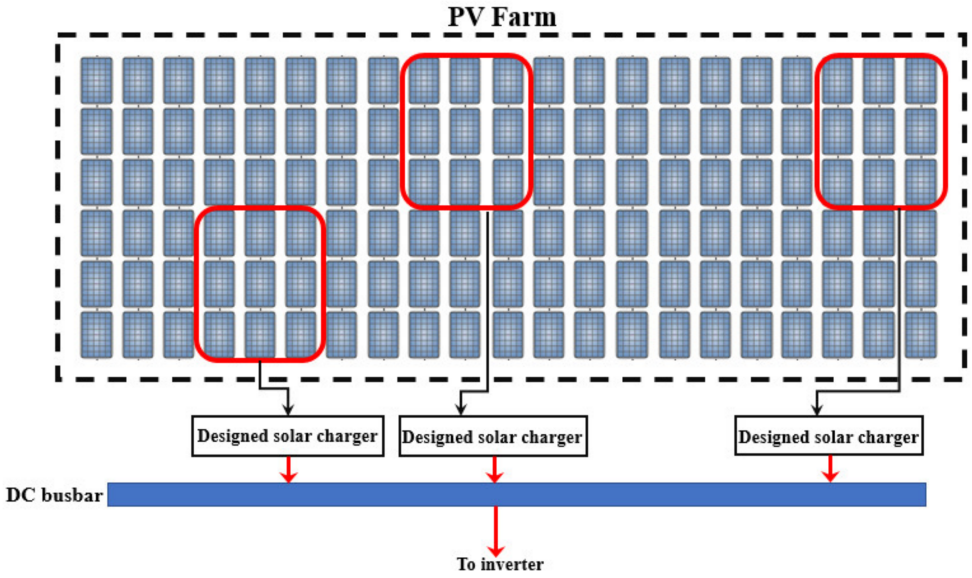

Figure 27. Expandability of the designed solar MPPT charger.

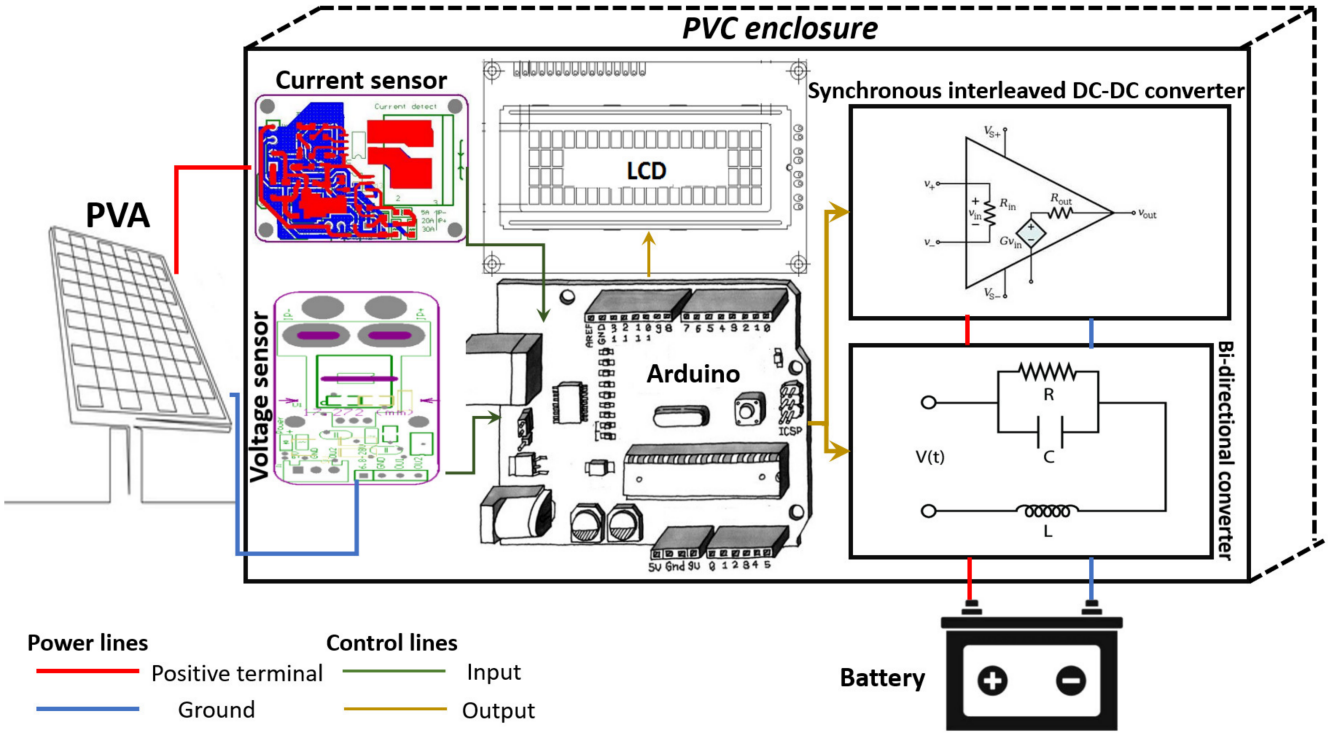

Figure 28. General overview of the suggested future design prototype.

10. Conclusions

This paper aimed to design an effective solar battery charger to be used in off-grid, standalone PV systems. After the setup of the 1.918 kWp PVA in SP configuration, an investigation is led for several SIPs, with fluctuating irradiances of 100 W/m^2 in 0.5 s time lapses. The novelty of the designed interleaved synchronous DC-DC converter granted smaller sizes of the needed inductors and capacitors, thus increasing the cost efficiency of the system. Low inductor ripple currents (20% of inductor current) with small output

voltage ripples (0.01 V) are obtained after the analysis of the output curves, furthering the design's simulation. The output of this converter hence produced a stubborn output voltage of 26 V, optimum to feed the 24 V, 150 Ah Li-I battery. For the sake of monitoring the battery charging current, a bi-directional DC-DC converter was successively used and controlled by I_{ref} method via a PI controller.

This in turn had led to a maximum safe charging current. At this stage, the V-I quantities are ensured to be at most optimum values, regardless of the irradiance fluctuations. In progress, a DoD control tactic was designed to ensure that the battery would never drain below 25% of complete charge, therefore sustaining its maximum life cycle. The mean efficiency of the MPPT ranged from a minimum of 87% to a maximum of 100%. In addition, this design has shown a flexibility in installation to adapt smaller/larger PV networks with a simple modification of the power electronics units. On the other side, and from a critical point of view, it can be said that the PVA of 1.918 kWp is too large to charge a battery of 150 Ah, but this was accounted for simulation purposes only. For instance, the designed DC-DC interleaved synchronous converter serves only to step down (i.e., Buck) the PVA's output voltage at a conventional range to feed the battery. Accordingly, this converter does not possess the ability to step up (i.e., Boost) the PVA's output voltage when it is below the recommended battery's voltage range. A better design would hence adopt both DC conversion techniques (i.e., Buck-Boost). The current design also did not encounter any partial shading conditions cases where it has only worked for uniform shading: the irradiance patterns, and despite their swift variations, are commonly objected to the entire PVA. In most real-world solar charging applications, designs are more often interfered with partial shading conditions, where the solar irradiance intensity over the PVA is inhomogeneous (i.e., some regions of the PVA receive more irradiance than others, and vice versa). This in turn lead to a more non-linearly disturbed P-V characteristic curve, in which the modified P&O would not function optimally. Another limitation of this work is that the PVA is always set under a working temperature of 25 °C, which is rarely the case for real-world PV applications: the temperature variations have also negative impacts on the P-V characteristic curve, where the modified P&O cannot also cope with.

As a final overview, this design has dealt with the process of Li-I battery charging, beginning with severe irradiance levels, to finally offering safe charging values at the fastest possible rate, while protecting the battery from accelerated ageing by a dedicated plug-out function. As for the future work, this model is encouraged to be manufactured and implemented in real-world PV applications, to furtherly analyze and investigate its real outcomes, when compared with the results obtained in this paper.

Author Contributions: Writing—original draft, K.O.; Writing—review & editing, A.H., M.A., T.L., B.C. and M.R.; Supervision, A.H., T.L., B.C. and M.R. All authors have read and agreed to the published version of the manuscript.

Funding: This research received no external funding.

Institutional Review Board Statement: Not applicable.

Informed Consent Statement: Not applicable.

Data Availability Statement: Data is unavailable due to privacy or ethical restrictions.

Conflicts of Interest: The authors declare no conflict of interest.

Nomenclature

Abbreviations

ADC	Analog to Digital Conversion
DC	Direct Current
DoD	Depth of Discharge
ESS	Energy Storage System
HC	Honey Comb

IGBT	Insulated Gate Bipolar Transistor
IP	Ingress Protection
LCD	Liquid Crystal Display
Li-I	Lithium-Ion
MOSFET	Metal Oxide Semi-conductor Field Effect Transistor
MPPT	Maximum Power Point Tracking
P&O	Perturb and Observe
PG	Proportional Gain
PCB	Printed Circuit Board
PI	Proportional Integral
PV	Photo Voltaic
PVA	PV Array
PVC	Polyvinyl Chloride
PVR	PV Reconfiguration
PWM	Pulse Width Modulation
SIP	Solar Irradiance Pattern
SoC	State of Charge
SP	Series Parallel
STC	Standard Test Conditions
TCT	Total Cross Tied
Units	
A	Ampere
s	Second
V	Volt
W	Watt
W/m^2	Irradiance, Watts per meter squared
Symbols	
CO_2	Carbon dioxide
I_{BAT_CHARGE}	Battery charging current
I_{ref}	Reference current

References

1. Pal, P.; Mukherjee, V.; Kumar, P.; Makhatha, M.E. Pre-feasibility analysis and performance assessment of solar photovoltaic (PV) modules for the application of renewable power generation. *Mater. Today Proc.* **2021**, *39*, 1813–1819. [CrossRef]
2. Gielen, D.; Boshell, F.; Saygin, D.; Bazilian, M.D.; Wagner, N.; Gorini, R. The role of renewable energy in the global energy transformation. *Energy Strategy Rev.* **2019**, *24*, 38–50. [CrossRef]
3. Boström, T.; Babar, B.; Hansen, J.B.; Good, C. The pure PV-EV energy system—A conceptual study of a nationwide energy system based solely on photovoltaics and electric vehicles. *Smart Energy* **2021**, *1*, 100001. [CrossRef]
4. Li, G.; Shittu, S.; Diallo, T.M.O.; Yu, M.; Zhao, X.; Ji, J. A review of solar photovoltaic-thermoelectric hybrid system for electricity generation. *Energy* **2018**, *158*, 41–58. [CrossRef]
5. Nwaigwe, K.; Mutabilwa, P.; Dintwa, E. An overview of solar power (PV systems) integration into electricity grids. *Mater. Sci. Energy Technol.* **2019**, *2*, 629–633. [CrossRef]
6. Osmani, K.; Haddad, A.; Lemenand, T.; Castanier, B.; Ramadan, M. A review on maintenance strategies for PV systems. *Sci. Total. Environ.* **2020**, *746*, 141753. [CrossRef] [PubMed]
7. Simonazzi, M.; Chiorboli, G.; Cova, P.; Menozzi, R.; Santoro, D.; Sapienza, S.; Sciancalepore, C.; Sozzi, G.; Delmonte, N. Smart soiling sensor for PV modules. *Microelectron. Reliab.* **2020**, *114*, 113789. [CrossRef]
8. Osmani, K.; Ramadan, M.; Haddad, A.; Lemenand, T.; Castanier, B. A Short Review on Mathematical Algorithms for Predictive Maintenance Techniques and Anomaly Detection in PV Systems. In Proceedings of the 31st European Safety and Reliability Conference, ESREL, Angers, France, 19–23 September 2021; pp. 3222–3229.
9. Pei, T.; Zhang, J.; Li, L.; Hao, X. A fault locating method for PV arrays based on improved voltage sensor placement. *Sol. Energy* **2020**, *201*, 279–297. [CrossRef]
10. Pratt, L.; Govender, D.; Klein, R. Defect detection and quantification in electroluminescence images of solar PV modules using U-net semantic segmentation. *Renew. Energy* **2021**, *178*, 1211–1222. [CrossRef]
11. Cole, W.; Greer, D.; Ho, J.; Margolis, R. Considerations for maintaining resource adequacy of electricity systems with high penetrations of PV and storage. *Appl. Energy* **2020**, *279*, 115795. [CrossRef]
12. Majeed, R.; Waqas, A.; Sami, H.; Ali, M.; Shahzad, N. Experimental investigation of soiling losses and a novel cost-effective cleaning system for PV modules. *Sol. Energy* **2020**, *201*, 298–306. [CrossRef]
13. Osmani, K.; Ramadan, M.; Haddad, A.; Lemenand, T.; Castanier, B. An Overview on the Use of Phase Change Material (PCM) for PV Cooling. *Key Eng. Mater.* **2022**, *922*, 3–9. [CrossRef]

14. de Oliveira, A.K.V.; Aghaei, M.; Rüther, R. Aerial infrared thermography for low-cost and fast fault detection in utility-scale PV power plants. *Sol. Energy* **2020**, *211*, 712–724. [CrossRef]
15. Alves, R.H.F.; Júnior, G.A.D.D.; Marra, E.G.; Lemos, R.P. Automatic fault classification in photovoltaic modules using Convolutional Neural Networks. *Renew. Energy* **2021**, *179*, 502–516. [CrossRef]
16. Maleki, A.; Haghighi, A.; Assad, M.E.H.; Mahariq, I.; Nazari, M.A. A review on the approaches employed for cooling PV cells. *Sol. Energy* **2020**, *209*, 170–185. [CrossRef]
17. Yurtseven, K.; Karatepe, E.; Deniz, E. Sensorless fault detection method for photovoltaic systems through mapping the inherent characteristics of PV plant site: Simple and practical. *Sol. Energy* **2021**, *216*, 96–110. [CrossRef]
18. Clavijo-Blanco, J.; Álvarez-Tey, G.; Saborido-Barba, N.; Barberá-González, J.; García-López, C.; Jiménez-Castañeda, R. Laboratory tests for the evaluation of the degradation of a photovoltaic plant of 2.85 MWp with different classes of PV modules. *Renew. Energy* **2021**, *174*, 262–277. [CrossRef]
19. Li, C.; Yang, Y.; Zhang, K.; Zhu, C.; Wei, H. A fast MPPT-based anomaly detection and accurate fault diagnosis technique for PV arrays. *Energy Convers. Manag.* **2021**, *234*, 113950. [CrossRef]
20. Osmani, K.; Haddad, A.; Lemenand, T.; Castanier, B.; Ramadan, M. Material Based Fault Detection Methods for PV Systems. *Key Eng. Mater.* **2020**, *865*, 111–115. [CrossRef]
21. Abdulmunem, A.R.; Samin, P.M.; Rahman, H.A.; Hussien, H.A.; Mazali, I.I. Enhancing PV Cell's electrical efficiency using phase change material with copper foam matrix and multi-walled carbon nanotubes as passive cooling method. *Renew. Energy* **2020**, *160*, 663–675. [CrossRef]
22. Ameur, A.; Berrada, A.; Loudiyi, K.; Aggour, M. Forecast modeling and performance assessment of solar PV systems. *J. Clean. Prod.* **2020**, *267*, 122167. [CrossRef]
23. Fares, E.; Bicer, Y. Comparative performance evaluation of c-Si and GaAs type PV cells with and without anti-soiling coating using energy and exergy analysis. *Renew. Energy* **2020**, *146*, 1010–1020. [CrossRef]
24. Thopil, G.A.; Sachse, C.E.; Lalk, J.; Thopil, M.S. Techno-economic performance comparison of crystalline and thin film PV panels under varying meteorological conditions: A high solar resource southern hemisphere case. *Appl. Energy* **2020**, *275*, 115041. [CrossRef]
25. Mirzaei, M.; Mohiabadi, M.Z. A comparative analysis of long-term field test of monocrystalline and polycrystalline PV power generation in semi-arid climate conditions. *Energy Sustain. Dev.* **2017**, *38*, 93–101. [CrossRef]
26. Brecl, K.; Bokalič, M.; Topič, M. Annual energy losses due to partial shading in PV modules with cut wafer-based Si solar cells. *Renew. Energy* **2021**, *168*, 195–203. [CrossRef]
27. Ansari, M.I.H.; Qurashi, A.; Nazeeruddin, M.K. Frontiers, opportunities, and challenges in perovskite solar cells: A critical review. *J. Photochem. Photobiol. C Photochem. Rev.* **2018**, *35*, 1–24. [CrossRef]
28. Sultan, S.; Kim, J.H.; Kim, S.; Kwon, Y.; Lee, J.S. Innovative strategies toward challenges in PV-powered electrochemical CO_2 reduction. *J. Energy Chem.* **2021**, *60*, 410–416. [CrossRef]
29. Babajide, A.; Brito, M.C. Solar PV systems to eliminate or reduce the use of diesel generators at no additional cost: A case study of Lagos, Nigeria. *Renew. Energy* **2021**, *172*, 209–218. [CrossRef]
30. Ghadikolaei, S.S.C. An enviroeconomic review of the solar PV cells cooling technology effect on the CO_2 emission reduction. *Sol. Energy* **2021**, *216*, 468–492. [CrossRef]
31. Gómez-Navarro, T.; Brazzini, T.; Alfonso-Solar, D.; Vargas-Salgado, C. Analysis of the potential for PV rooftop prosumer production: Technical, economic and environmental assessment for the city of Valencia (Spain). *Renew. Energy* **2021**, *174*, 372–381. [CrossRef]
32. Wang, M.; Mao, X.; Gao, Y.; He, F. Potential of carbon emission reduction and financial feasibility of urban rooftop photovoltaic power generation in Beijing. *J. Clean. Prod.* **2018**, *203*, 1119–1131. [CrossRef]
33. Gil, G.O.; Chowdhury, J.I.; Balta-Ozkan, N.; Hu, Y.; Varga, L.; Hart, P. Optimising renewable energy integration in new housing developments with low carbon technologies. *Renew. Energy* **2021**, *169*, 527–540. [CrossRef]
34. Dutta, R. *Use of Clean, Renewable and Alternative Energies in Mitigation of Greenhouse Gases*; Elsevier: Amsterdam, The Netherlands, 2020; Volume 3, pp. 821–834. [CrossRef]
35. Razmjoo, A.; Kaigutha, L.G.; Rad, M.A.V.; Marzband, M.; Davarpanah, A.; Denai, M. A Technical analysis investigating energy sustainability utilizing reliable renewable energy sources to reduce CO_2 emissions in a high potential area. *Renew. Energy* **2021**, *164*, 46–57. [CrossRef]
36. Huuki, H.; Karhinen, S.; Böök, H.; Ding, C.; Ruokamo, E. Residential solar power profitability with thermal energy storage and carbon-corrected electricity prices. *Util. Policy* **2021**, *68*, 101157. [CrossRef]
37. Akinsipe, O.C.; Moya, D.; Kaparaju, P. Design and economic analysis of off-grid solar PV system in Jos-Nigeria. *J. Clean. Prod.* **2021**, *287*, 125055. [CrossRef]
38. Osmani, K.; Haddad, A.; Jaber, H.; Lemenand, T.; Castanier, B.; Ramadan, M. Mitigating the effects of partial shading on PV system's performance through PV array reconfiguration: A review. *Therm. Sci. Eng. Prog.* **2022**, *31*, 101280. [CrossRef]
39. Al-Addous, M.; Dalala, Z.; Class, C.B.; Alawneh, F.; Al-Taani, H. Performance analysis of off-grid PV systems in the Jordan Valley. *Renew. Energy* **2017**, *113*, 930–941. [CrossRef]
40. Grande, L.S.A.; Yahyaoui, I.; Gómez, S.A. Energetic, economic and environmental viability of off-grid PV-BESS for charging electric vehicles: Case study of Spain. *Sustain. Cities Soc.* **2018**, *37*, 519–529. [CrossRef]

41. Satpathy, R.; Pamuru, V. *Chapter 7—Off-Grid Solar Photovoltaic Systems. Solar PV Power Design, Manufacturing and Applications from Sand to Systems*; Academic Press: Cambridge, MA, USA, 2021; pp. 267–315.
42. Osmani, K.; Ramadan, M.; Lemenand, T.; Castanier, B.; Haddad, A. Optimization of PV array tilt angle for minimum levelized cost of energy. *Comput. Electr. Eng.* **2021**, *96*, 107474. [CrossRef]
43. Said, Z.; Mehmood, A.; Waqas, A.; Hachicha, A.A.; Loni, R. Central versus off-grid photovoltaic system, the optimal option for the domestic sector based on techno-economic-environmental assessment for United Arab Emirates. *Sustain. Energy Technol. Assess.* **2021**, *43*, 100944.
44. Mulleriyawage, U.G.K.; Shen, W.X. Optimally sizing of battery energy storage capacity by operational optimization of residential PV-Battery systems: An Australian household case study. *Renew. Energy* **2020**, *160*, 852–864. [CrossRef]
45. El Kafazi, I.; Lafkih, M.; Bannari, R. PV generator and energy storage systems for laboratory building. *Energy Rep.* **2020**, *6*, 672–679. [CrossRef]
46. Barzegkar-Ntovom, G.; Chatzigeorgiou, N.G.; Nousdilis, A.I.; Vomva, S.A.; Kryonidis, G.C.; Kontis, E.O.; Georghiou, G.E.; Christoforidis, G.C.; Papagiannis, G.K. Assessing the viability of battery energy storage systems coupled with photovoltaics under a pure self-consumption scheme. *Renew. Energy* **2020**, *152*, 1302–1309. [CrossRef]
47. Wang, Y.; Das, R.; Putrus, G.; Kotter, R. Economic evaluation of photovoltaic and energy storage technologies for future domestic energy systems—A case study of the UK. *Energy* **2020**, *203*, 117826. [CrossRef]
48. Osmani, K.; Alkhedher, M.; Ramadan, M.; Choi, D.S.; Li, L.K.; Doranehgard, M.H.; Olabi, A.-G. Recent progress in the thermal management of lithium-ion batteries. *J. Clean. Prod.* **2023**, *389*, 136024. [CrossRef]
49. Liu, J.; Chen, X.; Yang, H.; Li, Y. Energy storage and management system design optimization for a photovoltaic integrated low-energy building. *Energy* **2020**, *190*, 116424. [CrossRef]
50. Yu, H.J.J. System contributions of residential battery systems: New perspectives on PV self-consumption. *Energy Econ.* **2021**, *96*, 105151. [CrossRef]
51. Aniello, G.; Shamon, H.; Kuckshinrichs, W. Micro-economic assessment of residential PV and battery systems: The underrated role of financial and fiscal aspects. *Appl. Energy* **2021**, *281*, 115667. [CrossRef]
52. Alsolami, M. A multi-input, multi-stage step-up DC-DC converter for PV applications. *Alex. Eng. J.* **2021**, *60*, 2315–2324. [CrossRef]
53. Raj, A.; Arya, S.R.; Gupta, J. Solar PV array-based DC–DC converter with MPPT for low power applications. *Renew. Energy Focus* **2020**, *34*, 109–119. [CrossRef]
54. Kumar, L.A.; Alexander, S.A.; Rajendran, M. *Power Electronic Converters for Solar Photovoltaic Systems*; Academic Press: Cambridge, MA, USA, 2021; pp. 207–234.
55. Celikel, R.; Yilmaz, M.; Gundogdu, A. A voltage scanning-based MPPT method for PV power systems under complex partial shading conditions. *Renew. Energy* **2022**, *184*, 361–373. [CrossRef]
56. Mirzaei, A.; Rezvanyvardom, M. High voltage gain soft switching full bridge interleaved Flyback DC-DC converter for PV applications. *Sol. Energy* **2020**, *196*, 217–227. [CrossRef]
57. Revathi, B.S.; Mahalingam, P.; Gonzalez-Longatt, F. Interleaved high gain DC-DC converter for integrating solar PV source to DC bus. *Sol. Energy* **2019**, *188*, 924–934. [CrossRef]
58. Cibira, G. PV cell electrical parameters dynamic modelling based on double-diode five-parameter reduced forms. *Appl. Surf. Sci.* **2018**, *461*, 98–101. [CrossRef]
59. Barth, N.; Jovanovic, R.; Ahzi, S.; Khaleel, M.A. PV panel single and double diode models: Optimization of the parameters and temperature dependence. *Sol. Energy Mater. Sol. Cells* **2016**, *148*, 87–98. [CrossRef]
60. de Oliveira, I.; Capovilla, D.A.; Moura, A.L.; Timóteo, V.S.; Carvalho, J.F.; Frejlich, J. Nonlinear photovoltaic effect in Sillenite photorefractive crystals. *Opt. Mater.* **2017**, *66*, 72–78. [CrossRef]
61. Wang, J.; Yang, B.; Li, D.; Zeng, C.; Chen, Y.; Guo, Z.; Zhang, X.; Tan, T.; Shu, H.; Yu, T. Photovoltaic cell parameter estimation based on improved equilibrium optimizer algorithm. *Energy Convers. Manag.* **2021**, *236*, 114051. [CrossRef]
62. Archila, L.M.P.; Rodríguez, J.D.B.; Correa, R. Implicit modelling of series-parallel photovoltaic arrays using double-diode model and its solution. *Sol. Energy* **2021**, *214*, 131–137. [CrossRef]
63. Amir, A.; Che, H.S.; Amir, A.; El Khateb, A.; Rahim, N.A. Transformerless high gain boost and buck-boost DC-DC converters based on extendable switched capacitor (SC) cell for stand-alone photovoltaic system. *Sol. Energy* **2018**, *171*, 212–222. [CrossRef]
64. Saravanan, S.; Babu, N.R. A modified high step-up non-isolated DC-DC converter for PV application. *J. Appl. Res. Technol.* **2017**, *15*, 242–249. [CrossRef]
65. Revathi, B.S.; Prabhakar, M. Non isolated high gain DC-DC converter topologies for PV applications—A comprehensive review. *Renew. Sustain. Energy Rev.* **2016**, *66*, 920–933. [CrossRef]
66. Tewari, N.; Sreedevi, V. A novel single switch dc-dc converter with high voltage gain capability for solar PV based power generation systems. *Sol. Energy* **2018**, *171*, 466–477. [CrossRef]
67. Dileep, G.; Singh, S. Selection of non-isolated DC-DC converters for solar photovoltaic system. *Renew. Sustain. Energy Rev.* **2017**, *76*, 1230–1247. [CrossRef]
68. Van De Sande, W.; Ravyts, S.; Sangwongwanich, A.; Manganiello, P.; Yang, Y.; Blaabjerg, F.; Driesen, J.; Daenen, M. A mission profile-based reliability analysis framework for photovoltaic DC-DC converters. *Microelectron. Reliab.* **2019**, *101*, 113383. [CrossRef]

69. Amir, A.; Amir, A.; Che, H.S.; Elkhateb, A.; Rahim, N.A. Comparative analysis of high voltage gain DC-DC converter topologies for photovoltaic systems. *Renew. Energy* **2019**, *136*, 1147–1163. [CrossRef]
70. Anita, S.J.; Ahmed, Y.S.; Prabhu, D.H.; Govind, S. Proposed modified solar based dc-dc quadratic boost converter for modern irrigation system. *Mater. Today: Proc.* **2020**, *33*, 4656–4662. [CrossRef]
71. Yang, Y.; Wu, Q.; Lin, W.; Chi, X.; Liu, D.; Jiang, A. Design and Simulation of a Kind of Wide, High Input Voltage DC-DC Converter for PV. *IFAC-PapersOnLine* **2017**, *50*, 2125–2130. [CrossRef]
72. Rezvanyvardom, M.; Mirzaei, A. High gain configuration of modified ZVT SEPIC-Boost DC-DC converter with coupled inductors for photovoltaic applications. *Sol. Energy* **2020**, *208*, 357–367. [CrossRef]
73. Mirza, A.F.; Ling, Q.; Javed, M.Y.; Mansoor, M. Novel MPPT techniques for photovoltaic systems under uniform irradiance and Partial shading. *Sol. Energy* **2019**, *184*, 628–648. [CrossRef]
74. Behera, M.K.; Saikia, L.C. A new combined extreme learning machine variable steepest gradient ascent MPPT for PV system based on optimized PI-FOI cascade controller under uniform and partial shading conditions. *Sustain. Energy Technol. Assess.* **2020**, *42*, 100859. [CrossRef]
75. Kamran, M.; Mudassar, M.; Fazal, M.R.; Asghar, M.U.; Bilal, M.; Asghar, R. Implementation of improved Perturb & Observe MPPT technique with confined search space for standalone photovoltaic system. *J. King Saud Univ.—Eng. Sci.* **2020**, *32*, 432–441. [CrossRef]
76. Abdel-Salam, M.; El-Mohandes, M.-T.; Goda, M. An improved perturb-and-observe based MPPT method for PV systems under varying irradiation levels. *Sol. Energy* **2018**, *171*, 547–561. [CrossRef]
77. Devi, V.K.; Premkumar, K.; Beevi, A.B.; Ramaiyer, S. A modified Perturb & Observe MPPT technique to tackle steady state and rapidly varying atmospheric conditions. *Sol. Energy* **2017**, *157*, 419–426. [CrossRef]
78. Ahmed, J.; Salam, Z. An improved perturb and observe (P&O) maximum power point tracking (MPPT) algorithm for higher efficiency. *Appl. Energy* **2015**, *150*, 97–108. [CrossRef]
79. Shahid, H.; Kamran, M.; Mehmood, Z.; Saleem, M.Y.; Mudassar, M.; Haider, K. Implementation of the novel temperature controller and incremental conductance MPPT algorithm for indoor photovoltaic system. *Sol. Energy* **2018**, *163*, 235–242. [CrossRef]
80. Tey, K.S.; Mekhilef, S. Modified incremental conductance MPPT algorithm to mitigate inaccurate responses under fast-charging solar irradiation level. *Sol. Energy* **2014**, *101*, 333–342. [CrossRef]
81. Murtaza, A.; Chiaberge, M.; Spertino, F.; Shami, U.T.; Boero, D.; De Giuseppe, M. MPPT technique based on improved evaluation of photovoltaic parameters for uniformly irradiated photovoltaic array. *Electr. Power Syst. Res.* **2017**, *145*, 248–263. [CrossRef]
82. Das, P. Maximum Power Tracking Based Open Circuit Voltage Method for PV System. *Energy Procedia* **2016**, *90*, 2–13. [CrossRef]
83. Fares, D.; Fathi, M.; Shams, I.; Mekhilef, S. A novel global MPPT technique based on squirrel search algorithm for PV module under partial shading conditions. *Energy Convers. Manag.* **2021**, *230*, 113773. [CrossRef]
84. Zhao, Z.; Cheng, R.; Yan, B.; Zhang, J.; Zhang, Z.; Zhang, M.; Lai, L.L. A dynamic particles MPPT method for photovoltaic systems under partial shading conditions. *Energy Convers. Manag.* **2020**, *220*, 113070. [CrossRef]
85. Mansoor, M.; Mirza, A.F.; Ling, Q. Harris hawk optimization-based MPPT control for PV systems under partial shading conditions. *J. Clean. Prod.* **2020**, *274*, 122857. [CrossRef]
86. Mansoor, M.; Mirza, A.F.; Ling, Q.; Javed, M.Y. Novel Grass Hopper optimization based MPPT of PV systems for complex partial shading conditions. *Sol. Energy* **2020**, *198*, 499–518. [CrossRef]
87. Senthilvel, A.; Vijeyakumar, K.; Vinothkumar, B. FPGA based implementation of MPPT algorithms for photovoltaic system under partial shading conditions. *Microprocess. Microsyst.* **2020**, *77*, 103011. [CrossRef]
88. Mirza, A.F.; Mansoor, M.; Ling, Q.; Yin, B.; Javed, M.Y. A Salp-Swarm Optimization based MPPT technique for harvesting maximum energy from PV systems under partial shading conditions. *Energy Convers. Manag.* **2020**, *209*, 112625. [CrossRef]
89. Titri, S.; Larbes, C.; Toumi, K.Y.; Benatchba, K. A new MPPT controller based on the Ant colony optimization algorithm for Photovoltaic systems under partial shading conditions. *Appl. Soft Comput.* **2017**, *58*, 465–479. [CrossRef]
90. da Rocha, M.V.; Sampaio, L.P.; da Silva, S.A.O. Comparative analysis of MPPT algorithms based on Bat algorithm for PV systems under partial shading condition. *Sustain. Energy Technol. Assess.* **2020**, *40*, 100761. [CrossRef]
91. Fathy, A.; Rezk, H.; Yousri, D. A robust global MPPT to mitigate partial shading of triple-junction solar cell-based system using manta ray foraging optimization algorithm. *Sol. Energy* **2020**, *207*, 305–316. [CrossRef]
92. Pal, R.S.; Mukherjee, V. Metaheuristic based comparative MPPT methods for photovoltaic technology under partial shading condition. *Energy* **2020**, *212*, 118592. [CrossRef]
93. Avila, L.; De Paula, M.; Trimboli, M.; Carlucho, I. Deep reinforcement learning approach for MPPT control of partially shaded PV systems in Smart Grids. *Appl. Soft Comput.* **2020**, *97*, 106711. [CrossRef]
94. Laxman, B.; Annamraju, A.; Srikanth, N.V. A grey wolf optimized fuzzy logic based MPPT for shaded solar photovoltaic systems in microgrids. *Int. J. Hydrog. Energy* **2021**, *46*, 10653–10665. [CrossRef]
95. Charin, C.; Ishak, D.; Zainuri, M.A.A.M.; Ismail, B.; Jamil, M.K.M. A hybrid of bio-inspired algorithm based on Levy flight and particle swarm optimizations for photovoltaic system under partial shading conditions. *Sol. Energy* **2021**, *217*, 1–14. [CrossRef]
96. Mohapatra, A.; Nayak, B.; Das, P.; Mohanty, K.B. A review on MPPT techniques of PV system under partial shading condition. *Renew. Sustain. Energy Rev.* **2017**, *80*, 854–867. [CrossRef]
97. Diab, A.A.Z.; Rezk, H. Global MPPT based on flower pollination and differential evolution algorithms to mitigate partial shading in building integrated PV system. *Sol. Energy* **2017**, *157*, 171–186. [CrossRef]

98. Yang, B.; Zhong, L.; Zhang, X.; Shu, H.; Yu, T.; Li, H.; Jiang, L.; Sun, L. Novel bio-inspired memetic salp swarm algorithm and application to MPPT for PV systems considering partial shading condition. *J. Clean. Prod.* **2019**, *215*, 1203–1222. [CrossRef]
99. Jose, B.K. Fuzzy Based Maximum Power Point Tracking of PV Array under Non-uniform Irradiance Conditions. *Mater. Today Proc.* **2020**, *24*, 1835–1842. [CrossRef]
100. Bharathi, K.; Sasikumar, M. Power flow control based on bidirectional converter for hybrid power generation system using microcontroller. *Microprocess. Microsyst.* **2021**, *82*, 103950. [CrossRef]
101. Siva Reddy, R.V. Microcontroller based bidirectional buck–boost converter for photo-voltaic power plant. *J. Electr. Syst. Inf. Technol.* **2018**, *5*, 745–758. [CrossRef]
102. Kanta, S.; Plangklang, B.; Subsingha, W. Design of a Bi-directional DC-DC 4 Phase Interleave Converter for PV Applications. *Energy Procedia* **2014**, *56*, 604–609. [CrossRef]
103. Chu, G.; Wen, H.; Jiang, L.; Hu, Y.; Li, X. Bidirectional flyback based isolated-port submodule differential power processing optimizer for photovoltaic applications. *Sol. Energy* **2017**, *158*, 929–940. [CrossRef]
104. Spier, D.; Oggier, G.; da Silva, S. Dynamic modeling and analysis of the bidirectional DC-DC boost-buck converter for renewable energy applications. *Sustain. Energy Technol. Assess.* **2019**, *34*, 133–145. [CrossRef]
105. Mao, M.; Zhang, L.; Yang, L.; Chong, B.; Huang, H.; Zhou, L. MPPT using modified salp swarm algorithm for multiple bidirectional PV-Cuk converter system under partial shading and module mismatch. *Sol. Energy* **2020**, *209*, 334–349. [CrossRef]
106. Kumar, L.A.; Alexander, S.A.; Rajendran, M. *Power Electronic Converters for Solar Photovoltaic Systems*; Academic Press: Cambridge, MA, USA, 2021; pp. 235–288.
107. Ajmal, A.M.; Babu, T.S.; Ramachandaramurthy, V.K.; Yousri, D.; Ekanayake, J.B. Static and dynamic reconfiguration approaches for mitigation of partial shading influence in photovoltaic arrays. *Sustain. Energy Technol. Assess.* **2020**, *40*, 100738. [CrossRef]
108. Yadav, A.S.; Mukherjee, V. Conventional and advanced PV array configurations to extract maximum power under partial shading conditions: A review. *Renew. Energy* **2021**, *178*, 977–1005. [CrossRef]
109. Krishna, G.S.; Moger, T. Reconfiguration strategies for reducing partial shading effects in photovoltaic arrays: State of the art. *Sol. Energy* **2019**, *182*, 429–452. [CrossRef]
110. Yadav, V.K.; Yadav, A.; Yadav, R.; Mittal, A.; Wazir, N.H.; Gupta, S.; Pachauri, R.K.; Ghosh, S. A novel reconfiguration technique for improvement of PV reliability. *Renew. Energy* **2022**, *182*, 508–520. [CrossRef]
111. Krishna, G.S.; Moger, T. Improved SuDoKu reconfiguration technique for total-cross-tied PV array to enhance maximum power under partial shading conditions. *Renew. Sustain. Energy Rev.* **2019**, *109*, 333–348. [CrossRef]
112. Meerimatha, G.; Rao, L. Novel reconfiguration approach to reduce line losses of the photovoltaic array under various shading conditions. *Energy* **2020**, *196*, 117120. [CrossRef]
113. Calcabrini, A.; Muttillo, M.; Weegink, R.; Manganiello, P.; Zeman, M.; Isabella, O. A fully reconfigurable series-parallel photovoltaic module for higher energy yields in urban environments. *Renew. Energy* **2021**, *179*, 1–11. [CrossRef]
114. Malathy, S.; Ramaprabha, R. Reconfiguration strategies to extract maximum power from photovoltaic array under partially shaded conditions. *Renew. Sustain. Energy Rev.* **2018**, *81*, 2922–2934. [CrossRef]
115. Potnuru, S.R.; Pattabiraman, D.; Ganesan, S.I.; Chilakapati, N. Positioning of PV panels for reduction in line losses and mismatch losses in PV array. *Renew. Energy* **2015**, *78*, 264–275. [CrossRef]
116. Nihanth, M.S.S.; Ram, J.P.; Pillai, D.S.; Ghias, A.M.; Garg, A.; Rajasekar, N. Enhanced power production in PV arrays using a new skyscraper puzzle based one-time reconfiguration procedure under partial shade conditions (PSCs). *Sol. Energy* **2019**, *194*, 209–224. [CrossRef]
117. Osmani, K.; Haddad, A.; Lemenand, T.; Castanier, B.; Ramadan, M. An investigation on maximum power extraction algorithms from PV systems with corresponding DC-DC converters. *Energy* **2021**, *224*, 120092. [CrossRef]
118. Jaschke, R. Conduction Losses in DC/DC-Converters as buckboost/boostbuck synchronous rectifier types. In Proceedings of the 2007 Compatibility in Power Electronics, IEEE, Gdansk, Poland, 29 May–1 June 2007. [CrossRef]
119. Ayachit, A.; Kazimierczuk, M.K. Averaged Small-Signal Model of PWM DC-DC Converters in CCM Including Switching Power Loss. *IEEE Trans. Circuits Syst. II Express Briefs* **2018**, *66*, 262–266. [CrossRef]
120. Panda, A.K.; Aroul, K. A Novel Technique to Reduce the Switching Losses in a Synchronous Buck Converter. In Proceedings of the 2006 International Conference on Power Electronic, Drives and Energy Systems, IEEE, New Delhi, India, 12–15 December 2006. [CrossRef]
121. Abu-aisheh, A.A.; Batarseh, M.G. *Chapter 15—DC-DC Converters. Electric Renewable Energy Systems*; Academic Press: Cambridge, MA, USA, 2016; pp. 337–353.
122. Available online: https://www.onsemi.com/pub/Collateral/AND9135-D.PDF (accessed on 1 April 2023).
123. Jadhav, S.; Devdas, N.; Nisar, S.; Bajpai, V. Bidirectional DC-DC converter in Solar PV System for Battery Charging Application. In Proceedings of the 2018 International Conference on Smart City and Emerging Technology (ICSCET), IEEE, Mumbai, India, 5 January 2018. [CrossRef]

Chapitre 4

Développement d'un algorithme innovant basé sur l'Intelligence Artificielle (IA) inspirée des mécanismes pathogènes de la maladie du Diabète de Type 1 (T1D) pour les applications de suivi du point de puissance maximale (MPPT)

Sur la base des résultats du **chapitre 3**, on peut affirmer que le chargeur solaire proposé peut optimiser les performances des systèmes PV, en fournissant une procédure de charge rapide et sûre pour la batterie Li-I, utilisée dans les systèmes PV hors-réseau. Cette amélioration des performances est principalement due à l'algorithme MPPT qui fournit des « Duty Ratios » précis pour le convertisseur électronique de puissance suivant, garantissant ainsi une extraction maximale de la puissance du réseau photovoltaïque.

C'est à partir de là qu'est née l'idée d'améliorer cet algorithme MPPT, en particulier parce que l'algorithme « P&O » modifié du **chapitre 3** ne fonctionnerait pas de manière optimale dans des conditions d'ombrage partiel. En d'autres termes, l'algorithme « P&O » modifié suggéré pour la conception du **chapitre 3** ne fonctionne que dans des conditions d'ombrage homogènes, d'où la nécessité de créer un algorithme MPPT plus flexible pour un fonctionnement dynamique dans des conditions d'ombrage partiel. Il est donc inspiré, sur la base du mécanisme pathogène du diabète de type 1 (T1D), la modification de l'algorithme conventionnel d'optimisation par essaimage de particules (PSO), pour une meilleure découverte de la courbe caractéristique PV, dans des conditions extrêmes d'ombrage partiel. Il convient de noter que cette étude est unique dans le domaine de la recherche sur le photovoltaïque.

La **section 1** de cette étude correspond à une analyse documentaire des techniques MPPT

existantes pour le fonctionnement dans des conditions d'ombrage partiel, avec les avantages et les inconvénients de chacune d'entre elles. La **section 2** révèle le comportement du PV dans des conditions d'ombrage partiel, sous la forme d'un modèle mathématique et de représentations graphiques (courbes). La **section 3** décrit le processus d'évolution de la T1D, où le comportement des différentes cellules présentatrices d'antigènes (APC) doit être imité pour les essaims dans l'algorithme PSO. La **section 4** présente l'approximation entre l'algorithme PSO (essaims) et la T1D (cellules). La **section 5** présente la simulation de la modification de l'algorithme PSO basée sur le T1D suggérée dans cinq conditions différentes d'ombrage partiel extrême. La **section 6** examine les résultats obtenus, tandis que les conclusions et les travaux futurs sont suggérés à la **section 7**.

L'algorithme proposé décompose les particules en deux ensembles principaux (cellules T effectrices), avec d'autres particules témoins autonomes. Les particules témoins servent de messagers pour les pics maximaux découverts précocement dans la courbe caractéristique de PV. La coordination entre les cellules effectrices et les cellules témoins (les particules dans l'algorithme PSO) garantit un tracé fluide et complet de la courbe caractéristique PV, ce qui permet d'extraire le maximum de puissance disponible. L'évolution du T1D est finalement traduite par un processus de modification continu et dynamique des poids d'inertie et des coefficients cognitifs et sociaux de toutes les particules.

Sous cinq pics locaux, cet algorithme a montré une convergence précise avec une efficacité de 98% et un temps d'exécution rapide de 5.817 S. Ainsi, il optimise définitivement la performance d'un système PV dans des conditions d'ombrage partiel, permettant une plus grande production d'énergie.

Développement d'un algorithme innovant basé sur l'Intelligence Artificielle (IA) inspirée des mécanismes pathogènes de la maladie du Diabète de Type 1 (T1D) pour les applications de suivi du point de puissance maximale (MPPT)

Cette étude devrait être soumise à « **Soft Computing** »

Résumé – Cet étude vise à améliorer le comportement de l'algorithme Particle Swarm Optimization (PSO) basé sur l'intelligence artificielle (IA) en termes de précision de convergence et de vitesse d'exécution, lors de son utilisation dans les applications Maximum Power Point Tracker (MPPT) dans les systèmes photovoltaïque (PV). La réaction des cellules PV dans des conditions d'ombrage partiel (PSC) inévitables est hautement non linéaire, ce qui entraîne des pertes d'extraction de puissance du générateur PV (PVA). Inspirée de l'évolution biologique de la maladie du diabète de type 1 (T1D), la courbe I-V caractéristique du PVA est entièrement tracée, ce qui donne une puissance d'extraction maximale sous différents PSC. L'imitation de l'attitude des immunocytes, qui se traduit par une destruction complète des cellules β pancréatiques, se reflète dans la conception de l'essaim PSO : au lieu d'adapter un seul essaim pour explorer la courbe I-V, deux essaims sont définis pour les lymphocytes T lymphatiques effecteurs (c'est-à-dire CD_4^+ et CD_8^+ cellules T), où les cellules présentant l'antigène (APC) sont attribuées à des particules témoins autonomes, servant de messagers pendant la phase d'exploration. La coopération synergique entre les lymphocytes T effecteurs et l'APC se reflète sous la forme d'une modification dynamique des poids d'inertie, des coefficients sociaux et cognitifs des vecteurs vitesse/positionnement des différentes particules. Sous quatre modèles PSC distincts avec cinq maximaux locaux dans la courbe I-V, le T1D-PSO effectue une opération efficace, avec une efficacité moyenne de ≅ 98 % et un temps d'exécution maximal de 5.817 s, résultant ainsi en une exploration complète de la courbe I-V. Les recommandations de

travaux futurs sont basées sur l'application de T1D-PSO dans un MPPT du monde réel. Les simulations ont été réalisées via Matlab.

A novel Artificial Intelligence (AI) based algorithm modification based on the pathogenic mechanisms of Type 1 Diabetes (T1D) disease for Maximum Power Point Tracking (MPPT) applications

Khaled Osmani[1], Ahmad Haddad[2,3], Thierry Lemenand[1], Bruno Castanier[1] and Mohamad Ramadan[2,3, *]

[1]LARIS EA 7315, Polytech Angers, UNIV Angers, France

[2]School of Engineering, International University of Beirut BIU, Beirut, Lebanon

[3]School of Engineering, Lebanese International University LIU, Bekaa, Lebanon

mohamad.ramadan@liu.edu.lb

Abstract: This paper aims at improving the behavior of the Artificial Intelligence (AI) based, Particle Swarm Optimization (PSO) algorithm in terms of convergence accuracy and speed of execution, upon its usage in Maximum Power Point Tracker (MPPT) applications in PhotoVoltaic (PV) systems. The reaction of PV cells under unavoidable Partial Shading Conditions (PSC) is highly non-linear, thus it leads to power extraction losses from the PV Array (PVA). Inspired by the biological evolution of Type 1 Diabetes (T1D) disease, the characteristic I-V curve of the PVA is completely traced yielding in a maximum power extraction under different PSC. The mimic of immunocytes' attitude which results in a complete pancreatic β cells destruction, is reflected on the PSO swarm's design: instead of adapting a single swarm to explore the I-V curve, two swarms are set for effector lymphatic T cells (i.e., $CD_4^+$and CD_8^+ T cells), where Antigen Presenting Cells (APC) are assigned to standalone witness particles, serving as messengers during the exploration phase. The synergistic cooperation between effector T cells and APC is mirrored as a dynamic modification for inertia weights, social, and cognitive coefficients of different particles' velocity/positioning vectors. Under four distinct PSC patterns with five maximum local peaks in the I-V curve, the T1D-PSO performed an efficient operation, with an average efficiency of ≅ 98% and a maximum execution time of 5.817 s, hence resulting in a complete exploration of the I-V curve. Future work recommendations are based on applying T1D-PSO in a real-world MPPT. Simulations were carried out via Matlab.

Keywords: Artificial intelligence, MPPT, GMPPT, Maximum power, Partial shading, PV, Algorithm

Nomenclature

A-IV	Approximating I-V	IDE	Improved Differential Evolution algorithm
AI	Artificial Intelligence	IGS	Improved Gravitational Search algorithm
AMA	Artificial Mountain Ape optimization	IOCVM-PO	Improved 0.8 Open Circuit Voltage Model and Perturb and Observe algorithm
ANN-MC-QCD	Artificial Neural Network assisted sequential Monte Carlo and Quickest Change Detection	I-V	Current-Voltage
ANN-PSO	Artificial Neural Network and Particle Swarm Optimization	KCL	Kirchoff's Current Law
APC	Antigen Presenting Cells	KVL	Kirchoff's Voltage Law
AV	Artificial Vision algorithm	LMPP	Local Maximum Power Point
BDS	Bypass Diode Scanning approach	MAKWO	Modified Artificial Killer Whale Optimization algorithm
BPD	ByPass Diode	MCSO	Modified Cat Swarm Optimization
CPV	Configuration of PV cells	MF	Modified Firefly algorithm
CSR-IV	Current Source Region detection of I-V curve	MFO	Moth-Flame Optimization algorithm
DC	Direct Current	MGA-FA	Modified Genetic Algorithm and Firefly Algorithm
DCs	Dendritic Cells	MHC	Major Histocompatibility Complex
DCS	Deterministic Cuckoo Search algorithm	MPP	Maximum Power Point

DR	Duty Ratio	MPT	Maximum Power Trapezium algorithm
EA-PO	Enhanced Adaptive Perturb and Observe	MPV-PSO	Modified Particle Velocity-based Particle Swarm Optimization
EB-MPPT	Enhanced Bayesian based Maximum Power Point Tracking	NK	Natural Killer
ES-MPP	Enhanced Scanning based Maximum Power Point Tracking	NOD	Non Obese Diabetic
FF	Fill Factor	OD-PSO	Overall Distribution and Particle Swarm Optimization algorithm
FOCV-SCC	Fractional Open Circuit Voltage-Short Circuit Current	P&O	Perturb and Observe
GG	Greenhouse Gas	PI	Power Increment algorithm
GMPP	Global Maximum Power Point	PPU	Power Processing Unit
GMPPT	Global Maximum Power Point Tracker	PSC	Partial Shading Conditions
GWO-FLC	Grey Wolf Optimization and Fuzzy Logic Controller	PSO	Partial Swarm Optimization
GWO-GSO	Grey Wolf Optimization and Golden-Section Optimization	PSO-OCC	Particle Swarm Optimization combined with One Cycle Control
HC	Hill Climb	PV	PhotoVoltaic
HGPR-J	Hybrid Gaussian Process Regression-Jaya algorithm	P-V	Power-Voltage
HGWO-BM	Hybrid Grey Wolf Optimization and Beta Method	PVA	PhotoVoltaic Array
HPSOGS	Hybrid Particle Swarm Optimization Gravitational Search algorithm	RES	Renewable Energy Sources

HPSO-GSA	Hybrid Particle Swarm Optimization and Gravitational Search Algorithm	SP	Series Parallel
HS-MPPT	High Speed Maximum Power Point Tracking	SSHC-ABC	Single current Sensor Hill Climbing and Artificial Bee Colony
HT	Hybrid Taguchi genetic algorithm	STCs	Standard Test Conditions
IC	Incremental Conductance	T1D	Type 1 Diabetes
ICSO	Improved Chicken Swarm Optimization	T1D-PSO	Particle Swarm Optimization modification according to T1D

Symbols

$V_i^{(t)}$	Initial velocity vector	Wit_Par_{DCs}	Witness particles of Dendritic Cells
$X_i^{(t)}$	Initial position vector	$Wit\_Par_{\mathrm{granzyme\,B}}$	Witness particles of granzyme B
CD_4^+	Autoreactive T cells	$Wit\_Par_{\mathrm{macrophages}}$	Witness particles of macrophages
CD_8^+	Cytotoxic T Lymphocyte	$X_i^{(t+1)}$	Updated position vector
FF_{total}	Resultant Fill Factor after all iterations	c_1	Cognitive coefficient
G_O	Irradiance at the Standard Test Conditions	c_{1_new}	Cognitive coefficient at next iterations
H_2O_2	Hydrogen Peroxide	c_2	Social coefficient
I_0	Diode saturation current	c_{2_new}	Social coefficient at next iterations
I_D	Diode current	$gbest^t$	Best position vector achieved by the entire swarm of particles
IFN_γ	Interferon gamma	n_S	Number of population
I_{Sh}	Shunt branch current	$pbest^t$	Best position vector achieved by the particle i
I_{SC}	Short circuit current	r_1	Random number
I_{cell}	PV Cell's current	r_2	Random number

I_{ph}	Light generated current	r_u	Uniform random distribution vector
K_i	Temperature coefficient	$w_{CD_4^+}$	inertia weight of CD_4^+
R_S	Series resistance	$w_{CD_8^+}$	inertia weight of CD_8^+
R_{Sh}	Parallel resistance	x_{hi}	maximum abscissa of the search region
T_0	Temperature at STC	x_{lo}	Minimum abscissa of the search region
TNF_α	Tumor necrosis factor	y_{hi}	Maximum ordinate of the search region
$V_{CD_4^+}^{(t+1)}$	Modified velocity vector equation of CD_4^+	y_{lo}	Minimum ordinate of the search region
$V_{CD_8^+}^{(t+1)}$	Modified velocity vector equation of CD_8^+	G	Actual irradiance
V_{OC}	Open circuit voltage	NO	Nitric Oxide
$V_i^{(t+1)}$	Updated velocity vector	T	Actual temperature
Wit_{Par} NK	Witness particles of Natural Killer	V	Single diode model output voltage
Wit_Par MHC class I	Witness particles of MHC class I	k	Boltzmann constant
Wit_Par MHC class II	Witness particles of MHC class I	q	Electron's charge
	Greek letters		
α	Diode's ideality factor	η_i	Efficiency of case i
η	Efficiency		

1. Introduction

Energy, aside than being a socio-economic development indicator of countries, is nowadays ranked between essential human life's necessities [1]. Particularly, the dictums of modern technologies, require continuous electrical power supply facilities. Conventional power generators (i.e., fuel based) might not be always resilient and available for this production process, due to shortage/unavailability in provisions. From the same perspective, non-renewable energy generators induce global warming, increase air toxicity as well as environmental pollution [2], due to the leftovers of the excessive burnout of gas/diesel. From such analyses, has aroused the idea of adapting environmentally friendly power supplies, referred to as Renewable Energy Sources

(RES). Among various RES forms (i.e., wind, tidal, etc.) PhotoVoltaic (PV) power systems are receiving a special attention, with the most anticipated growth potential, where China for instance aims at achieving a renewable energy share of up to 50% by year 2050 [3]. The market share of Chinese PV has also increased from 1% to 35% from 2002 to 2010, and the yield of PV power output increased from 2.6 MW in year 2000 to 2000 MW in year 2008 [4]. Nevertheless, the improved PV maintenance strategies [5], amelioration of PV cells' raw materials [6], and optimization of PV panels' tilt angles [7] have also contributed in elevating the popularity of PV systems. By adding precedent advantages to the silent performance, static architecture, non-detrimental nature of such systems [8], as well as the abundancy of solar irradiance [9], PV systems can well contribute into the transition towards a carbon-less future. An ability exists to reduce Greenhouse Gas (GG) emissions by up to 55% in Europe for example, upon usage of PV systems [10].

On the other hand, PV systems are of outdoor nature: they mainly depend on solar irradiance in order to convert light into electricity. The electricity generation process takes place when photons are absorbed (if their energies are equal or greater than the material's bandgap energy) by PV cells' materials (i.e., Silicon, Germanium, etc.) [11]. Electrons are hence excited into the conduction band. The problem resides in the non-homogeneity of solar irradiance. This is referred to as Partial Shading Conditions (PSC) where inhomogeneous light beams hit onto different regions of the PV panels' surfaces [12]. Possibly due to physical obstacles, whether dynamic or static (such as overhead poles, trees, buildings, passing clouds, birds, etc.) PSC result in non-homogeneous power production across the same panel. This fact reflects as the transformation of some regions of the panel into a load which dissipates its power from other regions of the same panel: hotspots formation [13]. In addition to the lowered efficiency of PVs when subjected to PSC, hence the inability to fully extract the maximum available power, the hotspots' makeup could lead to a permanent damage in the panel [14]. In some cases, hotspots could ignite a burnout: when the entire generating capacity of unshaded cells is dissipated in shaded cells, where local overheating gets created due to the enormous power dissipation in a small area (shaded region of the PV panel) [15]. Since PSC are practically unavoidable, they consist a major obstacle in front of PV systems in achieving their destined aim as resilient, and robust power supplies [16]. The resulting dynamical change on the level of inbuilt PV modules' series and parallel resistances (R_S and R_{Sh} respectively) [17] due to PSC is a threat to PV systems' sustainability.

In order to compensate the highly nonlinear behavior of PV cells, induced by PSC [18], Maximum Power Point Trackers (MPPT) were established under two parts: the MPPT algorithm, and the DC-DC converter. Particularly, Global Maximum Power Point Trackers (GMPPT) algorithms accomplish this aim when sunrays hit the PV panels' surfaces in dissimilar fashion. Four major divisions for GMPPT algorithms exist to locate the Global Maximum Power Point (GMPP), among many local Maximum Power Points (MPP) [19]:

- Intelligent and metaheuristic search algorithms
- Hybrid strategies
- Exploitation of characteristic curves
- Other GMPPTs

The first set contains algorithms such as Improved Chicken Swarm Optimization (ICSO) [20], Modified Cat Swarm Optimization (MSCO) [21], Improved Gravitational Search algorithm

(IGS) [22], Improved Differential Evolution algorithm (IDE) [23], Modified Particle Velocity-based Particle Swarm Optimization (MPV-PSO) [24], Modified Firefly algorithm (MF) [25], Deterministic Cuckoo Search algorithm (DCS) [26], Moth Flame Optimization algorithm (MFO) [27], Artificial Mountain Ape algorithm (AMA) [28], and Modified Artificial Killer Whale Optimization algorithm (MAKWO) [29]. These intelligent algorithms have shown great efficiency (up to 99.9%) in locating the Global Maximum Power Point (GMPP) by adapting a nature behavior inspired search. On the other hand, they require complex programming facilities (such as artificial intelligence, fuzzy logic, etc.).

The combination of two or more algorithms from within the intelligent and metaheuristic set, yields to the hybrid strategies in which the tracking performance is improved. This second set includes algorithms such as Hybrid Grey Wolf Optimization and Beta Method (HGWO-BM) [30], Modified Genetic Algorithm and Firefly Algorithm (MGA-FA) [31], Single current Sensor Hill Climbing and Artificial Bee Colony (SSHC-ABC) [32], Grey Wolf Optimization and Golden Section Optimization (GWO-GSO) [33], Overall Distribution and Particle Swarm Optimization algorithm (OD-PSO) [34], Particle Swarm Optimization combined with One Cycle Control (PSO-OCC) [35], Improved 0.8 Open Circuit Voltage model with Perturb and Observe algorithm (IVOC-PO) [36], Artificial Neural Network assisted Sequential Monte Carlo and Quickest Change Detection (ANN-SMC-QCD) [37], Hybrid Taguchi genetic algorithm (HT) [38], Artificial Neural Network and Particle Swarm Optimization (ANN-PSO) [39], Hybrid Particle Swarm Optimization Gravitational Search Algorithm (HPSO-GSA) [40], Grey Wolf Optimization and Fuzzy Logic Controller (GWO-FLC) [41], and Hybrid Gaussian Process Regression-Jaya algorithm (HGPR-J) [42]. Despite the greater convergence towards the GMPP, hybrid strategies involve more complexities in algorithm implementation. In other terms, the software production for any of these algorithms is at least of doubled difficulty when compared to each algorithm within the first set.

The third set corresponds to decomposing the search region within the characteristic Current-Voltage (I-V) and Power-Voltage (P-V) curves of a PV panel into smaller sub-regions. It includes methods such as Approximating I-V curve (A-IV) [43], Current Source Region detection of I-V curve (CSR-IV) [44], Maximum Power Trapezium algorithm (MPT) [45], Power Increment algorithm (PI) [46], Two Stage using Searching Technique and Bisection Method (TS-ST-BM) [47], and Enhanced Scanning based Maximum Power Point tracking (ES-MPP) [48]. When compared to the intelligent and hybrid strategies, these methods show less complexity. The GMPP search region is dissected into smaller sub-regions, where in each, the MPP is found and compared to its previous. The GMPP is hence achieved by numerical differentiations between several founded MPP. Although such methods reduce the time to locate the GMPP, with lesser complexities than in the first set, but on the other hand might show convergence error, due to the asynchronous timing between GMPP localization and time of calculations.

Other GMPPTs [49] include diligence algorithms such as Enhanced Bayesian based MPPT (EB-MPPT) [50], Artificial Vision algorithm (AV) [51], High Speed MPPT module (HS-MPPT) [52], Bypass Diode Scanning approach (BDS) [53], Enhanced Adaptive Perturb and Observe (EA-PO) [54], and Configuration of PV cells (CPV) [55]. Regardless the good feedback about these algorithms, still it is based on simulation results, where it needs more experimental approval (after implementation into real world MPPT applications).

Based on this small survey, it can be concluded that the higher the algorithms' accuracy in detecting the GMPP, the more complex is its implementation. Besides, intelligent algorithms with

excellent detection accuracy show the need for excess time in order to finalize their work. Therefore, an optimum GMPPT algorithm must have a high detection accuracy in addition to low operational time. Accordingly, this paper first grant from the high accuracy and intermediate complexity of AI methods, specifically the Particle Swarm Optimization (PSO) algorithm. To lower the processing time and overlapped searches of a conventional PSO, its modification is emphasized on mimicking the pathogenic mechanisms of Type 1 Diabetes (T1D). The particles' velocity, position, acceleration, and other factors are scripted with reference to the behavior of different hormonal as well as cellular entities during the progress of T1D disease. With a specific imitation of human antibodies reactions during insulin cells destruction process, a conventional PSO algorithm for GMPPT is improved. Referred to as T1D-PSO, results show a high degree of accuracy (convergence towards the optimum) with a reduced amount of operating time. Not only the optimum is located, but also the entire I-V curve is traced momentarily, to produce accurate time-based position vectors, hence exploring the global region underneath the I-V curve.

The remainder of this paper is as follows: Section 2 explores the behavior of a PV system when confronted with PSC, where Section 3 presents the pathogenic mechanisms for T1D. Section 4 reveals how the T1D emergence was approximated to the scenario of PSC with the modification of PSO. In Section 5 the Matlab simulation took place. Different results with discussions are presented in Section 6. Finally, conclusion and future works are conducted in Section 7.

2. PV behavior under PSC

To examine how the PSC affect a proper PV system's performance, the difference (in quantities and waveforms) between the PV cell current (I_{cell}) shown in Fig. 1 under isotropic irradiance, and I_{cell} under PSC, is a key index.

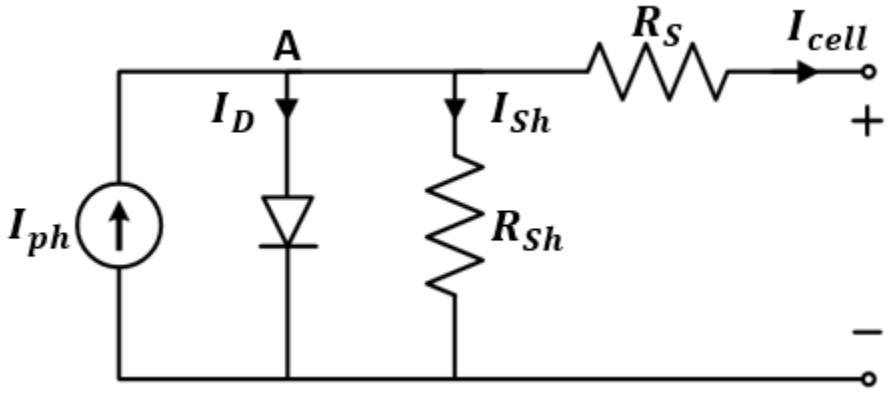

Fig. 1. Single diode model for a PV cell

By applying Kirchhoff's Current Law (KCL) at node A in Fig.1, the resulting PV cell's current I_{cell} can be expressed as in Eq.(1).

$$I_{cell} = I_{ph} - I_D - I_{Sh} \quad (1)$$

with I_{ph}, I_D, I_{sh} representing respectively the light generated, diode and shunt branch currents [56,57].

The light generated, diode, and shunt currents can be expanded as in Eqs.(2)-(4).

$$I_{Ph} = \frac{G}{G_O} \cdot [I_{SC} + K_i\ (T - T_0)] \tag{2}$$

$$I_D = I_0 \left[exp\left(\frac{q(V + R_s\ I_{cell})}{\alpha\ k\ T} \right) - 1 \right] \tag{3}$$

$$I_{Sh} = \frac{V + R_S\ I_{cell}}{R_{Sh}} \tag{4}$$

where G denotes the actual system's irradiance, G_O the irradiance at the Standard Test Conditions (STCs: $G_O = 1000\ \mathrm{W/m^2}$), I_{SC} the short circuit current, K_i the current temperature coefficient, T the actual system's temperature, T_0 the temperature at the STCs ($T_O = 25°\mathrm{C}$), I_0 the diode saturation current, k represents the Boltzmann constant, q the charge of electron, V the single diode model output voltage, R_S the series resistance, α the ideality factor of a diode, and R_{Sh} the shunt resistance [56,57].

The substitution of Eqs.(2)-(4) in Eq.(1), represent the expanded PV cell current shown in Eq.(5).

$$I_{cell} = \frac{G}{G_O} \cdot \left([I_{SC} + K_i\ (T - T_0)] - I_0 \left[exp\left(\frac{q(V + R_s\ I_{cell})}{\alpha\ k\ T} \right) - 1 \right] - \frac{V + R_S\ I_{cell}}{R_{Sh}} \right) \tag{5}$$

The factor $\frac{G}{G_O}$ corresponds to the formative reflection of PSC effects over the PV panels. Under homogeneous shading conditions, $\frac{G}{G_O}$ have a single value, regardless how intense the solar irradiance is. For example, when $G = 800\ \mathrm{W/m^2}$ this light intensity is similarly seen by the entire PV cells within the panel. Therefore, only a single peak exists in the I-V curve, thus locating this peak would compensate the nonlinearity (condemned by the presence of an exponential factor in Eq.(5)) of PV cells and extract the maximum available power.

Now considering different PSC, as elaborated in Fig. 2, the coefficient $\frac{G}{G_O}$ fluctuates between different PV cells. Accordingly, it takes several values, with respect to the differences between solar light intensities, due to physical barriers. Rather than obtaining a theoretically single value as an output of Eq.(5), many exist according to $\frac{G}{G_O}$ variations, exposed in Eq.(6).

$$\frac{G}{G_0} = \begin{cases} \text{value 1; resulting from PSC}_1 \\ \vdots \\ \text{value n; resulting from PSC}_n \end{cases} \quad (6)$$

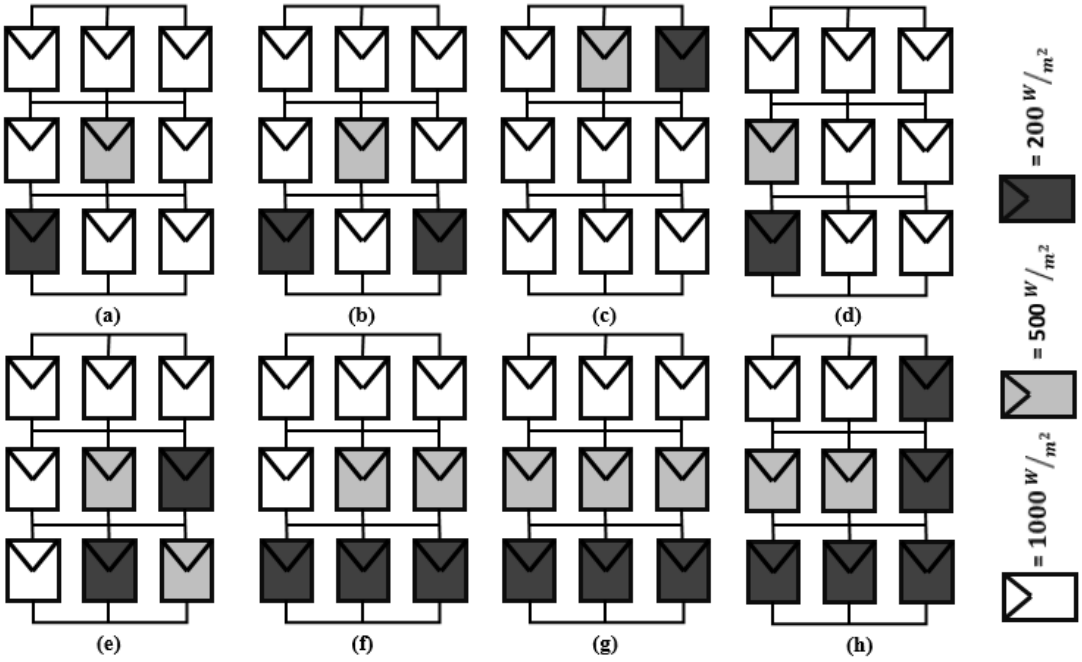

Fig. 2. Different shading patters, (a) random, (b) diagonal, (c) uneven row, (d) uneven column, (e) short and narrow, (f) short and wide, (g) long and narrow and (h) long and wide

When any of the shading patterns shown in Fig. 2 take place, I_{cell} (inside the shaded area) becomes lesser than zero, where the shaded solar cell goes into reverse bias mode, dissipates power, and gets destroyed due to overheating. Concerning such analysis, Fig. 3 displays the effects of PSC over a PV array's characteristics (P-V and I-V) curves. The black curve in Fig.3(a) represents an ordinary P-V curve under homogeneous shading, as defined in Eq.(4), where the maximum attainable power is of 4000 W (concerning the PV array's limitations). Also in the same figure, the red curve represents the effects of shading, where the maximum attainable power is reduced to below 2000 W, thus representing a power extractability droppage by more than 50%. The bottleneck arises with the blue curve of Fig.3(b), when many Local Maximum Power Points (LMPP) appear in the P-V curve due to the activation of Bypass Diodes (BPD).

By taking into consideration that the PV Array (PVA) output power is represented by the area underneath the P-V curve, it is clear that BPD add more area to this curve (blue-red curves combined) when compared to no BPD activation (red curve only). On the other hand, this resulting curve add more complexity to its analysis: the more existing LMPP, the higher the difficulties for a traditional MPPT algorithm to locate the GMPP.

For instance, a P&O algorithm will get stuck over the first LMPP of the blue curve in Fig.3(a), such that any succeeding LMPP is never spotted. In other terms, any available power, underlying to the right of the first LMPP cannot be located/extracted by means of conventional MPPT algorithms (P&O, IC, etc.): when applied into real PV applications, any Power Processing

Units (PPU) governed by such algorithms would lack the ability to produce accurate Duty Ratio (DR), to either buck or boost the PPU's output voltage. In other terms, the inaccuracy in voltage/current equalization by the PPU yields to a lower power extraction from the PVA, due to avoided search spaces from within the characteristic curve. An instantaneous GMPP tracker is hence needed to overcome these drawbacks.

The same logic applies for Fig.3(b), where the healthy I-V curve (black colored) is shrank to the red curve due to shading effects. Since the PVA's power is the product of voltages and currents (x-axis and y-axis quantities), it can be deducted from Fig.3(b) that the activation of BPD (blue curve) adds more area to the entire I-V curve resulting from anisotropic shading profiles (combination of blue and red curves).

Analytically, the added area resulting from BPD activation in Fig.3(b), which reflects an added output power from the PVA is located between currents 35 and 15 A and voltages between 0 and 100 V. A point-wise dissection of the combined red-blue curve of Fig.3(b), which is represented by Eq.(5), must be taken into consideration, in order to extract the highest Fill Factor (*FF*), which represents the ratio of the maximum output power over the product of short-circuit and open-circuit current and voltage respectively.

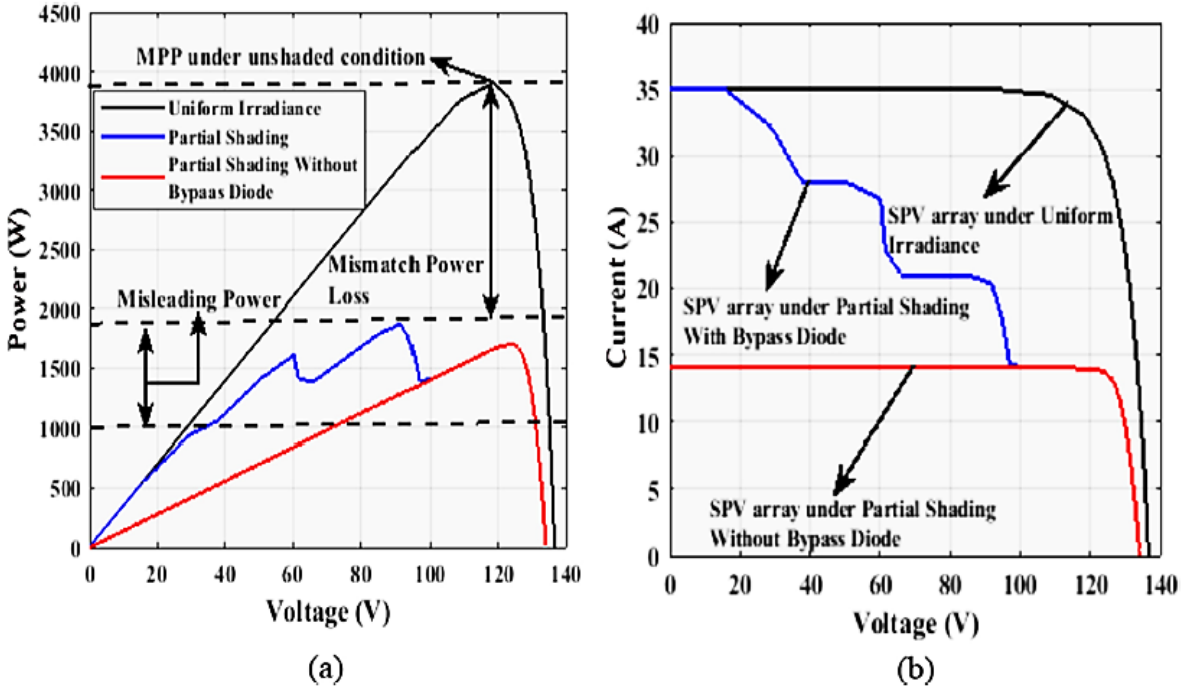

Fig. 3. Impacts of PSC over (a) P-V characteristic curve (b) I-V characteristic curve [58]

Concerning the first LMPP in Fig.3(b), represented as $P(x; y)$, belonging to the red-blue curve combination, where $x = 40$ V and $y = 28$ A, a specific DR must be defined by the GMPPT, after exploration of P by the algorithm. The produced DR for P is different for the succeeding LMPP, represented as $Q(x; y)$ where $x = 60$ V and $y = 26$ A.

After such analysis for the I-V curve under PSC, a good GMPPT algorithm must ensure to cover all points existing on the I-V curve (in this case, the red-blue curve) during the explorative

and exploitative phases, then produce accurate DR for the PPU operation, thus extracting the maximum available power from the PVA (as a real GMPPT application, which is not the purpose of this paper).

3. Pathogenic mechanisms for T1D

Type 1 Diabetes (T1D) is an organ-specific autoimmune disease representing self-failure from an erroneous discrimination, conducted by the immune system [59,60]. For Non Obese Diabetic (NOD) mice, as well as for humans [61,62], T1D is provoked by a cellular turnover/mutation of pancreatic β cells [63-65]. Located in islets of Langerhans [66,67], these β cells falsely expose as antigens [68]. Thus β cells autoantigens are presented to mononuclear immunocytes, such as T-lymphocytes [69,70]. This presentation process is done by means of Antigen Presenting Cells (APC) [71] such as:

- Major Histocompatibility Complex (MHC): which are proteins coding genes for cells identifying the presence of a foreign (intruding) substances [72].
- Macrophages: a type of white blood cells, constituting the mononuclear phagocyte system [73].
- Dendritic Cells (DCs): a special type of immune cells, known as accessory cells [74].
- B cells: known as B-lymphocytes, regarded as professional APC [75]. Granzyme B is the concern, among different B cells, which is involved in T1D progression [76].
- Natural Killer (NK) cells: a type of immune cells, existing as a part of white blood cells, containing granules with enzymes [77].

The major contributors in β cells destruction mechanism, are the effector T cells, which are decomposed into autoreactive CD_4^+ T cells [78], and Cytotoxic T Lymphocyte (CTL) CD_8^+ T cells [79]. These effectors T cells are chemically activated as follows:

- CD_4^+ activation: by means of MHC class II, and interleukin secretion by macrophages and DCs [80].
- CD_8^+ activation: by means of MHC class I [80], and granzyme B exocytosis [81].

When effector T cells are activated, they can distinguish autoantigens produced by mutated β cells and react accordingly [82]. A synergetic endeavor is hence done between APC and effector T cells, to ensure a progressive, yet complete, destruction of β cells:

- Macrophages: by release of Nitric Oxide (NO) and Hydrogen Peroxide (H_2O_2), which are inflammatory cytokines, onto the surface of β cells [83].
- NK: by release of cytotoxic molecules, such as Perforin [84].
- CD_8^+: by release of Perforin and granzymes exocytosis [85].
- CD_4^+: by secretion of pro-inflammatory cytokines, such as interferon gamma IFN_γ, tumor necrosis factor alfa TNF_α [85], etc.
- Granzyme B: by means of BH3-interacting domain death agonist (Bid) [81].

This combinatorial cellular interaction would yield to a stoppage in insulin secretion [86]. At this level, no ability exists in order to remove excess sugar from blood vessels (above 100 mg/dl) [87]: a condition that is referred to as hyperglycemia [88]. A clinical diabetes of type 1 is hence manifested [89]. The stated mechanisms of T1D pathogenesis are graphically presented in Fig. 4.

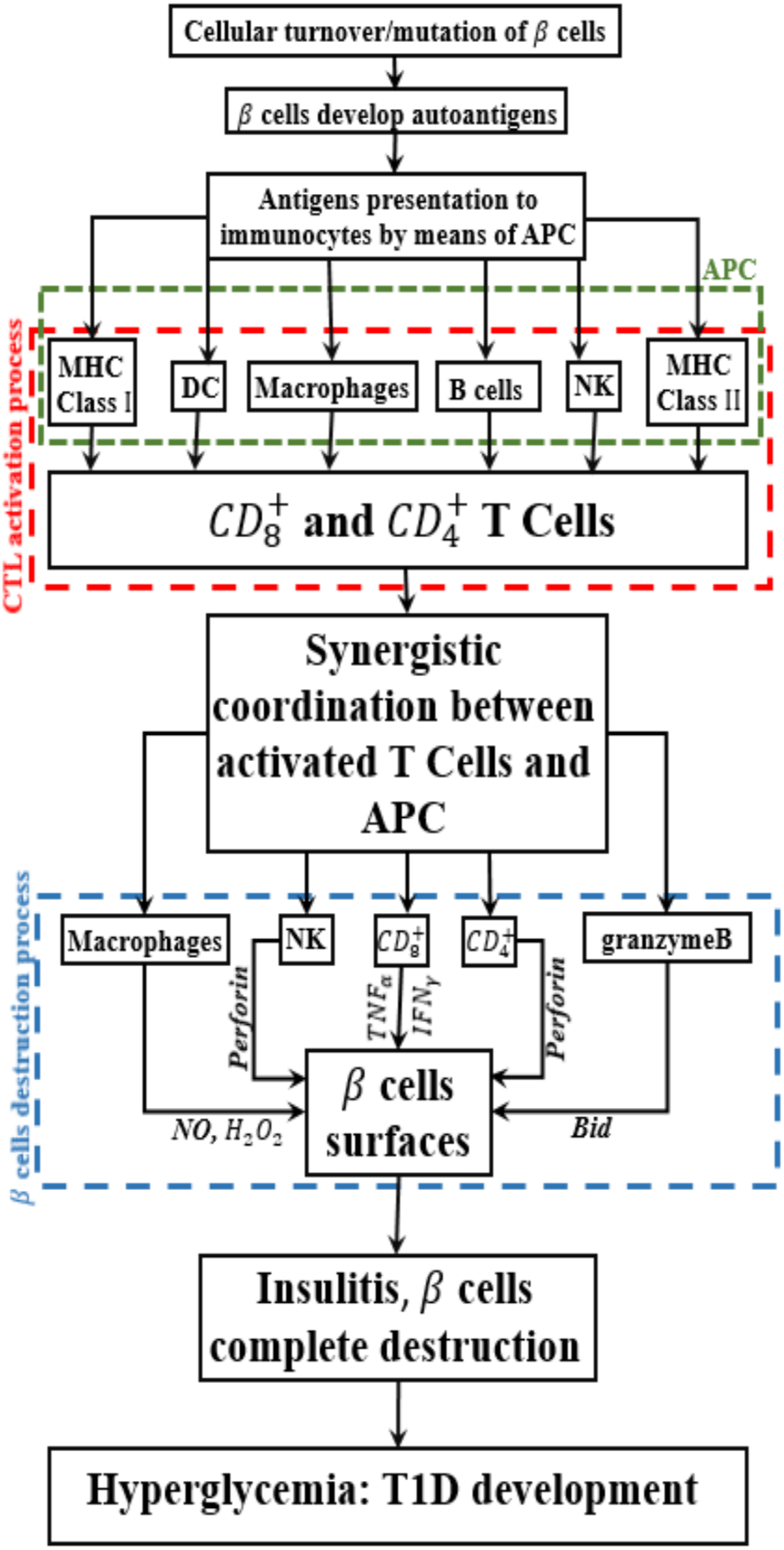

Fig. 4. T1D evolution flowchart

The hormonal interactions between different cells shown in Fig. 4, yield to a progressive destruction of the β cells mass function over time. The relation of this paper with respect to the stated biological phenomenon, is the analysis of the resulting mathematical curve describing T1D progression, presented in Fig. 5: incidentally, the orange curve in this figure resembles the I-V characteristic curve (red-blue curve) from Fig.3(b). Hyperglycemia arises after initial CD_8^+ kill solidification by APC and B cells autoantibodies CD_4^+ and CD_8^+ responses. Clinical diabetes is hence taking place after complete β cells destruction, reflected as momentarily exploration/exploitation by the killing agents. Accordingly, the stages from A to F in Fig. 5 are to be applied into the PSO modification.

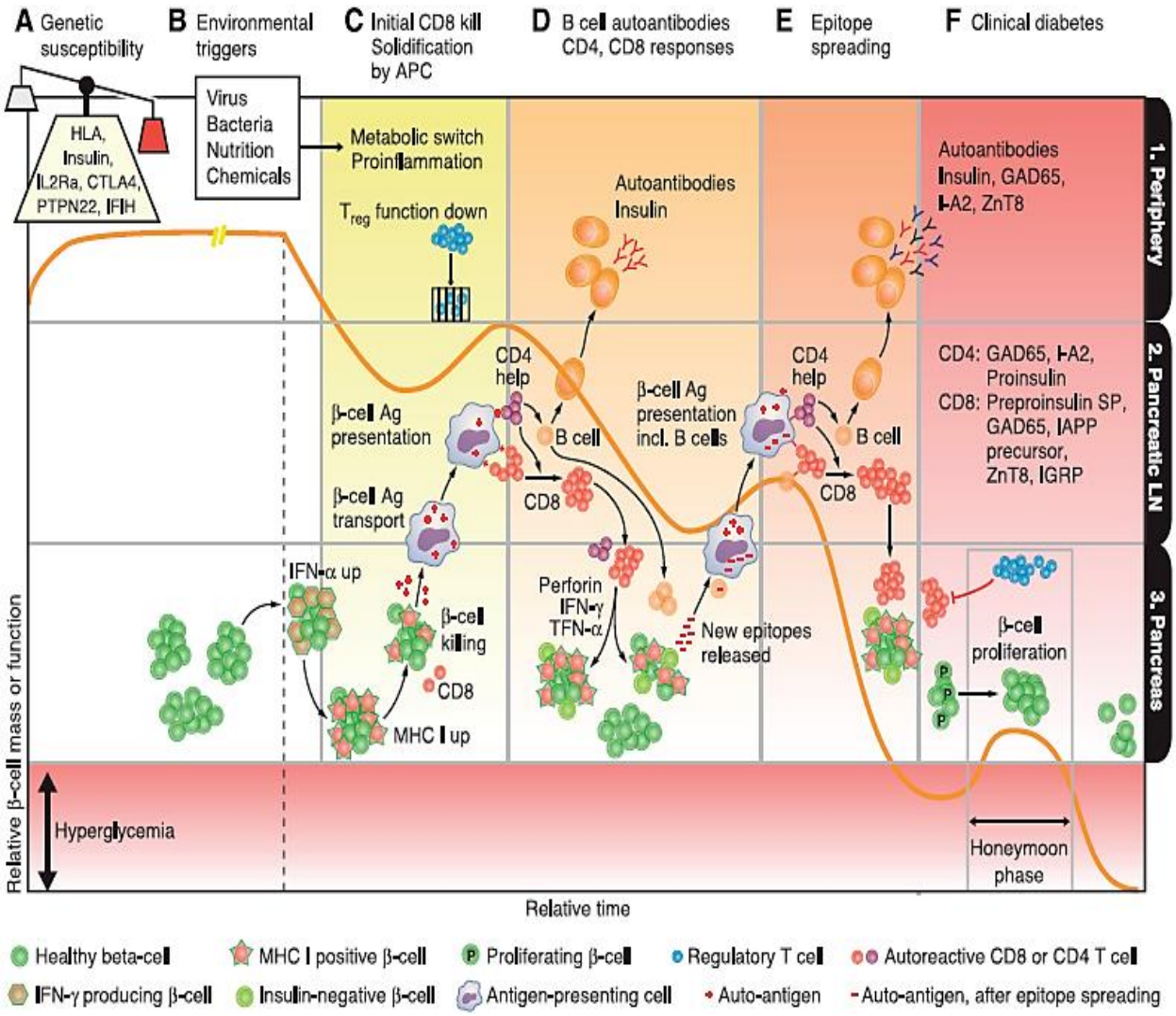

Fig. 5. Etiology and pathogenesis of T1D [90]

The PSO modification, according to T1D pathogenesis shown in Fig. 5, corresponds to two steps: first, the orange curve is to be approximated to the I-V characteristic curve under PSC, shown as the combined red-blue curve in Fig.3(b). Second, different cellular gatherings over the

curve are to be applied for particles swarms' motions, velocities, and positions. The overall aim is to achieve a sharper and faster momentarily I-V curve tracing under PSC, by mimicking the hierarchical cellular coordination seen in T1D evolution.

4. Approximation between PSO, T1D and PSC

A conventional PSO corresponds to a total number of i particles within a swarm: Each particle has an initial position vector $X_i^{(t)}$, and an initial velocity vector $V_i^{(t)}$ exposed in Eq.(7) and Eq.(8) which govern the dynamics of the swarm across the searching space [91].

$$X_i^{(t)} = \left(x_i^{(t)}, y_i^{(t)}\right) \tag{7}$$

$$V_i^{(t)} = \alpha \tag{8}$$

The coordinates of $X_i^{(t)}$ ensure that the population are restricted into the region of interest as shown in Eq.(9) and Eq.(10), where α denotes a numerical value, generally taken as zero, or chosen randomly within specific limits [92].

$$x_i^{(t)} = x_{lo} + r_u \cdot (x_{hi} - x_{lo}) \tag{9}$$

$$y_i^{(t)} = y_{lo} + r_u \cdot (y_{hi} - y_{lo}) \tag{10}$$

where r_u is a uniform random distribution vector included in $[0;1]$, x_{lo} and x_{hi} representing the minimum and maximum abscissas of the search region respectively, y_{lo} and y_{hi} indicating the minimum and maximum ordinates of the search region respectively.

Both position as well as velocity vectors are continuously updated until a stopping criterion is met, concerning the processes of exploration and exploitation of the search region. At succeeding iterations (i.e., $(t+1)$), the two vectors are updated as shown in Eq. (11) and Eq. (12) [93].

$$X_i^{(t+1)} = X_i^{(t)} + V_i^{(t+1)} \tag{11}$$

$$V_i^{(t+1)} = wV_i^{(t)} + c_1 r_1 \cdot \left(pbest^t - X_i^{(t)}\right) + c_2 r_2 \cdot \left(gbest^t - X_i^{(t)}\right) \tag{12}$$

such that w represents the inertia weight constant, c_1 and c_2 are the cognitive and social coefficients respectively, r_1 and r_2 are random numbers within the interval $[0,1]$, $pbest^t$ and $gbest^t$ are the best position vector achieved by the particle i yielding in the personal optimum value of the search region, and the best position vector achieved by the entire swarm of particles respectively at iteration t respectively [93].

The inertia weight constant in Eq. (12) is defined within the interval $]0,1[$ and determines how much should the particle stick to its previous velocity. The acceleration coefficients, c_1 and

c_2 determine how much weight should be given between refining the search results of the particle itself and recognizing the search results of the swarm respectively [93,94]. By grouping what has been preceding, the conventional PSO flowchart can be summarized as in Fig. 6.

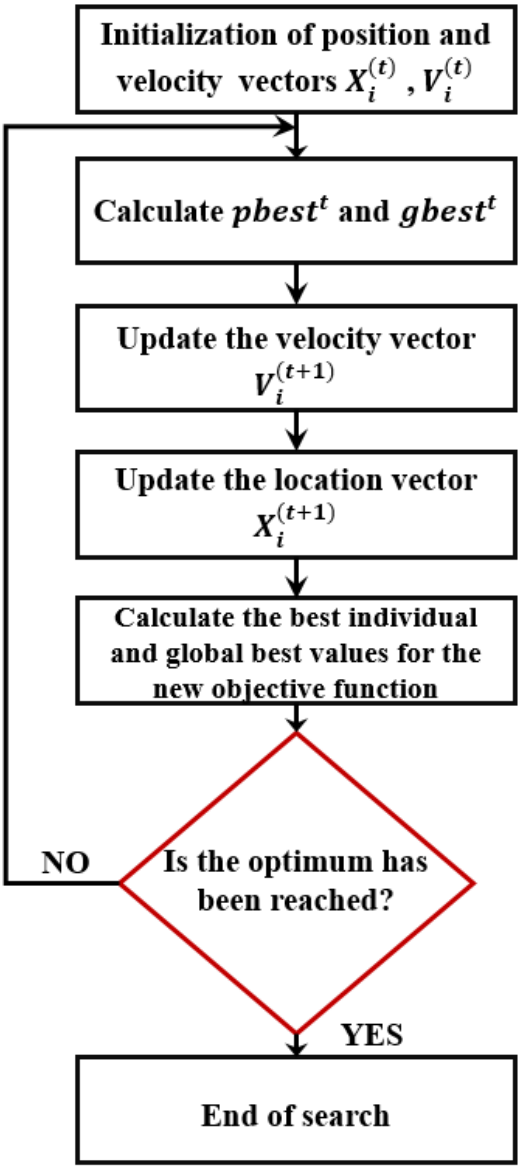

Fig. 6. Conventional PSO flowchart

The reflection of T1D pathogenesis on PSO modification is as follows:

- The single major swarm of particles is decomposed into sub-swarms, to mimic the diversity of cells which incorporate into the destruction of pancreatic β cells.
- The synergistic cooperation between activated T cells and APC is translated by means of dynamical modifications of:

i. Inertia weight w: to allow the manipulation of the exploration rate to save time and to ensure future convergence as the process develops [95].
ii. Cognitive coefficient c_1: to control the particle's self-confidence degree, therefore defining particles' trajectories [96].
iii. Social coefficient c_2: to control the neighbors' confidence degree with respect to current particles, what also defines particles' trajectories [96].

Regarding the general heuristic of population size, where the number of population n_S is included in the interval of $[10, 30]$ according to the reference [97], for this study, n_S is chosen to be of twenty-six particles. To be noted that the larger number of particles, yields in an increased probability of mutual collisions between the particles during the exploration phase, hence the increased per-iteration computational complexity. Concerning the optimization function of the PV panel under PSC as presented in Eq.(5), and since the optimal population size is problem-dependent, the current selection of n_S is based on a cross-validation between the search space, and the immunocytes which contribute in the evolution of T1D [97]. Concerning the algorithm process, the total set of twenty-six particles is decomposed into two major sets of ten particles each, and six standalone particles.

In other words, instead of admitting a total of twenty-six particles into a single swarm, to explore/exploit the I-V curve, which represent the search space (the optimization function), they are decomposed to sub-entities as follows:

- Each cell of APC is reflected as a single exploring particle, referred to as "*witness particle*".
- The major effector T cells (i.e., CD_8^+ and CD_4^+) are included in two swarms where each involves ten particles, to be guided by their relative witness particles.
- Witness particles of MHC class I, and granzyme B, denoted as $Wit\_Par_{\text{MHC class I}}$ and $Wit\_Par_{\text{granzyme B}}$ respectively serve as guides for CD_8^+cells particles.
- Witness particles of MHC class II, macrophages, NK, and DCs denoted as $Wit\_Par_{\text{MHC class II}}$, $Wit\_Par_{\text{macrophages}}$, Wit_Par_{NK}, and Wit_Par_{DCs} respectively guide CD_4^+cells particles through the I-V curve exploration process.
- The communication between witness and T cells particles is defined by mathematical relations of mutual inertia weights, and acceleration coefficients.

To be noted that taking more than a single witness particle for each swarm is not recognized as a duplication, since both cognitive and social terms of each particle are multiplied by the uniform random distribution vectors, what chaotically changes the value of $V_i^{(t+1)}$ for each particle in turns. Also, the witness-to-acknowledge process is a tradeoff between searching speed, and convergence accuracy. The modification of Eq.(8) to Eq.(12) for *witness particles* begins by assuming a zero initial velocity, where α in this case equals to zero, as expressed in Eq.(13).

$$V^{(t)}_{Wit\_Par_{\text{MHC class I}}} = V^{(t)}_{Wit\_Par_{\text{granzyme B}}} = \cdots = V^{(t)}_{Wit_{Par_{\text{DCs}}}} = 0 \tag{13}$$

Concerning the initialization of position vectors for all witness particles, the abscissas/ordinates constrictions in Eq.(9) and Eq.(10) are defined in Eq.(14).

$$\begin{cases} x_{lo} = y_{lo} = 0 \\ x_{hi} = V_{OC} \\ y_{hi} = I_{SC} \end{cases} \quad (14)$$

where V_{OC} and I_{SC} represent the PV array open-circuit voltage and short-circuit current respectively.

The velocity vector of witness particles at next iterations, written in Eq.(12), has the following requirements, concerning PSO modification based on T1D pathogenesis:

- The value of w is taken as the average value of the vector $]0,1[$: although the resulting value ($\cong 0.55$) for inertia weight amid the early exploration process is considered small [92] but would ensure an accurate exploration process which results would be later linked to w of effector T cells particles.
- The cognitive coefficient c_1 is taken as a positive integer, where the social coefficient c_2 is regarded as zero: each of the witness particles are independent of others and are more attracted to their own personal best position [92]. The negligence of c_2 is based on the fact that witness particles serve as messengers for CD_4^+ and CD_8^+ particles, hence no need for social interactions between other witness particles.

The personal best position $pbest^t$ is specific for the obtainment of each witness particle, such as the best personal position achieved by $Wit\_Par_{\text{MHC class I}}$ for example, is referred to as $pbest^{(t)}_{Wit\_Par_{\text{MHC class I}}}$. The best personal positions achieved by $Wit\_Par_{\text{MHC class II}}$, $Wit\_Par_{\text{macrophages}}$, Wit_Par_{NK}, and Wit_Par_{DCs} are mutually compared to each other, where the optimum position vector is considered as pre-calculated historic personal best for CD_4^+ particles, denoted by $pbest^{(t)}_{Wit\_Par\_CD_4^+}$. On the other hand, the best personal position achieved by $Wit\_Par_{\text{MHC class I}}$ and $Wit\_Par_{\text{granzymeB}}$ are also mutually compared to each other, where optimum position denoted by $pbest^{(t)}_{Wit\_Par\_CD_8^+}$ is considered the pre-calculated historic personal best for CD_8^+ particles.

On the opposite side, the effector T cells, encapsulated within the two major distinct swarms, have in turn their updated velocity vector equation of Eq.(12) modified according to the following conditions:

- The inertia weight w of CD_4^+ and CD_8^+ particles is expressed in Eq.(15):

$$w_{CD_4^+} = w_{CD_8^+} = 2 \cdot w_{Wit\_Part} - \varepsilon \quad (15)$$

where ε represents a small numerical value which ensures that $0 < w < 1$.

The inertia weight of effector T cells particles are doubled with respect to w of witness particles, in order to ensure a doubled speed of CD_4^+ and CD_8^+ particles while attaining to the I-V

search region, specifically to the latest and best updated position vector achieved by the witness particles. This is to ensure a convenient follow-back by effector T cells particles to the already spread out witness particles.

- Both acceleration coefficients, c_1 and c_2 are taken as positive integers. Since particles' social interaction is now a concern, in order to make both swarms attracted towards the global best position, the condition $c_2 > c_1$ must be taken into consideration. This statement can be explained in other words, as a linear increasing of c_2 and a linear decreasing of c_1 over time (as the search proceeds) [97]. Considering that c_1 and c_2 are bounded between c_{1_min} , c_{1_max}, and c_{2_min} , c_{2_max} respectively, the dynamical changes to the acceleration coefficients for effector T cells particles are expressed in Eq,(16) and Eq.(17).

$$c_{1\_new} = c_{1\_old} - \left(\text{ave} \begin{bmatrix} c_{1\_max} \\ \vdots \\ c_{1\_min} \end{bmatrix} \right) \tag{16}$$

$$c_{2\_new} = c_{2\_old} + \left(\text{ave} \begin{bmatrix} c_{2\_max} \\ \vdots \\ c_{2\_min} \end{bmatrix} \right) \tag{17}$$

where c_{1_new}, c_{2_new} represent the cognitive and social factors at next iterations respectively (i.e., at $(t+n)$), and c_{1_old}, c_{2_old} represent the same factors at previous iterations (i.e., at iteration (t)).

Accordingly, the modified velocity vectors equations of CD_4^+ and CD_8^+ particles are respectively shown in Eq.(18) and Eq.(19).

$$V_{CD_4^+}^{(t+1)} = w_{CD_4^+} V_i^{(t)} + c_{1\_new} r_1 \cdot \left(pbest_{Wit\_Par\_CD_4^+}^{(t)} - X_{CD_4^+}^{(t)} \right) + c_{2-new} r_2 \cdot \left(gbest^t - X_{CD_4^+}^{(t)} \right) \tag{18}$$

$$V_{CD_8^+}^{(t+1)} = w_{CD_8^+} V_i^{(t)} + c_{1\_new} r_1 \cdot \left(pbest_{Wit\_Par\_CD_8^+}^{(t)} - X_{CD_8^+}^{(t)} \right) + c_{2-new} r_2 \cdot \left(gbest^t - X_{CD_8^+}^{(t)} \right) \tag{19}$$

In relation with the T1D evolution, the reflected witness particles' (i.e., DCs, NK, etc.) intrinsic role in this PSO modification, is initially to explore the search space, hence deriving the personal best position vectors. From another part, witness particles aim to guide the main sets of swarms of CD_4^+ and CD_8^+ particles towards the succeeding optimum, within the same search space. Accordingly, and by utilizing the best personal position achieved by witness particles of each main swarms' sets, in conjunction with the modified acceleration coefficients/inertia weights, both equations (18) and (19) represent the final optimum velocity vectors update for CD_4^+ and CD_8^+ swarms respectively. The modified PSO can be related to T1D pathogenesis, as shown in Fig. 7 according to four steps:

i. Events of genetic susceptibility/environmental triggers which relatively represent the root cause of T1D evolution, are perceived as PSC inducers, due to physical light obstacles in front of PV panels' surfaces.

ii. The antigens presentation to immunocytes by means of APC is reflected by witness particles, returning optimum position and velocity vectors to the two swarms of CD_4^+ and CD_8^+ particles.

iii. The synergistic cooperation between effector T cells and APC is deliberated as modification of inertia weights and acceleration coefficients of CD_4^+ and CD_8^+ particles within the swarms.

iv. The occurrence of clinical diabetes is mirrored as a complete trace down of the corresponding I-V curve which represents the search region (optimization function).

The approximation between T1D and PSO is shown in Fig. 7, where the modified PSO algorithm is summarized in Fig. 8. The key note to bear in mind is that the jumping-jack between witness particles and effector T cells, regarded as continuous modification of w, c_1, and c_2 is an induced trade-off between the modified PSO's operational time, and its degree of convergence.

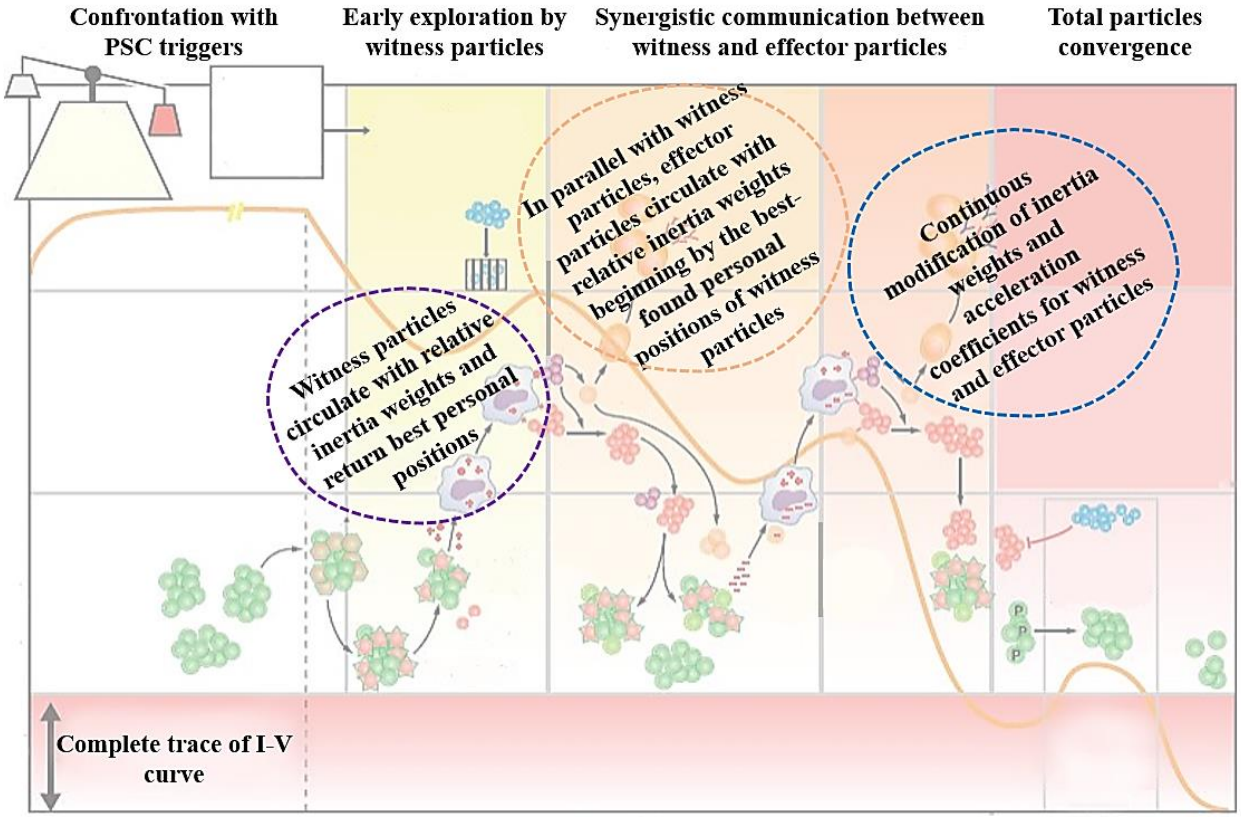

Fig. 7. Correlation between T1D pathogenesis chart and modified PSO

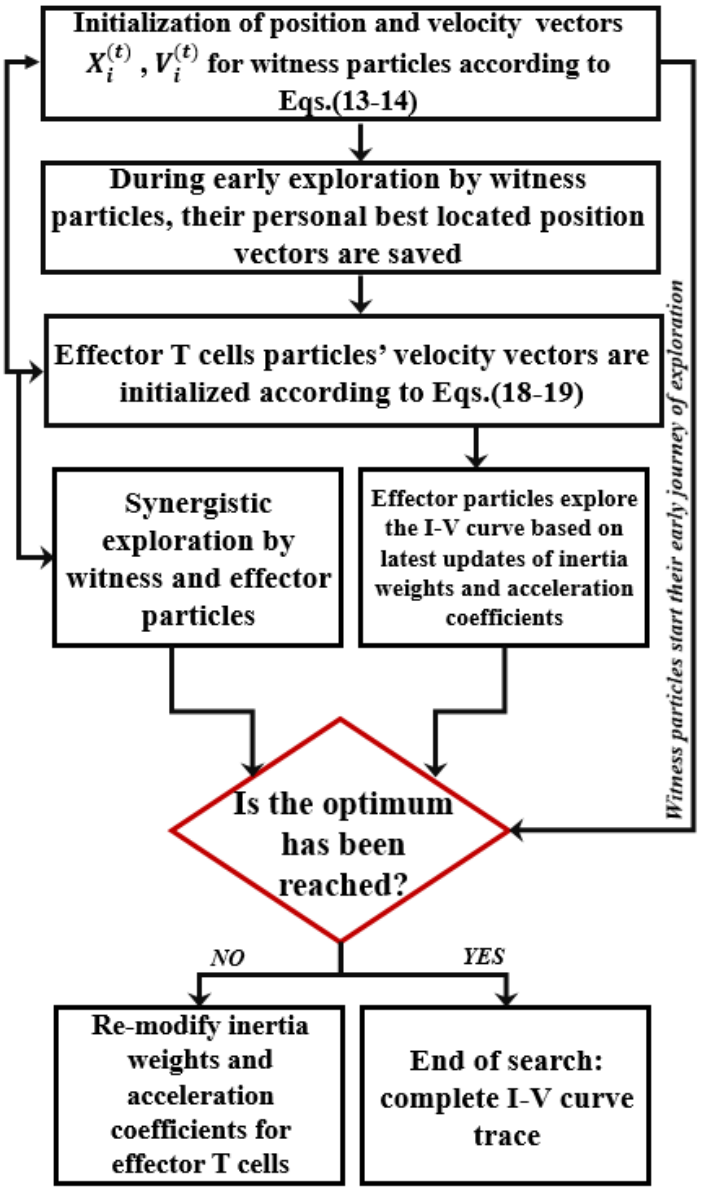

Fig. 8. Modified PSO flowchart

The core behind PSO algorithm's modification is not only to ensure a convergence towards the minimum of the search space, defined by the PV's I-V curve, but to also force all particles to trace the I-V curve from the beginning of the search process. In other words, witness as well as effector particles must coincide as much as possible with the I-V curve during the entire search process. For this case of study, the optimum destined for reaching, is a point within the nonlinear I-V curve located somewhere near the $(V_{OC}, 0)$ coordinates.

The T1D inspired PSO modification hence must certify that all twenty six particles do not conduct any motion outside the boundaries of the optimization function defined in Eq.(4) and Eq.(5), then these particles would point-to-point align with the I-V curve trajectory. Otherwise, all particles will chaotically move towards the point defined by $(V_{OC}, 0)$ aimlessly.

5. Matlab simulation of T1D-PSO algorithm

The initial step of T1D-PSO implementation in Matlab, is inducted by the characterization of the PV Array (PVA) that will be tested under different PSC. The response of PVA under different PSC scenarios (i.e., presentation of several peaks in the I-V curve) will be subjected to the developed algorithm to see its effects (i.e., speed, convergence, etc.). Both size and architecture of PVA would reveal different parameters needed to define the I-V function, as covered in Section 2 under the mathematical modeling of PV cell.

The equation set beginning by Eq.(1) to Eq.(5) are to be extracted from PVA characteristics then implemented as a Matlab function. The PVA is a set of PV modules interconnected all together to produce a single output. In turns, a PV module is a set of interconnected PV cells, where each's output current expressed in Eq.(5). In other terms, the PV module current output, is the same I_{cell} multiplied with number of cells N_S (since the number of parallel PV cells define the current output of the PV module). Accordingly, and for simulation purposes only, the characteristics of each PV module within the PVA are chosen as encapsulated in Table 1.

PV module parameter	Value
Number of cells N_S	60 cells
Open circuit voltage V_{OC}	36.3 Volts
Short circuit current I_{SC}	7.84 Amperes
Current temperature coefficient K_i	0.102
Temperature at STC T_0	298.15 Kelvin
Actual system's temperature T	298.15 Kelvin
Diode saturation current I_0	2.9273×10^{-10} Amperes
Diode ideality factor α	0.98119
Boltzmann constant k	1.380649×10^{-23} J$\cdot$K^{-1}
Electron charge q	$1.6021766 \times 10^{-19}$ Coulombs
Shunt resistance R_{Sh}	313.0553 Ohms
Series resistance R_S	0.39381 Ohms

Table 1. Characteristic parameters of the used PV module

The destined PVA is to be under Series-Parallel (SP) topology as shown in Fig. 9. A PV string consists of three series connected PV module as characterized in Table 1. Each string is to be repeated 15 times, thus creating a 15×3 SP PVA. The idea behind this design is for simulation purposes only, where bigger number of parallel strings allows a bigger range for PSC propositions. By applying KCL (Kirchoff's Current Law) and KVL (Kirchoff's Voltage Law) onto the entire PVA, the new I_{SC} is now equal to 120 Amperes, and new V_{OC} equals to 108 Volts. The obtained values of open/short-circuit voltage and current represent the (x, y) ranges for the I-V function.

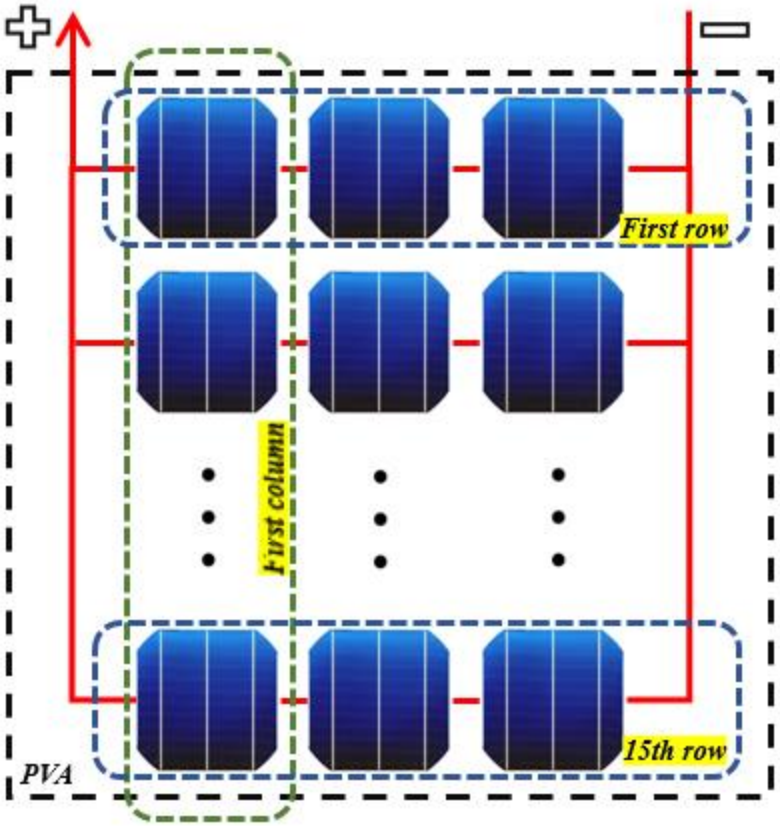

Fig. 9. The 15×3 PVA to be tested with different PSC

In order to test the T1D-PSO algorithm speed and convergence accuracy, the designed PVA shown in Fig. 9 is set to be exposed under four distinct PSC scenarios, in an evolving complexity. The first case of PSC is destined to have two peaks in the I-V characteristic curve, which is drawn using the parameters summarized in Table 1. The second PSC scenario would have three peaks, and the accumulation continues until last PSC scenario would involve an occurrence of five different peaks in the I-V curve.

The initialization process of each PSC is obtained after exposing different regions of the PVA to physical barriers that would result in a non-homogeneous quantities of solar irradiations, received by the surface of the PVA. For this purpose, clouds (physical light barriers) are supposed to cover different zones of the PVA, yielding in multiple peaks apparition in the I-V curve.

When a cloud interferes the total light absorption by the PVA, the corresponding reflection over the I-V curve for instance would be noticed as apparition of two peaks. Following the same perspective, the confrontation of four spaced clouds versus the PVA would result in the apparition of five different peaks within the I-V curve.

The choice of clouds' positioning over the PVA is randomly set, what is believed to better standardize the algorithm to be robust under any PSC pattern, as exposed in Fig. 2. All of four PSC scenarios are interpreted in Fig. 10. The presence of a cloud is an indicator that the affected PV panel is not receiving irradiance in the same amount as its neighbors do. This can be also

understood that each of the PSC correspond to a certain $\frac{G}{G_0}$ as revealed in Eq.(6), which is smaller than one.

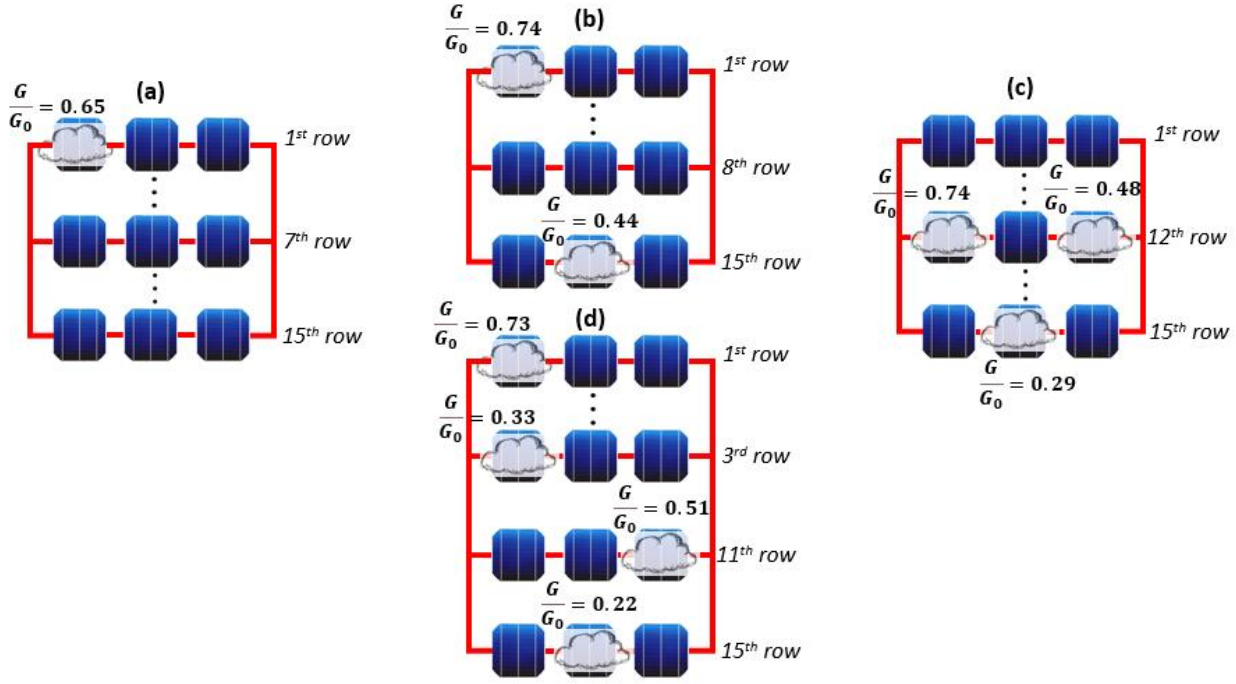

Fig. 10. Different PSC conditions: (a) Case 1 with 2 peaks, (b) Case 2 with 3 peaks, (c) Case 3 with 4 peaks, (d) Case 4 with 5 peaks

Concerning the Matlab simulation process, it consists of five scripts, from which some are mutually called by others. The functions were categorized as follows:

1. Modified T1D-PSO function: considered as the main function, in which the population size, number of movements, dimensions, and other swarm-related criteria are defined. Moreover, the pre-defined I-V characteristic function (Eq.(5)) is called with its corresponding abscissa/ordinates restrictive ranges, equivalently with the points plotter function which aims to plot the motion of different particles. After the identification of all the parameters that are required as initials for the searching process, and the call of different required function for visualizing the process (such as the plotting function), a loop is executed with relevance to the array size, defined by the total number of movements. Sub-sequentially, and with respect to the population size, an inner loop is established in which the velocity vectors of effector/witness particles (Eq.(18) and Eq.(19)) are defined. During this process, it is continuously checked (by vector comparison) the states of particles' fitness values (in terms of best attained position vectors), where the resultant optimum is taken into consideration, and updated for particles with minor fitness (presenting less optimum position vectors). Accordingly, Table 2 encapsulates a pseudo-code for the PSO main function.

```
clear
Population_size = 26;
Number_movements = 50;
Dimensions = 2;
⋮
[x_range,y_range] = IV_Ranges ; % call the coordinates restriction function of Eq.(14)
for i = 1: Population_size
set the position vectors for effector/witness particles
start the vector comparision of best found position vector for the particles
end
Deduce the optimum position vector after scalar comparison
Set the initial velocity vectors/weights value for APC particles
⋮
for movements = 1: Number_movements
for particle = i: Population_size
update the acceleration coefficients for the particles % as in Eqs.(16-17)
update the position vectors for witness/effector particles
update the velocity vectors for effector particles % according to Eqs.(18-19)
declare the found position vectors for each particle
if fitness( witness_particle(i)) < fitness(witness_optimum)
update the position vector for the witness particle
else if fitness( effector_particle(i)) < fitness(effector_optimum)
update the position vector for the effector particle
end
end
end
call the function plotter to plot the particles with modified velocities
```

Table 2. T1D-PSO main function pseudo-code

2. Coordinates restriction function: in this function, the particles are obliged to travel along the search space of the I-V function according to Eq.(14). Table 3 represents a pseudo-code for the 'IV_Ranges' function:

```
function [V,I] = IV_Ranges(func)
V = [0,108]
I = [0,120]
end
```

Table 3. Coordinates restriction function pseudo-code

3. Characteristic I-V curve function: the optimization function is referred to according to Eq.(5), with the corresponding reference values, having its pseudo-code represented in Table 4.

$function\ [I, ref\_value] = IV\_function(V, I)$
$[V\_range, I\_range] = IV\_Ranges(\text{func})$
$I = linspace\,(I\_range(1), I\_range(2), 101);$
$V = linspace\,(V\_range(1), V\_range(2), 101);$
⋮
$set\ xlabel$
$set\ ylabel$
⋮
$set\ the\ PVA\ parameters\ according\ to\ Table\ 1$ % define variables such as $\alpha, T_0,\ K_i, q, etc.$
$define\ a\ loop\ to\ make\ the\ \frac{G}{G_O}\ factor\ in\ Eq.(5)\ gradually\ decrease\ according\ to\ Fig.10\ while\ also\ taking\ into\ consideration\ the\ SP\ connection\ topology\ of\ the\ PVA$
$define\ the\ I-V\ function\ according\ to\ Eq.(5)$
end

Table 4. The I-V function pseudo-code

4. Population scaling function: in addition to the coordinates restriction, a population scaling function is used in this work to prevent the population (effector/witness particles) from bouncing outside of the search space (the I-V characteristic curve), which is defined by the voltage values (on the x-axis) and current values (on the y-axis). Table 5 denotes a pseudo-code for this function.

$function\ Population = Population\_scaling\,(Population, V, I)$
$Population(Population(:,1) < V(1), 1) = V(1);$
$Population(Population(:,1) > V(2), 1) = V(2);$
$Population(Population(:,2) < I(1), 2) = I(1);$
$Population(Population(:,2) > I(2), 2) = I(2);$
end

Table 5. Population scaling function pseudo-code

5. Points plotter: used to draw the motion of the effector/witness particles in scatter mode. Table 6 represents its pseudo-code.

$function\ Points = Points\_plotter(Population, points)$
$figure(1)$
cla
$hold\ on$
⋮
$points = scatter(Population(:,2), Population(:,1), \ldots, set\ marker\ face\ color, \ldots)$
$pause(0.1)$
$drawnow()$
end

Table 6. Points plotter function pseudo-code

5.1. Simulation results for Case 1

Assuming a total of twenty iterations, T1D-PSO propagation for Case 1 was intermittently paused, as the positions of the scattered points representing the particles were taken at first, tenth, fifteenth, and last iteration. This is shown in Fig. 11, Fig. 12, Fig. 13, and Fig. 14 respectively.

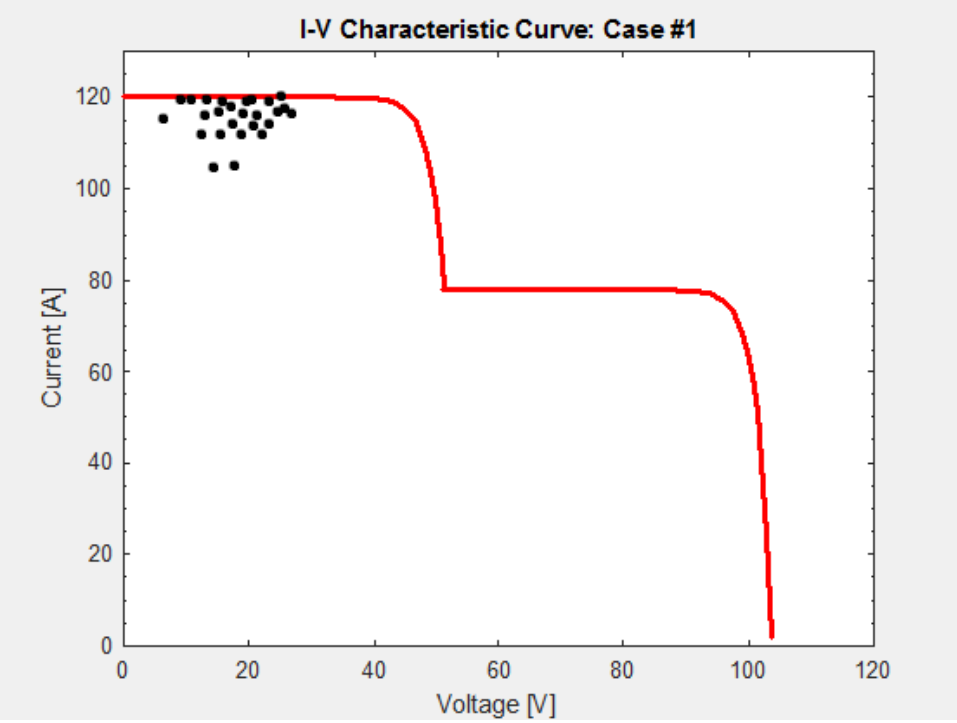

Fig. 11. Particles positioning for Case1 at the end of the first iteration

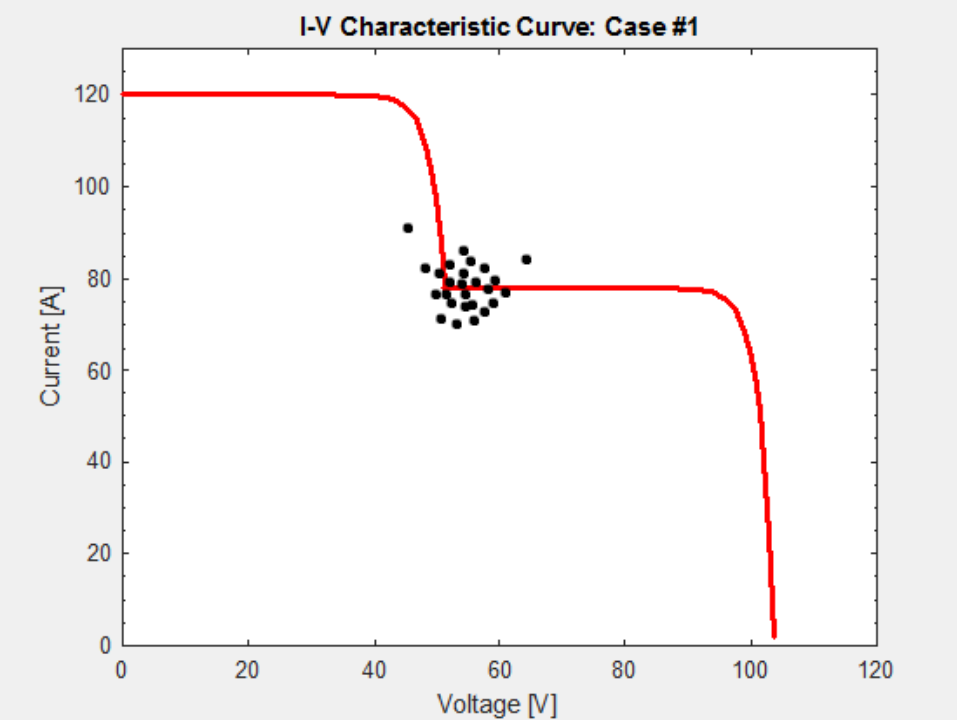

Fig. 12. Particles positioning for Case 1 at the end of the tenth iteration

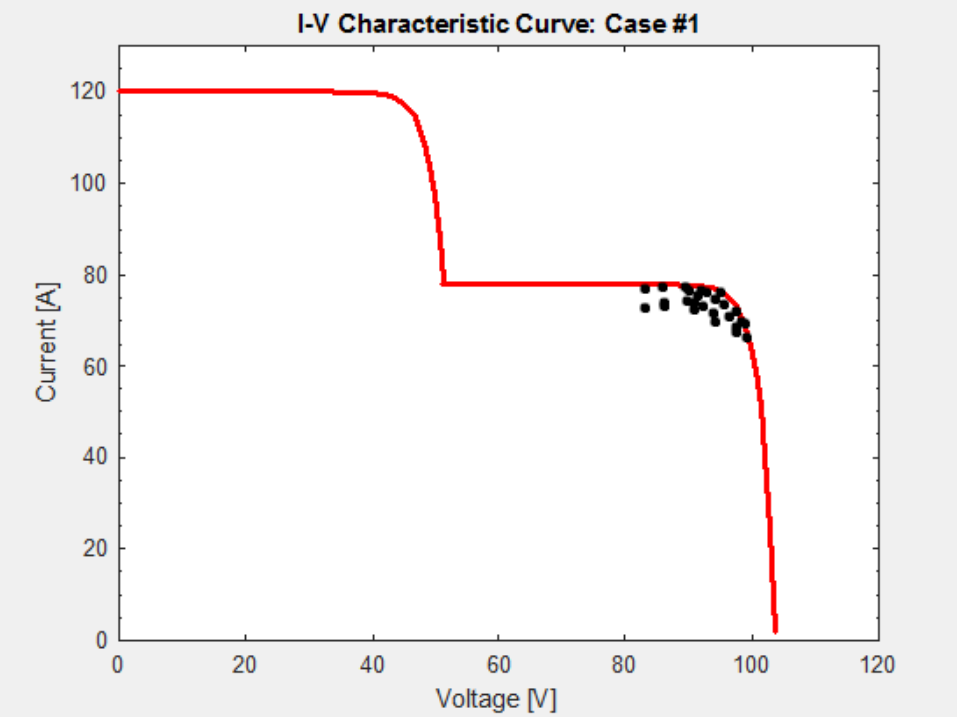

Fig. 13. Particles positioning for Case 1 at the end of the fifteenth iteration

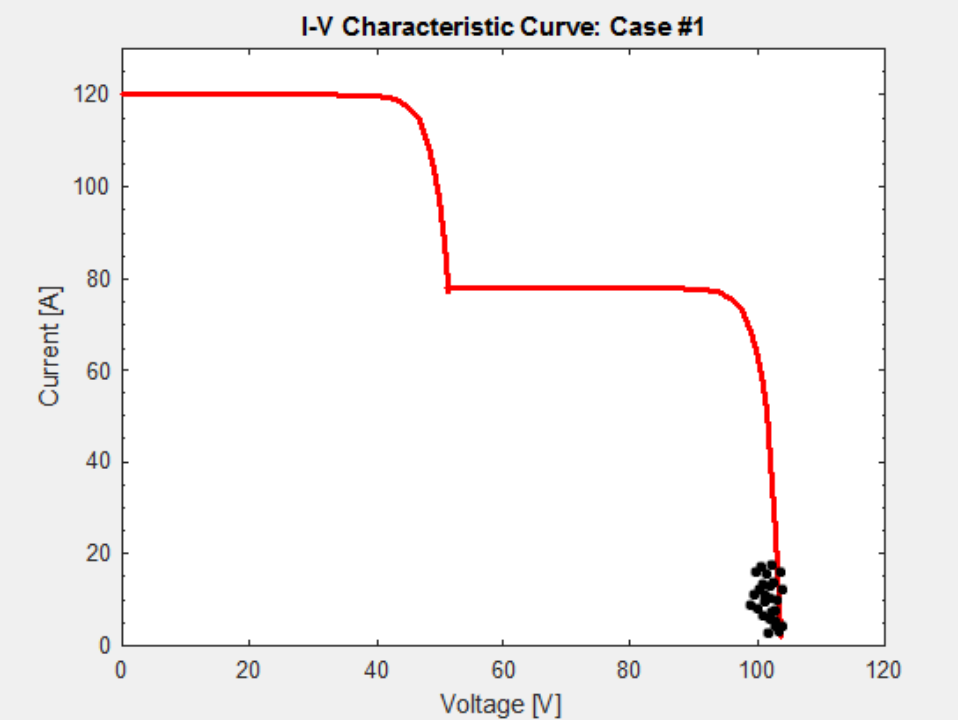

Fig. 14. Particles positioning for Case 1 upon completion of all iterations

5.2. Simulation results for Case 2

With the same number of twenty total iterations, the T1D-PSO propagation for Case 2 was intermittently paused, as the scattered points representing the positioning of the particles were taken at same iterations' time lapses of Case 1, shown respectively in Fig. 15, Fig. 16, Fig. 17, and Fig. 18.

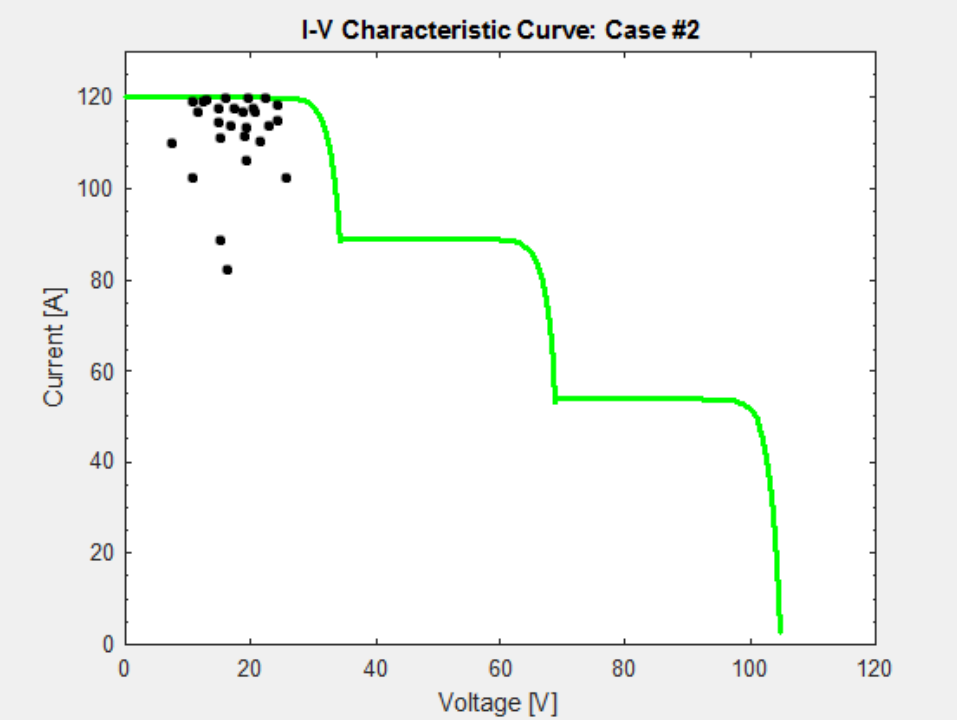

Fig. 15. Particles positioning for Case 2 upon the end of the first iteration

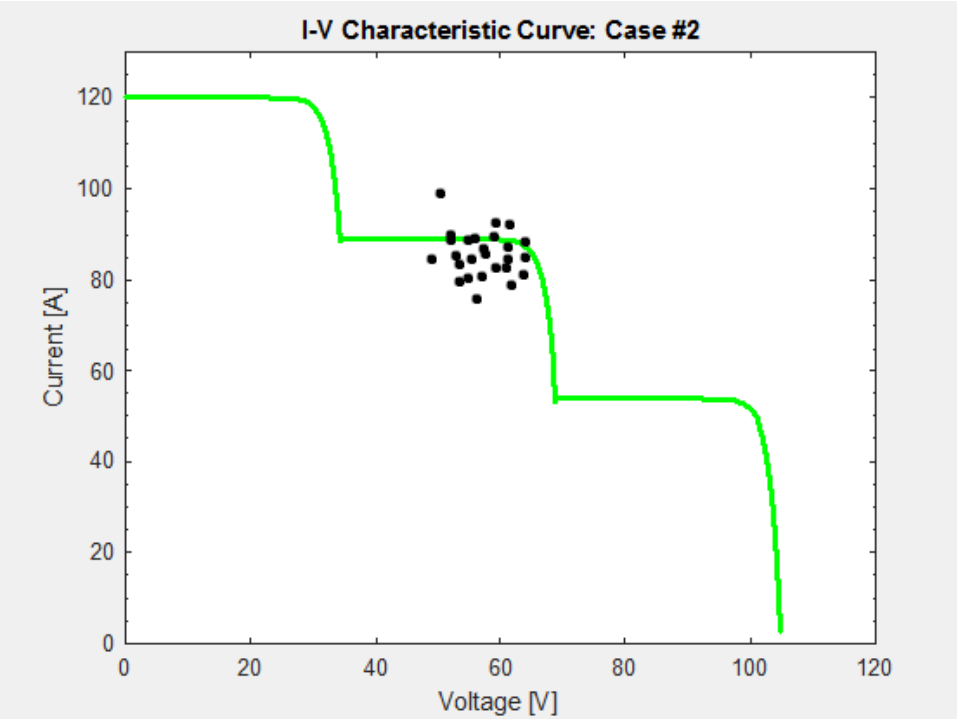

Fig. 16. Particles positioning for Case 2 upon the end of the tenth iteration

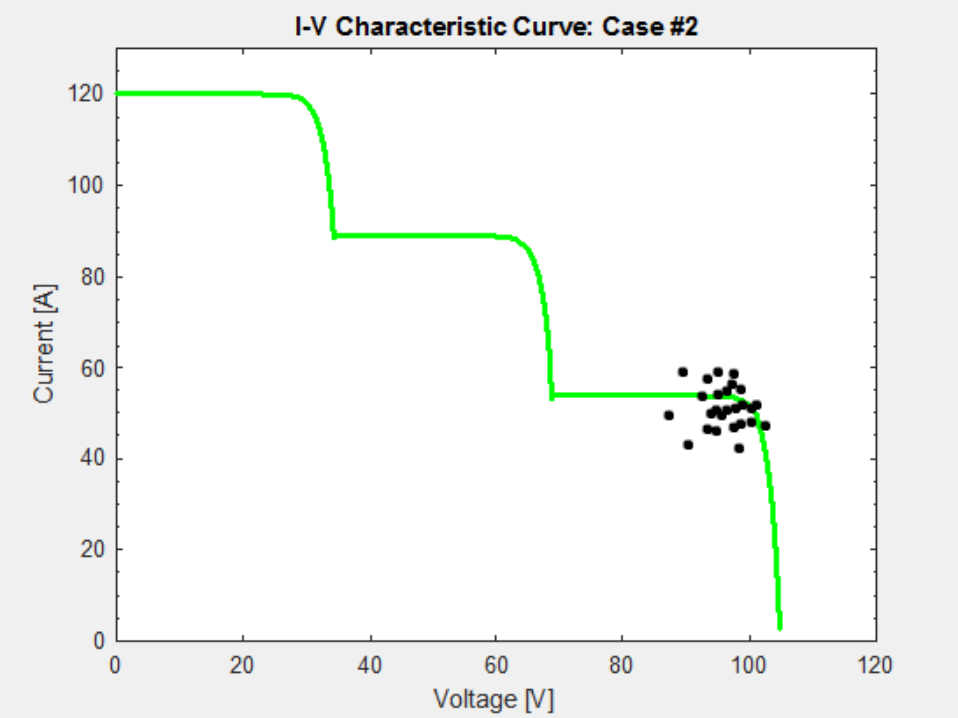

Fig. 17. Particles positioning for Case 2 upon the end of the fifteenth iteration

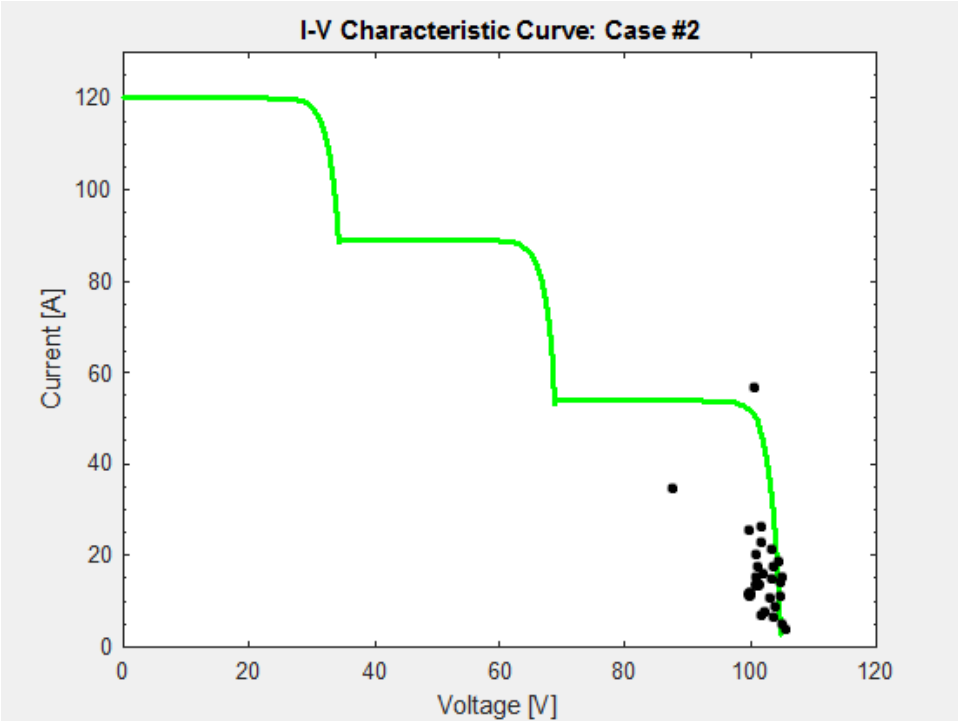

Fig. 18. Particles positioning for Case 2 upon completion of all iterations

5.3.Simulation results for Case 3

From the same perspective of Case 2 and Case 1, the T1D-PSO was intermittently paused at same iterations' milestones, where corresponding outputs are shown in Fig. 19, Fig. 20, Fig. 21, and Fig. 22.

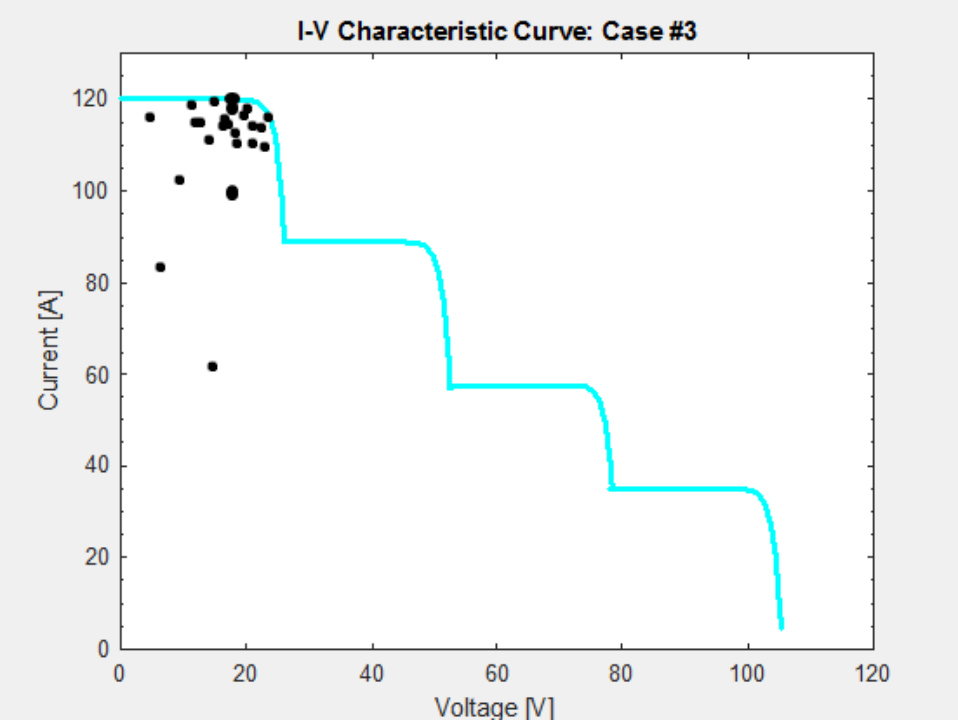

Fig. 19. Particles positioning for Case 3 upon completion of the first iteration

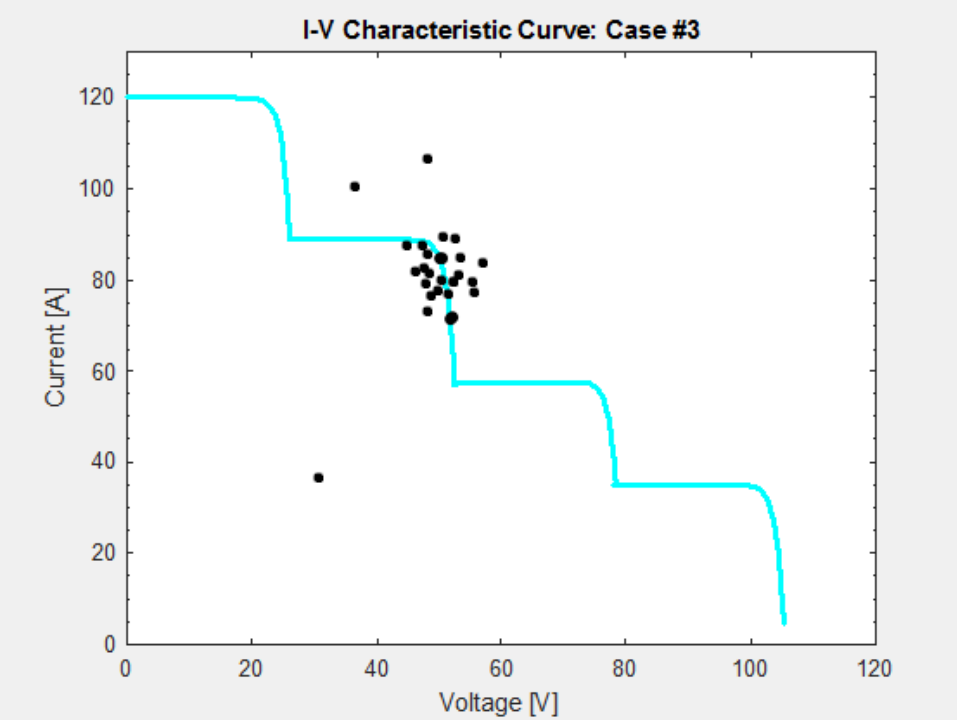

Fig. 20. Particles positioning for Case 3 upon completion of the tenth iteration

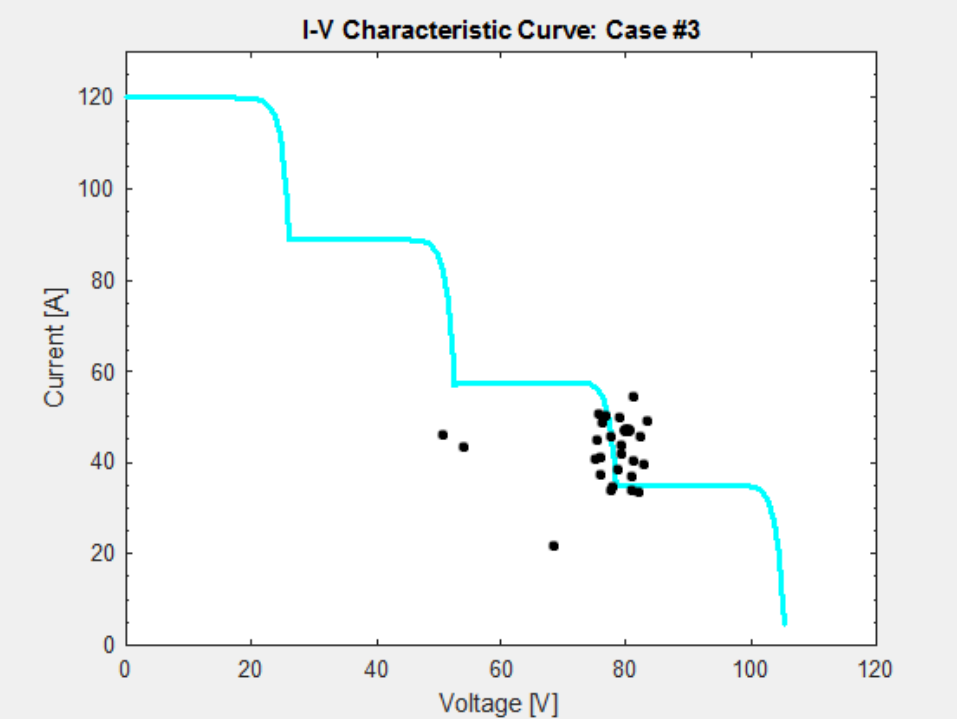

Fig. 21. Particles positioning for Case 3 upon completion of the fifteenth iteration

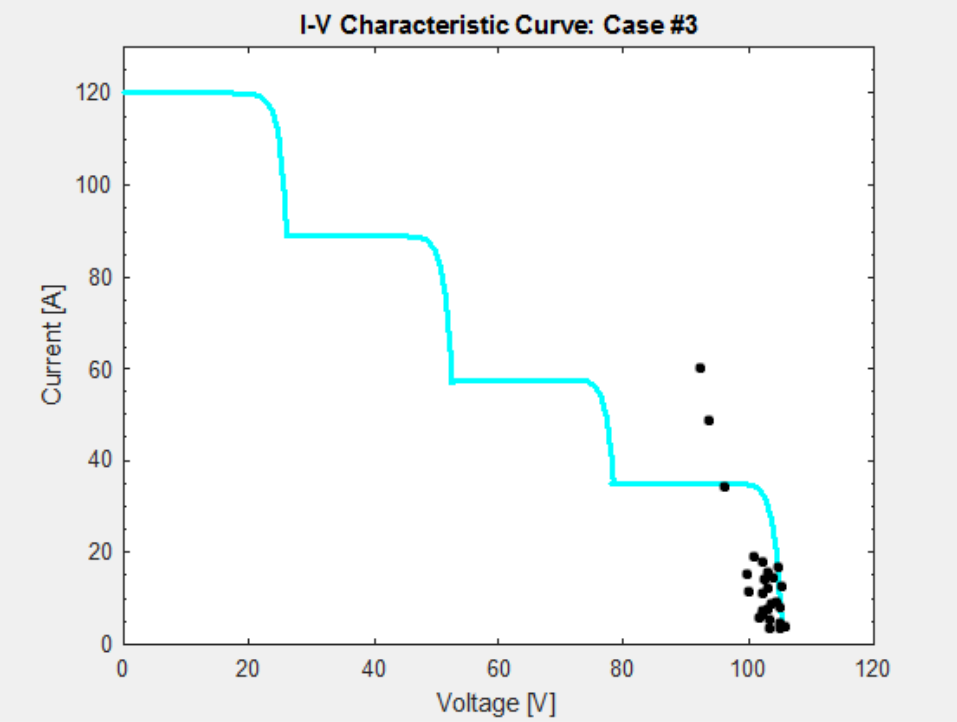

Fig. 22. Particles positioning for Case 3 upon completion of all iterations

5.4.Simulation results for Case 4

The last studied PSC, which corresponds to the apparition of five different peaks within the I-V curve and represent the closest similar to the curve in Fig. 5, have its applied T1D-PSO paused at same time lapses of all previous cases, where particles' positions are shown in Fig. 23, Fig. 24, Fig. 25, and Fig. 26.

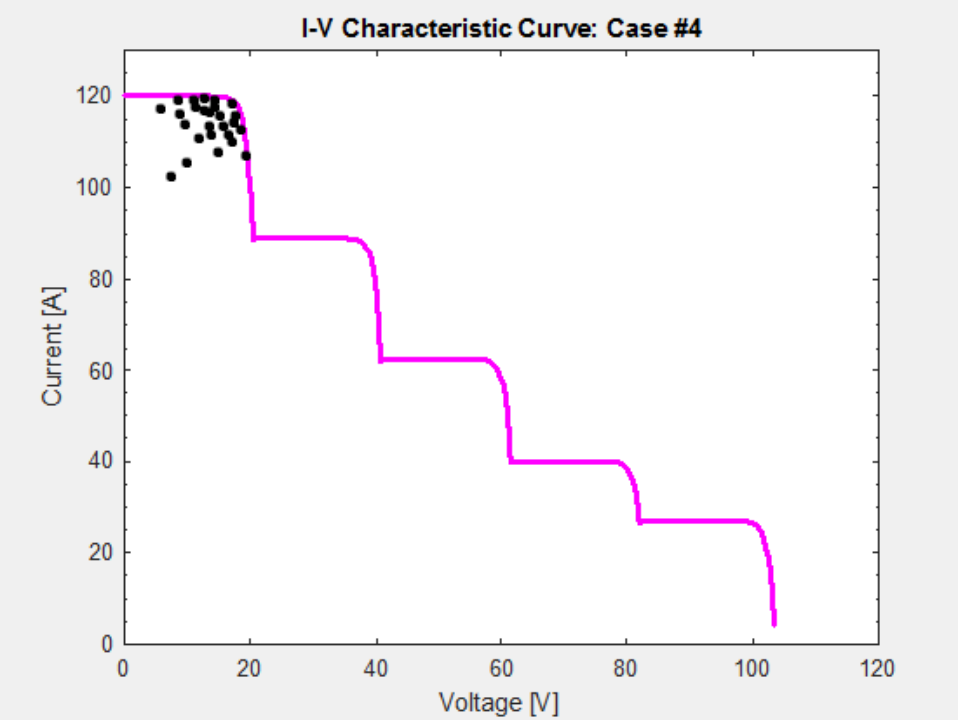

Fig. 23. Particles positioning for Case 4 upon completion of the first iteration

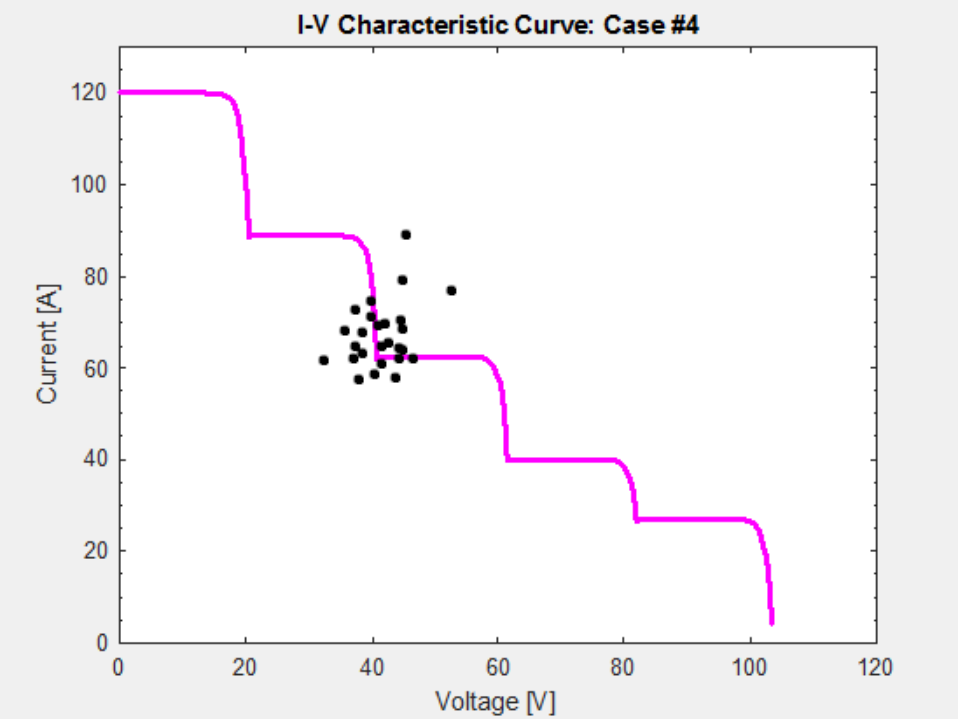

Fig. 24. Particles positioning for Case 4 upon completion of the tenth iteration

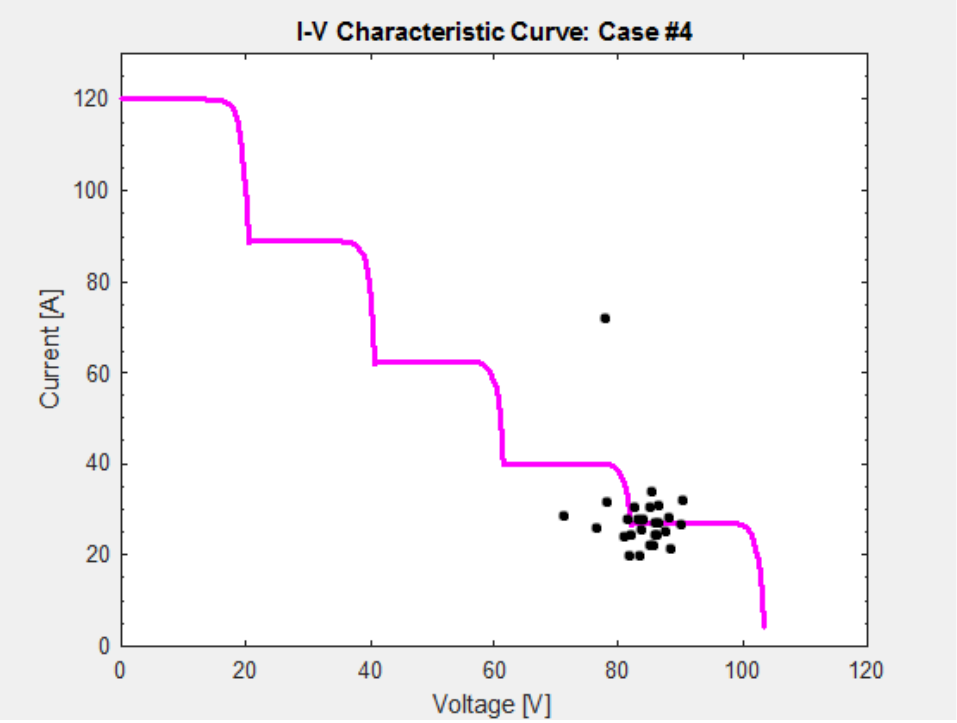

Fig. 25. Particles positioning for Case 4 upon completion of the fifteenth iteration

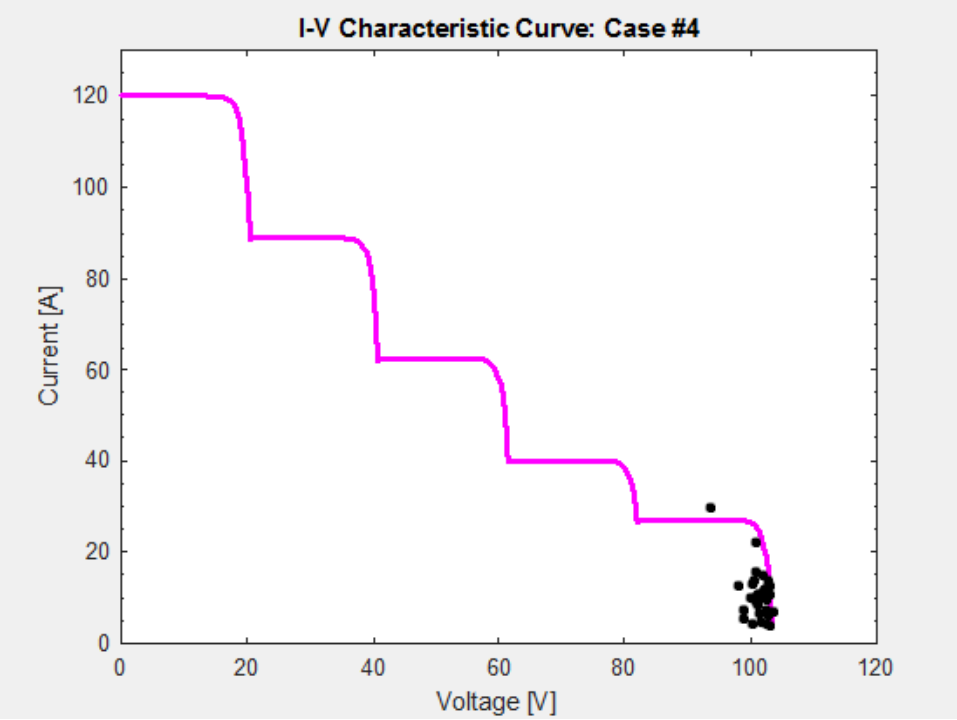

Fig. 26. Particles positioning for Case 4 upon completion of all iterations

6. Results and discussion

The analysis of the results for different PSC cases, ranging from Case 1 to Case 4, confirms that witness as well as effector particles respected the margins given for abscissas/ordinates axis. For instance, not a single particle has exceeded the border of the ordinate axis, denoted by $I_{SC} = 120$ A. From the same perspective, all particles lay to the left of the abscissas border, denoted by $V_{OC} = 108$ V. This fact supports the conclusion that no unnecessary trajectories were forced by the developed T1D-PSO algorithm, hence yielding in a better convergence, and a fast optimum search process.

Under all PSC cases, the coordination between witness and effector particles indicated a momentarily complete trace down of the entire I-V curve. This is clearly shown upon the inclusion of different paused time-lapsed iterations of the algorithm. In other words, the T1D-PSO process did not get stuck over any local peak, but instead, explored the entire region pointed by the I-V curve.

Since PSC scenarios were evolving in complexities, such that Case 1 was the simplest one (only two peaks) and Case 4 is the most complex (having biggest number of local MPPs), the criteria of algorithm's judgments (i.e., convergence accuracy, speed) were found different for each case. Table 7 encapsulates for each PSC scenario, different optimums found, the reflected efficiency, and the time needed to complete all iterations.

PSC case	Coordinates of the founded optimum $(x; y)$	Convergence accuracy [%] with respect to the reference optimum of $(108; 0)$	Execution time [s]
Case 1	$(106.22; 5.34)$	98.47%	2.403 s
Case 2	$(106.18; 5.77)$	98.45%	3.611 s
Case 3	$(105.73; 7.25)$	98.12%	4.730 s
Case 4	$(105.24; 8.77)$	97.77%	5.817 s

Table 7. Different optimums found for different PSC cases

Although the developed algorithm needs more time when confronted by more complex PSC scenarios, but still it ensures a complete I-V curve trace down, including all sampled points which constitute the curve. This in turn yields to a bigger extraction from the total available power under a certain PSC scenario, unlike the operation when a conventional MPPT gets stuck over a local MPP [19]. Therefore, the T1D-PSO offers bigger Fill Factor (*FF*), which represents the ratio of the actual maximum power to the product of voltage and current in open-circuit, short-circuit respectively upon each iteration, where the sum of all *FF* indicates an almost complete area coverage (power quantity) below the I-V curve. As an example, by taking the fourth case, Figs. 27-30 bear into consideration the same previous time lapses when pausing the flow of the algorithm, in order to check for resultant *FF*. The total extracted power is then the sum of all FF, where each *FF* represents the amount of extractable PVA's power under the investigated LMPP from the I-V curve.

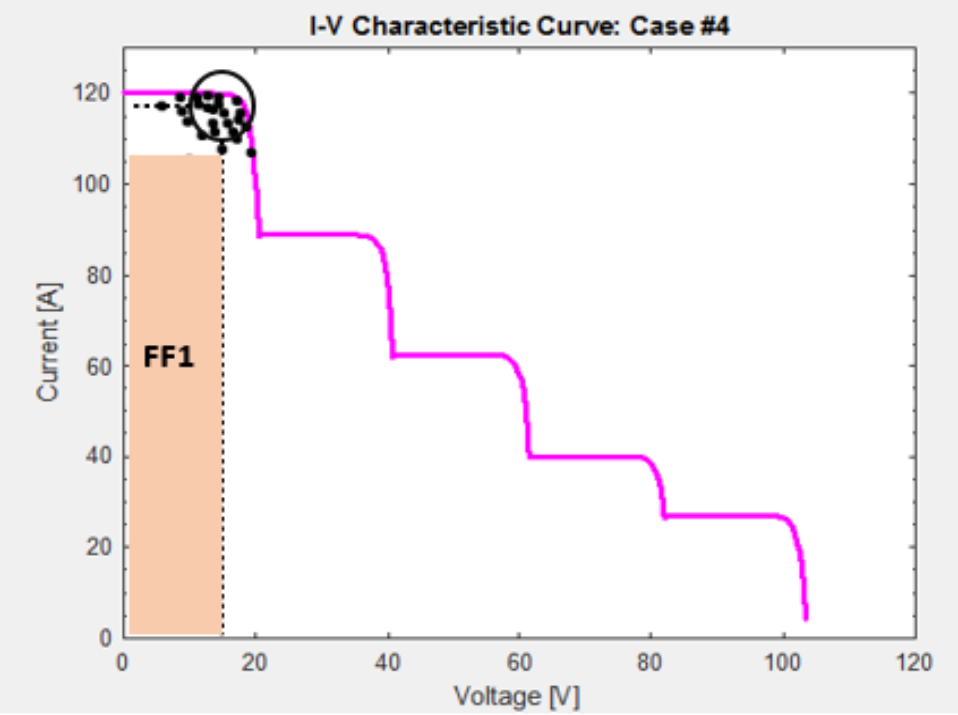

Fig. 27. Resulting fill factor from the first iteration of T1D-PSO

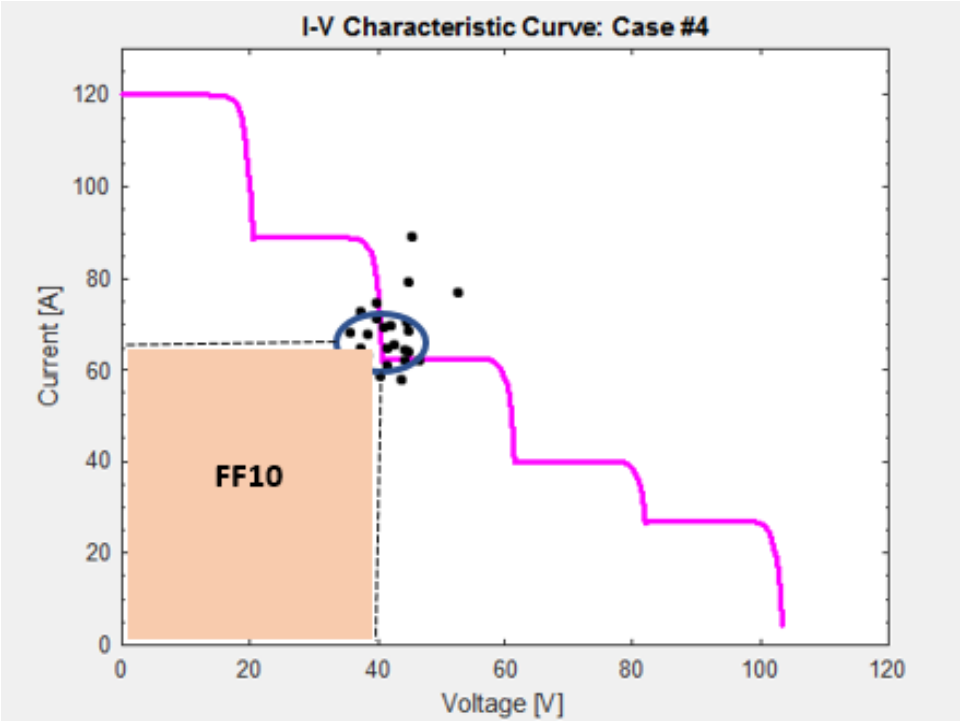

Fig. 28. Resulting fill factor from the tenth iteration of T1D-PSO

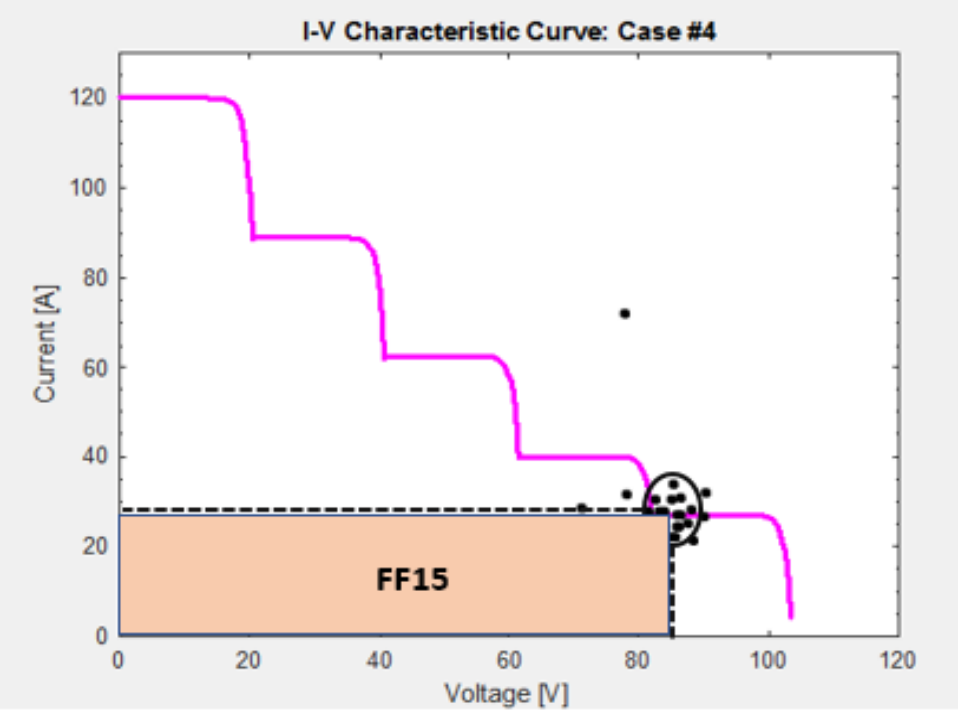

Fig. 29. Resulting fill factor from the fifteenth iteration of T1D-PSO

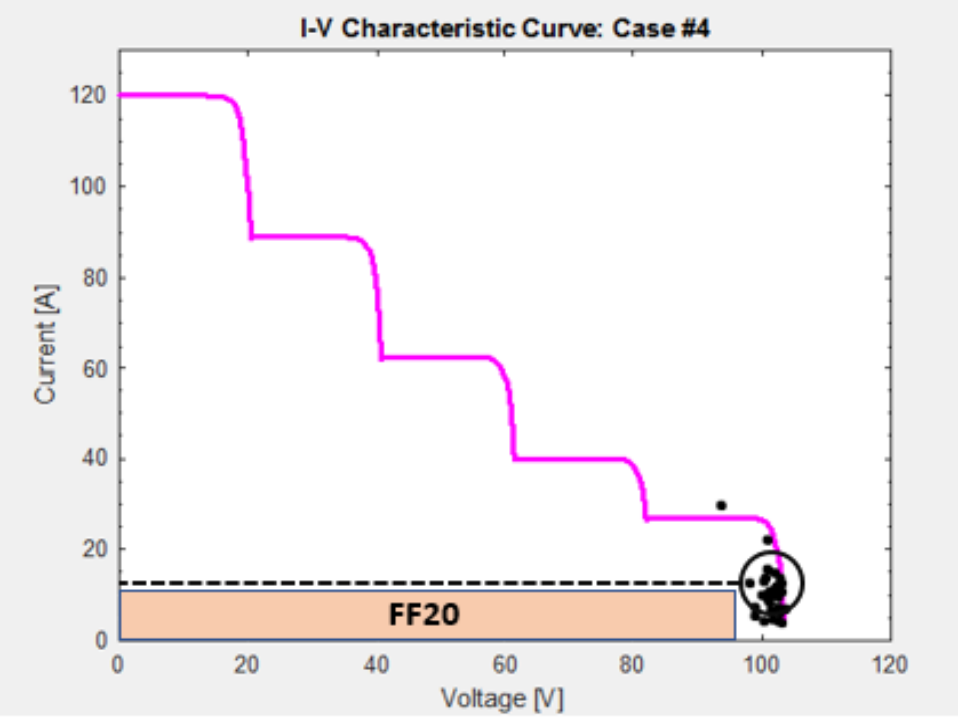

Fig. 30. Resulting fill factor from the final iteration of T1D-PSO

Upon completion of all iterations i, the resulting FF_{total}, which indicates the amount of power extracted, can be formalized as in Eq.(20).

$$FF_{total} = \sum_{i=1}^{20} FF_i \tag{20}$$

The continuity of the I-V curve under the different studied PSC cases, is momentarily discretized for each LMPP and all points which belong to that curve: at each point defined by voltage abscissa and current ordinate, exists a unique *FF*. The effect of T1D-PSO can be perceived as successive summations for the area underneath the I-V curve, represented by individual *FF*.

The stated T1D-PSO algorithm which lies under the intelligent based MPPT techniques [19], have shown superiority in extracting the maximum available power from the partially shaded PVA in terms of efficiency, execution time, and supported number of local peaks within the I-V curve.

For the execution time, and as compared with other relevant PSO modification algorithms [98-105], the highest execution time (for Case 4) is seen below 6 s, thus judged as being fast. As for the T1D-PSO efficiency η, a pseudo-code is presented in Table 8, in which different steps are presented upon its calculation: since the optimum is located at $(V_{OC}; 0)$, the modulus ratios of different found optimums $V_{optimum_i}$ and $I_{optimum_i}$ in Table 7 with respect to the modulus of the optimum coordinates represent the T1D-PSO efficiency in the referred case i of PSC, as expressed in Eq.(21). The average T1D-PSO efficiency is hence the sum of case-specified efficiencies over the total number of PSC cases, as shown in Eq.(22).

$$\eta_i = \frac{\sqrt[2]{(V_{optimum_i})^2 + \left(I_{optimum_i}\right)^2}}{\sqrt[2]{(V_{OC})^2 + (0)^2}} \tag{21}$$

$$\eta = \sum_{i=1}^{4} \frac{\eta_i}{i} \tag{22}$$

Define voltage vector: [10 20 40 60 80 110]
Define max iterations $= 20$
For iteration 1 to 20
Check whether or not the swarms are present in the i^{th} index of the voltage vector
Calculate η_i (Eq.(21))
Increase the voltage vector index
End loop when swarms have successively surpassed all voltage indices within the voltage vector
Calculate η (Eq.(22))

Table 8. Efficiency calculation procedure of T1D-PSO

The voltage vector is created in Table 3, to ensure that the particles are accurately travelling across the search space of the shaded I-V curve for all PSC scenarios, in order to avoid any

redundant calculations, and to ensure that the swarms are successively travelling across the search space from left to right without getting stuck into a LMPP. According to the stated outcomes, Table 9 presents a comparative assessment between T1D-PSO and other PSO-based MPPT techniques.

PSO-based MPPT strategy	Efficiency [%]	Execution time	Maximum number of local peaks	Ref.
T1D-PSO	$\cong 98\%$	Fast	5	Proposed
Improved PSO with reduced steady state oscillations	-	Fast	4	[98]
Improved PSO	-	Slow	4	[99]
PSO-FW	-	Moderate	2	[100]
PSO combined with Fireworks algorithm FWA	100%	Fast	3	[101]
Multicore PSO	Up to 99%	Slow	3	[102]
Accelerated PSO	Up to 99%	Fast	3	[103]
Modified PSO	-	Slow	2	[104]
PSO with modified particles initialization	$< 98\%$	Fast	3	[105]

Table 9. Performance comparison between T1D-PSO and other related MPPT techniques

As apparent from Table 9, the proposed T1D-PSO have shown a superiority in dealing with complex PSC profiles, as related to other PSO modification research. This fact can be noticed from the ability to deal with five LMPP as compared to other PSO related articles, where the range of LMPP was between two and four. With the resultant T1D-PSO efficiency (98%), regarding the PVA design shown in Fig. 9, as well as the complex and rare PSC scenarios in Fig. 10, the proposed PSO algorithm modification can be judged as flexible and resilient in front of many PSC.

When compared to the PSO modification of Ishaque *et al.* [98], the irradiance fluctuations were more extreme in this work. Unlike step changes in irradiances, the fluctuations in this work were more severe, as for the fourth case for example, the factor $\frac{G}{G_0}$ was massively decreased from 0.73 to 0.22 thus reflecting a robust performance of the proposed PSO modification in front of more complex irradiance profiles. The improved PSO work in Abdulkadir *et al.* [99] took more time to achieve the GMPP as compared to T1D-PSO.

The work of Wei *et al.* [100] did not involve extreme changing irradiance profiles, unlike the proposed T1D-PSO, where in the work of Chai *et al.* [101] the hybridization between PSO and FireWorks Algorithm (FWA) is perceived as difficult to implement, especially on the level of the balancing processes between exploration and exploitation. On the other hand, the work of Chao *et al.* [102] did not take into consideration the shading effects over large PV arrays, when compared to the 15×3 PVA studied in this work. Considering the work of Alshareef *et al.* [103], the used P&O algorithm as an accelerator for the PSO, might induce inaccurate peak identification, especially under swiftly changing irradiance conditions. The modified PSO of Rajasekar *et al.*

[104] pre-assumes initial constraints which might not always be accurate, unlike the proposed T1D-PSO which does not imply any need for initial power/environmental data, where finally, the work provided by Engel and Engel [105] did not take into consideration realistic shadowing scenarios, unlike the cases studied in this work, as illustrated in Fig. 10.

As a comparative summary between the proposed T1D-PSO and other PSO-related MPPT techniques, the developed work possesses the following advantages:

- A dynamical flexibility in front of random, and complex PSC
- An ability to counter react to a higher number of LMPP
- Less time needed to trace the I-V curve of a PV panel subject to various PSC
- Taken into consideration a large PVA design, with realistic shadowing scenarios, what makes it eligible for future hardware implementation in PV plants
- No false LMPP identifications, even under highly fluctuating irradiance conditions
- No need for initial power/environmental data attributes
- Traces the entire I-V curve, momentarily with regards to the subjected PSC, without blindly chasing a single optimum

In addition to the stated highlights, the proposed technique surpasses the complexity of chasing a GMPP, but instead, traces the entire I-V curve of the PV panel under test, from $(0, I_{SC})$ to $(V_{OC}, 0)$: all particles are forced to coincide with the I-V curve during the exploitation phase, according to the updated velocity vectors in Eq. (18) and Eq. (19). Moreover, by taking into consideration the abscissas/ordinates constriction in Eq. (14), as well as the Population scaling function in Table 5, all effector T cells particles (i.e., CD_4^+ and CD_8^+) as well as witness particles (i.e., macrophages, NK, granzymeB, etc.) are never allowed to have any position vectors outside the search space (i.e., the I-V characteristic curve). Accordingly, the stated T1D-PSO ensures a convergence towards $(V_{OC}, 0)$ in a reasonable time, which never exceeds a duration of 6 s for the most complex PSC (i.e., Case 4).

Aside than PSO-based MPPT, the stated T1D-PSO can be also compared with other MPPT schemes: for the example of the squirrel search algorithm, and regardless of the low execution time and high efficiency of the proposed model, it was only tested under three LMPP [106]. Accordingly, the T1D-PSO would perform in a more robust discipline in front of more complex PSC, with its workflow requiring less data initialization, such as the Levy flight and other parameters as in [106]. The radial basis function network MPPT algorithm on the other hand, requires a two-stage procedure training, in order to determine the final-layer units' weights [107]. This fact can be perceived as a computational complexity, where the T1D-PSO algorithm does not require any training procedures to converge towards the optimum, but instead it only updates the velocity vectors of the assigned particles. From another side, the MPPT algorithm in [108] utilizes a fuzzy positioning mechanism to determine the local neighborhoods of a GMPP, then succeed the searching phase with a modified Cuckoo Search algorithm, to establish local/global modes of GMPP locating. Such scheme can be regarded as computationally complex, and difficult to implement. The proposed T1D-PSO instead simply implies a jumping-jack between the inertia weights of effector/witness particles, to ensure a compatible, mutual, and smooth surfing of the entire I-V curve.

7. Conclusion and future work

Although the accurate causals for T1D evolution are medically not confirmed, still its pathogenic mechanisms can be approximated to PSC, hence the complete I-V curve tracing for a PVA. The momentarily point-wise curve tracing yields in turn to a maximum power exploration from the partially shaded PVA. Unlike nature-inspired MPPT algorithms, such as APA, MAKWO, ICSO, etc. the AI-based T1D-PSO algorithm is achieved after a focused study of a particular autoimmune disease, the T1D. The behavior of biological immunocytes, which destruct the β cells, is mimicked and applied onto a conventional PSO, leading to a complete exploration of the PV characteristic curve. This fact elevates the rank of novelty behind this work.

Unlike the conventional PSO algorithm's workflow progress, the unified swarm of particles is decomposed into two main entities, the CD_4^+ and CD_8^+ effector T cells. Aside, exist the standalone witness particles, which refer to APC, the mediators of cellular immune response during T1D development. The witness particles serve as messengers (to inform about the best found locations during the exploration phase), that when coordinated with effector particles, ensure a smooth and convergent trajectory along the I-V curve. By adapting a continuous dynamic modification processes for inertia weights, cognitive and social coefficients, for witness as well as effector particles, the overall final particles' trajectory converges toward the reference destination. This is done after ensuring that all zones of the I-V curve are examined. The robustness of the developed algorithm is ensured after its exposition to five different local peaks within the I-V curve. Its overall propagation was smooth with a fast execution time: the maximum held 5.817 s where its efficiency was solid in front of different PSC, exceeding 98% in most cases. The chosen PSC patterns indicate that the developed T1D-PSO algorithm can compensate the effects of having inhomogeneous shading across the PVA. In other words, this algorithm is practical versus almost any PSC pattern. When compared to similar PSO-based MPPT, T1D-PSO achieved superior efficiencies when confronted with a maximum number of Local Maximum Power Points (LMPP).

Apart of present results achieved by this work, it also serves as a rich background for real-case PV MPPT applications: the exocytosis phenomenon conducted by APC/effector T cells, such as the release of Perforin, NO, H_2O_2, etc. which chemically destroy the β cells can be reflected as the exploitation phase of this algorithm: generation of duty ratios that govern the operations of power processing units, such as DC-DC non-isolated buck/boost converters. At each iteration, under different PSC, the dynamic particles re-positioning, according to the newly found optimum, is transposed into a dynamic generation of duty cycles, hence when actuated by the converter, a maximum power is actually harvested from the PVA. Since a hardware implementation was not the objective behind this paper, the T1D-PSO algorithm can be coded into a microcontroller as a future work, that when accompanied by a suitable DC-DC converter, would present a novel real-world PV MPPT prototype. However, the exact outcomes (in terms of efficiency and execution time) of the recommended future work for the T1D-PSO algorithm into a hardware application cannot be accurately predicted, since the algorithm execution's performance will be related to the hardware configuration (i.e., processing memory, conversion channel resolution, data registers, etc.), and the suitability of the designed DC-DC converter.

References

[1] Walker G, Simcock N, Day R. Necessary energy uses and a minimum standard of living in the United Kingdom: Energy justice or escalating expectations? Energy Research & Social Science. 2016;18:129-38. https://doi.org/10.1016/j.erss.2016.02.007

[2] Fini MA, Gharapetian D, Asgari M. Efficiency improvement of hybrid PV-TEG system based on an energy, exergy, energy-economic and environmental analysis; experimental, mathematical, and numerical approaches. Energy Conversion and Management. 2022;265:e115767. https://doi.org/10.1016/j.enconman.2022.115767

[3] Yang XJ, Hu H, Tan T, Li J. China's renewable energy goals by 2050. Environmental Development. 2016;20:83-90. https://doi.org/10.1016/j.envdev.2016.10.001

[4] Liu Lq, Wang Zx, Zhang Hq, Xue Yc. Solar energy development in China-A review. Renewable and Sustainable Energy Reviews. 2010;14(1):301-11. https://doi.org/10.1016/j.rser.2009.08.005

[5] Osmani K, Haddad A, Lemenand T, Castanier B, Ramadan M. A review on maintenance strategies for PV systems. Science of the Total Environment. 2020;746:e141753. https://doi.org/10.1016/j.scitotenv.2020.141753

[6] Osmani K, Haddad A, Lemenand T, Castanier B, Ramadan M. Material Based Fault Detection Methods for PV Systems. Key Engineering Materials. 2020;856:111-5. https://doi.org/10.4028/www.scientific.net/KEM.865.111

[7] Osmani K, Ramadan M, Lemenand T, Castanier B, Haddad A. Optimization of PV array tilt angle for minimum levelized cost of Energy. Computers & Electrical Engineering. 2021;96(Part A):e107474. https://doi.org/10.1016/j.compeleceng.2021.107474

[8] Li G, Shittu S, Diallo TMO, Yu M, Zhao X, Ji J. A review of solar photovoltaic-thermoelectric hybrid system for electricity generation. Energy. 2018;158:41-58. https://doi.org/10.1016/j.energy.2018.06.021

[9] Liu Z, Zhang Y, Yuan X, Liu Y, Xu J, Zhang S, et al. A comprehensive study of feasibility and applicability of building integrated photovoltaic (BIPV) systems in regions with high solar irradiance. Journal of Cleaner Production. 2021;307:e127240. https://doi.org/10.1016/j.jclepro.2021.127240

[10] Jager-Waldau A, Kougias I, Taylor N, Thiel C. How photovoltaics can contribute to GHC emission reductions of 55% in the EU by 2030. Renewable and Sustainable Energy Reviews. 2020;126:e109836. https://doi.org/10.1016/j.rser.2020.109836

[11] Al-Subhi A. Parameters estimation of photovoltaic cells using simple and efficient mathematical models. Solar Energy. 2020;209:245-57. https://doi.org/10.1016/j.solener.2020.08.079

[12] Osmani K, Haddad A, Jaber H, Lemenand T, Castanier B, Ramadan M. Mitigating the effects of partial shading on PV system's performance through PV array reconfiguration: A review. Thermal Science and Engineering Progress. 2022;31:e101280. https://doi.org/10.1016/j.tsep.2022.101280

[13] Raina G, Sinha S. A comprehensive assessment of electrical performance and mismatch losses in bifacial PV module under different front and rear side shading scenarios. Energy Conversion and Management. 2022;261:e115668. https://doi.org/10.1016/j.enconman.2022.115668

[14] Sizkouhi AMM, Esmailifar SM, Aghaei M, Karimkhani M. RoboPV: An integrated software package for autonomous aerial monitoring of large scale PV plants. Energy

Conversion and Management. 2022;254:e115217. https://doi.org/10.1016/j.enconman.2022.115217
[15] Li C, Yang Y, Zhang K, Zhu C, Wei H. A fast MPPT-based anomaly detection and accurate fault diagnosis technique for PV arrays. Energy Conversion and Management. 2021;234:e113950. https://doi.org/10.1016/j.enconman.2021.113950
[16] Yang B, Ye H, Wang J, Li J, Wu S, Li Y, et al. PV arrays reconfiguration for partial shading mitigation: Recent advances, challenges and perspectives. Energy Conversion and Management. 2021;247:e114738. https://doi.org/10.1016/j.enconman.2021.114738
[17] Reddy AKVK, Narayana KVL. Investigation of a social group assisted differential evolution for the optimal PV parameter extraction of standard and modified diode models. Energy Conversion and Management. 2022;268:e115955. https://doi.org/10.1016/j.enconman.2022.115955
[18] Altwallbah NMM, Radzi MAM, Azis N, Shafie S, Zainuri MAAM. New perturb and observe algorithm based on trapezoidal rule: Uniform and partial shading conditions. Energy Conversion and Management. 2022;264:e115738. https://doi.org/10.1016/j.enconman.2022.115738
[19] Osmani K, Haddad A, Lemenand T, Castanier B, Ramadan M. An investigation on maximum power extraction algorithms from PV systems with corresponding DC-DC converters. Energy. 2021;224:e120092. https://doi.org/10.1016/j.energy.2021.120092
[20] Wu Z, Yu D, Kang X. Application of improved chicken swarm optimization for MPPT in photovoltaic system. Optimal Control Applications and Methods. 2018;39:1029–42. https://doi.org/10.1002/oca.2394
[21] Guo L, Meng Z, Sun Y, Wang L. A modified cat swarm optimization based maximum power point tracking method for photovoltaic system under partially shaded condition. Energy. 2018;144:501-14. https://doi.org/10.1016/j.energy.2017.12.059
[22] Li LL, Lin GQ, Tseng ML, Tan K, Lim MK. A maximum power point tracking method for PV system with improved gravitational search algorithm. Applied Soft Computing. 2018;65:333-48. https://doi.org/10.1016/j.asoc.2018.01.030
[23] Tey KS, Mekhlief S, Seyedmahmoudian M, Horan B, Oo AT, Stojcevski A. Improved differential evolution-based MPPT algorithm using SEPIC for PV systems under partial shading conditions and load variation. IEEE Transactions on Industrial Informatics. 2018;14:4322–33. https://doi.org/10.1109/TII.2018.2793210
[24] Sen T, Pragallapati N, Agarwal V, Kumar R. Global maximum power point tracking of PV arrays under partial shading conditions using a modified particle velocity-based PSO technique. IET Renewable Power Generation. 2018;12:555–64. https://doi.org/10.1049/iet-rpg.2016.0838
[25] Yang XS. Firefly Algorithms for Multimodal Optimization. In: Watanabe, O., Zeugmann, T. (eds) Stochastic Algorithms: Foundations and Applications. Lecture Notes in Computer Science, Berlin: Springer; 2009, p. 169–78. http://doi.org/10.1007/978-3-642-04944-6_14
[26] Peng BR, Ho KC, Liu YH. A novel and fast MPPT method suitable for both fast changing and partially shaded conditions. IEEE Transactions on Industrial Informatics. 2017;65(4):3240-51. https://doi.org/10.1109/TIE.2017.2736484
[27] Mirjalili S. Moth-flame optimization algorithm: a novel nature-inspired heuristic paradigm. Knowledge Based Systems. 2015;89:228–49. https://doi.org/10.1016/j.knosys.2015.07.006

[28] Gupta S, Saurabh K. Artificial Mountain Ape Optimization Algorithm for Maximum Power Point Tracking under Partial Shading Condition. 2017 International Conference on Energy, Communication, Data Analytics and Soft Computing (ICECDS). 2017, p. 1-6. http://doi.org/10.1109/ICECDS.2017.8389547
[29] Gharehchopog FS, Gholizadeh H. A comprehensive survey: Whale Optimization Algorithm and its applications. Swarm and Evolutionary Computation. 2019;48:1-24. https://doi.org/10.1016/j.swevo.2019.03.004
[30] Rocha MV, Sampaio LP, Oliveira da Silva SA. Maximum Power Point Extraction in PV Array Under Partial Shading Conditions Using GWO-Assisted Beta Method. Renewable Energies and Power Quality Journal. 2018;1:450–55. https://doi.org/10.24084/repqj16.346
[31] Daraban S, Petreus D, Morel C. A novel MPPT (maximum power point tracking) algorithm based on a modified genetic algorithm specialized on tracking the global maximum power point in photovoltaic systems affected by partial shading. Energy. 2014;74:374–88. https://doi.org/10.1016/j.energy.2014.07.001
[32] Goud JS, Kalpana R, Singh B. A hybrid global maximum power point tracking technique with fast convergence speed for partial-shaded PV systems. IEEE Transactions on Industry Applications. 2018;54:5367-76. https://doi.org/10.1109/TIA.2018.2845415
[33] Shi JY, Zhang DY, Ling LT, Xue F, Li YJ, Qin ZJ, et al. Dual-algorithm maximum power point tracking control method for photovoltaic systems based on grey wolf optimization and golden-section optimization. Journal of power electronics. 2018;3:841-52. https://doi.org/10.6113/JPE.2018.18.3.841
[34] Li H, Yang D, Su W, Lu J, Yu X. An overall Distribution Particle Swarm Optimization MPPT Algorithm for Photovoltaic System Under Partial Shading. IEEE Transactions on Industrial Electronics. 2018 ;66(1):265-75. https://doi.org/10.1109/TIE.2018.2829668
[35] Anoop K, Nandakumar M. A novel maximum power point tracking method based on particle swarm optimization combined with one cycle control. International Conference on Power, Instrumentation, Control and Computing (PICC). 2018, p. 1-6. https://doi.org/10.1109/PICC.2018.8384777
[36] Başoğlu ME, Cakir B. Hybrid global maximum power point tracking approach for photovoltaic power optimizers. IET Renewable Power Generation. 2018;12:875-82. https://doi.org/10.1049/iet-rpg.2018.0029
[37] Chen L, Wang X. Enhanced MPPT method based on ANN-assisted sequential Monte-Carlo and quickest change detection. IET Smart Grid. 2019;2(4):635-44. https://doi.org/10.1049/iet-stg.2019.0012
[38] Lee CT, Tsou HI, Chou TH, Weng KW. Application of the hybrid Taguchi genetic algorithm to maximum power point tracking of photovoltaic system. Proceedings of the IEEE International Conference on Applied System Innovation (ICASI). 2018, p. 231–34. https://doi.org/10.1109/ICASI.2018.8394575
[39] Said SZ. Maximum power point tracking of photovoltaic generators partially shaded using a hybrid artificial neural network and particle swarm optimization algorithm. International Journal of Energy and Power Engineering. 2017;66:91–9. https://doi.org/10.11648/j.ijepe.20170606.12
[40] Jiang S, Ji Z, Shen Y. A novel hybrid particle swarm optimization and gravitational search algorithm for solving economic emission load dispatch problems with various

practical constraints. International Journal of Electrical Power & Energy Systems. 2014;55:628-44. https://doi.org/10.1016/j.ijepes.2013.10.006
[41] Eltamaly AM, Farh HMH. Dynamic global maximum power point tracking of the PV systems under variant partial shading using hybrid GWO-FLC. Solar Energy. 2019;177:306-16. https://doi.org/10.1016/j.solener.2018.11.028
[42] Huang C, Wang L, Long H, Luo X, Wang JH. A hybrid global maximum power point tracking method for photovoltaic arrays under partial shading conditions. Optik. 2019;180:665-74. https://doi.org/10.1016/j.ijleo.2018.11.158
[43] Ghasemi MA, Ramyar A, Iman-Eini H. MPPT method for PV systems under partially shaded conditions by approximating I-V curve. IEEE Transactions on Industrial Electronics. 2017;65(5):3966–75. https://doi.org/10.1109/TIE.2017.2764840
[44] Aquib M, Jain S. A global maximum power point tracking technique based on current source region detection of I-V curve. IEEE, Proceedings of the IEEMA Engineer Infinite Conference (eTechNxT). 2018, p. 1-5. https://doi.org/10.1109/ETECHNXT.2018.8385346
[45] Furtado AMS, Bradaschia F, Cavalcanti MC, Limongi LR. A reduced voltage range global maximum power point tracking algorithm for photovoltaic systems under partial shading conditions. IEEE Transactions on Industrial Electronics. 2017;65(4):3252–62. https://doi.org/10.1109/TIE.2017.2750623
[46] Li X, Wen H, Chu G, Hu Y, Jiang L. A novel power-incremented based GMPPT algorithm for PV arrays under partial shading conditions. Solar Energy. 2018;169:353-61. https://doi.org/10.1016/j.solener.2018.04.055
[47] Ramana VV, Mudlapur A, Damodaran RV, Venkatesaperumal B, Mishra S. Efficient global peak tracking of PV system under mismatching conditions using searching technique and bisection method. IEEMA Engineer Infinite Conference (eTechNxT). 2018, p. 1-6. https://doi.org/10.1109/ETECHNXT.2018.8385358
[48] Başoğlu ME. An enhanced scanning based MPPT approach for DMPPT systems. International Journal of Electronics. 2018;105(12):2066-81. https://doi.org/10.1080/00207217.2018.1494332
[49] Belhachat F, Larbes C. Comprehensive review on global maximum power point tracking techniques for PV systems subjected to partial shading conditions. Solar Energy. 2019;183:476-500. https://doi.org/10.1016/j.solener.2019.03.045
[50] Keyrouz F. Enhanced Bayesian Based MPPT Controller for PV Systems. IEEE Power and Energy Technology Systems Journal. 2018;5(1):11-7. https://doi.org/10.1109/JPETS.2018.2811708
[51] Martin AD, Vasquez JR, Cano JM. MPPT in PV systems under partial shading conditions using artificial vision. Electric Power Systems Research. 2018;162:89–98. https://doi.org/10.1016/j.epsr.2018.05.005
[52] Selvakumar S, Madhusmita M, Koodalsamy C, Simon SP, Sood YR. High-speed maximum power point tracking module for PV systems. IEEE Transactions on Industrial Electronics. 2018;66(2):1119–29. https://doi.org/10.1109/TIE.2018.2833036
[53] Winston DP, Kumar BP, Christabel SC, Chamkha AJ, Sathyamurthy R. Maximum power extraction in solar renewable power system- a bypass diode scanning approach. Computers & Electrical Engineering. 2018;70:122–36. https://doi.org/10.1016/j.compeleceng.2018.02.034

[54] Ahmed J, Salam Z. An Enhanced Adaptive P&O MPPT for Fast and Efficient Tracking Under Varying Environmental Conditions. IEEE Transactions on Sustainable Energy. 2018;9(3):1487-96. https://doi.org/10.1109/TSTE.2018.2791968
[55] Ashouri-Zadeh A, Toulabi M, Dobakhshari AS, Taghipour-Broujeni S, Ranjbar AM. A novel technique to extract the maximum power of photovoltaic array in partial shading conditions. International Journal of Electrical Power & Energy Systems. 2018;101:500–12. https://doi.org/10.1016/j.ijepes.2018.03.035
[56] Yousri D, Babu TS, Allam D, Ramachandaramurthy VK, Etiba MB. A Novel Chaotic Flower Pollination Algorithm for Global Maximum Power Point Tracking for Photovoltaic System Under Partial Shading Conditions. IEEE Access. 2019;7:121432-45. https://doi.org/10.1109/ACCESS.2019.2937600
[57] Yang B, Wang J, Zhang X, Yu T, Yao W, Shu H, et al. Comprehensive overview of meta-heuristic algorithm applications on PV cell parameter identification. Energy Conversion and Management. 2020;208:e112595. https://doi.org/10.1016/j.enconman.2020.112595
[58] Manjunath, Suresh HN, Rajanna S. Reduction of mislead power and mismatch power loss under partial shading conditions using novel square matrix shade dispersion technique. Solar Energy. 2020;207:1364-83. https://doi.org/10.1016/j.solener.2020.07.036
[59] Delli AJ, Lernmark A. Chapter 39 – Type 1 (Insulin-Dependent) Diabetes Mellitus: Etiology, Pathogenesis, Prediction, and Prevention. Endocrinology: Adult and Pediatric (Seventh Edition). 2016, p. 672-90. https://doi.org/10.1016/B978-0-323-18907-1.00039-1
[60] Adi S, Gerard-Gonzalez A. Chapter 1 – Type 1 Diabetes Mellitus: An Overview. Nutritional Therapeutic Interventions for Diabetes and Metabolic Syndrome (Second Edition). Academic Press. 2018, p. 3-13. https://doi.org/10.1016/B978-0-12-812019-4.00001-5
[61] Pearson JA, Wong FS, Wen L. The importance of the Non Obese Diabetic (NOD) mouse model in autoimmune diabetes. Journal of Autoimmunity. 2016;66:76-88. https://doi.org/10.1016/j.jaut.2015.08.019
[62] Bresson D, von Herrath M. Mechanisms underlying type 1 diabetes. Drug Discovery Today: Disease Mechanisms. 2004;1(3):321-7. https://doi.org/10.1016/j.ddmec.2004.11.015
[63] Thomsen SK, Gloyn AL. The pancreatic β cell: recent insights from human genetics. Trends in Endocrinology & Metabolism. Cell Press. 2014;25(8):425-34. https://doi.org/10.1016/j.tem.2014.05.001
[64] Chen C, Cohrs CM, Stretmann J, Bozsak R, Speier S. Human beta cell mass and function in diabetes: Recent advances in knowledge and technologies to understand disease pathogenesis. Molecular Metabolism. 2017;6(9):943-57. https://doi.org/10.1016/j.molmet.2017.06.019
[65] Talchai C, Xuan S, Lin HV, Sussel L, Accili D. Pancreatic β Cell Dedifferentiation as a Mechanism of Diabetic β Cell Failure. Cell. 2012;150(6):1223-34. https://doi.org/10.1016/j.cell.2012.07.029
[66] Wieland FC, van Blitterswijk CA, van Apeldoorn A, LaPointe VLS. The functional importance of the cellular and extracellular composition of the islets of Langerhans.

Journal of Immunology and Regenerative Medicine. 2021;13:e100048. https://doi.org/10.1016/j.regen.2021.100048
[67] Carrero JA, Ferris ST, Unanue ER. Macrophages and dendritic cells in islets of Langerhans in diabetic autoimmunity: a lesson on cell interactions in a mini-organ. Current Opinion in Immunology. 2016;43:54-9. https://doi.org/10.1016/j.coi.2016.09.004
[68] Gu Y, Merriman C, Guo Z, Jia X, Wenzlau J, Li H, et al. Novel antibodies to the β-Cell surface epitope of ZnT8 in patients progressing to type-1 diabetes. Journal of Autoimmunity. 2021;122:e102677. https://doi.org/10.1016/j.jaut.2021.102677
[69] Boitard C. T-lymphocyte recognition of beta cells in type 1 diabetes: Clinical perspectives. Diabetes & Metabolism. 2013;39(6):459-66. https://doi.org/10.1016/j.diabet.2013.08.001
[70] Tang St, Tang Hq, Zhang Q, Wang Cj, Wang Ym, Peng Wj. Association of cytotoxic T-lymphocyte associated antigen 4 gene polymorphism with type 1 diabetes mellitus: A meta-analysis. Gene. 2012;508(2):165-87. https://doi.org/10.1016/j.gene.2012.07.044
[71] Getts DR, Getts MT, King NJC, Miller SD. Chapter 19 – Infectious Triggers of T Cell Autoimmunity. The Autoimmune Diseases (Fifth Edition). Academic Press. 2014, p. 263-74. https://doi.org/10.1016/B978-0-12-384929-8.00019-8
[72] Falta MT, Fontenot AP. Antigen Processing and Presentation. Comprehensive Toxicology (Second Edition). 2010;5:285-97. https://doi.org/10.1016/B978-0-08-046884-6.00616-3
[73] King TC. Inflammation, Inflammatory Mediators, and Immune-Mediated Disease. Elsevier's Integrated Pathology. 2007, p. 21-57. https://doi.org/10.1016/B978-0-323-04328-1.50008-5
[74] Schraml BU, e Sousa CR. Defining dendritic cells. Current Opinion in Immunology. 2015;32:13-20. https://doi.org/10.1016/j.coi.2014.11.001
[75] Ollila J, Vihinen M. B cells. The International Journey of Biochemistry & Cell Biology. 2005;37(3):518-23. https://doi.org/10.1016/j.biocel.2004.09.007
[76] Kataoka T, Nagai K. Molecular dissection of cytotoxic functions mediated by T cells. Progress in Biotechnology. 2002;22:13-23. https://doi.org/10.1016/S0921-0423(02)80039-9
[77] Bryceson YT, Bjorkstrom NK, Mjosberg J, Ljunggren HG. Chapter 13 – Natural Killer Cells. The Autoimmune Disease (Fifth Edition). Academic Press. 2014, p. 187-99. https://doi.org/10.1016/B978-0-12-384929-8.00013-7
[78] Levy O, Han E, Ngai J, Anandakumaran P, Tong Z, Ng KS, et al. Chapter 12 – Micro/Nano-Engineering of Cells for Delivery of Therapeutics. Micro- and Nanoengineering of the Cell Surface. 2014, p. 253-79. https://doi.org/10.1016/B978-1-4557-3146-6.00012-X
[79] Ashrafizadeh M, Farhood B, Musa AE, Taeb S, Najafi M. The interactions and communications in tumour resistance to radiotherapy: Therapy perspectives. International Immunopharmacology. 2020;87:e106807. https://doi.org/10.1016/j.intimp.2020.106807
[80] Moticka EJ. Chapter 20 – Activation of T Lymphocytes and MHC Restriction. A Historical Perspective on Evidence-Based Immunology. 2016, p. 169-79. https://doi.org/10.1016/B978-0-12-398381-7.00020-4

[81] Moticka EJ. Chapter 19 – B Lymphocyte Activation. A Historical Perspective on Evidence-Based Immunology. 2016, p. 159-68. https://doi.org/10.1016/B978-0-12-398381-7.00019-8
[82] Moticka EJ. Chapter 34 – Immune Responses Directed Against Self. A Historical Perspective on Evidence-Based Immunology. 2016, p. 299-308. https://doi.org/10.1016/B978-0-12-398381-7.00034-4
[83] Moticka EJ. Chapter 14 – Cell Collaboration in the Antibody Response: Role of Adherent Cells. A Historical Perspective on Evidence-Based Immunology. 2016, p. 113-20. https://doi.org/10.1016/B978-0-12-398381-7.00014-9
[84] Moticka EJ. Chapter 28 – Lymphocytes that Kill: Natural Killer (NK) and Natural Killer T (NKT) Lymphocytes. A Historical Perspective on Evidence-Based Immunology. 2016, p. 243-51. https://doi.org/10.1016/B978-0-12-398381-7.00028-9
[85] Moticka EJ. Chapter 27 – T-Lymphocyte-Mediated Effector Mechanisms. A Historical Perspective on Evidence-Based Immunology. 2016, p. 235-42. https://doi.org/10.1016/B978-0-12-398381-7.00027-7
[86] Hiriart M, Velasco M, Larqué C, Diaz-Garcia CM. Chapter Four – Metabolic Syndrome and Iconic Channels in Pancreatic Beta Cells. Vitamins & Hormones. 2014; 95:87-114. https://doi.org/10.1016/B978-0-12-800174-5.00004-1
[87] Stephens EA, Ryan T. Chapter 3 – Intensive Insulin Therapy. Endocrine Secrets (Fifth Edition). Mosby. 2009, p. 31-40. https://doi.org/10.1016/B978-0-323-05885-8.00003-9
[88] McMahon GT. Hyperglycemia. Decision in Making Medicine (Third Edition). Mosby. 2010, p. 128-131. https://doi.org/10.1016/B978-0-323-04107-2.50046-6
[89] Atkinson MA. Chapter 32 – Type 1 Diabetes Mellitus. Williams Textbook of Endocrinology (Thirteenth Edition). 2016, p. 1451-83. https://doi.org/10.1016/B978-0-323-29738-7.00032-0
[90] van Belle TL, Coppieters KT, von Herrath MG. Type 1 diabetes: etiology, immunology, and therapeutic strategies. Physiological reviews. 2011;91(1):79-118. https://doi.org/10.1152/physrev.00003.2010
[91] Yang XS. Chapter 8 – Particle Swarm Optimization. Nature-Inspired Optimization Algorithms, Academic Press, 2nd Edition. 2021, p. 111-21. https://doi.org/10.1016/B978-0-12-821986-7.00015-9
[92] Lindfield G, Penny J. Chapter 3 – Particle Swarm Optimization Algorithms. Introduction to Nature-Inspired Optimization, Academic Press. 2017, p. 49-68. https://doi.org/10.1016/B978-0-12-803636-5.00003-7
[93] Isiet M, Gadala M. Self-adapting control parameters in particle swarm optimization. Applied Soft Computing. 2019;83:e105653. https://doi.org/10.1016/j.asoc.2019.105653
[94] He M, Liu M, Wang R, Jiang X, Liu B, Zhou H. Particle swarm optimization with damping factor and cooperative mechanism. Applied Soft Computing. 2019;76:45-52. https://doi.org/10.1016/j.asoc.2018.11.050
[95] Houssein EH, Gad AG, Hussain K, Suganthan PN. Major Advances in Particle Swarm Optimization: Theory, Analysis, and Application. Swarm and Evolutionary Computation. 2021;63:e100868. https://doi.org/10.1016/j.swevo.2021.100868
[96] Kumar A, Pant S, Ram M, Singh SB. Chapter 6 – On solving complex reliability optimization problem using multi-objective particle swarm optimization. Mathematics Applied to Engineering. Academic Press. 2017, p. 115-31. https://doi.org/10.1016/B978-0-12-810998-4.00006-5

[97] Engelbrecht AP. Chapter 16 – Particle Swarm Optimization. Computational Intelligence: An Introduction. Wiley, 2nd Edition. 2007, p. 312-5. https://doi.org/10.1002/9780470512517.ch16
[98] Ishaque K, Salam Z, Amjad M, Mekhilef S. An Improved Particle Swarm Optimization (PSO) based MPPT for PV with Reduced Steady State Oscillation. IEEE Transactions on Power Electronics. 2012;27(8):3627-38. https://doi.org/10.1109/TPEL.2012.2185713
[99] Abdulkadir M, Yatim AHM, Yusuf ST. An Improved PSO-Based MPPT Control Strategy for Photovoltaic Systems. International Journal of Photoenergy. 2014;2014:e818232. https://doi.org/10.1155/2014/818232
[100] Wei T, Liu D, Zhang C. An Improved Particle Swarm Optimization(PSO)-Based MPPT Strategy for PV System. MATEC Web of Conferences, ICMITE. 2017. https://doi.org/10.1051/matecconf/201713900052
[101] Chai LGK, Gopal L, Juwono FH, Chiong CWR, Ling HC, Basuki TA. A novel global MPPT technique using improved PS-FW algorithm for PV system under partial shading conditions. Energy Conversion and Management. 2021;246:e114639. https://doi.org/10.1016/j.enconman.2021.114639
[102] Chao RM, Nasirudin A, Wang IK, Chen PL. Multicore PSO Operation for Maximum Power Point Tracking of a Distributed Photovoltaic System under Partially Shading Condition. International Journal of Photoenergy. 2016;2016:e9754514. https://doi.org/10.1155/2016/9754514
[103] Alshareef M, Lin Z, Ma M, Cao W. Accelerated Particle Swarm Optimization for Photovoltaic Maximum Power Point Tracking under Partial Shading Conditions. Energies. 2019;12(4):1-18. https://doi.org/10.3390/en12040623
[104] Rajasekar N, Vysakh M, Thakur HV, Azharuddin SM, Muralidhar K, Paul D, et al. Application of Modified Particle Swarm Optimization for Maximum Power Point Tracking under Partial Shading Condition. Energy Procedia. 2014;61:2633-9. https://doi.org/10.1016/j.egypro.2014.12.265
[105] Engel EA, Engel NE. Maximum photovoltaic array power point tracking algorithm based on modified particle swarm optimization under non-uniform irradiance. IOP Conference Series: Materials Science and Engineering. 2020;734:e012112. https://doi.org/10.1088/1757-899X/734/1/012112
[106] Fares D, Fathi M, Shams I, Mekhilef S. A novel global MPPT technique based on squirrel search algorithm for PV module under partial shading conditions. Energy Conversion and Management. 2021;230:e113773. https://doi.org/10.1016/j.enconman.2020.113773
[107] Saravanan S, Ramesh Babu N. RBFN based MPPT algorithm for PV system with high step up converter. Energy Conversion and Management. 2016;122:239-51. https://doi.org/10.1016/j.enconman.2016.05.076
[108] Zhao Z, Cheng R, Yan B, Zhang J, Zhang Z, Zhang M, et al. A dynamic particles MPPT method for photovoltaic systems under partial shading conditions. Energy Conversion and Management. 2020;220:e113070.

Chapitre 5

Faisabilité et implémentation des traqueurs solaires pour les systèmes photovoltaïques

Les techniques d'optimisation des systèmes photovoltaïques, présentées dans les **chapitres 3** et **4**, sont liées aux unités de traitement au sein d'un système photovoltaïque, et concernent l'application des algorithmes MPPT renforcés, qui sous-tendent les techniques d'optimisation basées sur l'irradiation. C'est également le cas pour l'optimisation de l'angle d'inclinaison présentée au **chapitre 2**. Ce chapitre de la thèse suit le même schéma d'optimisation (considéré par rapport à l'irradiation), mais traite plutôt des suiveurs solaires.

La popularité des suiveurs solaires est largement répandue dans le domaine de la recherche photovoltaïque, car ces équipements permettent de suivre la trajectoire du soleil (trajectoire due au mouvement de la terre autour du soleil). Par conséquent, la quantité d'irradiation solaire absorbée par les systèmes photovoltaïques équipés de suiveurs solaires est plus grande que pour les mêmes systèmes photovoltaïques sans suiveurs solaires. On peut donc considérer que les suiveurs solaires optimisent les performances des systèmes photovoltaïques en permettant une plus grande productivité énergétique.

En complément, cette étude prend en compte d'autres facteurs environnementaux associés à l'augmentation de l'irradiation (par exemple, l'augmentation de la température) et étudie ses effets sur le cycle de vie total du système photovoltaïque. En prouvant que l'application d'un suiveur solaire peut réduire le cycle de vie d'un système PV (en tenant compte de la proportionnalité

linéaire entre l'augmentation de l'irradiation et l'augmentation de la température absorbée), cette étude ne recommande pas l'application d'un suiveur solaire ou recommande une période de "pause" pour les suiveurs solaires pendant laquelle ils sont encouragés à être éteints.

La **section 1** présente une revue de la littérature sur les différents types de suiveurs solaires, en termes de mécanismes de contrôle, de systèmes de contrôle, de nombre d'axes mobiles et d'autres attributs, ainsi que le pourcentage d'augmentation de l'irradiation résultant de l'application de différents types de suiveurs. La **section 2** présente le déroulement et la méthodologie de l'étude. La **section 3** présente les données environnementales des zones d'installation des systèmes photovoltaïques dans lesquelles des suiveurs solaires réels ont été appliqués aux systèmes photovoltaïques avec une augmentation de l'irradiation enregistrée. La **section 4** présente le schéma de calcul de la température du module PV (supposée homogène entre chaque module PV au sein du système PV) en relation avec l'irradiation. La **section 5** présente l'estimation du cycle de vie des systèmes PV étudiés avec/sans l'application de suiveurs solaires ainsi que le calcul de la puissance globale pendant le cycle de vie complet de chaque système PV. Les résultats numériques sont discutés dans la **section 6**, et enfin les conclusions et les travaux futurs sont présentés dans la **section 7**.

Neuf régions différentes (dans lesquelles des systèmes PV réels avec des suiveurs solaires appliqués sont rapportés dans la recherche) constituent la base de l'étude et sont situées en Europe (Izana (Espagne), Carpentras (France), Toravere (Estonie), stations de Lerwick (Ecosse)) et aux Etats-Unis d'Amérique (Barstow (Californie), Quillayute (Washington), Denver (Colorado), Madison (Wisconsin), Jacksonville (Floride)). Le test de faisabilité des suiveurs solaires proposés est écrit dans une application Visual Basic (afin d'automatiser les procédures de calcul à l'aide d'un ordinateur). Les résultats ont montré que seuls les sites de Barstow, Quillayute, Jacksonville et Carpentras sont en mesure de produire un gain significatif dans la production globale d'énergie photovoltaïque au cours de la durée de vie calculée. Dans d'autres endroits comme Madison,

Toravere et Lerwick, il n'est pas recommandé d'installer des suiveurs solaires (car ils ne produiraient pas de gain de puissance significatif sur la durée de vie réduite après leur application, par rapport au comportement opérationnel normal des mêmes systèmes photovoltaïques sans suiveurs solaires).

Dans les autres zones d'installation étudiées (Denver et Izana), il est recommandé aux ST installés de "faire une pause" pendant cinq et dix-sept ans respectivement au cours de leur durée de vie. Cette caractéristique supplémentaire constitue un compromis entre la réduction du cycle de vie des systèmes photovoltaïques après une irradiation excessive, d'où un chauffage excessif (dû à l'application de suiveurs solaires), et la réduction de la production d'énergie sans l'application de suiveurs solaires.

C'est donc grâce aux résultats de cette étude que le cycle de vie des systèmes photovoltaïques peut être prolongé, avec une économie préventive pour l'application des suiveurs solaires ainsi qu’une maintenance réduite pendant le cycle de vie, pour certaines zones géographiques. Le travail futur suggéré pour cette étude, en termes de prototypage sous la forme d'une application pratique, qui peut être reliée à Internet afin d'obtenir les données environnementales nécessaires, permet d'optimiser le comportement des systèmes photovoltaïques dans une zone d'installation donnée.

Faisabilité et implémentation des traqueurs solaires pour les systèmes photovoltaïques

Cette étude devrait être soumise à « **Renewable and Sustainable Energy Reviews** »

Résumé – Cet article étudie l'effet des traqueurs solaires (ST) sur les systèmes PV en termes d'augmentation de la température du module PV, de réduction du cycle de vie et de diminution de la production globale d'énergie PV au cours de sa durée de vie. Neuf régions différentes, dans lesquelles des systèmes PV existants ont été installés avec un gain d'éclairement enregistré après confrontation avec des ST, constituent la base de cette enquête, et sont situées à : Barstow (États-Unis, Californie), Quillayute (États-Unis, Washington), Denver (États-Unis, Colorado), Madison (États-Unis, Wisconsin), Jacksonville (États-Unis, Floride), Izana (Espagne), Carpentras (France), Toravere (Estonie) et les stations de Lerwick (Écosse). Un processus d'étude est présenté et automatisé dans Microsoft Excel au moyen de scripts Visual Basic Application (VBA), qui évalue la mise en œuvre de la faisabilité des ST dans chacune des zones étudiées d'installations de systèmes PV. En conséquence, il est démontré que ce n'est qu'à Barstow, Quillayute, Jacksonville et Carpentras que les implémentations des ST sont réalisables en termes de production d'un gain significatif dans la production globale d'énergie PV pendant la durée de vie calculée. Au contraire, dans les stations de Madison, Toravere et Lerwick, les ST ne sont recommandés pour aucune application, tandis qu'à Denver et Izana, il est recommandé aux ST installés de «faire une pause» pendant cinq et dix-sept ans au cours de leur durée de vie respectivement. Enfin, les conclusions et les travaux futurs associés, en termes de transformation de l'étude présentée en une application smartphone/web sont présentés.

How feasible are the applications of solar trackers for PV systems?

Khaled Osmani[1], Mohamad Ramadan[2,3 *], Ahmad Haddad[2,3], Thierry Lemenand[1], Bruno Castanier[1]

[1]LARIS EA 7315, Polytech Angers, UNIV Angers, France

[2]School of Engineering, International University of Beirut BIU, Beirut, Lebanon

[3]School of Engineering, Lebanese International University LIU, Bekaa, Lebanon

***Corresponding author: mohamad.ramadan@liu.edu.lb (M. Ramadan)**

Abstract

This paper studies the effect of Solar Trackers (STs) over PV systems in terms of the increased PV module temperature, reduced lifecycle, and decreased overall PV power generation during its lifespan. Nine different regions, in which existing PV systems were installed with recorded irradiance gain after confrontation with STs, constitute the backbone of this investigation, and were located in: Barstow (USA, California), Quillayute (USA, Washington), Denver (USA, Colorado), Madison (USA, Wisconsin), Jacksonville (USA, Florida), Izana (Spain), Carpentras (France), Toravere (Estonia), and Lerwick stations (Scotland). A flow process is presented and automated in Microsoft Excel by means of Visual Basic Application (VBA) scripts, that judges the implementation of STs' feasibility in each of the surveyed zones of PV systems installations. Accordingly, it was shown that only in Barstow, Quillayute, Jacksonville, and Carpentras the STs' implementations are feasible in terms of producing a significant gain in the overall PV power production during the calculated lifespan. Contrarily, in Madison, Toravere, and Lerwick station the STs are not recommended for any application, while in Denver and Izana, the installed STs are recommended to "take-a-break" for five and seventeen years during their lifetime respectively. Finally, conclusions and related future work, in terms of transforming the presented flow into a smartphone/web application are presented.

Keywords: Solar tracker, PV power, lifecycle estimation, environmental impacts, energy gain, temperature effect

Nomenclature

Abbreviations		***Symbols***	
AI	Artificial Intelligence	G_g	Global irradiance coefficient
ANN	Artificial Neural Network	$P_{M_{STC}}$	PV module's power at STC
CNN	Convolution Neural Network	P_M	PV module's power
CNN-SVM	CNN with Support Vector Machine	$P_{PV,with\ ST,yearly}$	Yearly PV power production with ST
CSV	Comma Separated Value	$P_{PV,without\ ST,yearly}$	Yearly PV power production without ST
DATs	Double Axis Trackers	$P_{PV,lifespan,without\ ST}$	Overall power produced by the PV system without ST
ESS	Energy Storage System	$P_{PV,lifespan,with\ ST}$	Overall power produced by the PV system with ST
LCOE	Levelized Cost Of Energy	P_{PV}	PV power
LID	Light Induced Degradation	T_a	Ambient temperature
LSTM	Long Short-Term Memory	T_m	PV module's temperature
ML	Machine Learning	U_{L0}	Heat loss coefficient by convection
MPPT	Maximum Power Point Trackers	U_{L1}	Heat loss coefficient by radiation
NWP	Numerical Weather Prediction	$\Delta P_{PV,lifespan}$	Lifespan difference of produced power
PV	PhotoVoltaic	$\Delta P_{PV,yearly}$	Yearly difference of produced power
PVGIS	PV Global Information System		
SATs	Single Axis Trackers	***Greek letters***	
SMA	Shape Memory Alloy	γ_0	Arrhenius model parameter 0
STC	Standard Test Conditions	γ_1	Arrhenius model parameter 1
STs	Solar Trackers	γ	PV module's temperature parameter
TMY	Typical Meteorological Year	τ	Estimated lifecycle
VBA	Visual Basic Application	$\tau\alpha$	transmittance-absorptance product

VBE	Visual Basic Editor	v	Wind speed

Units

$\%/℃$	PV module's temperature parameter
W/m^2	global irradiance
$\frac{W}{m^2}/°C$	Convection heat loss coefficient
$\frac{Ws}{m^3}/°C$	Radiation heat loss coefficient
m/s	Wind speed
℃	Ambient temperature (Celsius)
W	Electric active power
K	Ambient temperature (Kelvin)

1. Introduction

The global energy demand inflation has led to a severe shortage in non-renewable energy supplies residuals [1]. Such demand is continuously increasing thus creating an urgent necessity to meet the huge load requirements while in parallel requesting safe and environmentally friendly power supplies [2]. This fact is due because of the extremely high greenhouse gases emissions and the environmental damages caused by the impacts of classic energy facilities [3].

Alternatively, the PhotoVoltaic (PV) technology presents a promising green source of sustainable energy [4]. Due to the abundancy of the solar radiations [5], in addition to the upgrading related field research, in the domain of PV array reconfiguration [6], tilt angle adjustments [7], Maximum Power Point Trackers (MPPT) [8], PV maintenance strategies [9], and integration with Energy Storage Systems (ESS) [10], PV systems gained more popularity over other forms of renewable energy supplies [11].

Solar Trackers (STs) from another side, help in improving the efficiency as well as the power output of PV systems [12]. By mechanically allowing the PV panels to track the varying locations of the sun during the day, hence confronting such panels to be as perpendicular as possible in front of the global irradiance, the amount of energy produced is then optimized [13], and the overall power generation increases [14]. Since a PV power plant's efficiency rate is based on its capability to transform the captivated solar irradiance into electricity, STs are designed to elevate such efficiency by allowing a dynamic movement of the PV panels, following the sun pattern [15], thus maximizing the amount of the absorbed solar energy [16].

As compared with a fixed PV system, STs allow more absorption of solar irradiance, since the sun's position varies through the day, due to the earth rotation around it, typically by the integration of four classification criteria:

- Control systems: such as Open-loop [17] and Closed-loop [18].
- Driving mechanisms: either passive by means of Freon [19], Shape Memory Alloy (SMA) [20], bimetallic strips [21], thermal actuator [22], and thermo-hydraulic actuators [23], or else active by means of motors [24] that physically displace the panels via mechanical shafts.
- Number of moving axis: such as Single Axis Trackers (SATs) [25] or Double Axis Trackers (DATs) [26].
- Tracking topology: that can be based on algorithms [27], date and time [28], sensors with date-time integration [29], bifacial solar cells [30].

An overall PV energy gain is increased upon its confrontation with a ST by 50% [31], 35% [32], 25% [33], 34% [34], 10% [35], 32.12% [36], 28.8% [37], 22% [38], 60% [39], and 35.78% [40]. Such studies ensure an increased output power productivity, hence a more significant return on investment for the installed PV system [41].

Therefore, STs serve in lowering the Levelized Cost Of Energy (LCOE) [42] for a PV plant: since the overall light to electricity efficiency increases, the electricity's cost decreases, thus solidifying the potential of PV systems in front of other alternative renewable sources [43]. In terms of cost efficiency, STs can on the other side reduce the overall cost of a PV power plant,

since less panels are required to generate the same amount of electricity produced by a fixed PV system [44], making solar power more accessible and extractable [45].

The stated reduction in the number of PV panels required to output the same energy as compared to fixed PV systems, has also environmental advantages [46], by shrinking the need of excessive solar panels, of which the manufacturing processes impact negatively on the environment [47]. Their allowance of bigger and more efficient usage of solar energy, achieves a better reduction in the carbon footprint of PV power plants, thus sustaining more such systems [48]. In addition, STs present reliable applications strategies, versatile enough to be employed in a wide range of facilities, such as residential, commercial, and utility-scale PV farms [49]. Intrinsically designed to withstand harsh environmental conditions [50], and operations under extreme weather fluctuations [51], STs are suitable for usage in different locations of the world [52].

On the controversy, when PV panels are exposed to prolonged periods of sunlight for extended periods, the Light Induced Degradation (LID) is often a drawback of the STs' applications: it can cause a reduction of the PV module's efficiency and overall performance [53]. In other words, STs contribute in exacerbating the LID for certain types of PV modules [54], due to the increased amount of light absorbed, which translates in an accelerated degradation process [55]. The excessive exposure to sunlight with its complications [56], causes defections on the level of PV cells. The resulting defected silicon crystal structure of the PV cells can trap electrons, thus reducing the efficiency of the cell [57], thus reducing the power output, while in the same time accelerating the entropy generation in PV cells [58]. Such exposure as well can lead to a parallel exposure to other negative environmental factors such as creation of inhomogeneous temperature across the same PV module [59].

Following the same trajectory of showing the negative side of STs application, this paper studies the increased temperature effects [60] after the incorporation of STs with PV systems, with the lifecycle estimation of such systems, and eventually the cumulative average power produced over the calculated lifetime. For each of the surveyed PV systems, the calculation are presented before/after the implementation of STs, in order to conclude a general remark about how feasible such application in each of the regions is. According to the process flow presented in this study, it is recommended for some of the PV installations' zones to "take-a-break" during several years within their estimated lifetime, as a way to compensate the effects of elevated temperature, reduced lifespan, and lowered PV power productivity. For other regions as well, STs are initially not recommended for application, due to the area-specific environmental conditions (irradiance, wind speed, ambient temperature), or to the decreased lifecycle estimation after the addition of STs.

The rest of this paper consists as follows: Section 2 represents the study methodology which reveals the reasoning behind the conducted process flow, including the Visual Basic Application (VBA) pseudo-codes which are used upon the application of each task. Section 3 shows the actual recorded data for the chosen sites of PV installation. Section 4 outputs the calculation methodology for PV module temperature, with/without STs. Section 5 involves the lifecycle estimation for each of the zones of installation as well as the PV produced power with/without STs. All results are discussed in Section 6, where the recommendations of "take-a-break" are clarified, and finally in Section 7, the conclusions and future work are established.

2. Study methodology

This ST feasibility study begins by the Typical Meteorological Year (TMY) data as its input for each of the studies areas from the PV Global Information System (PVGIS) [61]. Such data, that comes in the form of a large Excel table, have specific columns for environmental attributes, such as ambient temperature (℃), global irradiance (W/m^2), wind speed (m/s). For each of the studied zones' location, the data is available during the span from year 2005 to year 2015, recorded hourly (with a step change of one hour). In other words, during each day from year 2005 to year 2015, the TMY data is measured and recorded in each hour. As can be deducted, such data would be enormous for each PV installation zone that will be investigated.

Accordingly, even basic mathematical operations within the tabulated data, such as average, sum, etc. could be challenging due to the data's size. Therefore, a Visual Basic Application (VBA) is conducted in this work, as a way to automatize all of the needed calculations, following a main process that follows as:

a. Calculate the PV modules temperature with and without the implementation of ST.

b. Estimate the lifecycle of the PV modules with and without the implementation of ST.

c. Calculate the overall average power production, during the entire calculated lifespan, with and without the implementation of ST.

d. At this level, it can be stated whether or not the ST are of major significance in elevating the PV power production at the studied region (this can be done via a numerical comparison of the final produced power during the estimated lifecycle, with and without the implementation of ST).

e. For the region(s) where the overall power produced by the PV system without ST ($P_{PV,lifespan,without\ ST}$) during the estimated lifecycle, exceeds the overall power of the same system with ST ($P_{PV,lifespan,with\ ST}$), denote a non-feasibility tag, and try to modify the cyclic operation of the ST according to a "take-a-break" criteria as follows:

1. For each year of the previously calculated lifespan, check if the yearly PV power production without ST ($P_{PV,without\ ST,yearly}$) is bigger than the one with ST ($P_{PV,with\ ST,yearly}$). If such condition is satisfied, recommend a "take-a-break" for the ST during that year, then re-do the calculation of parts a, b, and c with the new numeric in relation with the shutdown of the ST.

2. When the condition in 1. is not applicable (i.e., $P_{PV,with\ ST,yearly} > P_{PV,without\ ST,yearly}$ in each of the years during the span from year 2005 to year 2015), but still the condition in e. applies ($P_{PV,lifespan,without\ ST} > P_{PV,lifespan,with\ ST}$), due to the reduced lifecycle after the implementation of ST, then propose to "take-a-break" during the year(s) in which the difference produced power ($\Delta P_{PV,yearly} = P_{PV,with\ ST,yearly} - P_{PV,without\ ST,yearly}$) is less than the average of all yearly ΔP_{PV} from year 2005 to year 2015. This can be justified as the insignificant power production after the implementation of the ST during the specified year, and

therefore shutting it down, in order to decrease the temperature effect on the PV modules, hence elevating the lifecycle estimation of the system.

3. Check $\Delta P_{PV,lifespan}$ for the studied system after the execution of step(s) 1 and/or 2: if such power difference has increased after the application of step 1, what means that the overall power generation during the entire lifespan of the PV system has increased with respect to the same value before the execution of step 1, then ST is recommended to "take-a-break" during the specified year(s). For all other conditions, the ST is not recommended at all to be implemented in the studied region.

Before translating the above mentioned steps as Excel VBA, it is worthy to mention that the following points are pre-assumed for each of the studied region (location at which the PV system is installed):

i. A homogeneous temperature distribution is assumed to be over the entire PV system: the temperature of a single PV module thus reflects the temperature of all other PV modules, hence the PV panels, and eventually the entire PV system.

ii. The TMY data for each of the studied regions of PV systems' installation, during the span from year 2005 to year 2015, is assumed to be the same in the next decade(s). In other words, and as an example, the TMY data from year 2016 to year 2027 is assumed to be the same as from year 2005 to 2015, with a year-to-year correlation (i.e., irradiance/temperature/wind speed data of year 2016 is the same as irradiance/temperature/wind speed data of year 2005). This was taken into consideration since the reference [61] does not occupy any real TMY data after year 2015, and to the fact that according to the PV systems' lifecycle estimation, some of its composers (years) exist in the future, where the actual data recording is not done yet.

To be noted that all TMY data from the reference [61] comes in Comma Separated Values (.CSV) format. With that being said, the following steps represent the path from the obtainment of .CSV files into the decision whether if or not the application of ST is feasible, and how:

I. **Transform the .CSV file into an excel workbook**: in order to have a clear tabulated data, readable under the format of a single table, the source file (.CSV) must be converted accordingly. This can be done by opening an Excel application, select "Data" tab: in the "Get & Transform Data" section, select "From Text/CSV". The .CSV file is to be imported, with its File Origin relates to the used operating system, with a comma delimited option. The "Load" button would create one big table that contains all of the environmental recorded data, from year 2005 to year 2015, with a step change of one hour per day. The obtained table is labelled as "tmy_latitude_longitude_startYear_endYear", that is to be acknowledged for further VBA scripts implementation.

II. **Remove all zeroes from the global irradiance column**: since the data record in the TMY data table is done on an hourly basis, during nights the recorded irradiance is zero. When it is intended to derive the average irradiance for example, the night recorded values (i.e., zeroes) would give a false image for that parameter. Since ST are designed to increment the amount of absorbed light during effective sun hours, and in order to carefully study the increase of irradiance absorbance with/without ST, the calculated average must not take into consideration the recorded irradiance during nights. With that being said, all zeroes

from the global irradiance column must be then replaced with blanks. The following pseudo VBA script presented in Table 1, serves for that purpose once implemented: it is to be written within the Visual Basic Editor (VBE) for Excel, and executed (Run) in the referred worksheet.

```
Sub ZeroReplacementWithBlank()
    Dim dataRange As Range
    Dim cell As Range
    Set dataRange = Range("A1:A1000")
    For Each cell in dataRange
        If cell.value = 0 Then
        cell.value = ""
        End If
    Next cell
End Sub
```

Table 1. VBA for replacing zeroes with blank in irradiance data

In the VBA of Table 1 (as well as in all others succeeding VBA), the function is started by the label *Sub* followed by the desired function name, and ended with *End Sub*. All variables that are needed for the logic execution are declared (in this VBA and all others) with *Dim*. The Range ("A1:A1000") in Table 1 is to be modified according to the actual location of the global irradiance data within the imported table ("A" represents the column label and the digits "1" and "1000" the start/end indices respectively). It is important to note that all of the zero values are to only be replaced by blanks, and never considering executing other similar function such as *EntireRow.Delete*, since other significant data beside the irradiance will get deleted, thus prohibiting further usages in other VBA.

III. Calculate the yearly average global irradiance without ST: After removing the zeroes from the irradiance column data, the workflow process of this study imply the calculation of the yearly average global irradiance during the span from year 2005 to year 2015 (to be involved later in PV module's temperature calculation). Regardless of the fact that the average calculation shall impose no problem, still, the enormous data that is quantified based on the "year-month-day:time" entitlement can add some difficulties over such calculation. With that being said, the VBA in Table 2 serves as a conditional average calculator, based on the "year" value in the "year-month-day:time" attribute. The "year" indicators are placed in a column that is situated to the left of the irradiance column.

```
Sub ConditionalAverage()
    Dim dataRange As Range
    Dim cell As Range
    Dim outputData As Range
    Dim sum As Double
    Dim count As Integer

    Set dataRange = Range ("i10:i10000")
```

```
    For Each cell in dataRange
        If Left(cell.Offset(0,-1),4) = "2015" Then
        sum = sum + cell.Value
        count = count + 1
        End If
    Next cell

    If count > 0 Then
        avg =  sum / count
    Else
        avg = 0
    End If

    Set outputData = Range ("k1")
    outputData.value = avg

End Sub
```

Table 2. VBA for conditional yearly average calculation (year-based)

The macro in Table 2 assumes that the filtered global irradiance data (i.e., zeroes are replaced with blanks) exist in the column 'i' from cell index 10 until cell index 10000. This is adjustable according to the actual data fitting space within the workbook. In cell 'k1' the average of all global irradiance data captured in year 2015 is stored. Under the same *dataRange* the conditional attribute "2015" can be changed to all other years during the supervised span, where the resulting conditional averages are stored successively in 'k2', 'k3', etc. At this stage, the yearly average global irradiance from year 2005 to year 2015 are all calculated and stored in column 'k'.

IV. Calculate the yearly global average irradiance with ST, yearly average ambient temperature, and yearly average wind speed: after the obtainment of the yearly average global irradiance for all years between year 2005 and year 2015 without ST, according to each zone's irradiance increase rate, the yearly global average irradiance with ST can be obtained (according to the percentage increase). The same fact applies for the yearly average ambient temperature, as well as the yearly average wind speed. Such data can be simply obtained using the same macro as in Table 2, where it is only needed to change the data range ("i10:i1000") and the placeholder (i.e., column) at which the calculated data is to be stored (in column "l" instead of "k" as in Table 2 for example). At this point, and for each studied region, all yearly average data of global irradiance with ST, global irradiance without ST, ambient temperature, and wind speed are obtained from year 2005 to year 2015.

V. Calculate the PV module temperature (with/without ST): the arrangement of all previous yearly average data for different environmental attributes, enables the calculation of the PV module's temperature (T_m) in each year during the span from 2005 to 2015. To be taken into acknowledgment that the PV module's temperature formula will be explained

thoroughly in Section 4, such that the aim here is to only provide a closed loop working process topology. Accordingly, Table 3 represents the macro needed to calculate T_m.

```
Sub modTemp()
    Range("M1:M11").Formula = "=0.9*A1/(30.02+6.28*D1)+C1"
End Sub
```

Table 3. VBA for PV module's temperature calculation

In the macro of Table 3, the cells from M1 to M11 store T_m of the studied region for the PV system without ST, from year 2005 to year 2015. The script automatically assign A1 (yearly average global irradiance without ST), D1 (yearly average wind speed), and C1 (yearly average temperature) for the stored T_m at cell M1 (year 2005), and A2, D2, C2 for the stored T_m at cell M2 (year 2006), and so on until year 2015 (cell M11). The T_m of the studied regions for the PV system with ST, can be obtained also with the same macro as in Table 3, where only the range should be changed ("M1:M11") and the attributes A1 should also be changed to the column which encapsulates the yearly average global irradiance with ST. The finalization of this part would yield in the yearly average T_m for all studied regions, with and without ST, from year 2005 to year 2015.

VI. Calculate the average PV module's temperature from year 2005 to year 2015 with and without ST: after having all the PV modules' temperatures, calculated with/without ST, during the span from year 2005 to year 2015 as in the previous step stored in ("M1:M11"), the aim in this phase is to get the average temperature of the entire span. Accordingly, each of the studied regions, would have two outputs, as in terms of PV modules temperatures covering the entire span, that will be used in the successive step to estimate the lifecycle of the PV system (with/without ST). For that purpose, Table 4 presents a macro to calculate the average temperature of the PV modules (with/without ST) during the entire span from year 2005 to year 2015.

```
Sub FullTempAvg()
    Dim YearlTemp1 As Range
    Dim YearlTemp2 As Range
    Dim AvgWithSt As Double
    Dim AvgWithoutSt As Double
    Dim FinalTemp1 As Range
    Dim FinalTemp2 As Range

    Set YearlTemp1 = Range("M1:M11")
    Set YearlTemp2 = Range("N1:N11")

    AvgWithSt = Worksheetfunction.Average(YearlTemp1)
    AvgWithoutSt = Worksheetfunction.Average(YearlTemp2)

    Set FinalTemp1 = Range("O1")
    Set FinalTemp2 = Range("P1")
```

```
    FinalTemp1.Value = AvgWithSt
    FinalTemp2.Value = AvgWithoutSt

End Sub
```

Table 4. VBA for calculating the PV modules average temperature from year 2005 to year 2015

By running the script in Table 4, the average T_m from year 2005 to year 2015 for the cases of PV systems installations with/without ST are calculated and stored in the cells "O1" and "P1" respectively. The latent, as well as the ranges for the yearly average T_m in ("M1:M11") and ("N1:N11"), can be changed from the VBA according to the current Excel workbook design requirements.

VII. Estimate the PV systems lifecycles with/without ST: after having the average T_m from year 2005 to year 2015 for the cases of PV systems installations with/without ST, each PV system's lifecycle can be estimated. The formula enrolled for such purpose will be thoroughly described in Section 5. The aim in this phase is to acknowledge the influence of the elevated T_m due to the application of ST, and how much it decreases the lifecycle estimation. Based on what has been precedent, Table 5 encapsulates the VBA for PV systems' lifecycles estimation.

```
Sub LifeCyEs()
    Range("Q1:Q11").Formula = "=EXP(5.23+(2102/O1))/8766"
    Range("R1:R11").Formula = "=EXP(5.23+(2102/P1))/8766"
End Sub
```

Table 5. VBA for PV systems' lifecycle estimation

The range in Table 5 that starts inside the "Q" column of index 1 until index 11, represent the cells in which the lifecycle has been estimated according to the average of T_m with ST. Similarly, the range that starts inside the "R" column of index 1 until index 11, represent the cells in which the lifecycle has been estimated according to the average of T_m without ST. The outcome of the VBA in Table 5 yields in the lifecycle estimation in years.

VIII. Calculate the yearly average PV power production during the estimated lifecycle with/without ST: from previous VBA, the existence of the yearly average global irradiance from year 2005 to year 2015 without ST (step III), and the yearly average global irradiance from year 2005 to year 2015 with ST (step IV), along with the T_m with/without ST (step V), permits the calculation of the yearly average PV power $\left(P_{PV,yearly}\right)$ with/without ST during the span from year 2005 to year 2015, in function of the power of the PV module at Standard Test Conditions - STC $\left(P_{M_{STC}}\right)$. The enrolled formula for this purpose will be

thoroughly examined in Section 5. The VBA in Table 6 encapsulates the script implementation for this calculation.

```
Sub powrCalc()
    Range("R1:R11").Formula = "=K1/1000*(1-0.05*((P1-273.15)-25))"
    Range("S1:S11").Formula = "=L1/1000*(1-0.05*((O1-273.15)-25))"
End Sub
```

Table 6. VBA for PV power calculation during the estimated lifecycle with/without ST

In the script of Table 6, the ranges "R1:R11" and "S1:S11" represent the cells in which the P_{PV} is produced without/with ST respectively, since columns 'K' and 'L' store the yearly average global irradiance data without/with ST respectively. Whereas columns 'P' and 'O' store the yearly average T_m without/with ST respectively.

IX. Calculate the cumulative average power during the entire lifecycle based on the produced power during the span from year 2005 to year 2015: after the calculation of P_{PV} during each year of the span, the 10-year cumulative without ST can be obtained using a sum function as revealed in Table 7 under the term *TenYrPowerNoSt.Value*, where the same entity with ST is referred to as *TenYrPowerWithSt.Value.*

```
Sub PowSum()
    Dim ColRange1 As Range
    Dim ColRange 2 As Range
    Dim CumlNoSt As Double
    Dim CumlWithSt As Double
    Dim TenYrPowNoSt As Range
    Dim TenYrPowSt As Range
    Dim LifeSpanPowNoSt As Range
    Dim LifeSpanPowSt As Range
    Dim EntLfSpanNoSt As Double
    Dim EntLfSpanSt As Double

    Set ColRange1 = Range("R1:R11")
    Set ColRange2 = Range("S1:S11")
    CumlNoSt = WorksheetFunction.Sum(ColRange1)
    CumlWithSt = WorksheetFunction.Sum(ColRange2)

    Set EntLfSpanNoSt = Range ("Q1")
    Set EntLfSpanSt = Range ("Q2")
    Set TenYrPowerNoSt = Range("T1")
    Set TenYrPowerSt = Range ("T2")
    Set LifeSpanPowerNoSt = Range("T3")
    Set LifeSpanPowerSt = Range("T4")
```

```
    TenYrPowerNoSt.Value =  CumlNoSt
    TenYrPowerWithST.Value  = CumlWithSt
    LifeSpanPowerNoSt.Value = TenYrPowerNoSt.Value * EntLfSpanNoSt / 10
    LifeSpanPowerSt.Value = TenYrPowerWithSt.Value * EntLfSpanSt / 10

End Sub
```

Table 7. VBA for cumulative average of produced PV power with/without ST

Progressively, and since it is pre-assumed that the environmental conditions from year 2005 to year 2015 are decade-repetitive, it will be possible to calculate the P_{PV} during the entire pre-calculated lifespan instead of only 10 years, as stored in the variable *LifeSpanPowerNoSt.Value* and *LifeSpanPowerSt.Value* for the entire PV power (P_{PV}) without/with ST ($P_{PV,lifespan,without\ ST}$, $P_{PV,lifespan,with\ ST}$) respectively. Such calculations depend on the previously calculated lifespan for the PV system without/with ST, as stored in cells "Q1" and "Q2" in the example of Table 7.

X. Highlight the negative value(s) resultant from subtracting $P_{PV,lifespan,without\ ST}$ from $P_{PV,lifespan,with\ ST}$: Since the PV power produced from the system with added ST must be larger than the power produced by the same system without ST, if $P_{PV,lifespan,with\ ST} - P_{PV,lifespan,without\ ST} < 0$ then highlight the row of that operation as an index that the ST application in that case is not practical due to the mixed environmental interactions of irradiance, ambient temperature, and wind speed. All rows (which reflect the operational years) that are highlighted in red after the execution of the VBA in Table 8, indicate a necessity to take-a-break action for the ST from the PV system at the indicated operational year.

```
Sub HighlightNegVal()
    Dim lastRow As Long
    Dim rng As Range
    Dim cell As Range

    lastRow = Range("J" & Rows.count).End(xlUp).Row
    Set rng = Range("J2:J" & lastRow)

    For Each cell In rng
        If cell.value  < 0 Then
        cell.Interior.Color = vbRed
        End If
    Next cell
End Sub
```

Table 8. VBA to highlight negative PV power produced with/without ST

The script in Table 8 bases on a pre-condition that the subtraction results of $\Delta P_{PV,lifespan} = P_{PV,lifespan,with\ ST} - P_{PV,lifespan,without\ ST}$ for different years inside the span from 2005 to 2015 are already stored in column "J" (as an example in this case). All red marked cells indicate the years during the span of study that within the ST must be turned off (take-a-break).

XI. Highlight the below than average $\Delta P_{PV,yearly}$ (with respect to all yearly ΔP_{PV} during the span from year 2005 to year 2015): sometimes the $\Delta P_{PV,yearly}$ of each year are all positive, but still the overall $P_{PV,lifespan,with\ ST}$ (during the entire calculated lifespan) is less that $P_{PV,lifespan,without\ ST}$ due to the reduced lifecycle estimation after the addition of ST. In such cases, the condition in step X cannot be applied. As an alternative solution-seeking method, the VBA in Table 9 aims to highlight the rows (i.e., years) in which the $\Delta P_{PV,yearly}$ is less than the average of all $\Delta P_{PV,yearly}$ during the span from year 2005 to year 2015. This can be understood as insignificance of power production after the addition of ST in that year, and that it is possible to take-a-break for the ST accordingly.

```
Sub BelowAverage()
    Dim LastRow As Long
    Dim i As Long
    Dim CColumn As Range
    Dim CColumnAverage As Double

    LastRow = Cells(Rows.Count, "C").End(xlUp).Row
    Set CColumn = Range ("C1:C" & LastRow)
    CColumnAverage = Application.WorksheetFunction.Average(CColumn)

       For i = 1 To LastRow
          If Cells(i,"C").Value < CColumnAverage Then
             Cells(i, "C").Interior.ColorIndex = 6
          End If
       Next i
End Sub
```

Table 9. VBA to highlight the years based on the below than average difference PV power production with/without ST

The script in Table 9 takes into consideration that all $\Delta P_{PV,yearly}$ from year 2005 to year 2015 are stored in column "C". The years that have not got any significant power production increase after the installation of ST, are hence highlighted in yellow (color index 6, to separate from the red highlighting in case of negative power production).

XII. **Modify the calculations based on the red/yellow highlighted rows:** according to the outcomes of steps X and/or XI (upon applicability), all of the highlighted years, that reflect the take-a-break action for the ST, are to have their T_m, lifecycle estimation, and P_{PV} re-calculated as in the case of using no ST (thus taking-a-break):

a. If the new average P_{PV} during the new calculated lifecycle estimation is bigger than the one without ST, then recommend the take-a-break during the highlighted years, by pointing out that with such action, the entire PV power generation will be more significant during its estimated lifecycle.

b. Else if even with the take-a-break recommendation, according to steps X and/or XI (upon applicability), it does not yield to a higher new average P_{PV} during the new calculated lifecycle estimation with respect to the same average P_{PV} without ST, then do not recommend at all the implementation of a ST at that location, since it is perceived as "environmentally non-feasible". This can be interpreted by the logic of environmental conditions combinatorics incompatibility between irradiance, ambient temperature, and wind speed.

The entire workflow process, as elaborated with steps I to XII, can be encapsulated according to the flowchart in Figure 1.

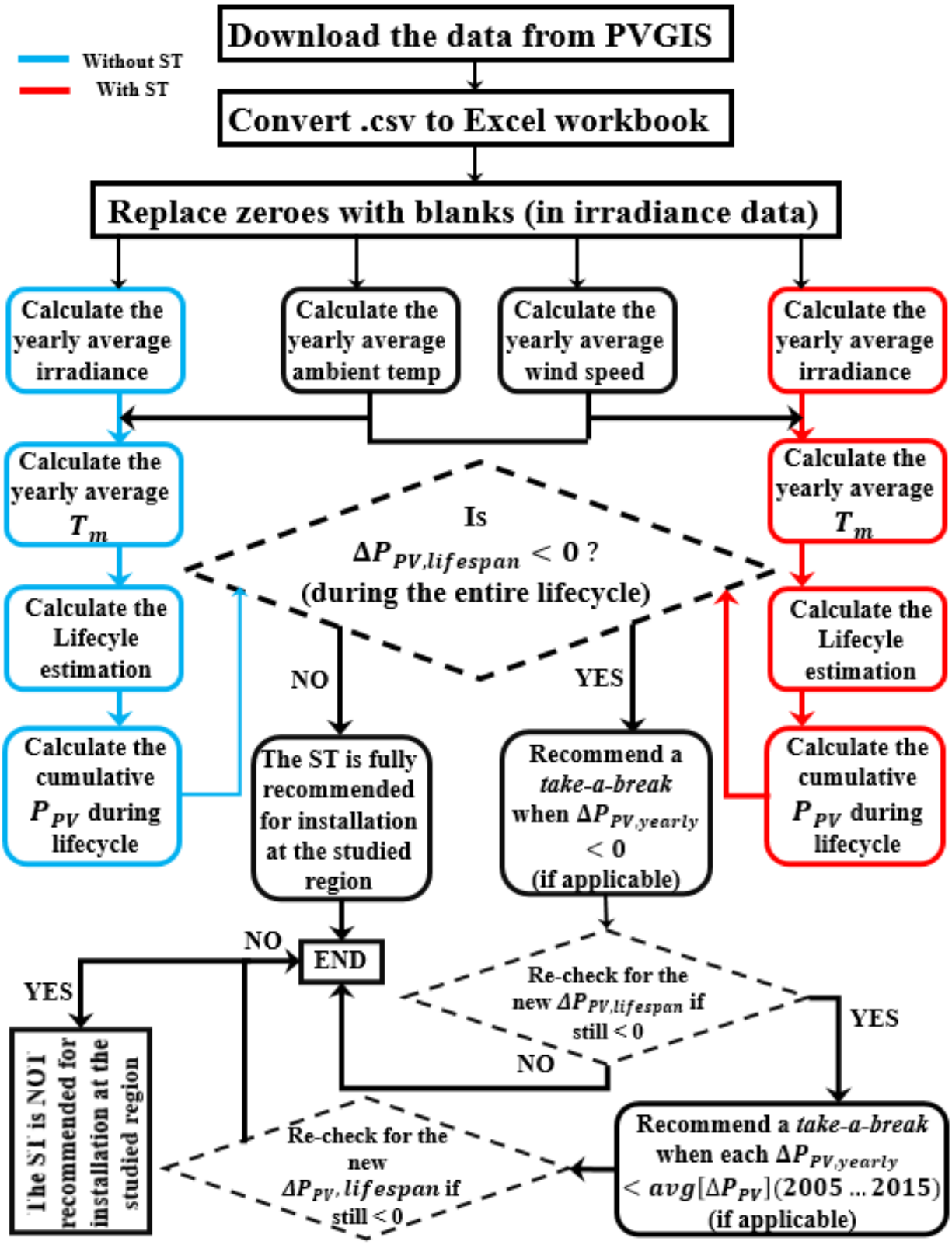

Figure 1. Flowchart of the calculation process

3. Data of PV systems with STs

In order to apply and test the model explained in Section 2, it is necessary to have actual recorded irradiance increase after the real implementation of STs onto real PV systems. In other words, to be able to calculate the span averaged P_{PV}, the irradiances captivated by the PV systems must be calculated before/after the implementation of STs. Therefore, a percentage irradiance increase is needed for each PV system to be studied. Since the scope of this manuscript does not interact with any physical data sampling, it has been projected into other studies of real irradiance measurements, which can lead to the needed percentage increase of captivated irradiance. As a key note, the broader the areas in which the PV systems were implemented, the better the sensitivity study of the model imaged in Figure 1. For this purpose, the irradiance data were used according to two studies: the first taken place in Europe with four different geographical zones at Izana, Toravere, Carpentras, and Lerwick [62]. The second, taken place in USA with five different geographical zones at Barstow, Quillayute, Denver, Madison, and Jacksonville [63].

Both studies serve for the acknowledgment of the irradiance increase percentage after the installation of STs at the studies regions. With this data, the process of Figure 1 can be started, with no ST application (intrinsic data from PVGIS) and ST application (VBA calculations after the employment of the irradiance increase data). Table 10 encapsulates the regional data information for all the surveyed geographical zones.

Table 10. Regional data information for the studied PV systems' installation sites

Region	Country	Latitude (°N)	Longitude (°W)	Hemisphere	Type of ST	Recorded irradiance increase per year	Ref.
Barstow	California (USA)	34.85°	-116.80°	Norther, Western	DAT	43%	[63]
Quillayute	Washington (USA)	47.93°	-124.57°	Norther, Western	DAT	29%	
Denver	Colorado (USA)	39.83°	-104.65°	Norther, Western	DAT	37%	
Madison	Wisconsin (USA)	30.95°	-95.95°	Norther, Western	DAT	31%	
Jacksonville	Florida (USA)	33.82°	-85.78°	Norther, Western	DAT	32%	
Izana	Spain (Europe)	39.32°	-4.80°	Norther, Western	SAT	39%	[62]
Carpentras	France (Europe)	44.08°	5.05°	Northern, Eastern	SAT	39%	
Toravere	Estonia (Europe)	58.25°	24.46°	Northern, Eastern	SAT	38%	
Lerwick	Scotland (Europe)	60.14°	-1.15°	Northern, Eastern	SAT	20%	

The irradiance gain information in Table 10, allows the beginning of the workflow of Figure 1, until the phase of T_m calculations. In other words, it is possible through Table 10, to expand all needed climatic data, from the span which begins by year 2005 to year 2015, in terms of irradiance with/without STs, yearly average temperature, yearly average wind speed. At each of the studied zones, the VBA of Table 1 is the primal step to obtain the irradiance for cases with/without STs. Then by applying the VBA of Table 2, all yearly average climatic data can be obtained. The only modification that must be done is the change of the ranges within the spreadsheet, in a way that data do not overlap. Finally, the application of the codes in Table 1 and Table 2, yields in the climatic data information as stored in Table 11, for each of the studied regions.

Region	Year	Yearly average global irradiance without ST (W/m^2)	Yearly average global irradiance with ST (W/m^2)	Yearly average ambient temperature (K)	Yearly average wind speed (m/s)
Barstow	2005	511.233	731.063	290.641	2.516
	2006	526.827	753.362	290.966	3.038
	2007	545.354	779.856	291.266	3.25
	2008	584.213	835.424	291.325	3.697
	2009	327.362	468.127	290.891	3.23
	2010	373.044	533.452	290.141	3.976
	2011	341.083	487.748	289.866	3.947
	2012	436.997	624.905	291.508	2.881
	2013	394.487	564.116	291.183	2.733
	2014	389.9	557.557	292.383	2.907
	2015	441.922	631.948	291.933	3.631
Quillayute	2005	265.885	342.991	284.3083	4.721
	2006	324.712	418.878	283.766	5.433
	2007	305.099	393.577	283.566	8.169
	2008	373.064	481.252	282.7083	6.128
	2009	315.177	406.578	283.383	5.456
	2010	333.611	430.358	283.791	4.885
	2011	318.087	410.332	283.433	4.512
	2012	299.344	386.153	283.508	3.142
	2013	349.312	450.612	283.858	2.952
	2014	285.554	368.364	284.791	4.404
	2015	298.041	384.472	285.3	2.557
Denver	2005	497.422	681.468	283.616	3.477
	2006	532.857	730.014	283.741	3.646
	2007	530.033	726.145	283.5	3.282
	2008	537.74	786.023	283.25	3.114
	2009	531.635	728.34	283	2.884
	2010	450.403	517.052	283.741	2.532

	2011	508.202	696.236	283.483	3.162
	2012	501.021	686.398	284.816	2.563
	2013	480.369	658.105	283.091	2.911
	2014	423.641	580.388	283.391	2.939
	2015	311.591	426.879	282.333	2.384
Madison	2005	466.538	611.164	283.575	4.214
	2006	422.017	552.842	283.825	3.425
	2007	377.988	495.164	283.416	4.662
	2008	526.619	689.87	281.833	4.48
	2009	511.244	669.729	281.975	4.05
	2010	586.713	768.594	283.466	3.909
	2011	567.662	743.637	283.175	4.028
	2012	481.033	630.153	284.975	2.692
	2013	459.051	601.356	281.766	2.885
	2014	581.352	761.571	281.1	4.297
	2015	565.104	740.286	283.15	4.172
Jacksonville	2005	429.154	566.483	293.966	2.991
	2006	405.926	535.822	294.475	3.225
	2007	418.042	551.815	294.391	5.092
	2008	479.463	632.891	294.041	4.886
	2009	414.943	547.724	293.958	4.627
	2010	545.136	719.579	293.025	3.488
	2011	545.707	720.333	294.55	3.136
	2012	497.881	657.202	294.475	2.895
	2013	323.575	427.119	294.25	3.457
	2014	561.988	741.824	293.775	3.046
	2015	533.667	704.44	295.091	4.443
Izana	2005	383.016	532.392	283.65	3.624
	2006	406.591	565.161	284.308	4.363
	2007	377.788	525.125	283.075	2.807
	2008	502.401	698.337	283.141	3.442
	2009	551.723	766.895	284.15	3.693
	2010	604.147	839.764	282.941	4.61
	2011	314.336	436.927	284.383	2.706
	2012	408.311	567.552	283.958	3.121
	2013	472.945	657.393	283.133	2.919
	2014	466.07	647.837	284.258	3.761
	2015	334.87	465.469	284.483	3.145
Carpentras	2005	470.014	653.494	287.875	3.832
	2006	468.774	651.595	288.983	4.283
	2007	436.468	606.69	288.441	3.941
	2008	448.053	622.793	288.308	4.663
	2009	444.76	618.216	288.808	2.946
	2010	457.76	636.286	287.475	3.221
	2011	508.002	806.227	288.883	3.346

	2012	522.377	726.104	288.283	3.712
	2013	444.378	617.685	287.933	3.435
	2014	442.575	615.179	289.208	2.878
	2015	436.5	606.735	288.958	3.022
Toravere	2005	202.384	279.289	279.258	4.773
	2006	184.964	255.25	280.041	5.503
	2007	392.438	541.564	280.108	3.742
	2008	211.07	291.276	280.55	4.249
	2009	221.95	306.291	279.141	3.859
	2010	460.503	635.494	277.916	3.731
	2011	236.505	326.376	279.958	3.14
	2012	115.344	159.714	278.516	3.817
	2013	137.421	189.641	279.75	3.041
	2014	332.675	459.091	280.016	3.865
	2015	122.58	169.16	280.525	4.509
Lerwick	2005	138.502	166.202	282.075	7.998
	2006	150.055	180.066	282.541	9.798
	2007	189.848	227.817	282.025	6.486
	2008	131.244	157.492	282.166	10.731
	2009	144.677	173.612	282.316	8.926
	2010	133.707	160.448	281.266	5.748
	2011	122.437	146.924	282.233	7.609
	2012	147.464	176.956	281.5	7.045
	2013	98.451	118.141	281.6	8.369
	2014	119.499	143.398	282.583	10.956
	2015	108.563	130.275	282.05	7.187

Table 11. Averages of climatic data for the studied regions of PV systems' installations

4. Calculation of PV module temperature

Towards the successive execution of the flowchart in Figure 1, the registered data in Table 11 allow the manifestation of the VBA in Table 3: the required data for calculating T_m can be accordingly employed. As for the mathematical model used for such calculation, it is based in this study on Eq.(1): such model considers the wind effect (as a cooling medium) on the PV module temperature, hence giving a better reflective image on the temperature estimation [64].

$$T_m = T_a + \frac{\tau\alpha \times G_g}{U_{L0} + U_{L1}\upsilon} \quad (1)$$

with T_a representing the ambient temperature, $\tau\alpha$ the transmittance-absorptance product, G_g the global irradiance coefficient, U_{L0} the heat loss coefficient by convection, U_{L1} the heat loss coefficient by radiation, and υ the windspeed [64].

This model is advantageous amongst others, since it does not rely on the efficiency of PV modules, or other PV cell intrinsic materials' coefficients to calculate T_m, and has a detection sensitivity of 98.77% [64]. The goal in this step is to calculate the yearly average T_m for each of the studied PV systems, before and after the implementation of STs. Therefore, for each year during the span from 2005 to 2015, exists a unique T_m with corresponding unique attributes of yearly average G_g, and yearly average υ. As can be noticed, all required data are already stored in Table 11.

From another side, other coefficients of Eq.(1) are labelled to constants, such as the $\tau\alpha$ product is in the range of 0.9, U_{L0} equals $30.02\frac{W}{m^2}/°C$, and U_{L1} equals $6.28\frac{Ws}{m^3}/°C$ [64]. By grouping the precedent information, Eq.(1) can be easily seen in the VBA of Table 3, where the range ("M1:M11") corresponds to the cells in the workbook that are to store T_m from year 2005 to year 2015 for the region under investigation, "A1" represents G_g, "D1" represents υ, and "C1" represents T_a. To be noted that the macro of Table 3 is applicable for all the studied regions, where the range ("M1:M11") is to be suitably changed, as well as for the cells in "A", "C", and "D" columns. By taking this into consideration, with the inclusion the Eq.(1) for each of the surveyed region, with their corresponding data position in Excel, T_m is calculated accordingly, in Table 12 for the PV systems without STs, and in Table 13 for the same systems integrated with STs. What differs for both calculations procedure is G_g since it is the only changing variable from Eq.(1), and due to its direct proportionality with T_m, it can be observed after the numerical comparison of both produced tables, how big did T_m evolve post the installation of STs.

Table 12. PV modules' temperatures without the implementation of STs

Yearly average T_m [K]											
	Without ST										
Region	2005	2006	2007	2008	2009	2010	2011	2012	2013	2014	2015
Barstow	300.682	300.6229	300.998	301.201	296.747	296.246	295.466	299.682	298.707	299.651	299.462
Quillayute	288.319	288.322	286.943	287.61	287.796	288.738	288.339	288.923	290.332	289.247	291.121
Denver	292.249	292.804	292.922	293.012	292.941	292.568	292.653	294.594	292.042	291.256	288.566
Madison	291.009	291.196	289.153	289.983	290.272	293.143	292.411	294.201	290.349	290.278	292.196
Jacksonville	301.88	301.742	300.46	301.15	300.279	302.474	304.429	303.771	299.88	304.066	303.383
Izana	290.181	290.681	290.211	291.898	293.482	292.161	290.4	291.364	291.936	292.078	290.538
Carpentras	295.696	296.395	295.613	295.108	297.058	295.674	297.842	297.098	295.685	297.49	296.976
Toravere	282.294	282.619	286.707	283.9	282.823	285.67	284.237	280.439	282.268	285.531	282.416
Lerwick	283.628	284.016	284.44	283.379	283.829	283.086	283.649	283.287	282.673	283.671	283.35

Table 13. PV modules' temperatures with the implementation of STs

Yearly average T_m [K]											
	With ST										
Region	2005	2006	2007	2008	2009	2010	2011	2012	2013	2014	2015
Barstow	305	304.775	305.184	305.448	299.266	298.872	297.875	303.198	301.943	302.777	302.7
Quillayute	289.482	289.644	287.922	289.031	289.075	290.172	289.761	290.493	292.21	290.539	292.81
Denver	295.443	296.157	296.408	297.519	296.619	293.875	296.046	298.212	295.354	294.166	290.872
Madison	293.313	293.481	290.931	292.509	292.844	296.142	295.274	297.061	293.009	293.124	295.001
Jacksonville	304.413	304.067	302.402	303.424	302.302	305.497	307.591	306.746	301.681	307.359	306.037
Izana	292.729	293.166	292.994	295.313	297.121	295.757	292.747	294.252	295.37	295.128	292.9
Carpentras	298.749	299.286	298.41	297.76	300.275	298.872	303.101	300.536	298.708	300.72	300.103
Toravere	283.448	283.598	289.215	285.173	284.222	288.616	285.864	281.178	283.225	287.626	283.135
Lerwick	283.939	284.311	284.923	283.621	284.131	283.45	283.933	283.645	282.888	283.889	283.61

5. Lifecycle estimation and PV power calculation

By moving forward within the flow of Figure 1, the data of Tables (12-13) permit the calculation of the estimated lifecycle for different PV systems, when incorporated and not, with STs. First, the T_m of each PV system, must be average-calculated during the span from year 2005 to year 2015 (since this is the available recorded data, constituting a reference base for determining as sensitive as possible an accurate image of T_m), thus the lifecycle estimation model depends solely on T_m. Forwardly, the acknowledgment of the lifecycle for each of the studied PV systems, allows in turn the determination of how significant the implementation of the ST is.

5.1. **Lifecycle estimation**

In order to calculate the average T_m during the span from year 2005 to year 2015, without/with the implementation of STs, the data of Tables (12-13) are to be used with the macro of Table 4: in this example, the range of ("M1:M11") represents the yearly average T_m of the PV systems with the implementation of STs (thus data of Table 13), where on the other hand, the range ("N1:N11") concerns the yearly average T_m of the PV systems without the implementation of STs (thus data of Table 12). Accordingly, the lifespan-averaged T_m of each of the PV systems without/with the implementation of STs are located in columns "P" and "O" respectively.

The lifecycle estimation is successively calculated, based on the data of columns "P" and "O", according to an accelerated life testing, based on Arrhenius acceleration law: the PV module life time (i.e., the entire PV system's lifetime which is composed of interconnected PV modules) is hence defined as in Eq.(2) [65].

$$\tau = e^{\gamma_0 + \frac{\gamma_1}{T_m}} \tag{2}$$

with γ_0 and γ_1 representing the Arrhenius model parameters (with $\gamma_0 = 5.23$ and $\gamma_1 = 2102$), and T_m the PV module's temperature [65]. Accordingly, the formula of the VBA in Table 5, and after its comparison with Eq.(2), it can be stated that the ranges ("Q1:Q11") and ("R1:R11") will encapsulate the estimated lifecycle for each of the studied PV systems with/without STs respectively. After executing both VBAs, of Table 4 and Table 5, the output data can be stored as in Table 14.

Calculated variable	Region								
	Barstow	Quillayute	Denver	Madison	Jacksonville	Izana	Carpentras	Toravere	Lerwick
Average T_m during the span from 2005 to 2015 without ST [K]	299.042	288.698	292.327	291.29	302.137	291.357	296.421	283.536	283.546
Average T_m during the span from 2005 to 2015 with ST [K]	302.458	290.103	295.515	293.88	304.683	294.316	299.683	285.027	283.849
Life time estimation of the PV system without ST [years]	24.058	30.949	28.274	29.007	22.387	28.959	25.601	35.335	35.326
Life time estimation of the PV system with ST [years]	22.222	29.876	26.164	27.22	21.122	26.933	23.699	33.991	35.048
Reduction in the lifecycle due to the application of ST [years]	1.836	1.072	2.11	1.787	1.264	2.026	1.902	1.344	0.278

Table 14. Calculated lifetime estimation for each of the PV systems with/without STs

As can be seen for Table 14, the implementation of ST onto a PV system is directly linked to an elevated temperature of the PV modules, in each of the studied PV systems. The highest T_m increase is recorded in the PV system located at Barstow (from 299.042 K to 302.458 K), where the lowest T_m increase is on the other side recorded in the PV system located at Lerwick (from 283.546 K to 283.849 K). The increased T_m in each of the PV systems, decreases their lifecycle expectancy, however it is not necessarily that the region with the highest T_m increase must yield to the highest decrease in the lifecycle expectancy for the PV system under study (Barstow). The reduced number of years in turn is only a difference between the lifecycle estimations of the PV system without/with ST, where the PV system located in Denver had scored the highest lifecycle estimation decrease of 2.11 years.

5.2. **PV power calculation**

Consecutively to the data obtained in Table 14, the process of the flowchart in Figure 1, can heads up toward the calculation of the generated PV power (P_{PV}), during the 10-year span from year 2005 to year 2015, then projected to the estimated lifecycle (as initially assumed that the environmental data during the span from year 2005 to year 2015 is decade-repetitive, as in Section 2). Firstly, the average P_{PV} is calculated for each of the surveyed PV systems, during each year of the span from year 2005 to year 2015. Therefore, the average P_{PV} during the 10-year span is the sum of the yearly average P_{PV}. In advance, the lifespan-average PV power production ($P_{PV,lifespan}$) can hence be calculated according to the data in Table 14. With that being said, the $P_{PV,lifespan}$ is to be calculated for each of the PV systems, with ST ($P_{PV,lifespan,with\ ST}$) and without ST ($P_{PV,lifespan,without\ ST}$).

The mathematical model used for P_{PV} calculation is shown in Eq.(3): it considers the maximum PV power at STC, the global irradiance, and the temperature of the PV module [66].

$$P_M = P_{M_{STC}} \times \frac{G_t}{1000} \times [1 - \gamma \times (T_m - 25)] \quad (3)$$

such that P_M represents the power of the module (hence the P_{PV} by taking into consideration the series-parallel interconnections of PV modules), $P_{M_{STC}}$ represents the P_{PV} at STC, G_t the global irradiance, γ the temperature parameter of the PV module at MPP (equals to $5\%/℃$ for the crystalline silicon modules, as the case for the studied PV systems), and T_m the PV module temperature (here in ℃) [66]. The constants 1000 and 25 represent the irradiance and the temperature at STC.

The yearly P_{PV} of each of the PV systems, can be hence calculated according to Eq.(3), after executing the VBA in Table 6: the ranges ("R1:R11") and ("S1:S11") represent therefore the cells at which the P_{PV} is yearly calculated, where columns "K" and "L" represent the irradiance data captured by the PV systems with/without STs respectively (Table 11), and columns "P" and "Q" represent the T_m for each of the PV systems without/with the application of STs respectively (Tables 12-13). Accordingly, the execution of the VBA in Table 6, results in the data encapsulated in Table 15, and Table 16. In order to standardize the outputs, all of the produced power calculations were in function of $P_{M_{STC}}$ (that is to multiply the obtained number

with $P_{M_{STC}}$ to have a Watt reading value), where such correlation does not perturb the numerical outcomes, since each of the PV system have a unique $P_{M_{STC}}$ according to the number of PV panels used in the design.

Region	Year										
	2005	2006	2007	2008	2009	2010	2011	2012	2013	2014	2015
Barstow	0.447	0.462	0.468	0.495	0.35	0.409	0.387	0.404	0.384	0.361	0.413
Quillayute	0.279	0.341	0.322	0.393	0.331	0.349	0.334	0.313	0.363	0.298	0.309
Denver	0.644	0.675	0.669	0.676	0.67	0.576	0.648	0.59	0.627	0.57	0.461
Madison	0.633	0.569	0.548	0.742	0.713	0.734	0.731	0.576	0.638	0.81	0.733
Jacksonville	0.349	0.333	0.37	0.408	0.371	0.427	0.374	0.358	0.296	0.396	0.394
Izana	0.536	0.558	0.528	0.659	0.681	0.785	0.436	0.547	0.62	0.608	0.462
Carpentras	0.528	0.51	0.492	0.516	0.469	0.514	0.516	0.55	0.499	0.457	0.462
Toravere	0.363	0.329	0.617	0.361	0.392	0.748	0.401	0.217	0.247	0.543	0.219
Lerwick	0.239	0.256	0.32	0.228	0.248	0.234	0.211	0.257	0.175	0.206	0.189

Yearly average P_{PV} in function of $P_{M_{STC}}$ ($\times P_{M_{STC}}$) without STs [W]

Table 15. Yearly average PV power production for each of the PV systems without STs

Region	Year										
	2005	2006	2007	2008	2009	2010	2011	2012	2013	2014	2015
Barstow	0.706	0.728	0.752	0.805	0.466	0.532	0.488	0.609	0.553	0.545	0.618
Quillayute	0.358	0.437	0.414	0.503	0.425	0.448	0.428	0.401	0.464	0.382	0.395
Denver	0.691	0.737	0.732	0.789	0.734	0.528	0.704	0.686	0.667	0.592	0.442
Madison	0.626	0.566	0.513	0.709	0.687	0.776	0.754	0.634	0.617	0.781	0.752
Jacksonville	0.549	0.52	0.54	0.616	0.536	0.693	0.686	0.629	0.42	0.708	0.677
Izana	0.547	0.579	0.539	0.708	0.771	0.85	0.449	0.579	0.667	0.658	0.478
Carpentras	0.652	0.648	0.606	0.624	0.612	0.634	0.786	0.717	0.616	0.607	0.601
Toravere	0.3	0.274	0.566	0.31	0.328	0.666	0.346	0.173	0.204	0.483	0.182
Lerwick	0.178	0.193	0.243	0.169	0.186	0.172	0.157	0.19	0.127	0.154	0.14

Yearly average P_{PV} in function of $P_{M_{STC}}$ ($\times P_{M_{STC}}$) with STs [W]

Table 16. Yearly average PV power production for each of the PV systems with STs

The obtainment of the data in Tables (16-17) allows the calculation of the cumulative average power during the entire lifecycle based on the produced power during the span from year 2005 to year 2015. This task is achievable by means of the VBA in Table 7: the cumulative average is first calculated over the 10-year span from year 2005 to year 2015, then projected towards the estimated lifecycle, as presented in Table 14. With what has been precedent, and after the execution of Table 7 VBA, the cumulative average PV power for each of the PV systems, with ST ($P_{PV,lifespan,with\ ST}$), as well as without ST ($P_{PV,lifespan,without\ ST}$) are presented in Table 17.

Region	$P_{PV,lifespan,without\ ST}$ ($\times P_{M_{STC}}$) $[W]$	$P_{PV,lifespan,with\ ST}$ ($\times P_{M_{STC}}$) $[W]$
Barstow	10.985	14.964
Quillayute	11.237	13.900
Denver	19.239	19.103
Madison	21.535	20.169
Jacksonville	9.120	13.883
Izana	18.584	18.373
Carpentras	14.113	16.826
Toravere	15.673	13.023
Lerwick	9.055	6.685

Table 17. Overall PV power production during the estimated lifecycle with/without STs

To have a better understanding of the values in Table 17, suppose a $P_{M_{STC}}$ value for any of the surveyed PV systems: for example, assume that the PV system located in Barstow, have a $P_{M_{STC}}$ of 10 kW (which is a rated power, and has not got anything to do with the implementation of ST): this system would produce, during its entire estimated lifecycle without ST (24.05 years) a cumulative-yearly-averaged power of 109.850 kW. If this same system is incorporated with ST, then during its entire estimated lifecycle (22.22 years), it would produce a cumulative-yearly-averaged power of 149.640 kW. As can be stated, the implementation of ST onto Barstow's PV system will yield in 39.790 kW more power than it would produce without the implementation of ST.

6. Results discussion with proposed ST application

After possessing the data of PV power production for each of the surveyed systems, and in order to flag a corresponding take-a-break recommendation, the process' flowchart in Figure 1, first searches for the case of $P_{PV,lifespan,with\ ST} < P_{PV,lifespan,without\ ST}$, then highlights in red the relevant years that are the reason behind such condition. Thus, the red-highlighted years of operation are to be considered with the numerical of PV system operational constants (i.e., PV

module's temperature) without the addition of ST. This can be automatically done by means of the VBA in Table 8. The take-a-break recommendation is hence validated after the new calculation of P_{PV}: if the resulting power generated exceeds the original $P_{PV,lifespan,with\ ST}$ and eventually $P_{PV,lifespan,without\ ST}$. In the second approach, and where there are not any $P_{PV,lifespan,with\ ST} < P_{PV,lifespan,without\ ST}$, the VBA in Table 9, then highlights in yellow the operational year in which $P_{PV,with\ ST,yearly} - P_{PV,without\ ST,yearly} < average\ all\ \Delta P_{PV,yearly}$. As in the previous logical condition, a new P_{PV} is hence calculated while taking the numerical of the PV system without ST in the highlighted year(s): the take-a-break recommendation is therefore justified, if the generated power exceeds the original $P_{PV,lifespan,with\ ST}$ and eventually $P_{PV,lifespan,without\ ST}$.

To be noted that the VBA of Tables (8-9) are only executed on the PV system of which the condition of $P_{PV,lifespan,with\ ST} < P_{PV,lifespan,without\ ST}$ applies. Consecutively, the Excel workbook detects an erroneous behavior of the PV systems ($P_{PV,lifespan,with\ ST} < P_{PV,lifespan,without\ ST}$) installed in Denver, Madison, Izana, Toravere, and Lerwick stations. All other PV systems are perceived as working as supposedly.

6.1. Case study of different regions of PV installations

6.1.1. Case of Denver

For the case of Denver, it was detected that during year 2010 and year 2015, the installed ST had produced a lower yearly average power compared to the same system without ST. Accordingly, the installed ST at that site, is recommended to take-a-break during the mentioned years. The corresponding new P_{PV} calculation is presented in Table 18.

6.1.2. Case of Madison

A negative $\Delta P_{PV,yearly}$ is witnessed in Madison, where by means of the VBA in Table 8, the affected years were 2005, 2006, 2007, 2008, 2009, 2013, and 2014. Accordingly, the ST installed in Madison's site is recommended to take-a-break during the mentioned years. However, even with the shutting down of the ST at these years, still, the $P_{PV,lifespan,with\ ST}$ calculated with the relevant data of climatic conditions as well as PV modules' temperatures of no ST, resulted in a power quantity that is still below $P_{PV,lifespan,without\ ST}$ as presented in Table 18. Therefore, for this site it is recommended to not apply any ST applications initially. This is due to the trilogy of irradiance-temperature-wind speed effect on the PV power generation.

6.1.3. Case of Izana

In Izana, each yearly P_{PV} of the system with ST exceeds the one for the system without ST. Still, a problem is due to the reduced lifecycle, due to the effect of T_m: despite that the yearly average power generation is bigger compared to itself without ST, but on the other hand, the reduced lifecycle due to ST application will yield in less power generation when compared with the lifecycle of the same system without ST. Therefore, for this particular region, the VBA of Table 8 is not applicable, where the flowchart of Figure 1 jumps to the next VBA in Table 9: to

recommend a take-a-break phase for this site, where the $\Delta P_{PV,yearly}$ is less than the average of all $\Delta P_{PV,yearly}$ during the span from year 2005 to year 2015. With that being said, the highlighted years were 2005, 2006, 2007, 2011, 2012, and 2015. When the ST is shutdown during these years, the overall PV power production, during the new lifecycle estimation will be greater than the one without ST application, as shown in Table 18.

6.1.4. Case of Toravere

As simple as it can be expressed, the VBA of Table 8 highlights each year of the span 2005 to 2015: as can be seen from Tables (15-16) the $P_{PV,lifespan,without\ ST}$ of each year is bigger than $P_{PV,lifespan,with\ ST}$ of the same year. Therefore, the flowchart of Figure 1 directly ends the solution method, while declaring a non-feasible application (since the recommendations are to shut down the ST during each year of the PV system's lifespan, that is equivalent of having no ST).

6.1.5. Case of Lerwick

Exactly as in the case of Toravere, the VBA of Table 8 also highlights each year of the span 2005 to 2015: as can be seen from Tables (15-16) the $P_{PV,lifespan,without\ ST}$ of each year is bigger than $P_{PV,lifespan,with\ ST}$ of the same year. That is to say that a ST application in Lerwick is not recommended, since the irradiance-temperature effect decrease from the generated power quantity.

The common fact for all of the problematic PV installation areas, is that when detected a negative $\Delta P_{PV,yearly}$, or the $\Delta P_{PV,yearly}$ is below the average, the entire calculations are to be re-considered beginning with the T_m calculations, to re-estimate the lifecycle, and finally to re-calculate the PV power production. This is equivalent to the re-execution of each of the VBA from Table 3 to Table 7. By following such procedure, Table 18 entitles the new calculations for each of the systems (if applicable) to finally conclude whether to recommend or not a take-a-break phase.

6.2. Self-criticism

Although the process presented in this study can give an automated insight about the feasibility whether to implement or not a ST on a PV system, based on the installation region's locations with the consequent calculated PV power productivity, still, it relies on historical measurement data: the time range of the data's measurement presented in this study lies in the interval of $[2005, \ldots, 2015]$. After year 2015, the data is supposed to be repetitive, re-beginning by the data of the year 2005. This composes a major drawback, for the fact that environmental data (irradiance, ambient temperature, wind speed) are fluctuating and cannot be perceived as standard or repetitive. Therefore, the decision to recommend a take-a-break would not be accurate, due to the reduced data measurements' sensitivity.

However, with the potential Artificial Intelligence (AI) trends, which include the Artificial Neural Network (ANN), and Machine Learning (ML), the solar irradiation on the first hand can be "predicted" with many forecasting models, such as deep generative model based on Long Short-Term Memory (LSTM) networks [67], Convolution Neural Network (CNN) based on

LSTM [68], regression-tree models [69], satellite cloud motion vectors [70], wavelet based time-frequency analysis integrated with deep learning [71], functional link broad learning system [72], federated learning and distributed computing [73], CNN with Support Vector Machine (CNN-SVM) [74], infinite hidden Markov model [75], statistical learning for Numerical Weather Prediction (NWP) [76], hybrid deep ensemble reinforcement learning algorithm [77], probabilistic irradiance forecasting based on XGBoost [78], encoder-decoder model [79], improved prophet algorithm [80], recurrent neural network [81], hybrid deep neural model [82], optical flow model [83], turbidity estimation method [84], real-time mapping model [85], regression unsupervised incremental learning algorithm [86], all-sky images pattern learning [87], adjusted combination of moving averages [88], regression analysis [89] and others [90]. The observation of the meteorological stations' data (i.e., PVGIS), which are presented here in this study in Table 11 for example, represents a main source for some ML models, as the reference data to conduct the solar irradiance predictions in the reference [91].

Following the same perspective, other needed climatic attributes that are used as input to the model presented in this work, such as temperature and wind speed can be also forecasted using AI models such as multi-objective algorithm and interpretability learning model [92], multi-objective feature selection approach [93], multifaceted feature fusion and transfer learning [94], deep learning with hybrid time series decomposition and multi-objective optimization [95], hybrid decomposition method with temporal convolutional networks [96], dynamic time scan forecasting [97], variational mode decomposition with improved echo state network [98], stacked denoising auto-encoders [99], generalized dynamical model [100], grey wolf optimizer [101], adaptive deep learning models [102], and other numerical models [103].

With that being said, and with the continuous improvement of meteorological data prediction models, based on AI learning algorithms, the required input data for the process of this paper shall provoke no future problem: it will be possible to obtain the needed environmental attributes (as presented in Table 11) ahead of time, without any physical data measurements. That is to say that even the extrapolation of the irradiance, ambient temperature, and wind speed, which is used in this work (i.e., to extrapolate the data of the span $[2005, \dots, 2015]$ over the estimated lifecycle) will not be necessary, since the fortified AI models should be subsequently able to determine by prediction the needed data years ahead (i.e., long-term prediction models). But on the other hand, the predicted data accuracy, might affect the data sampling, since all AI models would have a marginal error, as compared to the physically measured and recorded data.

As can be concluded from Table 18, a five years take-a-break recommendation for the PV system that is installed in Denver, would yield in an average cumulative PV power production of $19.432 \times P_{M_{STC}}$ after it initially was $19.103 \times P_{M_{STC}}$ (which is lower than the same power quantity produced by the same PV system without ST equal to $19.239 \times P_{M_{STC}}$): if assumed that the $P_{M_{STC}} = 10$ kW, the major power difference before/after the take-a-break recommendation will be 194.32 kW and 191.03 kW that is of more than 3 kW of produced power.

From another side, even with the take-a-break recommendations for the PV system that is installed in Madison, still, its $P_{PV,lifespan,with\ ST}$ $(21.393 \times P_{M_{STC}})$ is lower than $P_{PV,lifespan,without\ ST}$ $(21.535 \times P_{M_{STC}})$. Therefore, a ST is seen not feasible in Madison zone. As for Toravere and Lerwick, the implementation of STs is initially non-feasible since each $P_{PV,lifespan,with\ ST}$ during the estimated lifecycles is lower than $P_{PV,lifespan,without\ ST}$.

To be noted that the non-feasibility of the ST at some sites (e.g., Madison), has not got anything to do related with a singular environmental attribute, such as high/low irradiance, or high/low wind speed alone, or even any relation with the type of the applied ST (SAT, or DAT). In other words, it cannot be judged that a relatively high elevated ambient temperature in a particular zone, insists the non-feasibility of a ST application. Instead, the flowchart in Figure 1, with the different tabulated results obtained, reveals that the combination of the three meteorological attributes (irradiance, temperature, wind speed), together with the estimated lifecycle, determines the PV power produced, hence the judgment criteria.

Table 18. Results of the process flowchart

Region	Problematic operational years	New T_m [K]	New lifecycle estimation [years]	New $P_{PV,lifespan,with\ ST}$ $(\times P_{M_{STC}})$	$P_{PV,lifespan,without\ ST}$ $(\times P_{M_{STC}})$	Is take-a-break recommended?
Denver	2010;2015	295.187	26.37	19.432	19.239	YES: 5 years during the lifecycle
Madison	2005;2006;2007; 2008;2009;2013; 2014	292.338	28.26	21.393	21.535	NO: the implementation of STs in Madison is NOT recommended
Izana	2005;2006;2007; 2011;2012;2015	292.914	27.868	18.728	18.584	YES: 17 years during the lifecycle
Toravere	ALL	-	-	-	-	NO: the implementation of STs in Toravere is NOT recommended
Lerwick	ALL	-	-	-	-	NO: the implementation of STs in Lerwick is NOT recommended

7. Conclusion and future work

The traditional approach toward STs is their implementation onto PV systems in order to ameliorate the generated PV power. This is due to the linear correlation between the increased irradiance (due to the STs' dynamical projection of PV panels under the sun) and the higher power generation. Despite the proportional irradiance-power generation relation, that is seemed to be fortified upon the usage of STs, on the other hand exists a negatively induced relation between the PV module temperature and the PV power productivity.

The more irradiance is captivated due to the application of STs, the more heat is generated on the level of PV modules, the less the estimated lifecycle will be. Where the PV power generation is inversely proportional to the PV module temperature, in addition to the reduced lifecycle estimation, it was shown through this paper, that STs might not be feasible for application in some regions, and in others are recommended to take-a-break according to this work's flow process.

Amongst nine different surveyed regions with PV systems installations, located in Europe and America, five of them showed erroneous performance upon their confrontation with STs: Denver, Madison, Izana, Toravere, and Lerwick, after detection by the automated Excel workbook as presented in this study. By following the flow process's logic, results have indicated that the ST in Denver is to take-a-break for five years during its lifecycle, where the ST of Izana is also recommended to take-a-break for seventeen years during its lifecycle. Such recommendations come as an intermediate solution to compensate the reduced lifecycle and elevated PV module's temperature after being subjected to the ST. As for all other errored sites (i.e., Madison, Toravere, Lerwick), the application of STs is not recommended at all due to the irradiance-temperature-wind speed trilogy effect on PV modules.

Concerning the applicable future works behind this manuscript, the set of VBA scripts can be translated into an Android product for example, to produce a handy tool that studies the feasibility of STs applications, by means of smartphones. This thus would provide a practical and easy to use phone application, which does not require much space/memory to operate. The presented VBA pseudo-codes are to be re-written in Java, where with the work conducted in this paper, the backbone of the app will be ready initially. This targeted app can be as well linked with Google Maps, to provide an ability for a real-time area localization, with precise coordinates, thus yielding in better data extraction from PVGIS.

On a second attempt, the presented VBA can be also re-written in JavaScript in order to create a Google Chrome (or any other web browser) web application (extension), that interactively fetch the data from PVGIS to successively do the calculation and output the results concerning the feasibility of STs application in dynamic ways. The overall bottom line behind this paper is that STs are not necessarily a beneficial addon to PV systems, where in some cases their non-application yield to more PV power outcomes, with reduced technical/economical burdens (i.e., cost of ST, ST's maintenance, etc.).

References

[1] X. Yang, S. Liu, L. Zhang, J. Su, T. Ye. 2020. Design and analysis of a renewable energy power system for shale oil exploitation using hierarchical optimization. Energy. 206, Article ID: 118078.

[2] A.L. Konde, M. Kusaf, M. Dagbasi. 2022. An effective design method for grid-connected solar PV power plants for power supply reliability. Energy for Sustainable Development. 70, 301-13.

[3] J. Buss, N. Mansuy, J. Langaniere, D. Persson. 2022. Greenhouse gas mitigation potential of replacing diesel fuel with wood-based bioenergy in an arctic Indigenous community: A pilot study in Fort McPherson, Canada. Biomass and Bioenergy. 159, Article ID: 106367.

[4] A. Allouhi, S. Rehman, M.S. Buker, Z. Said. 2023. Recent technical approaches for improving energy efficiency and sustainability of PV and PV-T systems: A comprehensive review. Sustainable Energy Technologies and Assessments. 56, Article ID: 103026.

[5] S. Sreenath, A.M. Azmi, N.Y. Dahlan, K. Sudhakar. 2022. A decade of solar PV deployment in ASEAN: Policy landscape and recommendations. Energy Reports. 8, Supplement 10, 460-9.

[6] K. Osmani, A. Haddad, H. Jaber, T. Lemenand, B. Castanier, M. Ramadan. 2022. Mitigating the effects of partial shading on PV system's performance through PV array reconfiguration: A review. Thermal Science and Engineering Progress. 31, Article ID: 101280.

[7] K. Osmani, M. Ramadan, T. Lemenand, B. Castanier, A. Haddad. 2021. Optimization of PV array tilt angle for minimum levelized cost of energy. Computers & Electrical Engineering. 96, Part A, Article ID: 107474.

[8] K. Osmani, A. Haddad, T. Lemenand, B. Castanier, M. Ramadan. 2021. An investigation on maximum power extraction algorithms from PV systems with corresponding DC-DC converters. Energy. 224, Article ID: 120092.

[9] K. Osmani, A. Haddad, T. Lemenand, B. Castanier, M. Ramadan. 2020. A review on maintenance strategies for PV systems. Science of the Total Environment. 746, Article ID: 141753.

[10] K. Osmani, M. Alkhedher, M. Ramadan, D.S. Choi, L.K.B. Li, M.H. Doranehgard, A.-G. Olabi. 2023. Recent progress in the thermal management of lithium-ion batteries. Journal of Cleaner Production. 389, Article ID: 136024.

[11] M. Zhao, Y. Wang, X. Wang, J. Chang, Y. Chen, Y. Zhou, A. Guo. 2022. Flexibility evaluation of wind-PV-hydro multi-energy complementary base considering the compensation ability of cascade hydropower stations. Applied Energy. 315, Article ID: 119024.

[12] A. El Hammoumi, S. Chtita, S. Motahhir, A. El Ghzizal. 2022. Solar PV energy: From material to use, and the most commonly used techniques to maximize the power output of PV systems: A focus on solar trackers and floating solar panels. Energy Reports. 8, 11992-12010.

[13] J.M. Schwidtal, M. Agostini, M. Coppo, F. Bignucolo, A. Lorenzoni. 2023. Optimized operation of distributed energy resources: The opportunities of value stacking for Power-to-Gas aggregated with PV. Applied Energy. 334, Article ID: 120646.

[14] M. Vyas, S. Chowdhury, A. Verma, V.K. Jain. 2022. Solar Photovoltaic Tree: Urban PV power plants to increase power to land occupancy ratio. Renewable Energy. 190, 283-83.
[15] A. Awasthi, A.K. Shukla, M. Manohar S.R., C. Dondariya, K.N. Shukla, D. Porwal, G. Richhariya. 2020. Review on sun tracking technology in solar PV system. Energy Reports. 6, 392-405.
[16] Y. Yin, H. Chen, X. Zhao, W. Yu, H. Su, Y. Chen, P. Lin. 2022. Solar-absorbing energy storage materials demonstrating superior solar-thermal conversion and solar-persistent luminescence conversion towards building thermal management and passive illumination. Energy Conversion and Management. 266, Article ID: 115804.
[17] J. Wong, F. Bai, T.K. Saha, R.H.G. Tan. 2021. A feasibility study of the 1.5-axis tracking model in utility-scale solar PV plants. Solar Energy. 216, 171-9.
[18] R. F. Fuentes-Morales, A. Diaz-Ponce, M.I. Pena-Cruz, P.M. Rodrigo, L.M. Valentin-Coronado, F. Martell-Chavez, C.A. Pineda-Arellano. 2020. Control algorithms applied to active solar tracking systems: A review. Solar Energy. 212, 203-19.
[19] A.A. Elsayed, E.E. Khalil, M.A. Kassem, O.A. Huzzayin. 2021. A novel mechanical solar tracking mechanism with single axis of tracking for developing countries. Renewable Energy. 170, 1129-42.
[20] G.S. Rajput, J. Vora, P. Prajapati, B. Chaudhari. 2022. Areas of recent developments for shape memory alloy: A review. materialstoday: PROCEEDINGS. 62, Part 13, 7194-8.
[21] Z. Zhang, K. Pei, M. Sun, H. Wu, X. Yu, H. Wu, S. Jiang, F. Zhang. 2020. A novel solar tracking model integrated with bistable composite structures and bimetallic strips. Composite Structures. 248, Article ID: 112506.
[22] S. Tu, L. Xu, J.K. El-Demellawi, H. Liang, X. Xu, S. Lopatin, S. De Wolf, X. Zhang, H.N. Alshareef. 2020. Autonomous MXene-PVDF actuator for flexible solar trackers. Nano Energy. 77, Article ID: 105277.
[23] B. Mendecka, G. Di Ilio, V.K. Krastev, G. Bella. 2022. Evaluating the potential of phase-change induced volumetric expansion in thermal energy storage media for passive solar tracking in high-temperature solar energy systems. Applied Thermal Engineering. 212, Article ID: 118561.
[24] L.J. Piotrowski, F.A. Farret. 2022. Feasibility of solar tracking and fixed topologies considering the estimated degradation and performance of photovoltaic panels. Solar Energy Materials and Solar Cells. 244, Article ID: 111834.
[25] W. Ma, W. Zhang, X. Zhang, W. Chen, Q. Tan. 2023. Experimental investigations on the wind load interference effects of single-axis solar tracker arrays. Renewable Energy. 202, 566-80.
[26] C.-H. Wu, H.-C. Wang, H.-Y. Chang. 2022. Dual-axis solar tracker with satellite compass and inclinometer for automatic positioning and tracking. Energy for Sustainable Development. 66, 308-18.
[27] E.T. Tchao, S.A. Asakipaam, Y.A.K. Fiagbe, B. Yeboah-Akowuah, E. Ramde, A.S. Agbemenu, B. Kommey. 2022. An Implementation of an optimized dual-axis solar tracking algorithm for concentrating solar power plants deployment. Scientific African. 16, Article ID: e01228.

[28] A. Saymbetov, S. Mekhilef, N. Kuttybay, M. Nurgaliyev, D. Tukymbekov, A. Meiirkhanov, G. Dosymbetova, Y. Svanbayev. 2021. Dual-axis schedule tracker with an adaptive algorithm for a strong scattering of sunbeam. Solar Energy. 224, 285-97.
[29] C. Jamroen, C. Fongkerd, W. Krongpha, P. Komkum, A. Pirayawaraporn, N. Chindakham. 2021. A novel UV sensor-based dual-axis solar tracking system: Implementation and performance analysis. Applied Energy. 299, Article ID: 117295.
[30] J. Chantana, Y. Kawano, T. Nishimura, A. Mavlonov, T. Minemoto. 2022. Estimation of performance limit for bifacial single-junction solar cell. Optics & Laser Technology. 156, Article ID: 108500.
[31] A.R. Sagar, S. Al Saim, A.S.M. Ittehad, H.U. Zaman. 2017. A novel design of a Bi-level automatic solar tracker using rotations around orthogonal axes. 2017 8th International Conference on Computing, Communication and Networking Technologies (ICCCNT). IEEE. India.
[32] F.I. Mustafa, S. Shakir, F.F. Mustafa, A.T. Naiyf. 2018. Simple design and implementation of solar tracking system with two axis with four sensors for Baghdad city. 2018 9th International Renewable Energy Congress (IREC). IEEE. Tunisia.
[33] Z. Zengwei, Z. Zhen, J. Yongfeng, L. Haolin, Z. Shengcheng. 2019. Performance Analysis on Bifacial PV Panels With Inclined and Horizontal East-West Sun Trackers. IEEE Journal of Photovoltaics. 9(3), 636-42.
[34] K.E. Kanyarusoke, J. Gryzagoridis. 2016. The new hydro-mechanical solar tracker: Performance testing with a PV panel. 2016 International Conference on the Domestic Use of Energy (DUE). IEEE. South Africa.
[35] H. Allamehzadeh. 2019. An Update on Solar Energy and Sun Tracker Technology with a Dual Axis Sun Tracker Application. 2019 IEEE 46th Photovoltaic Specialists Conference (PVSC). IEEE. USA.
[36] P. Sharma, N. Malhotra. 2014. Solar tracking system using microcontroller. 2014 1st International Conference on Non Conventional Energy (ICONCE 2014). IEEE. India.
[37] H. Fathabadi. 2017. Novel Online Sensorless Dual-Axis Sun Tracker. IEEE/ASME Transactions on Mechatronics. 22(1), 321-8.
[38] I.H. Rosma, I.M. Putra, D.Y. Sukma, E. Safrianti, A.A. Zakri, A. Abdulkarim. 2018. Analysis of Single Axis Sun Tracker System to Increase Solar Photovoltaic Energy Production in the Tropics. 2018 2nd International Conference on Electrical Engineering and Informatics (Icon EEI). IEEE. Indonesia.
[39] I.H. Rosma, J. Asmawi, S. Darmawan, B. Anand, N.D. Ali, B. Anto. 2018. The implementation and Analysis of Dual Axis Sun Tracker System to Increase Energy Gain of Solar Photovoltaic. 2018 2nd International Conference on Electrical Engineering and Informatics (ICon EEI). IEEE. Indonesia.
[40] A. Masih, I. Odinaev. 2019. Performance Comparison of Dual Axis Solar Tracker with Static Solar System in Ural Region of Russia. 2019 Ural Symposium on Biomedical Engineering, Radioelectronics and Information Technology (USBEREIT). IEEE. Russia.
[41] F. Peprah, B. Aboagye, M. Amo-Boateng, S. Gyamfi, E. Effah-Donyina. 2023. Economic evaluation of solar PV electricity presumption in Ghana. Solar Compass. 5, Article ID: 100035.
[42] A. Abdallah, R. Opoku, C.K.K. Sekyere, S. Boahen, K.O. Amoabeng, F. Uba, G.Y. Obeng, F.K. Forson. 2022. Experimental investigation of thermal management

techniques for improving the efficiencies and levelized cost of energy of solar PV modules. Case Studies in Thermal Engineering. 35, Article ID: 102133.
[43] S. Al-Sanad, J. Parol, L. Wang, A. Kolios. 2023. Design optimisation of wind turbine towers with reliability-based calibration of partial safety factors. Energy Reports. 9, 2548-56.
[44] D. D'Agostino, F. Minelli, M. D'Urso, F. Minichiello. 2022. Fixed and tracking PV systems for Net Zero Energy Buildings: Comparison between yearly and monthly energy balance. Renewable Energy. 195, 809-24.
[45] A.N. Vargas, G.R. Francisco, M.A.F. Montezuma, L.P. Sampaio, L. Acho. 2022. Low-cost dual-axis solar tracker with photovoltaic energy processing for education. Sustainable Energy Technologies and Assessments. 53, Part B, Article ID: 102542.
[46] M.A.V. Rad, A. Toopshekan, P. Rahdan, A. Kasaeian, O. Mahian. 2020. A comprehensive study of techno-economic and environmental features of different solar tracking systems for residential photovoltaic installations. Renewable and Sustainable Energy Reviews. 129, Article ID: 109923.
[47] P. Majewski, W. Al-shammari, M. Dudley, J. Jit, S.-H. Lee, K. Myoung-Kug, K. Sung-Jim. 2021. Recycling of solar PV panels – product stewardship and regulatory approaches. Energy Policy. 149, Article ID: 112062.
[48] E.I.C. Zebra, H.J. van der Windt, B. Olubayo, G. Nhumaio, A.P.C. Faaij. 2023. Scaling up the electricity access and addressing best strategies for a sustainable operation of an existing solar PV mini-grid: A case study of Mavumira village in Mozambique. Energy for Sustainable Development. 72, 58-82.
[49] A. Costa, T.S. Ng, B. Su. 2023. Long-term solar PV planning: An economic-driven robust optimization approach. Applied Energy. 335, Article ID: 120702.
[50] A. Gholami, M. Ameri, M. Zandi, R.G. Ghoachani, S.F. Gerashi, H.A. Kazem, A.H.A. Al-Waeli. 2023. Impact of harsh weather conditions on solar photovoltaic cell temperature: Experimental analysis and thermal-optical modeling. Solar Energy. 252, 176-94.
[51] N. Aoun. 2022. Methodology for predicting the PV module temperature based on actual and estimated weather data. Energy Conversion and Management: X. 14, Article ID: 100182.
[52] R. Ramful, N. Sowaruth. 2022. Low-cost solar tracker to maximize the capture of solar energy in tropical countries. Energy Reports. 8, Supplement 15, 295-302.
[53] Z.Y. Yeo, Z.P. Ling, J.W. Ho, Q.X. Lim, Y.H. So, S. Wang. 2022. Status review and future perspectives on mitigating light-induced degradation on silicon-based solar cells. Renewable and Sustainable Energy Reviews. 159, Article ID: 112223.
[54] K. Osmani, A. Haddad, T. Lemenand, B. Castanier, M. Ramadan. 2020. Material based fault detection methods for PV systems. Key Engineering Materials. 865, 111-5.
[55] N. Bansal, S.P. Jaiswal, G. Singh. 2022. Prolonged degradation and reliability assessment of installed modules operational for 10 years in 5 MW PV plant in hot semi-arid climate. Energy for Sustainable Development. 68, 373-89.
[56] U.M. Damo, C.G. Ozoegwu, C. Ogbonnaya, C. Maduabuchi. 2023. Effects of light, heat and relative humidity on the accelerated testing of photovoltaic degradation using Arrhenius model. Solar Energy. 250, 335-46.

[57] A. Ouédraogo, B. Zouma, E. Ouédraogo, L. Guissou, D.J. Bathiébo. 2021. Individual efficiencies of a polycrystalline silicon PV cell versus temperature. Results in Optics. 4, Article ID: 100101.
[58] M.R. Kalateh, A. Kianifar, M. Sardarabadi. 2022. Energy, exergy, and entropy generation analyses of a water-based photovoltaic thermal system, equipped with clockwise counter-clockwise twisted tapes: An indoor experimental study. Applied Thermal Engineering. 215, Article ID: 118906.
[59] X. Ma, M. Li, Y. Peng, L. Sun, C. Chen. 2022. Development of thermo-electrical loss model for photovoltaic module with inhomogeneous temperature. Energy. 248, Article ID: 123542.
[60] K. Osmani, M. Ramadan, A. Haddad, T. Lemenand, B. Castanier. 2022. An overview on the use of phase change material (PCM) for PV cooling. Key Engineering Materials. 922, 3-9.
[61] Website: https://re.jrc.ec.europa.eu/pvg_tools/en/
[62] J. Antonanzas, R. Urraca, F.J. Martinez-de-Pison, F. Antonanzas. 2018. Optimal solar tracking strategy to increase irradiance in the plane of array under cloudy conditions: A study across Europe. Solar Energy. 163, 122-30.
[63] W.D. Lubitz. 2011. Effect of manual tilt adjustments on incident irradiance on fixed and tracking solar panels. Applied Energy. 88, 1710-9.
[64] M. Akhsassi, A. El Fathi, N. Erraisi, N. Aarich, A. Bennouna, M. Raoufi, A. Outzourhit. 2018. Experimental investigation and modeling of the thermal behavior of a solar PV module. Solar Energy Materials and Solar Cells. 180, 271-9.
[65] R. Laronde, A. Charki, B. David. 2011. Lifetime estimation of a photovoltaic module based on temperature measurement. 2nd IMEKO TC 11 International Symposium Metrological infrastructure. Proceedings, Croatia, pp. 1-6.
[66] K. Mertens. 2014. Chapter 6 – Solar Modules and Solar Generators. Photovoltaics Fundamentals, Technology, and Practice. Wiley. pp. 136-41.
[67] Y. Gao, S. Miyata, Y. Akashi. 2022. Multi-step solar irradiation prediction based on weather forecast and generative deep learning model. Renewable Energy. 188, 637-50.
[68] P. Kumari, D. Toshniwal. 2021. Deep learning models for solar irradiance forecasting: A comprehensive review. Journal of Cleaner Production. 318, Article ID: 128566.
[69] C. Voyant, F. Motte, G. Notton, A. Fouilloy, M.-L. Nivet, J.-L. Duchaud. 2018. Prediction intervals for global solar irradiation forecasting using regression trees methods. Renewable Energy. 126, 332-40.
[70] D. Aicardi, P. Musé, R. Alonso-Suarez. 2022. A comparison of satellite cloud motion vectors techniques to forecast intra-day hourly solar global horizontal irradiation. Solar Energy. 233, 46-60.
[71] F. Rodriguez, I. Azcarate, J. Vadillo, A. Galarza. 2022. Forecasting intra-hour solar photovoltaic energy by assembling wavelet based time-frequency analysis with deep learning neural networks. International Journal of Electrical Power & Energy Systems. 137, Article ID: 107777.
[72] R. Bisoi, D.R. Dash, P.K. Dash, L. Tripathy. 2022. An efficient robust optimized functional link broad learning system for solar irradiance prediction. Applied Energy. 319, Article ID: 119277.

[73] H. Wen, Y. Du, E.G. Lim, H. Wen, K. Yan, X. Li, L. Jiang. 2022. A solar forecasting framework based on federated learning and distributed computing. Building and Environment. 225, Article ID: 109556.
[74] S. Ghimire, B. Bhandari, D. Casillas-Pérez, R.C. Deo, S. Salcedo-Sanz. 2022. Hybrid deep CNN-SVR algorithm for solar radiation prediction problems in Queensland, Australia. Engineering Applications of Artificial Intelligence. 112, Article ID: 104860.
[75] A. Frimane, J. Munkhammar, D. van der Meer. 2022. Infinite hidden Markov model for short-term solar irradiance forecasting. Solar Energy. 244, 331-42.
[76] H. Verbois, Y.-M. Saint-Drenan, A. Thiery, P. Blanc. 2022. Statistical learning for NWP post-processing: A benchmark for solar irradiance forecasting. Solar Energy. 238, 132-49.
[77] S.M.J. Jalali, S. Ahmadian, B. Nakisa, M. Khodavar, A. Khosravi, S. Nahavandi, S.M.S. Islam, M. Shafie-khah, J.P.S. Catalao. 2022. Solar irradiance forecasting using a novel hybrid deep ensemble reinforcement learning algorithm. Sustainable Energy, Grids and Networks. 32, Article ID: 100903.
[78] X. Li, L. Ma, P. Chen, H. Xu, Q. Xing, J. Yan, S. Lu, H. Fan, L. Yang, Y. Cheng. 2022. Probabilistic solar irradiance forecasting based on XGBoost. Energy Reports. 8, Supplement 5, 1087-95.
[79] J. Tong, L. Xie, S. Fang, W. Yang, K. Zhang. 2022. Hourly solar irradiance forecasting based on encoder-decoder model using series decomposition and dynamic error compensation. Energy Conversion and Management. 270, Article ID: 116049.
[80] Y. Xinpei, L. Yiguo, S. Jiong. 2022. Forecasting Research on Long-term Solar Irradiance with An Improved Prophet Algorithm. IFAC-PapersOnLine. 55(9), 491-4.
[81] S.A. Haider, M. Sajid, H. Sajid, E. Uddin, Y. Ayaz. 2022. Deep learning and statistical methods for short- and long-term solar irradiance forecasting for Islamabad. Renewable Energy. 198, 51-60.
[82] X. Huang, Q. Li, Y. Tai, Z. Chen, J. Zhang, J. Shi, B. Gao, W. Liu. 2021. Hybrid deep neural model for hourly solar irradiance forecasting. Renewable Energy. 171, 1041-60.
[83] P.M.P. Garniwa, R.A. Rajagukguk, R. Kamil, H. Lee. 2023. Intraday forecast of global horizontal irradiance using optical flow method and long short-term memory model. Solar Energy. 252, 234-51.
[84] S. Chen, Z. Liang, P. Dong, S. Guo, M. Li. 2023. A transferable turbidity estimation method for estimating clear-sky solar irradiance. Renewable Energy. 206, 635-44.
[85] F. Wang, Z. Xuan, Z. Zhen, Y. Li, K. Li, L. Zhao, M. Shafie-khah, J.P.S. Catalao. 2020. A minutely solar irradiance forecasting method based on real-time sky image-irradiance mapping model. Energy Conversion and Management. 220, Article ID: 113075.
[86] B.K. Puah, L.W. Chong, Y.W. Wong, K.M. Begam, N. Khan, M.A. Juman, R.K. Rajkumar. 2021. A regression unsupervised incremental learning algorithm for solar irradiance prediction. Renewable Energy. 164, 908-25.
[87] T.-P. Chu, J.-H. Guo, Y.-G. Leu, L.-F. Chou. 2023. Estimation of solar irradiance and solar power based on all-sky images. Solar Energy. 249, 495-506.
[88] D.J. Pedregal, J.R. Trapero. 2021. Adjusted combination of moving averages: A forecasting system for medium-term solar irradiance. Applied Energy. 298, Article ID: 117155.

[89] D.R. Arumugham, P. Rajendran. 2021. Modelling global solar irradiance for any location on earth through regression analysis using high-resolution data. Renewable Energy. 180, 1114-23.
[90] F. von Loeper, P. Schamann, M. de Langlard, R. Hess, R. Basmann, V. Schmidt. 2020. Probabilistic prediction of solar power supply to distribution networks, using forecasts of global horizontal irradiation. Solar Energy. 203, 145-56.
[91] Y. Zhou, Y. Liu, D. Wang, X. Liu, Y. Wang. 2021. A review on global solar radiation prediction with machine learning models in a comprehensive perspective. Energy Conversion and Management. 235, Article ID: 113960.
[92] M. Li, Y. Yang, Z. He, X. Guo, R. Zhang, B. Huang. 2023. A wind speed forecasting model based on multi-objective algorithm and interpretability learning. Energy. 269, Article ID: 126778.
[93] S.-X. Lv, L. Wang. 2023. Multivariate wind speed forecasting based on multi-objective feature selection approach and hybrid deep learning model. Energy. 263, Part E, Article ID: 126100.
[94] T. Liang, C. Chen, C. Mei, Y. Jing, H. Sun. 2022. A Wind Speed Combination Forecasting Method Based on Multifaceted Feature Fusion and Transfer Learning for Centralized Control Center. Electric Power Systems Research. 213, Article ID: 108765.
[95] S.-X. Lv, L. Wang. 2022. Deep learning combined wind speed forecasting with hybrid time series decomposition and multi-objective parameter optimization. Applied Energy. 311, Article ID: 118674.
[96] D. Li, F. Jiang, M. Chen, T. Qian. 2022. Multi-step-ahead wind speed forecasting based on a hybrid decomposition method and temporal convolutional networks. Energy. 238, Part C, Article ID: 121981.
[97] M.A. Costa, R. Ruiz-Cardenas, L.B. Mineti, M.O. Prates. 2021. Dynamic time scan forecasting for multi-step wind speed prediction. Renewable Energy. 177, 584-95.
[98] H. Hu, L. Wang, R. Tao. 2021. Wind speed forecasting based on variational mode decomposition and improved echo state network. Renewable Energy. 164, 729-51.
[99] H. Jahangir, M.A. Golkar, F. Alhameli, A. Mazouz, A. Ahmadian, A. Elkamel. 2020. Short-term wind speed forecasting framework based on stacked denoising auto-encoders with rough ANN. Sustainable Energy Technologies and Assessments. 38, Article ID: 100601.
[100] V.E.L.A. Duca, T.C.O. Fonseca, F.L.C. Oliveira. 2021. A generalized dynamical model for wind speed forecasting. Renewable and Sustainable Energy Reviews. 136, Article ID: 110421.
[101] A. Altan, S. Karasu, E. Zio. 2021. A new hybrid model for wind speed forecasting combining long short-term memory neural network, decomposition methods and grey wolf optimizer. Applied Soft Computing. 100, Article ID: 106996.
[102] N. Abdulla, M. Demirci, S. Ozdemir. 2022. Design and evaluation of adaptive deep learning models for weather forecasting. Engineering Applications of Artificial Intelligence. 116, Article ID: 105440.
[103] H. Chen, Q. Zhang, Y. Birkelund. 2022. Machine learning forecasts of Scandinavian numerical weather prediction wind model residuals with control theory for wind energy. Energy Reports. 8, Supplement 13, 661-8.

Chapitre 6

Conclusions et perspectives

Les systèmes photovoltaïques représentent une voie prometteuse pour faire évoluer le paysage énergétique mondial vers un avenir plus propre et plus vert. En tant que ressources énergétiques renouvelables populaires, ils affichent une trajectoire de croissance constante, tant au niveau des applications que de la recherche. Cependant, et comme c'est le cas pour les systèmes physiques extérieurs, les systèmes photovoltaïques sont souvent confrontés à des défauts et à des conditions environnementales défavorables qui compromettent leur productivité énergétique et leur efficacité globale. Malgré ces obstacles, l'engagement continu à faire progresser la technologie PV, comme c'est l'objet de cette thèse, souligne son rôle vital dans l'élaboration d'un paradigme de production d'énergie plus propre et plus durable.

La partie de cette thèse consacrée à l'analyse de la littérature, en ce qui concerne les différents types de défauts qui peuvent intervenir dans le bon fonctionnement des systèmes PV, ainsi que les défauts de maintenance PV correspondants, représente une part importante de celle-ci. Après l'étude présentée, il est conclu que les stratégies d'optimisation basées sur l'irradiation pour les systèmes PV agiraient comme un schéma de maintenance préventive pour de tels systèmes, prolongeant ainsi leur cycle de vie. Ce fait est principalement dû à la difficulté de compenser les effets des fluctuations de l'irradiation sur la production d'énergie des systèmes PV (contrairement à l'augmentation de la température PV par exemple, qui peut être directement compensée par différentes techniques de refroidissement, comme cela a également été étudié dans cette thèse).

En conséquence, et en plus de six revues publiées, cette thèse a pris en considération la conception et la simulation de quatre études, qui permettent une performance maximale d'un système PV, dans des conditions extrêmement fluctuantes et d'ombrage partiel. Le schéma essentiel utilisé dans cette thèse, pour optimiser la performance des systèmes PV, est principalement basé donc sur l'irradiation.

Le mode de modification dynamique de l'angle d'inclinaison proposé permet d'augmenter l'irradiation arrivant à la surface des modules PV (c'est-à-dire l'irradiation normale directe), tandis que le nouveau chargeur solaire présenté permet de charger rapidement et en toute sécurité les systèmes de stockage d'énergie à base de Lithium-Ion pour les systèmes PV hors réseau. Le nouvel algorithme MPPT basé sur les mécanismes pathogènes du diabète de type 1 (T1D) a permis d'extraire une puissance maximale d'un réseau photovoltaïque dans des conditions d'ombrage partiel difficiles (reflétées par cinq pics locaux maximaux distincts dans la courbe caractéristique photovoltaïque). L'étude de faisabilité sur les suiveurs solaires, au stade final, a joué le rôle d'un décideur en termes d'installation d'un suiveur solaire pour un système PV, sur la base de la zone géographique d'installation, optimisant ainsi la performance du système en prolongeant son cycle de vie (en raison de la diminution de l'entropie des modules PV).

Les principaux résultats de cette thèse de doctorat sont résumés dans le tableau suivant :

Titre de l'étude	Méthodologie de l'étude	Résultats principaux
1.1 Revue des stratégies de maintenance pour les systèmes photovoltaïques	➢ Étudier les effets des différentes pannes photovoltaïques sur le fonctionnement des systèmes photovoltaïques. ➢ Explorer les différents types de stratégies de maintenance photovoltaïque.	✓ Une augmentation de 8,7 % de la production globale d'électricité, une réduction de 81 % des chutes de tension et une diminution de 2 % des distorsions sont obtenues grâce à l'application de différents types de programmes de maintenance photovoltaïque. ✓ Les techniques de maintenance prédictive et préventive des systèmes photovoltaïques devraient constituer la tendance future dans le domaine de la maintenance des systèmes photovoltaïques. ✓ La maintenance préventive joue un

		rôle important dans la prolongation du cycle de vie des systèmes photovoltaïques tout en optimisant leurs performances.
1.2 Revue des défauts des systèmes photovoltaïques et de leurs méthodes de détection correspondantes	➢ Classification et exploration des différents types de pannes photovoltaïques, internes, externes et électriques. ➢ Classification et exploration des différents types de techniques de détection des défauts photovoltaïques, principalement basées sur les zones photovoltaïques caractérisées électriquement comme AC ou DC. ➢ Évaluation comparative des données pour les défauts photovoltaïques et méthode de détection.	✓ Les pannes externes sont les plus courantes pour les systèmes photovoltaïques. ✓ Les défauts photovoltaïques liés à l'environnement ont la plus forte probabilité de se produire dans les systèmes photovoltaïques. ✓ Les pannes photovoltaïques basées sur l'irradiation sont les plus difficiles à détecter et à identifier. ✓ Les défauts basés sur l'irradiation (« hotspots ») ont les impacts négatifs les plus importants sur la performance d'un système photovoltaïque approprié.
1.3 Méthodes de détection des défauts basées sur les matériaux pour les systèmes photovoltaïques	➢ Aperçu des différents matériaux qui peuvent composer une cellule photovoltaïque. ➢ Comparaison des caractéristiques des matériaux photovoltaïques étudiés. ➢ Examen des types de défaillances photovoltaïques pouvant survenir au niveau des cellules photovoltaïques. ➢ Évaluation de l'applicabilité des méthodes de détection des défauts photovoltaïques étudiées en fonction des différents matériaux photovoltaïques.	✓ Les matériaux des cellules photovoltaïques déterminent l'efficacité globale du système photovoltaïque. ✓ Les défauts photovoltaïques induits par l'irradiation présentent des défauts de diodes de dérivation, quels que soient les matériaux photovoltaïques utilisés.
1.4 Brève revue des algorithmes mathématiques pour les techniques de maintenance prédictive et la détection d'anomalies dans les systèmes photovoltaïques.	➢ Caractérisation de différents algorithmes de détection prédictive de défauts pour les systèmes photovoltaïques, principalement basés sur l'historique des processus et sur des données quantitatives. ➢ Évaluation comparative des différentes techniques prédictives examinées en termes de niveau de détection, de types de défauts et de précision.	✓ La majorité des méthodes prédictives de détection des pannes photovoltaïques prennent en compte l'irradiation solaire dans leurs modèles de calcul. ✓ Les méthodes basées sur l'historique des processus sont les plus efficaces pour détecter les effets de l'irradiation sur la performance des systèmes photovoltaïques, en prédisant les défauts d'ombrage partiel et leurs conséquences.
1.5 Étude des algorithmes d'extraction de la puissance maximale d'un système photovoltaïque	➢ Revue des algorithmes MPPT classés pour un fonctionnement dans des conditions d'ombrage uniforme et partiel.	✓ Les conditions d'ombrage partiel réduisent fortement l'efficacité des systèmes photovoltaïques. ✓ Les conditions d'ombrage partiel sont difficilement évitables dans

avec les convertisseurs DC-DC correspondants	➢ Examen des convertisseurs DC-DC, classés en unités de traitement de puissance isolées et non isolées.	toute application photovoltaïque réelle. ✓ Les algorithmes MPPT basés sur le suivi du point de puissance maximale globale s'avèrent être les meilleurs pour compenser les effets de la fluctuation de l'irradiation avec une efficacité de détection allant de 97,36 % à 99,99 %. ✓ Les convertisseurs DC-DC non isolés ont un rendement de conversion supérieur à 95 % par rapport aux convertisseurs isolés qui ont un rendement de conversion de 91,2 %.
1.6 Atténuation des effets de l'ombrage partiel sur la performance du système PV grâce à la reconfiguration du réseau PV	➢ Aperçu spécialisé des effets des conditions d'ombrage partiel sur les performances des systèmes photovoltaïques (points chauds, pointes multiples, pertes par désadaptation électrique). ➢ Examen des méthodes de reconfiguration des panneaux photovoltaïques, classifiées comme techniques physiques, électriques et combinées physico-électriques. ➢ Discussion sur les différentes méthodes de reconfiguration photovoltaïque examinées en termes de facteur de remplissage, de pourcentage de perte de puissance, de ratio de performance, etc.	✓ Les conditions d'ombrage partiel accélèrent le processus de vieillissement des systèmes photovoltaïques. ✓ Les méthodes d'optimisation des systèmes photovoltaïques basées sur l'irradiation, telles que les techniques de reconfiguration des réseaux photovoltaïques étudiées, contribuent à l'augmentation de la production globale d'énergie PV. ✓ L'algorithme SD-PAR, parmi les différentes techniques de reconfiguration physique des réseaux photovoltaïques, résiste à tous les types d'ombrage possibles, avec une efficacité proche de 100 % et une amélioration de la puissance de 70 %. ✓ L'algorithme MHHO, parmi les méthodes PVR électriques basées sur des algorithmes, a produit la puissance DC de sortie la plus élevée ($82.2V_M I_M$) avec un facteur de remplissage élevé (75 %), des pertes de puissance minimales (16 %) et des pertes de désadaptation de puissance minimales (19 %). ✓ La future méthode de reconfiguration des panneaux photovoltaïques proposée : TCT-connecté avec une matrice de commutation contrôlée par l'algorithme MHHO aurait théoriquement un rendement proche de 100%, une augmentation de puissance de plus de 75%, des pertes de désadaptation réduites à 10%, des pertes de puissance réduites à 3%, et un facteur de remplissage élevé de 80%.

1.7 Aperçu de l'utilisation des matériaux à changement de phase (PCM) pour le refroidissement des systèmes photovoltaïques	➢ Etude des effets de la température sur la production d'énergie des panneaux photovoltaïques. ➢ Examen des différentes formes de PCM, classées comme organiques, inorganiques, eutectiques et commerciales. ➢ Évaluation critique de tous les types de PCM en termes de température de fusion, de conductivité thermique, etc. ➢ Établissement d'une approche de sélection des PCM pour le refroidissement du PV. ➢ Discussion sur la réduction de la température des modules PV avant/après l'application des PCM.	✓ La relation entre l'augmentation de la température des modules PV et leur rendement énergétique est inversement proportionnelle. ✓ Les techniques de refroidissement basées sur le PCM sont plus performantes que les autres méthodes de refroidissement telles que le refroidissement par l'air et l'eau. ✓ Il est suggéré de sélectionner le PCM destiné à abaisser la température des modules PV en fonction de ses critères de température de fusion. ✓ La gestion thermique des modules photovoltaïques est une approche plus simple et beaucoup plus facile que les techniques utilisées pour combattre les problèmes liés à l'irradiation.
1.8 Évaluation comparative de différents suiveurs solaires : Vers une conception rentable, facile à mettre en œuvre et à haut rendement	➢ Etude angulaire du rayonnement solaire en fonction du positionnement des modules PV. ➢ Classification des suiveurs solaires en fonction de leurs systèmes de contrôle, de leurs mécanismes d'entraînement, du nombre d'axes mobiles et des schémas de suivi. ➢ Discussion sur les avantages de l'utilisation des suiveurs solaires.	✓ Les techniques de contrôle en boucle fermée produisent un positionnement plus précis des modules PV que le contrôle en boucle ouverte. De même, les mécanismes de pilotage actifs produisent une meilleure orientation des modules PV que les techniques passives. ✓ Les suiveurs solaires à deux axes minimisent mieux l'irradiation perdue (radiations solaires non captées) que les suiveurs à un axe, où les stratégies de suivi basées sur un processeur possèdent la meilleure fiabilité et dynamique dans le suivi des positions solaires. ✓ Les suiveurs solaires optimisent les performances des PV en augmentant la quantité d'irradiation sur la surface des modules photovoltaïques.
2. Optimisation de l'angle d'inclinaison des panneaux photovoltaïques pour minimiser le coût d'énergie	➢ Définition de la procédure d'optimisation par augmentation manuelle et progressive de 5° de l'angle d'inclinaison jusqu'à l'obtention d'un seuil mathématique. ➢ Calcul de la puissance moyenne, du coût actualisé de l'énergie et de la perte de puissance pour chaque valeur des angles d'inclinaison. ➢ Définition du modèle mathématique qui permet d'installer le nombre maximum de modules PV (de même	✓ Le coût actualisé de l'énergie est réduit d'un facteur de 4,32, 3,73 et 4,35 pour Tripoli, Belfort et Tantan respectivement, après l'application du modèle suggéré. ✓ La puissance produite par les systèmes PV simulés à Tripoli, Belfort et Tantan est augmentée de 4,43%, 4,48% et 4,47% respectivement, après l'application du modèle suggéré.

	géométrie) dans une zone carrée sans ombrage mutuel. ➢ Simulation de l'ensemble du modèle pour trois zones géographiques distinctes (Belfort-France, Tantan-Maroc, et Tripoli-Liban).	
3. Conception d'un chargeur solaire innovant de batterie Lithium-Ion basé sur le MPPT pour un fonctionnement sous des conditions d'irradiations fluctuantes	➢ Mise en place du dimensionnement du réseau photovoltaïque à tester et création de modèles d'irradiation très fluctuants dans Matlab. ➢ Conception de l'électronique de puissance du convertisseur DC-DC. ➢ Mise en place de l'organigramme pour la modification de l'algorithme P&O. ➢ Conception de l'électronique de puissance du convertisseur bidirectionnel avec le schéma de suppression du courant. ➢ Simulation des cinq modèles d'irradiation solaire.	✓ La conception a montré une efficacité de performance globale dans des conditions d'irradiation fluctuantes irréalistes de 87% à 100%. On peut donc prédire qu'il sera encore plus performant dans des conditions d'irradiation réalistes, lorsqu'il sera appliqué en tant que prototype réel. ✓ La conception améliorée des circuits d'électronique de puissance et l'algorithme MPPT modifié ont permis de minimiser les ondulations des formes d'ondes de courant et de tension injectées dans les systèmes de stockage d'énergie. ✓ Grâce à l'amélioration de la conception des circuits (convertisseur DC-DC, convertisseur bidirectionnel, etc.), le chargeur global devient plus flexible pour les applications à taille limitée, lors de sa mise en œuvre dans une application réelle (en raison de la réduction du poids des composants électroniques). ✓ La conception peut être adaptée à des réseaux PV plus importants, ce qui permet d'optimiser les processus de charge pour les systèmes PV hors réseau à plus grande échelle.
4. Développement d'un algorithme innovant basé sur l'Intelligence Artificielle (IA) inspirée des mécanismes pathogènes de la maladie du Diabète de Type 1 (T1D) pour les applications de suivi du point de puissance maximale (MPPT)	➢ Étude du comportement des cellules photovoltaïques dans des conditions d'ombrage partiel. ➢ Étude des mécanismes pathogènes du diabète de type 1 (T1D). ➢ Approximation entre le processus d'évolution de T1D (en termes de comportement des cellules) et l'algorithme PSO (comportement des particules). ➢ Simulation Matlab du nouvel algorithme proposé dans quatre scénarios de conditions d'ombrage partiel.	✓ L'algorithme MPPT proposé trace complètement la courbe caractéristique PV, quel que soit le nombre de pics maximaux locaux. ✓ L'algorithme MPPT proposé a montré une précision de convergence de 98,47% avec un temps d'exécution rapide allant de 2,403 S à 5,817 S. ✓ Par rapport à d'autres algorithmes MPPT comparables, cette proposition peut gérer jusqu'à cinq pics locaux dans la courbe caractéristique du PV, sans se bloquer sur un pic quelconque. ✓ Le nouvel algorithme MPPT proposé optimise les performances des systèmes photovoltaïques, en particulier lorsqu'ils sont confrontés à des conditions d'irradiation

		indésirables.
5. Faisabilité et implémentation des traqueurs solaires pour les systèmes photovoltaïques	➢ Télécharger l'ensemble des données environnementales (vitesse du vent, température ambiante et irradiance) pour les zones géographiques à étudier, dans lesquelles des systèmes photovoltaïques sont déjà installés avec des données de performance. ➢ Calculer l'irradiation moyenne annuelle pour chacun des systèmes PV avec/sans l'application de suiveurs solaires. ➢ Calculer la température moyenne annuelle du module PV pour chaque système PV avec/sans application de suiveurs solaires. ➢ Calculer l'estimation du cycle de vie de chaque système photovoltaïque avec/sans l'application de suiveurs solaires. ➢ Calculer la puissance PV cumulée pour chaque système PV avec/sans l'application de suiveurs solaires. ➢ Vérifier la faisabilité de l'application des suiveurs solaires pour chaque système photovoltaïque, en indiquant s'il est recommandé de les installer, s'il n'est pas recommandé de les installer ou s'il est recommandé de les interrompre pendant le cycle de vie du système photovoltaïque.	✓ Les suiveurs solaires, après cette étude, s'avèrent ne pas être nécessairement recommandés pour une installation dans toutes les zones géographiques. ✓ Parmi les neuf zones d'installation de systèmes photovoltaïques analysées, seuls quatre sites, avec leurs attributs environnementaux correspondants, ont montré une augmentation significative de la puissance au cours de leur cycle de vie après l'installation de suiveurs solaires. ✓ Dans certaines zones géographiques, il n'est jamais recommandé d'installer des suiveurs solaires pour les systèmes photovoltaïques, alors que dans d'autres zones, il est recommandé de faire une pause dans le cycle de vie des suiveurs solaires pendant une période déterminée. ✓ Cette étude optimise la performance des systèmes photovoltaïques en prenant une décision pour la recommandation de l'implémentation de suiveurs solaires.

Les résultats indiqués dans le tableau ci-dessus récapitulent les résultats de cette thèse comme un bagage complet à ajouter aux systèmes PV, afin d'améliorer et optimiser leur performance, principalement en ce qui concerne l'irradiation. En d'autres termes, l'application du modèle dynamique de la modification de β, avec le chargeur solaire suggéré pour être contrôlé par la modification de l'algorithme MPPT basé sur T1D, simultanément avec une décision concrète d'implémenter ou non un suiveur solaire, rendrait définitivement le système PV plus immunisé contre les perturbations induites par l'irradiation sur son comportement opérationnel.

En ce qui concerne les travaux futurs (perspectives) qui peuvent être dérivés des résultats de cette thèse, ils peuvent être organisés et suggérés selon les **chapitres 2**, **3**, **4**, et **5**. En commençant par l'ajustement de l'angle d'inclinaison, il est encouragé d'utiliser cette étude sur des réseaux PV réels (décomposés en deux groupes, A et B) afin d'obtenir des données concrètes sur les effets et l'importance du modèle d'ajustement de l'angle d'inclinaison proposé dans les systèmes PV réels, comme suit :

1. Les panneaux photovoltaïques du groupe A doivent être installés sur des supports mobiles.
2. Les panneaux photovoltaïques du groupe B (ayant exactement les mêmes caractéristiques électriques et les mêmes dimensions que ceux du groupe A) doivent être installés sur des enceintes fixes.
3. Au cours de chaque saison, le support mobile doit être modifié manuellement en fonction de la valeur optimale β calculée au préalable.
4. La puissance produite en fonction de la saison doit être tabulée et comparée pour les panneaux photovoltaïques des groupes A et B. À ce niveau, il est possible de tester les résultats matériels de l'étude proposée au **chapitre 2**, et sa faisabilité pour une application dans des systèmes photovoltaïques plus importants.
5. Il peut également être suggéré d'automatiser le processus de positionnement du support en fonction du β optimal calculé au moyen de moteurs industriels, dans le cas de systèmes photovoltaïques de grande taille.

En ce qui concerne la conception du chargeur solaire présentée au **chapitre 3**, elle peut également être améliorée pour soutenir des systèmes de stockage d'énergie plus importants pour les systèmes photovoltaïques hors réseau. Après tout, le rôle d'un tel chargeur est d'optimiser les performances des systèmes photovoltaïques en fonctionnement, lorsque ceux-ci impliquent un banc de batteries

de plus de 150 Ah. Dans un premier temps, chacun des circuits d'électronique de puissance présentés doit être modifié pour pouvoir traiter des bancs de batteries plus importants. En outre, la conception du buck-convertisseur présentée au **chapitre 3** est toujours envisagée pour abaisser la tension d'alimentation du banc de batteries créée par le réseau PV relativement élevé. À cette fin, il est également encouragé, dans le cadre des travaux futurs de cette étude, de concevoir un convertisseur buck-boost non isolé, capable de supporter des bancs de batteries plus puissants, même avec des panneaux photovoltaïques plus petits, conformément aux lignes directrices suivantes :

1. Déterminer la plage de tension d'entrée des panneaux photovoltaïques et spécifier les plages de niveaux de tension et de courant de sortie requis.
2. Les inducteurs, les condensateurs, les diodes et les transistors sont sélectionnés en fonction des nouvelles exigences en matière de gestion de la puissance et de la fréquence de commutation.
3. Choisir une stratégie de contrôle. Par exemple, le convertisseur buck-boost doit être "programmé" comment et quand augmenter/diminuer sa tension de sortie.

D'autre part, le nouveau MPPT (modification PSO basée sur T1D) qui est présenté et simulé dans le **chapitre 4**, est encouragé à être appliqué sur un contrôleur de charge réel. Il peut s'agir par exemple de le fusionner avec le prototype de la future conception du **chapitre 3** : l'algorithme T1D-PSO agirait alors comme un gouverneur pour le futur convertisseur buck-boost suggéré, fournissant ainsi les « duty ratios » les plus précis en fonction de l'état des conditions d'ombrage partiel. En d'autres termes, le T1D-PSO peut être intégré à un contrôleur physique qui dicte les états de commutation des interrupteurs à semi-conducteurs du convertisseur buck-boost, ce qui permet d'obtenir une meilleure extractibilité de la puissance sous cinq pics maximaux locaux dans la courbe caractéristique du PV. Voici quelques étapes de clarification à cette fin :

1. Les fonctions, les routines d'appel, les variables et toutes les tâches de programmation connexes présentées au **chapitre 4** doivent être téléchargées sur un petit système informatique.
2. Ce système informatisé (RaspBerry Pi par exemple), après avoir téléchargé le flux de travail logique, doit avoir ses entrées analogiques connectées au côté du générateur photovoltaïque (tension et courant photovoltaïques)..
3. Les ports de sortie numériques de ce système informatisé doivent être reliés aux commutateurs à semi-conducteurs du convertisseur buck-boost conçu (conception améliorée du **chapitre 3**).
4. Les ports de sortie analogiques qui seront à leur tour connectés au système de stockage d'énergie.
5. Dans l'ensemble, le circuit général proposé permettrait de charger efficacement et rapidement le système de stockage d'énergie, même dans des conditions d'ombrage partiel.

Enfin, l'étude présentée au **chapitre 5** peut être encodée dans une application pour smartphone ou codée comme une application pour navigateur web. Bien que le flux de travail de l'étude de faisabilité des suiveurs solaires présentée soit automatisé au moyen de VBA, il nécessite toujours un ordinateur pour fonctionner. C'est pourquoi il est suggéré d'intégrer cette étude dans une application pratique, ce qui permettrait aux ingénieurs photovoltaïques de disposer d'une fonction plus flexible pour déterminer l'applicabilité des suiveurs solaires en fonction de la région d'installation des systèmes PV.

Références

[1] Bridge BA, Adhikari D, Fontenla M. Electricity, income, and quality of life. The Social Science Journal 2016;53:33-9. doi: doi.org/10.1016/j.soscij.2014.12.009.

[2] Adedeji BP. Electric vehicles survey and a multifunctional artificial neural network for predicting energy consumption in all-electric vehicles. Results in Engineering 2023;19: 101283. doi: doi.org/10.1016/j.rineng.2023.101283.

[3] Khan AA, Zan J, Fang X, Zhang W, Jadoon UF. Global warming drove the Mid-Miocene climate humidification in the northern Tibetan Plateau. Global and Planetary Change. 2023;226: 104135. doi: https://doi.org/10.1016/j.gloplacha.2023.104135.

[4] Hosseini SE. Chapter 1 – Fossil fuel crisis and global warming. Fundamentals of Low Emission Flameless Combustion and Its Applications 2022:1-11.doi: https://doi.org/10.1016/B978-0-323-85244-9.00001-0.

[5] Bórawski P, Holden L, Bełdycka-Bórawska A. Perspectives of photovoltaic energy market development in the european union. Energy 2023;270: 126804. doi: https://doi.org/10.1016/j.energy.2023.126804.

[6] Bhatia SC. Chapter 2 – Solar radiations. Advanced Renewable Energy Systems 2014:32-67.

[7] Hajji M, Yahyaoui Z, Mansouri M, Nounou H, Nounou M. Fault detection and diagnosis in grid-connected PV systems under irradiance variations. Energy Reports 2023;9:4005-17.

[8] Aboagye B, Gyamfi S, Ofosu EA, Djordjevic. Investigation into the impacts of design,

installation, operation and maintenance issues on performance and degradation of installed solar photovoltaic (PV) systems. Energy for Sustainable Development 2022;66:165-76.

Liste des annexes

Annexe 1.1

Revue des stratégies de maintenance pour les systèmes photovoltaïques

Science of the Total Environment 746 (2020) 141753

Contents lists available at ScienceDirect

Science of the Total Environment

journal homepage: www.elsevier.com/locate/scitotenv

A review on maintenance strategies for PV systems

Khaled Osmani [a,b], Ahmad Haddad [a,b], Thierry Lemenand [c], Bruno Castanier [c], Mohamad Ramadan [a,b,*]

[a] School of Engineering, International University of Beirut BIU, Beirut, Lebanon
[b] School of Engineering, Lebanese International University LIU, Bekaa, Lebanon
[c] LARIS, Polytech Angers, France

HIGHLIGHTS

- Maintenance strategies aim to avoid the decrease in efficiency that is caused by potential faults.
- Four types of maintenance strategies may be identified, preventive, predictive, corrective and urgent.
- The study presents a review on the main developed techniques under each of the four maintenance categories.

GRAPHICAL ABSTRACT

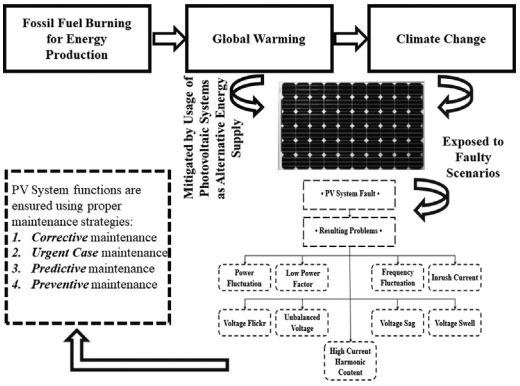

ARTICLE INFO

Article history:
Received 10 May 2020
Received in revised form 13 August 2020
Accepted 15 August 2020
Available online 22 August 2020

Editor: Abdul Ghani Olabi

Keywords:
Maintenance
Photovoltaic
Performance
Corrective
Preventive
Predictive

ABSTRACT

PV (PhotoVoltaic) systems gained popularity in being eco-friendly power supplies, reducing toxic gas emissions for energy production. Unfortunately it's been seen that efficiency reduction and output deficit are two common scenarios for PV systems when confronted with faulty events: this fact creates the crucially important need of knowing types of different possible faults and be able to detect them according to their ways of striking, timing and density of their leftovers. What comes after is fixing the damages, by preventing them from happening repeatedly and stop them from reaching the surface. Since knowing the fault without correcting it is counterproductive, maintenance strategies can reduce competencies of the system, accelerate operation time, and compensate the system in a way that prevents lowering in efficiency and consequently financial losses. This paper aims to present different schemes used in fault intervention categorized by preventive, corrective, predictive and urgent case faults maintenance methods with corresponding effects on environment. A critical comparison between different strategies is presented as well as an economical assessment of the maintenance costs and energy production increase. Each type is individually clarified to reveal what area of PV faults types it can withstand. With a recommendation on maintenance choice, an informative reference for researchers in the field is established to optimally maintain a sustainable PV system.

1. Introduction

Obligations of modern life requirements led to a high energy demand (Emodi et al., 2019). Consequently, fossil fuel consumption increased in turn (Erdiwansyah et al., 2019). This fact led to depletion of ozone layer and caused other harmful residuals mainly global warming

* Corresponding author at: School of Engineering, International University of Beirut BIU, Beirut, Lebanon.
E-mail address: mohamad.ramadan@liu.edu.lb (M. Ramadan).

https://doi.org/10.1016/j.scitotenv.2020.141753
0048-9697/

Nomenclature

AC	Alternating Current
ACO	Ant Colony Optimization
ANN	Artificial Neural Network
BES	Battery Energy Storage
BESS	Battery Energy Storage Systems
DC	Direct Current
DVR	Dynamic Voltage Regulator
EDS	Electrostatic Dust removal System
ESS	Energy Storage System
EV	Electric Vehicle
FLC	Fuzzy Logic Controller
FMEA	Failure Mode and Effect Analysis
GCPVS	Grid Connected Photovoltaic Systems
LSP	Load Shedding Period
LV	Low Voltage
MG	Micro Grids
MPPT	Maximum Power Point Tracker
NGV	Neutral Ground Voltage
PA	Predictive Algorithm
PEG	Power Electric Grid
PEMCS	Predictive Energy Management and Control System
PI	Proportional Integral
PIC	Peripheral Interface Controller
PLC	Programmable Logic Controller
PO	Predictive Optimization
PSO	Particle Swarm Optimization
PV	Photo Voltaic
RCM	Reliability Centered Maintenance
RMS	Root Mean Square
RPN	Risk Priority Number
SAPF	Shunt Active Power Filter
SEPIC	Single Ended Primary Inductor Converter
SMES	Superconductive Magnetic Energy Storage
STATCOM	Static Synchronous Compensator
THDC	Total Harmonic Distortion Current
UPQC	Unified Power Quality Conditioner
UPS	Uninterruptible Power Supply
VAR	Volt Ampere Reactive

and climate change. The resulting increase in earth's temperature destabilizes energy balance. Negative impacts are noticed on the level of dried agriculture, rising sea levels and increased heavy precipitations (Koutroulis, 2019). This fact influences animal/insect life cycle, evolving an abnormal expand of their mortality rates thus perturbing overall nature process. This scenario is the result of excessive burning and combustion of non-renewable power supplies of oil and gas to fulfill bulky energy needs (Wilberforce et al., 2019a). As a result, higher amounts of CO_2 are present in the airspace (Wilberforce et al., 2019b).

When CO_2 emissions are not carefully dictated, rainfall and wind movements are driven to extreme states, where it is seen that rainy areas became dryer by the time, thus affecting food production mainly by overkilling agriculture and plants seeding (Zhi et al., 2020).

From another perspective, to compensate the human needs in energy (mainly electricity) especially in populated areas (China, India, etc.) electrical power generation using fuel-based generators are seen to cause human diseases. Since generators involves noisy electromechanical parts to produce power, they contribute in one way or another in increasing noise pollution and hence mounting stress levels, causing civilizations to be more drug dependent. The need for ecofriendly energy supply systems, got inflated by result (Olabi et al., 2020).

Fortunately solar energy is capable in supplying electrical needs, by removing the deficits of conventional power supplies (based on non-renewable residues) (Bazan et al., 2018). This happens with the usage of PV (Photovoltaic) modules that converts directly the light into energy. Therefore PV systems gained wide popularity in moving towards a non-carbon future, eliminating the threats of global warming, food production, drug needs and effects on animal/insects mortality rates (Mekonnen et al., 2016). This is because solar radiations are the most common along all regions of the globe (Lee et al., 2020). High demands for PV systems installations are taking place, as to reduce large electricity bills and fees and to have a private supply of energy production. In parallel with the challenge of high capital cost, and reduced chances of full commercialization disadvantages (Wilberforce et al., 2019c) a standalone PV system with no regular maintenance becomes fatigued by time, with diminished available efficiency in sustaining a solid energy supply.

These systems often interact with faulty scenarios, causing them to deteriorate over time, become less productive in addition to causing other sided deficiencies of burning, electrocution and different scripts of electrical faults, perturbations and power system fluctuations that weren't present at the first instance. In other words, a non-maintained PV system cannot positively contribute to the environment without a proper maintenance strategy (Munoz-Ceron et al., 2018). Such systems often don't run as they are supposed to.

Non-optimal performance means that the overall energy production would be less, in terms of open-circuit voltage, current leakage and energy storage within specified banks (batteries, capacitor banks, etc.). This erroneous running scheme would not meet users' expectancies to avoid power consumption from the grid and hence lower their fees and bills. In other words, the faulty conditions reverse the economic user's strategy where he no longer benefits from such system, therefore the entire process becomes useless.

Accordingly, ample research about fault detection methods took place, to inform users/designers *when* and *where* a fault has taken place, and of *which* type. This is tremendously important since knowing the source of the problem is halfway solving it. The actions after acknowledging a fault (plus its destructive effect) are of core importance.

Developing ways to remove bad impacts from within the system, to restore its correct functionality, is what permits users to benefit from to the maximum. To solve faults problems means an uninterrupted energy source, a fact that elevates its reliability and durability and provides users with a stable energy source. Solving mechanisms, referred to as maintenance techniques for PV systems, sometimes intervention methods, are ways to mitigate faults impacts on the system.

This paper shows four different families of fault maintenance for PV systems, beginning with Corrective methods, proceeding to Urgent case methods, then Predictive methods and ending at Preventive methods. Each set of methods will be clearly identified, showing its sub-parts, description, target and contribution in maintaining the desired optimum environmental conditions.

1.1. Problems associated with PV system faults

The power quality is labeled to as measuring of standard power delivered. It is not sufficient to produce power from PV arrays alone, since their outputs are small sized DC voltages that when associated with consumable AC voltages (loads) lead to power quality events, presented in Fig. 1. Such destructive circumstances are common for all types of PV cells (mono-crystalline, poly-crystalline…) since they take place at final destination of PV systems (outcomes of inverters). Therefore, any disturbances from PV systems can affect the overall production leading to erroneous functioning. The first problem is the power fluctuation where the generated power is unstable. This is mainly due to the fact that PV cells output are environment related in terms of irradiance, temperature, humidity and other surrounding factors.

Beginning with Power Fluctuations, due to intrinsic composition of PV cells, sometimes the power production is not stable mainly due to shading, sizing and topology of PV system (Farhoodnea et al., 2013;

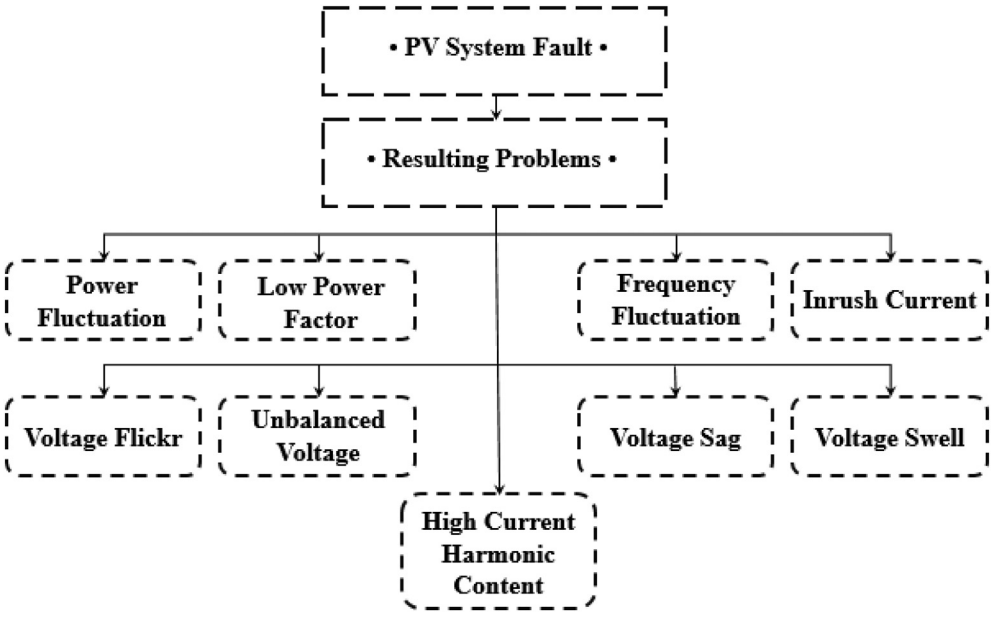

Fig. 1. Different power quality events resultant from PV system faults.

Marcos et al., 2012). On the other hand, THDC (Total Harmonic Distortion Current) is frequently found in grid-tied PV systems that are results of inverting the primitive DC voltage from PV arrays to AC quantities by the usage of inverters. The inverter switching mechanisms cause the creation of these harmonics producing distortions in current waveform (González et al., 2011; Golovanov et al., 2013). Also, reversed power flow operation (from load to source) injects large amount of THDC into the grid (Anwari et al., 2009). On the other hand, wind speed and cloud movements certainly lead to varying output power levels of PV modules (Shivanshankar et al., 2016) causing generated power to be intermittent and unreliable especially when connected to grid.

From another angle, we see a low power factor as leading/lagging below unity when the PV system encounters a fault, especially when grid-tied. The phase displacement and effects of THDC cause this issue: PV systems inject active power to the power system that reduces the original active power generated in center power plants and hence the misbalance. Similarly, the variable power factor function of the inverter gives similar malfunction (Gerritt, 2009).

Moving forward, we notice frequency fluctuations issue due to unbalancing between the supply power and demand. Frequency fluctuates in conjunction with irradiance. Another power quality issue is seen when variation in output power production yields to voltage fluctuations. This is noted as voltage flicker, where shading and clouds moving frequency lead to variation in output power productivity which cause the undesired effect that the majority of installed PV systems suffer from (Stewart et al., 2012; Pan et al., 2012).

The most user-complaint issues among consumers (80% of total complaints) refer to voltage sag (Mathnani et al., 2010; Gao et al., 2013): a decrease of RMS voltage below standard values of a given power system. Such phenomenon is greatly seen to happen when interconnecting PV output to micro-grids, the fact that immensely affect customers/critical loads in different zones of distribution (Mohammadi et al., 2017).

Beside from the voltage sag event, it is seen that grid connected PV systems prolongs the voltage swell scenario as well (Dugan et al., 2012). This can be understood as the contradictory of voltage sag, which is an instantaneous increase of RMS voltage when a heavy load turns off in the network. This is more likely to happen in summer (high irradiance) and under low load conditions in LV (Low Voltage) distribution networks (Vegunta et al., 2013). If the network is unbalanced (poor phases' organization towards loads) voltage swell takes place on the lightest loaded phase with high PV penetration (Alam et al., 2012). In the last decade voltage is examined to surge when PV outputs are penetrated onto low voltage grid resulting in abnormal operation of distribution networks (Kharrazi et al., 2020).

Voltage unbalance, according to IEEE (Institute of Electrical and Electronics Engineers) is the inequality in voltage magnitudes or dissymmetry in phase angles between different phase voltages. It must not surpass 2% according to (Block et al., 2014; Pansakul and Hongesombut, 2014). This is more likely to happen when PV penetration level up to 85%. This effect causes derivable other negative impacts as it increases NGV (Neutral Ground Voltage) (Alam et al., 2013). When present, these unbalances also in turn increase the output ripple of PV inverter due to negative sequence voltage and hence produced current is attacked by high order harmonic content (Hao and Yonghai, 2014a). Also, when micro-grids work as power-island, they are seen to experience a heavy voltage unbalance when reconnected to the grid (Lidula and Rajapakse, 2014).

The last abuse of PV systems fault is the occurrence of inrush current in them (Tseng and Chen, 2012; Shrivastava et al., 2014). This happens due to the need of power transformer energizing during start up. This transformer itself experiences a high value of transient current which is considered as major event. The inrush current can have tenfold value of the rated. From another side, penetration of DG (Distributed Generation) in power system make rise for fault current level yielding to further complications in systems' performances (Sahebi et al., 2017).

1.2. Maintenance and intervention methods

The mentioned problems associated with faulty PV systems must be mitigated in order to complete the overall performance with maximum efficiency. With proper maintenance scheme an immediate damage/malfunction will be localized and hence a rapid restoration would take place. Since problems associated with PV systems are directly related to financial losses, a good maintenance will avoid any form of profit losses.

From a similar financial point of view, when the maintenance methods succeed in minimizing the possibility of technical problems of the equipment this also in turn reduces the economic burden of repairs.

According to relativity between accidental events and faults, when properly maintaining the PV system, the chances for accidents to happen (as fire, injuries, electrification…) would be reduced.

At last, intervention techniques help in exporting useful conclusions and creation of pro-actions plans that ensure the smooth functioning of PV installation, achieved by processing periodic reports' history on productivity and optimum operation.

Table 1 groups different categories of PV maintenance topologies while describing for each, when to take place and the expected results after execution.

2. Corrective maintenance

The Corrective maintenance covers up the activities performed by labors (service/maintenance) teams to restore a PV plant system malfunctioning or blackout due to an event. An event is generally the result of PV system faults occurring at different levels/nodes of the network. This form of maintenance takes places *after* the identification of a so-called event (failure detection). It is a direct approach maintenance mechanism where specialists manually intervene to either fix, replace, or change in algorithm and other tasks. Table 2 exposes first the relation between different events (that happens on the level of the PV system) and applicability of the corrective technique and second, the procedure(s) taking place within each technique.

2.1. Artificial intelligence

When PV arrays are grid-tied, negative impacts can be seen on the power quality forms. In order to explore the highest capability of the mixed electrical system, the mentioned power quality events must be mitigated in a way to suppress undesired leftovers. Fig. 2 exposes different artificial intelligence related techniques.

Each of the above mentioned methods, has a unique control algorithm (since artificial intelligence deals with machine language and computer encoding) which accordingly is targeted to a unique power system (whether single/three phase, balanced/unbalanced systems).

2.1.1. Inverter reconfiguration

Since the inverter within a PV system is the core of delivering AC signal, it was found that certain configurations yield to different specific situations (Rendroyoko and Rusli, 2013) by varying the output and hence mitigating the power events resulting from faults. Eight different control algorithm were found where each proceed a way to diminish error from faults, recapitulated in Fig. 3.

The Direct Source Current Shaping improves the power factor to unity and eliminates harmonic quantities in current (Shen and Wang, 2006). It works for three phased power systems. For the Flexible Active and Reactive Power Control, this algorithm opposes inversely between power fluctuations and output harmonic current by a certain way of programming in which the power fluctuations are decreased when harmonics in output current is increased and vice-versa (Huang et al., 2014). The Hysteresis Current Control is found to solve voltage fluctuations (overvoltage during PV system start up/under-voltage after PV disconnection) and maintaining a fixed voltage profile for load reduction (Pyo et al., 2008). From another side, the Flexible Positive and Negative Sequence Control is seen to have control over power fluctuations instead (reactive and active) by altering "k" (a variable limited between −1 and 1 that sets a linear relation between constants used in output power calculations of PV inverter) the control parameter (Hao and Yonghai, 2014b). As for the Advanced Instantaneous Power Theory, it stabilizes the power fluctuation to a 10% rate, reduces third harmonic content by 0.4% and possesses two coefficients for current adjustments (Shou et al., 2013). On the other hand, the Spatial Iterative Learning plays on converging load voltage error to 0 and maintaining load voltage waveform somehow fixed in a voltage sag environment (Dasgupta et al., 2010). The Fuzzy Reasoning minimizes the frequency deviation to 0.2 Hz (Senjyu et al., 2007) in a three-phase islanding system and lastly the Particle Swarm Optimization maintains both good voltage and frequency profiles, as well as supply of active power (Al-Saedi et al., 2012).

Among different control algorithms implemented for Inverter Reconfiguration, it is concluded that they share the same aimed function: to adjust the obtained AC waveform according with system requirements and need. What differs is the programming flowchart and data acquisition to perform that task. Both Spatial Iterative Learning and Fuzzy Reasoning require the most complex algorithm, under machine learning topology, while maintaining healthier frequency balances. Other algorithms as Flexible Active and Reactive Power Control and Direct Source Current Shaping focus more on maintaining a good power factor with less complexity in programming. The Flexible Positive and Negative Sequence Control is a tradeoff between the two previous sets, as less complexity in algorithm derivation and reduced power fluctuations. The Advanced Instantaneous Power Theory for instance share with Direct Source Current Shaping algorithm solely in reducing harmonic effects. The choice of which algorithm to implement depends on actual harmonic contents in the system, and perturbations occurring in the AC waveform.

2.1.2. Dynamic voltage regulator (DVR)

A DVR is an additional electronic device noted as a compensator that works on regulating power profiles on permissible levels. Voltage sags that are often caused by low active power injection are compensated by its usage. Composed of mainly two parts, control circuit (in which algorithm is fed into) and a power circuit including storage bank, inverter, filter and power transformer (Choi et al., 2010). Five different control algorithms are summarized in Fig. 4.

The Two Fast Vector Control uses twelve active switches to compensate voltage sags (recorded at 22% for 100 W active power injection) (AlMathnani et al., 2010). Otherwise, the Vector Control mitigates 22% voltage drops (Al-Mathani et al., 2008). When Fuzzy Logic is used, no harmonic contents were shown in both current and voltage waveforms, as it was able to compensate voltage sags up to 50% and voltage swell up to 150% without polluting the power system (Farsadi et al., 2013). Other studies show mitigation of voltage sag up to 10% and voltage swell to 90% with the ability of using the DVR as UPS (Uninterruptible Power Supply) (Ramasamy and Thangavel, 2012). The Particle Swarm Optimization from another part injects power without harmonic distortion and reduces the need of power by 12% to compensate voltage sag of 20% (Kumar et al., 2009). At the end, the PSO Based Phase Advancement Compensation was able to mitigate voltage sag of up to 60% in a 17 MW power distribution system (Raj et al., 2008).

Unlike Inverter Reconfiguration technique, the DVR concentrates mainly on maintaining the optimum voltage profile. The aim of this technique relies on restraining voltage fluctuations (over-voltage, under-voltage) while dynamically studying the active voltage output. All of algorithms inside DVR share the same process of mitigation

Table 1
Overview of different maintenance methods.

Maintenance strategy	Description	Goals
Corrective	Takes place after a failure event, and include fixing, repairing, replacing and other correction tasks	Make corrections to avoid major equipment damaging
Urgent case	Takes places after a Major Force event, and requires fixing, replacing and other correction tasks	Make corrections in a hurry, prior to anything else to prevent bigger damages
Predictive	Evaluates the conditions of the system by performing scheduled/continuous real-time monitoring	To predict the optimal time to perform maintenance and hence elevating the equipment uptime
Preventive	Performs maintenance on a pre-scheduled time interval regardless of the condition	To reduce the possibility of any failure

Table 2
Event-task relation for each corrective technique type.

	Corrective techniques					
	Artificial intelligence	Water cleaning	Dry cleaning	Snow removal	Equipment technical maintenance	Shading mitigation
Events						
Snow accumulation				✓		
Dust/particles accumulation		✓	✓			
Shading	✓					✓
Equipment failure					✓	
Corrective tasks						
Replace					✓	
Fix				✓	✓	
Remove		✓	✓	✓	✓	
Repair				✓	✓	✓
Code	✓					✓

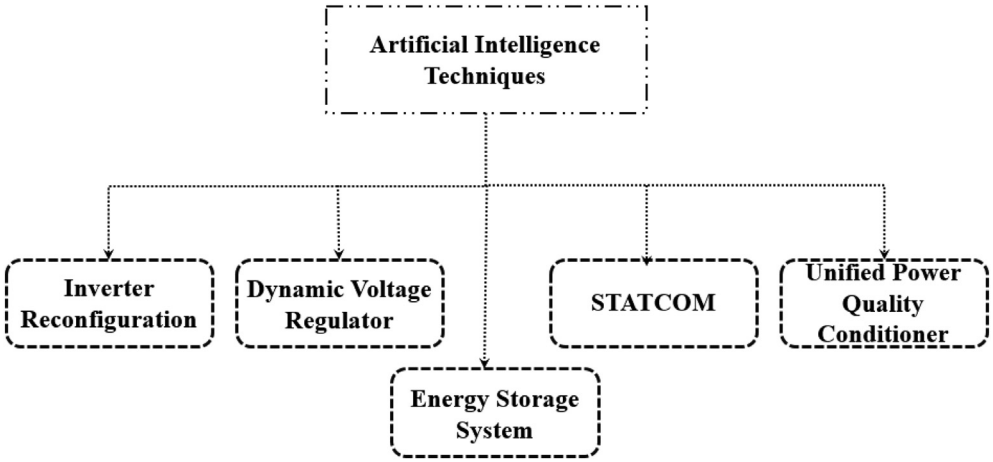

Fig. 2. Different Artificial Intelligence techniques.

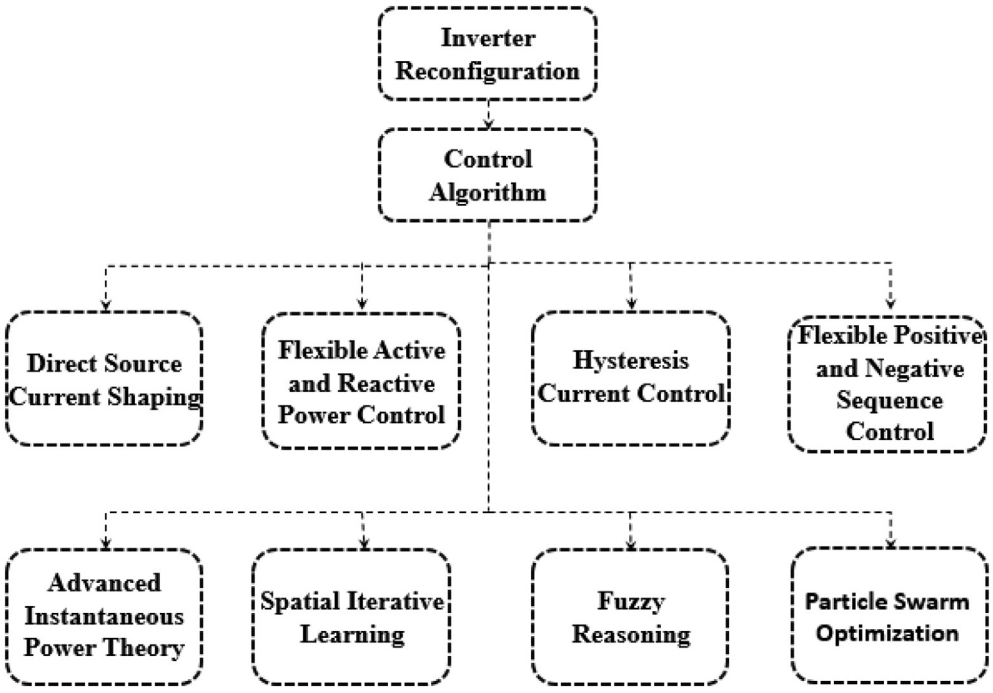

Fig. 3. Different control algorithms for Inverter Reconfiguration.

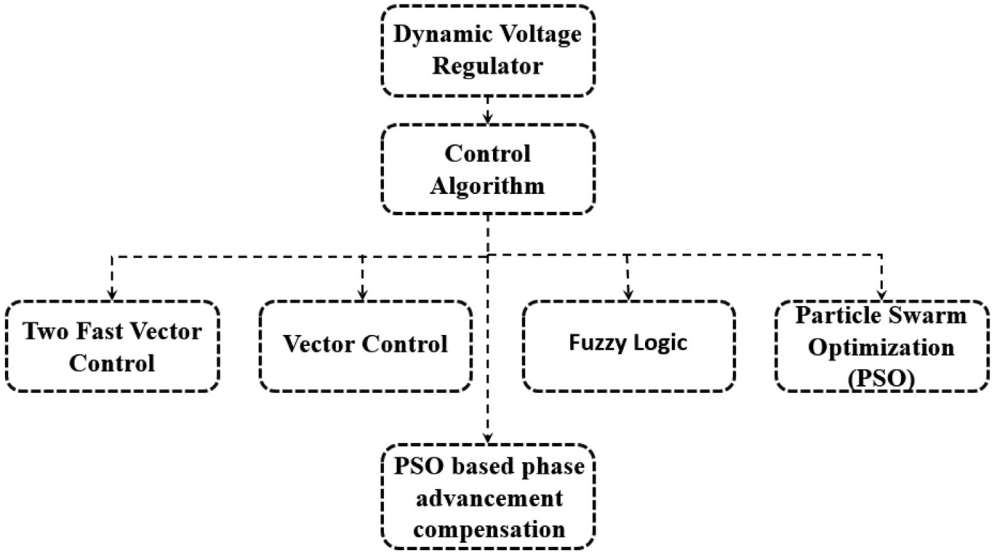

Fig. 4. Different control algorithms for Dynamic Voltage Regulator.

voltage drops/sags. What differs is the percentage of mitigation (from 10% to 150%) with respect to response time and system rated power.

2.1.3. Static synchronous compensator (STATCOM)

By operating as a source and sink of reactive power, a STATCOM enhances power factor and poor voltage regulation caused by inability of the power system distribution to meet reactive load power demand (Sumathi, Bansilal, 2009a). By sink/source it is meant that the STATCOM absorbs reactive power from the grid when its voltage is greater than nominal voltage and injects VAR (Volt Ampere Reactive) when it is lower. To do that, complex algorithm process must be done to achieve exact levels of accuracy. There were six different algorithms control agendas to feed in STATCOM machine coding summarized in Fig. 5.

The Single Phase Synchronous Reference Frame reduces voltage unbalance factor for below 4% regulate current THD to 0.7% and voltage THD (Total Harmonic Distortion) to 0.5% (Chidurala et al., 2013). On the other hand, the Current Control with Hysteresis Band Modulation Technique was found to obtain power factor above 0.9, has a good transient response which improves voltage dip in a fast manner and maintains good voltage profile (5%) during inductive load startup and voltage sag/swell events (Varma et al., n.d.). In (Varma et al., 2012), it was concluded that the STATCOM used makes current/voltage THD <2% with voltage profile regulation in 1.5 cycles. From another side, the Least Mean Square injects reactive power (compensate VAR (Volt Ampere Reactive)) which results in regulating voltage and maintaining a fixed power factor (Arya et al., 2012). Apart, the Artificial Neural Network control method achieves a unity power factor within 0.01 s (Xiao-ping et al., 2006) and eliminates oscillation caused by disturbances within 0.01 s (Sharma et al., 2014). Penultimate point, the Supervised Neural Network have a similar performance as conventional method with the addition of maintaining high bus voltage 1.05 p.u. (per unit) for different load factor in both voltage control and reactive

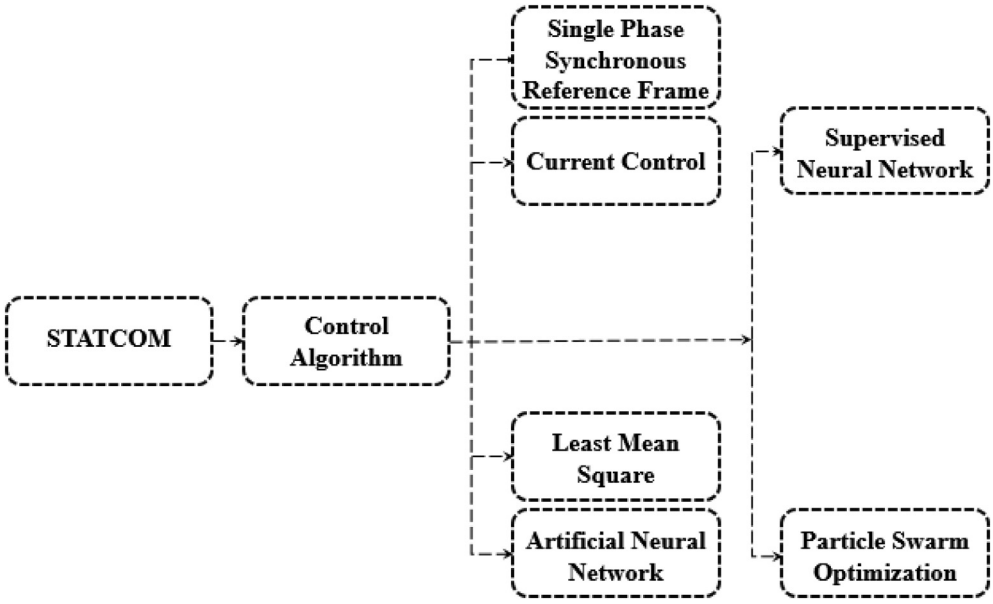

Fig. 5. Different control algorithms for STATCOM.

power control modes (Sumathi, Bansilal, 2009b). Lastly, the Particle Swarm Optimization can be used to allocate multiple STATCOM units, reduce power losses by 20% and increase stability limit by about 0.8 loading factor (compared to situation with absence of STATCOM) (Kumarasamy and Raghavan, 2012). At the same pace, the particle position can be calculated within one sampling period, reduced overshoot voltage by 0.7 V compared to PI controller and is applicable in all types of loading ranging from light to high (Liu and Hsu, 2010).

The STATCOM algorithms take into consideration reactive power compensation. The algorithms involved in this area centralize on feeding PV system's needs of reactive power while lowering THD. The execution of such algorithms take advantage of maintaining a good voltage profile with a good power factor just like in Inverter Reconfiguration and DVR processes.

2.1.4. Unified power quality conditioner (UPQC)

A UPQC that is alternatively known as SAPF (Shunt Active Power Filter), is a universal active filter that possesses multifunction in power conditioning that can be used to compensate voltage disturbances, fluctuations, and to prevent harmonic loaded current to enter to the power system (Kamran and Habelter, 1998). It consists of two voltage-source converters with a common DC link designed in multi-phase configurations. Having nine different control algorithms topologies summarized in Fig. 6.

For the State Vector Modulation, it had shown the ability to compress a voltage sag event for up to 7% while maintaining a good voltage profile after a significant change in load (Kumar and Sinha, 2012). In the Synchronous Detection Method and P-Q Theory results show that the THD are eliminated (0%) and power factor was maintained to unity, with no return current in the neutral wire (Kabir and Mahbub, 2011). From another part, the Voltage Angle Control topology alleviated voltage swell event up to 26% while mitigating voltage sag up to 81% (Bhargavi, 2011). For the D-UPFC scheme, it is concluded that this method has potential in mitigating voltage sag/swell events (Lee et al., 2006a; Lee et al., 2006b). The ANN algorithm alone was shown to reduce current harmonics (Sabo et al., 2013) and when mixing Fuzzy Logic with ANN (Artificial Neural Network), THD were eliminated in short response time with high frequency (Kumar and Sastry, 2011). The TS (Takagi-Sugeno) Fuzzy also reduces THD of current while having faster dynamic response (Shang and Wu, 2011). The PSO (Particle Swarm Optimization) Fuzzy on the other hand, showed similar results to those for TS in reducing harmonics in current and fast compensation of voltage sag (Shen et al., 2009a; Shen et al., 2009b). The PSO Based Adaptive Neuro-Fuzzy Inference System algorithm is able to compensate voltage sag with reduced storage size and phase jump due to ground and line-to-line faults (Kumar et al., 2011a; Kumar et al., 2011b). Finally, the PSO Based Feedback Controller reduces both THD of current and voltage with high efficiency (Karanki et al., 2010).

The benefits of applying Inverter Reconfiguration, DVR and STATCOM can all be achieved by using a UPQC. As seen to reduce current harmonics, lower THD, maintain a good power factor and spare any disturbances in voltage perturbations. Such algorithms are the most complex to implement, requiring extra actuators to fulfill desired functions. This can be considered as an economic burden, with increased overall system functioning costs when applying UPQC.

2.1.5. Energy storage system (ESS)

ESS are means to preserve energy produced while not being consumed. In other terms, ESS is the group of batteries, capacitors and flywheels (Ariyaratna et al., 2019; Mahmoud et al., 2020). Since voltage fluctuations are mainly related to intermittent PV power output, an accurate storage system immensely mitigate these fluctuations resulting in more efficient power forms, with less carbon emissions (Uctug and Azapagic, 2018; Lamnatou et al., 2020). This was considered as a corrective maintenance technology under Artificial Intelligence field since different algorithms can be fed into a controller so that according to a given specifics, laws are formed to switch on/off some of the ESS i.e. plug in/out a bank of capacitor or switch the battery bank to another in order to accommodate power fluctuations resultant from shading and other disturbances in power profiles. Eight different control algorithms for ESS are presented in Fig. 7.

The time-window is directly proportional to rated power of ESS in the Discrete Fourier Transform where shorter time-window is able to track actual output power closely in order that longer time-window is 3.3 times more in output power form than the precedent (Cao et al., 2014). A reduction of fast cloud impact in voltage profile is found after using the PI Controller Reactive Power Injection to the grid control algorithm where voltage profiles are maintained in sunny as well as cloudy days (Abdelkarim et al., 2013). In the Micro Energy Management System, the output power fluctuations are suppressed without sacrificing in system's efficiency (Noro et al., 2012). As for Coordinated Control, peak load shaving is achievable with shorter time response (Liu et al., 2012). The ANN algorithm reduces electrical costs by forecasting predicted marginal price and availability of solar irradiance (Liu et al., 2014; Pazikadin et al., 2020). Alternatively, the Generic Algorithm (according to its name) mitigate power fluctuations in a substation (Zhang et al., 2012) as the Matrix Real-Coded Genetic Algorithm

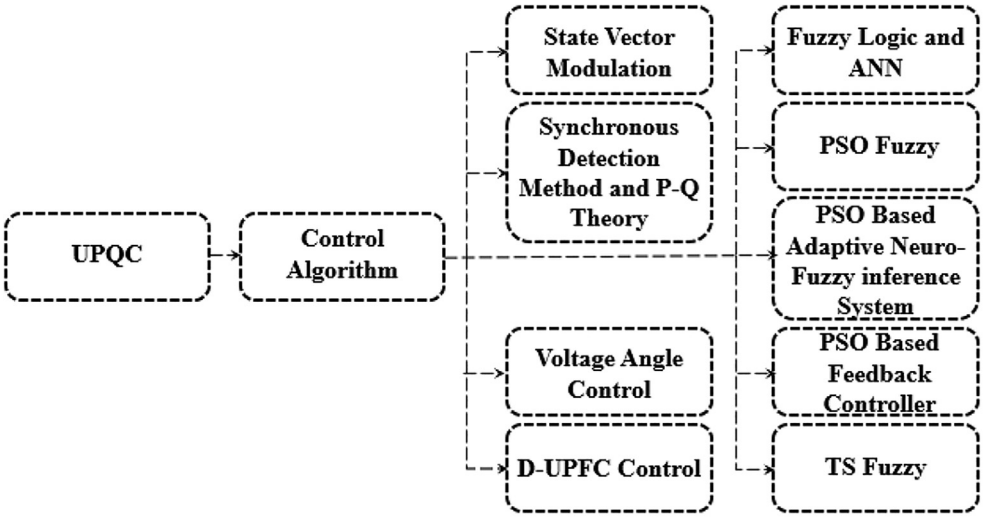

Fig. 6. Different control algorithms for UPQC.

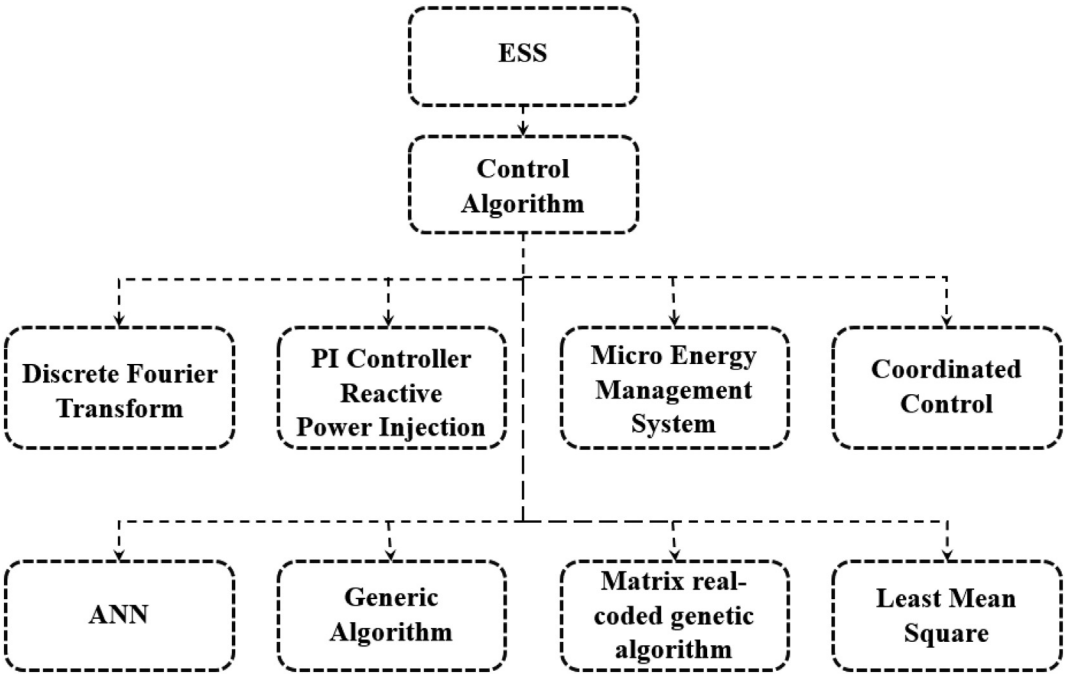

Fig. 7. Different control algorithms for ESS.

determines optimal parameters of ESS in micro grid (what banks to choose, at what time with which switching techniques) (Chen et al., 2011). Lastly, the Least Mean Square eliminate harmonics in current to below 5% where the inverter control algorithm is based on predicted output power (Chen et al., 2008).

The BES (Battery Energy Storage), another form of ESS works under the principle of storing surplus power during extra peak power production i.e. maximum solar irradiance in a sunny day, and return it back to the network when peak load demand occurs and corresponding power production is intermittent (low radiations, cloudy day) (Barzegkar-Nvotom et al., 2020). There are three main battery categories acting as energy reservoirs (Chaudhary and Rizwan, 2018):

- Conventional Batteries (widely used with types as Lead Acid, Nickel Cadmium, Lithium Ion and others…)
- High Temperature Batteries
- Flow Batteries

Following equations are for charging and discharging characteristics that are taken into consideration when designing/using BES as a form of overvoltage suppression:

$$E\,(t+\Delta t) = E(t) + \Delta t \cdot P_c \cdot \eta_c \tag{1}$$

$$E\,(t+\Delta t) = E(t) - \Delta t \cdot P_d / \eta_d \tag{2}$$

where P_c is the charging power and P_d is the discharging power, whereas E is the stored energy, t the time taken to store the energy, η_c and η_d are charging and discharging efficiencies (Chaudhary and Rizwan, 2018).

Power limits of battery storage systems are defined by the following power constraints:

$$0 \le P_d(t) \le P_{d\ max} \tag{3}$$

$$0 \le P_c(t) \le P_{c\ max} \tag{4}$$

For an example of 120 Ah (Ampere Hour) battery, the supposed charging current is estimated at 10% of total Ah rating, therefore assumed at 12 A with a charging voltage of 14 V (that is 2.35 V for each 2 V cell) the maximum charging power $P_{c\ max}$ is 168 W (regardless of charging efficiency and neglecting charging losses). The discharge power is load related, and in some cases dictated by DOD (Depth of Discharge) that is commonly referred at 50% and battery C-rating (related to manufacturing process) therefore for the same 120 Ah battery example, the maximum discharge power $P_{d\ max}$ is 720 W.

ESS are considered as solution for off-grid PV system. When expanding the storage capacity, PV users are expected to gain more power functioning days, under low solar irradiance and shading scenarios. Since batteries are at the highest costs of PV system requirements, ESS are believed to be the most expensive solution for PV system optimization.

2.2. PV panels water cleaning

PV panels' cleaning (for dust/droppings removal) is of crucial importance at elevating overall system output power. Since dust and other accumulated particles act as a blocking interface to solar irradiance from reaching destined cells, voltage drop and other disturbances are seen once panels become dirty. Since natural cleaning can often take place (such as raining, etc.) the "man-made" term is derived in a way to confront that the process was intentional using floating water pumps and other media as shown in Fig. 8.

Such correction method (for external faults resulting from dust or leaves accumulation) alleviates much the overall power output as the Table 3 indicates. Among sixteen different monthly readings, we only see a negative percentage difference between clean and dirty panels output power, over the span of the three hottest summer months. The reason can be referred to PV panel sets localization: due to notable change in incident solar radiation angle within July, August and September compared to other months, the position of the dirty panels in the study is assumed to receive more sunrays than clean ones. Whereas in the remaining months, it was seen that the output power for clean panels are larger than dirty ones. By adding all gathered percentage differences and dividing them over the number of samples (sixteen months) we arrive at an 8.7% percentage difference. Said differently, there is a larger power

Fig. 8. Cleaning process for PV panels (Alnaser et al., 2018).

production for clean panels than that of power production for dirty panels by 8.7%.

This cleaning process can be expanded to achieve wider forms of PV panels' purification and dust/bacteria removal as indicated in Fig. 9.

Core focusing on the Artificial Cleaning Methods, and starting by manual cleaning, it is considered as the most primitive form since it only requires a worker with a soft cloth and water to clean panels. For small-scale PV power plants this is one of most efficient techniques of cleaning (Mohamed and Hasan, 2012). For larger plants, jets and brushes are used with the ability to add detergent formulas as a way to improve cleaning for hard soiling (El-Nashar, 1994; Kimber, 2007).

The Self-Cleaning set of methods, on the other hand, states techniques where the human worker can be replaced by automotive systems and sometimes robots to achieve higher efficiencies in water consumption saving.

The Active Cleaning set corresponds to all cleaning techniques that requires continuous power to execute function, beginning with the Mechanical Methods. They are equipped with mopping, brushing and blowing. A system compromising a central processor, a gearbox and a stepper motor rotates in a way that keeps solar irradiance normal to the PV module surface. When rotating 180° the brush rotates due to gravitational force and cleans the PV surface. The other cleaning process held by the brush is at different times executed at 360 degrees (Tejwani and Solanki, 2010).

Table 3
Difference between solar produced powers from clean vs. dirty panels in (Alnaser et al., 2018).

Month/year	Clean panels: actual solar electricity (kWh)	Dirty panels: actual solar electricity (kWh)	Percentage difference
Nov 2013	1.1365	1.0717	5.70
Dec 2013	1.0809	1.0194	5.69
Jan 2014	1.1344	1.0685	5.81
Feb 2014	1.2382	1.1865	4.18
Mar 2014	1.1735	1.1343	3.34
Apr 2014	1.2196	1.1569	5.14
May 2014	1.1862	1.1412	3.79
Jun 2014	1.1048	1.1035	0.12
Jul 2014	0.9201	0.9355	−1.67
Aug 2014	0.7544	0.7619	−0.99
Sep 2014	0.6810	0.7106	−4.35
Oct 2014	1.2093	0.6631	45.17
Nov 2014	0.9560	0.6026	36.97
Dec 2014	1.0479	0.9785	6.62
Jan 2015	1.0487	0.9821	6.35
Feb 2015	1.2037	1.1512	4.36
Overall	1.0612	0.9687	8.72

To eliminate dust and bird droppings, an integrative system of PLC (Programmable Logic Controller) and PIC (Peripheral Interface Controller) can be used where its first structure groups wipers, darkness and movement sensors are controlled all together by the PLC. Its other structure uses roller brush and alarms controlled by the PIC (Lamont and El Chaar, 2011).

Moving to the Electrostatic Shields cleaning techniques, it is based on the theory of the traveling wave resultant from electric field that carries charged air dust elements in a transverse way (Masuda et al., 1972; Masuda and Matsumoto, 1973). The EDS (Electrostatic Dust removal System) consists of two parallel electrodes each reciprocally charged, made from specific chemical components placed in specific environment where the negative electrode induces the negative charge on dust elements present at the PV surface. The dust accumulations exist currently at the positive electrode after attraction. The result is a contact-less removing technique showing that for 80% of dust removal the performance of each PV module increases by 90% (Mazumder et al., 2007; Mazumder et al., 2013).

At the last sub-part of Active Techniques, the Robotic Cleaning consisting of an electric motor and brush showed effectiveness in decreasing water usage upon cleaning while alleviating the power generation (Ju and Fu, 2011).

On the other hand, the Passive Cleaning methods family is based on the relation between modifying the surface property of PV module with the super hydrophobic feature. This feature is for surfaces having the properties of water rejection and high water droplet mobility. The fabrication of such cleaning surfaces requires nanostructures. For the Super Hydrophilic Surfaces, the water draws on its surface carrying along dust particles away at the reverse operation topology than the hydrophobic structures. The difference is within chemical elements and reaction used in fabrication. Each corresponds to specific set of geographical areas, where rain floods heavily or rarely (Nayshevsky et al., 2018).

The water cleaning process is cheap and simple. It requires no expertise in labors and no special equipment to perform it. From Table 3, an 8.7% difference of power output between clean and dirty PV panels can demonstrate that applying a scheduled cleaning routines is worthy. The water and labor costs for cleaning is compensated with elevated power outcomes. The note to be taken into consideration is that, cleaning, must be merely done with water. Adding soap or other cleaning detergents can lead to future accumulation on the top surface of PV panels, causing extra futuristic failures. Some chemical detergents can leave traces on the glass mounting, causing light deviation and other failures.

2.3. PV panels dry cleaning

Without water usage, PV panels can be dust-wiped using dry robotic cleaning system that uses a Silicon brush to remove dust particles.

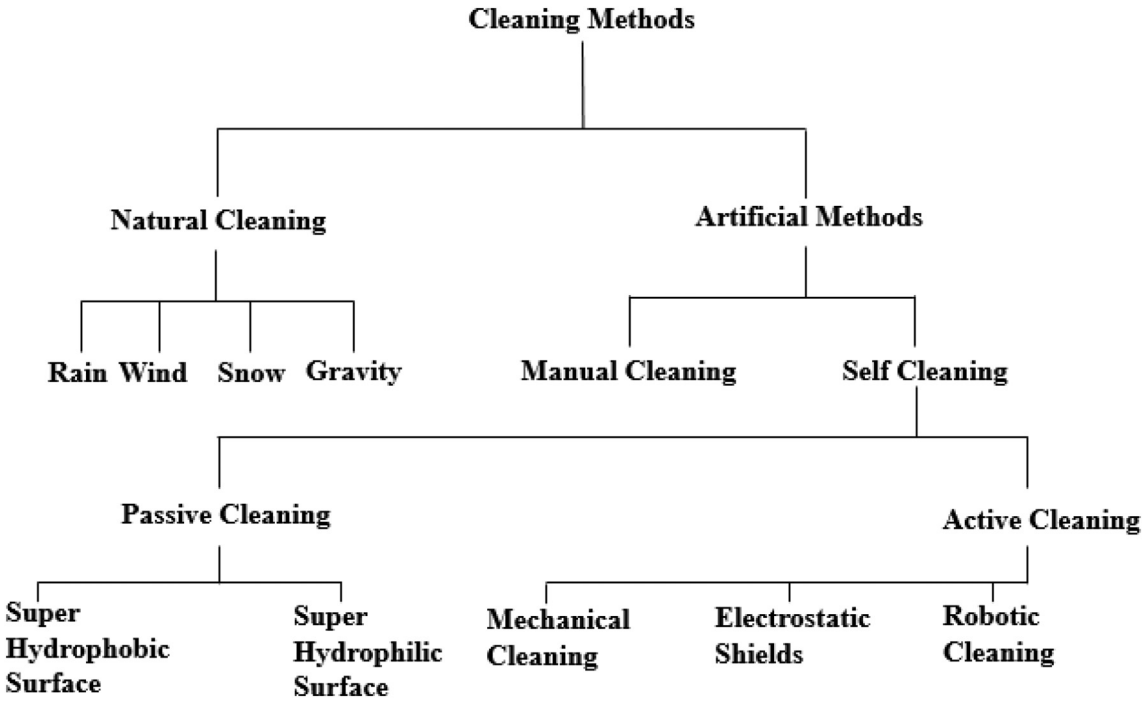

Fig. 9. Different cleaning strategies (Jamil et al., 2017).

Fig. 10 shows a simulated prototype for a dry cleaning robot, indicating all mechanical parts, installation over PV panels mount rack and its rotating motors driving circuitry.

The Silicon rubber foam brush used, demonstrated high resistance to collections of dust/debris on the brush, absorption of water and high cleaning efficiency.

From the same perspective, an automated water-free solar cleaning service unit is made by using a microcontroller. Its algorithm commands a dual DC (Direct Current) motor drivers, in a way that the robot senses its live position and automatically manages the degree of panels cleaning using pre-defined sets of data. The control process is held using a Bluetooth module judging the driving apparatus to operate in the lateral direction (parallel to panels) (Deb and Brahmbhatt, 2018). Fig. 11 shows the actual prototype of the water-free cleaning robot.

Dry cleaning is considered as an advanced technology over water cleaning. Its drawbacks, however, are the need for extra machinery (robots, electronics) and continuous surveillance, maintenance and monitoring of the machines performance. This adds extra costs for PV system maintenance performance which is considered as economical drawback.

2.4. Snow removal

Not only dust and bird droppings affect the power output of a PV power plant. In cold areas, snow accumulation over PV panels greatly reduces their overall power output (Marion et al., 2013). Due to huge difference between dust and snow constitution, the techniques used to mitigate negative impact of dust/accumulations does not work for removing snow from above PV surfaces (Andrews et al., 2013).

Among the eight techniques recapitulated in Fig. 12, increasing the Tilt Angle yields to faster sliding of the accumulated snow and hence reduction of power production losses (Ross, 1995; Ross and Usher, 1996). This is done at night (no solar irradiance and no power dependencies on PV outputs) where the day after the angle is restored to its original pace (to achieve higher absorption of irradiance). Since the back of the PV panel is always clear of snow, we can force the back

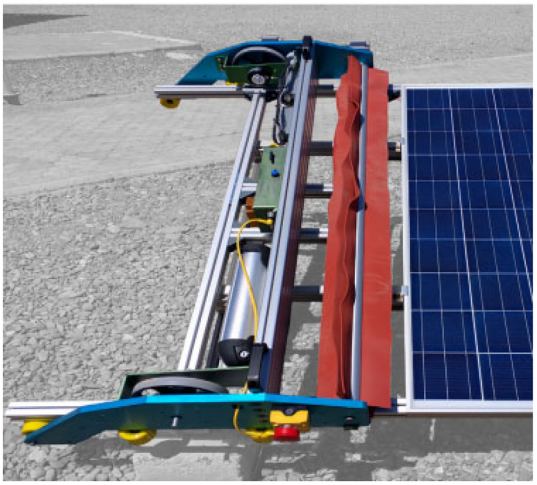

Fig. 10. Dry cleaning robot (Parrott et al., 2018).

Fig. 11. Water-free service unit (Deb and Brahmbhatt, 2018).

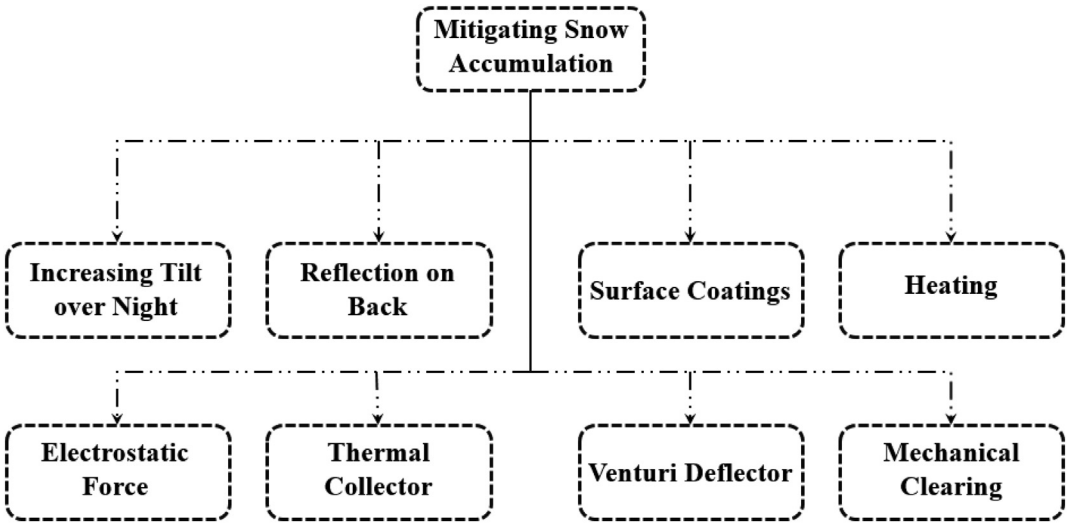

Fig. 12. Snow removal techniques.

surfaces of the panels to absorb the diffused light, reflected from the ground behind the panels what results in an increased PV temperature and hence quickening the melting process of the snow on the front of the PV panels (Chaudhary and Rizwan, 2018; Takehara et al., 2000).

The Surface Coatings used are forms of adhesion reduction and friction by absorbing quantities of solar radiations to breakdown the snow cover. Alternatively, Heating processes are straightforward schemes to remove snow from PV panels. Two general forms to achieve the removing task exist as:

- Voltage Application Heating: by taking benefit from the resistive properties of PV panels, a voltage source is applied across after snow falling inducing them to produce heat (Takehara et al., 2000).
- External Heating Source: done by adding external resistive heaters to the front or back surfaces of the panel (Garvison and Warfield, 2005). This strategy reduces losses of heat due to cold surrounding environment resulting in a fast more focused snow removal.

Electrostatic Force: after integrating conductors in the PV panel glass and charging them with high alternating voltages, an electrostatic repulsion occurs between PV surface and small ice blocks, lifting them off the surface (Higashiyama et al., 1998).

The Thermal Collector process applies the theory of heat transfer from a vertical metallic panel in the same sense of snow fall (does not collect snow) where solar irradiance causes the absorber (collector) to warm up and thus transfer heat through conductive paths to the snow covered panel that at the end results in snow melting, as described in Fig. 13.

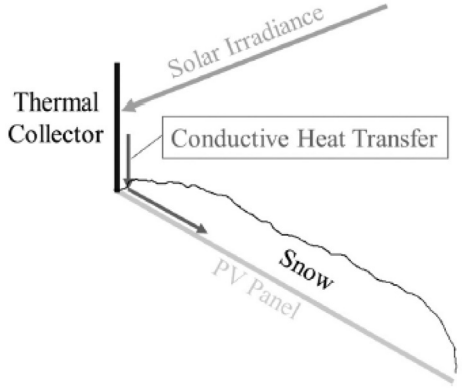

Fig. 13. Thermal collector (Pawluk et al., 2019).

The Venturi Deflector, a simple device with no moving parts, uses unidirectional wind to push air down front the PV panel and thus preventing snow from accumulating (Pawluk et al., 2019).

Chemical treatment (spraying of brine and salt) is found effective in de-icing but could somehow degrade the PV module (Borrebaek et al., 2020).

Such corrective technique is a must in cold, snowy areas. Snow piling on top of PV surfaces blocks the absorption of solar radiation. All techniques presented in this strategy require electro-mechanical equipment mounting on the rack of the panels except for surface coating. Using a resistance free, sliding surface coating would block the bulking of the snow without any power requirement for heating or vibrating. On the other hand, techniques with electrostatic force and heating initiators, might decrease the system overall power output by portioning some of the fabricated power to operate the equipment. Heating mechanisms can cause serious burning and provoke permanently damaged PV panels if the operating temperature is not carefully studied.

2.5. Equipment technical maintenance

Upon equipment failure, denoted by alarms signals and based on sensors notifications, a corrective technical maintenance is needed by a set of labors (service team) to manually intervene in replacing, switching off/on modules and fixing faulty equipment.

Table 4 reveals different physical aspects that are required to be put in place when maintaining equipment failure. Driving to the faulty site comes first, then inside equipment lodge, operators can contribute in problem solving by fixing the damage, replacing corrupted equipment, and setting an order for a new equipment. The actions recapitulated in Table 4 cover up the red dashed part of the PV system, shown in Fig. 14.

Within the red dashed zone in Fig. 18 lies the greatest part of equipment from DC-DC charge controller, safety elements, inverter and

Table 4
Actions held by service team during technical maintenance (Peters and Madlener, 2017).

Action	Effect
Drive	Drive to/from power plant
Switch on/off	Array changes state
Order	Item available after lead time
Replace	Item renewed
Fix	Item fixed

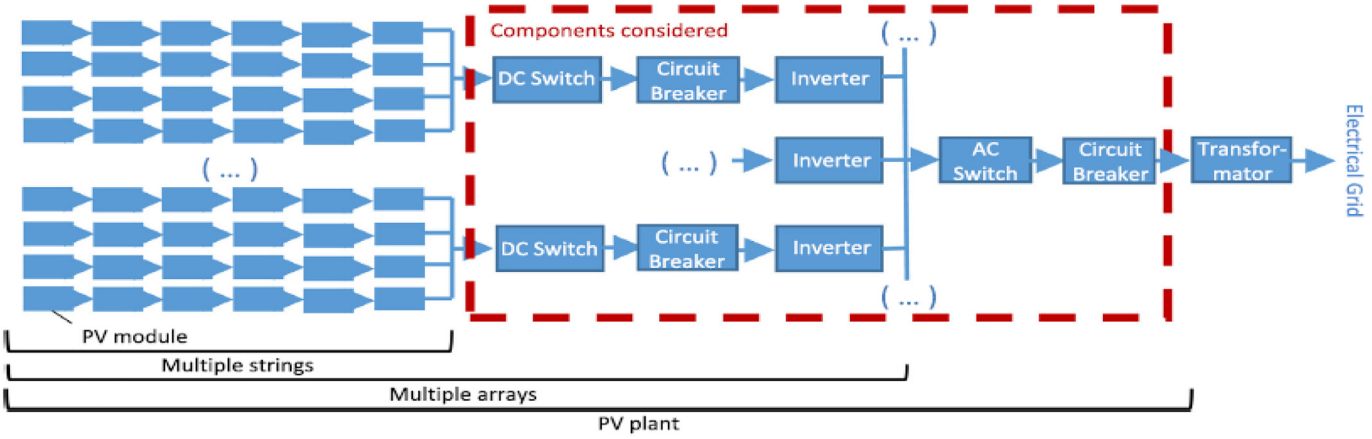

Fig. 14. Targeted PV system level for technical maintenance (Peters and Madlener, 2017).

breakers. Accordingly, the biggest equipment failure coincides within this zone, having larger fault probabilities than other zones (on the left side exist the pure DC zone with PV modules and their accessories, and other right side is the consumable AC zone).

Unlike Snow Removal technique, equipment maintenance is required for PV system regardless of ambient temperature and weather conditions. If an item is missed or damaged, it must be replaced, or fixed under all circumstances. The flow (which begins by driving to the fault location and ends up by fixing the fault) seen in Table 4, to maintain an equipment failure, can be improved by previously storing required items quantities in warehouses so the ordering task can be withdrawn leading to improved maintenance time operation response. The technical team in charge can be well trained to directly identify the problem, whether it is to replace or fix the damage.

2.6. Shading mitigation techniques

To reduce negative effects of shading on PV panels (caused by clouds, trees, and other forms of aerial obstacles) means reducing the rate of having a flat voltage profile. This in turn leads to a more efficient power productivity. The procedure can be decomposed into two family sets of methods as described in Fig. 15.

- Circuit Based Topologies
- Modified MPPT (Maximum Power Point Tracker) Based Techniques

Since we cannot remove clouds or other barriers from shading onto the panels, the above mentioned sets of methods compensate the decrease in solar radiation (whether it was a complete or a partial shading) by acting as a power conditioning unit, especially on the MPPT level.

The Circuit Based Topologies generally optimize the tracking efficiency under partial shading scenarios. The Bypass Diodes permits PV arrays to execute multiple local maxima (Murtaza et al., 2014). To track the local peak of each singular PV module, a DC-DC voltage chopper is used (Dhople et al., 2010).

The need for such converter is neglected when using the AC/micro inverter circuit, as AC modules take into consideration the efficiency, safety and cost design parameters where each PV module has a dedicated DC-AC converter instead (Gross et al., 1997). The Bypass diode can be removed and a set of Multiple Input/DC-DC converter is used to track the maximum power point of each PV module (Poshtkouhi and Trescases, 2011). The circuit transforms to Injection of Bias voltage on string level for MPPT scheme, when the dedicated DC-DC converter is used, for each string rather than for each module, where a diode is forward biased (for each string) in case of shaded module (Karatepe et al., 2008). Under PSC (Partial Shading Condition), a GMPP (Global Maximum Power Point) tracker is seen to overcome the problem of having multiple local peaks in PV module characteristic curve P—V (Power-Voltage) using meta-heuristic algorithms (Mohamed et al., 2019). The usage of a GMPP tracker ensures extraction of the maximum available power from PV system under PSC.

The PV equalizer depends on battery equalizer system in a way that energy distribution in both shaded/unshaded PV cells is effected by a single inductor and current inverter topology (Park et al., 2009).

In the EAR (Electrical Array Reconfiguration) PV generator scheme, the PV array is reconfigured in two forms depending on the status of the shading (partial, total, etc.) as 'fixed array' or 'adaptive array' using a switching matrix existing half way between the two array forms (Nguyen and Lehman, 2008).

The integrated Capacitor method tracks instantaneous power from PV array output and compares it to a previous value. This is done through charging mode. Until the capacitor is fully charged, the instant global peak (and voltage) is acquainted (Mahmoud, 2006). The charging time of the capacitor depends on open circuit voltage and short circuit current of the panel:

$$t_c = 2C^{V_{OC}}/_{I_{SC}} \tag{5}$$

with C, V_{OC} and I_{SC} denoting capacitance, open-circuit voltage and short-circuit current respectively.

From a different perspective, in the Multilevel Inverter technique, the DC link is controlled through a virtual-vector based pulse width modulation method. Its scheme corresponds to four-level, three-phase diode clamped inverter (Cavalcanti et al., 2012). As for Voltage Equalization technique, it extracts maximum power under non-uniform irradiance using a SEPIC (Single Ended Primary Inductor Converter) (Pragallapati et al., 2013).

At the end of Circuit topology group of methods, the Current Equalization approach is used to mitigate partial shading obstacles by connecting a synchronous fly-back converter across each PV module. This regulates the maximum power point under partially shaded conditions (Sharma et al., 2012).

The MPPT based techniques are algorithm-based methods to extract maximum power point under uniform irradiance conditions, through the power conditioning unit. Global MPPT strategies, are in advance, working for non-homogeneous shading conditions (i.e. where the P—V curve have multiple peaks). This in turn gives the PV system more flexibility and precision in achieving the maximum available power (Rezk et al., 2019).

Shading is considered to be the most common problem for all PV systems. Since clouds and barriers cannot be physically displaced, it is of crucial importance to eliminate any cause of hotspots, hence reducing PV burning casualties. Usage of PV panels with internally implemented bypass diodes, blocks the possibility of PV burning when

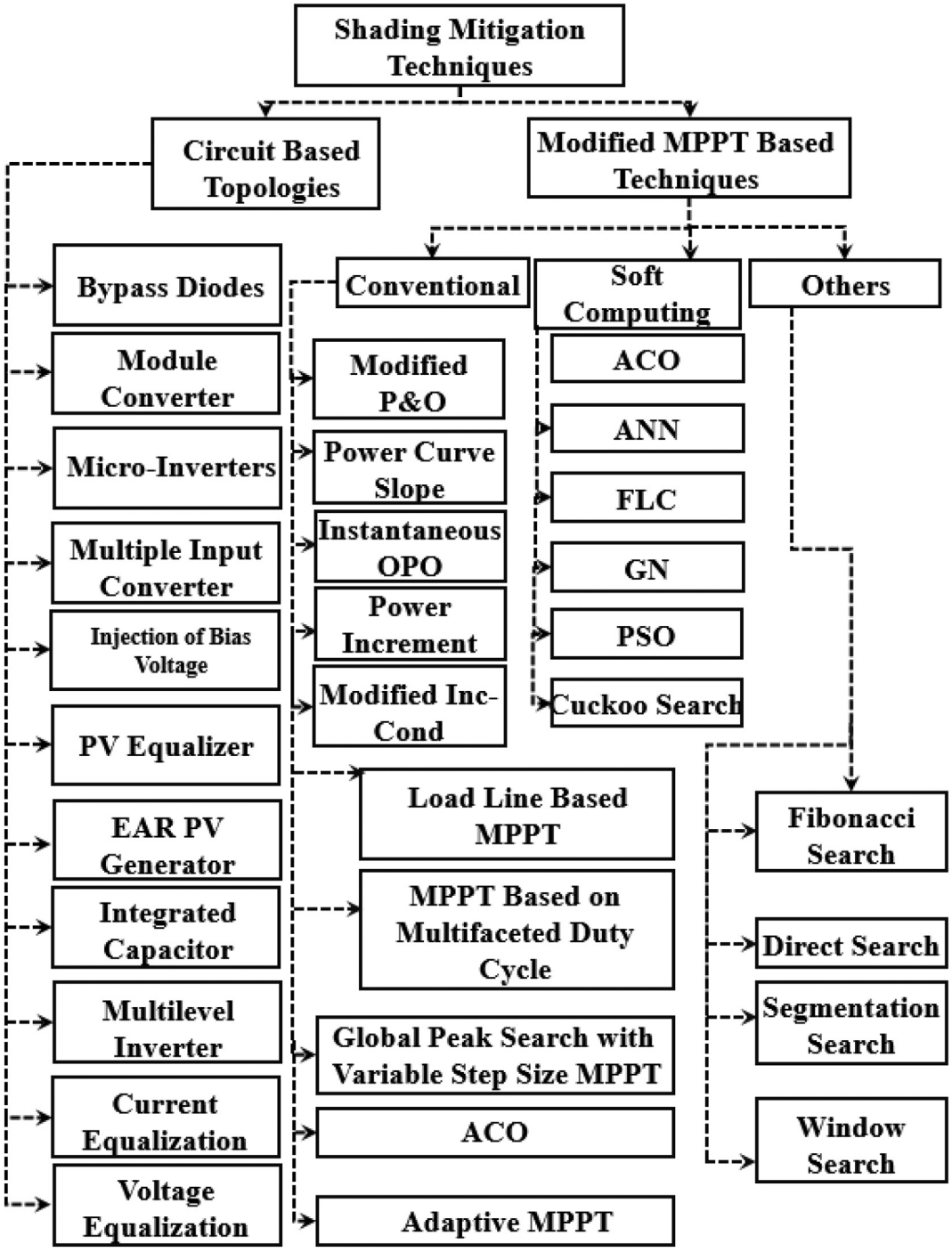

Fig. 15. Classification of different Shading Mitigation Techniques (Das et al., 2017).

non-homogeneous radiation strike upon PV surfaces. Although this type of panels is more expensive than traditional ones, but it could relief the need of buying a new PV panel if a hotspot occurred. To ensure the maximum power extraction of PV system, the MPPT is found effective in commanding the system to operate at highest point of peak power, due to the fact that the P—V characteristic curve of PV panels is non-linear. A 100 W panel can supply its maximum capability of rated power only by usage of an MPPT. That is to say, if no MPPT was involved in PV system design, only a fraction of the rated power is achievable, especially under shading conditions. The high cost of MPPT is returned with increased power output when used.

Corrective maintenance is the basic form among different maintenance schemes. It is also the most common for all PV systems, regardless of system power capability, design criteria and equipment used. Since faults can happen at any time, adaptive corrective maintenance should take place to immediately mitigate fault leftovers. A good initially designed PV system could help in lowering the need for such maintenance. To benefit the most from corrective maintenance, a scheduled PV cleaning is recommended within an interval of 15 days. The cleaning process is advised to be done with water only. For warm climate areas, snow removal techniques are of no need. An internally coupled bypass diodes PV panels are advised for the PV system design to reduce any

risk of future hotspots. To ensure the maximum power withdrawal from PV system, an MPPT is proposed to be installed within the system, what would accelerate the cost of return period, while leaving no fragments of available power unused. A DVR controlled by an integrated circuit comparator, can achieve desired voltage profile with less need of complex programming. This analog circuitry can continuously perform a differentiation between actual and reference voltage levels to drive shafts of center tapped transformers into accurate positioning.

Unlike urgent case maintenance costs and energy production relation, corrective maintenance cost help in increasing energy production, rather than reproducing power from complete outage. For instance, the additive costs of water and labor expenses are less compared to 8.7% power increase versus non cleaned panels as shown in Table 3. Of equal importance, the cost of repairing damaged or partially damaged equipment results in elevating power outcomes, making the system more sustainable with much more increased life expectancy.

3. Urgent case maintenance

Besides Corrective Maintenance, the Urgent Case Maintenance differs with respect to its higher priority: such actions are mandatory when major unpredictable events take place in the power plant, hence require vociferous manual actions (corrective) to restore normal working conditions in the system (Taljan and Gubina, 2009). In other words, this type of maintenance is in the first part corrective, but in the second it has higher priority and needs to be accomplished before any other maintenance of whatever forms, since the drawbacks are the most toxic. For any given plant, the reasons triggering this type of maintenance gives highest degree of potential leaving the system without intervention in distressed mode, detailed in Fig. 16.

The fall from height trigger example in Fig. 20 requires immediate site visit, hence rapid maintenance of the damage, since the fallen PV modules could have affected neighbors or other people properties such as cars or belongings and even PV related items such as combiner boxes or cable ducts which leads to compound system errors. Similarly, events like theft and sabotage induce a warning sign to directly make the right actions that sometimes require dealing with local authorities to avoid future likely actions. Earthquakes for example could leave PV module chassis holders in unstable conditions yielding a fall, shadowing other PV modules or damaging partial zones of the system. Therefore whenever this happens, a speedy check must be made at the system's site to ensure that everything is still under control.

The results of such triggers are most hazardous if not treated urgently, and can affect different factors, recapitulated in Table 5.

In Table 5, consequent risks are cause related, affecting either the system itself, the working field employees or random passengers near system's installation. They can be biological (i.e. striking the human body, like act of burning, body fractions and others) or purely physical, hitting only materials as PV system components.

The maintenance approach in this scheme is identical to the corrective one, but instead the process passes through different steps, including an important risk decisions making.

The operation and maintenance shown in Fig. 17 was, to begin with, a tool for military purposes but then got spread for any types of operations that may introduce risks. Beginning by the identification of hazards, this process should present all the critical conditions that may lead to severe risks. In the risk assessment task, it would be the process that describes numerically the severity of a scenario that might occur. Then, to make risk decisions, the decision maker tells what mitigation techniques may reduce the level of risk based on a mathematical study of the risk (i.e. if manageable or not). Moving forward, the control implementation includes engineering/administrative controls that help in eliminating the hazard of the risk. When no control scheme is applicable, PPE (Personal Protective Equipment) is used. The final step of this methodology is to continuously supervise and monitor if the assessment was accurate and check the effectiveness of the control.

Concerning the hazard identification function, three categories related to PV operations are taken into consideration. The first talks

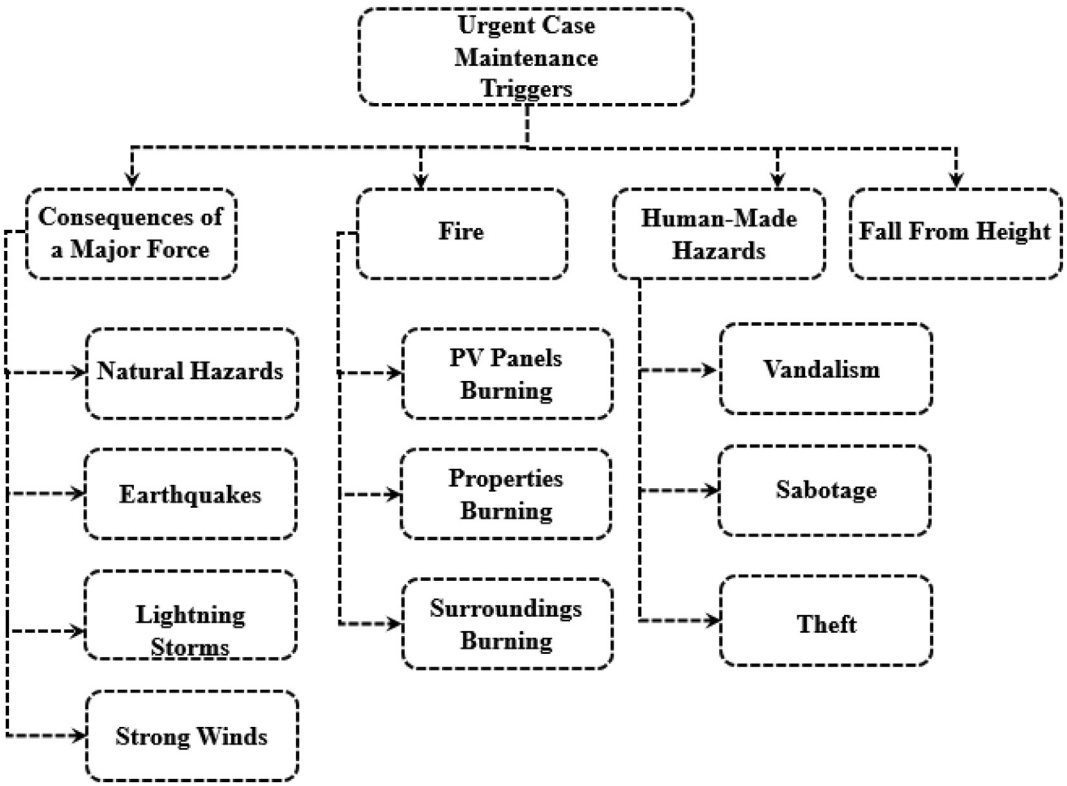

Fig. 16. Reasons behind Urgent Maintenance need.

Table 5
Relation between affected criteria, risks and initial cause.

Cause	affected criteria					Risks	
	PV system	Employees	Passengers	Damage of PV system	Health hazards	Mishaps	Burns
Consequences of a major force	✓			✓		✓	
Fire	✓	✓	✓	✓	✓		✓
Human-made hazards		✓	✓	✓	✓	✓	
Fall from Height		✓	✓		✓	✓	

about the source of the hazard, the second is related to its effect and the final is based on the process of operations (repair, fix, etc.) (Kamenopoulos and Tsoutsos, 2015).

On the other hand, for the hazard assessment task, a matrix is constructed that relates events to probabilities, recapitulated in Table 6.

In Table 6, an event is related to the causing condition yielding to different types of erroneous results of different severities (level of affection on PV system's performance) and weights (contribution in decreasing system's efficiency). The last three columns of Table 6 are up to the PV system safety designers that correspond to different numerical values for each system's topology, area and functioning. To be able to fill the three columns (assessing the hazards) there exists a three-step process to do so, recapitulated in Table 7.

To fully identify an event, like the poor safety program, experts working in PV system design will be able (after inspection and studies) to set its probability to happen from Table 7. For example, if good cable shielding is missing without a proper precaution, then the probability will be ranked as (A), the corresponding severities would be catastrophic (since a bolted short circuit will take place, hence electrocution causing death and loss of power fabrication would be the consequences) and the weight is maximal at that point of value 1.

Just like Corrective Maintenance, this is also a basic form of mandatory maintenance with highest priority among all other sort of maintenance schemes. It has nothing to do with artificial intelligence, machine learning or any complex method of fault intervention. The corresponding practical aspects concern site visit, and immediate replacement/fixing of stolen/damaged equipment. The probability of occurrence for this type of maintenance is less than the one for the corrective techniques, since major forces are less likely to happen compared to normal faulty scenarios.

The energy production at this stage centers entirely on cost of maintenance. That is to say, in cases of major forces events, if no urgent case maintenance costs are paid, no energy is produced at all (complete black out). Whereas if no purchase and replacement of a completely damaged PV panel, will certainly yield to a null power production.

4. Predictive maintenance

This particular form of PV plants maintenance mathematically evaluates the risk of failure of system components (equipment) before it happens, by taking into consideration data from scheduled system monitoring. The collected data sets a predictive plan to perform maintenance routines, to reduce the hazardous defects that will happen in future time while the system is still working. This greatly lowers the cost of post maintenance and prevents bigger failures.

The five different predictive maintenance techniques are recapitulated in Fig. 18.

Fig. 17. Steps for urgent case maintenance (Kamenopoulos and Tsoutsos, 2015).

Predictive Energy Management and Control System (PEMCS).

The stated PEMCS is composed of a two-part solution: PO (Predictive Optimization) and PA (Predictive Algorithm). It runs along three different modes over a full day (24 h) interval where each has its own requirements (Syed and Raahemifar, 2016) as summarized inFig. Fig. 19.

In the first mode (Mode-1) a major interaction from PV, BESS (Battery Energy Storage Stations) and PEG (Power Electric Grid) is formed. As for Mode-2 the PEG is unavailable where load is directly supplied from PV/BESS with the ability to keep surplus (if present) into BESS (if there is room). In Mode-3, on the contrary, load is supplied from PEG and PV (if available) with forbidden access to the energy within BESS.

In the PO (Predictive Optimization) function of PEMCS, the critical task to achieve is to ensure that during LSP (Load Shedding Period) there would be no energy shortage due to surplus. The optimal operational decisions are made while PEMCS is in Mode-1. The focus of Mode-2 is to ensure no energy supply shortage/curtailment while the Mode-3 is active.

The objective function of the proposed PO (Kamenopoulos and Tsoutsos, 2015):

$$J(U,k) = \sum_{k=LSi}^{LSf} P_{CF}(k)\Delta t \tag{6}$$

where $P_{CF}(k)$ is the forecasted shortage power during time interval Δt that equals to the difference between forecasted PV ($P_{PVF}(k)$) and load ($P_{DF}(k)$)

$$P_{CF}(k) = P_{PVF}(k) - P_{DF}(k) \tag{7}$$

Eq. (6) runs PO during Mode-1 hence minimizes the forecasted curtailment or shortage of power, thus representing Mode-2 operational resources. In Eq. (7) $P_{CF}(k)$ is minimized through predicted power from/to BESS.

The final sub-part of the PEMCS corresponds to PA (Predictive Algorithm), where it runs in Mode-1 as a way to minimize shortage during Mode-2. In other terms, the futuristic forecasted surplus in Mode-2 is injected into PEG during Mode-1.

In summary, the three modes differ primarily according to solar irradiance intervals, as in Mode-3 there is no usage of BESS energy, referred to as No-PEMCS mode that is scheduled from 10 PM to 6 AM (no solar irradiance) to make sure that during future LSP (Load Shedding Period) there will still be enough energy for the user to grant from. From 11 AM to 2 PM (during highest solar irradiance period) load is supplied from PV where surplus is stored into BESS (Battery Energy Storage Systems) if there is space. For Mode-1, scheduled from 6 AM to 11 AM then from 2 PM to 10 PM all energy supplies interact with each other (PV with BESS and PEG) for a continuous load supply. The different time intervals for the three modes add all together to form the continuous 24 h interval.

Fig. 20 reveals combinational analysis of PO and PA with different three modes of operation, to ensure at last that there would be no energy shortage nor curtailment during LSP.

Table 6
Event-Probability matrix (Kamenopoulos and Tsoutsos, 2015).

Event (1)	Condition (2)	Result (3)	Probability (4) A,B,C,D	Severity (5) I, II, III, IV	Weight (6)
Poor Safety Program	Not followed sops during maintenance (lockout/tag-out, PPEs)	Electric shock electrocution			
Gnawing electric cables by rats	Live elements or wires/circuits are not protected/damaged	Damage of the PV system fire			
Not followed basic electrical requirements (electrical code –NEC)	Live elements or wires/circuits are not protected / damaged	Electric shock electrocution			
Not followed basic electrical requirements (electrical code –NEC)	Not safe distance	Electric shock electrocution			
Not followed basic electrical requirements (electrical code –NEC)	Not grounded	Damage of the PV system fire electric shock electrocution			
Not followed basic electrical requirements (electrical code –NEC)	Not appropriate wiring	Damage of the PV system fire			
Not followed basic electrical requirements (electrical code –NEC)	Not overcurrent protection GFDI	Damage of the PV system fire electric shock electrocution			

Table 7
The 3-step process for hazards identification (Kamenopoulos and Tsoutsos, 2015).

Step	Description	Local	Levels of probabilities/severities & weight
1	Assess the probability	Column 4 of Table 6	A. Likely to occur immediately or within a short period B. Probably will occur in time C. May occur in time D. Unlikely to occur
2	Assess the severity	Column 5 of Table 6	I. Catastrophic: may cause death or loss of PV facility II. Critical: may cause severe injury, occupational illness or PVP (PV Panel) damages III. Marginal: may cause minor injury, occupational illness or PVP damages IV. Negligible: probably would not affect personal safety or health but it is a violation of a safety standard
3	Provide weights	Column 6 of Table 6	The weight should be a number from 0 to 1 with a weight step at 0.05

The PEMCS contribute in power durability at users' side, with less outage/shortage corresponding to solar irradiance levels. The energy prediction covers 24 h daily interval where all forms of possible shortage/outage is negotiated with respect to load shedding, and irradiance level. With no PEMCS, interaction between ESS, PV and PEG is missed, leading to load demand injection from ESS at high irradiation intervals, that in turn, results in blackout during night and low solar radiation due to intensive drainage of reserved supplies. On the other hand, any energy surplus is failed to be stored into ESS at peak radiation intervals, causing inability to withstand load demand under shading conditions

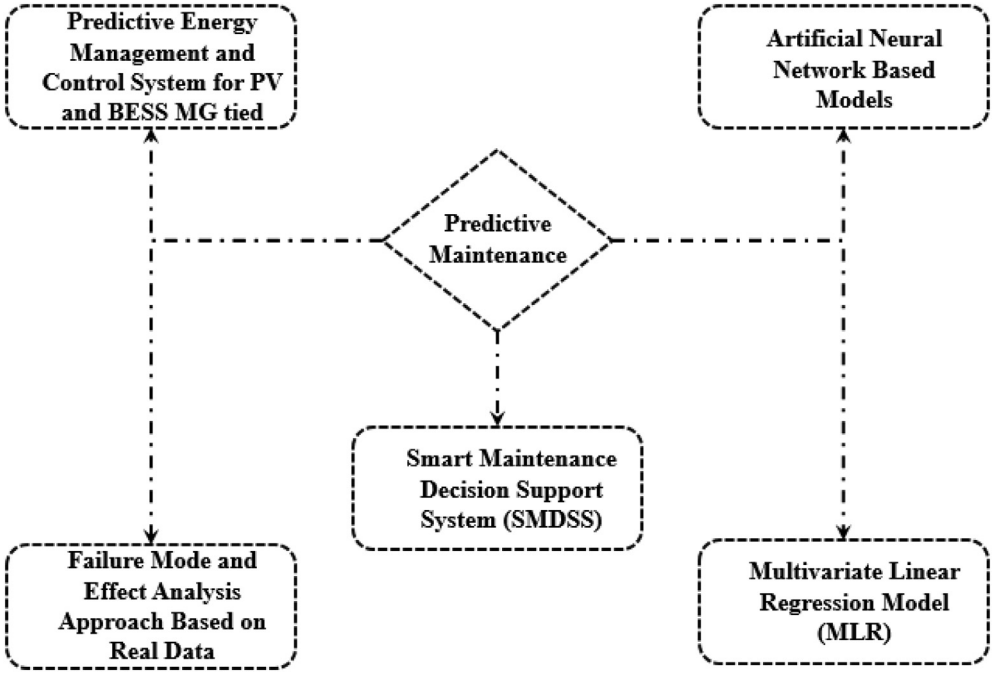

Fig. 18. Different Predictive maintenance methods.

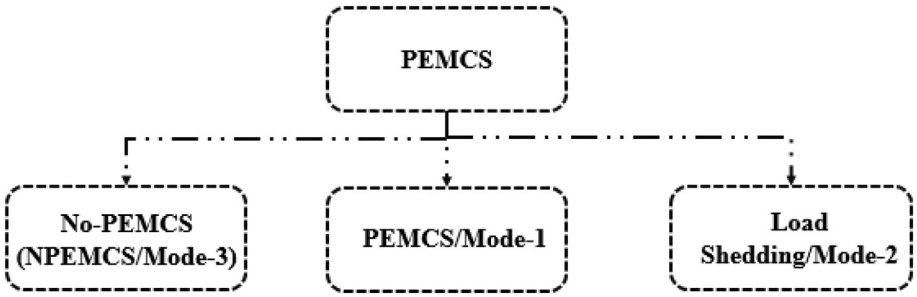

Fig. 19. Predictive Energy Management and Control System (PEMCS) modes of operation.

and night times. The predictive optimization algorithm is of minor complexity in software implementation as it only manages the energy feeder for loads between PEG, PV and ESS.

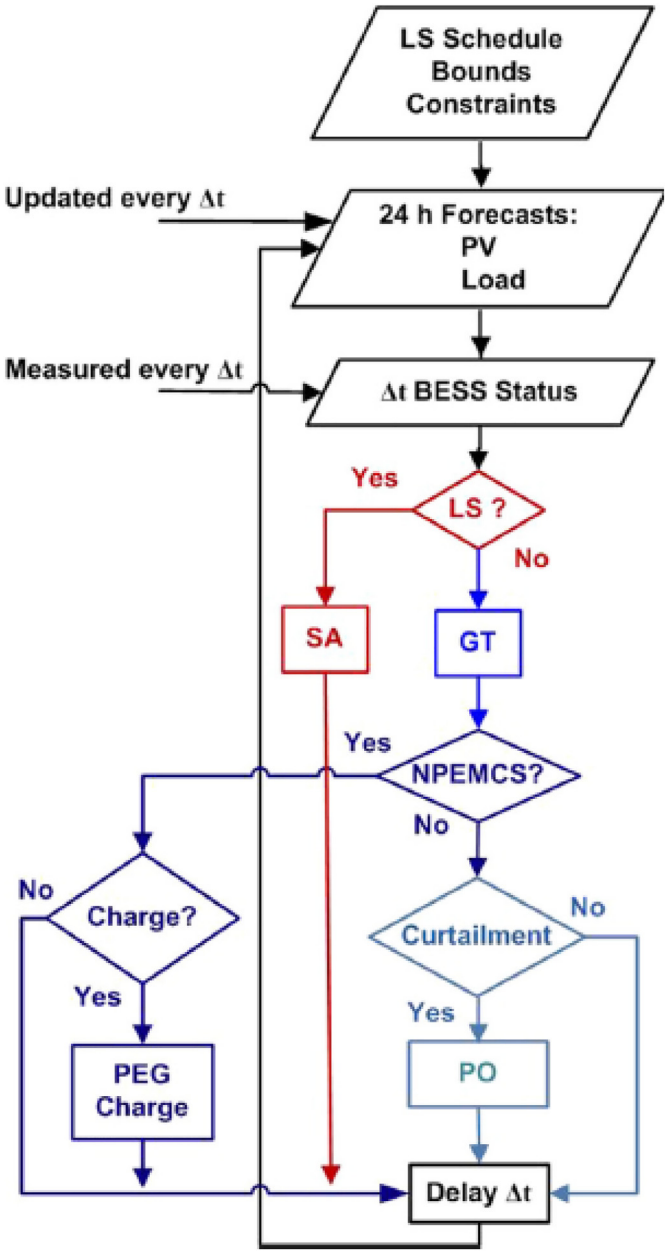

Fig. 20. PEMCS with PO and PA (light blue path corresponds to Mode-1, red path corresponds to Mode-2 and dark blue path to Mode-3) (Syed and Raahemifar, 2016). (For interpretation of the references to colour in this figure legend, the reader is referred to the web version of this article.)

4.1. Failure mode and effect analysis (FMEA)

The RCM (Reliability Centered Maintenance) applied to FMEA (Failure Mode and Effect Analysis) allows the analysis of each system sub-component as a detective investigation for its pre-failure: by identification of the various failure modes affecting each part, co-related with its cause and resultant consequences (Livera et al., 2019). The entire study relies on real experimental data from different solar plant worldwide as a way to derive a general algorithm of probability for the risk of failure (Villarini et al., 2017; Colli, 2015), decomposed into three sectors: Severity/Occurrence/Detection.

The method first study the severity that is translated into the seriousness of the end effect of component failure as described in Table 8.

Secondly, the occurrence indicates the frequency of happening criteria, recapitulated in Table 9.

At the end, the detection is the possibility of failure detection before it happens, shown in Table 10.

Each rating is measured on a subjectively defined scale where the RPN (Risk Priority Number) is the multiplication of total three criteria of Severity (S), Occurrence (O) and Detection (D):

$$RPN = S \times O \times D \tag{8}$$

By computing RPNs, disastrous failures can be prevented by core focusing primarily on high RPNs (having highest priority). Severities

Table 8
Severity ranking criteria (Villarini et al., 2017).

Rank of severity	Description
1–2	Minor failure/degradation, hardly detected, no influence on the system performance
3–4	Failure/degradation will be detected by the plant owner/operator and/or will cause small deterioration of parts or system performance.
5–6	Failure/degradation will be detected by the plant owner/operator, and will create dissatisfaction, and/or will cause deterioration of parts or system performance
7–8	Failure/degradation will be easily detected by plant owner/operator, and will create high dissatisfaction, and/or will cause extended deterioration of parts and system relevant non-functionality/loss of performance
9–10	Failure/degradation will result in a non-operation of the system or severe loss of performance

Table 9
Occurrence ranking criteria (Villarini et al., 2017).

Rank of occurrence	Description
1–2	Unlikely – Probability of occurrence <0.001
3–4	Remote probability – 0.001 < Probability of occurrence <0.01
5–6	Occasional probability – 0.01 < Probability of occurrence <0.10
7–8	Moderate probability – 0.10 < Probability of occurrence <0.20
9–10	High probability – 0.20 < Probability of occurrence

Table 10
Detection ranking criteria (Villarini et al., 2017).

Rank of detection	Description
1–2	Very high probability that the problem will be detected
3–4	High probability that the problem will be detected
5–6	Moderate probability that the problem will be detected
7–8	Low probability that the problem will be detected
9–10	None or minimal probability that the problem will be detected

ranked from 1 (minor damage) to 10 (major damage) are recapitulated in Table 8. The various probabilities for a failure to occur can be seen inside Table 9. For Table 10 the examination of a likelihood of pre-detecting a failure before happening is achieved. Grouping collected data from Table 7 to Table 9 we gather, *O* and *D* respectively resulting in RPN calculation then accordingly defining high priority failure mode.

Unlike PEMCS that requires machine learning, the FMEA analyses the system components' situation to predict its date of failure. The prediction is estimated on the probability of a future faulty event to occur, affecting certain system component. Equipment can be seen as functional, degraded or nearly damaged. The change, fix and replace activities would take place prior to equipment damage or malfunctioning, which will reduce future system shutdown costs and ensure energy sustainability. When both PEMCS and FMEA are adapted, the optimum power distribution and equipment safety are both guaranteed.

4.2. Artificial neural network (ANN)

With a high accuracy in predictive control of high-complex real world applications, the mathematical models of Artificial Neural Network consist first of fixed input/output layers, and one or many hidden layers that yields in processing information (prediction of a fault) in non-linear feature, high parallelism with learning and generalizations capabilities (Basheer and Hajmeer, 2000; Zhang et al., 1998). As a way to predict system failure, ANN models used here not only rely on environmental conditions as temperature and radiation but also on assets' conditions variables (Hernandez-Perez et al., 2020). Using this scheme benefits designers to detect early degradation scenarios and compute risks before it happens. To achieve these targeted results, using ANN models, there must be a back-propagation training process of the network, then comes the turn for the overall prediction methodology (Polo et al., 2015).

At first instance, the back-propagation is a learning mechanism to solve predictions that bases on the following logistic function:

$$Z = f(x) = \frac{e^x}{e^x + 1} \tag{9}$$

Eq. (9) referred to as Sigmoid function, is often used in logistic regression (a statistical modeling of a binary dependent variable that estimates the parameters of a logistic model) where its usage is to model the probability of an event happening. This learning training consists of two steps (Basheer and Hajmeer, 2000):

Forward Steps: the output of the output layer is:

$$\hat{y}_d = f(n_{\hat{y}d}) = f\left(\sum_{j=1}^{J}\left(w_{\hat{y}_d,k} \times a_k\right)\right) \tag{10}$$

where $\hat{y}_d$is the obtained output, $w_{\hat{y}d,\,k}$ is the weight corresponding to each obtained output, a_k is the output produced by the nucleus of each neuron and y_d is the real output. Fig. 21 is a graphical interpretation of Eq. (10).

Backward Steps: in this step the error between the obtained output and real output is calculated as the weights are adjusted in order to decrease the error reversely.

As for the logic selection tool, the RCM (Reliability Centered Maintenance) presents a generic process for the logic selection of maintenance actions to prevent failure occurrence.

The simulation of ANN is the core function where ANN prediction comes afterwards as a result, beginning by setting of input/output

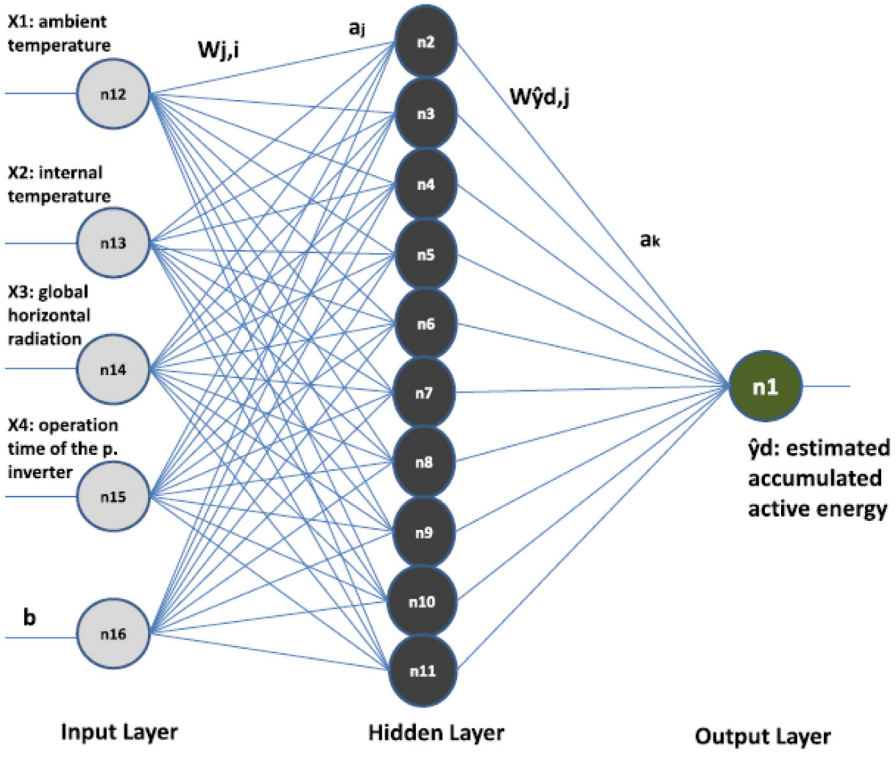

Fig. 21. Back-propagation perception multi-layer ANN (Polo et al., 2015).

data, to divide collected data to be processed in the correct category of training, testing and validation processes (Meenal and Selvakumar, 2018; Moretti et al., 2019). After that comes the development of ANN models for input/output analysis. Data of input/output are normalized between a range of −1 to 1. Then the model is trained with the normalized data (Ghritlahre and Prasad, 2018).

The ANN model becomes ready for prediction after being optimally selected between different models on the basis of statistical performance of predicted data with lowest values of different errors. Fig. 22 organizes steps to accomplish, beginning by input and output definition to arrive at the ability for network prediction.

By requiring heavy programming language, back-propagation and machine learning steps, ANN is seen less attractive for predicting future fault status for PV system with respect to PEMCS and FMEA. While using PEMCS combined with FMEA, simple structured program with visual inspection/detection of any equipment degradation, are effective in predetecting post failures, while maintaining optimum energy balance.

4.3. Multivariate linear regression model (MLR)

Under the regression type analysis, MLR builds a mathematical function that relates response variable to causal variables (set of predictors). In other terms, the independent variables are mathematically equated to dependent variables, where those are results of daily system conversion efficiency and dust effect in terms of exposure days and ambient temperature, forming the causal variables (Hammad et al., 2018). The resultant MLR model can be investigated in Eq. (11).

$$\eta_n = \mu_0 + \mu_1 D_n + \mu_2 T_n + \varepsilon_n \tag{11}$$

where D_n and T_n are the dust effect and average daily ambient temperature in day n respectively, η_n is the daily efficiency of day n, μ_0 is the regression model intercept, μ_1 and μ_2 are the regression coefficients and finally ε_n is the difference between actual and predicted efficiencies of the PV system in the nth day.

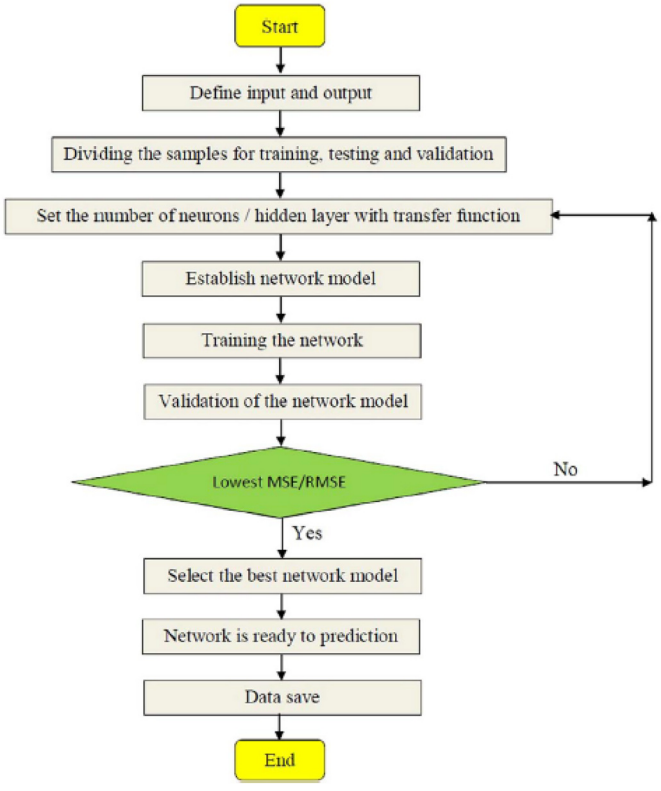

Fig. 22. Steps of data prediction using ANN (Ghritlahre and Prasad, 2018).

Compared to ANN, the MLR uses a straightforward mathematical function, simple but effective enough to acknowledge the set of predictors with affected variables. True that MLR model is not as precise as the ANN, but it could give PV system operators a brief idea about what might cause a failure.

4.4. Smart maintenance decision support system (SMDSS)

The SMDSS is a set of layers, consisting of dependent component model (DCM), analytical hierarchy process model (AHP), an expert system (ES), a full cost model (FCM) and a marketing information system (MkIS) (Bumblauskas et al., 2017).

$$SMDSS = DCM + AHP + ES + FCM + MkIS \tag{12}$$

Each term of Eq. (12) possesses a unique function: the DCM provides output in terms of actions. The AHP provides output in term of maintenance priority and altogether forms requirements for ES and FCM. At the end, the MkIS outputs a maintenance quotation based on the DCM and AHP outputs.

Similar to MLR, the SMDSS uses a mathematical model relating dependent variables to independent ones, outputting priority of maintenance for possibly failing zone within PV system.

On the contrary of corrective maintenance topology, predictive maintenance is less seen in today's PV systems, since it majorly involves machine learning processes, and require mathematical models. The cause-effect relation between fault contributor and damaged equipment is recommended to be implemented in larger PV systems, having wider areas of installation with standard power levels rated in megawatts. The larger the PV system the more the corresponding components, hence it becomes harder to visually inspect or detect degradations, system pre-failures or any other critical aspect. The machine learning techniques could help system designers in identifying which side of PV system the fault exists. For PV systems taking place at thousands of squared meters, detecting such faults without ANN and similar techniques is time and energy consuming.

Predictive maintenance are less compulsory than corrective and urgent case maintenance methods. Some PV system operate without any predictive interventions. The maintenance costs inside this set relies majorly on price of software and coding implementations. Paid costs for such maintenance are greatly seen in larger PV installations, where provided with fault localization and pre-determined intervention technique (replacing or fixing) could help mitigate larger future faults. Maintenance cost of return for such techniques is not directly noticed, as time is needed to observe the financial benefit in the long term of using them.

5. Preventive maintenance

The preventive maintenance is used in pre-failure mode, to decrease bigger damages that might occur after execution of a probabilistic future damaging event. Fig. 23 recapitulates the different four schemes used for such type of maintenance.

5.1. PV panels cooling

For varying climatic conditions, an inhomogeneous temperature distribution will be present across cells (Halawachs et al., 2019). The system will work normally as no form of any dysfunctionality would take place at any given moment, but if temperature still increases, the form factor as well as the open-circuit voltage would decrease (Bahaidarah et al., 2016). This phenomenon is due to the inverse relation between temperature and chemical bonding inside each cell. To spare the agony of that scenario, cooling methods exist in two forms to benefit from lowering the temperature, before system failure what results in a

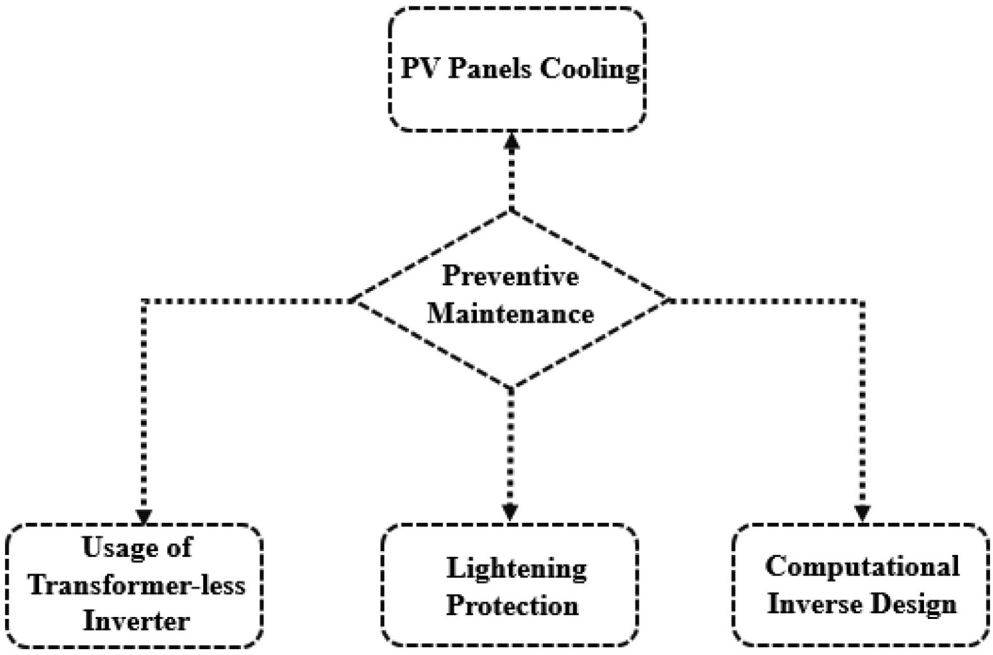

Fig. 23. Different preventive maintenance strategies.

better overall performance of the PV system, as follows (Hernandez-Callejo et al., 2019; Wu et al., 2018):

- Passive Cooling techniques:
  - Presence of fins; heat sinks, heat separators: achieve a cell temperature at 37 °C
  - Cooling by phase change materials: provides uniform cooling
- Active Cooling techniques:
  - Improved design of heat exchange: offers unified temperature distribution
  - Immersion inside a dielectric cooling liquid: cools down the panels in the range of 20–45 °C
  - Impact cooling: possesses high extraction capacity
  - Cooling with a heat pipe: achieve cells temperature in an acceptable range

The central panel cooling system coupled to the ground generates cold air circulation (cooled through a heat exchanger coupled to the floor) through a fan, passing it towards the surface of PV panels, resulting in heat dissipation (Sahay et al., 2015). A heat sink has also the same result as it sucks off extra accumulated heat over a particular region of the PV array (Hernandez-Perez et al., 2020).

Regardless of the methodology, to continuously cool a PV panel signifies extending its life cycle. Since semi-conductive material that allows passage of electrons upon light striking (Silicon, Germanium, etc.) does not accommodate heat, cooling serves as a refresher for these elements to operate at optimum conditions. Between different cooling techniques, the immersion of PV panels inside a dielectric liquid or simply throwing cold water at its surfaces is recommended the most, since it gathers benefits of cleaning the panels while simultaneously cooling them.

5.2. Usage of transformer-less inverter

Since the significant power to be used at the end of any PV system is generally of AC form (residential, commercial and domestic loads within the grid) and because of the DC form of the power gifted from PV arrays, the role of inverters to replace from DC to AC cannot be swapped (Howlader et al., 2018). In many inverters designs, transformers exist to achieve a galvanic isolation between DC and AC components, and in other circumstances the transformers are to boost DC voltage from PV output to higher values. This fact reduces the overall inverter efficiency, even though the system would work fine without any failure (Obi and Bass, 2016).

In other words, we can change the inverter type when transformers are needed (depending on the open-circuit voltage of PV panels) to transformer-less inverters that achieve complete galvanic isolation between DC and AC sides using power electronics instead.

So even if the GCPVS (Grid Connected Photovoltaic Systems) works fine, showing no failure, the transformer problems still exists (leakage current, hysteresis losses, eddy currents…). Therefore, in order to reduce further complications, the inverter is changed to one without a transformer.

This sub-technique is more involved into electrical performance of PV system rather than cell behavior like in water cooling. The usage of a transformer-less inverter could spare away agony of transformer related problems, contributing in neater power supply. Regardless of absence of galvanic isolation, a transformer-less inverter is recommended in PV designs.

5.3. Lightning protection

Since a PV system can run optimally without similar protective techniques, their implementation helps to prevent any damages that will occur if lightning strikes. When occurred, lightning results in direct strike, over-voltage and heat burning to PV modules, causing in turn to degrade the electric characteristics of the system and to deteriorate the output voltage to zero. Therefore, a proper design of lightning protection guarantees the performance of the system with the least lightning hazards (Santhakumari and Sagar, 2019).

The protective system can be decomposed into two sub-parts: as external and internal, shown in Fig. 24.

For the external lightning protection process, a low impedance metallic rod is to be placed in earth, developing a quick path for any surge (resultant from a lightning strike) to circulate in it rather than damaging equipment when that huge amount of energy flows inside system's components. For the internal system, by taking example of the separation distance, it is done by creating enough space between

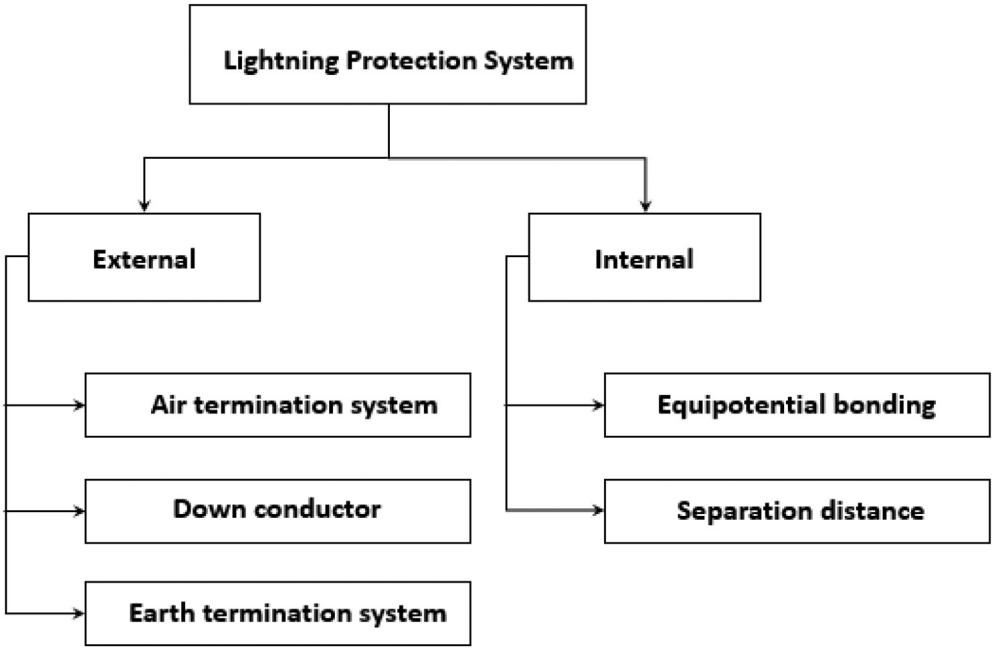

Fig. 24. Classification of Lightning protection system (Ahmad et al., 2018).

cells conduction path for them to not be entirely merged in (faulted all together) when a strike hit.

Compared with snow removal technique for snowy areas in the corrective maintenance set, the lightning protection is only recommended in heavy thunder regions. Its application could avoid any system post failure, burning, damage and breakout due to lightning strike.

5.4. Computational inverse design

To avoid the non-feasible trial-and-error approach to come up with optimum viable arrangements for a given application (here the constructive material of PV panels) the material characterization technique that enhances the relation between structure and electro-optical properties can solve the mentioned problem (Brito et al., 2019).

Numerical simulations make the transition from quantum scale to the desired macroscopic properties, possible. This is to select a special configuration that is the nearest to the target functionality (maximum open-circuit voltage with minimum losses) (Visa et al., 2016). This strategy selects the structure that has the target functionality while calculating a small portion of million-level possible configurations.

Without this design, a regularly-manufactured PV panel can work, but this adds a future failure preventive method by first choosing cell building blocks (atoms, oxides, etc.) then computing the target property (doping level, transmission) then finally using an optimization method to reach the destined level of performance (Santhakumari and Sagar, 2019).

This is to fabricate cells that are flexible with unpleasant environmental conditions (such as heat, humidity…) to prevent future failures (mainly due to soiling) and hence achieve maximum power extraction. To do so, two different strategies are established: where one is the reciprocal of the other: the forward strategy takes into account, first the material building blocks, to material morphology to ending up with macroscopic properties. The inverse strategies work inversely starting from macroscopic properties to arrive at the fabrication processes (Jain et al., 2014). An optimally identified triple-junction cell design for instance, allows the absorption of different wavelength lights. This in turns permit a more concentrated power production on the cellular level of each PV array composition (Fathy et al., 2019) under various shading scenarios.

The engineered chemical design for PV cells, from the moment of production, could help restraining erroneous non-linear behavior in them while in future operations (Alami et al., 2019). The recommendation to adjust computational inverse design are dedicated for PV manufacturers, to take into consideration the established strategies to produce reliable PV cells, solid in front of elevated heat levels and increased humidity.

The preventive maintenance scheme is the most valuable among others, since it inhibits the possibility of faults to occur, hence partially removes the need of all other tactics. A good initial PV system design can be included within preventive maintenance, by choosing reliable PV cells, a corresponding transformer-less inverter and other aspects.

In term of costs, preventive maintenance is cheapest among other strategies, since its design requirement are included in PV system initial cost of installation. Unlike corrective maintenance, preventive one is paid once for all, at prior system design and installation.

6. Conclusion and discussion

To properly maintain an environmentally healthy status, this paper first examined the contribution of a PV system towards a carbon free future. It was shown that a standalone PV system does not operate perfectly (as designed) without a proper maintenance scheme. Then the examination proceeded with the supportive relation between adapting a maintenance system in parallel with the PV system itself. It was shown through tabulated data, that PV system output is greatly improved when exposed to the proper sort of maintenance: an increase of 8.7% of overall power production is seen when applying maintenance, while mitigating voltage sag up to 81% and lowering distortions to 2%.

Since PV systems deal with real-world scenarios that are mostly interfered with disturbances, defects, climate instability and other factors contributing to the interruption of the desired system's performance in terms of efficiency, productivity, reliability and durability, designers must find ways to counteract these issues; this is the role of maintenance and intervention methods. It was shown that the maintenance process has four major strategies where each has a set of sub-strategies.

Corrective methods focused on the level of energy purity, especially under artificial intelligence techniques, where methods relied on the form of energy output, such as maintaining the sinusoidal waveform

for voltage output at the inverter as neatly as possible (with minimum wave perturbation and malformation). Efficient power quality is also ensured within these methods. Other methods like cleaning (with and without water), snow removal and shading mitigation techniques emphasized on extracting as largest power as available from the PV system either by removing obstacles (physical barriers), or compensating low irradiance scenarios by means of power processing units (DC-DC converters). Ending with the direct manual approaches (like fixing, replacing and interventions on the software level) which help to mitigate blackouts, corrupted system's performance and delayed operations. Therefore a continuously corrected PV system (dust/snow removal) is able to achieve higher energy production rates, lowering the global warming critical issue, by lowering CO_2 emissions.

A thermally cooled PV module can stabilize output voltage and ensure a maximum power productivity, hence lowering air pollution.

It is true that Urgent case methods have similar materialistic ways of maintaining a PV system, but what makes them different is their priority: an urgent event due to a major force (fall from height, lightning, sabotage…) requires an immediate interference and breakthrough system appliances to reduces errors, since their futuristic effects are the most damaging (fire, mishaps, electrification…).

The Predictive maintenance, differs from the two precedents by time-advance property, therefore executing scheduled maintenance routines, collected by informative data and historic records of system's performance. It reduces the larger failure risks that will happen in future time, according to acquainted data. It also develops mathematical models with discrete outputs that negotiate possible faulty events. This for instance cannot solve pre-damaged equipment or in other words, replace corrective maintenance schemes.

Predicting a fault in a PV system, enables its expansion for future upgrade, therefore allowing more energy production, serving more communities hence reducing the need of combustion in generators as alternative.

The Preventive maintenance at the end, is the set of methods that would help in avoiding the three precedent methods, as a way to intervene on the system without occurrence of any fault (like cooling the panels before they get overheated to get rid of voltage drop issue…).

A fault-preventing designed PV system helps individuals in rural areas to have their corresponding need of energy without relying on bulky power transmission by using expensive electrical transmission lines. When transmission lines are less needed, this results in needing less carbon emitters production facilities what yields in regulating toxic emissions.

For future trends corresponding to each maintenance technique, both corrective and urgent case maintenance methods, will witness less evolution compared to other maintenance strategies. Corrective and urgent case tactics will remain at same priority, since damaged equipment cannot be surpassed or ignored. After all, aspects of fixing, replacing, modifying software will remain almost the same for any period of time. Whether now or in the future, the act of replacing a burnt PV panel would be the same. On the other hand, predictive and preventive maintenance strategies will develop exponentially due to rise in machine learning techniques, surge of artificially intelligent and computer controlled systems. The future expectancy of supervisory, monitoring and controlling systems is machine based. Algorithms would keep improving to have higher degree of accuracy in smaller response time.

A good supportive maintenance system is of great importance, as it minimizes all forms of malfunction and consequently reduce operating costs. Corrective and urgent case maintenances are found suitable for any PV system, since it's a must after any fault detection. Other maintenance methods (predictive/preventive) are recommended for systems at initial installation period, as they need private adjustments on the level of algorithm implementation, during system's design.

To take maximum advantage from detailed PV maintenance sets, a recommendation for systems operators is to build on each collection aside. Beginning with preventive methods, the initial choice of cells architecture would be for reliable, temperature and humidity flexible ones. The inverter on the other hand is engineered to be in transformer-less architecture. In this manner, all problems related to non-linear behavior of cells, and electrical problems related with transformers (leakage current, eddy losses…) would be restrained. A scheduled PV cooling process is also advised to ensure optimum power output. Heading towards predictive maintenance strategies, a combination of PEMCS with FMEA would ensure a decent power distribution with future fault indicator for all equipment. A scheduled visual inspection is advised to keep track of any degradation of equipment. From the corrective maintenance set, an MPPT enabled PV system, with internally coupled bypass diodes within PV panels and with continuous scheduled PV panel cleaning, would achieve highest power productivity with less probabilities of panels burning due to hotspots. Nevertheless, the urgent case intervention is always executed upon need.

This combinational process between four different strategies, would ensure a durable, sustainable PV system with highest achievable efficiency and less impacts of faulty scenarios.

CRediT authorship contribution statement

Khaled Osmani: Writing - original draft, Investigation, Writing - review & editing, Visualization. **Ahmad Haddad:** Writing - review & editing, Visualization, Supervision. **Thierry Lemenand:** Writing - review & editing, Visualization, Supervision. **Bruno Castanier:** Writing - review & editing, Visualization, Supervision. **Mohamad Ramadan:** Conceptualization, Writing - review & editing, Visualization, Supervision, Project administration.

Declaration of competing interest

The authors declare that they have no known competing financial interests or personal relationships that could have appeared to influence the work reported in this paper.

References

Abdelkarim, E., Aly, M.M., Abdel-Akher, M., Ziadi, Z., Senjyu, T., 2013. Supersession of large penetration photovoltaic power transients using storage batteries. Proceedings of IEEE 10th International Conference on Power Electronics and Drive System (PEDS), Kitakyushu, pp. 78–83.

Ahmad, N.I., Abdul-Kadir, M.Z.A., Izadi, M., Azis, N., Radzi, M.A.M., Zaini, N.H., Nasir, M.S.M., 2018. Lightning protection on photovoltaic systems: a review on current and recommended practices. Renewable Sustainable Energy 82, 1611–1619.

Alam, M.J.E., Muttaqi, K.M., Sutanto, D., 2012. A Comprehensive Assessment Tool for Solar PV Impacts on Low Voltage Three Phase Distribution Networks. Proceedings of 2nd International Conference on the Developments in Renewable Energy Technology. ICDRET, Dhaka, pp. 1–5.

Alam, M.J.E., Muttaqi, K., Sutanto, D., 2013. Effectiveness of traditional mitigation strategies for neutral current and voltage problems under high penetration of rooftop PV. IEEE Power and Energy Society General Meeting (PES), Vancouver 1–5.

Alami, A.H., Rajab, B., Abed, J., Faraj, M., Abu Hawili, A., Alawadhi, H., 2019. Investigating various copper oxides-based counter electrodes for dye sensitized solar cell applications. Energy 174, 526–533.

Al-Mathani, A.O., Hannan, M.A., Al-Dabbagh, M., Ali, M.A.M., Mohamed, A., 2008. Development of new control strategy for voltage sag mitigation. Proceedings of 2nd IEEE international conference on power and energy. JohorBaharu 318–323.

AlMathnani, A., Shareef, H., Mohamed, A., Ali, M.A.M., Hannan, M.A., 2010. Power Quality Improvement Using DVR With Two Fast Vector Control. Proceedings of 4th International Power Engineering and Optimization Conference. ShahAlam. Selangor. IEEE, Malaysia, pp. 376–381.

Alnaser, N.W., Al Othman, M.J., Dakhel, A.A., Batarseh, I., Lee, J.K., Najmaii, S., Alothman, A., Al Shawaikh, H., Alnaser, W.E., 2018. Comparison between performance of man-made and naturally cleaned PV panels in a middle of a desert. Renew. Sust. Energ. Rev. 82, 1048–1055.

Al-Saedi, W., Lachowicz, S.W., Habibi, D., Bass, O., 2012. Power quality enhancement in autonomous micro grid operation using particle swarm optimization. Electrical power and energy system 42, 139–149.

Andrews, R., Pollard, A., Pearce, J.M., 2013. The effects of snowfall on solar photovoltaic performance. Sol. Energy 92, 84–97.

Anwari, M., Hamid, M.I., Rashid, M.I.M., Taufik, 2009. Power quality analysis of grid connected photovoltaic system in adjustable speed drive. Proceedings of the IEEPES/IAS conference on sustainable alternative energy (SAE) 1–5.

Ariyaratna, P.M., Muttaqi, K.M., Sutanto, D., 2019. The simultaneous mitigation of slow and fast voltage fluctuations caused by rooftop solar PV by controlling the charging/discharging of an integrated battery energy storage system. Journal of Energy Storage 26 (4–8).

Arya, S.R., Singh, B., Chandra, A., Al-Haddad, K., 2012. Control of DSTATCOM using adjustable step least mean square control algorithm. Proceedings of IEEE Fifth Power India Conference, Murthal, pp. 1–6.

Bahaidarah, H.M.S., Baloch, A.A.B., Gandhidasan, P., 2016. Uniform cooling of photovoltaic panels: a review. Renewable Sustainable Energy 1520–1544.

Barzegkar-Nvotom, G.A., Chatzigeorgiou, N.G., Nousdilis, A.I., Vomva, S.A., Kryonidis, G.C., Kontis, E.O., Georgihou, G.E., Christoforidis, G.C., Papagiannis, G.K., 2020. Assessing the viability of battery energy storage systems coupled with photovoltaics under a pure self-consumption scheme. Renew. Energy 152, 1302–1309.

Basheer, I.A., Hajmeer, M., 2000. Artificial neural networks: fundamentals, computing, design, and application. Journal Microbiological Methods 43, 3–31.

Bazan, J., Rieradevall, J., Gabarrell, X., Vazquez-Rowe, I., 2018. Low-carbon electricity production through the implementation of photovoltaic panels in rooftops in urban environments: a case study for three cities in Peru. Sci. Total Environ. 622-623, 1448–1462.

Bhargavi, R.N., 2011. Power quality improvement using interline unified power quality conditioner. Proceedings of 10th International Conference on Environment and Electrical Engineering, Rome, pp. 1–5.

Block, P., Lopez-Salamanca, H.L., Teixeira, M., Dahlke, D.B., Shiono, O., Donadon, A.R., 2014. Power quality analyses of a large scale photovoltaic system. Proceedings of 5th international renewable energy congress (IREC), Hammamet 1–6.

Borrebaek, P.A., Jelle, B.P., Zhang, Z., 2020. Avoiding snow and ice accretion on building integrated photovoltaics – challenges, strategies, and opportunities. Solar Energy Material and Solar Cells 206 (7–8).

Brito, P.P., Diniz, A.S.A.C., Kazmerski, L.L., 2019. Materials design and discovery: potential for application to soiling mitigation in photovoltaic systems. Sol. Energy 183, 791–804.

Bumblauskas, D., Gemmill, D., Igou, A., Anzengruber, J., 2017. Smart maintenance decision support systems (SMDSS) based on corporate big data analysis. Expert Syst. Appl. 7–20.

Cao, M., Xu, Q., Zeng, P., Xu, X., Yuan, X., 2014. An energy storage system configuration method to stabilize power fluctuation in different operation periods. National Harbor 1–5.

Cavalcanti, M.C., Farias, A.M., Oliveira, K.C., Neves, F.A.S., Afonso, J.L., 2012. Eliminating leakage currents in neutral point clamped inverters for photovoltaic systems. IEEE Transactions Industrial Electron 59, 35–43.

Chaudhary, P., Rizwan, M., 2018. Voltage regulation mitigation techniques in distribution system with high PV penetration: a review. Renew. Sust. Energ. Rev. 82, 3279–3287.

Chen, X., Fu, Q., Yu, S., Zhou, L., 2008. Unified control of photovoltaic grid connection and power quality managements. Workshop on Power Electronics and Intelligent Transportation System, Guangzhou, pp. 360–365.

Chen, C., Duan, S., Cai, T., Liu, B., Hu, G., 2011. Optimal allocation and economic analysis of energy storage system in micro grids. IEEE Transactions Power Electronics 26, 2762–2773.

Chidurala, A., Saha, T.K., Mithulananthan, N., 2013. Power quality enhancement in unbalanced distribution network using solar DSTATCOM. Proceedings of the Australasian Universities Power Engineering Conference, Hobart, pp. 1–6.

Choi, S.S., Li, B.H., Vilathgamuwa, D.M., 2010. Dynamic voltage restorer with minimum energy injection. IEEE Transactions Power System. 15, 51–57.

Colli, A., 2015. Failure mode and effect analysis for photovoltaic systems. Renew. Sust. Energ. Rev. 50, 804–809.

Das, S.K., Verma, D., Nema, S., Nema, R.K., 2017. Shading mitigation techniques: state-of-art in photovoltaic applications. Renew. Sust. Energ. Rev. 78, 369–390.

Dasgupta, S., Sahoo, S.K., Panda, S.K., 2010. Design of a spatial iterative learning controller for single phase series connected PV module inverter for grid voltage compensation. Proceedings of the international power electronics conference, Sapporo 1980–1987.

Deb, D., Brahmbhatt, N.L., 2018. Review of yield increase of solar panels through soiling prevention, and a proposed water-free automated cleaning solution. Renew. Sust. Energ. Rev. 82, 3306–3313.

Dhople, S.V., Ehlmann, J.L., Davoudi, A., Chapman, P.L., 2010. Multiple-input boost converter to minimize power losses due to partial shading in photovoltaic modules. IEEE Energy Convers Congress and Exposition (ECCE) 2633–2636.

Dugan, R.C., McGranaghan, M.F., Santoso, S., Beaty, H.W., 2012. Electrical Power System Quality. 3rd edition. The McGraw Hill Companies, United States of America.

El-Nashar, A.M., 1994. Effect of dust accumulation on the performance of evacuated tube collectors. Sol. Energy 53, 105–115.

Emodi, N.V., Chaiechi, T., Beg, A.B.M. Rabiul Alam, 2019. The impact of climate variability and change on the energy system: a systematic scoping review. Sci. Total Environ. 676, 545–563.

Erdiwansyah, R. Mamat, Sani, M.S.M., Sudhakar, K., 2019. Renewable energy in southeast Asia: policies and recommendations. Sci. Total Environ. 670, 1095–1102.

Farhoodnea, M., Mohamed, A., Shareef, H., Zayandehroodi, H., 2013. Power Quality Analysis of Grid-connected Photovoltaic systems in Distribution Networks. Prz Elektrotech, pp. 208–213.

Farsadi, M., Shahrak, A.G., Tabrizi, S.D., 2013. DVR with fuzzy logic controller and photovoltaic for improving the operation of windfarm. Proceedings of 8th International Conference on Electrical and Electronics Engineering. Bursa, pp. 191–195.

Fathy, A., Abd Elaziz, M., Sayed, E.T., Olabi, A.G., Rezk, H., 2019. Optimal parameter identification of triple-junction photovoltaic panel based on enhanced moth search algorithm. Energy 188, 116025.

Gao, T., Cao, J., Xu, Y., Zhang, H., Yu, P., Yao, S., 2013. From power quality to power experience. Proceedings of fourth international conference on networking and distributed computing, LosAngelos, USA 116–120.

Garvison, P., Warfield, D.B., 2005. Photovoltaic Module Mounting Unit and System.

Gerritt, L., 2009. How PV grid-tie inverters can zap utility power factor. Renew. Energy 1, 14–16.

Ghritlahre, H.K., Prasad, R.K., 2018. Application of ANN technique to predict the performance of solar collector systems – a review. Renew. Sust. Energ. Rev. 84, 75–88.

Golovanov, N., Roscia, M., Lazaroiu, G.C., 2013. Power quality assessment in small scale renewable energy sources supplying distribution systems energies. Energies. 6, 634–645.

González, P., Romero-Cadaval, E., González, E., Guerrero, M., 2011. Impact of grid connected photovoltaic system in the power quality of a distribution network. Proceedings of the Second IFIPWG5.5/SOCONET Doctoral Conference on Computing Electrical and Industrial Systems, (DoCEIS) 466–473.

Gross, M.A., Martin, S.O., Pearsall, N.M., 1997. Estimation of output enhancement of a partially shaded BIPV array by the use of AC modules. IEEE In Photovoltaic Specialists Conference. 26, 1381–1384.

Halawachs, M., Neumaier, L., Vollert, N., Maul, L., Dimitriadis, S., Voronko, Y., Eder, G.C., Omazic, A., Muhleisen, W., Hirschl, Ch., Schwark, M., Berger, K.A., Ebner, R., 2019. Statistical evaluation of PV system performance and failure data among different climate zones. Renew. Energy 139, 1040–1060.

Hammad, B., Al-Abed, M., Al-Ghandoor, A., Al-Sardeah, A., Al-Bashir, A., 2018. Modeling and analysis of dust and temperature effects on photovoltaic systems' performance and optimal cleaning frequency: Jordan case study. Renew. Sust. Energ. Rev. 82, 2218–2234.

Hao, H., Yonghai, X., 2014a. Control strategy of PV inverter under unbalanced grid voltage sag. Proceedings of the IEEE energy conversion congress and exposition (ECCE), Pittsburgh 1029–1034.

Hao, H., Yonghai, X., 2014b. Control strategy of PV inverter under unbalanced grid voltage sag. Proceedings of the IEEE energy conversion congress and exposition (ECCE), Pittsburgh 1029–1034.

Hernandez-Callejo, L., Gallardo-Saavedra, S., Alonso-Gomez, V., 2019. A review of photovoltaic systems: design, operation and maintenance. Sol. Energy 188, 426–440.

Hernandez-Perez, J.G., Carrillo, J.G., Bassam, A., Flota-Banuelos, M., Patino-Lopez, L.D., 2020. A new passive PV heatsink design to reduce efficiency losses: a computational and experimental evaluation. Renew. Energy 147, 1209–1220.

Higashiyama, Y., Yanase, S., Sugimoto, T., 1998. Behavior of water droplets located on a hydrophobic insulating plate under DC field. Proceedings of the Conference Record of 1998 IEEE Industry Applications Conference. Thirty-Third IAS Annual Meeting (Cat. No.98CH36242).

Howlader, A.M., Sadoyama, S., Roose, L.R., Sepasi, S., 2018. Distributed voltage regulation using Volt-Var controls of a smart PV inverter in a smart grid: an experimental study. Renew. Energy 127, 145–157.

Huang, H., Yonghai, X., Lin, Y., 2014. Control scheme of PV inverter under unbalanced grid voltage. National Harbor 1–5.

Jain, A., Bollinger, J.A., Truskett, T.M., 2014. Inverse methods for material design. AICHE J. 60, 2732–2740.

Jamil, W.J., Abdul Rahman, H., Shaari, S., Salam, Z., 2017. Performance degradation of photovoltaic power system: review on mitigation methods. Renewable Sustainable Energy 876–891.

Ju, F., Fu, X., 2011. Research on impact of dust on solar photovoltaic (PV) performance. International Conference on Electrical and Control Engineering (ICECE), Yichang, China, pp. 3601–3606.

Kabir, Md.A., Mahbub, U., 2011. Synchronous detection and digital control of shunt active power filter in power quality improvement. Proceedings of IEEE power and energy conference, Illinois, Champaign 1–5.

Kamenopoulos, S.N., Tsoutsos, T., 2015. Assessment of the safe operation and maintenance of photovoltaic systems. Energy 93, 1633–1638.

Kamran, F., Habelter, T.G., 1998. Combined deadbeat control of a series-parallel converter combination used as universal power filter. Proceedings of the IEEE power electronic specialist conference (PESC). IEEE Trans. Power Electron. 13, 160–168.

Karanki, S.B., Mishra, M.K., Kumar, B.K., 2010. Particle swarm optimization-based feedback controller for unified power quality conditioner. IEEE Transactions Power Delivery 25, 2814–2824.

Karatepe, E., Hiyama, T., Boztepe, M., Colak, M., 2008. Voltage based power compensation system for photovoltaic generation system under partially shaded insolation conditions. Energy Conversion Management 49, 2307–2316.

Kharrazi, A., Sreeram, Y., Mishra, Y., 2020. Assessment techniques of the impact of grid-tied rooftop photovoltaic generation on the power quality of low voltage distribution network – a review. Renew. Sust. Energ. Rev. 120 (1–10).

Kimber, A., 2007. The effect of soiling on photovoltaic systems located in arid climates. Proceedings of the 22nd European PV Solar Energy Conference. Milan, Italy, WIP, Germany.

Koutroulis, A.G., 2019. Dryland changes under different levels of global warming. Sci. Total Environ. 655, 482–511.

Kumar, K.S.R., Sastry, S.V.A.R., 2011. Application of PI, fuzzy logic and ANN in improvement of power quality using UPQC. Proceedings of the international conference on sustainable energy and intelligent system, Chennai 316–319.

Kumar, R., Sinha, A.K., 2012. Unified power quality conditioner controller for enhancement of power system voltage stability using state vector modulation. Proceedings of the annual IEEE India conference, Kochi 891–896.

Kumar, R.A., Kumar, G.S., Kumar, B.K., Mishra, M.K., 2009. Compensation of voltage sags and harmonics with phase jumps through DVR with minimum VA rating using particle swarm optimization. Proceedings of the world congress on nature biologically inspired computing, Coimbatore 1361–1366.

Kumar, G.S., Kumar, B.K., Mishra, M.K., 2011a. Mitigation of voltage sags with phase jumps by UPQC with PSO-BASED ANFIS. IEEE Transaction on Power Delivery 2761–2773.
Kumar, G.S., Kumar, B.K., Mishra, M.K., 2011b. Power quality improvement by UPQC with minimum real power injection. Proceedings of 14th European Conference Power Electronics and Applications, Birmingham, pp. 1–10.
Kumarasamy, K., Raghavan, R., 2012. Particle swarm optimization algorithm for voltage stability improvement using multiple STATCOM. Proceedings of the International conference on emerging trends in electrical engineering and energy management, Chennai 235–242.
Lamnatou, Chr., Notton, G., Chemisana, D., Cristofari, C., 2020. Storage systems for building-integrated photovoltaic (BIPV) and building-integrated photovoltaic/thermal (BIPVT) installations: environmental profile and other aspects. Sci. Total Environ. 699 (2–5).
Lamont, L.A., El Chaar, L., 2011. Enhancement of a stand-alone photovoltaic system's performance: reduction of soft and hard shading. Renew. Energy 36, 1306–1310.
Lee, K., Koizumi, H., Kurokawa, K., 2006a. Voltage sag/swell controller by means of D-UPFC in the distribution system. Proceedings of the Conference Record of the 2006 IEEE 4th World Conference on Photovoltaic Energy Conversion, Waikoloa, pp. 24–35.
Lee, K., Koizumi, H., Kurokawa, K., 2006b. Voltage control of D-UPFC between a clustered PV system and distribution system. Proceedings of 37th IEEE Power Electronics Specialists' Conference, Jeju, pp. 1–5.
Lee, J., Wang, W., Harrou, F., Sun, Y., 2020. Reliable solar irradiance prediction using ensemble learning-based models: a comparative study. Energy Convers. Manag. 208 (1–2).
Lidula, N.W.A., Rajapakse, A.D., 2014. Voltage balancing and synchronization of micro grids with highly unbalanced loads. Renew. Sust. Energ. Rev. 31, 907–920.
Liu, C.H., Hsu, Y.Y., 2010. Design of a self-tuning PI controller for a STATCOM using particle swarm optimization. IEEE Trans. Ind. Electron. 57, 702–715.
Liu, X., Aichborn, A., Liu, L., Li, H., 2012. Coordinated control of distributed energy storage system with tap changer transformers for voltage rise mitigation under high photovoltaic penetration. IEEE Transactions Smart Grid 3, 897–906.
Liu, M., Quilumba, F.L., Lee, W.J., 2014. Dispatch scheduling for a wind farm with hybrid energy storage based on wind and LMP forecasting. Proceedings of IEEE Industry Applications Society Annual Meeting, Vancouver, pp. 1–8.
Livera, A., Theristis, M., Makrides, G., Georghiou, G.E., 2019. Recent advances in failure diagnosis techniques based on performance data analysis for grid-connected photovoltaic systems. Renew. Energy 133, 126–143.
Mahmoud, M., 2006. Transient analysis of a PV power generator charging a capacitor for measurement of the I–V characteristics. Renew. Energy 31, 2198–2206.
Mahmoud, M., Ramadan, M., Olabi, A.G., Pullen, K., Naher, S., 2020. A Review of Mechanical Energy Storage Systems Combined With Wind and Solar Applications Energy Conversion and Management. vol. 210 p. 112670 Article.
Marcos, J., Marroyo, L., Lorenzo, E., Garcia, M., 2012. Smoothing of PV power fluctuations by geographical dispersion. Program Photovoltaic Resource Application 226–237.
Marion, B., Schaefer, R., Caine, H., Sanchez, G., 2013. Measured and modeled photovoltaic system energy losses from snow for Colorado and Wisconsin locations. Sol. Energy 97, 112–121.
Masuda, S., Matsumoto, Y., 1973. Contact-Type Electric Curtain for Electro-Dynamical Control of Charged Dust Particles. 2nd International Conference on Static Electricity. No. 72. (March). Frankfurt, Germany, pp. 1370–1409.
Masuda, S., Fujibayashi, K., Ishida, K., Inaba, H., 1972. Confinement and transportation of charged aerosol clouds via electric curtain. Electrical Engineering Japan 92, 43–52.
Mathnani, A.O., Shareef, H., Mohamed, A., Ali, M.A.M., Hannan, M.A., 2010. Power quality improvement using DVR with two fast vector control. Proceedings of 4th International Power Engineering and Optimization Conference. IEEE, Malaysia, pp. 376–381.
Mazumder, M.K., Sharma, R., Biris, A.S., Zhang, J., Calle, C., Zahn, M., 2007. Self-cleaning transparent dust shields for protecting solar panels and other devices. Part Scientific Technologies 25, 5–20.
Mazumder, M., Horenstein, M.N., Stark, J.W., Girouard, P., Sumner, R., Henderson, B., Sadder, O., Hidetaka, I., Biris, A.S., Sharma, R., 2013. Characterization of electrodynamic screen performance for dust removal from solar panels and solar hydrogen generators. IEEE Transactions Industrial Applications 49, 1793–1800.
Meenal, R., Selvakumar, A.I., 2018. Assessment of SVM, empirical and ANN based solar radiation prediction models with most influencing input parameters. Renew. Energy 121, 324–343.
Mekonnen, M.M., Gerbens-Leenes, P.W., Hoekstra, A.Y., 2016. Future electricity: the challenge of reducing both carbon and water footprint. Sci. Total Environ. 569-570, 1282–1288.
Mohamed, A.O., Hasan, A., 2012. Effect of dust accumulation on performance of photovoltaic solar modules in Sahara environment. Journal of Basic and Applied Scientific Research 11030–11036.
Mohamed, M.A., Diab, A.A.Z., Rezk, H., 2019. Partial shading mitigation of PV systems via different meta-heuristic techniques. Renew. Energy 1159–1175.
Mohammadi, Y., Moradi, M.H., Leborgne, R.C., 2017. Locating the source of voltage sags: full review, introduction of generalized methods and numerical simulations. Renew. Sust. Energ. Rev. 77, 821–844.
Moretti, L., Polimeni, S., Meraldi, L., Raboni, P., Leva, S., Manzolini, G., 2019. Assessing the impact of a two-layer predictive dispatch algorithm on design and operation of off-grid hybrid micro grids. Renew. Energy 143, 1439–1453.
Munoz-Ceron, E., Lomas, J.C., Aguilera, J., de la Casa, J., 2018. Influence of operation and maintenance expenditures in the feasibility of photovoltaic projects: the case of a tracking PV plant in Spain. Energy Policy 121, 506–518.
Murtaza, A., Chiaberge, M., Spertino, F., Boero, D., De Giuseppe, M., 2014. A maximum power point tracking technique based on bypass diode mechanism for PV arrays under partial shading. Energy Build 73, 13–25.
Nayshevsky, I., Xu, Q.F., Lyons, A.M., 2018. Hydrophobic-hydrophilic surfaces exhibiting dropwise condensation for anti-soiling applications. IEEE 45th Photovoltaic Specialists Conference (PVSC).
Nguyen, D., Lehman, B., 2008. A reconfigurable solar photovoltaic array under shadow conditions. IEEE In Applied Power Electron Conference and Exposition APEC. 23, 980–986.
Noro, Y., Naoi, S., Toba, K., Kimura, M., Minegishi, T., Shimuzu, M., Aoki, S., Okuda, Y., 2012. Power fluctuation suppression system for large scale PV. Proceedings of IEEE PES Transmission and Distribution Conference and Exposition (TD), Orlando, pp. 1–6.
Obi, M., Bass, R., 2016. Trends and challenges of grid-connected photovoltaic systems – a review. Renew. Sust. Energ. Rev. 58, 1082–1094.
Olabi, A.G., Mahmoud, M., Soudan, B., Wilberforce, T., Ramadan, M., 2020. Geothermal based hybrid energy systems, toward eco-friendly energy approaches. Renew. Energy 147, 2003–2012.
Pan, A., Tian, Y., Zhao, H., Yang, X., Jin, J., 2012. Power Quality Analysis of PV System of Summer and Winter CIRED 2012 Workshop Integration of Renewables into the Distribution Grid: Lisbon. pp. 1–4.
Pansakul, C., Hongesombut, K., 2014. Analysis of voltage unbalance due to rooftop PV in low voltage residential distribution system. Proceedings of the international electrical engineering congress, Chonbuti 1–4.
Park, S.H., Kim, T.S., Park, J.S., Moon, G.W., Yoon, M.J., 2009. A new buck-boost type battery equalizer. IEEE In Applied Power Electron Conference and Exposition, APEC. 24, 1246–1250.
Parrott, B., Zanini, P.C., Shehri, A., Kotsovos, K., Gereige, I., 2018. Automated, robotic dry-cleaning of solar panels in Thuwal, Saudi Arabia using a silicone rubber brush. Sol. Energy 171, 526–533.
Pawluk, R.E., Chen, Y., She, Y., 2019. Photovoltaic electricity generation loss due to snow – a literature review on influence factors, estimation and mitigation. Renew. Sust. Energ. Rev. 107, 171–182.
Pazikadin, A.R., Rifai, D., Ali, K., Malik, M.Z., Abdella, A.N., Faraj, M.A., 2020. Solar irradiance measurement instrumentation and power solar generation forecasting based on artificial neural networks (ANN): a review of five years research trend. Sci. Total Environ. 715 (7–10).
Peters, L., Madlener, R., 2017. Economic evaluation of maintenance strategies for ground-mounted solar photovoltaic plants. Appl. Energy 199, 264–280.
Polo, F.A.O., Bermejo, J.F., Fernandez, J.F.G., Marquez, A.C., 2015. Failure mode prediction and energy forecasting of PV plants to assist dynamic maintenance tasks by ANN based models. Renew. Energy 81, 227–238.
Poshtkouhi, S., Trescases, O., 2011. Multi-input single-inductor DC-DC converter for MPPT in parallel-connected photovoltaic applications. IEEE In Applied Power Electron Conference and Exposition (APEC) 26, 41–47.
Pragallapati, N., Sharma, P., Agarwal, V., 2013. A new voltage equalization based distributed maximum power point extraction from a PV source operating under partially shaded conditions. IEEE In Photovoltaic Specialists Conference (PVSC) 39, 2921–2926.
Pyo, G.C., Kang, H.W., Moon, S.I., 2008. A new operation method for grid-connected PV system considering voltage regulation in distribution system. IEEE Power and Energy Society General Meeting – Conversion and Delivery of Electrical Energy in the 21st Century, Pittsburgh, pp. 1–7.
Raj, P.A., Kumar, S.S., Raja, J., Sudhakaran, M., Palanivelu, T.G., 2008. Particle swarm optimization based energy optimized dynamic voltage restorer. Proceedings of the Joint international conference on power system technology and IEEE power india conference, NewDelhi 1–6.
Ramasamy, M., Thangavel, S., 2012. Photovoltaic based dynamic voltage restorer with energy conservation capability using fuzzy logic controller. Proceedings of the international conference on emerging trends in science, engineering and technology, Tiruchirappalli 485–492.
Rendroyoko, I., Rusli, M., 2013. Development of power quality control procedures and standards to control the connection of non-linear loads in electrical systems. Proceedings of 2nd International Conference on Electricity Distribution, Stockholm, pp. 1–6.
Rezk, H., AL-Oran, M., Gomaa, M.R., Tolba, M.A., Fathy, A., Abdelkareem, M.A., Olabi, A.G., Hashema, A., El-Sayed, M., 2019. A novel statistical performance evaluation of most modern optimization-based global MPPT techniques for partially shaded PV system. Renewable and Sustainable Energy Reviews 115 (Article: 109372).
Ross, M.M.D., 1995. Snow and ice accumulation on photovoltaic arrays: an assessment of the TN conseil passive melting technology. Golden Colorado. United States: Energy Diversification Research Laboratory. CANMET, Natural Resources Canada.
Ross, M.M.D., Usher, E.P., 1996. Modelled and observed operation of a passive melting technology for photovoltaic arrays. Proceedings of the 7th International Workshop on Atmospheric Icing of Structures, pp. 245–250.
Sabo, A., Abdul-Wahab, N.I., Radzi, M.A.M., Mailah, N.F., 2013. A modified artificial neural network (ANN) algorithm to control shunt active power filter (SAPF) for current harmonic reduction. Proceedings of IEEE conference on clean energy and technology, Langkawi 348–352.
Sahay, A., Sethi, V.K., Tiwari, A.C., Pandey, M., 2015. A review of solar photovoltaic panel cooling systems with special reference to ground coupled central panel cooling system (GC-CPCS). Renew. Sust. Energ. Rev. 42, 306–312.
Sahebi, A., Samet, H., Ghanbari, T., 2017. Evaluation of power transformer inrush currents and internal faults discrimination methods in presence of fault current limiter. Renew. Sust. Energ. Rev. 68, 102–112.
Santhakumari, M., Sagar, N., 2019. A review of the environmental factors degrading the performance of silicon wafer-based photovoltaic modules: failure detection methods and essential mitigation techniques. Renewable and Sustainable Energy 110, 83–100.
Senjyu, T., Datta, M., Yona, A., Sekine, H., Funabashi, T., 2007. A new method for smoothing output power fluctuations of PV system connected to small power utility. Proceedings of 7th International Conference on Power Electronics, Daegu, pp. 829–834.

Shang, Y., Wu, A., 2011. TS-fuzzy-controlled shunt active-power filter for power quality improvement. Proceedings of the international conference on electrical and control engineering, Yichang 1869–1872.
Sharma, P., Peter, P.K., Agarwal, V., 2012. Exact maximum power point tracking of partially shaded PV strings based on current equalization concept. IEEE In Photovoltaic Specialists Conference (PVSC) 38, 1411–1416.
Sharma, P., Hoff, B., Meena, R., 2014. ANN based reactive power control of an autonomous wind-diesel hybrid power plant using PMIG and SG. Power and energy systems, towards sustainable energy, Bangalore 1–6.
Shen, C.L., Wang, J.Y., 2006. A 3phase 3wire Half Bridge Single Stage Grid Connected PV Power Inverter with Direct Source Current Shaping Algorithm to Improve Power Factor. Proceedings of IEEE Region 10 Conference. TENCON, Hong Kong, pp. 1–4.
Shen, H., Wan, J., Yuan, C., Liu, Y., Li, G., 2009a. Harmonic signal detection algorithm in parallel of UPQC studies based on PSO-fuzzy. Proceedings of the Asia Pacific power and energy engineering conference, Wuhan 1–4.
Shen, H., Wan, J., Liu, Y., Yuan, C., Li, G., 2009b. UPQC signal detection algorithm studies based on PSO-fuzzy. Proceedings of 4th IEEE Conference on Industrial Electronics and Applications, Xi'an, pp. 2236–2240.
Shivanshankar, S., Mekhilef, S., Mokhlis, H., Karimi, M., 2016. Mitigating methods of power fluctuation of photovoltaic (PV) sources – a review. Renew. Sust. Energ. Rev. 59, 1170–1184.
Shou, T., Wang, H., Zhu, T., Zhu, L., Wang, Q., Lou, X., Wang, J., Zhou, N., 2013. Harmonic current suppression for three phase PV generation system under unbalanced grid voltage. Proceedings of the Asia-Pacific power and energy engineering conference (APPEEC), Kowloon 1–6.
Shrivastava, S., Khan, A., Mahor, A., 2014. Transformer inrush current and related challenges. International Journal of Emerging Technology and Advanced Engineering. 4, 450–452.
Stewart, E., Aukai, T.P., MacPherson, S.D.J., Quach, B.P., Nakafuj, D., Davis, R., 2012. Realistic Irradiance-based Voltage Flicker Analysis of PV Applied to Hawaii Distribution Feeders. Proceedings of IEEE Power and Energy Society General Meeting, SanDiego, pp. 1–7.
Sumathi, Bansilal, S., 2009a. Artificial neural network application for control of STATCOM in power systems for both voltage control mode and reactive power mode. Proceedings of 3rd International Conference on Power Systems, Kharagpur, pp. 1–4.
Sumathi, Bansilal, S., 2009b. Artificial neural network application for control of STATCOM in power systems for both voltage control mode and reactive power mode. Proceedings of 3rd International Conference on Power Systems, Kharagpur, pp. 1–4.
Syed, I.M., Raahemifar, K., 2016. Predictive energy management and control system for PV system connected to power electric grid with periodic load shedding. Sol. Energy 136, 278–287.
Takehara, N., Manabe, N., Kaisha, C.K., 2000. Photovoltaic Power Generating System (US09/258,210).
Taljan, G., Gubina, A.F., 2009. Energy-based system well-being analysis for small systems with intermittent renewable energy sources. Renew. Energy 34, 2651–2661.
Tejwani, R., Solanki, C.S., 2010. 360° sun tracking with automated cleaning system for solar PV modules. Photovoltaic Specialists Conference (PVSC), 35th IEEE.
Tseng, H.T., Chen, J.F., 2012. Voltage compensation type inrush current limiter for reducing power transformer inrush current. IET Electric Power Application 6, 101–110.
Uctug, F.G., Azapagic, A., 2018. Environmental impacts of small-scale hybrid energy systems: coupling solar photovoltaics and lithium-ion batteries. Sci. Total Environ. 643, 1579–1589.
Varma, R.K., Siavashi, E.M., Das, B., Sharma, V., 2012. Real-time digital simulation of a PV solar system as STATCOM (PV-STATCOM) for voltage regulation and power factor correction. Proceedings of IEEE Electrical Power and Energy Conference, London, pp. 157–163.
R.K. Varma, B. Das, I. Axente, T. Vanderheide. Optimal 24-hr utilization of a PV solar system as STATCOM (PV-STATCOM) in a distribution network. Proceedings of IEEE Power and Energy Society General Meeting, SanDiego. pp. 1–8.
Vegunta, S.C., Twomey, P., Randles, D., 2013. Impact of PV and load penetration on LV network voltages and unbalance and potential solutions. Proceedings of 22nd International Conference on Electricity Distribution, Stockholm, pp. 1–4.
Villarini, M., Cesarotti, V., Alfonsi, L., Introna, V., 2017. Optimization of photovoltaic maintenance plan by means of a FMEA approach based on real data. Energy Convers. Manag. 152, 1–12.
Visa, I., Burduhos, B., Neagoe, M., Moldovan, M., Duta, A., 2016. Comparative analysis of the infield response of five types of photovoltaic modules. Renew. Energy 95, 178–190.
Wilberforce, T., El Hassan, Z., Durrant, A., Thompson, J., Soudan, B., Olabi, A.G., 2019a. Overview of ocean power technology. Energy 175, 165–181.
Wilberforce, T., Baroutaji, A., Soudan, B., Al-Alami, A.H., Olabi, A.G., 2019b. Outlook of carbon capture technology and challenges. Sci. Total Environ. 657, 56–72.
Wilberforce, T., Baroutaji, A., El Hassan, Z., Thompson, J., Soudan, B., Olabi, A.G., 2019c. Prospects and challenges of concentrated solar photovoltaics and enhanced geothermal energy technologies. Sci. Total Environ. 659, 851–861.
Wu, S.Y., Chen, C., Xiao, L., 2018. Heat transfer characteristics and performance evaluation of water-cooled PV/T system with cooling channel above PV panel. Renew. Energy 125, 936–946.
Xiao-ping, Y., Yang-ru, Z., Yan, W., 2006. A novel control method for DSTATCOM using artificial neural network. Proceedings of 5th International Power Electronics and Motion Control Conference, Shanghai, pp. 1–4.
Zhang, G., Patuwo, B.E., Hu, M.Y., 1998. Forecasting with artificial neural networks: the state of the art. Int. J. Forecast. 14, 35–62.
Zhang, M.D., Xie, J., Gan, D.Q., 2012. Optimal ESS operation strategy in distribution system with wind power. Proceedings of the International Conference on Sustainable Power Generation and Supply, Hangzhou, pp. 1–6.
Zhi, L., Gonghuan, F., Yaning, C., Weili, D., Yerbolat, M., 2020. Agricultural water demands in Central Asia under 1.5 °C and 2.0 °C global warming. Agric. Water Manag. 231 (2–4).

Annexe 1.2

Revue des défauts des systèmes photovoltaïques et de leurs méthodes de détection correspondantes

A critical review of PV systems' faults with the relevant detection methods

Khaled Osmani[1], Ahmad Haddad[2,3], Thierry Lemenand[1], Bruno Castanier[1], Mohammad Alkhedher [4], and Mohamad Ramadan[2,3, *]

[1]LARIS EA 7315, Polytech Angers, UNIV Angers, France

[2]School of Engineering, International University of Beirut BIU, Beirut, Lebanon

[3]School of Engineering, Lebanese International University LIU, Bekaa, Lebanon

[4]Mechanical Engineering Department, Abu Dhabi University, United Arab Emirates

mohamad.ramadan@liu.edu.lb

Abstract. PhotoVoltaic (PV) systems are often subjected to operational faults which negatively affect their performance. Corresponding to different types and natures, such faults prevent the PV systems from achieving their nominal power output and attaining the required level of energy production. Regarding the operational optimization of PV systems, this paper aims primarily at surveying and categorizing different types of PV faults, classified as electrical, internal, and external, where each is thoroughly investigated: internal faults occur at the PV cellular level, and can either be short circuit, open circuit, bridging, or bypass diode faults. External faults on the other side are mainly classified as temporary (i.e., clouds shading, snowstorms, etc.) or permanent (e.g., glass breakage, frame defects, etc.) mismatch faults. Lastly, electrical faults involve common circuitry problems, such as short circuits (e.g., line to ground, line to line, etc.), power processing units' faults (e.g., inverter faults), and arc faults. As for the detection methods, six major fault detection methods are investigated for the AC side of the PV system with twenty-nine total AC based fault detection methods. On the other hand, eleven major fault detection methods are surveyed for the DC side of PV systems with seventy-three total DC based fault detection methods. The investigated methods are critically analyzed, and compared relevantly to each other, within the mutual sub-sets. The resulting tabulated comparative data assessments for PV faults (i.e., cause-effect relationships, impact on the PV system performance), as well as for faults detection methods (i.e., priority for application, etc.) compose a rich background for related PV systems' performance security fields, where a nexus future work is also suggested.

Keywords: PV faults, fault detection, detection methods, fault type, PV troubleshooting

Nomenclature

ABCO	Artificial Bee Colony Optimization	IR	Infra-Red
AC	Alternating Current	I-V	Current-Voltage
AFCI	Arc Fault Circuit Interrupter	KELM	Kernel Extreme Learning Machine
AITs	Artificial Intelligence Techniques	kNN	k-Nearest Neighbors
ANFIS	Adaptive Neuro-Fuzzy Inference System	LAPART-FD	LAterally Primed Adaptive Resonance Theory - Fault Detection
ANFIS-SM	Adaptive Neuro-Fuzzy Inference System-Sugeno Model	LCD	Liquid Crystal Display
ANN	Artificial Neural Network	LF	Low Frequency
ANOVA	ANalysis Of VAriance	L-G	Line-to-Ground
APRE	Absolute Performance Ratio Error	LIT	Lock In Thermography
AR	Auto Regressive	L-L	Line-to-Line
BPNN	Back Propagation Neural Network	LOF	Local Outlier Factor
CART	Classification And Regression Time	MBDM	Model Based Difference Measurement
CBs	Circuit Breakers	MEWMA	Modified Exponentially Weighted Moving Average
CCC	Current Carrying Conductor	ML	Machine Learning
CDIT	Climatic Data Independent Technique	MPPT	Maximum Power Point Tracker
CM	Common Mode	MRAS	Model Reference Adaptive System
CMM	Comparison between Measured and Modeled	MSDP	Multistate Data Processing
CR	Capacitive Region	MWPT	Modified Wavelet Packet Transform
DC	Direct Current	NDZ	Non Detection Zones
DC-DCFI	DC-DC converters Fault Identification	NOCT	Normal Operating Cell Temperature
DE	Deviation Error	OC/SC	Open/Short-Circuited
DFI	Degradation Fault Identification	OCPD	Over Current Protection Device
DLL	Dourly Lower Limit	Onm/offm	Online/offline model
D-S	Dampster-Shefer	OPC	Object linking and embedding for Process Control
DSP	Digital Signal Processor	PCC	Points of Common Coupling
DT	Decision Tree	PIC	Peripheral Interface Controller
DUL	Dourly Upper Limit	PLA	Power Loss Analysis
ECM	Earth Capacitance Measurement	PNN	Probabilistic Neural Network
EGC	Earth Ground Conductors	PPs	Peak Points
EI	Electroluminescence Imaging	PPU	Power Processing Unit

ELM	Extreme Learning Machine	PS/CS	Partial/Complete Shading
EM	Electrical Measurement	PSMFD	Partially Shaded Modules Fault Detector
EMI	Electro Magnetic Interference	PV	PhotoVoltaic
EMR	Electro Magnetic Resonance	P-V	Power-Voltage
ERV	Estimating Randomness in the Voltage signal	PVA	PhotoVoltaic Array
EWMA	Experimentally Weighted Moving Average	PVLOF	LOF based on PV string current
FBI/RBI	Forward Bias Imaging/Reverse Bias Imaging	Q-f	Reactive power-frequency
FDC	Fault Detection and Classification	RCDs	Residual Current Devices
FDD	Fault Detection and Diagnosis	RCM	Reliability Centered Maintenance
FDTI	Fault Detection Techniques for three-phase Inverters	RDM	Real-time Difference Measurement
FF	Fill Factor	RF	Random Forest
FFT	Fast Fourier Transform	RPS	Residential Photovoltaic System
FIRBPS	Finite Impulse Response Band Pass Filter	SCADA	Supervisory Control And Data Acquisition
FPGA	Field Programmable Gate Array	SFA	Subsection Fluctuation Analysis
FRSA	FRequency Spectrum Analysis	SFS	Sandia Frequency Shift
FSA	Frequency Spectrum Analysis	SHLFNNs	Single Hidden Layer Feedforward Neural Networks
FTD	Flash Test Driver	SM	Sugeno Model
GCPVS	Grid Connected PhotoVoltaic System	SMS	Slip Mode frequency Shift
GFDI	Ground Fault Detection and Interruption fuse	SPM	Signal Processing Methods
GISTEL	GIsement Solaire par TELedetection	SR	Shunt Resistance
GUI	Graphical User Interface	SSTDR	Spread Spectrum Time Domain Reflectometry
HET	Heat Exchange and Temperature	STCs	Standard Test Conditions
HF	High Frequency	STFT	Short Time Fourier Transform
HIGF	High Impedance Ground Fault	TDR	Time Domain Reflectrometery
HMI	Human Machine Interface	THD	Total Harmonic Distortion
HV/LV	High/Low Voltage	TSKFR	Takagie-Sugeno Kahn Fuzzy Rule
ICCD	Intensified Charge Coupled Device	TSKFRBS	Takagie-Sugeno Kahn Fuzzy Rule Based System

ICR	Inductance Capacitance Resistance	UIM	Ultrasonic Inspection Method
IDTs	Islanding Detection Techniques	WOEWMA	Wavelet Optimized Exponentially Weighted Moving Average
IGBT	Insulated Gate Bipolar Transistor	WPT	Wavelet Packet Transform
IMR	Insulation Monitoring Relay	WT	Wavelet Transforms
In/ThI	Infrared/Thermal Imaging		

I. Introduction

Population growth and modern life commitments have led to an excessive consumption of fossil fuels. This in turn caused higher emissions of greenhouse gases, leaving future generations in danger [1]. The need for alternative power resources peaked as a result, due to the increase in electricity demand on one hand, and to the underproductive performances of existing generating units (diesel and gas-based engines) on the other hand. [2]. Consequently, a worldwide increase in renewable energy studies, usages, and optimization has emerged [3].

Among different types of renewable energy supplies (wind, hydro, etc.) PhotoVoltaic (PV) systems are considered the cleanest and safest technology [4]. This is due to the fact that such systems do not involve any mechanically moving parts (i.e., actuators, shafts, etc.) and work silently. Thus, such systems in particular have achieved a global interest and a massive popularity as a promising solution for offsetting the underproductive problem of existing power resources and are considered to have a potential contribution to the future electricity mix [5].

Unfortunately, many obstacles exist and impede PV systems from functioning properly. Environmental factors, such as dust, temperature, snowfall, and humidity reduce the PV systems' capability in power production and cause various failure modes in the PV panels [6]. For instance, the dust accumulated over the PV modules' surfaces during the span of eight weeks under the desertic environment in Saharan environment, decreases the PV maximum power output by 8.41% as compared to the same PV system without dust accumulation [7]. In other words, the stated environmental leftovers, aside than possibly damaging the PV panels, could create consequent problems for PV systems, preventing their power production sustainability: as another example, a power drop of 9.99% and an average power reduction of 2.93% is witnessed for an uncleaned PV system (from dust and dirt) in a Mediterranean climate based region of installation, when compared to the same cleaned PV system [8].

Other than environmental implications, PV systems are seen to encounter inner faults for example, ranging from basic electrical faults (open-short/circuit) to Power Processing Units (PPU) faults such as Maximum Power Point Tracker (MPPT), and inverter malfunction [9-10]. Consequently, such faults disturb the produced power waveforms and could eventually cause drastic interruptions on the users' end.

Regardless of the fault's types, their recurrence on PV systems, leaves bad impacts such as harmonics distortion, voltage unbalancing, current leakages, deviated waveforms, smaller consumable power quantities than expected and service interruption by partial/total blackouts. For a healthy state of PV systems, with an extended lifecycle and an acceptable performance, abundant research is taking place to mitigate fault residues on such systems: for example, in order to reduce the partial shading conditions consequences' (i.e., caused by the movements of clouds), which partially shade the sunrays for up to 75% of the total PV array space, different PV array reconfiguration techniques can be adapted [11]. From a thermal optimization point of view, the decreased PV cell efficiency by 0.45% for each temperature rise of 1°C (due to high temperature environmental conditions) can be compensated by the application of phase change material, that are used to cool down the PV panels' operating temperature [12]. Adjusting the PV tilt angle from another side is recorded elevating the PV produced power by up to 50.36% for different regions of PV systems installations, thus compensating the lost solar irradiance due to positioning and self-shading [13].

As intended to optimize the performance and extend the longevity of PV systems with minimum fault occurrences, it is imperative to know first the difference types of possible PV faults, then accordingly acknowledge the corresponding PV fault detection methods (that are to be applied in real PV applications). For this purpose, ample research took place in order to quantify different PV faults, with the relevant detection techniques: for instance, the work in the reference [290] has categorized all possible PV faults into five main categories, as mismatch, ground, line-to-line, arc, and other types of faults. As for the fault detection methods in the same study, the presented survey classified all fault detection techniques as either visual/thermal or electrical based methods, without considering the model-based measurements methods, for example. From another side, the similarly related work in [291], takes into consideration only the failure modes in the PV inverter's power modules. Moreover, the authors in [292] have only reviewed the PV fault detection methods through the application of artificial neural networks, such that the review in [293] has grouped the PV faults either as optical degradation, electrical mismatch, or other electrical and hardware faults, having only imaging technologies based resultant fault detection methods. From a different approach, the work in [294] focused mainly on the outer physical degradation of the PV encapsulant, while the most reviewed fault detection methods emphasized on the visual inspection. Accordingly, and for the purpose of a broader PV faults classification with better expanded faults detection methods, throughout this paper, different faults will be first categorized as either internal, external, or electrical. The consequences of each will be clearly presented in tabulated data, in order to record the affected parts of a PV system. Moreover, two major fault detection techniques classifications will take place, as either detection at the AC side of the PV system or at the DC side. For each part, there exist various sets of methods, and sometimes sub-methods. Each technique will be uniquely identified, investigated, and compared to others within the same set. A critical comparison between detection schemes and targeted faults will be presented. The rest of this paper consists as follows: Section 2 presents a general overview for a PV system with a fault detection scheme, Section 3 classifies and investigate all possible PV faults, where in Section 4 the fault detection methods are expanded and analyzed. Section 5 presents a discussion based on the results of the different reviewed faults and fault detection methods with a future work recommendation, where finally in Section 6 conclusions are derived.

II. Overview of a typical PV system with a fault detection structure

As an additive to a typical off/on-grid PV system, a fault detector is an extra equipment, with the ability to guide the PV system's operators about the existence of a fault, its type and location within the PV system. Consisting of different sensors, processing units, actuators, transducers, and different protective relays and circuit breakers, such a system can be installed at any node indicated by the dashed polylines in Figure 1. On its output level, the fault detector contains a set of alarms, buzzers, and different forms of Graphical User Interface (GUI) to acknowledge the workers in the field about any fault incident. The full process of fault detection takes place within two distinct steps: monitoring and diagnosis.

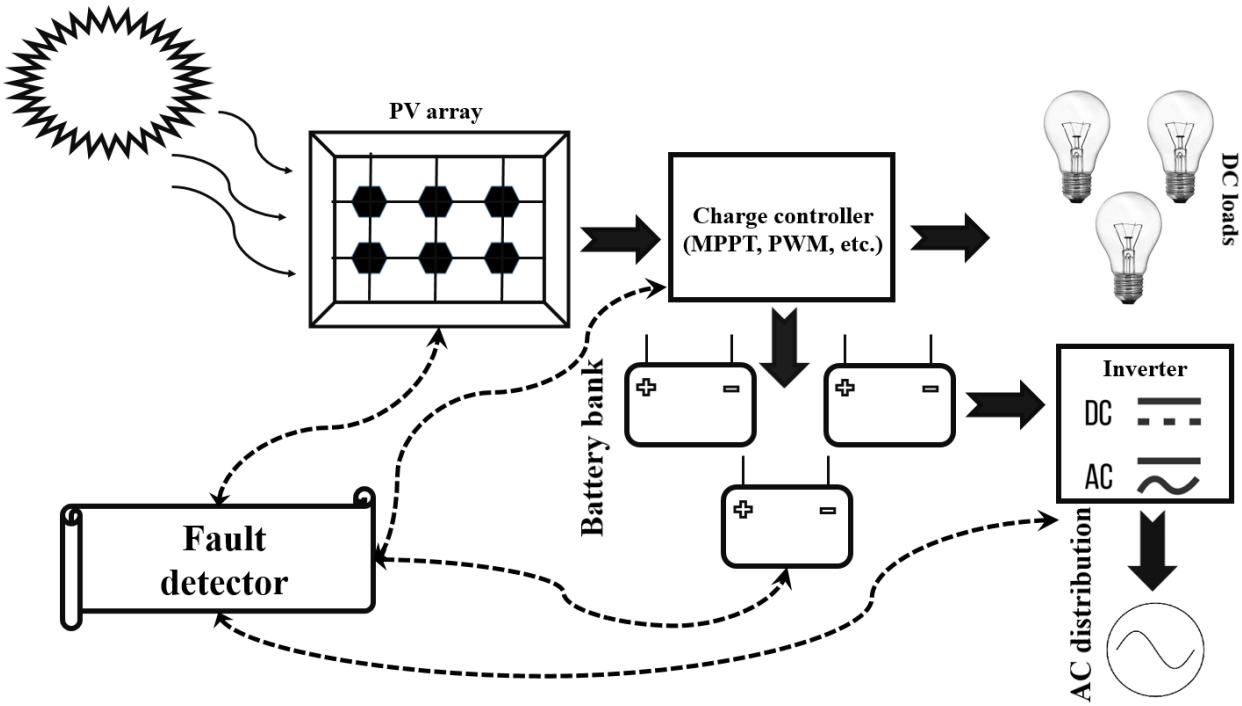

Figure 1. Fault detector allocation in an off-grid PV system

2.1.Monitoring

To evaluate the PV system's performance, the monitoring system collects and analyzes a set of different parameters (voltage, current, power, etc.) [14]. This process is crucially important, as a prior step before detecting the fault, with a continuous tracking on the electrical power generation. For data acquisition of various attributes, sensors are the first input to the monitoring system. The data are then transferred through signal processing units, where at final stage, they would be stored for further investigations [14-15]. Figure 2 reveals the cascaded monitoring process for a PV system, embedded within a fault detection scheme.

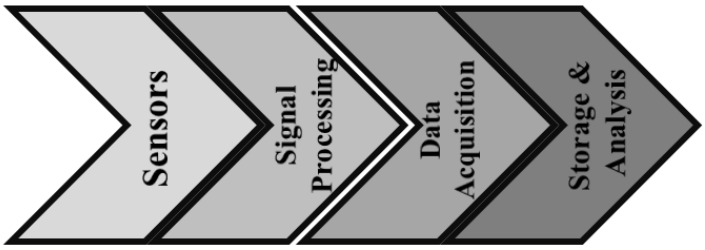

Figure 2. Block diagram of PV monitoring system

2.2.Diagnosis

The results of the monitoring system (in form of acquainted information) are injected to the fault diagnosis scheme as primal data. When compared with reference values, the inputted data can either declare a fault or not [16-17]. Its source of acquisition (whether from the DC or the AC side of the PV system) guides the fault detector about how to investigate upon it. Figure 3 reveals the different steps of PV fault diagnosis in a cascaded form, beginning by information analysis to alarm launching.

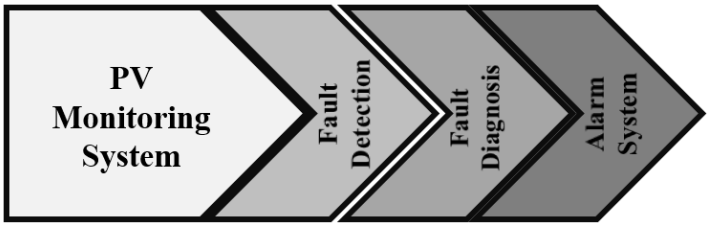

Figure 3. Block diagram of PV fault diagnosis scheme

III. Different PV system's faults

Due to their outdoor nature, PV systems encounter diverse faults, causing a massive decrease in the PV energy outcome, potential reduction, and most importantly the inability to satisfy various load demands. The fault classification can be mainly classified into three categories as follows:

- Internal
- External
- Electrical

The internal PV faults take place inside a PV module (underneath the protective glass), on the level of PV cells, and strings. External faults localize outside the PV module protective glass and are perceived as either temporary mismatch or permanent mismatch faults. Electrical faults on the other hand, refer to the perturbations of physical entities (i.e., voltage, current, power, etc.) in terms of quantities and waveforms. Figure 4 entitles the triggers for each set of PV faults.

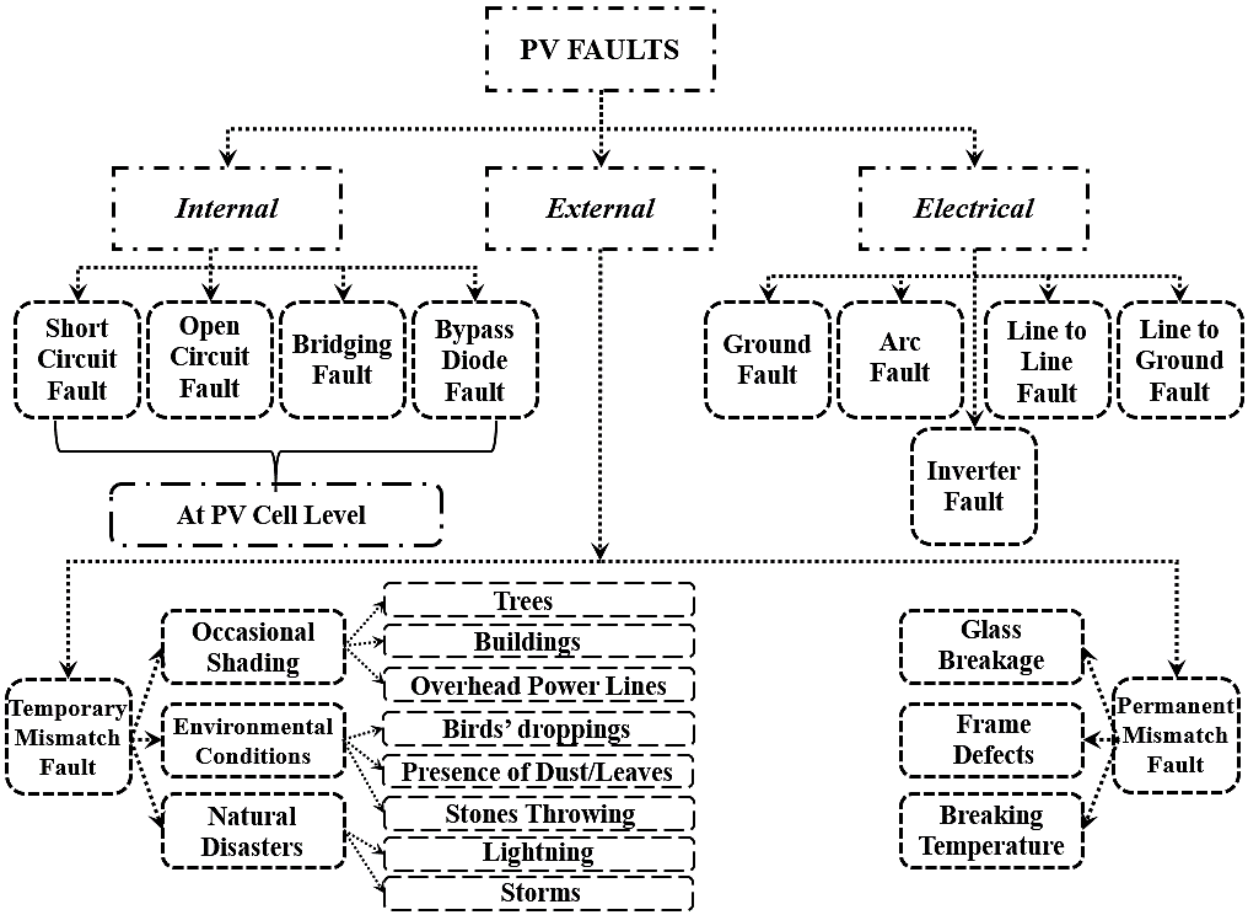

Figure 4. Summarizing block diagram representation of PV fault types and characterization

3.1. Internal PV faults

Internal PV faults take place inside the PV module itself. Their initial cause is the manufacturer's defects, poor quality of fabrication, damages due to inconvenient packaging, and

improper methods of wiring. Regardless of their root cause, internal faults are classified according to the effects they impose on a PV system, as either open/short-circuit, bridging and bypass diode faults. Table 1 groups the causes to consequences of different internal faults.

Table 1. Cause-effect relationship of different PV internal faults

Internal faults			
Types	Causes	Results	Consequences
Short circuit	Manufacturer's defects	Low impedance/bolted path between internal power rails	Inability to deliver power to DC load or to the power conditioning unit
Bridging	Manufacturer's defects/improper wiring	Creation of impedance faulted linking path	Null power output
Bypass diode	Manufacturer's defects/improper wiring	Bypass diode cannot be forward biased	Inability to mitigate hotspots events
Open circuit	Manufacturer's defects	Absence of link between power paths	Inability to deliver power to DC load or to the power conditioning unit

3.1.1. Short circuit fault

Improper connections (low impedance and sometimes bolted pathways) between the solar cells, or defects from initial manufacturing circuitry [18-19], lead to a short circuit on the module or on the bypass diode [20].

3.1.2. Bridging fault

Improper connection (high impedance and sometimes complete open circuit) between PV modules [21], causes such types of faults where the output tends to become null.

3.1.3. Inverted bypass diode fault/bypass diode fault

Faulty wiring made by the operator [22-23], resulting in bypass diode fault, reflects as abnormal voltage conditions on the output level.

3.1.4. Open circuit with/without bypass diode fault

An open circuit fault, reflected as maximum cell's output voltage, with no ability of current to flow (hence no power output) is often caused by broken cells, damaged connections between them, loose connections, and defected power cables due to aging. The excessive plugging/unplugging routines, yield to faulty open-circuited terminals mainly at junction boxes [23].

3.2. External PV faults

Due to the fact that PV systems need to be installed outdoors to receive direct solar radiation, they often interact with undesired environmental conditions. The weather for instance can fluctuate, ranging from hot (elevated ambient temperature) to cold (rain/snow accumulation). Accordingly, PV modules would rarely operate under the Standard Test Conditions (STCs), thus their nameplate power is never attained.

Moreover, natural disasters like intense lightning can burn PV panels. On the other hand, dust/leave accumulation results in partial shading/impedance mismatch. From another part, PV panels fall from height as well as abuse by stones throwing inflects a permanent damage (glass/frames breakage). Table 2 encapsulates the causes-to-consequences relation for different external faults.

Table 2. Cause-effect relationship of different PV external faults

External faults			
Types	Causes	Results	Consequences
Temporary mismatch fault	• Occasional shading • Environmental conditions • Natural disasters	Non homogeneous power production across PV surfaces and creation of hotspots	Low power production compared to standard values and risk of burning
Permanent mismatch fault	Equipment permanent damage	Null power production	Complete blackout

3.2.1. Temporary mismatch fault

When the irradiation varies, the PV system performance (i.e., in terms of power production) changes accordingly (e.g., low irradiation reflects lower power production, and vice-versa). Some regions of the PV system (i.e., zones of PV arrays) produce larger power quantities than others [24]. Even though, faulty PV regions due to temporary mismatch do not produce power as rated values or even close. This can be referred to a non-homogeneous PV output due to non-homogeneous shading [25-27].

This heterogeneity in power production which is caused by physical light barriers, such as trees, buildings, and overhead power lines, results in detrimental effects over the PV panels [28]. Depending on the climate conditions and geographical locations, snow can cover some panels of the PV system as well. From another part, biological conditions such as bird's droppings, and

leaves accumulation on the surfaces of the PV modules can also lead to partial shading conditions [29-30]. Dust and dirt from another side, can cover the PV arrays' surfaces, and sometimes sudden natural disasters as lightning and storms can also leave a PV system with a non-uniform irradiance distribution [31-32].

3.2.2. Permanent mismatch fault

Unlike partial mismatch fault conditions, a permanent mismatch cannot be reversed. It can be a result of bad soldering, degradation of modules, glass breakage, delamination, discoloration, defects in frame, cell breakage and micro-cracks.

These triggers have a wide range of causes, of which some are manifested by bad operations such as manual soldering of the cell at a breaking temperature, or poor packaging during transportation. Permanent mismatch faults can also be triggered during manufacturing processes, like inconvenient wafer slicing, cell production stringing and other embedded operations that eventually lead to cell cracks.

Such causes are referred to manufacturing defects. Environmental conditions can lead also to permanent mismatch faults. For instance, heavy snow loads in cold regions can break PV modules. Also, frequent temperature changes can wear out the cell interconnections [33-34]. Figure 5 reveals the physical delamination (indicated by red arrows) of the front encapsulation of a PV module, caused by external faults.

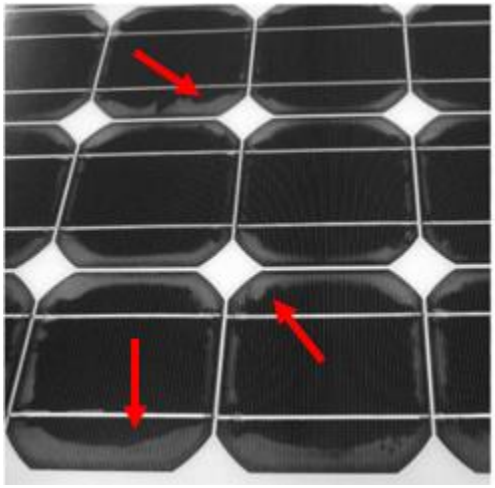

Figure 5. Delamination of the PV module's front encapsulation [51]

3.3. Electrical PV faults

Aside than the physical PV faults occurrence, driven by physical barriers (dust/snow/leaves accumulation) and internal manufacturing defects, PV systems also encounter intrinsic electrical faults. According to the PV system's electrical network distribution, electrical faults can occur as ground, line to line, line to ground, arc, and power conditioning units' faults. Table 3 summarizes the causes-to-consequences relation for different electrical faults.

Table 3. Cause-effect relationship of different electrical faults

Electrical faults			
Types	Causes	Results	Consequences
Ground fault	Improper wiring of ground/earth connections	Existence of a large feedback current in the ground	Risk of operator electrocution and voltage instability
Line to line fault	Existence of a faulty connection link between different power rails	Power loss on the output level (three-phase system)	Risk of equipment burning and wire damage
Line to ground fault	Short circuit between current carrying conductor and the ground	Power loss on the output level (single-phase system)	Risk of equipment burning and wire damage
Arc fault	Loose connections/loss of conductivity	Creation of arc current/sparks	Risk of burning/fire
Power conditioning units fault	Malfunctioning of PPUs due to internal fault	Inability to efficiently charge the battery bank and existence of disturbances on the output AC waveform	Lowering the PV system efficiency and decreasing its standby time

3.3.1. Ground faults

The PV system includes parts that aren't designed nor supposed to be exposed to any current, like the metallic part of a PV array, the enclosures and other equipment [35-36]. These non-current carrying labels are protected using Earth Ground Conductors (EGC) in order to eliminate any possibility for an electric shock which the operators might examine when working in field, such that the sudden electric current find its way to the ground instead of being trapped inside the equipment [37-38]. When the ground contains active currents, the analysis turns to the case of a fault [39-40]. This type can be decomposed into two sub-parts:

- Upper ground fault: an unintentional low impedance or bolted path between the Current Carrying Conductors (CCC) of the last two modules in a PV string and the ground [41].
- Lower ground fault: an unintentional low impedance or bolted path between the CCC of the second and third modules in a PV string and the ground with large feedback current [41].

3.3.2. Line to line faults

The cascading of PV modules creates PV strings, which in turn are wired in parallel to create an array, in order to deliver higher power outputs. The Line to Line (L-L) faults denote erroneous connection between different strings/arrays potentials. By taking an example of a PV string, a L-L cross string fault exists between one string and another. Such faults are very hard to detect and cause severe losses in the overall output before being distinguished [42]. It can be summarized by unintentional connections between two or more nodes of the PV strings/arrays [43-44] and is considered as a top reason for inducing open-circuit faults (due to electrical switchgear tripping mechanisms).

3.3.3. Line to ground faults

When there is a physical connection between the current carrying conductor and the ground, whether directly or through a low impedance path, a Line to Ground (L-G) fault takes place [45]. A L-G fault is extremely hazardous, as it causes a massive electron flow, in a timely manner, across a faulty small path when compared to the total system's wiring, what would generally result in fire hazards.

3.3.4. Arc faults

The conductors used in electrical circuits, often confront corrosion and lack of conductivity due to their chemical reaction with the surrounding environments, and damages resulting of excessive usage. This phenomenon creates an arc current high enough to ignite the surrounding material [46-47]. Such faults are chaotic, random, and might be active for a dangerous amount of time before being detected or resolved. When there is an insulation breakdown, parallel arc faults are ignited. Series arc faults on the other hand, take place when the connections get loose, the connection cables are damaged, or in the event of hotspots [47]. The resultant spontaneous faulty current is often too small to be detected by safety equipment such as Residual Current Devices (RCDs) [48-49].

3.3.5. Power processing units' faults

The Power Processing Units (PPUs) are equipment that work on shaping the resultant signals waveforms or modifying their quantities. For PV systems, two main PPUs exist:

- Inverter: used to transform the original DC power to consumable AC power (since most industrial/residential loads operate on AC).
- Maximum Power Point Tracker (MPPT): included in charge controllers, to extract the maximum available power under partial shading conditions.

These elements in turn, can interact with faulty scenarios, prohibiting them from achieving their destined functions. The PPUs faults are summarized in Table 4.

Table 4. Cause-effect relationship of different PPUs faults

Power conditioning units faults			
Types	Causes	Results	Consequences
Inverter failure	• High temperature for prolonged amount of operating time • Excessive operations	Failure in switching mechanisms	• Disturbance in the resulting AC waveform • Load malfunctioning
MPPT failure	• Sensors malfunctioning • Algorithm bugs	• Delayed time for battery bank charging • Battery bank over-charging	• Shortening the life cycle of the batteries • Batteries permanent damage • Lowering the standby time under low irradiance conditions

a) Inverter failure

Inverters can have their efficiency reduced, with faulty operational behavior, when exposed for example to continuous high temperatures for a prolonged amount of time, and when experiencing an excessive mechanical stress on their power switches. For instance, when Insulated Gate Bipolar Transistor (IGBT) fails as a solid-state switch in conduction for example, the algorithm conducting other IGBTs resets and the entire power electronics switching circuit fails, hence the inverter fault [50].

b) MPPT fault

The MPPT works in collaboration with sensors and charge controllers, to be able to identify the Peak Points (PPs) in the characteristic Current-Voltage (I-V) curve of the PV module and calibrate the charging process of the batteries [52]. When sensors get disconnected/defected, and the MPPT's algorithm experiences an erroneous workflow, the MPPT zone within the PV system gets faulty [53].

When the MPPT fails, it often leads to a damage on the level of the battery bank: the charge controller abnormally selects reference voltage levels. This yields to over-charging where the bank is exposed to higher than standards voltage inputs, for prolonged amounts of time. Under-charging from another part also takes place when the MPPT fails: consequently, the electrodes are damaged inside the batteries due to low input voltage feeding [54]. Since each type of the faults affects the

performance of the PV system in a specific severity, Table 5 in accordance provides a comparative assessment between the different reviewed PV faults.

Table 5: Comparison of different types of PV fault consequences

Reason						Possibility of occurrence	Fault severity			
Manufacturer defects		Circuitry					Complete blackout	Partial blackout	Non homogeneous power production	Impurities in output signals
Low quality	Bad design	L-L	L-G	Arc	MPPT					
✓	✓					Depending on the level of manufacturer fabrication and expertise in labor		✓	✓	
						High	✓	✓	✓	
		✓	✓	✓	✓	Medium to high (depending on circuitry design and safety precautions)	✓	✓		✓

Type	Reason								
	Environmental			Weather			Physical		
	Leaves	Dust	Soil	Snow	Storms	Lightning	Stones	Bird dropping	Shading
	.								
Internal PV faults									
External PV faults	✓	✓	✓	✓	✓	✓	✓	✓	✓
Electrical PV faults									

IV. Fault Detection Methods

The approaches to detect faults in PV systems are classified to work in either the DC or the AC regions of the PV system [246]. The entirety of techniques can be summed up as in Figure 6, where six major techniques are listed on the AC side and eleven techniques on the DC side of the PV system.

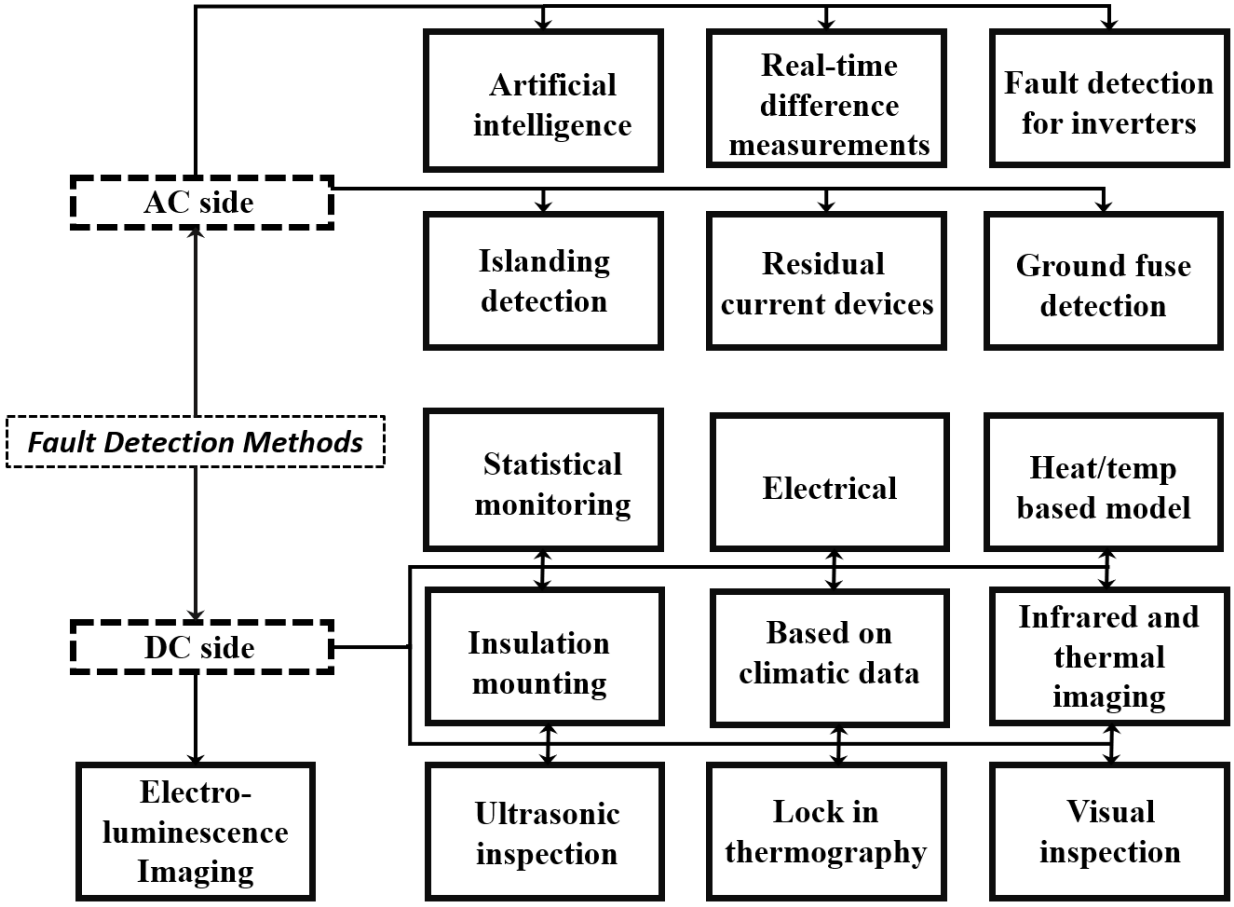

Figure 6. Complete PV fault detection methods at AC/DC sides of the PV system

4.1. Detection at AC Side

This set of fault detection techniques covers up the zone in PV systems where all AC quantities exist. The red dashed area in Figure 7 enfolds the referred region for detection. The output of the inverter is fed and distributed into the AC grid, by means of Main Distribution Boards (MDBs). Any power failure in the red dashed zone, needs AC relevant protective equipment, such as Circuit Breakers (CBs), Residual Current Devices (RCDs), and others protective switchgear. To be able to send tripping/switching commands to the AC safety switchgear, specific algorithms are required, which rely under Artificial Intelligence Techniques (AITs), Real-time Difference Measurement models (RDM), Fault Detection Techniques for three-phase Inverters (FDTI) and Islanding Detection Techniques (IDTs).

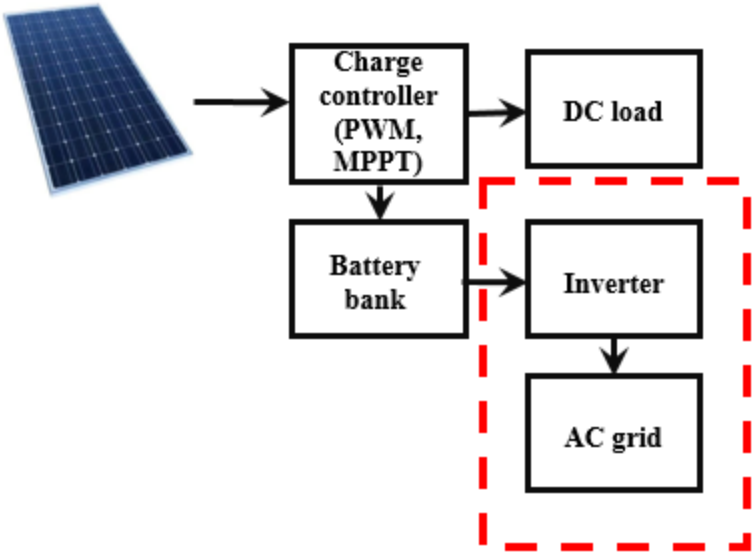

Figure 7. AC detection zone

4.1.1 Artificial Intelligence Techniques (AIT)

Artificial intelligence used in PV systems' fault detection aims to transfer a certain knowledge into computers and make decisions accordingly. Based on computational algorithms, this set of techniques allows computers to learn using human-inspired reasoning. When applied, their implementation results in a faster and more accurate decision making [278]. The following methods represent some examples about AIT for PV fault detection:

a) PIC based extension matter
b) SCADA for Ground Connected Photo Voltaic Systems GCPVS/NUI algorithm based on SCADA inputs
c) Automated diagnostic signal software tool based on comparison of APRE
d) SA-RBF Kernel Extreme Learning Machine KELM
e) Predictive Maintenance and Anomaly detection
f) ANN model detecting operational and environmental faults

a) PIC based extension matter

b) A Peripheral Interface Controller (PIC) is implemented for fault diagnosis. By combination of PIC micro-controller, coded in assembly, with a ZigBee wireless sensor, a remote access is granted on monitoring the occurring faults in the AC parts of PV systems. The power generation of a PV system is firstly analyzed under normal/defected operations. Then by relying on extension theory, a matter-element model (problem solving tactic based on human thinking) is constructed from the initial data collections. This PV fault diagnosis only requires small amounts of data to construct the matter-element model, while providing a high fault detection accuracy [55]. Recent evolution in computerized and embedded systems has led to more powerful micro-controllers than the one used in [55], where in terms of computational

speed, a programmable logic controller is better used to detect the PV faults.*SCADA for Ground Connected Photo Voltaic Systems GCPVS/NUI algorithm based on SCADA inputs*

This algorithm based model feeds input signals to a Supervisory Control And Data Acquisition (SCADA) system to categorize and identify different electrical faults such as string fault, short circuit fault and line to line fault for Grid Connected PhotoVoltaic System (GCPVS). The needed attributes are ambient temperature, irradiation (measured via a pyranometer), and power ratio [56]. The synoptic scheme for this model is shown in Figure 8.

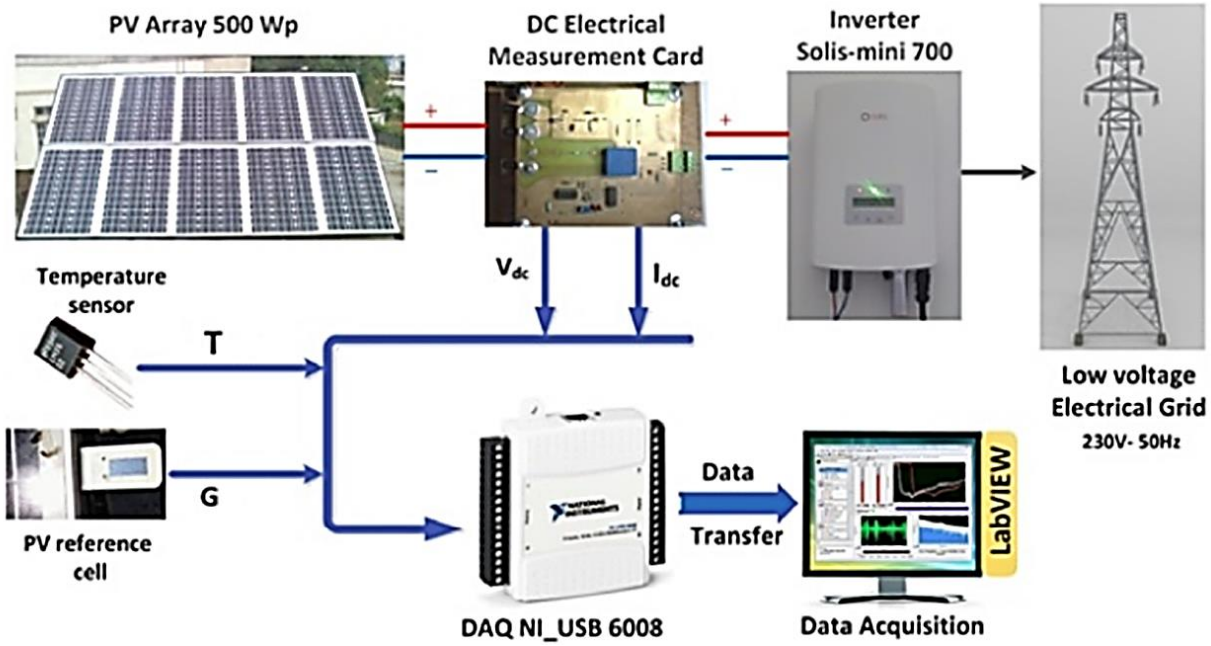

Figure 8. Synoptic scheme for GCPVS [56]

The fault detection model has achieved a high detection accuracy of 99.80%, but this value may fluctuate due to the major system's dependability on meteorological/electrical sensors, which might give false readings due to false/inaccurate calibration [56]. Similarly, a fault detector for PV plants using a web server relying on Non-Uniformity Index (NUI) can also act as a remote server based on SCADA inputs. The NUI algorithm which allows remote supervision and fault detection has been examined and with such model, the faulty PV zones within a PV farm can be identified according to their produced energy levels either as acceptable or not. With the usage of special temperature/irradiance models, this system seems to have diminished the required number of sensors for PV fault identification [164].

c) Automated diagnostic signal software tool based on comparison of APRE

Using certain electrical quantities (i.e., voltage, current) as reference values, an automated diagnostic signal tool to detect non-recoverable faults at AC sides of a PV system can be established [57]. The failure identification process takes place with the two indicators R_C (DC current) and R_V (DC voltage) as shown in Eq. (1) and Eq. (2) respectively.

$$R_C = \frac{I_{pv\_sim}}{I_{pv\_meas}} \quad (1)$$

$$R_V = \frac{V_{pv\_sim}}{V_{pv\_meas}} \quad (2)$$

with I_{pv_sim} , I_{pv_meas} denoting the simulated and measured array's DC current respectively and V_{pv_sim} , V_{pv_meas} the simulated and measured array's DC voltage respectively. A set of comparison takes place for the two equations where each translates into a specific fault situation. The entire procedure is based on Absolute Performance Ratio Error ((APRE) which represents a performance metric for machine learning), where the fault is located inside a GCPV plant by monitoring the DC and AC power ratio. The model has resulted in a good detection accuracy with a great potential for future adaptation as a widespread tool for GCPV [57].

d) SA-RBF Kernel Extreme Learning Machine (KELM)

This intelligent fault diagnostic tool uses simulated annealing algorithm based on radial function Kernel Extreme Learning Machine (KELM). The method begins by establishing the fault model and optimizes it using the Simulated Annealing (SA) algorithm [62]. The adopted KELM function Ω_{ELM} is shown in Eq. (3).

$$\Omega_{ELM} = \exp\left(-\frac{|x - x_i|^2}{2\sigma^2}\right) \quad (3)$$

where σ is the radial width parameter and x, x_i composers of target value vector. The SA algorithm optimizes the parameters for radial basis function KELM, where the resultant algorithm can quickly and effectively identify short circuit, aging and PV faults related to partial shading [62].

e) Predictive maintenance and anomaly detection

Working upon historical data, specifically using the actual two-year measurements of irradiance, temperature, and other climatic conditions as historical data to be fed into a predictive algorithm database, a learning-approach-based model can detect any reduced output fault by comparing both measured and predicted values of AC power [63]. Two normal operation limits were classified as Dourly Lower Limit (DLL) and Dourly Upper Limit (DUL), are expressed in Eq. (4) and Eq. (5) respectively.

$$DLL = 3\sigma_d \quad (4)$$
$$DUL = 5\sigma_d \quad (5)$$

where σ_d denotes a daily-equivalent standard deviation index. Samples which are numerically compared to the thresholds DLL and DUL represent normal/faulty operations of the PV system [63].

f) ANN model detecting operational and environmental faults

A two-layer Artificial Neural Network (ANN) based model that works as a Supervisory Control and Data Acquisition (SCADA) system, operates as a monitoring tool on PV assets as well as on their environmental conditions. This methodology can perform also economic evaluations about the current PV system's states, also on upgrading the previously designed PV systems to supply larger loads. It consists of a two-layer ANN model that states any lack of insulation, or

solar tracker blockage using a private logic decision making [66]. Figure 9 reveals the connections between the input/output layers of the algorithm, where b represents the bias, n the neuron, $W_{j,i}$ the weight of the input (j,i), and $W_{\hat{y}_d,j}$ the output weight of the ANN.

Different attributes, such as internal and ambient temperatures, radiation and time of performance are mutually linked to different nodes within the hidden layer. The probabilities of occurrence of an attribute within a specific node, are all taken into consideration. This would finally result in an estimated accumulated active energy level, to deduce the fault impact on the overall power production.

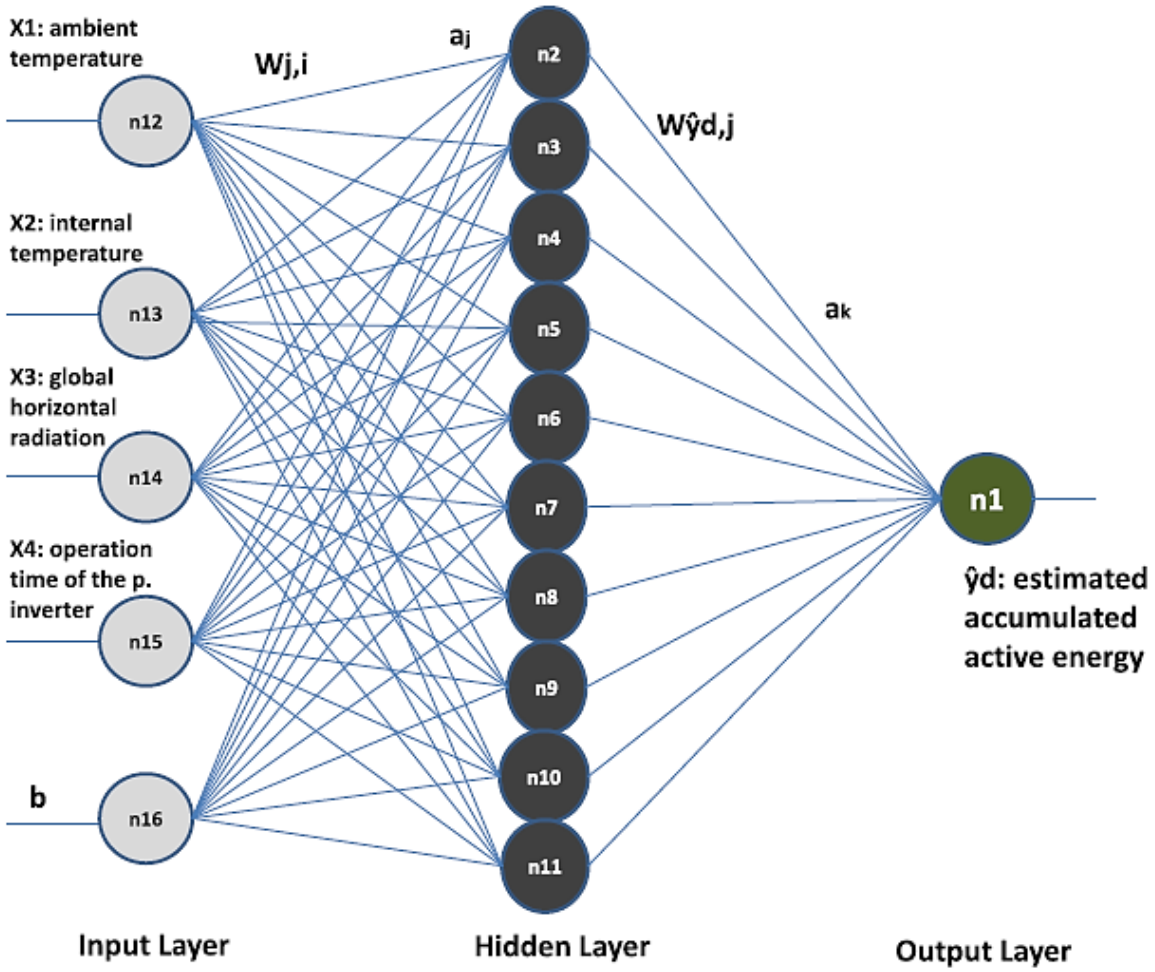

Figure 9. Multi-layer ANN back propagation [66]

4.1.2 Real-time Difference Measurement (RDM)

Real-time difference measurement systems acquire instantaneous physical samples (voltage, current, etc.), resulting from experimental/analytical measurements to dynamically provide data concerning the process of PV functioning (fault detection). This set of methods contains the following sub-methods:

a) Using AC output data
b) Using capacitance change criteria

a) Using AC output data

Using AC output data in PV system, a preliminary method consisting of three sub-methods used entirely to detect faults. The first sub-method relies on comparing both measured output values and estimated values. The second deals with present and past performance ratios and finally the last relies on comparing present and past output differences. By combining these three sub-methods, the resultant model overcomes the erroneous fault identification of other AC based PV fault methods for specific PV circuitry [68].

b) Using capacitance change criteria

Using AC parameter characterization, hot spots in PV systems can be detected by noticing the capacitance change within a single cell (that is comprised of series/parallel resistances and parallel capacitance). The measuring the AC impedance value in the range of 10-70 kHz the capacitance change is detected by monitoring first a High Frequency (HF) in the Capacitive Region (CR) and Low Frequency (LF) in DC impedance region. Such a fault detection system does not only help in identifying the formation of hotspots but can also help in the optimization of MPPT algorithms [155].

4.1.3 Fault Detection Techniques for three-phase Inverters (FDTI)

Embodying the raw source of AC power in a PV system, good monitoring and control techniques are required for inverters for a safe switch off, and an optimum overall performance of the system. Locating the fault of the inverter enables the usage of standby equipment (to get rid of blackouts) and modifications in the functional strategy [80-88]. There are two general ways to detect faults in inverters:

I. Signal-based methods
    1. By measurements of inverter's output voltages
    2. By measurements of load currents
II. Models-based methods

I. Signal-based methods

These methods require the measurements of inverter output voltages [110-116], or load currents [117-120], [173-181].

1. Measurements of inverter's output voltages

a) Mass center of the voltage pattern

To identify an open switch fault inside the inverter, an analysis of the pattern mass center derives an algorithm for that aim. First the algorithm starts by acquiring the AC voltages of the inverter and results of histograms created according to Eq. (6) [89].

$$\begin{cases} PR\ oj_{V_a(V_a)} = n_k \\ PR\ oj_{V_b(V_b)} = n_k \\ PR\ oj_{V_c(V_c)} = n_k \end{cases} \quad (6)$$

where PR represents the reference for the inverter's histogram voltage representations, V_a, V_b and V_c are the voltage magnitudes for each phase and n_k is the sample's number during one period of the signal. Successively, the left and right mass centers are calculated. From the mass center of each zone, the normalized diagnostic variables are calculated where any transistor open fault is identified by means of a Schmitt-trigger circuit. This method is characterized by its low computational requirements [89].

b) Open circuit fault identification rule for the inverter

Depending on the voltage variation of PV arrays, residual voltage errors are calculated. Basing on the amount of such errors, an open circuit fault identification rule is identified for the inverter as shown in Eq. (7).

$$R_i = [sign\ (r_i) + 1] \cdot \left(p_{min} - p_{pOi}\right) \quad (7)$$

where R_i represents the improved judgment criterion, $sign$ refers to the signum function, r_i is the voltage residual error, p_{min} the minimum output power of PV and p_{pOi} the *i*-th PV panel power. Designed for grid-connected PV systems, this method has shown reliability and flexibility, with a robustness in detecting PV faults under maximum power points variations [94].

2. Measurements of load currents

a) Current comparator method

By comparing the current between any two identical branches inside the AC distribution network, the inverter fault can be detected based on the fact that these two currents must be equal [90]. By setting a small constraint ε which corresponds to a maximum tolerance level, the difference between two nodes' currents $\Delta \mathrm{I}_{\mathrm{Nm}}$ must obey the inequality of Eq. (8).

$$\Delta \mathrm{I}_{\mathrm{Nm}} < \varepsilon \quad (8)$$

with N, m representing the currents' nodes. Therefore, when the difference between the two nodes' currents $\Delta \mathrm{I}_{\mathrm{Nm}}$ equals or surpasses ε an inverter fault is detected [90], [99].

b) State observer method

To detect an open-circuit fault for an inverter in a grid-tied PV, a mathematical model is first built for the converter. Then, a state observer is constructed with the aim to generate any occurring current residuals. The fault is detected by means of a comparison between the residual error with the setting threshold. For PV inverters open-circuit faults, this method is validated with a good feasibility [92].

c) Knowledge-based models

Based on a knowledge-model, an inverter's fault detection technique is established by using two approaches, the current vector trajectory, and the instantaneous frequency. Hence, an open transistor fault in the inverter is detected [96]. For three phase inverters, fault diagnosis is based

on the most probable defect, as a way to overcome the lack of Fourier analysis in proceeding explicit determination of the fault [97].

d) Similarity measurements based methods

When inverters interfere with failures, the semiconductor devices' based topologies become non symmetrical. Therefore, the resultant three phase current become nonsymmetrical in turn. Based on the residuals of current ordered-sequence Mannharden distance, the measuring algorithm can detect and locate the open-circuit faults [98].

e) Based on information fusion

For inverters' open-circuit fault detection, an improvement of Dempster-Shafer (D-S) evidence theory is achieved by the mixture of Back-Propagation Neural Network (BPNN) with Classification And Regression Tree (CART) algorithms. The load current signals are processed using Wavelet Transforms (WT). In other words, WT is used to extract fault characteristics (such as transistor faults in inverters). At a second order, BPNN and CART are used to diagnose the open-circuit faults. The improvement to the decision level concerning fault detection is held by means of the improved D-S [100-103].

f) Park's Vector method

The open-circuit fault as well as other defects in the power switches (IGBT, MOSFET, etc.) are detected by calculating the position of the current trajectory's midpoint. The Park's vector transformation allows the obtainment of both magnitude and phase angle of the pre-calculated three-phase average currents. An open fault exists if the magnitude of the space vector is nonzero and greater than a threshold [104-107].

II. Model-based methods

These methods require the accurate system model's design to achieve an optimum algorithm and consist of four distinct sub-methods.

a) Observer-based diagnosis scheme

As a way for detecting faults related to power switches inside an inverter, a directional residual evaluation in the frame is employed [108]. The fault detection process is held by residual vector evaluation shown in windowed norm as in Eq. (9).

$$\left|\left|r_{dq}\right|\right|_{2,t,T} = \sqrt{\int_{t-T}^{t} ||r_{dq}||^{2}\, dt} \tag{9}$$

where r_{dq} is the current residual vector and t, T are time constants. The algorithm for the inverter's fault detection used in this model is independent of the load torque, where simultaneous faults can be isolated, in a quantitative way with no need of extra measurements for voltage/current required for implementation [108], [91].

b) MRAS-based diagnosis

The open-switch inverter faults are detected by the employment of a permanent magnet synchronous motor. The model relies on reference adaptive system techniques, corresponding to normal voltage balancing/sequencing in each phase. In other words, in order to detect open circuit faults, this method takes into account the input voltages to the inverter and observes any voltage distortion at the output level. This proposed method can be well combined with the corrective maintenance schemes, such as the reconfiguration of inverter, while demanding less extra circuitry (e.g., voltage/current sensors), and low computing facility [109].

c) Multistate data processing and subsection fluctuation analysis for photovoltaic inverter

Composed of three distinct blocks: Multistate Data Processing (MSDP), Subsection Fluctuation Analysis (SFA) and Artificial Neural Network (ANN), the MSDP retains the main fault features and abducts the influence of load's change (to distinguish between this scenario and a fault). Secondly, the SFA classifies the different states of the inverter's switches. Finally, ANN combines MSDP and SFA to adapt an intelligent classification of faults [93].

d) Combination of a model-based and data processing perspective

Different fault scenarios (under model-based topology) are estimated by means of an additive model, which employs in turn sliding-mode proportional-integral observers. Then by performing a directional residual evaluation within a fixed reference frame, through data processor, faults can be detected in the inverter [95].

4.1.4 Islanding Detection Technique (IDT)

An over-current fault is noticed inside the AC region of the PV system, by means of Circuit Breakers (CBs). The CBs tripping, provided by an internal electro-mechanical mechanism, is executed to reduce any wires/equipment damaging. Islanding consists of switching off a faulty zone in the AC distribution panel, similarly to the operation of CBs. To detect islanding means to figure out where the fault has taken place, hence allowing its quick removal, therefore restoring power back to the faulty zone. The islanding detection technique possesses two different sub-techniques:

a) Central remote techniques
    1. System state monitoring
    2. Switch rate monitoring
    3. Inter-tripping
b) Local islanding techniques
    1. Passive techniques
    2. Active techniques
    3. Hybrid techniques

a) Central remote techniques

1. System state monitoring

Unintentional islanding here can be detected using parameter distribution quantity measurements such as voltage, frequency and transients in these two labels [185]. This method plays a complementary role to the SCADA and needs fewer number of state measurements [121-

123]. Machine language can be as well added to the monitoring process of the system's state by means of Decision Tree (DT) algorithms [182-184].

2. Switch rate monitoring

A tripped CB is a clear indicator about an over-current fault, yielding in islanding some zones of the PV system. Hence, a transfer trip detection technique scheme can be used to monitor all CBs that might cause the islanding of the PV inverter. The integration of a SCADA with the trip detection technique would help in the monitoring process [124-126].

3. Inter-tripping

Figured on a special communication between sensors and generating units, this method detects any open-circuits at the points of disconnection and generates a feedback signal to the sites' data monitors [127-128].

b) Local islanding techniques

1. Passive techniques

This area of research has four main categories of measurements that help revealing a local islanding fault. The first method takes into consideration the voltage and frequency fluctuations, above and under optimum values. It is considered as a primitive method in detecting unbalances, using protective relays that indicate a fault based on the power flow at Points of Common Coupling (PCC) between the utility and the inverter [129].

The second detects any voltage phase jump, where it monitors the difference between the current and the terminal voltage of the inverter to identify any surge occurrence [130].

The third category in this part is about harmonics measurements. It measures any change in the Total Harmonic Distortion (THD) at PCC, where the careful selection of the basis threshold reduces any false tripping [131]. Extra monitoring parameters can be added as THD of the current and unbalanced voltage to detect any islanding fault [132] that in turns present a harmonic impedance measuring [133] of the electric system, what results in islanding fault detection.

The last sub-part of this set of techniques operates by detecting the voltage unbalance, due to changes in the network topology and load [134], [135] that could result in islanding sub-parts of the PV systems. Such operation is achieved by continuously analyzing the output three-phase voltage at low time cycles [136].

2. Active techniques

Beginning with the impedance measurement technique, where source impedance is calculated using short circuit current and reduced supply voltage (due to islanding) [137], islanding detection zones can be identified, but not all of them, as this method have Non Detection Zones (NDZ) [138]. On the other hand, the Slip Mode frequency Shift (SMS) is considered as an active technique used to detect islanding, by taking advantage of a positive feedback carrying info about frequency, amplitude, and phase detection.

An improvement to this method (since it presents phase shift perturbation leading to measurement inaccuracy) is called improved SMS [139] where an additional phase shift is maintained that results in lower NDZ.

3. Hybrid techniques

Presenting a total of four different hybrid techniques, the first hybrid IDT bases on the voltage unbalance and THD, to identify an islanded AC zone due to CBs tripping. It can be added to a positive feedback based technique [140]. The limitation of each technique (hybrid-positive feedback) is overcome when both of the methods operate simultaneously.

A second hybrid technique is based on voltage and real power shifting where it is considered as a solution to overcome the limitations of other IDT techniques and takes advantages of individual passive and active techniques. This method uses an average rate of the real power shift in active technique and voltage change in passive one [141]. Such working methodology can lead to islanding detection even for multiple generating units.

The third method states that after the injection of an intentional voltage fluctuation by means of a high impedance load [142], a rate of change is afterwards calculated for voltage and a correlation factor, using digital signal processing, yielding eventually to islanding detection.

The last one represents a curve modeling for islanding detection, based on Sandia Frequency Shift (SFS) and reactive power versus frequency (Q-f) proposal [143]: this method reduces the NDZ by calculating the optimum SFS where the bacterial foraging algorithm is used to derive the optimal SFS gain.

4.1.5 Residual Current monitoring Devices (RCD)

Any residual between entering and leaving currents from a node inside the AC network, indicates a leakage, where the RCD's coil is sufficiently energized and tripped to stop that phenomenon. For a PV system, an RCD protects against L-L and L-G faults where it can be installed either for the entire string or one complete array [213]. The RCD sensitivity must be carefully chosen to avoid any false tripping [214].

4.1.6 Ground Fault Detection and Interruption fuse (GFDI)

In a complete circuit, the current created from the supply feeds the load and returns in the ground conductor. When there is any abnormality in this return current, the GFDI operates to immediately switch off the inverter [215],[216]. Sometimes leakage currents exist, inducting a false GFDI tripping. There are also certain environmental conditions such as relative humidity, ambient temperature, and salt mist, which negatively affect a proper operation of a GFDI fuse, causing a false tripping. Therefore, the sensitivity of the GFDI must also be properly selected [217], [218].

The classification of AITs (Artificial Intelligence Techniques) sub-methods rely on the algorithm of implementation. Whether ANN, DT, KELM or others, the back-propagation, data-mining, and decision making with the corresponding degrees of accuracy and data acquisition time is what characterize each. They all share a complex programming process in common. Different RDM based techniques aim to detect various electrical faults. Beginning with open-circuit/short-current faults, arriving at detecting failures in power conditioning units, they differentiate in their accuracy and data acquisition time.

Regardless that FTDI attributed methods might contain implemented artificial intelligence algorithms, they differentiate from AIT with their case-specified algorithms. The learning/decision algorithms are driven according to each converter datasheet. On the AC side of a PV system, the CBs are a must to neglect any form of overloading. This in turn reduces the potential of equipment damaging and cable burning. The islanding detection techniques give the possibility to figure out the faulty zone, hence restoring normal functioning at the load side (e.g., reduce any form of partial/complete blackout). The application of IDT gives the system a more reliable and consistent performance.

The RCDs and GFDI based techniques refer to fault detection methods by means of safety switchgear. From one side, RCDs reduce any possibility of current leakages, hence avoiding any risk of personnel electrocution. On the other hand, GFDI ensures that no current is present in the ground. This avoids in turn any voltage unbalancing. The safety switchgear (CBs, RCDs, GFDI) cannot be avoided in the AC side of the PV system. No fault detection at the AC side of the PV system can be set for execution without such devices (whether actively or remotely via SCADA). The electro-mechanical tripping phenomenon of these devices is the clear indicator for a fault detection.

The islanding detection technique can be mixed with RCDs and GFDI by means of Residual Current Breaker with Over-current devices (RCBOs). When RCBOs are used, any trip can be detected using islanding detection, at the same time while avoiding any personnel electrocution, voltage unbalancing and equipment (wires, loads) damaging. This would reduce the need of extra components, causing a more financially affordable PV protective system. Table 6 reveals the potential need for applying different fault detection methods and the consequences when not being applied.

Table 6. Consequences of not applying different AC fault detection techniques

Detection technique	**Necessity for application**	**Consequences when *not* applied**	**Effects**
AIT	Optional	Errors between measured and predicted electrical quantities	Reduction in system's financial competencies
RDM	Optional	Errors between measured and calculated electrical quantities	Reduction of system overall efficiency
FDTI	Medium to high	Converters internal failure	Distorted AC waveforms
IDT	Must	CBs excessive false tripping	Partial/complete blackout
RCD	Must	Presence of current leakages	Personnel electrocution
GFDI	Must	Abnormal quantities of return current	Voltage unbalancing

4.2. Detection at DC Side

With DC detection techniques, the entire DC zone within a PV system is monitored. The blue dashed area in Figure 10 entitles the corresponding region for fault detection. The received DC power from the solar module in Figure 10 is fed into the charge controller. DC loads are supplied from the charge controller, at the same time while the battery bank gets charged and monitored.

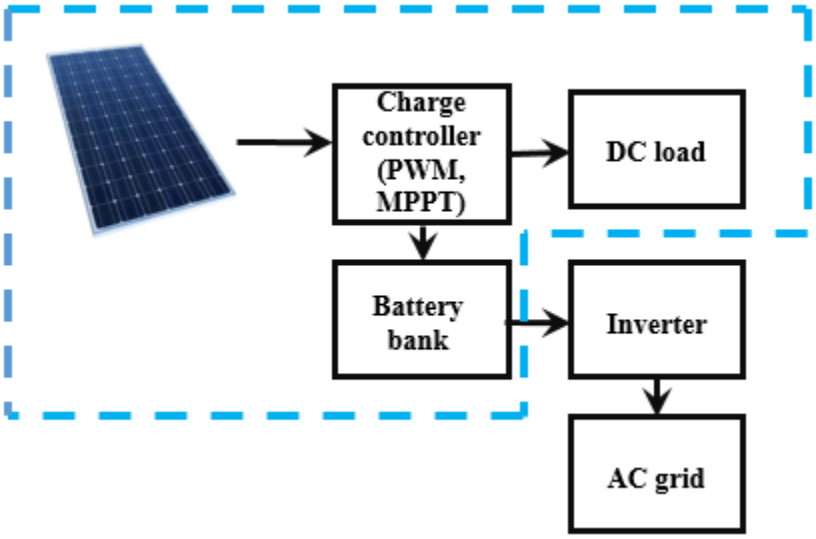

Figure 10. DC detection zone

4.2.1 Statistical monitoring method

Statistical monitoring based fault detection methods for PV systems rely on collecting PV performance data, calculate a statistic test to define the acceptance/rejection regions of the data set, then draw a final conclusion accordingly. A statistical monitoring method relying on Modified Exponentially Weighted Moving Average (MEWMA) algorithm can detect non-recoverable faults at the DC side of a PV system. The tactic starts with the one-diode model identification, to simulation of PV system, and end up with applying the algorithm [169]. Figure 11 exposes the fault detection/identification phases of MEWMA algorithm.

The procedure shown in Figure 11, indicates that the PV system is running optimally if no residuals from the compared outputs exist between the simulated version of the prototype and the real hardware itself. In case of any differences in the outputs, the MEWMA algorithm can classify the existence of a fault, as either faulty module, faulty string, or partial shading due to ageing. This strategy was tested experimentally on a GCPV showing a good capacity in PV fault detection [169].

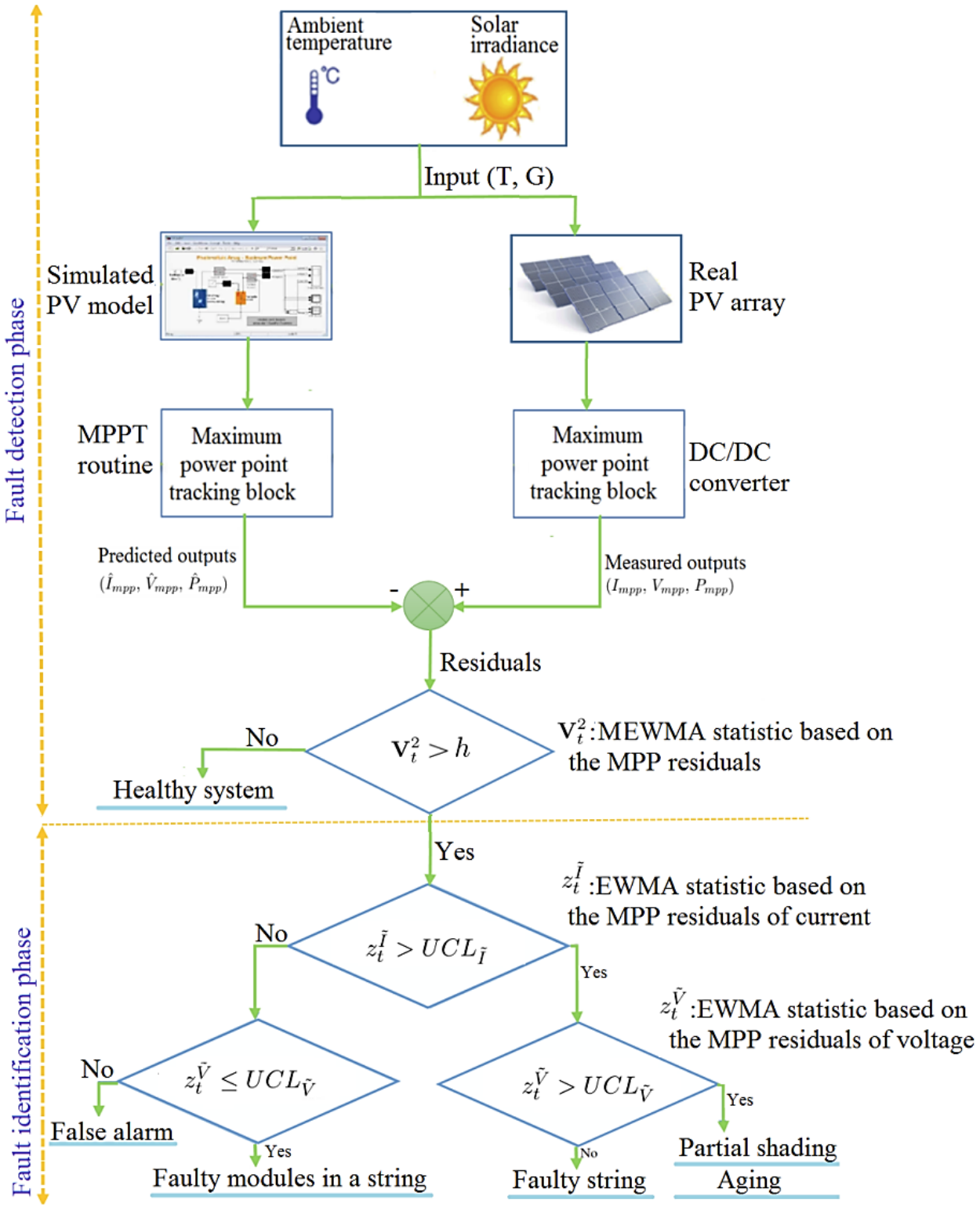

Figure 11. MEWMA flowchart [169]

4.2.2 Electrical methods

This set of methods rely on Current-Voltage (I-V) characteristics analysis, to detect a fault in the DC detection zone. It covers up the following sub-methods:

a) Model Based Difference Measurement (MBDM)
    1. DC to AC power ratio monitoring
    2. Comparison between DC voltage/current deviated error with respect to reference values
    3. Base fault diagnosis combined with Wald-test technique
    4. Comparison of simulated I-V characteristic curve with experimental data
    5. Comparison of measured values with model prediction results
    6. MPPT fault locator
    7. Shading fault detector based on Deviation Error (DE)
    8. Short circuit current detector
    9. Dynamic I-V characteristics based fault diagnosis
    10. Shading and electrical faults detector based on Bishop model
    11. Experimentally Weighted Moving Average (EWMA) control for shading effect on PV modules detection
    12. T-test statistical method for physical fault detection/algorithm for fault detection
    13. Electrical and environmental fault detection based on WOEWMA
    14. OPC monitoring
    15. Comparison between Measured and Modeled (CMM) PV system outputs
    16. Analysis of solar photovoltaic power generation
b) Spread Spectrum Time Domain Reflectometry (SSTDR)
c) Estimating Randomness in the Voltage signal (ERV)
d) Power Loss Analysis technique (PLA)
e) Electrical current-voltage I-V Measurement (EM)
f) Open/Short-Circuited modules in PV string (OC/SC)
g) High/Low Voltage fault diagnosis sections (HV/LV)
h) Partial/Complete Shading fault detector (PS/CS)
i) Online/offline model (Onm/offm)
j) Degradation Fault Identification (DFI) based on string current
k) DC-DC converters Fault Identification (DC-DCFI)

a) Model Based Difference Measurement (MBDM)

Model based difference measurement methods consist of modelling the optimum cases (theoretical) for current/voltage values (reference values). The second modelling includes the actual experimental values for the quantities being studied. The difference between these two models yields to a clear representation of the deviation error. The value of the deviated error represents in turn a clear sign of the fault's type.

1. DC to AC power ratio monitoring

By monitoring the DC to AC power ratio, the location of a fault in a Grid Connected PhotoVoltaic (GCPV) system is located. Accompanied with a developed software tool the identification of different sub-faults in the different regions of the PV system (on the level of PV

string, module, MPPT, etc.) is enabled. The failures taking place at the DC side of the system are indicated by means of capture losses L_c given in Eq. (10).

$$L_c = Y_r - Y_a \tag{10}$$

where Y_r and Y_a denote the reference yield and energy produced by PV array over a specific time period respectively. Accordingly, the calculated values of losses yield in a clear representation of the fault's type and its causals (e.g., soil, electrical interconnections, etc.) [187].

2. Comparison between DC voltage/current deviated error with respect to reference values

Relying on the comparison between the simulated and measured data of the PV system's performance a fault is detected then identified by analyzing and comparing the number of errors deviated between the DC voltage and current with respect to the evaluated thresholds of a reference fault-free system. For capture losses monitoring, the error parameter EL_c is established as shown in Eq. (11).

$$EL_c = |L_{c_{meas}} - L_{c_{sim}}| \tag{11}$$

with $L_{c_{meas}}$ and $L_{c_{sim}}$ correspond to measured and simulated power losses respectively. The different established thresholds for fault detection and diagnosis procedures the most likely occurring fault can be determined [188].

3. Base fault diagnosis combined with Wald-test technique

Targeting for Residential Photovoltaic System (RPS) fault detection, an algorithm emphasizing on active and passive parts of the PV system, is used to first diagnose the problem using a base fault diagnosis to check for any fault's alarm signal using an arbitrary data. After so, in the passive part, and in order to investigate the temporary mismatch resulting fault, Wald-test technique is statistically used. Then a proposed Flash Test Driver (FTD) device is used on the power conditioning units to increase the efficiency as well as the reliability of the RPS. The suggested flash test method can be integrated with artificial intelligence-based techniques, thus expanding its PV fault detection types, cost-effectively [189].

4. Comparison of simulated I-V characteristic curve with experimental data

Targeting the faults that might occur on the level of a PV array such as temporary mismatch and electrical faults, different intended fault scenarios were exerted on the system. The comparison between the Matlab simulated I-V characteristic curve and the generated experimental data of the same PV system, helps in identifying the nature of the fault. The categorization of different faults is generated from normal operation to bypass diode fault. Such PV fault detection technique can lead designers to an accurate prediction of possible faults [191].

5. Online comparison of measured values with model prediction results

On the level of PV panels, a fault detector is established by comparing the measured values with model prediction results. The prediction relies on the theoretically calculated PV power production resulting from solar irradiance and PV panel temperature measurements. With a low complexity and high fault detection rate, this method results in a fault detection rate greater than 90% for different irradiance intervals models [192].

6. MPPT fault locator

For shading and converter faults in PV arrays, when comparing the Maximum Power Point Tracker (MPPT) output under shading conditions with respect to the same output under normal irradiance, faults are detected (e.g., the PV power output is smaller compared to standard conditions). If the PV load is too small, the fault cannot be accurately identified, hence, a defined voltage ratio technique takes place over the normal difference method [193].

From another point of view, the modification of the MPPT algorithm is another way to detect the PV faults in the DC region. Basing the algorithm on the variation of the aspect ratio of the rectangle parametrized by the origin $(0;0)$ and the Maximum Power Point (MPP) $(V_{MPP};I_{MPP})$ within the Power-Voltage (P-V) characteristic curve, the non-recoverable faults as faulty interconnections, bridge earth, and shunt path development can be detected [262]. The MPPT algorithm can be adjusted as well to detect different physical faults on the level of PV cell, such as shading, aging, degradation, and possible hotspots, due to environmental triggers [263]. On the other hand, a faulty MPPT can negatively affect the PV system's efficiency and reliability (i.e., false decision making, inaccurate duty ratios signaling, etc.). Accordingly, in order to restore a proper MPPT operation, the standard activation must be allowed [70].

7. Shading fault detector based on Deviation Error (DE)

When partial shading occurs on the level of PV cells, the PV modules in turn overheat and bypass diodes get activated. Accordingly, the mathematical equation corresponding to the normalized error DE resulting from comparing the actual I-V curve data with reference ones can lead to error identification. By means of this method, shading faults can be online dissociated between homogeneous and non-homogeneous. In addition, the bypass diodes activation is detected with a derivative calculation between the standard error and the PV module voltage [194].

8. Short circuit current detector

The output current of a PV system is highly dependable on external climatic conditions, therefore faulty currents can be misinterpreted by PV current fluctuation (high values under high irradiance profiles, low values under cloudy days). In order to eliminate such confusion, a dynamic state estimation-based algorithm can be a solution to identify the short circuit currents especially when the series fuse is not operating due to the reduced value of the short circuit current which is limited by the blocking diode. The proposed algorithm is effective for a PV fault on the cellular level [195].

9. Dynamic current-voltage characteristics based fault diagnosis

A simultaneous way of investigation between sampled data of voltage-current characteristics of a PV panel and the determination of its intrinsic parameters can lead to a dynamic fault diagnosis. With a fast parameter estimation, this technique allows a deep knowledge upon the state of the PV panel, what reflects as identifying the different sorts of external faults [196].

10. Shading and electrical faults detector based on Bishop model

By relying on the least squares method, the diagnosis of Solar Energy Production Source System (SEPSS), based on Bishop model is exposed where shading faults, as well as different electrical faults are taken into consideration. When the direct signal analysis (i.e., by temporal

power/voltage variations) does not contribute well in the PV fault detection, the proposed least square based fault detection overcomes such obstacles. In the process of fault detecting decision, a fuzzy logic approach is employed, with less needed time for calculation and ease of implementation [197].

11. Experimentally Weighted Moving Average (EWMA) control for shading effect on PV modules detection

For an early detection of shading effects on PV modules, as well as other faults on the DC side of the system, the usage of a mixed combination of the simple one-diode model in collaboration with the extended capacity of the EWMA control scheme, can detect the mentioned faults [199]. First, the one-diode model is used to make a reference of a healthy PV array maximum power coordinates. Then, all residuals (resulting from the difference of measurements between predicted and actually measured data) serve as fault indicators. When uncorrelated residuals exist, EWMA executes to identify the fault's type.

12. T-test statistical method for physical fault detection/algorithm for fault detection

To detect faults on the DC sides of a Grid Connected PhotoVoltaic (GCPV) system, a fault detection algorithm based on T-test statistical method is used to detect different types of physical faults [201] where for a given solar irradiance and temperature inputs, attributes such as voltage and power ratio of the PV strings, are measured. The needed inputs of the algorithm are solar irradiance, modules temperatures, voltage, and power ratios [166].

13. Electrical and environmental fault detection based on WOEWMA

Using the upgraded Wavelet Optimized Exponentially Weighted Moving Average (WOEWMA) algorithm, electrical as well as environmental faults of PV grid connected systems can be detected [163]. The overall system can classify false alarms and missed detection rates. Figure 12 presents the two online/offline monitoring phases for the WOEWMA algorithm. Control limits are calculated from the off-line modeling phase and compared with the detection chart obtained during the on-line monitoring phase. The fault is declared after violating the permissible threshold between the detection chart and its control limits.

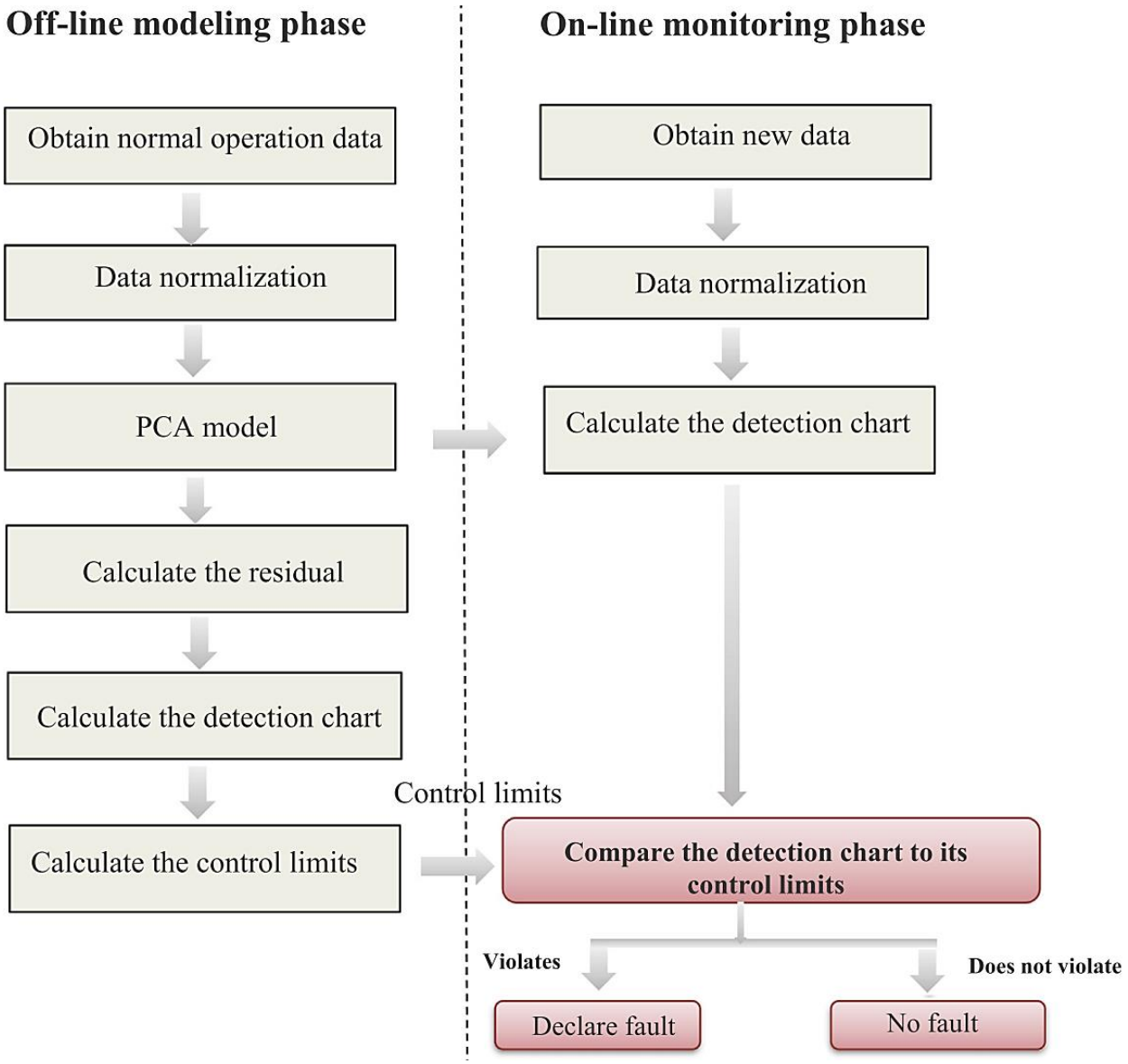

Figure 12. General diagram of detector scheme [163]

14. OPC monitoring

In an Object linking and embedding for Process Control (OPC) environment for PV simulation, a remote supervision and fault detection technique based on voltage/current comparison tactic is proposed [165]. The system itself is a decision maker where it analyses the monitored data and evaluates the expected behavior of PV arrays in terms of output voltage, current and produced power. The current and voltage indicators that were used for fault detection are shown in Eq. (12) and Eq. (13) respectively.

$$NR_c = \frac{I_m}{I_{scg}} \tag{12}$$

$$NR_v = \frac{V_m}{V_{ocg}} \quad (13)$$

with I_m and V_m representing the current and voltage quantities at the maximum power point respectively while I_{scg} and V_{ocg} representing the real-time measured current and voltage quantities. This method was experimentally tested on a real PV system, where the root mean square errors between real/simulated data were below 3.6% [165].

15. Comparison between Measured and Modeled PV system outputs (CMM)

The analysis of the difference between actual PV measured values (i.e., DC current and voltage) and modeled ones, could predict the electrical fault within a PV system. Predictive models get simulated with aid of computers, to fabricate a theoretical threshold. In other words, a reference value for which all non-equal values, represents a specific fault type. Based on the reference thresholds for fault detection as well as diagnosis procedures, the most likely PV fault to occur can be identified [251]. Under the same perspective, based on an extended correlation function and on the matter model [253] predictive PV faults detection are improved.

16. Analysis of solar photovoltaic power generation

Under dynamic PV systems operations, sometimes exists an inability to distinguish between the effects of undesirable environmental conditions (i.e., clouds, snow accumulation, etc.), which lead to the same results of fault conditions (i.e., decrease in power generation capacity). Accordingly, for a proper operation description the test method based on the analysis of solar photovoltaic power generation performance reveals a voltage and current based fault detection method. Unlike conventional voltage/current based PV fault detection methods, this scheme is able to distinguish between environmental factors and concrete PV cell faults [69].

b) Spread Spectrum Time Domain Reflectometry (SSTDR)

The fault is detected using a plot, which in turns is created using the incident and reflected signals. Referred to as "auto-correction plot", it can be used to identify different faults without the need to disconnect the inverter, as it checks the losses/disturbances between the two signals. The fault is hence identified after the analysis of the plot's changes [204].

From the same perspective, the incorporation of a fault detection algorithm with SSTDR results in a tool to detect wiring faults even with the existence of impedance varieties throughout the PV system. Such combined system can detect PV ground faults for different PV systems' architectures and distinguish ground faults that GFDI cannot detect [205].

Similarly, mixing the Time Domain Reflectrometery (TDR) principle with Earth Capacitance Measurement (ECM) a fault detector for disconnection and degradation problem is achieved [247]. The model investigated can be implemented in a PV system in two ways, the first as a fault inspector, the second as a temporary detector to find the degradations in the PV system.

c) Estimating Randomness in the Voltage signal (ERV)

A Finite Impulse Response Band Pass Filter (FIRBPS) can detect an arc fault in the DC wiring, by estimating the corruption between the output signal with reference to the input signal. If the difference is low/high in comparison with a threshold, arc faults' existence can be investigated [206].

The randomness in the voltage signal can be estimated as well by means of a modified one-diode model. The one-diode model can be completed by combining the Artificial Bee Colony Optimization (ABCO) and Differential Evolution (DE) algorithms to digitally model a PV array and extract the ABCO-DE parameter [207]. Hence, an I-V curve based PV module fault detector can be launched as a fault detector using ABCO-DE parameter extraction technique.

d) Power Loss Analysis technique (PLA)

PV Faults can be detected based on power losses. This can be done by comparing the monitored data (e.g., DC output power) with the simulation outcomes [242]. Basing on PLA, the faults occurring between the PV array and the converter can be detected [250], [243]. Current and voltage ratios can also be used as a skeleton for PLA based fault detection algorithm [244].

e) Electrical current-voltage I-V Measurement (EM)

PV faults can be detected by depending only on I-V measurements on the output level [255]. The EM based methods can be as well ameliorated using a micro-controller [256] as a central decision making unit [257]. Such methods are also applicable for GCPV [258], where the derivatives of I-V indicators signal the detection partial shading phenomenon [259]. The addition of other performance indicators (e.g., Fill Factor (FF)), and electrical characteristics (e.g., Shunt Resistance (SR)) to the crude I-V measurements, yields in a wider overview of the PV system's performance [260].

Following the same perspective, by comparing the actual electrical parameters (e.g., voltage, current) from the I-V characteristic curve and theoretical ones, faulty connections can be investigated. The technique relies on analyzing the shape of the I-V characteristic of a PhotoVoltaic Array (PVA) [254].

f) Open/Short-Circuited modules in PV string (OC/SC)

By emphasizing only on the quantity of transducers, such as the number of sensors and power meters, a simple diagnostic technique is achieved [71] to detect the number of open/short circuited modules in a PV string.

Also based on current and voltage indicators, a procedure to calculate the thresholds needed to identify the fault is presented [72] where the PV array that is formed from series and parallel interconnection of PV modules, forms a reference for the thresholds' calculation. For an automatic process to identify OC/SC modules, without any manual interventions, the design's principles and runtime control algorithm are presented [73] to detect the bypass PV cell faults.

g) High/Low Voltage fault diagnosis sections (HV/LV)

The localization of the defected PV modules is done by analyzing the terminal I-V curve, which is divided into high and low voltage fault diagnosis sections. In each section, the healthy and defected working points of string modules are analyzed for both of I-V sides [74] where at the end, any faulty PV module is located by probing into different working points.

Therefore, faulty conditions are regionally characterized inside the detection zones within the I-V characteristic curves [75]. Such zones are defined after subtracting the measured from the maximum set point values of I-V signals.

h) Partial/Complete Shading fault detector (PS/CS)

Using three input variables, such as measured values of array voltage, current and irradiance, a method to detect faults and partial shading under every irradiance situation is established [76]. Such method is able to classify the status of PV arrays into three states as normal, partially shaded, or faulty mode. From another side, and based on DC power measurements, shading faults are detected by focusing on real-time fault diagnosis (i.e., instantaneous power measurement under real PV working conditions). Accordingly, the detection, location, and identification of different types of PV shadows patterns are injected to the output DC power analysis, hence yielding in timely PV fault detections [77].

i) Online/offline model (Onm/offm)

After evaluating three PV coefficients (current, voltage, and power coefficients), a two-step model relies first on an offline step that uses a PV simulated model. From the other side, the online step compares real measured PV coefficients with respect to those obtained in offline step. The combination of both online and offline steps results in a differential PV fault detector [78].

j) Degradation Fault Identification based on string current (DFI)

Based on the degradation faults, a fault diagnostic method that takes into account the relationship between the level of degradation and PV plant faults (including current faults), identifies the process between PV degradation and the decrease in a PV string current. In other words, the relationship between the level of PV modules' degradation and the PV plant's faults is investigated. After intentional short circuit scenarios, this method succeeds in identifying different PV faults, that were undetectable when using conventional protection settings [79].

k) DC-DC converters Fault Identification (DC-DCFI)

Apart from MPPTs, old techniques for battery charging control relies on Pulse Width Modulation (PWM). The purpose of PWM is to efficiently extract power from PV arrays while safely charging the battery bank [203], providing various ranges of output stages [248]. Labeled as DC-DC converters, such devices can encounter faults, preventing them from functioning or implying an erroneous behavior [249]. To detect the fault within such devices, the diagnosis can rely on:

- Magnetic component voltages equation [170]
- Short-circuit fault diagnosis [171]
- DC-link current pulse shapes [172]

To conclude on this section, Table 7 encapsulates a comparative assessment of different electrical sub-methods.

Table 7. Comparative assessment of different electrical based fault detection methods

Detection manner		Targeted faults	Scalability of PV system	Detection level	Algorithm -based	Simulation	Model-type
MBDM	1. [187]		GCPV	PV string/ module/M PPT	●		
	2. [188]						Deviated error Comparative
	3. [189]		RPS		●		Statistical
	4. [191]	Bypass Diode		PV array		●	
	5. [192]			PV panel			Experimental Predictive
	6. [193], [262], [263], [70]	External, PPUs		DC/DC DC/AC	●		
	7. [194]			PV cells			Deviated error, Mathematica l
	8. [195]	Short-Circuit			●		
	9. [196]	External		PV Panel			Experimental Tabulated data
	10. [197]	Shading electrical		PV module	●		
	11. [199]			PV module	●		Deviated error
	12. [166], [201]	External	GCPV		●		Statistical Experimental
	13. [163]	Electrical External	Grid-tied		●		
	14. [165]	Electrical		PV array	●		
	15. [251,253]						Deviated error, Experimental
	16. [69]	External		PV array			Experimental
SSTDR	[204-205], [247]	Electrical External			●	●	Hardware
ERV	[206-207]	Arc			●		Deviated error

PLA	[242,244], [250]			PV array converter	●		
EM	[254-260]	Partial shading	GCPV				Mathematical, software
OC/SC	[71,73]	Electrical		PV string			Hardware
HV/LV	[74,75]	Electrical		PV string PV array			Experimental Comparative
PS/CS	[76,77]			PV array			Comparative Real-time
Onm/offm	[78]					●	Comparative
DFI	[79]	External		PV string			Mathematical
DC-DCFI	[170-172], [248-249], [203]	Electrical		DC/DC	●	●	Real-time Hardware Comparative

4.2.3 Signal Processing Methods (SPM)

PV faults can be detected by the analysis of the output signals, such as current and voltage waveforms, by means of mathematical interpretation and the recordings of measured quantities. The synthesis of the recorded signals gives a clear representation on its status (whether normal or corrupted), what results in various faults detection. This set of methods contains the following sub-methods:

a) Wavelet transform/Wavelet transform with multi-level decomposition/GCPV fault detector
b) S-transform
c) Local Outlier Factor LOF/PVLOF
d) High Impedance Ground Fault detection HIGF
e) Generalized local likelihood ratio test algorithm
f) Differential current based fault detection

a) Wavelet transform with multi-level decomposition

The wavelet transform represents a mathematical modelling for dynamic signals using small waves [144]. It comprehends both frequency and time information simultaneously, which accordingly, it can detect discontinuities in the varying signals that are results to islanding. By correlating discontinuities with respect to time, the localization of islanding is performed for PV systems [145], using five decomposition levels [146].

When the raw wavelet transform is decomposed to a multi-level decomposition wavelet transformation, different faults can be detected using a diagnostic function based on the normalized standard deviation of the wavelet coefficients [153]. Since wavelet-based transforms are accurate at detecting discontinuities in signal waveforms, the random, dynamic, and non-periodic arc faults are efficiently discovered. In a particular case, the wavelet decomposition and arc discrimination are presented as algorithms for an arc detector platform using Digital Signal Processor (DSP) [159]. The fault identification accuracy of a wavelet based PV fault detector can be as well improved by means of wavelet packets using the available data of the PV array's I-V curve [162]. Accordingly, the fault detector becomes then able to distinguish between undesired environmental conditions and PV faults.

When creating a modification on the Wavelet Packet Transform (WPT), the resultant tool becomes able to detect the disturbances resulting from faults in Grid Connected PhotoVoltaic System (GCPVS) [167], as shown in Figure 13. Such scheme compares the results between WPT and Modified Wavelet Packet Transform (MWPT), yielding in fault identification by means of indices' calculation, such as energy and standard deviation.

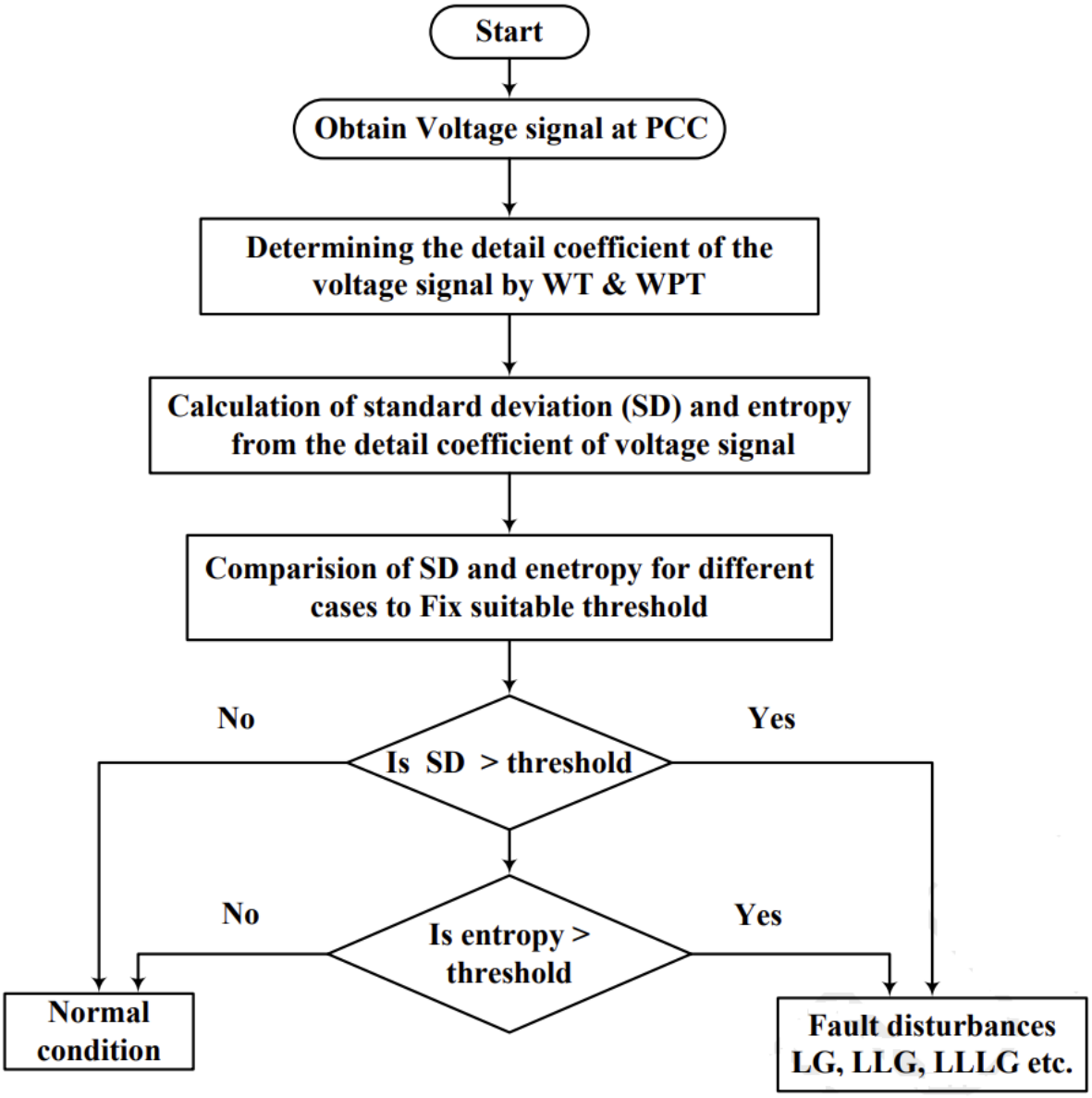

Figure 13. MWPT flowchart [167]

b) S-transform

The S-transform is simply an improved version of the previous WT transform, which eliminates the inability of islanding detection under noisy conditions [147,148]. It produces dual axis representation of time: the real and the frequency dependent resolution which constitutes the imaginary spectra. During an islanding, the voltage sequence becomes negative (backward on the x-y plane). In order to calculate both voltage and current sequences, they are both processed through the S-transform and the spectral energy content is used within the calculation [149].

c) Local Outlier Factor (LOF/PVLOF)

By relying on the instantaneous PV string current, without the need for weather measurement inputs, outlier detection rules are proposed as fault diagnostic methods. Specifically, the 'Hampel'

identifier and Boxplot rule are the most recommended among other outlier detection based methods to detect faults in PV systems [150].

When discussing the transient state and post-fault behavior in the DC side of the PV system, it can be noticed that some of the hotspots becomes undiscoverable (i.e., the occurring fault is not detectable by an Over Current Protection Device (OCPD)). When outlier statistic rules are applied, false alarms may be caused. Accordingly, the Local Outlier Factor (LOF) is developed inside a PV installation [151]. The addition of a specific algorithm to the LOF based on PV string current (PVLOF) to determine the electrical and shading faults on smaller scaled PV plants, the fault detection rate is better enhanced where the fault range is identified through seven steps [168].

d) High Impedance Ground Fault detection (HIGF)

With cost efficiency improvement, apart from the GFDI and SSTDR based PV fault detection methods, while implying on the Common Mode (CM) model of the full-wave inverter, the High Impedance Ground Fault (HIGF) detection scheme is accomplished. The CM model includes a simplified model for the transformer-less circuitry employed in a PV system architecture. This model includes the CM voltage source, ground capacitors and a capacitive path for an Electro Magnetic Interference (EMI) filter. This model detects the ground faults in PV systems [152].

e) Generalized local likelihood ratio test algorithm

By imposing a change detection algorithm (based on the generalized local likelihood ratio test) on the vector Auto Regressive (AR) model, the time correlation of the faulty signal and signal correlation among different meters (that are employed to measure different output signals of the system) are exploited. Hence this framework detects any sequential change and provide a PV fault detection algorithm [156].

f) Differential current based fault detection

A differential current-based fault detection, with a fast acting DC switch as an actuator can calculate the distance to fault by calculating the unknown cable resistance, relying on non-iterative Moore-Penrose pseudo inverse technique. In addition, with the special DC cable connected to the PV system, the DC arc faults could also be identified [160].

4.2.4 Machine Learning (ML) techniques

Enabling PV systems to learn from past experiences of faults existence, Machine Learning (ML) techniques allow such systems to learn new knowledge which is not already pre-programmed. This happens by means of large observations, learning algorithms and data mining [279]. Through this survey, twenty different ML techniques were found as follows:

a) Takagie-Sugeno Kahn Fuzzy Rule (TSKFR)
b) Decision Tree algorithm (DT)
c) Probabilistic Neural Network (PNN)
d) Multiple-layer ANN
e) LAterally Primed Adaptive Resonance Theory based Fault Detection (LAPART-FD)
f) Nelder-Mead optimization technique

g) Adaptive Neuro-Fuzzy Inference System-Sugeno Model (ANFIS-SM)
h) Fuzzy logic
i) Random Forest algorithm (RF)
j) DC arc faults
    1. Based on Tsallis entropy factor
    2. Based on electromagnetic radiation
    3. Based on a joint detection method
    4. Based on Frequency Spectrum Analysis (FSA) of V/I waveforms
k) Partially Shaded Modules Fault Detector (PSMFD)
l) GISTEL combined with fuzzy logic
m) ANN based fault locator using electrical attributes
n) String Current Algorithm for OC/SC fault detection
o) Mamdani-Sugeno fuzzy Logic
p) Electrical and Partial Shading faults based on kNN rule
q) Neuro-fuzzy bypass/blocking diodes faults classifier
r) Third-order polynomial function samples with fuzzy logic classification
s) Multiresolution signal decomposition
t) Multiresolution signal decomposition with two-stage support vector machine

a) Takagie-Sugeno Kahn Fuzzy Rule (TSKFR)

This ML based technique inspire learning by training, then occupying the acquainted information into the central processor unit (e.g., microprocessor, microcontroller, etc.). Each new faulty scenario (e.g., decreased power generation) can be referred to an old existing one [221]. This is done using a recursive algorithm that could train a model for several power input/output patterns, to eliminate the difficulty of detecting a fault in changing climatic conditions [222]. To classify the obtained fault within a PV array, Artificial Neural Network (ANN) is used [223].

b) Decision Tree algorithm (DT)

In the Decision Tree (DT) algorithm, the PV array voltage, current, operating temperature, and irradiance (referred as attributes) are used in the training and test sets where DT accurately detect and classify PV faults during the test set. This particular process of model training is easy to implement, where the resultant trained model detects PV faults by an accuracy up to 99.98%, and a classification accuracy of 99.8% [232].

c) Probabilistic Neural Network (PNN)

To detect and classify PV faults as short/open-circuit in real time, the Probabilistic Neural Network (PNN) is used, which requires specific information from the PV manufacturers' datasheet under Normal Operating Cell Temperature (NOCT) conditions and STCs [233]. Such model is able to represent the characteristics of PV systems under different environmental as well as electrical conditions.

d) Multi-layer (ANN)

To overcome the low PV fault detection efficiency of manual checking, and to ensure that the PV system is functioning at its best, a three-layered ANN is injected into a fault diagnostic

algorithm [234]. The performance of this three-layered ANN model surpasses the single ANN model which does not provide accurate precision for PV fault detection.

Similarly, and using only a two-layered ANN model, an automatic fault detector can provide detailed fault information with high accuracy about PV fault's types and locations. The multi-layered ANN plays the role of a comparator between both predicted power and the measured one. Based on this diagnosis, tasks are achieved in a way that the open circuit voltage and short circuit current of each PV string are to be determined using analytical equations. The resultant current/voltage data end up categorizing six different fault types [235]. Other algorithms such as Takagie-Sugeno Kahn Fuzzy Rule Based System (TSKFRBS), three-layered ANN can be found in [224-231].

e) LAterally Primed Adaptive Resonance Theory based Fault Detection (LAPART-FD)

To increase the reliability of PV systems an important factor is to design the PV fault detection system with the minimum number of sensors and data acquisition for Reliability Centered Maintenance (RCM) [237]. Accordingly, a Fault Detection and Diagnosis (FDD) tool based on Laterally Primed Adaptive Resonance Theory based Fault Detection (LAPART-FD) can be used. This tool automatically discovers different PV faults, such as temporary mismatch faults on the module level, and it relies on the algorithm which in turns is based on actual and synthetic data tests. The LAPART-FD PV fault detection probability recorded at highest an efficiency value of 86% [236].

f) Nelder-Mead optimization technique

The physical faults (i.e., degradation, partial shading, and short/open-circuit faults) in a PV system can be detected using the I-V characteristics' curves. Such a process requires the implementation of these characteristics on a Kernel extreme learning machine with the addition of Nelder-Mead simplex optimization technique [238]. The resultant fault detections can be simulated on a Single Hidden Layer Feedforward Neural Networks (SHLFNNs) based fault diagnosis model. The algorithm begins with the fundamentals of Extreme Learning Machine (ELM), returns to parameter optimization of the Kernel Extreme Learning Machine (KELM), heads toward data pre-processing and feature selection, and finally, establishes the fault diagnosis model.

g) Adaptive Neuro-Fuzzy Inference System-Sugeno Model (ANFIS-SM)

Combining the Adaptive Neuro-Fuzzy Inference System (ANFIS) with its common architecture, the Sugeno model, a faulty curve can be drawn inside the MPPT rectangle to identify shading faults, such as the reduction in the power extractability area. For this purpose, the model has to have six attributes to work accordingly, such as maximum power point current (I_{Mpp}), maximum power point voltage (V_{Mpp}), short circuit current (I_{SC}), open circuit voltage (V_{OC}), I-V step curve, S1 and S2 [239]. The sets of inputs/outputs are firstly classified, then the ANFIS is generated, to later on trains and tests itself.

h) Fuzzy logic

A fuzzy logic algorithm based model detects PV short circuits faults by taking voltage and power ratios as inputs. The correspondent fuzzy logic consists of voltage/power ratio inputs, where the membership for each input is decomposed into five fuzzy sets. Including machine learning

and targeting for Grid Connected PhotoVoltaic System (GCPVS), the proposed system can detect Short Circuit Faults (SCF) by means of theoretical curves of voltage and power ratios. Additionally, the suggested algorithm is capable of detecting hotspots formation in PV system, where its minimum detection accuracy is of 98.8% [240].

i) Random Forest algorithm (RF)

A Random Forest (RF) algorithm detects PV array faults using array voltage and string currents. Implemented in Matlab, the system can detect electrical faults as well as temporary mismatch faults, as presented in its flowchart in Figure 14. The RF combines multiple learning algorithms and takes only real-time values of voltage and current. The results of such algorithm indicate its superiority over the DT algorithm in detecting and classifying a PV array's faults [241].

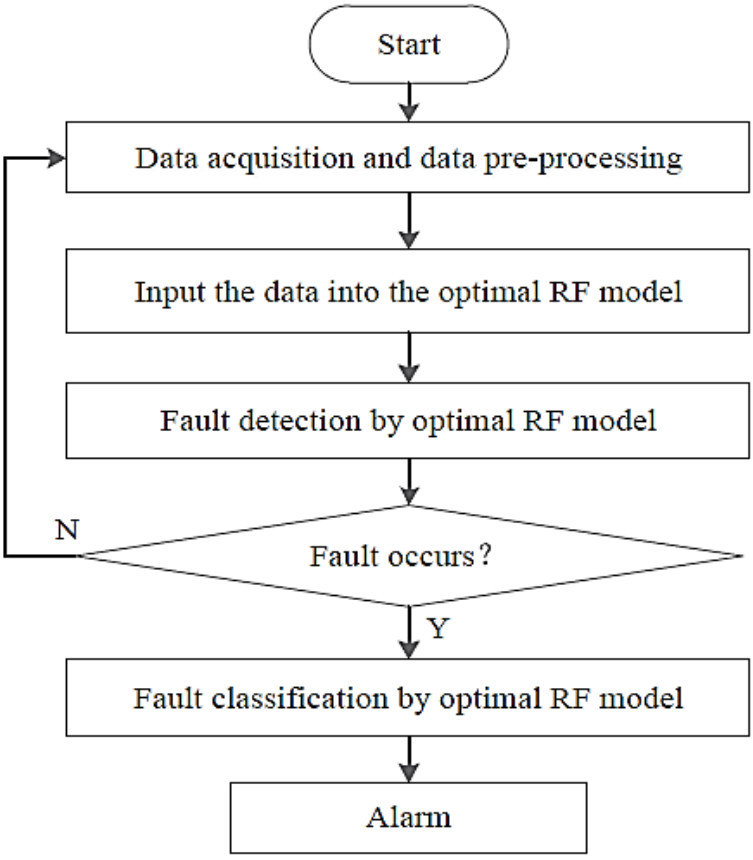

Figure 14. The RF flowchart [241]

j) DC arc faults

The detection of DC arc faults can be achieved with a method that uses Fast Fourier Transform (FFT), Short Time Fourier Transform (STFT) and wavelet transforms to create a statistic model under Artificial Neural Network (ANN) routine [59]. The decision making takes its final step after sensing elements and acquaint different PV physical data, while the model simulation is injected for signal processing purposes. Under the same point of view, and by using

the time and frequency characteristics of a parallel capacitor current, DC arc faults are detected and classified as series and switch arc faults, where this entire system is upgradable to easily investigate harmonics [264]. Generally, DC arc faults in PV systems are detected according to the four following major schemes:

1. Based on Tsallis entropy factor

The presence of an arc fault is identified by calculating the modified Tsallis entropy factor of the PV panel's current under the quantum probability model theory [154]. When the current fluctuations are random, the algorithm can differentiate between arc and no-arc states, as it does not need any prior information about the PV system working in progress.

2. Based on electromagnetic radiation

Electromagnetic radiation signals can detect DC arc faults with the help of a fourth order Hilbert curve fractal antenna, which captures Electro Magnetic Resonance (EMR) signals resulting from DC arcs [161]. As for the detection parameter of a DC arc fault, the characteristic frequency of the EMR signal distinguishes between PV arc fault from switch operation.

3. Based on joint detection method

To notice series arc faults in PV systems, a joint detection method is provided to an Arc Fault Circuit Interrupter (AFCI). Series PV arc faults are hence recorded by an Intensified Charge Coupled Device (ICCD). The fault definitions and diagnostics are hence derived by a statistic method from the time domain and Short Time Fourier Transform (STFT). For each sub-method a detection variable is proposed for an accurate arc fault identification [158].

4. Based on Frequency Spectrum Analysis (FSA) of V/I waveforms

PV arc faults are related to frequency contents. Due to signal variations induced by environmental conditions (i.e., irradiance, partial shading, etc.) certain lower frequencies limit ranges are not taken into consideration for false tripping [208]. Also, the upper frequency range is also excluded for its interactions with Radio Frequency (RF) noise. Between lower and upper borderlines, the middle frequency range is partially excluded since converters and charge controllers provide harmonics that affect the frequency [209]. The choice of AFCIs activating frequencies must be well studied according to the FRequency Spectrum Analysis (FRSA), mainly to ignore the disturbances and neglect false tripping [210-211].

k) Partially Shaded Modules Fault Detector (PSMFD)

By comparing between reference I-V and measured values, the proposed ANN model can detect faulty conditions on PV modules when being partially shaded. If the residual error between the estimated values developed by the ANN model and the measured ones exceeds thresholds values, this indicates that the PV module is subject to PSC [64].

l) GISTEL combined with fuzzy logic

Using experimental parameters (i.e., temperature, irradiance, etc.) PV electrical faults are located, by means of a hybrid model, which is created by combining GIsement Solaire par TELedetection (GISTEL) model and fuzzy logic based fabricated algorithm. This system estimates solar radiation data using GISTEL, and has its overall efficiency improved by fuzzy

logic algorithm [58]. By estimating on solar radiation, the GISTEL model is introduced to remotely locate and inform about any fault occurring on the level of PV battery bank [245], as revealed in Figure 15. By comparing the estimated solar irradiance data from satellite images with actual DC power output, failures within a PV system can be identified [190], [252]. The detection technique relies on comparing the simulated in verses with real measured DC output power.

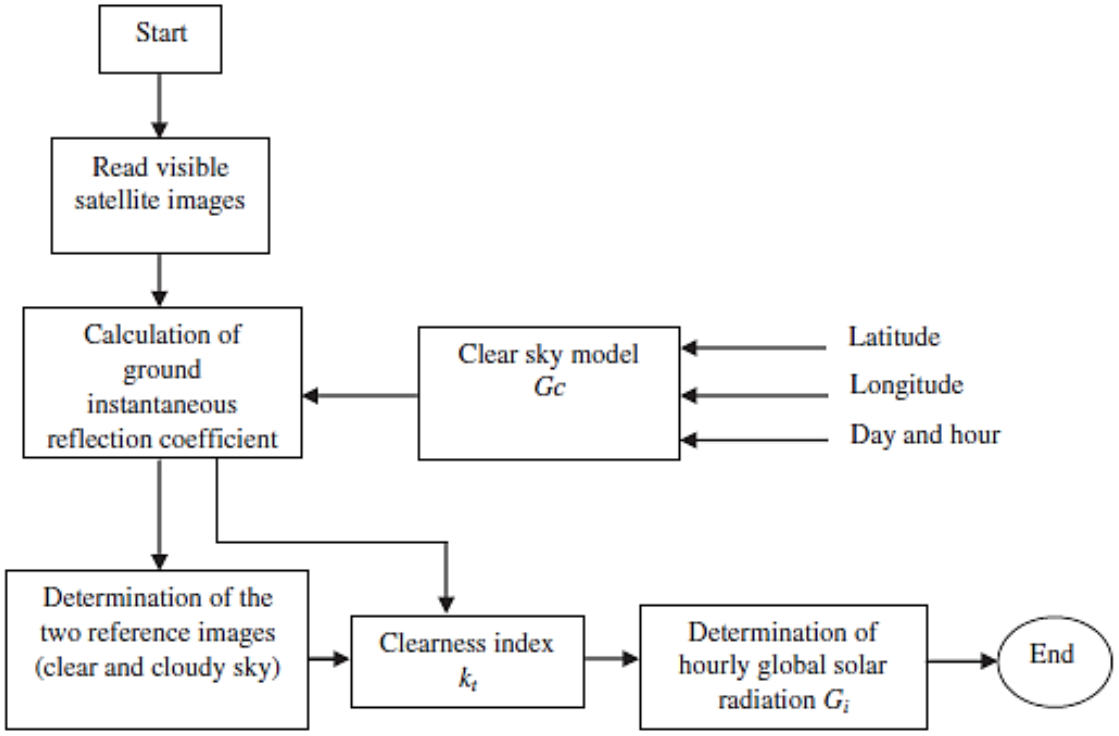

Figure 15. GISTEL steps [245]

m)ANN based fault locator using electrical attributes

Based on a Field Programmable Gate Array (FPGA), a sum of eight different PV operating faults are detected, using electrical attributes identification. For a set of PV working conditions, such as solar irradiance and working temperature, electrical attributes (i.e., voltage, current, etc.) are simulated first then later on compared with field measurement [60]. Figure 16 presents the attributes' calculation for a two-layer ANN algorithm. The attributes are calculated by differential comparison between the physical quantities of voltage, and current data, with the simulated ones. Resultant attributes are injected into the double layer ANN algorithm, in order to classify the detected faults.

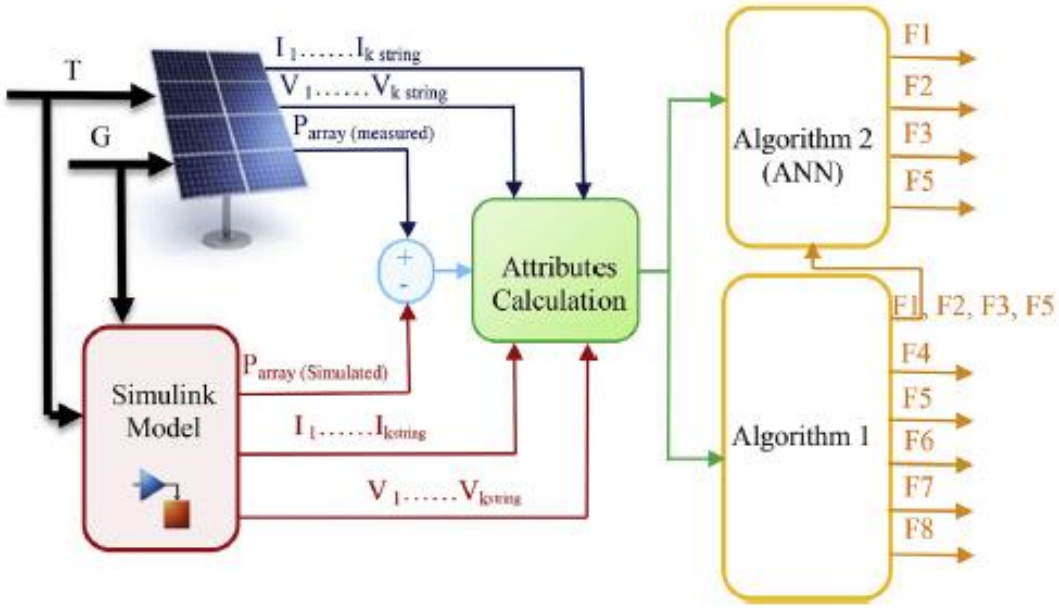

Figure 16. Two-algorithm ANN proposed fault classifier [60]

n) String Current Algorithm for OC/SC fault detection

A model for Open Circuit/ Short Circuit (OC/SC) PV fault detection is established using real tabulated data to store backup info in the system. This model relies on Genetic Algorithm, Tabu Search and Grey Wolf Optimization algorithms as strategies to program the ANN to be able to detect OC and SC with less needed monitoring parameters [61]. Figure 17 represents the flowchart for the string current algorithm, where its included error estimation, is the result of comparing between both simulated and actual power received by the solar system, representing hence the fault indicator.

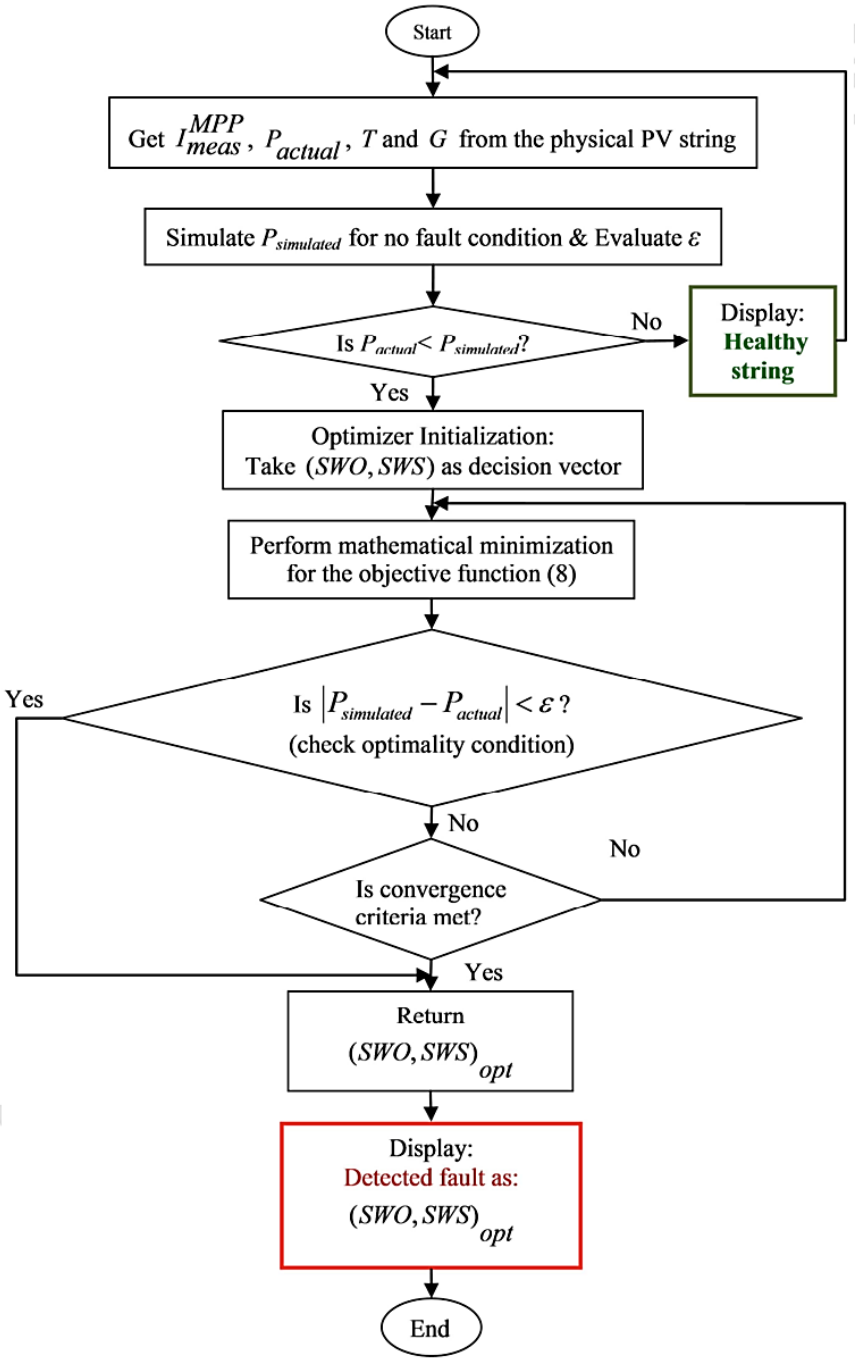

Figure 17. Solution flowchart [61]

o) Mamdani-Sugeno fuzzy Logic

By taking advantages from the ANN topology and fuzzy logic system interface combination, an environmental as well as electrical PV fault detector is created. The method begins by data acquisition from the PV plant, modelling the DC side of the PV system using five-parameter model, creation of power and voltage ratios, to finally implement the ANN model. The suggested

algorithm is able to detect different PV faults such as faulty PV modules and PSC with a maximum detection accuracy of 92.1% [65].

p) Electrical and Partial Shading faults based on kNN rule

A Fault Detection and Classification (FDC) technique relies on machine learning, dictated by the k-Nearest Neighbors (kNN) rule, traces the abnormalities within the I-V characteristic curve. The FDC models and simulates the PV system using STCs and NOCT, yielding in PV fault localization and characterization. The absolute error between the measured data and the developed in the range 0.61 to 6.5% with an average fault classification's accuracy of 98.70% [67].

q) Neuro-fuzzy bypass/blocking diodes faults classifier

A neuro-fuzzy classifier detects faults at the PV cells' level, such as series losses, bypass and blocking diode faults, basing on electrical parameters such as maximum power, and open circuit voltage deviations. The corresponding fault identification/discrimination processes take into consideration four electrical parameters, where the classifier has shown an ability to work with different irradiance/temperature levels [198].

r) Third-order polynomial function samples with fuzzy logic classification

After that different attributes are measured, a third-order polynomial function is used to classify higher and lower detection limits for PV voltage and power ratios faults. Samples are aftermath processed by a fuzzy logic classification to gain one output membership function. The correspondent maximum detection accuracy for this algorithm is equal to 95.27% [202].

s) Multiresolution signal decomposition

In a cascaded PV system, a fuzzy inference system indicates if a fault has occurred by giving an order decision to a multiresolution signal decomposition technique which in turns extracts the needed necessary features. Such method is based on a pattern recognition approach. The system uses fuzzy logic to interpret the monitored data and an online resource to acknowledge the faults. The suggested fault detection scheme is able to detect the DC-sided short circuit fault of a PV system, which are generally undetectable under low irradiance conditions [157].

t) Multi-resolution signal decomposition with two-stage support vector machine

To reduce the fire hazards due to faulty PV currents (being undetected in low irradiance conditions) with the presence of a MPPT, the multi-resolution signal decomposition for fault extraction is combined with two-stage Support Vector Machine (SVM) classifiers to detect the occurrence of Line-to-Line (L-L) faults. The required data for the algorithm is obtained from the total voltage and current from a PV array, with other labeled data to train the SVM. This method is found to be economical for requiring a smaller number of sensors, yet effective in detecting L-L faults under various operating conditions [186].

4.2.5 Insulation Monitoring Relays (IMR)

A continuous monitoring measurement is held between Current Carrying Conductor (CCC) and ground: whenever the resulting resistance value is smaller than a threshold, an alarm is set,

thus informing that a short circuit exists in the PV system. Such instrumentation is effective in detecting short circuited paths in PV systems, preventing further electrical complications [212].

4.2.6 Heat Exchange and Temperature based model (HET)

The Heat Exchange and Temperature based model (HET) detects a PV fault according to the change in the PV module temperature, due to the correlation between a PV fault and its temperature changing like in the case of hotspots. All heat exchange is scheduled within the fault detection technique. Using a finite element method, the physical defects of different types of PV cells are modeled [219], [220].

4.2.7 Climatic Data Independent Technique (CDIT)

The Climatic Data Independent Technique (CDIT) is attributes-independent, where it does not need any solar irradiance, temperature, humidity, and other climatic data. It relies coarsely on external meters as Inductance Capacitance Resistance (ICR) meters, Earth Capacitance Measurement (ECM) [265], Time Domain Reflectometery (TDR) [266], and ANalysis Of VAriance (ANOVA) [267] techniques. Fault detection is hence accomplished after analyzing the different effects of signal generators on the PV system, without any dependability on climatic factors, such as irradiance and temperature.

4.2.8 Infrared / Thermal Imaging (In/ThI)

Across a resistor, any power loss is noted as joule loss, where current passed is transformed into heat. Similarly, any loose contact shortening across PV cells can result to the same effect: loss in terms of overheating where affected cells produce less current as compared with normal ones and become reverse biased. Through temperature monitoring, the fault can be identified, in two ways: Forward Bias Imaging/Reverse Bias Imaging (FBI/RBI). Each of FBI/RBI techniques has its private method for calculating the shorted/faulty current in order to identify hotspots creation. This can be done in both methods by using Infra-Red (IR) cameras to record IR images, then performing image processing which results in identifying the PV fault nature and locating it within the PV system [268].

As a first approach, to identify the PV fault's type, and its frequency of occurrence, an IR thermography considers the panels' attributes under investigation, leading to fault identification [269], with the ability to investigate the existence of dust accumulated particles [261].

For hotspot cells exerting a reverse voltage with opened bypass diode, the inability to identify which PV module is defected, is solved by a technique described in the reference [270]. PV modules correspondingly do not need to be tested individually, where the detection relies on the observation of the total modules' surface temperature changes. Hence, the abnormal PV modules with open bypass diodes are identified using DC power supply and an IR camera [270].

To acknowledge the PV modules' actual temperature values, a thermal camera is connected in cascade with electrical sensor which measure different V-I values. Therefore, a diagnostic model

can identify different PV faults using the established parameter based model, which in turn is composed of an electrical model expressed by an energy balance equation of a PV module [271]. The measured parameters are compared to a reference performance estimation model, and the derived error can indicate the occurrence of a PV fault. Figure 18 exposes the process of fault identification using a thermal camera over a PV module. A model parameter calculation is thus achieved by combining the data captured from the electrical sensors with the values captured from the thermal camera. Fault diagnosis is hence completed after evaluating the performance estimation model [271].

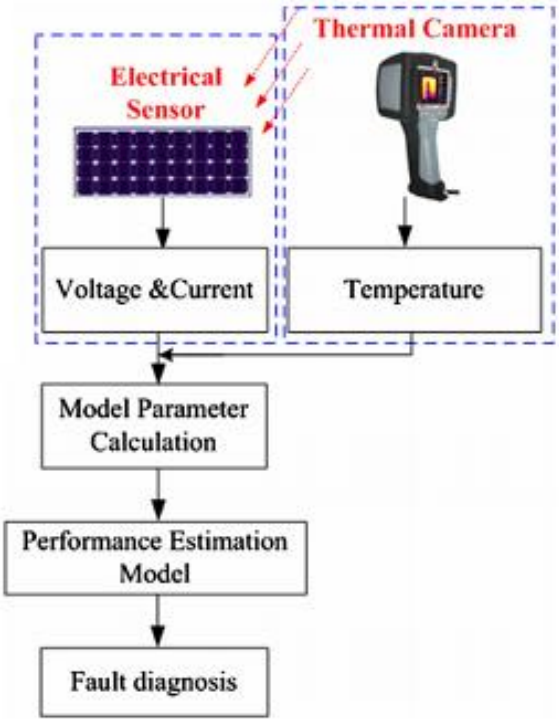

Figure 18. Thermal imaging [271]

4.2.9 Electroluminescence Imaging (EI)

To detect the aging process of PV modules, related to time entropy or reactions with the front glass cover, 2D-luminescence imaging can detect any defected PV modules by reflecting inhomogeneous luminescence patterns [272]. This type of detection reveals the degradation pattern of the encapsulation material, which gives a clear idea about the modules' lifetime energy output efficiency. The amount of light harvested by the PV modules, and its translation into DC power generation, reflects an indicator upon the health of PV modules [273].

When the excited carriers recombine within a PV cell, their emitted photons retrieve the EI imaging. An EI effect happens then by means of an injected current, which in turn yields to the carriers' excitation [275]. The Photo Luminescence (PL) effect can also give a clear idea about the amount of light beam being absorbed by the PV modules [276]. The emission intensity of EI

images is proportional to the PV current density and carrier lifetime, hence the ability to detect non-uniform currents sourced from poor PV inter-connections.

4.2.10 Ultrasonic Inspection Method (UIM)

When cracks/micro-cracks are present in the cells of a PV module, their response to ultrasonic vibrations followed by an excitation, is different from healthy cells. There are two modes to detect cracked PV cells by Ultrasonic Inspection Method (UIM): pulse-echo and transmission [274]. An ultrasonic transducer is present in both techniques to generate and distribute the pulses. In the first mode, the pulses are passed through a PV module to record the reflected pulses from the defected cells. In the second mode, the attenuated signals are recorded, yielding in locating the defected PV cells [200].

4.2.11 Lock In Thermography (LIT)

Lateral PV power loss is found using the Lock In Thermography (LIT) after injection of discontinuous pulsed currents into solar cells. Corrupted cells respond to these pulsed currents by appearing as local temperature generators, where by using different modulations, the defected PV cells appear. The pre-breakdown sites' visibility in LIT was better than that in reverse-bias EI [277].

The different fault detection methods of IMR, HET, CDIT, In/ThI, UIM, EI and LIT share all in common the need for external devices (transducers, cameras, etc.) in order to detect a fault. This fact could add extra financial burden on the fault detection prototype what decreases the cost efficiency of the PV system.

5. Discussion and recommendation

The surveyed types of PV faults would present a rich background to be fed into any PV fault detector database. As compared to other PV faults recurrence dataset, as in the work of [295], this paper did not estimate/record the frequency of occurrence of different PV faults, as posted in Table 8: the recorded data from real PV systems under operation, concerning the frequency of occurrence of PV faults would be treasurable for PV fault detection methods' databases, especially the ones classified under the AIT. The presented data in Table 8 for instance [295], would accelerate the learning paths for ML based PV fault detection methods, requiring the last for less self-learning processes. On the other side, however, the work in [295] focused only on specific PV faults and did not take into consideration broader types of faults, such as MPPT and inverter failures, contrarily to the surveyed PV faults in this paper.

Time *t* (in years: duration of the PV system installation)					
5	6	7	8	9	10
Disconnections, discoloration	Corrosion, disconnections, degradation, burn, delamination	Corrosion	Discoloration, delamination	-	Defective bypass diode
degradation	-	Burn marks	-	-	-
-	-	-	-	-	-
-	-	-	-	-	-
-	-	-	-	-	-
Cell cracks	-	-	-	-	-
-	-	Glass breakage, bypass diode	-	-	-

Frequency of occurrence (number of times)	1	2	3	4
1	Corrosion	Degradation, burn marks, defective backsheet	Discoloration, corrosion	Delamination, cell cracks, burn marks
1.5	-	-	-	-
2	Potential induced shunts	Defective bypass diode, Corrosion	Cell cracks, bypass diode	Bypass diode
2.5	Glass breakage,	-	-	-
3	-	-	-	Disconnections
3.5	-	-	-	-
4	Cell cracks	Cell cracks	Degradation	Degradation

Table 8. PV faults occurrence recording data [295]

Concerning the fault detection methods, not a set of techniques can replace the other. For instance, AC faulty scenarios cannot be detected by means of DC sensors, transducers, or any form of DC data capturers. Likewise, for DC faulty conditions, CBs, RCDs and GFDIs for example cannot trip or declare any form of fault detection based on continuous signals. From another side, online (real-time) PV fault diagnosis offers a higher fault detection accuracy than offline diagnosis, but in turns require extra hardware equipment in order to be able to cope with the larger amount of instantaneous operational data from the PV system. To only implement one form of fault

detection techniques leaves a full region within the PV system (whether it was the AC zone or DC zone) unmonitored with a probability to excessively have repeated faulty scripts.

Recent research in the field of PV faults detection methods emphasize on identifying untraditional PV faults. For example, by means of a wave shape based statistical algorithm, which analyzes the superimposed PV array power curve shape using the kurtosis function, short-circuit faults (i.e., electrical) of low values can be detected. Other types of faults (i.e., internal, external) can be as well detected, such as partial shading, blocking diodes, and others [282]. By following the same concern of detecting PV faults with small magnitudes, the triple exponentially weighted moving average statistical monitoring technique, when fused with other latent variable regression methods shows a good efficiency. Such incorporated method can detect string faults, inverter disconnection, circuit breakers faults, short circuit faults and others, from an actual 9,54 kW PV plant [283]. As a form of PV preventive maintenance, the statistical monitoring approach, initiated by a Hartigan's dip test, can identify any PV abnormal operating conditions, priorly than becoming actual failures [284], as similar is the case for the work in [285] where the suggested models offer quick and accurate prediction of different fault conditions. From another perspective, both DC and AC parts of a PV system can be monitored through a nonparametric approach using kernel density estimation, where different types of faults can be detected, such as string fault, partial shading, and loss of energy due to an inverter's disconnection [286]. Similarly, faults at both the DC side of the PV system, such as soiling and partial shading, as well as on its AC side, such as circuit breaker faults and inverter disconnection, can be detected via parametric models with double exponentially smoothing based scheme [287]. Contrarily, in order to have better focused PV faults detection on the DC side of a PV system (e.g., short circuit, open circuit, and shading faults), the generated residuals of current, voltage, and power, capture the difference between the actual and maximum power point of the same quantities. Successively, when the resulting fault indicators are subjected to an exponentially weighted moving average algorithm, the stated DC faults are identified [288], and better acknowledged due to the reduced measurement noise after the usage of a multiscale representation [289].

Despite the numerous advantages presented by the recent PV faults detection research field, very few methods from the massive presented literature review, present any solution in troubleshooting the PV system from its both AC and DC sides. Under working conditions, a PV system may encounter having multiple faults in both AC as well in DC regions. Accordingly, and for an efficient fault tracking process, a dual AC-DC fault detector is recommended to be installed in the PV system as shown in Figure 19.

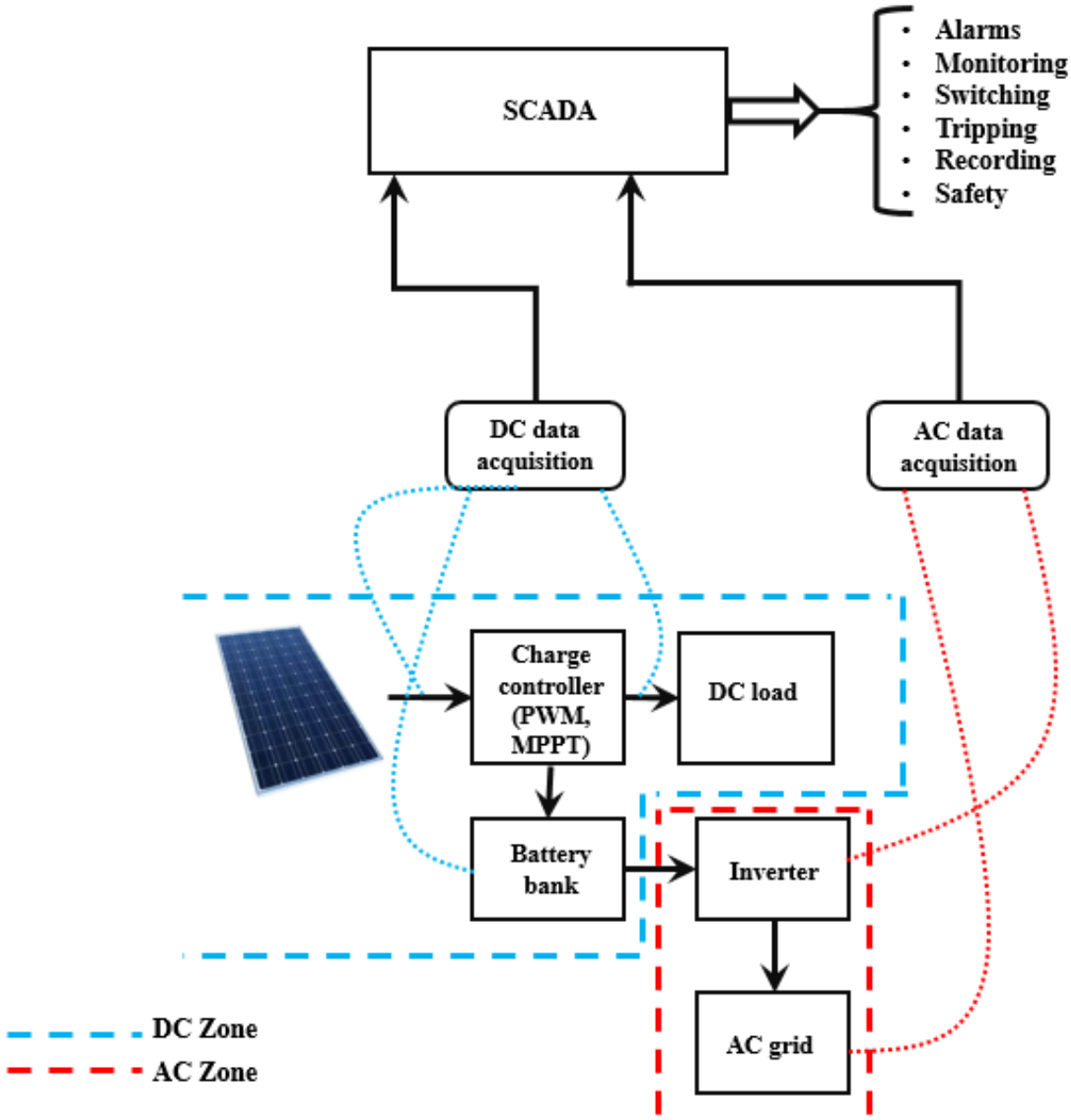

Figure 19. The suggested AC-DC fault detection general overview

The dual fault detector shown in Figure 19, implies some sensors/transducers installation at the DC side of the PV system in order to capture various DC faults. On the other hand, RCBOs and different AC switchgear can be coordinated with remoted applications, IoT-based (Internet of Things) to remotely access to AC-sided faults. In other terms, future directions are recommended based on the utilization of addressable protective switchgear for both sides of the PV systems, that can be remotely networked, controlled, and current-state acknowledged. Such protective devices can for example be assigned to a local area network, and accessed via internet protocol addressing (as an example), with an ability for a remote access through a virtual private network certification. A registered user can hence configure and read the different states of the AC as well as the DC protective switchgear. Therefore, the actual states of these tripping devices can hence be network

sent to a SCADA, over the same local area network, through a data block messenger that actually carries the "status" of the tripping devices (i.e., open contacts reflect the presence of a fault through a logic TRUE; closed contacts reflect normal working conditions through a logic FALSE). Other information (i.e., integer data type) can be as well carried to the SCADA from other protective devices, such as under/over-voltage sensors, temperature sensors (i.e., to acknowledge the states of electrical cables overheating), and power factor recorders.

The SCADA in turns gather the processed acquainted data with a distinguishing algorithm between the two-sided faults zones in the PV system's regions, and set accordingly the corresponding needed fault alarms, signals, and switching mechanisms to declare the detected fault. The obtained fault type can be graphically represented on a Liquid Crystal Display (LCD) or any Human Machine Interface (HMI), with an ability to set sirens for heavy/risky faults. Accordingly, the bottom line of the suggested AC-DC dual fault diagnostic tool for PV systems consists of network addressable protective switchgear for both sides of the PV systems, connected (database-wise) to a SCADA (that can be programmed via visual basic application for example) through a data block carrier over the same network. Each zone of the PV system can be uniquely graphed, where each protective device would have its own representative graphical images, that is to be animated according to the real-time status of the device (i.e., intermittent red colored animations denote the presence of a short circuit, where static green colors indicate a non-tripping mechanism, for example). With the aforementioned suggested architecture, such fault diagnostic tool can be set to be controlled by means of programmable logic controllers, which in turn can be remotely accessed via webservers, thus enabling the ability for PV system fault detection/monitoring from smartphones.

The proceeding step which comes after the fault identification and detection is the corresponding fault maintenance technique, that is classified under four different topologies [280], for different types of PV cell raw materials [281]:

- Corrective maintenance
- Urgent case maintenance
- Preventive maintenance
- Predictive maintenance

Table 9 encapsulates a comparative characterization of different PV maintenance techniques. The different PV faults acknowledgment, with various fault detection methods, and fault maintenance represent a complete package, which yields in a more robust performance for PV systems.

Table 9: Overview of different maintenance methods [280]

Maintenance strategy	Description	Goals
Corrective	Takes place after a failure event, and includes fixing, repairing, replacing and other correction tasks	Make corrections to avoid major equipment damaging
Urgent case	Takes places after a major force event, and requires fixing, replacing and other correction tasks	Make corrections in a hurry, prior to anything else to prevent bigger damages
Predictive	Evaluates the conditions of the system by performing scheduled/continuous real-time monitoring	Predict the optimal time to perform maintenance and hence elevating the equipment uptime
Preventive	Performs maintenance on a pre-scheduled time interval regardless of the condition	Reduce the possibility of any failure

6. Conclusions

PV systems are a lifetime investment with a great cost of installation. In order to grant the predicted energy saving during a PV system's lifecycle, and to ensure a reliable payback period, the PV system is assumed to work optimally, with no faults occurrence. However, PV systems often interact with various faulty scenarios that reduce their competencies and prohibit their cost effectiveness.

Throughout this paper, the different PV faults were classified as either internal, external, or electrical faults. Internal faults are mainly due to the manufacturer's defects: the impurities in the PV cells raw material, as well as the low semiconductor's quality used during the fabrication process, yield eventually to further complications under the operation of the PV system. With that being said, their probability of occurrence is indirectly proportional to the fabrication's quality class (i.e., higher PV raw materials reflect lower probability of internal faults occurrence), where they affect the performance of the PV system from its DC side. On the other hand, external faults are directly related to undesired environmental conditions: weather fluctuations, accumulation of dust, soil, and snow, for example, affect the proper functioning of PV system also from its DC side: the PV cells are not able as supposedly to convert light into a DC voltage, due either to the presence of physical obstacles (i.e., temporary mismatch faults), or to the damage induced on the level of the PV modules (i.e., permanent mismatch faults). External faults are the most common for PV systems, mainly due to the chaotic and random aspects of the PV systems' environmental surroundings In addition, electrical fault can affect both the DC and the AC sides of the PV system: possessing a spontaneous criteria, electrical faults provoke abnormal quantities of currents (i.e., in the events of short circuits) and voltages (i.e., in the event of open circuits, voltage superimposing, etc.), thus affecting furtherly the load dissipation, as well as the safety of the wiring circuits.

The presented PV fault characterization helped in investigating the applicability of a corresponding fault detection system on both sides of a PV system. The DC-sided fault detection methods, on the first hand, in majority rely on sensory data acquisition- the statistical monitoring methods for example collect the PV performance data, that when compared to a reference, a fault can be detected. Electrical based methods are the most abundant in the literature, where such methods can detect each of the three major types of faults. Signal processing and ML based techniques are the most complex, since they imply on waveforms interpretation and data mining respectively. The easiest DC detection methods correspond to IMR, HET, CDIT, In/ThI, EI, UIM, LIT, since they are based only on installing readily available hardware. For that, such techniques, when incorporated with a SCADA, would present the most efficient and reliable PV fault detection method at the DC side of a PV system. .

As concerning the PV fault detection methods at the AC side of the PV system, unlike AIT and RDM based methods that are complex to implement and require heavy computational facilities respectively, the IDT, RCD, GFDI have more priority for installation in a PV system, while at the same time being the easiest to adapt: higher reliability is presented using these techniques, since they rely only on ready equipment. The keynote is that newer RCD and GFDI and other relevant equipment are fabricated with a small embedded system in each, where they can be address assigned and remote controlled (i.e., networked). With that being said, such devices can be graphically assigned to the SCADA, in a way that when an RCD trips for example, a site operator can graphically visualize this issue, directly locate the source of error, and be able to send remote alarms for further fault acknowledgment. Therefore, through this paper, it has been seen that a dual AC-DC fault detection system can be easily applied to a PV system, simply by the usage of fault indicator devices (e.g., RCD, RCBO, MCB, LIT, etc.) that possess the feature of remote addressing (e.g., through local area network, peer-to-peer communication, etc.). Such devices, hence, serving on both sides of the PV system, can be thus reflected to a visual SCADA which also have its own set of data blocks to be networked with. The tripping mechanisms can be hence inspected remotely, while directly localizing the source of error, for further on-site commissioning.

The reliability, durability, and sustainability of PV systems are greatly improved by continuous monitoring, and faults' identification processes. When equipped with fault detecting tools, like the one suggested in this paper, PV systems ensure robust power production, and a safer performance.

7. References

[1] R. Venkateswari, S. Sreejith. 2019. Factors influencing the efficiency of photovoltaic systems. Renewable and Sustainable Energy Reviews. 101, 376-94.

[2] S. Sulaemany, E. Brown, R. Quispe-Abad, N. Muller. 2019. Floating PV system as an alternative pathway to the amazon dam underproduction. Renewable and Sustainable Energy Reviews. 135, 1-5.

[3] K.K. Jaiswal, C.R. Chowdhury, D. Yadav, R. Verma, S. Dutta, K.S. Jaiswal, SangmeshB, K.S.K. Karuppasamy. 2022. Renewable and sustainable clean energy development and impact on social, economic, and environmental health. Energy Nexus. 7, Article ID: 100118.

[4] M.H. Shubbak. 2019. Advances in solar photovoltaics: Technology review and patent trends. Renewable and Sustainable Energy Reviews. 115, 1-5.

[5] M. Adar, M.-A. Babay, S. Touairi, Y. Najih, M. Mabrouki. 2022. Experimental validation of different PV power prediction models under Beni Mellal climate, implications for the energy nexus. Energy Nexus. 5, Article ID: 100050.

[6] N. Yarar, M. Yagci, S. Bahceci, A. Onen, T.S. Ustun. 2023. Artificial neural networks based harmonics estimation for real university microgrids using hourly solar irradiation and temperature data. Energy Nexus. 9, Article ID: 100172.

[7] M. Dida, S. Boughali, D. Bechki, H. Bouguettaia. 2020. Output power loss of crystalline silicon photovoltaic modules due to dust accumulation in Saharan environment. Renewable and Sustainable Energy Reviews. 124, 1-3.

[8] A. Juaidi, H.H. Muhammad, R. Abdallah, R. Abdalhaq, A. Albatayneh, F. Kawa. 2022. Experimental validation of dust impact on-grid connected PV system performance in Palestine: An energy nexus perspective. Energy Nexus. 6, Article ID: 100082.

[9] T.K. Roy, M.A.H. Pramanik, S.K. Ghosh. 2022. Design of an integral terminal-based sliding mode controller for PV and BESS-based DC microgrids. Energy Nexus. 7, Article ID: 100130.

[10] K. Osmani, A. Haddad, T. Lemenand, B. Castanier, M. Ramadan. 2021. An investigation on maximum power extraction algorithms from PV systems with corresponding DC-DC converters. Energy. 224, Article ID: 120092.

[11] K. Osmani, A. Haddad, H. Jaber, T. Lemenand, B. Castanier, M. Ramadan. 2022. Mitigating the effects of partial shading on PV system's performance through PV array reconfiguration: A review. Thermal Science and Engineering Progress. 31, Article ID: 101280.

[12] K. Osmani, M. Ramadan, A. Haddad, T. Lemenand, B. Castanier. 2022. An Overview on the Use of Phase Change Material (PCM) for PV cooling. Key Engineering Materials. 922, 3-9.

[13] K. Osmani, M. Ramadan, T. Lemenand, B. Castanier, A. Haddad. 2021. Optimization of PV array tilt angle for minimum levelized cost of energy. Computers & Electrical Engineering. 96, Part A, Article ID: 107474.

[14] S.R. Madeti, S.N. Singh. 2017. Monitoring system for photovoltaic plants: A review. Renewable and Sustainable Energy Reviews. 67, 1180-207.

[15] P. Hacke, S. Lokanath, P. Williams, A. Vasan, P. Sochor, G.S.T. Mani, H. Shinohara, S. Kurtz. 2018. A status review of photovoltaic power conversion equipment reliability,

safety, and quality assurance protocols. Renewable and Sustainable Energy Reviews. 82, 1097-112.

[16] S. Shivashankar, S. Mekhilef, H. Mokhlis, M. Karimi. 2016. Mitigating methods of power fluctuations of photovoltaic (PV) sources – A review. Renewable and Sustainable Energy Reviews. 59, 1170-84.

[17] A. Colli. 2015. Failure mode and effect analysis for photovoltaic systems. Renewable and Sustainable Energy Reviews. 50, 804-9.

[18] A. Dhoke, R. Sharma, T.K. Saha. 2019. An approach for fault detection and location in solar PV systems. Solar Energy. 194, 197-208.

[19] T. Pei, J. Zhang, L. Li, X. Hao. 2020. A fault locating method for PV arrays based on improved voltage sensor placement. Solar Energy. 201, 279-97.

[20] Y. Zhao, B. Lehman, J.F. de Palma, J. Mosesian, R. Lyons. 2011. Fault analysis in solar PV arrays under: Low irradiance conditions and reverse connections. In: Proceedings of the 37th photovoltaic specialists' conference (PVSC), IEEE. pp. 2-4.

[21] M. Davarifar, A. Rabhi, A. El-hajjaji. 2013. Comprehensive modulation and classification of faults and analysis their effect in DC side of photovoltaic system. Energy and Power Engineering. 5, 230-36.

[22] A. Triki-Lahiani, A.B.B. Abdelghani, I. Slama-Belkhodja. 2018. Fault detection and monitoring systems for photovoltaic installations: A review. Renewable and Sustainable Energy Reviews. 82, 2680-92.

[23] E. Diaz-Dorado, J. Cidras, C. Carrillo. 2017. Discretized model for partially shaded PV arrays composed of PV panels with overlapping bypass diodes. Solar Energy. 157, 103-15.

[24] S.N. Deshkar, S.B. Dhale, J.S. Mukherjee, T.S. Babu, N. Rajasekar. 2015. Solar PV array reconfiguration under partial shading conditions for maximum power extraction using genetic algorithm. Renewable and Sustainable Energy Reviews. 43, 102–10.

[25] B.I. Rani, G.S. Ilango, C. Nagamani. 2013. Enhanced power generation from PV array under partial shading conditions by shade dispersion using Su Do Ku configuration. IEEE Transactions on Sustainable Energy. 4, 594–601.

[26] J.P. Ram, N. Rajasekar. 2017. A new global maximum power point tracking technique for solar photovoltaic (PV) system under partial shading conditions (PSC). Energy. 118, 512–25.

[27] J.P. Ram, N. Rajasekar. 2017. A novel flower pollination based global maximum power point method for solar maximum power point tracking. IEEE Transactions on Power Electronics. 32, 8486–99.

[28] X.H. Nguyen. 2015. Matlab/Simulink based modeling to study effect of partial shadow on solar photovoltaic array. Environmental Systems Research. 4, 1-5.

[29] Y. Hu, J. Zhang, W. Cao, J. Wu, G.Y. Tian, S.J. Finney, J.L. Kirtley. 2015. Online two section PV array fault diagnosis with optimized voltage sensor locations. IEEE Transactions on Industrial Electronics. 62, 7237–46.

[30] N. Heidari, J. Gwamuri, T. Townsend, J.M. Pearce. 2015. Impact of snow and ground interference on photovoltaic electric system performance. IEEE Journal of Photovoltaics. 5, 1680–85.

[31] M.S. Arani, M. Akhavanhejazi. 2016. The Comprehensive Study of Electrical Faults in PV Arrays. Journal of Electrical and Computer Engineering. Article ID: 8712960.

[32] A.M. Omer. 2007. Renewable energy resources for electricity generation in Sudan. Renewable and Sustainable Energy Reviews. 11, 1481–97.

[33] V. Sharma, S.S. Chandel. 2013. Performance and degradation analysis for long term reliability of solar photovoltaic systems: a review. Renewable and Sustainable Energy Reviews. 27, 753–67.

[34] D.S. Pillai, N. Rajasekar. 2018. A comprehensive review on protection challenges and fault diagnosis in PV systems. Renewable and Sustainable Energy Reviews. 91, 18-40.

[35] H. Liu, M. Mitolo, J. Qiu. 2013. Ground-fault loop impedance calculations in low-voltage single-phase systems. IEEE Transactions on Industry Applications. 50, 1331-37.

[36] W.I. Bower, J.C. Wiles. 1994. Analysis of grounded and ungrounded photovoltaic systems. Proceedings of 1994 IEEE 1st World Conference on Photovoltaic Energy Conversion - WCPEC. IEEE. pp. 809–12.

[37] D.E. Collier, T.S. Key. 2002. Electrical fault protection for a large photovoltaic power plant inverter. Conference Record of the Twentieth IEEE Photovoltaics Specialists Conference.

[38] S.E. Forman. 1982. Performance of experimental terrestrial photovoltaic modules. IEEE Transactions on Reliability. 31, 235–45.

[39] Y. Zhao, R. Lyons. 2011. Ground-fault analysis and protection in PV arrays. Proceedings of Photovoltaics Protection. pp: 1–4.

[40] A. McEvoy, T. Markvart, L. Castaner. 2011. Practical handbook of photovoltaics: fundamentals and applications, 2nd edition. Elsevier.

[41] M.K. Alam, F. Khan, J. Johnson, J. Flicker. 2015. A comprehensive review of catastrophic faults in PV arrays: types, detection, and mitigation techniques. IEEE Journal of Photovoltaics. 5, 982–97.

[42] M. Cotterell. 2012. Installation guidelines: electrical. Practical Hand book of Photovoltaics, 2nd edition, chapter 3. pp. 819–34.

[43] Y. Zhao, J.F. de Palma, J. Mosesian, R. Lyons, B. Lehman. 2012. Line-Line Fault Analysis and Protection Challenges in Solar Photovoltaic Arrays. IEEE Transactions on Industrial Electronics. 60, 3784-95.

[44] D.S. Pillai, R. Natarajan. 2019. A Compatibility Analysis on NEC, IEC, and UL Standards for Protection Against Line-Line and Line-Ground Faults in PV Arrays. IEEE Journal of Photovoltaics. 9, 864-71.

[45] S.R. Madeti, S.N. Singh. 2017. A comprehensive study on different types of faults and detection techniques for solar photovoltaic system. Solar Energy. 158, 161-85.

[46] K.M. Armijo, J. Johnson, M. Hibbs, A. Fresquez. 2014. Characterizing fire danger from low power PV arc-faults. 2014 IEEE 40th Photovoltaic Specialist Conference (PVSC). IEEE.

[47] J. Johnson, J. Kang. 2012. Arc-fault detector algorithm evaluation method utilizing prerecorded arcing signatures. 2012 38th IEEE Photovoltaic Specialist Conference. IEEE. pp. 1378–82.

[48] J. Flicker, J. Johnson. 2013. Electrical simulations of series and parallel PV arc-faults. 2013 IEEE 39th Photovoltaic Specialist Conference (PVSC). IEEE. pp. 3165–72.

[49] D.A. Dini, P.W. Brazis, K.H. Yen. 2012. Development of arc-fault circuit-interrupter requirements for photovoltaic systems. 2011 37th IEEE Photovoltaic Specialist Conference. IEEE. pp. 1790–94.

[50] F. Chan, H. Calleja. 2006. Reliability: A new approach in design of inverters for PV systems. 2006 IEEE International Power Electronics Congress. IEEE. pp. 1–6.

[51] A. Omazic, G. Oreski, M. Halwachs, G.C. Eder, C. Hirschl, L. Neumaier, G. Pinter, M. Erceg. 2019. Relation between degradation of polymeric components in crystalline silicon PV module and climatic conditions: A literature review. Solar Energy Materials and Solar Cells. 192, 123-33 .

[52] K. Osmani, A. Haddad, M. Alkhedher, T. Lemenand, B. Castanier, M. Ramadan. 2023. A Novel MPPT-Based Lithium-Ion Battery Solar Charger for Operation under Fluctuating Irradiance Conditions. Sustainability. 15(12), Article ID: 9839.

[53] Z. Alam, L. Khan, Q. Khan, S. Ullah, S. Ahmed, M.A. Khan. 2020. Integrated Fault-Diagnoses and Fault-Tolerant MPPT Control Scheme for a Photovoltaic System. 2019 15th International Conference on Emerging Technologies (ICET). IEEE. pp. 2-5.

[54] K. Osmani, M. Alkhedher, M. Ramadan, D.S. Choi, L.K.B. Li, M.H. Doranehgard, A.-G. Olabi. 2023. Recent progress in the thermal management of lithium-ion batteries. Journal of Cleaner Production. 389, Article ID: 136024.

[55] K.-H. Chao, C.-T. Chen. 2017. A remote supervision fault diagnosis meter for photovoltaic power generation systems. Measurement. 104, 93-104.

[56] R. Benkercha, S. Moulahoum. 2018. Fault detection and diagnosis based on C4.5 decision tree algorithm for grid connected PV system. Solar Energy. 173, 610-34.

[57] W. Chine, A. Mellit, A.M. Pavan, S.A. Kalogirou. 2014. Fault detection method for grid-connected photovoltaic plants. Renewable Energy. 66, 99-110.

[58] M. Tadj, K. Benmouiza, A. Cheknane, S. Silvestre. 2014. Improving the performance of PV systems by faults detection using GISTEL approach. Energy Conversion and Management. 80, 298-304.

[59] S. Lu, B.T. Phung, D. Zhang. 2018. A comprehensive review on DC arc faults and their diagnosis methods in photovoltaic systems. Renewable and Sustainable Energy Reviews. 89, 88-98.

[60] W. Chine, A. Mellit, V. Lughi, A. Malek, G. Sulligoi, A.M. Pavan. 2016. A novel fault diagnosis technique for photovoltaic systems based on artificial neural networks. Renewable Energy. 90, 501-12

[61] A. Hazra, S. Das, M. Basu. 2017. An efficient fault diagnosis method for PV systems following string current. Journal of Cleaner Production. 154, 220-32

[62] Y. Wue, Z. Chen, L. Wu, P. Lin, S. Cheng, P. Lu. 2017. An Intelligent Fault Diagnosis Approach for PV Array Based on SA-RBF Kernel Extreme Learning Machine. Energy Procedia. 105, 1070-76.

[63] M. De Bendetti, F. Leonardi, F. Messina, C. Santoro, A. Vasilakos. 2018. Anomaly Detection and Predictive Maintenance for photovoltaic systems. Neuro Computing, 310, 59-68

[64] H. Mekki, A. Mellit, H. Salhi. 2016. Artificial neural network-based modelling and fault detection of partial shaded photovoltaic modules. Simulation Modelling Practice and Theory. 67, 1-13.

[65] M. Dhimish, V. Holmes, B. Mehrdadi, M. Dales. 2018. Comparing Mamdani Sugeno fuzzy logic and RBF ANN network for PV fault detection. Renewable Energy. 117, 257-74.

[66] F.A.O. Polo, J.F. Bermejo, J.C.G. Fernandez, A.C. Marquez. 2015. Failure mode prediction and energy forecasting of PV plants to assist dynamic maintenance tasks by ANN based models. Renewable Energy. 81, 227-38.
[67] S.R. Madeti, S.N. Singh. 2018. Modeling of PV system based on experimental data for fault detection using kNN method. Solar Energy. 173, 139-51.
[68] T. Shimakage , K. Nishioka, H. Yamane, M. Nagura, M. Kudo. 2011. Development of fault detection system in PV system. Proceedings of 33rd international telecommunications energy conference (INTELEC). IEEE. pp. 1–5.
[69] X. Xu, H. Wang, X. Xu, Y. Zuo. 2011. Method for diagnosing photovoltaic array fault in solar photovoltaic system. Proceedings of Asia-Pacific power and energy engineering conference (APPEEC). IEEE. pp. 1–5.
[70] M. Omana, D. Rossi, G. Collepalumbo, C. Metra, F. Lombardi. 2012. Faults affecting the control blocks of PV arrays and techniques for their concurrent detection. Proceedings of international symposium on defect and fault tolerance in VLSI and nanotechnology systems (DFT). IEEE. pp. 199–204.
[71] N. Gokmen, E. Karatepe, B. Celik, S. Silvestre. 2012. Simple diagnostic approach for determining of faulted PV modules in string based PV arrays. Solar Energy. 86, 3364–77.
[72] S. Silvestre, M.A. da Silva, A. Chouder, D. Guasch, E. Karatepe. 2014. New procedure for fault detection in grid connected PV systems based on the evaluation of current and voltage indicators. Energy Conversion Management. 86, 241–9.
[73] X. Lin, Y. Wang, M. Pedram, J. Kim, N. Chang. 2013. Designing fault-tolerant photovoltaic systems. IEEE Design & Test. 31, 76–84.
[74] Y. Hu, J. Zhang, W. Cao, J. Wu, G.Y. Tian, S.J. Finney, J.L. Kirtley. 2015. Online two-section PV array fault diagnosis with optimized voltage sensor locations. IEEE Transactions on Industrial Electronics. 62, 7237–46.
[75] M. Alajmi, I. Abdel-Qader. 2016. Fault detection and localization in solar photovoltaic arrays using the current-voltage sensing framework. Proceedings of international conference on electro information technology (EIT). IEEE. pp. 307–12.
[76] R. Hariharan, M. Chakkarapani, G.S. Ilango, C. Nagamani. 2016. A method to detect photovoltaic array faults and partial shading in PV systems. IEEE Journal of Photovoltaics. 6, 1278–85.
[77] M. Bressan, Y. El-Basri, C. Alonso. 2015. A new method for fault detection and identification of shadows based on electrical signature of defects. In: Proceedings of the 17th European conference on power electronics and applications (EPE'15 ECCE-Europe). IEEE. pp. 1–8.
[78] E. Garoudja, K. Kara, A. Chouder, S. Silvestre, S. Kichou. 2016. Efficient fault detection and diagnosis procedure for photovoltaic systems. In: Proceedings of the 8th international conference on modelling, identification and control (ICMIC). IEEE. pp. 851–6.
[79] A. Dhoke, R. Sharma, T.K. Saha. 2018. PV module degradation analysis and impact on settings of overcurrent protection devices. Solar Energy. 160, 360–7.
[80] D. Kastha, B.K. Bose. 1994. Investigation of fault modes of voltage-fed inverter for induction motor drive. IEEE Transactions on Industrial Applications. IEEE. 30, 1028-38.

[81] J.H. Choi, S. Kim, D.S. Yoo, K.H. Kim. 2015. A diagnostic method of simultaneous open-switch faults in inverter-fed linear induction motor drive for reliability enhancement. IEEE Transactions on Industrial Electronics. IEEE. 62, 4065-77.
[82] A.R. Haitham, S.K.M. Ahmed, A. Iqbal, M. Rahimian, H.A. Toliyat. 2010. Incipient bearing fault diagnostics for inverter fed induction motor drive using ANFIS. Electrical Machines (ICEM) International Conference. IEEE. pp. 1-5.
[83] Q.T. An, L.Z. Sun, K. Zhao, L. Sun. 2011. Switching function model-based fast-diagnostic method of open-switch faults in inverters without sensors. IEEE Transactions on Power Electronics. 126, 119-26.
[84] X. Zhang. 2015. A new diagnostic method of open switch faults in inverters using sliding mode observer and MLD model. 2015 IEEE Magnetics Conference (INTERMAG). IEEE. pp. 1-2.
[85] A. Babel, A. Muetze, R. Seebacher, K. Krischan, E.G. Strangas. 2014. Condition monitoring and failure prognosis of IGBT inverters based on on-line characterization. 2015 IEEE 2nd conference Future Energy Electronics Conference (IFEEC). IEEE. pp. 1-7.
[86] S.C. Yang. 2015. On-line stator turn fault detection for inverter-fed electric machines using neutral point voltage differences. 2015 IEEE 2nd International, Future Energy Electronics Conference (IFEEC). IEEE. pp. 1-7.
[87] R. Riberio, C. Jacobina, E. Da Silva, A. Lima. 2003. Fault detection of open-switch damage in voltage-fed PWM motor drive systems. IEEE Transactions on Power Electronics. IEEE. 18, 587-93.
[88] F.W. Fuchs. 2003. Some diagnosis methods for voltage source inverters in variable speed drives with induction machines-A survey. Proceedings of IEEE/IE Annual Meeting. IEEE. pp. 1378-85.
[89] V.F. Pires, D. Foito, T.G. Amaral. 2015. Fault detection and diagnosis in a PV grid-connected T-type three level inverter. International Conference on Renewable Energy Research and Applications (ICRERA). IEEE. pp. 1-5.
[90] O.J. Aworo, A. Kwasinski. 2018. Fault Detection Strategy for Grid-Tie Three-Phase Photovoltaic Inverter. International Conference on Renewable Energy Research and Applications (ICRERA). IEEE. pp. 1-6.
[91] A.F. Ebrahim, T. Youssef, S.M.W. Ahmed, S.E. Elmasry, O.A. Mohammed. 2014. Fault detection and compensation for a PV system grid tie inverter. North American Power Symposium (NAPS). IEEE. pp. 1-6.
[92] Z. Li, T. Peng, J. Yang, Z. Lin, P. Zhang. 2014. Open fault detection for interleaved flyback micro-inverter based on state observer. Proceedings of the 33rd Chinese Control Conference. IEEE. pp. 1-4.
[93] Z. Huang, Z. Wang, H. Zhang. 2018. Multiple Open-Circuit Fault Diagnosis Based on Multistate Data Processing and Subsection Fluctuation Analysis for Photovoltaic Inverter. Transactions on Instrumentation and Measurement. IEEE. 67, 516-26.
[94] M. Dong, H. Dong, L. Wang, J. Yang, L. Li, Y. Wang. 2017. A Simple Open-Circuit Detection Strategy for a Single-Phase Grid-Connected PV Inverter Fed From Power Optimizers. Transactions on Power Electronics. IEEE. 33, 2798-802.
[95] J.A.P. Sanchez, D.U. Campos-Delgado, D.R. Espinoza-Trejo, A.A. Valdez-Fernandez, C.H. De Angelo. 2019. Fault diagnosis in grid-connected PV NPC inverters by a model-based and data processing combined approach. Power Electronics. IET. 12, 3254-64.

[96] R. Peuget, S. Courtine, J. Rognon. 1998. Fault detection and isolation on a PWM inverter by knowledge-based model. IEEE Transactions on Industrial Applications. IEEE. 34, 1318-26.
[97] A.C. Renfrew, J.X. Tian. 1993. The use of a knowledge-based system in power electronic circuit fault diagnosis. Proceedings of the 5th European conference on Power Electronics & Applications, Brighton, UK. pp. 57-62.
[98] C. Hang, L. Ying, N. Shu. 2018. Transistor open-circuit fault diagnosis in two-level three-phase inverter based on similarity measurement. Microelectronics Reliability. 91, 291-97.
[99] C. Yong, J.J. Zhang, Z.Y. Chen. 2020. Current observer-based online open-switch fault diagnosis for voltage-source inverter. ISA Transactions. 99, 445-53.
[100] M. Wang, J. Zhao, F. Wu, H. Yang. 2017. Transistor open-circuit fault diagnosis of three phase voltage-source inverter fed induction motor based on information fusion. 12th IEEE Conference on Industrial Electronics and Applications (ICIEA). IEEE. pp. 1-4.
[101] H. Weiwei, Q. Jin, M. Haowen, S. Yufeng. 2012. Information fusion method in fault modes. 2012 IEEE Conference on Prognostics and System Health Management (PHM). IEEE. pp. 1-5.
[102] Z. Yao, H. Pan. 2014. Engine fault diagnosis based on the weighted DS evidence theory. IEEE 7th International Workshop on Computational Intelligence and Applications (IWCIA). IEEE. pp. 219-23.
[103] Z. Lin, Z. Feng, Z. Xiao, Q. Zhong. 2010. Method of analog circuits fusion diagnosis based on BP network and DS theory. 2010 6th International Conference on Natural Computation. IEEE. pp. 389-93.
[104] K. Rothenhagen, F.W. Fuchs. 2005. Performance of diagnosis methods for IGBT open circuit faults in three phase voltage source inverters for ac variable speed drives. 2005 European Conference on Power Electronics and Applications. IEEE. pp. 1-10.
[105] H. Yan, Y. Xu, F. Cai, H. Zhang, W. Zhao, C. Gerada. 2019. PWM-VSI fault diagnosis for a PMSM drive based on the fuzzy logic approach. IEEE Transactions on Power Electronics. IEEE. 34, 759-68.
[106] N.M.A. Freire, J.O. Estima, A.J.M. Cardoso. 2011. Multiple open-circuit fault diagnosis in voltage-fed PWM motor drives using the current park's vector phase and the currents polarity. 8th IEEE Symposium on Diagnostics for Electrical Machines, Power Electronics & Drives. IEEE. pp. 1-5.
[107] R.P.S. Ventura, A.M.S. Mendes, A.J.M. Cardoso. 2011. Fault detection in multilevel cascaded inverter using park's vector approach with balanced battery power usage. Proceedings of the 2011 14th European Conference on Power Electronics and Applications. IEEE. pp. 2-4.
[108] D.U. Campos-Delgado, D.R. Espinoza-Trejo. 2010. An Observer-Based Diagnosis Scheme for Single and Simultaneous Open-Switch Faults in Induction Motors Drives. IEEE Transactions on Industrial Electronics. IEEE. 58, 671-79.
[109] S.M. Jung, J.S. Park, H.W. Kim, K.Y. Cho, M.J. Yoon. 2012. An MRAS-Based Diagnosis of Open-Circuit Fault in PWM Voltage-Source Inverters for PM Synchronous Motor Drive Systems. IEEE Transactions on Power Electronics. IEEE. 28, 2514-26.
[110] S. Karimi, A. Gaillard, P. Poure, S. Saadate. 2008. FPGA-Based Real-Time Power Converter Failure Diagnosis for Wind Energy Conversion Systems. IEEE Transactions on Industrial Electronics. 55, 4299-308.

[111] R.L.A. Ribeiro, C.B. Jacobina, E.R.C. da Silva, A.M.N. Lima. 2003. Fault detection of open-switch damage in voltage-fed PWM motor drive systems. IEEE Transactions on Power Electronics. IEEE. 18, 587-93.
[112] O.S. Yu, N.J. Park, D.S. Hyun. 2006. A novel fault detection scheme for voltage fed PWM inverter. Proceedings of Industrial Electronics Society Conference. pp. 2654-59.
[113] A.Q.T. Sun, L.Z. Zhao, K.L. Sun. 2011. Switching function model based fast diagnostic method of open-switch faults in inverters without sensors. IEEE Transactions on Power Electronics. 26, 119-26.
[114] M. Trabelsi, M. Boussak, M. Gossa. 2012. PWM-switching pattern-based diagnosis scheme for single and multiple open-switch damages in VSI-fed induction motor drives. ISA Transactions. 51, 333-44.
[115] M. Trabelsi, M. Boussak, P. Mestre, M. Gossa. 2011. An improved diagnosis technique for IGBTs open-circuit fault in PWM-VSI-fed induction motor drive. Proceedings of International Symposium on Industrial Electronics Conference. pp. 2111-17.
[116] U.M. Choi, H.G. Jeong, K.B. Lee, F. Blaabjerg. 2012. Method for detecting an open-switch fault in a grid-connected NPC inverter system. IEEE Transactions on Power Electronics. 27, 2726-39.
[117] A.M.S. Mendes, A.J.M. Cardoso. 1999. Fault diagnosis in a rectifier-inverter system used in a variable speed ac drives, by the average current Park's vector approach. Proceedings of European Conference on Power Electronics and Applications. pp. 1-9.
[118] S. Abramik, W. Sleszynski, J. Nieznanski, H. Piquet. 2003. A diagnostic method for on-line fault detection and localization in VSI-fed ac drives. Proceedings of European Conference on Power Electronics and Applications. pp. 2-4.
[119] K. Rothenhagen, F.W. Fuchs. 2004. Performance of diagnosis methods for IGBT open-circuit faults in voltage source active rectifiers. Proceedings of Power Electronics Specialists Conference. pp. 4348-54.
[120] X. Chen, J. Liu, Z. Deng, S. Song, S. Du, D. Wang. 2020. A diagnosis strategy for multiple IGBT open-circuit faults of modular multilevel converters. IEEE Transactions on Power Electronics. 36, 191-203.
[121] I.J. Balaguer-Alvarez, E.I. Ortiz-Rivera. 2010. Survey of distributed generation islanding detection methods. IEEE Latin America Transactions. 8, 565–70.
[122] A. Llaria, O. Curea, J. Jimenez, H. Camblong. 2009. Survey on Microgrids: analysis of technical limitations to carry out new solutions. Power Electronics and Applications, EPE'09. 13th European Conference. pp. 1–8.
[123] A. Timbus, A. Oudalov, C.N. Ho. 2010. Islanding detection in smart grids. Energy Conversion Congress and Exposition (ECCE). pp. 3631–37.
[124] P. Mahat, Z. Chen, B. Bak-Jensen. 2008. Review of islanding detection methods for distributed generation. Electric Utility Deregulation and Restructuring and Power Technologies, DRPT Third International Conference. pp. 2743–2748.
[125] R.S. Kunte, W. Gao. 2008. Comparison and review of islanding detection techniques for distributed energy resources. Power Symposium, NAPS'08. 40th North American. pp. 1–8.
[126] M. Ezzt, M.I. Marei, M. Abdel-Rahman, M.M. Mansour. 2007. A hybrid strategy for distributed generators islanding detection. 2007 IEEE Power Engineering Society Conference and Exposition in Africa, PowerAfrica. IEEE. pp. 1–7.

[127] S.P. Chowdhury, S. Chowdhury, P.A. Crossley. 2009. Islanding protection of active distribution networks with renewable distributed generators: A comprehensive survey. Electric Power Systems Research. 79, 984–92.
[128] F. Coffele, P. Moore, C. Booth, A. Dysko, G. Burt, T. Spearing, P. Dolan. 2010. Centralised Loss of Mains protection using IEC-61850. Developments in Power System Protection. IET. pp. 3-5.
[129] H.H. Zeineldin, E.F. El-Saadany, M.M. Salama. 2006. Impact of DG interface control on islanding detection and non-detection zones. IEEE Transactions on Power Delivery. 21, 1515–23.
[130] W. Hu, Y.L. Sun. 2009. A compound scheme of islanding detection according to inverter. Power and Energy Engineering Conference, Asia-Pacific. pp. 1–4.
[131] G. Yin. 2005. A distributed generation islanding detection method based on artificial immune system. In: Transmission and Distribution Conference and Exhibition: Asia and Pacific. IEEE/PES. pp. 1–4.
[132] S.I. Jang, K.H. Kim. 2004. An islanding detection method for distributed generations using voltage unbalance and total harmonic distortion of current. IEEE Transactions on Power Delivery. 19, 745–52.
[133] R.R.S. de Oliveira, H.M. Monteiro, R.R. Alexio, L.R.M. Silva, C.A. Duque. 2017. Islanding detection using impedance measurements techniques based on wavelet injection. 2017 Brazilian Power Electronics Conference (COBEP). IEEE. pp. 1-5.
[134] P. Mahat, Z. Chen, B. Bak-Jensen. 2011. Review on islanding operation of distribution system with distributed generation. Power and Energy Society General Meeting. IEEE. pp. 1–8.
[135] H.J. Kim, D.H. Kim, B.M. Han. 2015. Islanding detection method with negative-sequence current injection under unbalanced voltage grid. International Future Energy Electronics Conference (IFEEC). IEEE. pp. 1-5.
[136] P.P. Vergara, J.M. Rey, H.R. Shaker, J.M. Guerrero, B.N. Jorgensen, L.C.P. da Silva. 2018. Distribution Strategy for Optimal Dispatch of Unbalanced Three-Phase Islanded Microgrids. Transactions on Smart Grid. IEEE. 10, 3210-25.
[137] N. Liu, A.S. Aljankawey, C.P. Diduch, L. Chang, M. Mao, P. Yazdkhasti, J. Su. 2014. Performance evaluation for grid impedance based islanding detection method. International Power Electronics Conference (IPEC-Hiroshima 2014 – ECCE Asia). IEEE. pp. 1-5.
[138] M. Ropp, J. Ginn, J. Stevens, W. Bower, S. Gonzalez. 2006. Simulation and experimental study of the impedance detection anti-islanding method in the single-inverter case. Photovoltaic Energy Conversion, Conference Record of the IEEE 4th World Conference. 2, pp. 2379–82.
[139] F. Liu, Y. Kang, Y. Zhang, S. Duan, X. Lin. 2010. Improved SMS islanding detection method for grid-connected converters. IET Renewable Power Generation 4, 36–42.
[140] V. Menon, M.H. Nehrir. 2007. A hybrid islanding detection technique using voltage unbalance and frequency set point. IEEE Transactions on Power Systems. IEEE. 22, 442–48.
[141] G.K. Hung, C.C. Chang, C.L. Chen. 2003. Automatic phase-shift method for islanding detection of grid-connected photovoltaic inverters. IEEE Transactions on Energy Conversion. IEEE. 18, 169–73.

[142] W.Y. Chang. 2010. A hybrid islanding detection method for distributed synchronous generators. International Power Electronics Conference – ECCE ASIA -. IEEE. pp. 1326–30.
[143] H. Vahedi, R. Noroozian, A. Jalilvand, G.B. Gharehpetian. 2010. Hybrid SFS and Q-f Islanding Detection Method for inverter-based DG. International Conference on Power and Energy. IEEE. pp. 672–76.
[144] R. Polikar. 1999. The story of wavelets. Physics and modern topics in mechanical and electrical engineering. pp. 192–7.
[145] A. Pigazo, V.M. Moreno, M. Liserre, A. Dell'Aquila. 2007. Wavelet-based islanding detection algorithm for single-phase photovoltaic (PV) distributed generation systems. Industrial Electronics, ISIE 2007. IEEE International Symposium. pp. 2409–413.
[146] A. Pigazo, M. Liserre, R.A. Mastromauro, V.M. Moreno, A. Dell'Aquila. 2009. Wavelet based islanding detection in grid-connected PV systems. IEEE Transactions on Industrial Electronics. 56, 4445–55.
[147] P.K. Ray, S.R. Mohanty, N. Kishor, H.C. Dubey. 2010. Coherency determination in grid connected distributed generation based hybrid system under islanding scenarios. Power and Energy (PECon), IEEE International Conference. pp. 85–88.
[148] P.K. Ray, N. Kishor, S.R. Mohanty. 2010. S-transform based islanding detection in grid connected distributed generation based power system. Energy Conference and Exhibition (EnergyCon), IEEE International Conference. pp. 612–17.
[149] S.R. Samantaray, A. Samui, B.C. Babu. 2010. S-transform based cumulative sum detector (CUSUM) for islanding detection in Distributed Generations. Power Electronics, Drives and Energy Systems (PEDES) & 2010 Power India, 2010 Joint International Conference. pp. 1–6.
[150] Y. Zhao, B. Lehman, R. Ball, J. Mosesian, J.F. de Palma. 2013. Outlier detection rules for fault detection in solar photovoltaic arrays. Proceedings of twenty-eighth annual applied power electronics conference and exposition (APEC). IEEE. pp. 2913–20.
[151] Y. Zhao, F. Balboni, T. Arnaud, J. Mosesian, R. Ball, B. Lehman. 2014. Fault experiments in a commercial-scale PV laboratory and fault detection using local outlier factor. Proceedings of 40th photovoltaic specialist conference (PVSC). IEEE. pp. 3398–403.
[152] G. Wang, C.C. Youn, A.M. Stankovic. 2015. DC-side high impedance ground fault detection for transformerless single-phase PV systems. Proceedings of North American power symposium (NAPS). IEEE. pp. 1–6.
[153] I.S. Kim. 2016. On-line fault detection algorithm of a photovoltaic system using wavelet transform. Solar Energy. 126, 137–45.
[154] N.L. Georgijevic, M.V. Jankovic, S. Srdic, Z. Radakovic. 2016. The detection of series arc fault in photovoltaic systems based on the arc current entropy. IEEE Transactions on Power Electronics. IEEE. 31, 5917–30.
[155] K.A. Kim, G.-S. Seo, B.-H. Cho, P.T. Krein. 2016. Photovoltaic hot-spot detection for solar panel substrings using AC parameter characterization. IEEE Transactions on Power Electronics. IEEE. 31, 1121–30.
[156] L. Chen, S. Li, X. Wang. 2016. Quickest fault detection in photovoltaic systems. IEEE Transactions on Smart Grid. IEEE. 9, 1835-47.

[157] Z. Yi, A.H. Etemadi. 2017. Fault detection for photovoltaic systems based on multi-resolution signal decomposition and fuzzy inference systems. IEEE Transactions on Smart Grid. 8, 1274–83.
[158] S. Chen, X. Li. 2016. PV series arc fault recognition under different working conditions with joint detection method. Proceedings of the 62nd Holm conference on electrical contacts (Holm). IEEE. pp. 25–32.
[159] H. Zhu, Z. Wang, R.S. Balog. 2016. Real time arc fault detection in PV systems using wavelet decomposition. Proceedings of 43rd photovoltaic specialists conference (PVSC). IEEE. pp. 1761–6.
[160] S. Dhar, R.K. Patnaik, P.K. Dash. 2017. Fault detection and location of photovoltaic based DC microgrid using differential protection strategy. IEEE Transactions on Smart Grid. IEEE. 9, 4303-12.
[161] Q. Xiong, S. Ji, L. Zhu, L. Zhong, Y. Liu. 2017. A novel DC arc fault detection method based on electromagnetic radiation signal. IEEE Transactions on Plasma Science. 45, 472–8.
[162] B.P. Kumar, G.S. Ilango, M.J. Reddy, N. Chilakapati. 2018. Online fault detection and diagnosis in photovoltaic systems using wavelet packets. IEEE Journal of Photovoltaics. 8, 257–65.
[163] M. Mansouri, A. Al-khazraji, M. Hajji, M.F. Harkat, H. Nounou, M. Nounou. 2018. Wavelet optimized EWMA for fault detection and application to photovoltaic systems. Solar Energy. 167, 125-36.
[164] C. Ventura, G.M. Tina. 2016. Utility scale photovoltaic plant indices and models for on-line monitoring and fault detection purposes. Electric Power Systems Research. 136, 43-56.
[165] S. Silvestre, L. Mona-Lopez, S. Kichou, F. Sanchez-Pacheco, M. Dominguez-Pumar. 2016. Remote supervision and fault detection on OPC monitored PV systems. Solar Energy. 137, 424-33.
[166] M. Dhimish, V. Holmes, M. Dales. 2017. Parallel fault detection algorithm for grid-connected photovoltaic plants. Renewable Energy. 113, 94-111.
[167] P.K. Ray, A. Mohanty, B.K. Panigrahi, P.K. Rout. 2018. Modified wavelet transform based fault analysis in a solar photovoltaic system. Optik. 168, 754-63.
[168] H. Ding, K. Ding, J. Zhang, Y. Wang, L. Gao, Y. Li, F. Chen, Z. Shao, W. Lai. 2018. Local outlier factor-based fault detection and evaluation of photovoltaic system. Solar Energy. 164, 139-48.
[169] F. Harrou, Y. Sun, B. Taghezouit, A. Saidi, M.-E. Hamlati. 2018. Reliable fault detection and diagnosis of photovoltaic systems based on statistical monitoring approaches. Renewable Energy. 116, Part A, 22-37.
[170] S. Nie, X. Pei, Y. Chen, Y. Kang. 2014. Fault diagnosis of PWM DC–DC converters based on magnetic component voltages equation. IEEE Transactions on Power Electronics. 29, 4978–88.
[171] X. Pei, S. Nie, Y. Kang. 2015. Switch short-circuit fault diagnosis and remedial strategy for full-bridge DC–DC converters. IEEE Transactions on Power Electronics. 30, 996–1004.
[172] S.Y. Kim, K. Nam, H.S. Song, H.G. Kim. 2008. Fault diagnosis of a ZVS DC–DC converter based on DC-link current pulse shapes. IEEE Transactions on Industrial Electronics. 55, 1491–94.

[173] W. Sleszynski, J. Nieznanski. 2007. Open-transistor fault diagnostics in voltage-source inverters by analyzing the load currents. Proceedings of International Symposium on Diagnosis for Electric Machines. pp. 70-3.
[174] W. Sleszynski, J. Nieznanski, A. Cichowski. 2009. Open-transistor fault diagnostics in voltage-source inverters by analyzing the load currents. IEEE Transactions on Industrial Electronics. IEEE. 56, 4681-88.
[175] B.G. Park, K.J. Lee, R.Y. Kim, T.S. Kim, J.S. Ryn, D.S. Hyun. 2011. Simple fault diagnosis based on operating characteristic of brushless direct-current motor drives. IEEE Transactions on Industrial Electronics. IEEE. 58, 1586-93.
[176] M.S. Kanniche. 2004. Wavelet-fuzzy based algorithm for condition monitoring of voltage source inverters. Electronics Letters. 40, 267-68.
[177] C.M. Wolf, M.W. Degner, F. Briz. 2015. Analysis of current sampling errors in PWM VSI drives. IEEE Transactions on Industry Applications. IEEE. 51, 1551-60.
[178] Z. Li, P. Wheeler, A. Watson, A. Costabeber, B. Wang, Y. Ren, Z. Bai, H. Ma. 2020. A fast diagnosis method for IGBT faults and current sensor faults in grid-tied three-phase inverters with two current sensors. IEEE Transactions on Power Electronics. IEEE. 35, 5267-78.
[179] J.O. Estima, A.J.M. Cardoso. 2013. A new algorithm for real-time multiple open-circuit fault diagnosis in voltage-fed PWM motor drivers by the reference current errors. IEEE Transactions on Industrial Electronics. IEEE. 28, 3496-505.
[180] F. Zidani, D. Diallo, M.E.H. Benbouzid, R. Nait-Said. 2008. A fuzzy-based approach for the diagnosis of fault modes in a voltage-fed PWM inverter induction motor drive. IEEE Transactions on Industrial Electronics. IEEE. 55, 586-93.
[181] Q.T. An, L.Z. Sun, K. Zhao, L. Sun. 2015. Current residual vector-based open-switch fault diagnosis of inverters in PMSM drive systems. IEEE Transactions on Power Electronics. IEEE. 30, 2814-27.
[182] N. Senroy, G.T. Heydt, V. Vittal. 2006. Decision tree assisted controlled islanding. IEEE Transactions on Power Systems. 21, 1790–97.
[183] K. El-Arroudi, G. Joos, I. Kamwa, D.T. McGillis. 2007. Intelligent-based approach to islanding detection in distributed generation. IEEE Transactions on Power Delivery. 22, 828–35.
[184] N.W. Lidula, A.D. Rajapakse. 2010. A pattern recognition approach for detecting power islands using transient signals—Part I: Design and implementation. IEEE Transactions on Power Delivery. 25, 3070–77.
[185] J.P. Pham, N. Denboer, N.W. Lidula, N. Perera, A.D. Rajapakse. 2011. Hardware implementation of an islanding detection approach based on current and voltage transients. Electrical Power and Energy Conference (EPEC). pp. 152–57.
[186] Z. Yi, A.H. Etemadi. 2017. Line-to-Line Fault Detection For Photovoltaic Arrays Based on Multiresolution Signal Decomposition and Two-Stage Support Vector Machine. IEEE Transactions on Industrial Electronics. 64, 8546–5.
[187] E. Kymakis, S. Kalykakis, T.M. Papazoglou. 2009. Performance analysis of a grid connected photovoltaic park on the island of Crete. Energy Conversion and Management. 50(3), 433-38.
[188] S. Silvestre , A. Chouder ,E. Karatepe. 2013. Automatic fault detection in grid connected PV systems. Solar Energy. 94, 119–27.

[189] M. Davarifar, A. Rabhi, A. El Hajjaji, M. Dahmane. 2013. New method for fault detection of PV panels in domestic applications. Proceedings of the 3rd international conference on systems and control (ICSC). IEEE. pp. 727–32.
[190] J.M. Bright, S. Killinger, D. Lingfors, N.A. Engerer. 2018. Improved satellite-derived PV power nowcasting using real-time power data from reference PV systems. Solar Energy. 168,
[191] W. Chine A. Mellit, A.M. Pavan, V. Lughi. 2015. Fault diagnosis in photovoltaic arrays. Proceedings of international conference on clean electrical power (ICCEP). IEEE. pp. 67–72.
[192] R. Platon, J. Martel, N. Woodruff, T.Y. Chau. 2015. Online fault detection in PV systems. IEEE Transactions on Sustainable Energy. IEEE. 6, 1200–7.
[193] M. Hosseinzadeh, F.R. Salmasi. 2016. Determination of maximum solar power under shading and converter faults—a prerequisite for failure-tolerant power management systems. Simulation Modelling and Practice Theory. 62, 14–30.
[194] M. Bressan, Y. El Basri, A.G. Galeano, C. Alonso. 2016. A shadow fault detection method based on the standard error analysis of IV curves. Renewable Energy. 99, 1181–90.
[195] A. Umana, A.S. Meliopoulos. 2016. Detection of cell-level fault conditions within a photovoltaic array system. Proceedings of transmission and distribution conference and exposition (T&D), IEEE/PES. IEEE. pp. 1–5.
[196] W. Wang, A.C.-F. Liu, H.S.-H. Chung, R.W.-H. Lau, J. Zhang, A.W.-L. Lo. 2016. Fault diagnosis of photovoltaic panels using dynamic current–voltage characteristics. IEEE Transactions on Power Electronics. 31, 1588–99.
[197] T. Andrianajaina, E.J.R. Sambatra, C.B. Andrianirina, T.D Razafimahefa, N. Heraud. 2016. PV fault detection using the least squares method. Proceedings of international conference and exposition on electrical and power engineering (EPE). IEEE. pp. 846–51.
[198] A. Belaout, F. Krim, A. Mellit. 2016. A Neuro-fuzzy classifier for fault detection and classification in photovoltaic module. Proceedings of the 8th international conference on modelling, identification and control (ICMIC). IEEE. pp. 144–9.
[199] E. Garoudja, F. Harrou, Y. Sun, K. Kara, A. Chouder, S. Silvestre. 2017. Statistical fault detection in photovoltaic systems. Solar Energy. 150, 485–99.
[200] B. Du, R. Yang, Y. He, F. Wang, S. Huang. 2017. Nondestructive inspection, testing and evaluation for Si-based, thin film and multi-junction solar cells: An overview. Renewable and Sustainable Energy Reviews. 78, 1117-51.
[201] M. Dhimish, V. Holmes, B. Mehrdadi, M. Dales. 2017. Simultaneous fault detection algorithm for grid-connected photovoltaic plants. IET Renewable Power Generation. 11, 1565–75.
[202] M. Dhimish, V. Holmes, B. Mehrdadi, M. Dales. 2017. Multi-layer photovoltaic fault detection algorithm. High Voltage. 2, 244-52.
[203] M.E. Basoglu, B. Cakir. 2016. Comparisons of MPPT performances of isolated and non-isolated DC-DC converters by using a new approach. Renewable and Sustainable Energy Reviews. 60, 1100-13.
[204] M.K. Alam, F.H. Khan, J. Johnson, J. Flicker. 2014. PV arc-fault detection using spread spectrum time domain reflectometry (SSTDR). Energy Conversion Congress and Exposition (ECCE), IEEE conference. pp. 3294–300.

[205] S. Roy, M.K. Alam, F. Khan, J. Johnson, J. Flicker. 2017. An irradiance independent, Robust ground fault detection scheme for PV arrays based on spread spectrum time domain reflectometry (SSTDR). IEEE Transactions on Power Electronics. IEEE. 33, 7046-57.
[206] F. Schimpf, L.E. Norum. 2009. Recognition of electric arcing in the DC-wiring of photovoltaic systems. Telecommunications Energy (INTELEC) International IEEE Conference. IEEE. pp. 1–6.
[207] O. Hachana, G.M. Tina, K.E. Hemsas. 2016. PV array fault Diagnostic Technique for BIPV systems. Energy and Buildings. 126, 263-74.
[208] J. Johnson, S. Kuszmaul, W. Bower, D.A. Schoenwald. 2011. Using PV module and line frequency response data to create robust arc fault detectors. Proceedings of the 26th European Photovoltaic Solar Energy Conference and Exhibition. pp. 5–9.
[209] J.C. Gu, D.S. Lai, J.M. Wang, J.J. Huang, M.T. Yang. 2019. Design of DC series arc fault detector for photovoltaic system protection. IEEE Transactions on Industry Applications. 55, 2464-71.
[210] G.S. Seo, H. Bae, B.H. Cho, K.C. Lee. 2012. Arc protection scheme for DC distribution systems with photovoltaic generation. Renewable Energy Research and Applications (ICRERA). IEEE International Conference. pp. 1–5.
[211] M. Kavi, Y. Mishra, M. Vilathgamuwa. 2018. DC arc-fault detection in PV systems using multistage morphological fault detection algorithm. IECON 2018 – 44th Annual Conference of the IEEE Industrial Electronics Society. IEEE. pp. 1-5.
[212] D.K.J.S. Jayamaha, N.W.A. Lidula, A.D. Rajapakse. 2020. Protection and grounding methods in DC microgrids: Comprehensive review and analysis. Renewable and Sustainable Energy Reviews. 120, 12-14.
[213] S. Czapp, K. Borowski. 2019. Verification of safety in low-voltage power systems without nuisance tripping of residual current devices. Electric Power Systems Research. 172, 260-68.
[214] J.C. Hernandez, P.G. Vidal, F. Jurado. 2005. Guidelines for protection against electric shock in PV generators. IEEE Power Engineering Society General Meeting. 24 (1), 274–82.
[215] J. Flicker, J. Johnson. 2016. Photovoltaic ground fault detection recommendations for array safety and operation. Solar Energy. 140, 34-50.
[216] J.C. Hernández, P.G. Vidal, A. Medina. 2010. Characterization of the insulation and leakage currents of PV generators: Relevance for human safety. Renewable Energy. 35, 593–601.
[217] D.S. Pillai, J.P. Ram, N. Rajasekar, A. Mahmud, Y. Yang, F. Blaabjerg. 2019. Extended analysis on Line-Line and Line-Ground faults in PV arrays and a compatibility study on latest NEC protection standards. Energy Conversion and Management. 196, 988-1001.
[218] J. Flicker, J. Johnson, M. Albers, G. Ball. 2015. Recommendations for isolation monitor ground fault detectors on residential and utility-scale PV systems. 2015 IEEE 42nd Photovoltaic Specialist Conference (PVSC). IEEE. pp. 4-6.
[219] J.F. Martinez, M. Steiner, M. Wiesenfarth, S.W. Glunz, F. Dimroth. 2018. Thermal analysis of passively cooled hybrid CPV module using Si cell as heat distributor. IEEE Journal of Photovoltaics. 9, 160-6.

[220] S. Vergura, G. Acciani, O. Falcone. 2012. A finite-element approach to analyze the thermal effect of defects on silicon-based PV cells. IEEE Transactions on Industrial Electronics. 59, 3860–67.
[221] L. Liu, M. Zan, Y. Bai. 2019. A recursive ensemble model for forecasting the power output of photovoltaic systems. Solar Energy. 189, 291-98.
[222] Y. Yagi, H. Kishi, R. Hagihara, T.Tanaka, S. Kozuma, T. Ishida, M. Waki, M. Tanaka, S. Kiyama. 2003. Diagnostic technology and an expert system for photovoltaic systems using the learning method. Solar Energy Materials and Solar Cells. 75, 655–63.
[223] Z. Li, Y. Wang, D. Zhou, C. Wu. 2012. An intelligent method for fault diagnosis in photovoltaic array. System Simulation and Scientific Computing. 327, 10–16.
[224] P. Ducange, M. Fazzolari, B. Lazzerini, F. Marcelloni. 2011. An intelligent system for detecting faults in photovoltaic fields. 11th International Conference on Intelligent Systems Design and Applications (ISDA). IEEE. pp. 1341–46.
[225] A. Belaout, F. Krim, A. Mellit, B. Talbi, A. Arabi. 2018. Multiclass adaptive neuro-fuzzy classifier and feature selection techniques for photovoltaic array fault detection and classification. Renewable Energy. 127, 548-58.
[226] A. Ameur, A. Berrada, K. Loudiyi, M. Aggour. 2020. Forecast modeling and performance assessment of solar PV systems. Journal of Cleaner Energy Production. 267, 5-10.
[227] E. Garoudja, A. Chouder, K. Kara, S. Silvestre. 2017. An enhanced machine learning based approach for failures detection and diagnosis of PV systems. Energy Conversion and Management. 151, 496-513.
[228] M. Dhimish, V. Holmes, B. Mehrdadi, M. Dales. 2017. Diagnostic method for photovoltaic systems based on six layer detection algorithm. Electric Power Systems Research. 151, 26-39.
[229] M. Mittal, B. Bora, S. Saxena, A.M. Gaur. 2018. Performance prediction of PV module using electrical equivalent model and artificial neural network. Solar Energy. 176, 104-17.
[230] I.E. Kaid, A. Hafaifa, M. Guemana, N. Hadroug, A. Kouzou, L. Mazouz. 2018. Photovoltaic system failure diagnosis based on adaptive neuro fuzzy inference approach: South Algeria solar power plant. 204, 169-82.
[231] Y. Zhao, R. Ball, J. Mosesian, J.-F. de Palma, B. Lehman. 2015. Graph-based semi-supervised learning for fault detection and classification in solar photovoltaic arrays. IEEE Transactions on Power Electronics. 30, 2848–58.
[232] Y. Zhao, L. Yang, B. Lehman, J.-F. de Palma, J. Mosesian, R. Lyons. 2012. Decision tree-based fault detection and classification in solar photovoltaic arrays. Proceedings of twenty-seventh annual applied power electronics conference and exposition (APEC). IEEE. pp. 93–9.
[233] M.N. Akram, S. Lotfifard. 2015. Modeling and health monitoring of DC side of photovoltaic array. IEEE Transactions on Sustainable Energy. IEEE. 6, 1245–53.
[234] Syafaruddin, E. Karatepe, T. Hiyama. 2011. Controlling of artificial neural network for fault diagnosis of photovoltaic array. Proceedings of the 16th international conference on intelligent system application to power systems (ISAP). IEEE; pp. 1–6.
[235] L.L. Jiang, D.L. Maskell. 2015. Automatic fault detection and diagnosis for photovoltaic systems using combined artificial neural network and analytical based methods. In: Proceedings of international joint conference on neural networks (IJCNN).

IEEE. pp. 1–8.

[236] C.B. Jones, J.S. Stein, S. Gonzalez, B.H. King. 2015. Photovoltaic system fault detection and diagnostics using laterally primed adaptive resonance theory neural network. Proceedings of the 42nd photovoltaic specialist conference (PVSC). IEEE. pp. 1–6.

[237] G. Han, F.M. Ham, L.V. Fausett. 1994. Fuzzy LAPART supervised learning through inferencing for stable category recognition. Proceedings of 1994 IEEE 3rd International Fuzzy Systems Conference. IEEE. pp. 1-5.

[238] Z. Chen, L. Wu, S. Cheng, P. Lin, Y. Wu, W. Lin. 2017. Intelligent fault diagnosis of photovoltaic arrays based on optimized kernel extreme learning machine and I-V characteristics. Applied Energy. 204, 912-31.

[239] L. Bonsignore, M. Davarifar, A. Rabhi, G.M. Tina, A. Elhajjaji. 2014. Neuro-Fuzzy Fault Detection Method for Photovoltaic Systems. Energy Procedia. 62, 431-44.

[240] M. Dhimish, V. Holmes, B. Mehrdadi, M. Dales, P. Mather. 2017. Photovoltaic fault detection algorithm based on theoretical curves modelling and fuzzy classification system. Energy. 140, 276-90.

[241] Z. Chen, F. Han, L. Wu, J. Yu, S. Cheng, P. Lin, H. Chen. 2018. Random forest based intelligent fault diagnosis for PV arrays using array voltage and string currents. Energy Conversion and Management. 178, 250-64

[242] Y. Ueda, K. Kurokawa, T. Tanabe, K. Kitamura, H. Sugihara. 2008. Analysis results of output power loss due to the grid voltage rise in grid-connected photovoltaic power generation systems. IEEE Transactions on Industry Electronics. 55, 2744-51.

[243] S.R. Madeti, S.N. Singh. 2017. Comparative analysis of solar photovoltaic monitoring systems. AIP Conference Proceedings. 1859(1), 020116.

[244] L. Shen, Z. Li, T. Ma. 2020. Analysis of the power loss and quantification of the energy distribution in PV module. Applied Energy. 260, 4-8.

[245] M. Tadj, K. Benmouiza, A. Cheknane. 2014. An innovative method based on satellite image analysis to check fault in a PV system lead–acid battery. Simulation Modelling Practice and Theory. 47, 236-47.

[246] S. Silvestre. 2018. Advances in Renewable Energies and Power Technologies. Chapter 7: Strategies for Fault Detection and Diagnosis of PV Systems", Book Chapter. pp. 231-55.

[247] T. Takashima, J. Yamaguchi, K. Otani, T. Oozeki, K. Kato, M. Ishida. 2009. Experimental studies of fault location in PV module strings. Solar Energy Materials and Solar Cells. 93, 1079-82.

[248] T. Arunkumari, V. Indragandhi. 2017. An overview of high voltage conversion ratio DC-DC converter configurations used in DC micro-grid architectures. Renewable and Sustainable Energy Reviews. 77, 670-87.

[249] A. Nouri, I. Salhi, S. El Beid, N. Essounbouli, E. Elwarraki. 2016. A fault tolerant strategy for multilevel dc-dc converters to improve the PV system efficiency. IFAC-PapersOnLine. 49, 704-9.

[250] A. Chouder, S. Silvestre. 2010. Automatic supervision and fault detection of PV systems based on power losses analysis. Energy Conversion Management. 51, 1929–37.

[251] K. Osmani, M. Ramadan, A. Haddad, T. Lemenand, B. Castanier. 2021. A Short Review on Mathematical Algorithms for Predictive Maintenance Techniques and Anomaly

Detection in PV Systems. In Proceedings of the 31st European Safety and Reliability Conference, ESREL, Angers, France. pp. 3222-9.
[252] A. Drews, A.C. de Keizer, H.G. Beyer, E. Lorenz, J. Betcke, W.G.J.H.M. van Sark, W. Heydenreich, E. Wiemken, S. Stettler, P. Toggweiler, S. Bofinger, M. Schneider, G. Heilscher, D. Heinemann. 2007. Monitoring and remote failure detection of grid-connected PV systems based on satellite observations. Solar Energy. 81, 548–64.
[253] K.H. Chao, S.H. Ho, M.H. Wang. 2008. Modeling and fault diagnosis of a photovoltaic system. Electric Power Systems Research. 78, 97–105.
[254] A. Mellit, G.M. Tina, S.A. Kalogirou. 2018. Fault detection and diagnosis methods for photovoltaic systems A review. Renewable and Sustainable Energy Reviews. 91, 1-17.
[255] P. Lin, Y. Lin, Z.C. Chen, L. Wu, L. Chen, S. Cheng. 2017. A density peak-based clustering approach for fault diagnosis of photovoltaic arrays. International Journal of Photo Energy. 9, 1-14.
[256] M. Benghanem, A. Maafi. 1998. Data acquisition system for photovoltaic systems performance monitoring. IEEE Transactions on Instrumentation and Measurements. 47, 30–3.
[257] R. Mukaro, D. Tinarwo. 2008. Performance evaluation of a hot-box reflector solar cooker using a microcontroller-based measurement system. International Journal of Energy Research. 32, 1339–48.
[258] M.A. Eltawil, Z. Zhao. 2010. Grid-connected photovoltaic power systems: Technical and potential problems—A review. Renewable and Sustainable Energy Reviews. 14, 112-29.
[259] M. Miwa, S. Yamanaka, H. Kawamura, H. Ohno. 2006. Diagnosis of a power output lowering of PV array with a (-dI/dV)-V characteristic. Photovoltaic Energy Conversion, Conference Record of the IEEE 4th World Conference. IEEE. 2, 2442–5.
[260] S. Kaplanis, E. Kaplani. 2011. Energy performance and degradation over 20 years performance of BP c-Si PV modules. Simulation Modelling Practice and Theory. 19, 1201–11.
[261] Z.A. Jeffery, A.K. Dubey, Irshad, A. Haque. 2017. Scheme for predictive fault diagnosis in photo-voltaic modules using thermal imaging. Infrared Physics & Technology. 83, 182-87.
[262] B. Nehme, N.C. Msirdi, A. Naamane, T. Akiki. 2017. Analysis and Characterization of Faults in PV Systems. Energy Procedia. 111, 1020-29.
[263] J. Solorzano, M.A. Egido. 2013. Automatic fault diagnosis in PV systems with distributed MPPT. Energy Conversion and Management. 76, 925-34.
[264] Q. Xiong, S. Ji, X. Liu, X. Feng, F. Zhang, L. Zhu, A.L. Gattozi, R.E. Hebner. 2018. Detecting and localizing series arc fault in photovoltaic systems based on time and frequency characteristics of capacitor current. Solar Energy. 170, 788-99.
[265] T. Takashima, J. Yamaguchi, K. Otani, K. Kato, M. Ishida. 2006. Experimental studies of failure detection methods in PV module strings. Photovoltaic Energy Conversion, Conference Record of the IEEE 4th World Conference. 2, 2227–30.
[266] L. Schirone, F.P. Califano, M. Pastena. 1994. Fault detection in a photovoltaic plant by thermal effect of defects on silicon-based PV cells. IEEE Transactions on Industrial Electronics. 59, 3860–67.

[267] S. Vergura, G. Acciani, V. Amoruso, G. Patrono. 2008. Inferential statistics for monitoring and fault forecasting of PV plants. IEEE International Symposium on Industrial Electronics. IEEE. pp. 2414–19.
[268] E. Kaplani. 2012. Detection of degradation effects in field-aged c-Si solar cells through IR thermography and digital image processing. International Journal of Photoenergy. pp. 3-10.
[269] F. Ancuta, C. Cepisca. 2011. Fault analysis possibilities for PV panels. Proceedings of the 3rd international youth conference on energetics (IYCE). IEEE. pp. 1–5.
[270] R. Kase, S. Nishikawa. 2016. Fault detection of bypass circuit of PV module—Detection technology of open circuit fault location. Proceedings of the 19th international conference on electrical machines and systems (ICEMS). IEEE. pp. 1–4.
[271] Y. Hu, B. Gao, X. Song, G.Y. Tian, K. Li, X. He. 2013. Photovoltaic fault detection using a parameter based model. Solar Energy. 96, 96-102.
[272] J.C. Schlothauer, K. Grabmayer, I. Hintersteiner, G.M. Wallner, B. Roder. 2017. Non-destructive 2D-luminescence detection of EVA in aged PV modules: Correlation to calorimetric properties, additive distribution and a clue to aging parameters. Solar Energy Materials and Solar Cells. 159, 307-17.
[273] Z. Liu, M. Peters, V. Shanmugam, Y.S. Khoo, S. Guo, R. Stangl, A.G. Aberle, J. Wong. 2016. Luminescence imaging analysis of light harvesting from inactive areas in crystalline silicon PV modules. Solar Energy Materials and Solar Cells. 144, 523-31.
[274] P. Acevedo, M. Vasquez, J. Duran, R. Petrearce. 2015. A Pulse Generator Based on An Arduino Platform for Ultrasonic Applications. Physics Procedia. 70, 1096-99.
[275] T. Kirchartz, A. Helbig, W. Reetz, M. Reuter, J.H. Werner, U. Rau. 2009. Reciprocity between electroluminescence and quantum efficiency used for the characterization of silicon solar cells. Progress in Photovoltaics: Research and Applications. 17, 394–402.
[276] M. Kasemann, D. Grote, B. Walter, W. Kwapil, T. Trupke, Y. Augarten, R.A. Bardos, E. Pink, M.D. Abbott, W. Warta. 2008. Luminescence imaging for the detection of shunts on silicon solar cells. Progress in Photovoltaics: Research and Applications. 16, 297–305.
[277] O. Breitenstein, J. Bauer, T. Trupke, R.A. Bardos. 2008. On the detection of shunts in silicon solar cells by photo-and electroluminescence imaging. Progress in Photovoltaics: Research and Applications. 16, 325–30.
[278] G. Kayakutlu, E. Mercier-Laurent. 2016. Intelligence in Energy. Chapter 3: Intelligence for Energy. pp. 37-77
[279] M. Sharifzadeh, A. Sikinio-Lock, N. Shah. 2019. Machine-learning methods for integrated renewable power generation: A comparative study of artificial neural networks, support vector regression, and Gaussian Process Regression. Renewable and Sustainable Energy Reviews. 108, 513-38.
[280] K. Osmani, A. Haddad, T. Lemenand, B. Castanier, M. Ramadan. 2020. A review on maintenance strategies for PV systems. Science of the Total Environment. 746, 3-4.
[281] K. Osmani, A. Haddad, T. Lemenand, B. Castanier, M. Ramadan. 2020. Material Based Fault Detection Methods for PV Systems. Key Engineering Materials. 865, 111-5.
[282] A. Maleki, I. Sadeghkhani, B. Fani. 2019. Statistical sensorless short-circuit fault detection algorithm for photovoltaic arrays. Journal of Renewable and Sustainable Energy. 11, Article ID: 053501.

[283] B. Bouyeddou, F. Harrou, B. Taghezouit, Y. Sun, A.H. Arab. 2022. Improved Semi-Supervised Data-Mining-Based Schemes for Fault Detection in a Grid-Connected Photovoltaic System. energies. 15(21), Article ID: 7978.
[284] S. Vergura. 2018. A Statistical Tool to Detect and Locate Abnormal Operating Conditions in Photovoltaic Systems. Sustainability. 10(3), Article ID: 608.
[285] M. Green, C.B. Jones, J. Dore, E. Brill. 2017. Improving Efficiency of PV Systems Using Statistical Performance Monitoring. International Energy Agency, Photovoltaic Power Systems Programme. ISBN 978-3-906042-48-0.
[286] B. Taghezouit, F. Harrou, Y. Sun, A.H. Arab, C. Larbes. 2020. Multivariate statistical monitoring of photovoltaic plant operation. Energy Conversion and Management. 205, Article ID: 112317.
[287] B. Taghezouit, F. Harrou, Y. Sun, A.H. Arab, C. Larbes. 2021. A simple and effective detection strategy using double exponential scheme for photovoltaic systems monitoring. Solar Energy. 214, 337-54.
[288] F. Harrou, Y. Sun, B. Taghezouit, A. Saidi, M.-E. Hamlati. 2018. Reliable fault detection and diagnosis of photovoltaic systems based on statistical monitoring approaches. Renewable Energy. 116, Part A, 22-37.
[289] F. Harrou, B. Taghezouit, Y. Sun. 2019. Robust and flexible strategy for fault detection in grid-connected photovoltaic systems. Energy Conversion and Management. 180, 1153-66.

[290] Y.-Y. Hong, R.A. Pula. 2022. Methods of photovoltaic fault detection and classification: A review. Energy Reports. 8, 5898-929.
[291] A. Malik, A. Haque, V.S.B. Kurukuru, M.A. Khan, F. Blaabjerg. 2022. Overview of fault detection approaches for grid connected photovoltaic inverters. e-Prime – Advances in Electrical Engineering, Electronics and Energy. 2, Article ID: 100035.
[292] B. Li, C. Delpha, D. Diallo, A. Migan-Dubois. 2021. Application of Artificial Neural Networks to photovoltaic fault detection and diagnosis: A review. Renewable and Sustainable Energy Reviews. 138, Article ID: 110512.
[293] I. Høiaas, K. Grujic, A.G. Imenes, I. Burud, E. Olsen, N. Belbachir. 2022. Inspection and condition monitoring of large-scale photovoltaic power plants: A review of imaging technologies. Renewable and Sustainable Energy Reviews. 161, Article ID: 112353.
[294] N. Bansal, S.P. Jaiswal, G. Singh. 2021. Comparative investigation of performance evaluation, degradation causes, impact and corrective measures for ground mount and rooftop solar PV plants – A review. Sustainable Energy Technologies and Assessments. 47, Article ID: 101526.

[295] M. Köntges, G. Oreski, U. Jahn, M. Herz, P. Hacke, K.-A. Weiss, G. Razongles, M. Paggi, D. Parlevliet, T. Tanahashi, R.H. French. 2017. Assessment of Photovoltaic Module Failures in the Field. International Energy Agency, Photovoltaic Power Systems Programme. ISBN 978-3-906042-54-1.

Annexe 1.3

Méthodes de détection des défauts basées sur les matériaux pour les systèmes photovoltaïques

Key Engineering Materials
ISSN: 1662-9795, Vol. 865, pp 111-115
doi:10.4028/www.scientific.net/KEM.865.111

Submitted: 2019-11-08
Revised: 2019-11-09
Accepted: 2020-01-12
Online: 2020-09-30

Material Based Fault Detection Methods For PV Systems

Khaled Osmani[1,2,a], Ahmad Haddad[1,2,b], Thierry Lemenand[3,c], Bruno Castanier[3,d] and Mohamad Ramadan[1,2,e *]

[1]School of Engineering, International University of Beirut BIU, Beirut, Lebanon

[2]School of Engineering, Lebanese International University LIU, Bekaa, Lebanon

[3]LARIS, Polytech Angers, France

[a]khaled.ossmany@gmail.com, [b]ahmad.haddad@liu.edu.lb, [c]thierry.lemenand@univ-angers.fr, [d]bruno.castanier@univ-angers.fr, [e]mohamad.ramadan@liu.edu.lb

Keywords: Semiconductor materials, PV cells, faults detection, algorithms.

Abstract. The overall efficiency of a PV system is strongly affected by the PV cell raw materials. Since a reliable renewable energy source is expected to produce maximum power with longest lifetime and minimum errors, a critical aspect to bear in mind is the occurrence of PV faults according to raw material types. The different failure scenarios occurring in PV system, decrease its output power, reduce its life expectancy and ban the system from meeting load demands, yielding to severe consecutive blackouts. This paper aims first to present different core materials types, material based fault occurring on the PV cell level and consequently the fault detection techniques corresponding to each fault type.

Introduction

PV cells manufacturing process can rely on a variety of different materials, where they all connect for the primitive role of harvesting solar irradiance into significant electrical energy. Regardless from material diversity, the common matter for this fabrication is the Silicon that has semiconducting properties. Among different types, three dominant PV cell technologies rule the fabrication process: monocrystalline silicon, polycrystalline silicon and thin film. Other substances take sub-part of the mentioned materials.

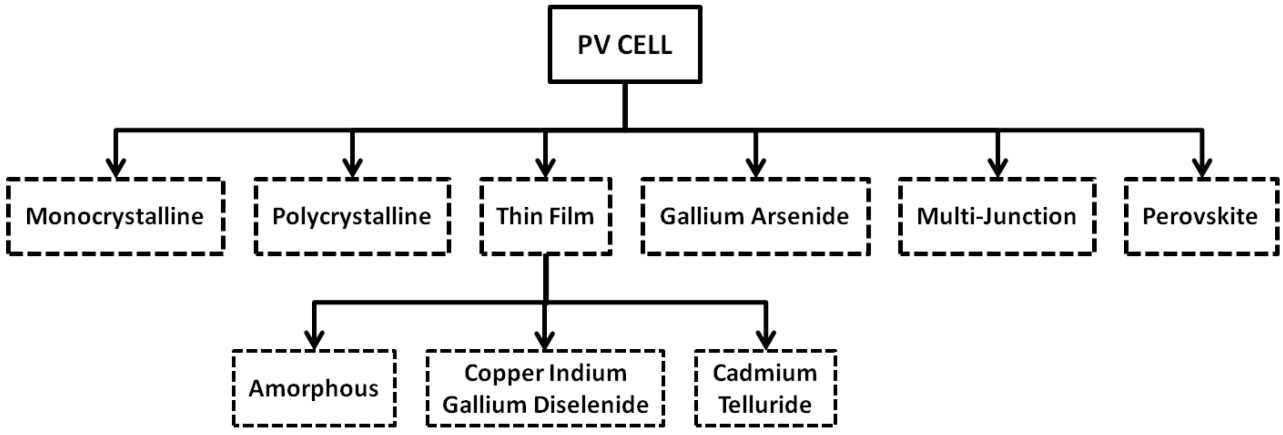

Fig. 1: Different materials used in PV cell fabrication

The Monocrystalline have the purest form of Silicon, where its seed crystal is transformed into a cylindrical ingot result from molten Silicon that later on is transformed into wafers creating a p-n junction after polish and doping. From other side, the Polycrystalline noted as multi-crystalline these cells contains groups of small grain of crystals, where once pulled out of molten Silicon are mechanically transformed into a cube-shaped ingot and later on doped and packaged. The amorphous Silicon is produced by dropping thin layers of Silicon onto a glass substrate. The resulted cell is ultra-thin and mechanically flexible, leaving dangling bonds with less order. Within same material architecture, the copper indium gallium di-selenide CIGS and cadmium telluride

CdTe are included that offer higher efficiencies with less safety as they contain toxic elements. Conversely to Silicon, the Gallium Arsenide GA is an alternative semiconductor having similarities in crystal structure but obtained in different chemical bonding. Multi-junction substances have two or more p-n junctions layered on top of each other allowing different paths for energy collection. In opposition to common crystal structure, the Perovskite cells are produced from organic materials mainly iodine. They consist of layers of polymers that have the option of production as semi-transparent film.

Table 1: Comparison between different PV cells materials

PV Material	Advantages	Disadvantages
Monocrystalline	High efficiency, live long, space-efficiency	Expensive, fragile, sensitive to climate changes
Polycrystalline	Simple manufacturing process, less sensitive to heat than monocrystalline	Efficiency at maximum 16%, less efficiency in space
Amorphous	Flexible mechanical manifestation	Reduced efficiency
CIGD	High efficiency	Contain toxic elements
CdTe	High efficiency	Contain toxic elements
GA	Can operate at higher temperature levels	Expensive to fabricate
Multi-junction	Allows multiple paths for flow of energy	Applicable only in concentrated PV systems
Perovskite	Cheap to produce	Relatively low efficiencies

Different Types of Faults at PV Cell Level

Physical faults bases on the intrinsic material of PV cell fabrication. It focuses on the inner construction of cells, and how it can lead to performance fluctuations as increasing/decreasing system overall efficiency. On this level, four different types of fault exist as shown in Fig.2.

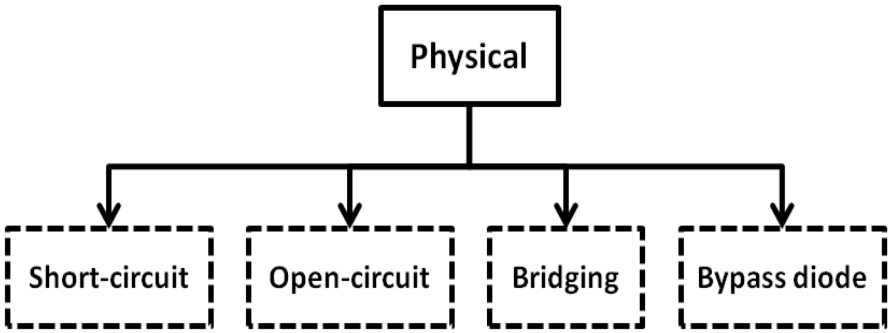

Fig. 2: Different physical PV cells faults

- Short circuit fault in PV modules or Bypass diode: Improper connection (low impedance and sometimes severe short circuit between the solar cells, or defects from manufacturing outcomes [1, 2], leads to a short circuit on the module or on the by-pass diode [3].
- Bridging fault: Improper connection (high impedance and sometimes complete open circuit between PV modules or cabling [4], causes such types of faults where output tends to become null.
- Inverted bypass diode fault: Faulty wiring made by the operator [5, 6] resulting in bypass diode fault, translates to abnormal voltage conditions on the output level.

- Open circuit with/without bypass diode fault: An open circuit fault, reflected as maximum output voltage, with no ability of current flow (hence no power output) is often caused by broken cells, damaged connections between them, loose connections, defected power cables due to aging and excessive plugging unplugging yields to faulty terminal mainly at junction boxes.

Material Based Fault Detection Techniques

The fault detection techniques that are based on PV material are summarized in the following:

1. Ultrasonic inspection technique UIT: When cracks and micro-cracks are present in the cells of PV module, their response to ultrasonic vibrations followed by an excitation, differentiate from those un-cracked. There are two modes for this method: pulse-echo and transmission. An ultrasonic transducer is present in both to generate and distribute the pulses. In the first the pulses are passed through PV module to record reflected back pulses from defected cells. In the second the attenuated signals are recorded, therefore in both techniques the X-Y location of the defected cells can be presented [7].
2. Lock in thermography LIT: Lateral power loss is found here after injection of discontinuous pulsed current into solar cell. Corrupted cells respond to this by appearing as a local temperature modulation where by using different modulations, different defected cells appear [8].
3. Electroluminescence Imaging EL: When excited carriers recombine into a solar cell, it emits photons then accordingly EL imaging is obtained. An EL effect happens then by means of an injected current that yields the excitation [9]. Light can also exists due to PL effect [10]. The emission intensity of EL images are proportional to current density and carrier lifetime, hence one can detect non-uniform current sourced from poor connections or other defects.
4. Infrared Thermal Imaging ITH: Across a resistor a power loss is noted as joule loss, where current passed is transformed into heat, therefore the loss. Similarly, any loose contact, shortening across PV cells can result to same effect: loss in terms of overheating where affected cells produce less current as compared with normal ones and becomes reverse biased. Through temperature monitoring, the fault can be identified, in two ways: FBI/RBI where each has its private method of calculating shorted/faulty current to identify hotspots accordingly, using IR cameras (in both) to record IR images, to perform image processing resulting in locating the fault knowing its type [11]. To identify fault type, and frequency of occurrence, an approach based on IR thermography that takes into account the panels under investigation leads to an ability in detecting different faults [12] with the help putting hotspots and local dust accumulated particles into the analyzing process. For hotspot cells exerting a reverse voltage, and due to the opening of bypass diode, the inability to identify which module is defected, is solved by [13] where there is no more need to measure the modules one by one, replaced by observing the surface temperature change of the PV modules, the abnormal modules with open bypass circuit are identified using DC power supply and infrared camera. To get temperature values, a thermal camera is connected cascaded with electrical sensor to know V-I values, hence a diagnostic model can identify faults using parameter based model established by electrical model and energy balance equation of a PV [14]. The measured parameters are compared to a performance estimation model hence error can be derived.

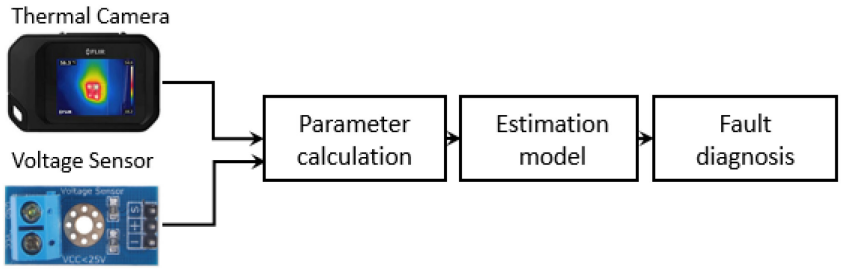

Fig. 3: Thermal Imaging

5. Machine Learning techniques MLT: The physical faults as degradation and partial shading as well as short/open-circuit faults in PV system can be detected using V-I characteristics: By implementing them on a Kernel extreme learning machine [15] with the addition of Nelder-Mead simplex optimization technique. Faults results can be simulated on SLNF based fault diagnosis model. The algorithm begins by imposing on fundamentals of ELM. Its next step is returning to parameter optimization of KELM. Finally data pre-processing and feature selection arrive at the establishment of the fault diagnosis model. A neuro-fuzzy classifier, is hence created to detect faults at the PV cells levels, as series losses, bypass and blocking diode faults based on parameters as maximum power, and open circuit voltage deviations [16].
6. Heat exchange and temperature based model HET: For the fact of correlation between a PV fault and PV temperature, i.e. When a fault happens in a PV array, its temperature changes. All heat exchange is scheduled within the fault detection technique. Using a finite element method, the physical defects of different types of PV cells are modeled [17].

The fault detection techniques discussed above are not all applicable to different PV materials. The mapping between detection methods and PV fabrication material is shown in Table 2.

Table 2: Applicability of fault detection methods based on fabricating material

Detection Method	PV Cell Material					
	Monocrystalline	Polycrystalline	Thin film	Gallium Arsenide	Multi-Junction	Perovskite
UIT	●	●	●			
LIT	●	●	●	●		
EL	●	●	●		●	
ITH	●	●	●	●	●	
MLT	●	●	●		●	●
HET	●	●	●	●		

Conclusion

It was seen that the radical substances used in PV cell fabrication plays a crucial role in determining the overall efficiency of the PV system. Different faults exists for each material that relies mainly on inner cell structure. Studied faults ranged from open-short/circuit to bypass diode errors. This paper has presented different physics used in cell manufacturing and ranged the faults that might occur. Accordingly, fault detection techniques have been presented. Moreover, it was shown how to select a fault detection technique depending on the nature of the fault.

References

[1] Jiang, L.L. et al.,"Automatic fault detection and diagnosis for photovoltaic systems using combined artificial neural network and analytical based methods". International Joint Conference on Neural Networks, IEEE International Joint Conference, 2015, vol. 12, p. 1–8.

[2] Wolgemuth J., "Failure modes of crystalline Si modules", PV Module Reliability Workshop, 2010.

[3] Zhao Y et al., "Fault analysis in solar PV arrays under: Low irradiance conditions and reverse connections". In: Proceedings of the 37th photovoltaic specialists' conference (PVSC). IEEE; 2011. p. 2–5.

[4] Davarifar M et al., "Comprehensive modulation and classification of faults and analysis their effect in DC side of photovoltaic system". Energy Power Engineering, 2013, issue 5, vol.4, p. 230.

[5] Chine W. et al., Fault diagnosis in photovoltaic arraysIn: Clean Electrical Power (ICCEP), International Conference on 2015, p. 67–72.

[6] Alam MK et al., "A comprehensive review of catastrophic faults in PV arrays: types, detection, and mitigation techniques". IEEE J Photovoltaic.

[7] Hund, T.D. et al., "Analysis techniques used on field degraded photovoltaic modules". NASA STI/Recon Technical Report N, 1995, p. 96.

[8] Breitenstein O. et al, "On the detection of shunts in silicon solar cells by photo-and electroluminescence imaging". Progress in Photovoltaics Research and Applications, 2008, issue 16, vol.4, p. 325–330.

[9] Kirchartz, T. et al., "Reciprocity between electroluminescence and quantum efficiency used for the characterization of silicon solar cells". Progress in Photovoltaics Research and Applications, 2009, 17 (6), p. 394–402.

[10] Kasemann, M. et al., "Luminescence imaging for the detection of shunts on silicon solar cells". Progress in Photovoltaics Research and Applications, 2008, issue 16, vol. 4, p. 297–305.

[11] Kaplani E., "Detection of degradation effects in field-aged c-Si solar cells through IR thermography and digital image processing". Int. J. Photoenergy, 2012.

[12] Ancuta F. et al., "Fault analysis possibilities for PV panels". In: Proceedings of the 3rd international youth conference on energetics (IYCE). IEEE; 2011, p. 1–5.

[13] Kase R. et al., "Fault detection of bypass circuit of PV module—Detection technology of open circuit fault location". In: Proceedings of the 19th international conference on electrical machines and systems (ICEMS), 2016. IEEE; 2016. p. 1–4.

[14] Yihua Hu et al., "Photovoltaic fault detection using a parameter based model", Research article, Solar Energy, vol. 96, 2013, p. 96-102

[15] Zhicong Chen et al., "Intelligent fault diagnosis of photovoltaic arrays based on optimized kernel extreme learning machine and I-V characteristics", Research article, Applied Energy, 2017, vol. 204, p. 912-931.

[16] Belaout A. et al., "A Neuro-fuzzy classifier for fault detection and classification in photovoltaic module". In: Proceedings of the 8th international conference on modelling, identification and control (ICMIC). IEEE; 2016, p. 144–9.

[17] Hu, Y. et al., 2013. "Photovoltaic fault detection using a parameter based model". Solar Energy, 1996, p. 96–102.

Annexe 1.4

Brève revue des algorithmes mathématiques pour les techniques de maintenance prédictive et la détection d'anomalies dans les systèmes Photovoltaïques

A short review on mathematical algorithms for predictive maintenance techniques and anomaly detection in PV systems

Khaled Osmani

LARIS EA 7315, Polytech Angers, UNIV Angers, France. E-mail: khaled.alosmani@etud.univ-angers.fr

Mohamad Ramadan

School of Engineering, International University of Beirut BIU, Beirut, Lebanon.
School of Engineering, Lebanese International University LIU, Bekaa, Lebanon. E-mail: mohamad.ramadan@liu.edu.lb

Ahmad Haddad

School of Engineering, International University of Beirut BIU, Beirut, Lebanon.
School of Engineering, Lebanese International University LIU, Bekaa, Lebanon. E-mail: ahmad.haddad@liu.edu.lb

Thierry Lemenand

LARIS EA 7315, Polytech Angers, UNIV Angers, France. E-mail: thierry.Lemenand@univ-angers.fr

Bruno Castanier

LARIS EA 7315, Polytech Angers, UNIV Angers, France. E-mail: bruno.castanier@univ-angers.fr

The applicability of PhotoVoltaic (PV) systems as an efficient renewable energy supply for an average lifespan of twenty-five years, is backpedalled after being confronted with fault events. Just like all outdoor systems, PVs are often subject to various types of faults and undesired working conditions. At any instance, PV modules can interact with different electrical faults. On the other hand, harsh external conditions can also affect a proper PV system functioning. Efficiency reduction and output deficits are most common results of PV system's interaction with faulty events, reflected as improper behaviour of the system. From this point, arises the need for a diagnostic and prediction system, which estimates the possibility of a future achievable potential and partially observable fault among a large set of possible failure modes, prior from happening, regardless of the PV cells raw materials being used. In the interest of a sustainable and reliable PV system design, this paper aims at exploring different mathematical models of fault predictive techniques. Underlying the artificial intelligence and algorithm-based decision making, various predictive algorithms are surveyed and compared with reference to their event risk's accuracy. For instance, Markov chains based probabilistic model computes failures rates, where convolutional neural networks indicate a malfunctioning panel, and supervised machine learning based automated barcode detection algorithms detect PV module's defects. The critical assessment between different models would serve as an informative background when choosing a PV fault predictive technique.

Keywords: Maintenance, PV, predictive, corrective, durability, error, efficiency, faults.

1. Introduction

Renewable energy sources are top contributors towards a carbon-less future. PV (PhotoVoltaic) systems in particular are the most popular compared to other supplies (wind, tidal, etc.) due to their non-detrimental nature and the abundancy of solar radiations, Maleki et al. (2020). With a direct conversion from light to electricity, such systems do not need any mechanical actuators to operate, with zero noise emissions, Do Nascimento et al. (2020). PV systems help in reducing climate change, as well as global warming by reduction of greenhouse gas emissions. The presence of toxic gas in air is reduced after adapting PV systems for power generation, where excessive burning of oil/petrol reservoirs is decreased, while still maintaining load demands, Bazan et al. (2018). The underproductive issue of existing power resources is offset upon adaptation of PV systems, possessing a potential contribution to the future electricity mix.

However, these systems are often confronted with scenarios which block them from fulfilling their destined goals. When encountered by bad environmental factors such as dust accumulation, elevated temperature, snowfall, partial shading conditions and other unpleasant biological conditions such as bird droppings, leave and soil accumulation, PV systems' efficiency are reduced, Conceicao et al. (2020). Aside from environmental implications, PV systems are faced with inner faults, beginning from manufacturing defects to electrical faults, arriving to power processing units malfunction (trackers, inverters, etc.), Manohar et al. (2019). Regardless of faults types, victimizing a proper behaviour of PV systems, they all share a bad impact over such systems, ranging from voltage unbalancing, deviated waveforms, current leakage,

Proceedings of the 31th European Safety and Reliability Conference
Edited by Bruno Castanier, Marko Cepin, David Bigaud and Christophe Berenguer
 Published by Research Publishing, Singapore
ISBN: 981-973-0000-00-0 :: doi: 10.3850/981-973-0000-00-0 esrel2021-paper

harmonic distortion, reduced quantities of produced power to service interruption (complete/partial blackouts), Kaushal et al. (2020).

Various fault intervention techniques were conducted to maintain a reliable and sustainable PV clean energy production, Osmani et al. (2020). Corrective techniques on the first side, include the set of labour activities of service restoration after a fault event, striking on different levels of the network. Categorized as a direct approach maintenance form, its mechanism is involved with manual fixation or replacement of damaged equipment. Aside than algorithm modification within inverters and other power conditioning units as dynamic voltage regulators, unified power quality conditioners, maximum power point trackers and energy storage systems, Mukhopadhyay et al. (2020), this technique does not involve any machine learning based processes. For instance, the inverter algorithm can be reconfigured to better adapt load demands, by controlling it via direct source current shaping, fuzzy reasoning, particle swarm optimization and hysteresis current control. From the same perspective, various algorithms can be fed into the charge controller of batteries, Osmani et al. (2020), to plug in or out the capacitors' bank and parts of the storage system, to accommodate power fluctuations resultant from disturbances in power profiles. It includes genetic algorithm, micro-energy management procedures and modification of energy storage/release from the batteries, Osmani et al. (2020).

The physical fault mitigation includes the panels water cleaning, by removal of blocking barriers (dust, particles, etc.) in front of solar irradiance. The water cleaning operation can be man-made, using floating water pumps, or automated via cleaning robots, consisting of electric motors, brushes, and other cleaning facilities. An elevation of 8.7% in overall PV system's efficiency is seen when adapting a water cleaning strategy, applied for the same system in clean/dirty modes, Alnaser et al. (2018). Cleaning activity also includes a dust-wiping driven robotic system, which uses a silicon brush to gently remove dust particles, Osmani et al. (2020).

For colder areas, the corrective maintenance includes snow removal, which aims to remove the blocking barrier (snow instead of dust particles) facing solar radiations, Yan et al. (2020). The snow accumulation can be withdrawn by usage of surface coatings, heating systems, tilt angle modification overnight and by means of electrostatic forces, which slide the snow off the PV panels' surfaces, Pawluk et al. (2019). Upon equipment failures, the service-team driven intervention is categorized by replacing, switching, and fixing faulty equipment denoted by alarm signals which are based on sensors data acquisition, Pei et al. (2020). The malfunction item is targeted to be renewed or fixed. Urgent case maintenance on the other hand, works with the same principles as corrective maintenance does, but with higher priority. When a PV panel is fallen from a height, stolen, sabotaged, or been set to fire due to lightnings or because of surrounding fires, Manzini et al. (2015), this fault is prioritized with respect to any other occurring fault. The escalated priority for urgent case maintenance is due to avoid any personnel threats and for the general safety, Osmani et al. (2020).

By focusing on the level of energy purity, corrective maintenances emphasise on an efficient power quality, dedicated to ensuring high energy production rates. Even though they succeed in eliminating faults leftovers, but their actions are taken post faults incidence. In other words, these techniques cannot bypass any fault driven loss or be able to avoid power production intermittency.

For a PV system better reliability and robustness in performance, this paper aims at exploring different mathematical models of predictive maintenance techniques, that differ from corrective techniques in a time-advanced property. Rather than intervening after a fault incidence, predictive models reduce larger failure risks, by a convenient decision making, regarding the pre-actions. With the help of mathematical models, fault events can be investigated prior from happening, by collection of informatic data and historic records of system's performance. In other words, rather than generalizing the overview of different types of fault intervention methods, Osmani et al. (2020), this work instead focuses solely on discussing, investigating, analysing, and comparing various maintenance techniques, relying under the predictive category.

The rest of this paper is organized as follows: in Section 2 a general overview of predictive maintenance techniques is explored, with mathematical detailing of each sub-method individually. Section 3 represents a comparative assessment of different predictive algorithms, which results are to be concluded in Section 4.

2. Overview of predictive maintenance techniques

The risk of any possible failure, in any node of the PV network, whether on the modules' side, power conversion level or at the consumable produced power zone is scalarly computed by means of mathematical formulas and discrete outputs, Gonzalo et al. (2020). In such techniques, the cost of post maintenance is lowered while bigger failures are prevented. Fig. 1 encapsulates two major predictive maintenance schemes, labelled as process-history and quantitative based.

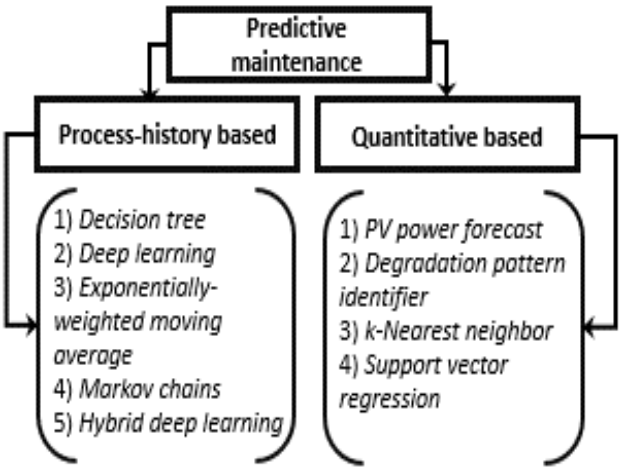

Fig. 1. Classification of different predictive techniques

2.1. *Process-history based methods*

Adapting both statistical and machine learning approaches, the process-history based family of methods involves the following sub-methods:

- Decision tree
- Deep learning
- Exponentially weighted moving average
- Markov chains
- Hybrid deep learning

2.1.1. *Decision Tree (DT)*

A decision tree model is constructed according to four consecutive steps starting by data acquisition, in which the training and test sets are obtained from previous experiments. Right after comes the data pre-processing that includes data sampling, clearing and attributes related tasks. The third stage corresponds to the training process of the DT by usage of 66% of randomly chosen pre-processed data. The testing step is its destination in which the pre-processed data remainder is used, Zhao et al. (2012).

The DT model development is established by means of attribute selection (fill factor, PV power, etc.), where attributes are filtered within the data pre-processing stage and selected only if they possess high correlation with class-label attributes, with low redundancy. The selection phase is governed by Eq. (1) representing the information for data classification Dj into class Ci ranging from 1 to m.

$$\mathrm{Info}(\mathrm{D_j}) = -\sum_{i=1}^{m} \mathrm{p_i} \log_2(\mathrm{p_i}) \qquad (1)$$

with p_i representing the probability of Ci in Dj. To split D into v number of partitions beginning from one, the information shown in Eq. (1) is redefined as in Eq. (2).

$$\mathrm{Info_A(D)} = \sum_{j=1}^{v} \frac{|\mathrm{D_j}|}{\mathrm{D}} \mathrm{Info}(\mathrm{D_j}) \qquad (2)$$

After the application of different steps, the overall flowchart of the DT model is seen in Fig. 2. The DT model showed easiness in a real-world implementation with up to 99.98% detection accuracy. Despite being a straightforward and easy to implement detection model, DT lacks model optimization and integration with PV inverters, Zhao et al. (2012).

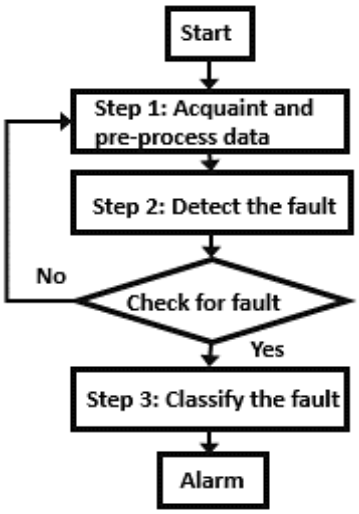

Fig. 2. Flowchart of the DT proposed model

2.1.2. *Deep Learning (DL)*

Each PV panel within the network is classified as healthy/damaged by means of a Convolutional Neural Network (CNN) derivative-based algorithm. The algorithm indicates a faulty panel, when a mean square error exists after subtraction of time series power output of the suspected panel, from the same output resulting from spatial neighbouring panels, Huuhtanen et al. (2018).

The power measurement for each PV panel is categorized as P(t,d,s) with t denoting the daytime in minutes, d the date and s the spatial location of the panel being investigated.

The CNN algorithm is designed using two layers, with a two-dimensional input data signal. The two layers can either be fully convolutional as indicated in Eq. (3) or fully convolutional for the first layer only, having unshared convolution for the second layer.

$$\mathrm{y(t,s;l)} = \sigma\left(\sum_{i=0}^{I-1}\sum_{j=0}^{J-1}\sum_{k=0}^{K-1}(\mathrm{x(t-i,s-j,k)} \cdot \mathrm{h(i,j,k;l)}\right) \qquad (3)$$

The term x in Eq. (3) indicates the input, y the output, h the convolutional kernel and σ the activation function. Indexes

such as t represents the time, s the spatial mapping of the panel, l the different features maps in the current layer, and k the different features maps in the previous layer.

For the unshared convolution layer, the output equation differs in having the convolutional kernel h as a function of time t. The predictor for a targeted panel is hence achieved by calculation of the power average of two adjacent panels, intended to minimize the mean square error ε.

Unlike sequential data processor as recurrent neural networks and long short-term memory networks, this algorithm is dependent on the absolute time, with ability to be applied onto larger real-life data set. Still, more research is needed to tune the algorithm's performance gain, Huuhtanen et al. (2018).

2.1.3. *Exponentially Weighted Moving Average (EWMA)*

The EWMA control chart can detect fault occurrences by a statistical examination, held between actual and non-faulty measurements. By taking into consideration the set $\{x_1,x_2,...,x_n\}$ as the collected observations, EWMA control chart can be computed according to Eq. (4), Garoudja et al. (2017).

$$\begin{cases} z_t=\lambda x_t+(1-\lambda)z_{t-1} \text{ if } t>0 \\ z_0=\mu_0 \text{ if } t=0 \end{cases} \quad (4)$$

with z_t representing the chart's output, x_t the actual time observation of the monitored process, λ the forgetting parameter, and μ_0 the mean of the free fault process' data. The expanded chart in Eq. (4) indicates, whether if the monitored process is under control at time t or not, by referencing the inclusion/exclusion of λ in the range of [LCL,UCL]. The terms LCL and UCL denote the Lower Control Limit and Upper Control Limit, respectively.

The boundaries control limits (LCL,UCL) can be calculated according to Eq. (5).

$$\begin{cases} \text{LCL} = \mu_0 - L\sigma_{z_t} \\ \text{UCL} = \mu_0 + L\sigma_{z_t} \end{cases} \quad (5)$$

with L representing the control limit's width and σ_{z_t} the standard deviation, calculated as in Eq. (6).

$$\sigma_{z_t} = \sigma_0 \sqrt{\frac{\lambda}{(2-\lambda)}(1-(1-\lambda)^{2t})} \quad (6)$$

with σ_0 representing the free fault dataset's standard deviation.

The flowchart of the entire EWMA's control is shown in Fig. 3. EWMA-based algorithms own a high ability in detecting small shifts in the monitored process, and a great flexibility, reflected in the possibility of accurate obtainment of results, by few parameters adjustments. However, accurate detection is particular for short-circuit, open-circuit and partial shading faults, Garoudja et al. (2017).

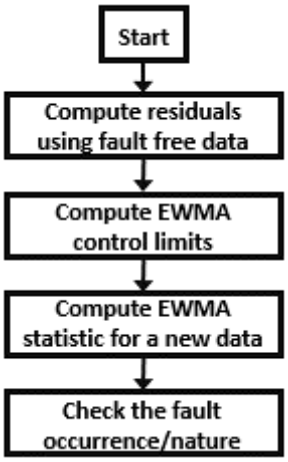

Fig. 3. Flowchart of the EWMA control

2.1.4. *Markov Chains (MC)*

For any element within the PV network, its behaviour is described either as normal or corrupted, according to a succession of states. The historical knowledge of a system's states, during the time vector $\{t_1, t_2, \dots, t_n\}$ permits the acknowledging of the state at any time t, Opera et al. (2019).

The Markov process' evolution to know the state of the system at time t (whether in failure or normal mode) depends on its current state and the way reaching it. A probability of a process in the states ξ and e at moments θ and t respectively, is denoted by $P(t,e,\theta,\xi)$. When the condition in Eq. (7) is not met, the Markov processes are not homogeneous and referred to as Markov chains.

$$P(t,e,\theta,\xi) = P(t+t_1,e,\theta+t_1,\xi) \quad (7)$$

Accordingly, the probability of the system to be in state j at the moment s_1 while already knowing it was in state i in the moment s with $s < s_1$ is shown in Eq. (8).

$$p_{ij}(s,s_1) = P\{x(s_1) = j; x(s) = i\} \quad (8)$$

Based on this model, the reliability indicators, such as mean total duration of successful/failure operations over the reference period are calculated as in Eqs. (9)-(10) respectively.

$$M[\alpha(T)] = P_S \times T \quad (9)$$

$$M[\beta(T)] = P_F \times T \quad (10)$$

Such that P_S and P_F represent the probability of success and failure respectively, with T the reference period. Such indicators are used as a monitoring key to the behaviour of the system. The algorithm grouping previous steps, which aims to calculate the maximum number of failures and maximum duration of one failure, starts with the probability P_0 assuming that all elements are normally operating.

This probabilistic Markov chains-based model is able to detect failures and classify them according to the dysfunction source (panels, wires, inverters, etc.), while informing the duration of each service interruption, if taken place. On the other hand, the results of such algorithm might not be accurate due to limited data gathered from the PV system, Opera et al. (2019).

2.1.5. *Hybrid Deep Learning (HDL)*

The PV power prediction can also be applied using a hybrid deep learning algorithm, consisting of Convolutional Neural Network (CNN), integrated with Long-Short Term Memory (LSTM). The CNN facilitates the PV power production by taking advance from historical power data, where the LSTM usage consists of modelling the temporal changes in latest PV data. The mixture of CNN with LSTM constructs the prediction model based on intrinsic power data of the PV system, Li et al. (2020).

Beginning with CNN model, which consists of a convolution, pooling and fully connected layers, the predicted power output data P_{d-K}^{m+1} for different $(\mathrm{d}-\mathrm{K})^{th}$ day on $(\mathrm{m}+1)^{th}$ time on that day can be grouped into the vector X_d as shown in Eq. (11).

$$X_d = [P_{d-1}^{m+1}, P_{d-2}^{m+1}, \dots, P_{d-K}^{m+1}]^T \quad (11)$$

For the LSTM model, used to predict the next output power P_d^{m+1} it has inputs as grouped in the input vector X_m shown in Eq. (12).

$$X_m = [P_d^{m+1}, P_d^{m-1}, \dots, P_d^{m-F}]^T \quad (12)$$

Such that P_d^m is the output power at the m^{th} time on d^{th} day, with X_m and F denoting the window size of LSTM. The final predicted output power, as a result of mixing CNN with LSTM models is shown in Eq. (13).

$$p^f = \alpha P_{CNN}^f + \beta P_{LSTM}^f \quad (13)$$

with P_{CNN}^f and P_{LSTM}^f representing the predicted output power from CNN and LSTM models respectively, and α, β representing two non-negative models assigned weights.

Prediction accuracy is calculated after comparison of the predicted power p^f with measured one P_n^m, according to indicators indexes formulas, such as the Mean Average Error (MAE), Root Mean Square Error (RMSE) as shown in Eqs. (14-15) respectively.

$$MAE = \frac{1}{N}\sum_{n\in N} |\, P_n^m - P_n^f \,| \quad (14)$$

$$RMSE = \sqrt{\frac{1}{N}\sum_{n\in N}\left(P_n^m - P_n^f\right)^2} \quad (15)$$

with N representing the total number of test samples. This hybrid model suffered from small prediction error when compared with other artificial intelligence-based methods such as Radial Basis Function Neural Network (RBFNN) and Back Propagation Neural Network (BPNN), but offers on the counterpart real-time parameters extraction capability, Li et al. (2020).

The process-history based methods can evaluate partial shading conditions, detect short circuit fault occurrence, and predict the soiling effects on PV performance. However, this category requires a historical data to operate accordingly, which might not always be available.

2.2. *Quantitative based methods*

The fault detection manner under this category, is based on the comparison between the real and expected performances of the PV system, while residual error implies the presence of a certain fault. It comprises the following sub-methods:

- PV power forecasting
- Degradation pattern identification
- k-nearest neighbour
- Support vector regression

2.2.1. *PV Power Forecasting (PVPF)*

To keep the PV system under control, power forecasting is a tool to predict the performance of the system, hence confirming or not the possibility of a fault occurrence. The error estimation resulting from comparison of actual and predicted power measurements, is the key indicator for a faulty event, Kene et al. (2017).

The inputs to the Artificial Neural Network (ANN) shown in Fig. 4, are defined by the vector $\{\mathrm{x}_1,\mathrm{x}_2,\dots,\mathrm{x}_\mathrm{n}\}$ which is correlated with the PV system inputs (temperature,

irradiance), and the output y with the maximum power output of the system.

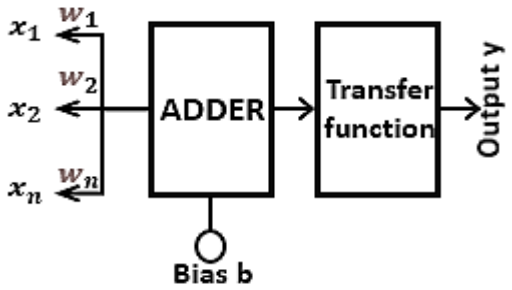

Fig. 4. ANN structure

The input vectors are processed along with their corresponding weight vectors ω_n in the adder, which in turns is biased by the threshold b. The equation of the total adder's input is shown in Eq. (16).

$$u=\sum_{j=1}^{n} x_j w_j \quad (16)$$

The output is then produced according to the transfer function, as shown in Eq. (17).

$$y=f(xw+b)=f(G+T) \quad (17)$$

with G and T representing the PV system's inputs of irradiance and temperature, respectively.

The simple computational technique of this ANN model, has shown accuracy in modelling the input/output relationship for the PV system, hence predicting any possible future failure, but did not take into specification any case narrowed fault detection type (on the level of PV modules, inverter, etc.) instead, it was generic, Kene et al. (2017).

2.2.2. *Degradation Patterns Identification (DPI)*

In terms of residual vector, the numeric difference between actual and real-time power production from the PV plant and the data estimated by a model of the inverters developed *ad hoc* is computed. The inverter model is developed using ANN, trained with historical data of solar irradiance, temperature and produced power, De Benedetti et al. (2018).

The calculated residual vector is hence applied to a Triangular Moving Average (TMA), for the sake of identifying future anomalies within the network. The detection algorithm flowchart is explored in Fig. 5.

In the computation of daily residuals task, a per-day aggregation modelling is executed on the residual vector.

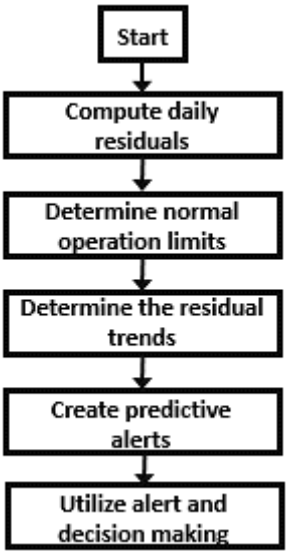

Fig. 5. Degradation patterns identification steps

The operational limits are then classified as Daily Lower Limit (DLL) and Daily Upper Limit (DUL) as shown in Eqs. (18-19) respectively.

$$DLL = 3\sigma_d \quad (18)$$
$$DUL = 5\sigma_d \quad (19)$$

with σ_d representing the daily-equivalent standard deviation index, as a function of the hourly dataset σ_h, seen in Eq. (20).

$$\sigma_d = K\sigma_h \quad (20)$$

where K represents the factor of prediction accuracy. The extraction of daily residual trends is based on a data filtering process, held by the TMA. Successively, the areas of degradation are found based on the derivative of the trend signal. The precedent data analysis is at final stage conditionalized in order to ensure the presence of a fault.

This model presents a validation error or 2.3% with a detection rate of over 90%, but on the other hand, implies a single model for all acquainted data, De Benedetti et al. (2018).

2.2.3. *k-Nearest Neighbour (k-NN)*

A lazy learning algorithm is used for function approximation/classification. The unknown points values of a function f can be predicted based on a sampling of the function itself, as shown in Eq. (21).

$$\{(x_i, y_i)|y_i = f(x_i)\} \quad (21)$$

where for an unknown point x the value of $f(x)$ is estimated based on the k-NN, by means of a suitable voting average. Regardless of its high accuracy, this process needs multi-algorithms combination and requires heavy training sets, Isapour et al. (2019).

2.2.4. *Support Vector Regression (SVR)*

Reinforcing both linear and non-linear mapping schemes, the Support Vector Regression (SVR) is obtained as a linear combination of samples or by means of kernels, respectively, Ferrari et al. (2013). The regression is solved by minimizing the loss function, which is governed by the following items:

(i) Accuracy ε
(ii) Trade-off C
(iii) Kernels σ

The mapping of the Support Vector Regression (SVR) is hence modelled as a linear addition of kernels' Gaussian function as shown in Eq. (22).

$$f_{SVR}(x) = \sum_{i=1}^{L} \beta_i G(x; \mu_i, \sigma) + b \qquad (22)$$

with β_i representing the corresponding coefficient, μ_i the optimal solution, L the units' number and b a constant. The SVR model showed better performance and prediction accuracy than k-Nearest Neighbour, still both needs to be enriched by more data, Ferrari et al. (2013).

Qualitative based fault prediction techniques can detect faults existence on the Direct Current (DC) as well as the Alternative Current (AC) sides of the PV system, by data approximation/comparison. On the other side, such methods require heavy computational functionalities to continuously monitor and estimate error rates.

3. Discussion

The variety of predictive maintenance techniques for PV systems induces a challenge when choosing a suitable scheme. The key points to be taken into consideration are the detection level (panels, power conditioners, energy storage systems or AC sides of the PV system) and the fault type (internal, external, or electrical). From another side, the maintenance scheme's cost of implementation and required acquaintances are another key elements, modifying its choice.

For instance, all process-history based techniques, require complex programming routines, to develop a self-training model. This fact could increase the implementation cost. The developed model requires in turn a large amount of historical data, in order to produce training routines.

Quantitative based models on the other hand do not involve such programming complexity. Instead, they require heavy computational facilities, to perform approximation/differencing between different measurement sets (predicted, simulated, measured, etc.). Despite the technical challenges (complex programming) as well as hardware challenges (need of extra equipment), both sub-techniques would offer a better opportunity in reducing the probability of fault occurrence in PV systems.

Table 1 standardizes the comparative assessment between different predictive techniques.

Table 1. Comparative assessment for different predictive techniques.

	Method	Detection level	Fault type	Accuracy
Process-history based methods	DT	Entire DC zone: electrical	1) Line-line 2) Ground 3) Mismatch	93.55% to 99.98%
	DL	DC zone: PV panel	Reduced power output	-
	EWMA	Entire DC zone: electrical	1) Short-circuit 2) Open-circuit 3) Partial shading	-
	MC	DC and AC zones	1) Power conditioning and protective units failure 2) Reduced PV panel power output	-
	HDL	DC zone: electrical	Reduced PV power output	-
Quantitative based methods	PVPF	DC zone: electrical	Reduced PV module output power	98.12% to 99.77%
	DPI	AC zone	Reduced power output	90%
	k-NN	DC and AC zones	Power perturbation	-
	SVR	DC and AC zones	Power perturbation	-

4. Conclusion

A PV system can be viewed as sets of interconnections between different sub-networks. The DC side, comprising the PV array, the charge controller, and the battery bank, is linked to the inverter to deliver consumable power at the AC side. The fault event possibility is higher at the DC side, since internal, external, and electrical faults might occur on the level of the array, rather than almost pure electrical

faults which might happen at the AC side. Since PV systems are of outdoor nature, the array can interact with many failure events, especially ones due to environmental instability. As a PV system can well operate without a predictive maintenance scheme, it is recommended to adapt a failure predictor mainly for large PV farms, with emphasize on detecting DC zone related failures, since they are the hardest to recognize. When generated power is in megawatts, an earlier failure interruption could save immense profitability resulting from power loss/intermittency. The choice between process-history or quantitative technique's architecture refers to the dataset availability of solar irradiance, temperature, and other efficiency related criteria. Finally, one of the challenges that we propose to take up in the future work is the definition and implementation of a decision-making scheme from data collection and processing to the maintenance decision in a global context of photovoltaic plant management.

References

Maleki, A., A. Haghighi, M.E.H. Assad, I. Mahariq and M.A. Nazari (2020). A review on the approaches employed for cooling PV cells. *Solar Energy 209*, 170-185.

Do Nascimento, A.D.J. and R. Ruther (2020). Evaluating distributed photovoltaic (PV) generation to foster the adoption of energy storage systems (ESS) in time-of-use frameworks. *Solar Energy 208*, 917-929.

Bazan, J., J. Rieradevall, X. Gabarrell, and I. Vazquez-Rowe (2018). Low-carbon electricity production through the implementation of photovoltaic panels in rooftops in urban environment: A case study for three cities in Peru. *Science of the Total Environment 622-623*, 1448–1462.

Conceicao, R., I. Vazquez, L. Fialho, and D. Garcia (2020). Soiling and rainfall effect on PV technology in rural Southern Europe. *Renewable Energy 156*, 743-747.

Manohar, M., E. Koley, and S. Ghosh (2019). Enhancing resilience of PV-fed microgrid by improved relaying and differentiating between inverter faults and distribution line faults. *International Journal of Electric Power & Energy Systems 108*, 271-279.

Kaushal, J. and P. Basak (2020). Power quality control based on voltage sag/swell, unbalancing, frequency, THD and power factor using artificial neural network in PV integrated AC microgrid. *Sustainable Energy, Grids and Networks 23*, Article ID: 100365.

Osmani, K., A. Haddad, T. Lemenand, B. Castanier and M. Ramadan (2020). Material Based Fault Detection Methods for PV Systems. *Key Engineering Materials 865*, 111-115.

Osmani, K., A. Haddad, T. Lemenand, B. Castanier and M. Ramadan (2020). A review on maintenance strategies for PV systems. *Science of The Total Environment 746*, Article ID: 141753.

Osmani, K., A. Haddad, T. Lemenand, B. Castanier and M. Ramadan (2021). An investigation on maximum power extraction algorithms from PV systems with corresponding DC-DC converters. *Energy 224*, Article ID: 120092.

Yan, C., M. Qu, Y. Chen, and M. Feng (2020). Snow removal method for self-heating of photovoltaic panels and its feasibility study. *Solar Energy 206*, 374-380.

Pawluk, R.E.., Y. Chen, and Y. She (2019). Photovoltaic electricity generation loss due to snow – A literature review on influence factors, estimation and mitigation. *Renewable and Sustainable Energy Reviews 107*, 171-182.

Pei, T., J. Zhang, L. Li, and X. Hao (2020). A fault locating method for PV arrays based on improved voltage sensor placement. *Solar Energy 201*, 279-297.

Manzini, G., P. Gramazio, S. Guastella, C. Liciotti, and G.L. Baffoni (2015). The Fire Risk in Photovoltaic Installations – Checking the PV Modules Safety in Case of Fire. *Energy Procedia 81*, 665-672.

Alnaser, N.W., M.J. Alothman, A.A. Dakhel, I. Batarseh, J.K. Lee, S. Najmaii, A. Alothman, H. AlShawaikh and W.E. Alnaser (2018). Comparison between performance of man-made and naturally cleaned PV panels in a middle of a desert. *Renewable and Sustainable Energy Reviews 82*, 1048-1055.

Mukhopadhyay, B., and D. Das (2020). Multi-objective dynamic and static reconfiguration with optimized allocation of PV-DG and battery energy storage system. *Renewable and Sustainable Energy Reviews 124*, Article ID: 109777.

Gonzalo, A.P., A.P. Marugan, and F.P.G. Marquez (2020). Survey of maintenance management for photovoltaic power systems. *Renewable and Sustainable Energy Reviews 134*, Article ID: 110347.

Zhao, Y., B. Lehman, J.F. de Palman, J. Mosesian and R. Lyons (2012). Decision tree-based fault detection and classification in solar photovoltaic arrays. Paper presented at *2012 Twenty-Seventh Annual IEEE Applied Power Electronics Conference and Exposition Volume number*, Orlando, USA. DOI: 10.1109/APEC.2012.6165803

Huuhtanen, T. and A. Jung (2018). PREDICTIVE MAINTENANCE OF PHOTOVOLTAIC PANELS VIA DEEP LEARNING. Paper presented at *2018 IEEE Data Science Workshop*, Lausanne. DOI: 10.1109/DSW.2018.8439898

Garoudja, E., F. Harrou, Y. Sun, K. Kara, A. Chouder and S. Silvestre (2017). A statistical-based approach for fault detection and diagnosis in a photovoltaic system. *Proceedings of 2017 6th International Conference on Systems and Control, 7-9 May 2017*. Batna. DOI: 10.1109/ICoSC.2017.7958710

Opera, S.V., A. Bara, D. Preotescu, and L. Elefterescu (2019). Photovoltaic Power Plants (PV-PP) Reliability Indicators for Improving Operation and Maintenance Activities. A Case Study of PV-PP Agigea Located in Romania. *IEEE Access 7*, 39142-39157.

Li, G., S. Xie, B. Wang, J. Xin, Y. Li and S. Du (2020). Photovoltaic Power Forecasting With a Hybrid Deep Learning Approach. *IEEE Access 8*, 175871-175880.

Kene, R.O., T.O. Olwal, and S.P.D. Chowdhury (2017). Performance prediction of photovoltaic arrays. Paper presented at *2017 52nd International Universities Power Engineering Conference, 28-31 Aug*, Heraklion. DOI: 110.1109/UPEC.2017.8231991

De Benedetti, M., F. Leonardi, F. Messina, and C. Santoro (2018). Anomaly detection and predictive maintenance for photovoltaic systems. *Neurocomputing 310*, 59-68.

Isapour, E. and S.M.M. Tafreshi (2019). A Hybrid Model Based on Neural networks to Predict the Power Output of Photovoltaic Systems. Paper presented at *2019 Iranian Conference on Renewable Energy & Distributed Generation, 11-12 June 2019*, Tehran, Iran. DOI: 10.1109/ICREDG47187.2019.194227

Ferrari, S., M. Lazzaroni, V. Piuri, A. Salman, L. Cristaldi and M. Faifer (2013). A data approximation based approach to photovoltaic systems maintenance. Paper presented at *2013 IEEE Workshop on Environmental Energy and Structural Monitoring Systems, 11-12 Sept. 2013*, Trento, Italy. DOI: 10.1109/EESMS.2013.6661694

Annexe 1.5

Étude des algorithmes d'extraction de la puissance maximale d'un système photovoltaïque avec les convertisseurs DC-DC correspondants

Energy 224 (2021) 120092

Contents lists available at ScienceDirect

Energy

journal homepage: www.elsevier.com/locate/energy

An investigation on maximum power extraction algorithms from PV systems with corresponding DC-DC converters

Khaled Osmani [c], Ahmad Haddad [a, b], Thierry Lemenand [c], Bruno Castanier [c], Mohamad Ramadan [a, b, *]

[a] School of Engineering, International University of Beirut BIU, Beirut, Lebanon
[b] School of Engineering, Lebanese International University LIU, Bekaa, Lebanon
[c] LARIS EA 7315, Polytech Angers, UNIV Angers, France

ARTICLE INFO

Article history:
Received 8 August 2020
Received in revised form
1 February 2021
Accepted 9 February 2021
Available online 13 February 2021

Keywords:
MPPT
GMPPT
Maximums
Extraction
DC-DC
Converters

ABSTRACT

This paper aims at exploring different approaches utilized to track the Maximum operating Power Point (MPP) of PV (Photovoltaic) modules, fulfilling the largest amount of available power extraction, hence achieving cost and energy efficiencies of PV systems. This procedure takes place within two divisions: algorithm implementation and DC-DC Power Processing Units (PPUs) design. First and foremost, all MPP algorithms fall under two major categories: local MPP (happens during homogeneous solar radiations) and global MPP (occurs with partial shading conditions). Each of the two groups possesses various methodologies for algorithm generation. Secondly, PPUs were generally classified as either isolated or non-isolated DC-DC converters. Each collection reigns a buck, boost and buck-boost converters with diverse circuit layouts. A critical assessment and comparison were conducted for algorithms and converters in terms of efficiency, reliability and complexity. After analysis and comparison of different maximum power point tracking schemes, it is found that the best algorithm to be adapted is from the global maximum power point tracking set, under exploitation of characteristic curve topologies. For PPUs architecture, it is concluded that a non-isolated buck-boost converter is the best to be chosen while designing an MPP tracker.

1. Introduction

PV systems are top ranked among renewable energy sources, with continuous increasing annual electricity generation [1]. By lowering carbon dioxide foot print [2], with convenient energy storage systems [3,4] such systems present flexibility in hybridization with other renewable energy supplies as well, thus meeting larger load demands [5]. These systems depend on different climatic conditions, mainly temperature and irradiance levels [6]. Environmental conditions continuously fluctuate, as solar radiations striking on the PV panels' surfaces and ambient temperature values are inconstant. Accordingly, the characteristic curve I–V (Current-Voltage) of a PV cell exhibits a nonlinear behavior resulting in a time varying maximums. In other words, the standard power written on the datasheet of each PV module is never fully attained unless interfered by a maximum power tracker [7]. This drawback backpedals the cost efficiency of any PV system, where it leaves some amount of the total available power untouchable [8].

Included in charge controllers (for off-grid PV systems), these trackers work on adjusting the solar operating voltage/current close to the maximum power point voltage/current (V_{MPP}/I_{MPP}) under changing atmospheric conditions [9]. First trackers were labeled as shunt controllers that either inject the output PV voltage to the batteries, or cut it off, with no regulation. Then came the PWM (Pulse Width Modulation) trackers that regulate only the output array voltage to be close to V_{MPP} [10]. That is to say that if solar irradiance is relatively high, the PWM would shut down the value of PV output voltage to be the closest possible to V_{MPP}. Therefore, the extra voltage is dissipated and never used. Such systems were less dynamic as they need the same voltage specification between the PV array and the battery bank. The PWM module works on the voltage conservation theory where input voltage V_{in} equals output voltage V_{out}.

The improved version of these trackers is labeled as MPPT

* Corresponding author. School of Engineering, International University of Beirut BIU, Beirut, Lebanon.
E-mail address: mohamad.ramadan@liu.edu.lb (M. Ramadan).

https://doi.org/10.1016/j.energy.2021.120092
0360-5442/

Nomenclature

A-IV	Approximating I–V
AMA	Artificial Mountain Ape optimization
ANN-MC-QCD	Artificial Neural Network assisted sequential Monte Carlo and Quickest Change Detection
AV	Artificial Vision algorithm
BDS	Bypass Diode Scanning approach
CPV	Configuration of PV cells
CSR-IV	Current Source Region detection of I–V curve
DC	Direct Current
DCS	Deterministic Cuckoo Search algorithm
EA-PO	Enhanced Adaptive Perturb and Observe
EB-MPPT	Enhanced Bayesian based Maximum Power Point Tracking
ES-MPP	Enhanced Scanning based Maximum Power Point Tracking
FVI	Fractional Open Circuit Voltage/Short Circuit Current
GWO-GSO	Grey Wolf Optimization and Golden-Section Optimization
HC	Hill Climb
HGWO-BM	Hybrid Grey Wolf Optimization and Beta Method
HPSOGS	Hybrid Particle Swarm Optimization Gravitational Search algorithm
HS-MPPT	High Speed Maximum Power Point Tracking
HT	Hybrid Taguchi genetic algorithm
HTGPR-J	Hybrid Gaussian Process Regression-Jaya Algorithm
IC	Incremental Conductance
ICSO	Improved Chicken Swarm Optimization
IDE	Improved Differential Evolution algorithm
IGS	Improved Gravitational Search algorithm
IVOC-PO	Improved 0.8 Open Circuit Voltage Model and Perturb and Observe algorithm
MAKWO	Modified Artificial Killer Whale Optimization Algorithm
MCSO	Modified Cat Swarm Optimization
MF	Modified Firefly algorithm
MFO	Moth-Flame Optimization algorithm
MGA-FA	Modified Genetic Algorithm and Firefly Algorithm
MPT	Maximum Power Trapezium algorithm
MP-VB-PSO	Modified Particle Velocity-Based Particle Swarm Optimization
OD-PSO	Overall Distribution and Particle Swarm Optimization algorithm
P&O	Perturb and Observe
PI	Power Increment algorithm
PPU	Power Processing Unit
PSA-OCC	Particle Swarm Optimization combined with One Cycle Control
PV	Photovoltaic
QIDO	Quad Input Dual Output
SEPIC	Single Ended Primary Inductor Converter
SMPS	Switched Mode Power Supply
SSHC-ABC	Single current Sensor Hill Climbing and Artificial Bee Colony
TS-ST-BM	Two Stage using Searching Technique and Bisection Method

(Maximum Power Point Tracker), where it regulates both the voltage and current coming from the solar panels, going to the batteries [11]. It works under power conservation theory where its input power P_{in} equals its output power P_{out} [12]. Their primary role is to manage charging the battery bank. It prevents it from over-charging (under high irradiance conditions) and under charging (during cloudy days). MPPTs became an essential part of any off-grid system: at night, the battery bank voltage is larger than the array voltage that it is connected to, where the MPPT blocks reverse power flow (from batteries to PV) [13]. Similarly, MPPTs are a must during cloudy days, with low solar irradiation [14,15]. Under unpredictably fluctuating climatic conditions, MPPTs in conjunction with solar power forecasting methods accelerate the pace of PSCs' (Partial Shading Conditions) effects mitigation. Solar power forecasting methods play an essential role, in estimating an irradiance mapping model. For instance, pixels in sky image, are filtered to map the relationship between the image and irradiance [16]. The resultant minute level PV power forecasting model, with extracted inputs from instantaneous sky images, can produce high average measures for clouds existence/passage predictions. The period of ahead power forecasting can vary from minutes to a full day in advanced as described in Wang et al. [17]. The correspondent partial daily pattern prediction framework involves deep learning modeling and time correlation principles, as a manner to overcome disadvantages from conventional Artificial Intelligence (AI) based models. Under three steps establishing model upgrading and parameters modifying, PV output power data can be estimated in advanced [17]. By taking into consideration the resulting mapping model, with the intelligent shading pattern prediction technique, a robust MPPT design can be achieved.

In addition to PSCs, when batteries are deeply discharged (below standard depth of discharge for each battery) an MPPT is also a must [18], where it guarantees battery life cycle extension, by supplying maximum charging current.

An MPPT induces a multi-stage charging [19]. The optimized charging of lithium-ion battery for electric vehicles starts by full flow when battery is low, slows down when close to full and trickles when completely charged. It works according to the four following stages:

- Bulk: the MPPT sends all available power from solar output
- Absorption: tapering down the current level to safer values when the battery reaches the regulation voltage
- Equalization: happening at high voltage values, still when the battery is not fully charged, the MPPT will periodically boost to complete the inner chemical reactions inside the battery
- Float: at this final destination, the MPPT reduces the charging voltage

The battery charging procedure stated above, can be understood by comparing it to a manual gear car, with different speed leveled road scenario: the car driver must choose the optimum gear level, to safely run the motor, and achieve the desired speed, in minimum time, with lowest fuel consumption; beginning with first gear, then at each speed upgrade interval, the gear is changed until maximum allowed speed is acquired, no speed boosting is made.

In its entirety, an MPPT consists of algorithm implementation, inside a computer-based chip (processor/controller) to perform different ADCs (Analog to Digital Conversions) in order to sense the PV system's surrounding temperature, irradiance levels and equivalent output PV voltage/current. The "decision-making" is designed by a set of rules to be followed in calculations or problem-solving operations. In other words, it is the programming language executed on the hardware level based on a pre-scripted code that

decides how and when to operate after the behavior of reference scenario.

The decision made is then transferred to power electronic conditioners PPUs, (either buck, boost or combination of both) to output from DC-DC converter an optimum voltage value, to charge the battery bank [20]. The battery bank charging is continuously monitored by MPPT, detecting any change in climatic conditions, to modify the corresponding charging values (voltage/current).

Moreover, the integration of PV supplies with the grid, referred to as Distributed Photovoltaic System (DPVS), can make it hard to recognize the load pattern of residential customers. The estimation of an accurate Customer Baseline Load (CBL), is of crucial importance for the demand response program [21]. A precise CBL can be held by decoupling PV-load, where the difference between actual load pattern and power output of DPVS can be efficiently calculated. This in turns help in better acknowledgment of PV system sizing and requirement for the load demand. The results of such researches can be granted for MPPT design sizing as well, after accurately identifying power outputs of the PV system, to be later fed into the tracker [21].

The proposed CBL estimation can be enhanced to become more resilient versus increased penetration of small-scaled DPVS, by employing a machine learning tactic, to separate the output power of each DPVS from net load data [22]. This process is done under two stages, resulting in PV output power estimation. The resultant data, such as maximum current/power, can also be granted from, during the design stage of any solar tracking controller.

The rest of this paper is decomposed as follows: in Section 2 a brief overview of off-grid PV systems is executed, where in Section 3, MPPT algorithms are explored either under uniform irradiance or partial shading conditions. In Section 4, different power processing units are surveyed majorly under isolated and non-isolated DC-DC converters architectures. Section 5 presents the discussion of obtained results from the two precedent sections where finally in Section 6 the overall conclusion is derived.

2. Overview of off-grid PV systems

An off-grid PV system uses a bank of batteries as a back-up during nights and low irradiance climatic conditions [23], where they are not directly connected to the grid (offline) [24]. Fig. 1 entitles the general block diagram of an offline PV system.

The PV array is consisted of many PV modules which in turn are the results of serial/parallel connections of PV cells. In Fig. 1, the output of the array (current, voltage) is primarily fed to the MPPT controller. Accordingly, the duty cycle is regulated to maintain a proper output of the DC-DC converter. This process stabilizes the output of the boost converter, regardless of irradiance fluctuations on the array level. Therefore, the input of the inverter is instantaneously fixed for optimal operation, yielding in maximum power extraction from the PV array. Fig. 2 represents the single diode model for a PV cell.where V_{PV} and I_{PV} are the generated voltage and current respectively from the PV cell. The relation between these quantities is presented in Eq. (1) [26]:

$$I_{PV} = I_{ph} - I_o\left(e^{q\left(\frac{V_{PV}+I_{PV}R_S}{AkT}\right)} - 1\right) - \frac{(V_{PV}+I_{PV}R_S)}{R_{sh}} \quad (1)$$

In Eq. (1), R_S and $R_{sh}$are the series and shunt resistances respectively, q the charge of electron, A the diode ideality factor, T the cell temperature and k the Boltzmann constant.

The corresponding PV array voltage/current outputs are the

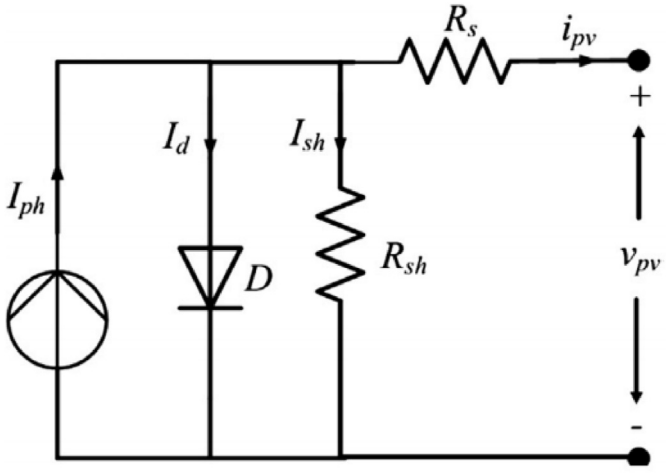

Fig. 2. Single diode model for PV cell [26].

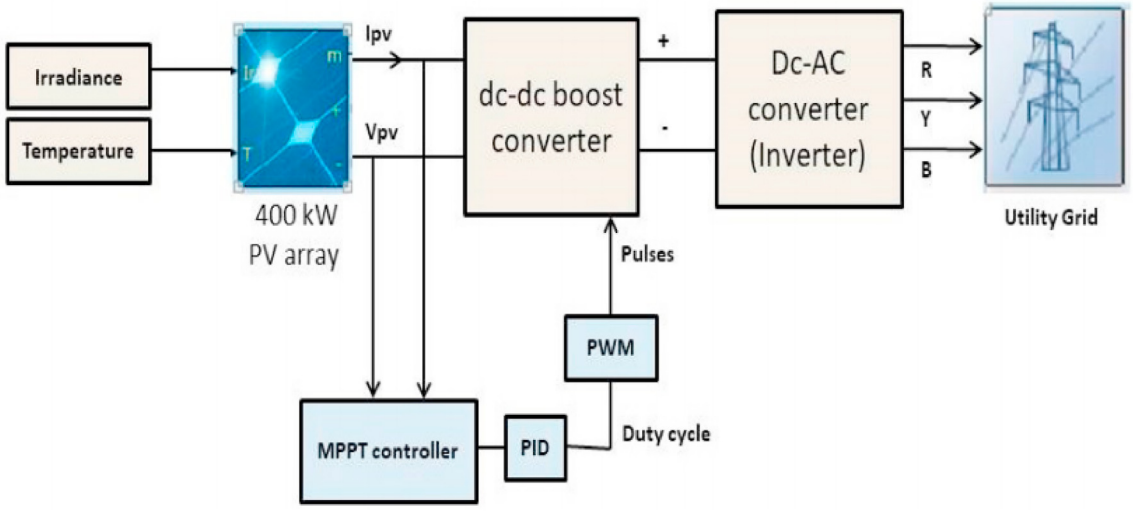

Fig. 1. General representation of an offline PV system with MPPT [25].

combinations (series/parallel) of each cell V_{PV}/I_{PV} output. They present the input variables for the maximum power point controller.

The maximum tracker in an off-grid PV system comes half-way between the output of the PV arrays and the load. Its general role is to provide an impedance matching between the resistance seen at the end of the PV array terminals R_{PV} and load resistance R_{LOAD}. By this, the maximum power transfer theorem ($R_{PV} = R_{LOAD}$)is satisfied hence, the largest amount of available power drawn from PV array output is guaranteed. Fig. 3 shows the position of MPPT implementation in an off-grid (offline) PV system.

The DC-DC converter part of MPPT contains active elements such as inductors and capacitors whose impedances are changed (increased/decreased) with relation to the frequency. Where an inductor impedance is $Z_L = j\omega L$ and capacitor impedance is$Z_C = {}^{1}/_{j\omega C}$ with L and C corresponding inductances and capacitances respectively and ω the angular frequency that equals to $2\pi f$. With the accurate duty ratio (switching frequency of the solid-state switch within DC-DC converters) the overall circuit from PV terminals to MPPT becomes a sequential circuit of adding/dividing resistors equivalently in serial/parallel combinations, to have the closest possible value to R_{LOAD}.

3. MPPT algorithm review

The MPPT (Maximum Power Point Tracking) procedure is confronted with two scenarios:

- *Uniform irradiance conditions*: whether under complete radiation or total shading, uniform irradiance conditions are when PV cell absorbs light equally hence producing a homogeneous power [27].
- *Partial shading conditions*: this happens when sunrays hit the PV panel surface in a dissimilar fashion. This incident is conducted by the presence of physical barriers like dust, snow accumulation, leaves and different shadowing resultant from trees, overhear power lines, buildings and clouds [28].

Because of this fact, the reaction of each PV cell inside each PV module produces a unique power generation [29]. Accordingly, the status of the PV system is said to be under partial mismatch fault [30]. Fig. 4 describes a graphical explanation of unshaded versus shaded PV array, where shading is highlighted with a darker color.

3.1. Under uniform irradiance conditions

The approaches to track MPP (Maximum Power Point) under uniform irradiance conditions (with either complete shading or complete irradiance conditions) uses two distinct algorithm schemes:

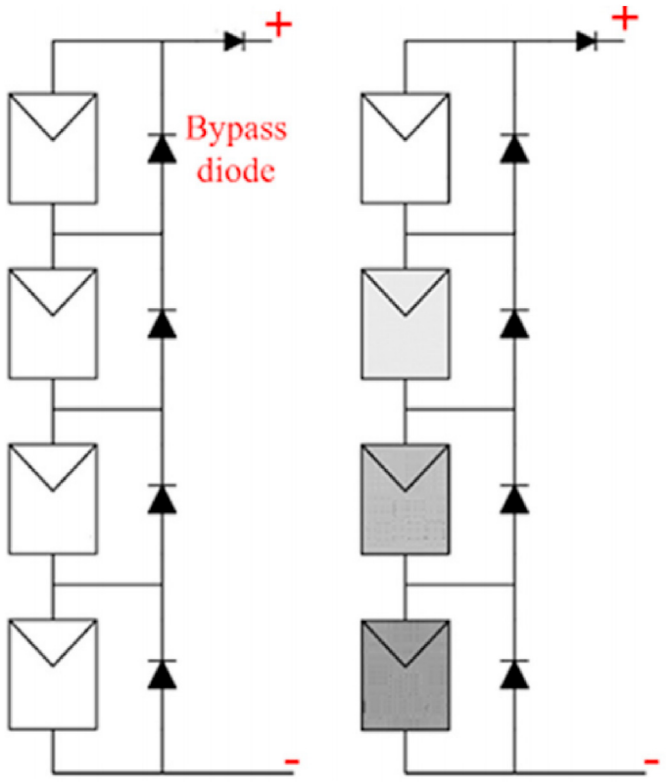

Fig. 4. Unshaded PV array (on the left) versus shaded PV array (on the right) [31].

- Metaheuristic algorithms: are of easy computational implementation and use as input data the V–I (Voltage-Current) of the PV panel in use to determine the increase/decrease in the control variable.
- Model based algorithms: can be used also under uniform irradiance conditions where they use mathematical expressions to calculate V/I (voltage/current) at MPP (maximum power point) using as input data the previously measured voltage and current values of the PV module.

Fig. 5 demonstrates the waveform of a PV cell under uniform irradiance in both V–I and P–V curves.

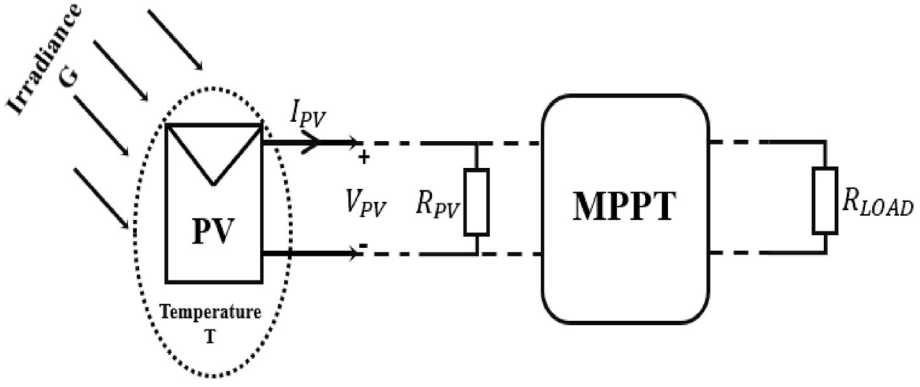

Fig. 3. MPPT positioning in off-grid PV systems.

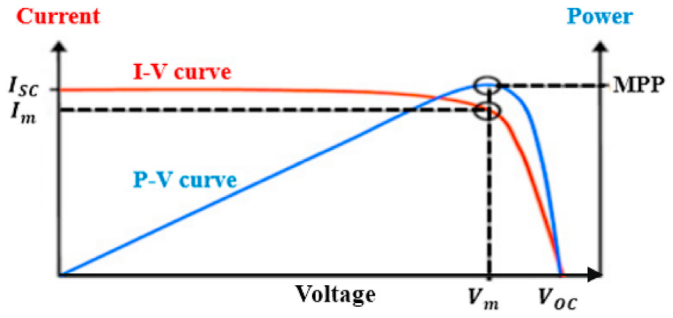

Fig. 5. Uniformly irradiated PV cell waveform behavior [32].

In Fig. 5, there exists a single peak corresponding to MPP (Maximum Power Point) that has V_m value (maximal voltage) ranged between zero and V_{OC} (open circuit voltage) on the X-Axis and I_m value (maximal current) ranged between zero and I_{SC} (short circuit current) on the Y-Axis.

In other words, such algorithms rely on V–I quantities (derived from V–I sensors at the input level) to create a basis for mathematical operations/calculations inside the decision making units (controller, micro-processors) in order to reach specific leveled signals at the output level to be transferred to PPU (Power Processing Units). Fig. 6 encapsulates different algorithms under this category.

3.1.1. Perturb and observe (P&O)

The P&O (Perturb and Observe) algorithm moves the operating point (corresponding to a location defined by V–I (Voltage–Current) values on the V–I curve that, by identification, corresponds in turn to the same location on the P–V curve) in the direction at which output power is increasing [33]. The V–I are continuously sensed at regulated time intervals and compared to change in power. The procedure continues as long as power is observed to increase along with voltage increase [34]. This operation stops when the following equation is satisfied:

$$dP/dV = 0 \tag{2}$$

The difference in perturbation size yields in different P&O algorithm classification. Table 1 summarizes different types of such algorithms according to perturbation size.

Fig. 7 shows the conventional P&O algorithm flowchart. This is one of the most basic algorithms to detect MPP at the lowest cost and ease of installation but, using this algorithm, the operating point fluctuates around the MPP (Maximum Power Point) and gives false data at swiftly changing irradiations [36].

3.1.2. Hill climb (HC)

In a similar fashion to the P&O algorithm, the HC (Hill Climb) algorithm is perturbed in the duty cycle of the converter whereas the P&O perturbations occur in the operating V/I (Voltage/Current) of the array [37]. In this manner, new variables are involved, $d(k)$(duty cycle) and Φ (fixed step-size), where these two variables are perturbed in the direction of increasing power. The perturbation direction is left under two ways:

- Forward perturbation direction: executed when the power at the duty cycle is larger than the one at the previous duty cycle. This signifies that the tracking is moving towards the MPP (Maximum Power Point).
- Reverse perturbation direction: happens when the power at the duty cycle is smaller than the one at the previous duty cycle. This signifies that the tracking is moving away of the MPP (Maximum Power Point).

The following set of equations describes the above-mentioned procedures [38]:

$$d(k) = d(k+\Phi),\ if\ P(k) > P(k-1) \tag{3}$$

$$d(k) = d(k-\Phi),\ if\ P(k) < P(k-1) \tag{4}$$

Despite the fact that HC (Hill Climb) algorithms are among the most commonly used algorithms in partial PV power system, due to their ease of implementation and low cost, they are affected by a different problem: they cannot track the exact MPP (Maximum Power Point) under varying irradiations and drain energy from the PV array [38].

3.1.3. Incremental conductance (IC)

According to Ohm's law across a resistor given by Eq. (5):

$$V = R \cdot I \tag{5}$$

with R equivalent to the resistance (opposing of current flow) equals to V/I, the conductance is referred to as the inverse of R that is the current conduction given by Eq. (6) as:

$$Conductance = {}^{1}/_{R} = {}^{I}/_{V} \tag{6}$$

The incremental conductance algorithm uses the incremental conductance of PV based on the mathematical fact that the derivative of the PV module (according to I–V curve) is zero at MPP (Maximum Power Point), positive at the left of MPP (rising curve with positive slope of the tangent at it) and negative at the right of the MPP (falling curve with negative slope of the tangent). Fig. 8

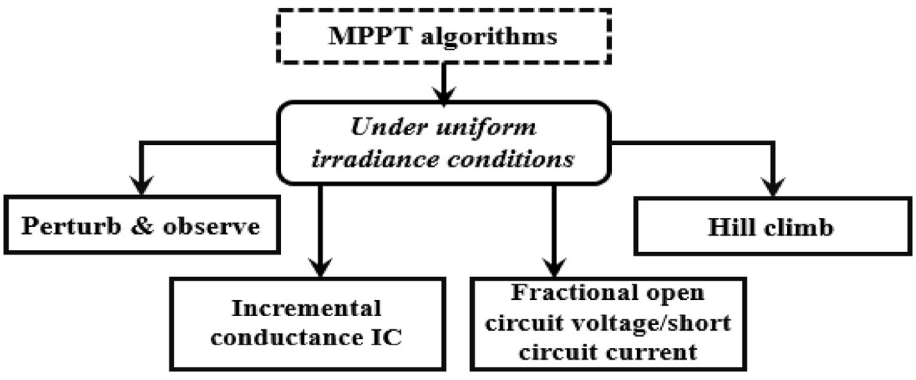

Fig. 6. Different algorithms to track MPP (Maximum Power Point) under uniform irradiance conditions.

Table 1
Different P&O algorithms characterization.

P&O classification	Perturbation size
Conventional	The perturbation size is fixed
Adaptive P&O method	Uses long and small perturbation sizes to attend MPP in small time and near the MPP respectively
Three point weighted method	The perturbing value is dictated by three different points

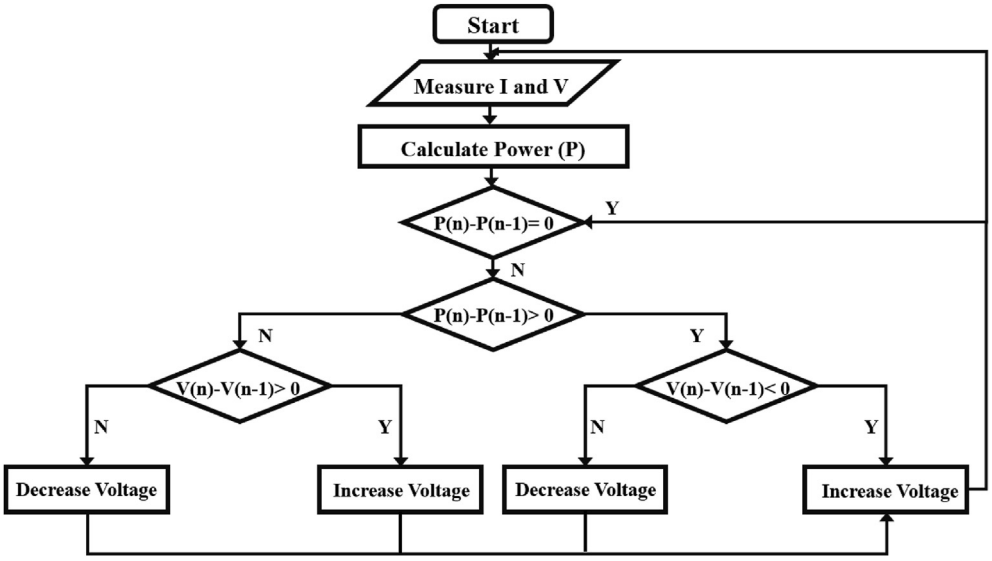

Fig. 7. Perturb and Observe algorithm flowchart [35].

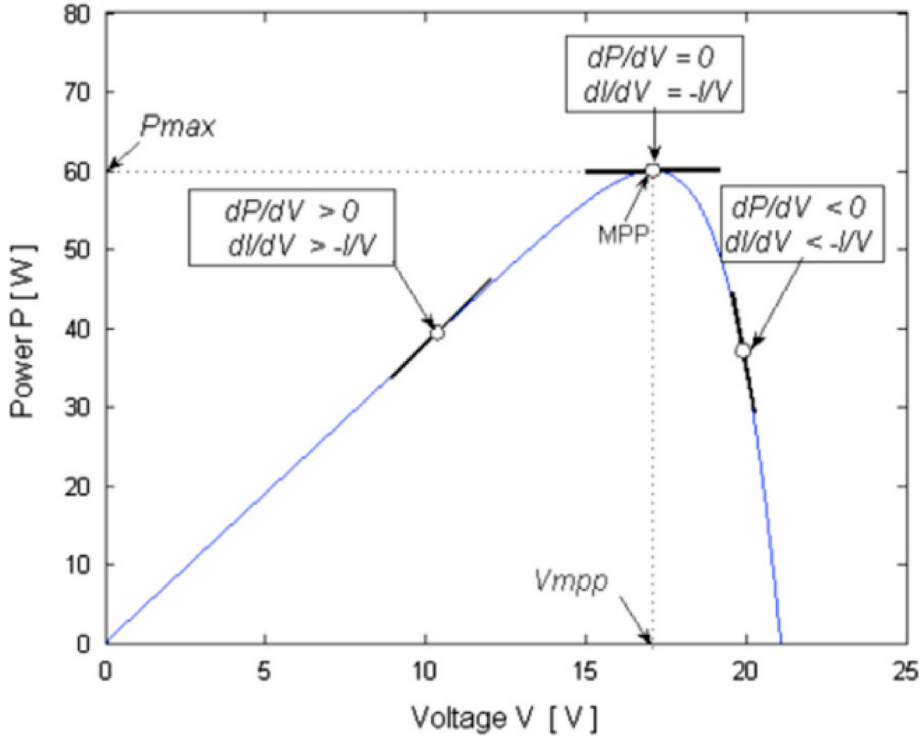

Fig. 8. Relation between incremental conductance and position of the operation point on P–V curve [39].

represents a graphical interpretation of the algorithm working principle.

The decomposition of the I–V (current-voltage) curve of the PV module into three different zones: left of MPP, at MPP, right of MPP enables this algorithm to overcome the limitations of P&O algorithm by using the relation between the instantaneous

conductance I/V and incremental conductance $\Delta I/\Delta V$ described by the following set of Eq. (7) [40]:

$$\begin{cases} \Delta I/\Delta V + I/V = 0 \text{ at MPP} \\ \Delta I/\Delta V + I/V > 0 \text{ at left of MPP} \\ \Delta I/\Delta V + I/V < 0 \text{ at right of MPP} \end{cases} \quad (7)$$

The incremental conductance is found to track MPP (Maximum Power Point) in varying weather conditions, with less oscillatory behavior near the MPP, as found to happen in P&O algorithm. On the other hand, it was found to give false results under low irradiation values [41].

To overcome this drawback, a modified IC (Incremental Conductance) technique with a proportional integral (PI) controller tuned by a swarm-based technique and referred to as whale optimization algorithm (WOA), is initialized. The optimization algorithm has the ability to determine best gain parameters of different modes of PI controller as I, P and Fractional order PI (FOPI) according to performance indices.

The chase for MPPT consists of two phases: exploration and exploitation. During the exploration step, the algorithm searches for the space globally. By space, it is meant the power area beneath the I–V (Current-Voltage) curve corresponding to the PV panel output. The function to extract the most power possible from the panel (the largest area under the I–V curve corresponding to the MPP at the knee of curve) is regarded to the exploitation phase: in this part, the aim is to obtain the optimal values of K_p (proportional gain) and K_i (integral gain) for the following equation of PI controller transfer function:

$$G_C(S) = K_p + K_i/S \quad (8)$$

where S corresponds to Laplace transform $S = j\omega$. The fractional PI (FOPI) is established to obtain an improved system performance rather than PI controller, where it tunes K_p, K_i and λ which refers to a fractional integrator order regrouped in the following equation:

$$G_C(S) = K_p + K_i/S^{\lambda} \quad (9)$$

The mentioned FOPI controller had a better power performance for the PV system rather than PI controller, since it seemed to nearly eliminate the overshoot (which is an undesired surge in signal that is common for all PI controllers) with a higher settling time [41].

However, the implementation of controllers of all types (whether integral, proportional, derivative and any mixture of these three) have a reluctant voltage error and a notable time domain error, since the Integral and Proportional blocks of the PI (Proportional Integral) controller needs time to execute mathematical calculations which in turn lags the error diminishing time.

3.1.4. Fractional open circuit voltage/short circuit current (FVI)

Due to the fact that both V_{OC} (open circuit voltage) and V_{MPP} (Maximum power voltage) both rely on the X-axis that corresponds to the voltage axis (horizontal) of the V–I curve of a PV module, it can be concluded that a linear relation exists between these two different quantities as given with Eq. (10):

$$V_{MPP} = K_1 \cdot V_{OC} \quad (10)$$

where K_1 is the proportional constant depending on the PV cell type and meteorological conditions [42]. According to statistical approaches covering different types of PV cell technologies and common weather conditions, K_1 is found to be in the range between 0.71 and 0.78 [43].

The main limitation of this algorithm is the intermittent power loss across PV system output terminals. This happens because the computing system must regularly check for the value of V_{OC} that couldn't be accomplished when a load is connected. To prevent this drawback, a pilot PV cell must be included within the PV module as it only monitors the value ofV_{OC} (open circuit voltage) as no load is connected across that cell terminals. This solution in turn, creates larger drawbacks as the pilot cells must be carefully chosen to accommodate meteorological conditions thus creating more burden on the module fabrication [44].

Just like the fractional open circuit voltage method, the fractional short circuit current begins from the fact that both I_{MPP} (maximum power current) and I_{SC} (short circuit current) lies on the Y-axis (vertical) of the V–I curve that corresponds to the current axis. Therefore, a linear relation also exists between these two different quantities, governed by Eq. (11):

$$I_{MPP} = K_2 \cdot I_{SC} \quad (11)$$

where the constant of proportionality K_2 (specific to the PV module in use) is found to be between 0.78 and 0.92 [42].

Although this algorithm is a direct approach and doesn't need any complex mathematical computations to be solved (likewise in fractional open circuit voltage), it needs in turn a switch to short circuit the PV terminals and a current sensor to periodically measure I_{SC} (short circuit current) what reflects as an increase of components hence elevating prototype's cost [45].

3.2. Under partial shading conditions

In addition to metaheuristic and model based algorithms found in MPPT (Maximum Power Point Tracking) under uniform irradiance, the algorithms topology to track MPP (Maximum Power Point) under partial shading conditions involve soft computing techniques: a fast and efficient training based algorithms developed in computerized processing units involving artificial intelligence procedures.

The sampled data obtained from PV system output (for example a relation between solar irradiance and PV power output) helps in building training data, which allows the ability for the algorithm to make predictions/decisions without being pre-scripted (programmed) in the algorithm itself to perform any desired task [46]. Fig. 9 shows the waveform behavior of a PV cell under partial shading conditions.

In Fig. 9, we see occurrence of multiple peaks, where each corresponds to a MPP (Maximum Power Point). The investigation in this figure permits to tell the existence of a peak point defined by V = 17 V (volts) and P = 42 W (watts). Table 2 encapsulates different

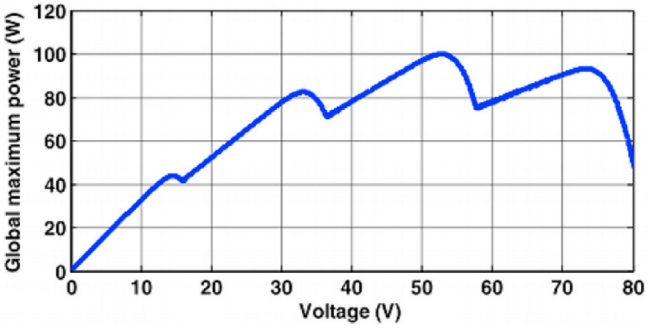

Fig. 9. Power waveform shape in a PV cell under partial shading conditions [47].

Table 2
Localization of different maximum power points.

MPP	Coordination in X–Y plane Voltage (V) - Power (W)
1	17 V - 42 W
2	33 V - 81 W
3	53 V - 100 W
4	75 V - 95 W

MPPs (Maximum Power Points) corresponding to Fig. 9.

Among different Maximum Power Points found in Table 2, the third MPP identified with its Y-axis reference (power axis) is found to have the highest power (100 W) compared to other MPPs. Referred to as GMPP (Global Maximum Power Point) the function of any algorithm under this type of irradiance is to achieve GMPP uniquely. From such perspective, it can be concluded that MPPT (Maximum power point tracking) algorithms have no efficiency for such curves, since they will have no identification of the next occurring MPP. The characterization of GMPPT (Global Maximum Power Point Tracking) techniques bases on four different divisions [47]:

- Intelligent and metaheuristic search algorithms
- Hybrid strategies
- Methods based on exploitation of characteristic curves
- Other GMPPTs [48].

3.2.1. Intelligent and metaheuristic search algorithms

This family of algorithms seeks to find optimal solution under pre-defined conditions (temperature, solar irradiance meta-heuristic data and other information about PV cell topology). Fig. 10 encloses different algorithms to obtain the GMPP (Global Maximum Power Point) using the intelligent and metaheuristic search algorithms.

Inspired by the behavior of chickens towards reaching food, the ICSO (Improved Chicken Swarm Optimization) lead to GMPP (Global Maximum Power Point) detection by mimicking of the individual attempts to reach the forage within each group of chickens: it consists of one rooster, one hen and many chickens. From that arrangement the rooster (having the best fitness) is the most likely to proceed swiftly to the largest portion of the forage. Reflecting to a PV system, the ICSO algorithm translates the behavior of the rooster, towards reaching the GMPP (Global Maximum Power Point) [49]. The cubic equation in Eq. (12) arranges the initial position of individuals in the chickens group:

$$L_{ij} = 4 \times x_{ij}^2 - 3 \times x_{ij} \tag{12}$$

where x_{ij} is the position of the i^{th} individual in j^{th} dimension space and L_{ij} is the chaotic sequence. When Eq. (12) $\neq 0$, the sequence is considered as valid and will return to the optimization space in Eq. (13):

$$x_{ij} = \frac{1}{2(b-a)} L_{ij} + \frac{1}{2(b+a)} \tag{13}$$

where b is the upper limitation of the optimization and a the lower limitation. Since less-fit individuals worsen the procedure to locate an extremum, which is reflected in PV system as increasing calculation time to locate the GMPP, the improved update of chickens is derived in Eq. (14):

$$x_{ij}(t+1) = x_{ij}(t) + FL(t) \times \left(x_{mj}(t+1) - x_{ij}(t)\right) \tag{14}$$

with $FL(t)$ an added coefficient described in Eq. (15):

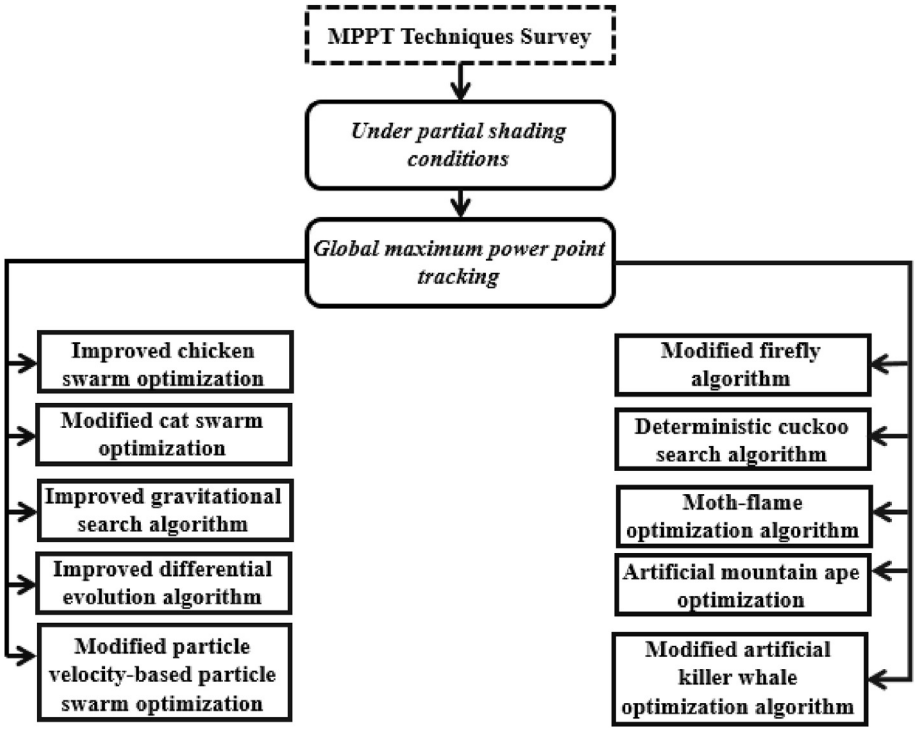

Fig. 10. Different algorithms to track MPP (Maximum Power Point) under partial shading conditions.

a) Improved chicken swarm optimization (ICSO)

$$FL(t) = 0.1 \times rand + 0.4 \tag{15}$$

The ICSO is found better than traditional CSO (Cat Swarm Optimization) resulting in less deviations and smaller iteration time of optimization [49].

b) Modified cat swarm optimization (MCSO)

The MCSO (Modified Cat Swarm Optimization) is an EA (Evolutionary Algorithm) population based on different cats where the most fit cat (having highest fitness factor) reaches food most swiftly. Corresponding to a PV system, the optimal fitness function $f(X)$ means best GMPP (Global Maximum Power Point) seeking. The population begins with a defined number of cats NP where each defines a candidate. The entire set of cats is defined by X_i where i ranges from 1 to total number of cats NP in N-dimensional space. Aside from position each cat has a velocity V_i function defined by Eq. (16) [50]:

$$V_i = [V_{i,1}, V_{i,2}, \ldots, V_{i,n}] \tag{16}$$

The algorithm uses two distinct searching modes:

- Seeking mode (SM)
- Tracking mode (TM)

The output of seeking mode is to find the best fitness value $X_{BestCopy}$ from along the fitness function exposed in Eq. (17) [50]:

$$f(X_j),\ j = 1, 2, \ldots, SMP \tag{17}$$

with SMP (Seeking Memory Pool) is a variable determining the amount of copies that will be created for each cat.

The tracking mode is corresponding to a cat in haunting mode: to track food, the cat would move quickly to a new position. To know the movement of the i^{th} cat, its velocity is modified as:

$$V_{i,d} = w \times V_{i,d} + r_1 \times c_1 \times (X_{best,d} - X_{i,d}) \tag{18}$$

such that$X_{best,d}$ is the best position found by all cats, r_1 a random number ranging from 0 to 1, c_1 acceleration constant and w inertia value. After that step, the velocity is checked if exceeding a threshold value, where if it does, this resultant scalar is considered the new threshold value.

This proposed algorithm was found eligible to deal with PSC (Partial Shading Condition) and can track maximum point in high speed and accuracy [50].

c) Improved gravitational search algorithm (IGS)

This algorithm relies on Newton's gravitational law where particles are attracted to each other by force of gravity and, the larger the gravitational force, the larger the mass of the particle. In other words, all particles move towards the particle with larger mass where itself occupy the optimum position. That larger mass particle is referred in PV system under PSC (Partial Shading Condition) as GMPP (Global Maximum Power Point) [51].

The procedure of IGSA (Improved Gravitational Search Algorithm) progresses as follows [51]:

$$\alpha_i(t) = \begin{cases} \alpha_{min} + \dfrac{(\alpha_{max} - \alpha_{min}) \times (fitness_i(t) - worst(t))}{average(t) - worst(t)}, & fitness_i(t) > average(t) \\ \alpha_{max}, & fitness_i(t) < average(t) \end{cases} \tag{19}$$

such that α_i is the gravitational constant change factor, α_{min} and α_{max} are the minimum and maximum values of α_i respectively, $fitness_i(t)$ is the fitness value of particle i at time t, and $worst(t)$ and $average(t)$ are respectively the worst fitness value and average fitness values at time t.

1. Generate the initial population
2. Calculate the fitness of each particle as described in Eq. (19):
3. Update $G_i(t)$ (Gravitational constant) and $M_i(t)$ (Inertial mass)
4. Calculate the total force from other particles
5. Update particles position
6. Repeat from step 2 until maximum numbers of iterations T is reached.

The application of this algorithm showed improvement upon tracking time/accuracy of GSA (Gravitational Search Algorithm) however, it showed no design integration between algorithm and PPU (Power Processing Unit) [51].

d) Improved differential evolution algorithm (IDE)

The IDE (Improved Differential Evolution) algorithm suits well for determining a GMPP (Global Maximum Power Point) in a PV system since it is dedicated to solve non-linear problems (like the current-voltage and power-voltage curves characteristics of a PV module). Labeled as EA (Evolutionary Algorithm), that needs few parameters to tune: four particles are used in the target vector (that is equivalent to converter duty cycles) [52]. Eq. (20) defines target vectors $D_{i,G}$:

$$D_{i,G};\ i = 1, 2, 3, 4 \tag{20}$$

According to each $D_{i,G}$ a $P_{i,G}$ (output power of PV array) is calculated. The highest obtained power is labeled as P_{best} corresponding to the best duty cycle D_{best}. The searching process will end if the differences in power and duty cycles respectively $\Delta P_{i,G}$ and $\Delta D_{i,G}$ are both larger than 0.005. If that condition is not satisfied, the duty cycle is maintained as D_{best} hence the iterations stop at that level. The following step after reaching that condition is to differentiate between best obtained power and output of PV array according to Eq. (21):

$$|P_{best} - P_{PV}|/P_{best} > 0.005 \tag{21}$$

When Eq. (21) is not satisfied, re-initiate with the new obtained D_{best}. If satisfied, a calculation in current-voltage derivatives are compared with 0 according to Eq. (22) and Eq. (23):

$$dV > 0\ \&\ dI < 0 \tag{22}$$

$$dV > 0 \;\&\; dI > 0 \tag{23}$$

If one of Eq. (22) and Eq. (23) is satisfied, a new duty cycle is obtained. If not, original target vectors $D_{i,G}$ is re-initialized. When the condition of the searching process is not verified i.e. $\Delta P_{i,G}$and $\Delta D_{i,G}$ are less than 0.005, a donor vector $DV_{i,G}$ is created from the original target vectors $D_{i,G}$. At this point, a crossover vector of $DV_{i,G}$ generates a new trial vector $DU_{i,G}$ described in Eq. (24):

$$DU_{i,G} = \begin{cases} DV_{i,G}\,; if\ rand \ \geq CR \\ D_{i,G}; else \end{cases} \tag{24}$$

where*rand* is a random number between [0,1] and *CR* a constant crossover rate.

The trial vector at this stage becomes compared to either of Eq. (25) and Eq. (26):

$$DU_{i,G} = D_{i,G} \tag{25}$$

$$DU_{i+1,G} = DU_{i,G} \tag{26}$$

If any of the two equations (25) and (26) are satisfied, the resultant power $PU_{i,G}$ from the trial vector$DU_{i,G}$ is equal to $P_{i,G}$ (array power resultant from target vector $D_{i,G}$) and accordingly $PU_{i+1,G}$ becomes equal to $PU_{i,G}$. When Eq. (25) and Eq. (26) are not satisfied, re-obtain the $PU_{i,G}$ from $DU_{i,G}$ then select the best value among $DU_{i,G}$ and $D_{i,G}$. With updated $D_{i,G}$ re-obtain newer values for $P_{i,G}$and repeat the sequence from that point.

The proposed algorithm showed a fast track (within 2 s) of a GMPP (Global Maximum Power Point) and responded swiftly (within 0.1 s) to irradiance/load variations [52].

e) Modified particle velocity-based particle swarm optimization (MP-VB-PSO)

The MP-VB-PSO (Modified Particle Velocity-Based Particle Swarm Optimization) bases on the conventional PSO (Particle Swarm Optimization) with the addition of limiting randomness by modification of velocity equation. This algorithm makes several adjustments (addition of adaptive values) which neglects the need for tuning the weight factor [53]. Results showed that this algorithm has better performance than conventional PSO.

f) Modified firefly algorithm (MF)

A metaheuristic swarm intelligence algorithm inspired by the behavior of fireflies glowing that applies population-based iterations with different factors [54]. The movement of a firefly *i* towards a more attractive firefly *j* is defined by Eq. (27):

$$x_i^{t+1} = x_i^t + \beta_0 e^{-\gamma r^2}\left(x_j - x_i\right) + \alpha\varepsilon_i \tag{27}$$

where β_0 is the degree of attractiveness defined by Eq. (28):

$$\beta_0 = \beta_{0max} + (\beta_{0min} - \beta_{0max}) \times \frac{Iter}{MaxIt} \tag{28}$$

and α a parameter of a randomizer vector defined by Eq. (29):

$$\alpha_0 = \alpha_{0max} + (\alpha_{0min} - \alpha_{0max}) \times \frac{Iter}{MaxIt} \tag{29}$$

with x_j and x_i the locations of fireflies *i* and *j* respectively. The last expression in Eq. (29) corresponds to a randomizer parameter with ε_i a randomizer vector obtained from a Gaussian distribution.

The reflection of two fireflies heading towards each other, is understood in PV system as the movement of a random operation point in the I–V (current-voltage) curve of a PV module towards GMPP (Global Maximum Power Point). This proposed modification of firefly algorithm has accelerated the convergence speed at each iteration by linearly reducing values of β and α what increases its efficiency versus the traditional firefly algorithm [54].

g) Deterministic cuckoo search algorithm (DCS)

The DCS (Deterministic Cuckoo Search) algorithm upgrades from traditional CS (Cuckoo Search) algorithm by beginning a set with three particles arranged from lowest to highest voltages [55]. After measurement of I_{PV} (current of PV panel) and V_{PV} (voltage of PV panel) the power for each of the three particles are calculated.

The particles are re-arranged according to their obtained power values, labeled as P_a (power of first particle), P_b (power of second particle) and P_c (power of third particle). The voltage command (activated by change-side mechanism) is updated according to P_a: when $P_a$is at leftmost or rightmost the voltage command is updated according to Eq. (30):

$$\begin{cases} P_{a,new} = P_a \\ P_{b,new} = P_b + \alpha(P_a - P_b) \\ P_{c,new} = P_c + \alpha\left(P_{a,new} - P_{b,new}\right) \end{cases} \tag{30}$$

where α is a multiplication constant. The voltage command is changed according to Eq. (31) when P_a is in the middle:

$$\begin{cases} P_{a,new} = P_a \\ P_{b,new} = P_b + \alpha(P_a - P_b) \\ P_{c,new} = P_c + \alpha(P_a - P_c) \end{cases} \tag{31}$$

A check of GMPP (Global Maximum Power Point) tracking stoppage must be made. If the stop criterion is satisfied, the tracking must stop, as the system will wait for any change in irradiance level. The algorithm stops finally the perturbation when both $(P_a - P_b)$ and $(P_a - P_c)$ are lower than a threshold value *dV*. With only one parameter to be tuned, and three particles to be investigated, this algorithm works in a simple structure with high speed and accuracy according to traditional Cuckoo search [55].

h) *Moth-flame optimization algorithm (MFO)*

The MFO algorithm is based on the moth behavior to converge towards a light source. The population in study here is within two forms: the number of moths, grouped in matrix M, and sets of flames, organized by matrix F. The two matrices (M and F) are of $n \times d$ dimension where n represents the moths number and d is the searching space [56,57]. The M and F matrices are described by Eq. (32) and Eq. (33) respectively:

$$M = \begin{bmatrix} M(1,1) & \cdots & M(1,d) \\ \vdots & \ddots & \vdots \\ M(n,1) & \cdots & M(n,d) \end{bmatrix} \tag{32}$$

$$F = \begin{bmatrix} F(1,1) & \cdots & F(1,d) \\ \vdots & \ddots & \vdots \\ F(n,1) & \cdots & F(n,d) \end{bmatrix} \tag{33}$$

Vector M is updated through a new vector *OM* that in turn is updated into another vector *OF* described in Eq. (34) and Eq. (35) respectively:

$$OM = [OM_1, \ldots, OM_i, \ldots OM_n] \tag{34}$$

$$OF = [OF_1, \ldots, OF_i, \ldots OF_n] \tag{35}$$

This algorithm executes several iterations [56] to get the best gain value K_i hence reducing the error $\left(dI/dV + I/V\right)$. In terms of tracking ability, efficiency and steady-state this algorithm showed superior performance in detecting GMPP (Global Maximum Power Point) compared to PSO (Particle Swarm Optimization) [57].

i) Artificial mountain ape optimization (AMA)

Inspired by mountain apes' groups organizations, where a set of apes is labeled as troop that is governed by a silverback (decision maker). The silverback communicates with other adult apes when he finds food, orders (the troop) to wait and then leaves its position toward a newer one to find more food. If he fails, he comes back to its previous position to start food intake with the troop.

Likewise, in a PV module the silverback is considered the operating point belonging to the I–V (Current-Voltage) curve of a PV module [58]. The first food reach is considered as a local MPP (Maximum Power Point). When the silverback is going to a new position for aiming to get more food, if reached, this position is considered as another MPP (Maximum Power Point) with higher power than the previous. If failed, the operating point is considered the MPP (Maximum Power Point).

The procedure of AMAO (Artificial Mountain Ape Optimization) goes as follows [58]:

$$Y_J^K = \frac{1.04}{T_A} \times L \times U\left[(d_{max} - d_{min}) + X_J^{K-1}\right] \tag{36}$$

such that d_{max} and d_{min} corresponds to duty ratios' maximum and minimum values respectively 0.95 and 0.005, L a multiple directions belonging to the range of [-6;6], U the factor's adjusting factor belonging to the range of [-2;2] and K the iteration number ranging from 1 to K_{max}.

1. Variables initialization: in which T_A corresponds to the member size in troops and Y_J as the position of the silverback
2. Searching process: where the definition of the position of the silverback in the K^{th} iteration as stated in Eq. (36):
3. Food amount calculation: to check if the amount of food needs more of adult apes within the troop to help in gathering it or not.
4. Decision to go back to the previous position of the silverback at Y_J^{K-1} (the amount of food is smaller than the previous) or head towards a new position (accordingly, this happens when the new operating point in the current-voltage curve of PV module shows less power than the older position on the curve).
5. Stopping criteria: among fifteen different iterations, the algorithms would stop searching hence the PPU (Power Processing Unit) will be set at latest found duty ratio.
6. Restart of the searching pattern: happens when any change in irradiance is observed (through voltage/current sensor and power calculation).

The proposed AMAO (Artificial Mountain Ape Optimization) took less time to converge into a global maximum than other conventional algorithms with lesser perturbations at the maximum power point [58].

j) Modified artificial killer whale optimization algorithm (MAKWO)

Influenced by the behavior of the killer whales (labeled as catchers) to roll the prey whales (the herders) the MAKWO (Modified Artificial Killer Whale Optimization) algorithm is derived. Catchers are found to communicate with other killer whales using the lob tailing behavior, if they find the prey, they kill it and move on to another [59]. The procedure of this algorithm follows the following steps [60]:

$$X_J^K = \frac{2}{K_w} \times h \times c\left[(D_{max} - D_{min}) + X_J^{K-1}\right] \tag{37}$$

1. Variables initialization: killer whales' population are initialized and labeled as K_w. Their position is denoted as X_J that corresponds to duty cycle in PV power analysis.
2. Locating the killer whales: the location of killer whales is shown in Eq. (37):

Such that D_{max} andD_{min} represents the maximum and minimum duty ratios' value of respectively 0.95 and 0.005, h a value representing different directions belonging to the interval of $[-\pi; \pi]$, J the position of the artificial killer whale, c an adjusting factor belonging to the interval of $[0; 2]$ and K the iteration number ranging from 1 to K_{max}.

$$X_J^{K+1} = X_J^K \tag{38}$$

3. Duty ratio: that corresponds to output power of PV panel.
4. Catchers position: when catchers catch a prey, their position is remembered as reference in artificial whale positions. If not, catchers go back to old position described in Eq. (38):
5. Stopping criteria: the algorithm would stop searching for maximums when no increase in power is seen after twelve consecutive iterations.
6. Restart the search process: happens at any change in irradiance pattern on PV panels.

The tracking speed of MAKWO (Modified Artificial Killer Whale Optimization) was faster than the one in conventional PSO (Particle Swarm Optimization). It also had reduced the problem of large output power fluctuations [60].

3.2.2. Hybrid strategies

The performance of GMPPT (Global Maximum Power Point Tracking) methods presented in Fig. 10 are improved by using hybrid strategies: the tracking performance is upgraded by combination of two or more algorithms [61]. Fig. 11 entitles different hybrid strategies.

A standalone beta method compares an intermediate variable β with beta referenceβ^*. These two variables are declared in Eq. (39) and Eq. (40) respectively [62]:

$$\beta = \ln\left(\frac{I_{PV}}{V_{PV}}\right) - C \times V_{PV} \tag{39}$$

$$\beta^* = \ln\left(\frac{I_{MPP}}{V_{MPP}}\right) - C \times V_{MPP} \tag{40}$$

with C a constant in both equations, I_{PV} and V_{PV} the PV current and voltage respectively and I_{MPP} and V_{MPP} the current and voltage at maximum power point respectively.

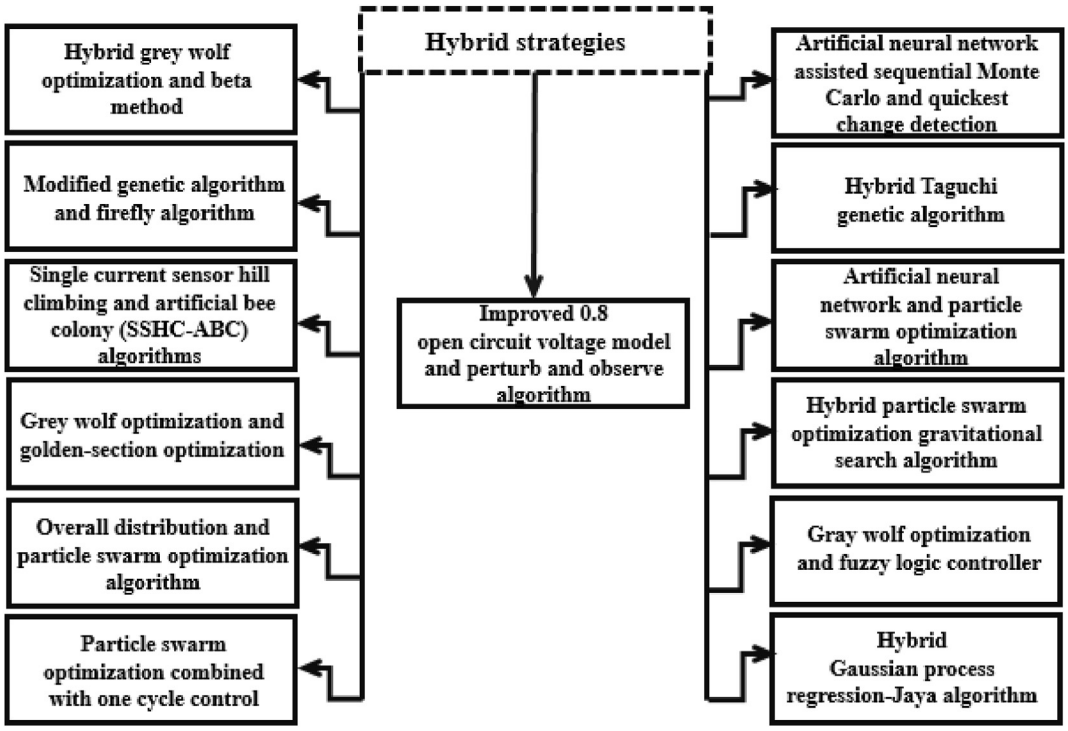

Fig. 11. Various hybrid strategies to improve tracking performance of GMPP (Global Maximum Power Point) under partial shading conditions.

a) Hybrid grey wolf optimization and beta method (HGWO-BM)

The comparison result between β and β^*drives the PI (Proportional-Integral) controller to generate a duty cycle used by the boost converter to alleviate voltage at specific rate. This methodology limits the power extraction from the PV array, and blocks operation of PV at MPP. When GWO (Grey Wolf Optimization) is mixed with beta method, this limitation is spared in a way that GWO achieves GMPP (Global Maximum Power Point) and uses beta method to calculate voltage and current at that point [62].

b) Modified genetic algorithm and firefly algorithm (MGA-FA)

The GA (Genetic Algorithm) alone works on elevating both the convergence speed and the accuracy to detect a GMPP (Global Maximum Power Point) under PSCs (Partially Shaded Conditions) by starting with a reduced population size, simplifying the mutation processes as well as the calculations of crossover and attractive processes [63,64].

On the other hand, the FA (Firefly Algorithm) converges to the best solution by attractiveness rate. When mixing these two different algorithms, the MGA-FA (Modified Genetic Algorithm and Firefly Algorithm), the convergence judgment becomes directly related to the mutation process and the initial fitness is calculated twice and compared to adapt a selection through the population [64]. The proposed algorithm tends to overcome the problem of declined accuracy of GA (Genetic Algorithm) with decreasing processing time [65].

c) Single current sensor hill climbing and artificial bee colony (SSHC-ABC) algorithms

For SSHC (Single current Sensor Hill Climbing) algorithm, its role is to detect any event of PSC (Partial Shading Condition) and to track the MPP (Maximum Power Point) during any uniform insolation condition. The ABC (Artificial Bee Colony) search space is reduced when collaborated with SSHC what results in increasing the convergence speed [66].

d) Grey wolf optimization and golden-section optimization (GWO-GSO)

The GWO-GSO algorithm first starts with GWO (Grey Wolf Optimization): the hunting is accelerated where the weight of wolf leaders is adjusted according to hunting progression. At the second stage, the algorithm switches to GSO (Golden Section Optimization) to adapt the local search, which avoids in turn unnecessary search. The mixed algorithm enhanced the reliability of GMPPT (Global Maximum Power Point Tracking) with higher accuracy under varying irradiance conditions [67].

e) Overall distribution and particle swarm optimization algorithm (OD-PSO)

This algorithm is a mixture between OD (Overall Distribution), where it is employed to rapidly detect the search region around GMPP (Global Maximum Power Point), and PSO (Particle Swarm Optimization), that has a role in finding and continuously updating best power found with best global peak [68].

The combination of the two stated algorithms benefits from solving the short-term optimization (OD) and outputting the best-found peak power (PSO). That yields to eliminate the steady-state oscillations and obtain the ability to detect any change in irradiation [68].

f) Particle swarm optimization combined with one cycle control (PSO-OCC)

Beginning with the OCC (One Cycle Control) an SR flip-flop (logic

gate) generates the switching pulse with D as duty ratio of switching [69]. The output Q of the flip-flop is fed to the converter. This entire procedure is governed by T_{ON} (ON period, corresponding to a true logic) in the switching period. The flip-flop remains on until V_{OUT} (output voltage) is equal to V_{ref} (reference voltage).

For the PSO (Particle Swarm Optimization) the duty ratio is taken as the solution space and the position of particle is defined as a possible solution.

When mixing OCC with PSO, the duty ratio is swapped with the PV panel current (new control parameter). This algorithm can track the GMPP (Global Maximum Power Point) more effectively and accurately than the solo performance of each sub-algorithm [69].

g) Improved 0.8 open circuit voltage model and perturb and observe algorithm (IVOC-PO)

This algorithm decomposes the search area for MPP (Maximum Power Point) into three distinct regions [70]:

- Left
- Middle
- Right

Accordingly, the duty ratios are calculated for the leftmost and rightmost MPP regions. With ΔD_1 and ΔD_2, the equivalent duty ratio differences in both leftmost and rightmost regions, the algorithm derives a smart power scanning with sampling different modulations of powers at different iterations, which enables a power differentiation between each iteration to outcome the highest power reached. The proposed algorithm showed high tracking efficiency [70].

h) Artificial neural network assisted sequential Monte Carlo and quickest change detection (ANN-SMC-QCD)

The SMC (Sequential Monte Carlo) executes the state estimation filtering and the improvement of MPP (Maximum Power Point) is helped by a set of predictions directed by ANN (Artificial Neural Network) [71]. The GMPP (Global Maximum Power Point) is predicted by a state-space model for the sequential estimation of peaks, where its estimation is held by SMC and where in turn, the ANN bases on observed voltage, current and irradiance.

The proposed algorithm achieved high efficiency and seen solid in front of rapid irradiance changes [71].

i) Hybrid Taguchi genetic algorithm (HT)

Due to the fact that a solo GA (Genetic Algorithm) is an extremely active algorithm in searching for a GMPP (Global Maximum Power Point) and is less likely to fall for a local peak, it is more improved by mixing Taguchi algorithm along with it to enhance the calculation abilities for GMPP.

It is seen that this hybrid algorithm has upgraded PV system performance in terms of overall power efficiency conversion [72].

j) Artificial neural network and particle swarm optimization algorithm (ANN-PSO)

In order to detect a global peak in a shaded PV system, a combination of PSO (Particle Swarm Optimization) and ANN (Artificial Neural Network) is proposed where the G_{best} (best of global peaks) is achieved using the PSO according to P_{best} (personal best of population) and the ANN with feedforward topology is used to fit an input-output relationship. The mixed algorithm showed effectiveness in detecting a GMPP (Global Maximum Power Point) under PSC (Partially Shaded Condition) PV system [73].

k) Hybrid particle swarm optimization gravitational search algorithm (HPSO-GSA)

The proposed approach of combining PSO (Particle Swarm Optimization) and GSA (Gravitational Search Algorithm) incorporates the essence of PSO with the motion mechanism of GSA, yielding to a global power peak detection that reduces blackouts and low power production from a PV system [74].

l) Grey wolf optimization and fuzzy logic controller (GWO-FLC)

FLC (Fuzzy Logic Controller) soft tunes the generated output power at the GMPP (Global Maximum Power Point) tracked by GWO (Grey Wolf Optimization). The FLC helps in re-initializing the GWO and that results in lowering the oscillations around the GMPP [75].

The mixture of GWO with FLC showed superior performance in dynamic GMPP catching and power efficiencies under PSCs (Partially Shaded Conditions) [75].

m) Hybrid Gaussian process regression-Jaya algorithm (HTGPR-J)

The combination of GPR (Gaussian Process Regression) with Jaya algorithm makes the last an attractive stochastic tool [76]. The GPR in turn is merged into the operating voltages for the PV system and serves as a predictor for PV power generation. All candidates, who are failing to output an increased level of power during different iterations, are discarded by GPR. This makes the Jaya algorithm not in need of any algorithm-specific controlling parameters, which decreases the complexities of coding. In terms of convergence speed and dynamical efficiency the GPR-Jaya demonstrated high performance [76].

3.2.3. Exploitation of characteristic curves

This set of methods utilizes the characteristic curves of I–V (current-voltage) and P–V (power-voltage) and sets mathematical approaches, dividing the search region into smaller sub-regions and decomposing the panel characteristics, to detect the global peak in a PV system under partial shading. Fig. 12 annotates different tactics used to attain the desired function.

The search for V_{MPP}(Maximum Power Point Voltage) within the voltage range is divided into smaller sub-regions with the aid of samples from P–V (Power-Voltage) curve of a PV module [77]. In each sub-region an I–V (Current-Voltage) curve is approximated to derive an upper limit for array power. A comparison is held between each peak of all sub-regions to finally achieve the GMPP (Global Maximum Power Point).

This algorithm showed faster convergence towards GMPP than artificial intelligence techniques [77].

b) Current source region detection of I–V (current-voltage) curve (CSR-IV)

The operating voltage is localized either within CSR (Current Source Region) or VSR (Voltage Source Region). The algorithm at this point is divided in two sub-algorithms [78]:

- When the operating voltage lies in CSR, the algorithm moves to the next operating voltage and skips the settling of PV voltage at V_{ref} (reference voltage).

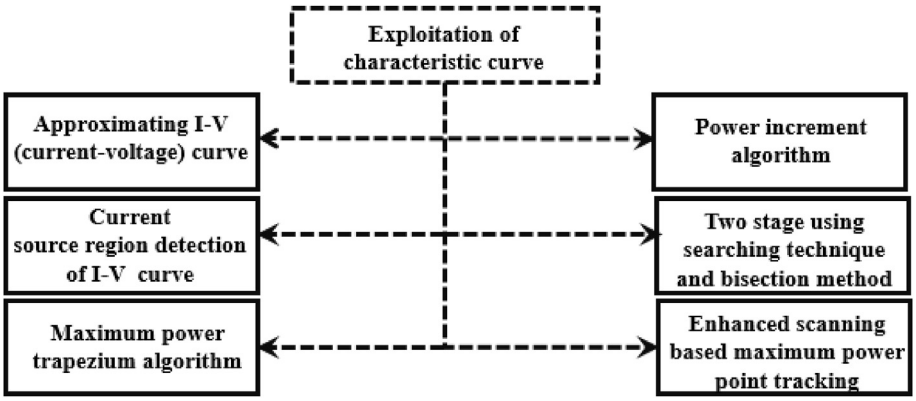

Fig. 12. Different GMPPTs (Global Maximum Power Point Tracking) algorithms based on characteristic curve exploitation.

a) Approximating I–V (current-voltage) curve (A-IV)

- When the operating voltage lies in VSR, the algorithm uses P&O (Perturb and Observe) to find a peak whenever the operating voltage moves from VSR to CSR.

The global peak is understood after comparison of different local peaks. The proposed algorithm can detect power peaks with less tracking time while serving to detect peaks under uniform irradiance conditions [78].

c) Maximum power trapezium algorithm (MPT)

Genuinely introducing the MPT (Maximum Power Trapezium], the proposed algorithm helps in finding a GMPP (Global Maximum Power Point) with special PSC (Partial Shading Conditions) that is a special condition of irradiance yielding more than the three conventional local peaks in P–V (Power-Voltage) curve of a PV module [79].

MPT (Maximum Power Trapezium Algorithm) decomposes the P–V plane into a trapezoidal area. It avoids scanning unnecessary voltage ranges (inside the plane) using progressive voltage range reduction.

In terms of tracking time and energy loss, the proposed algorithm showed uniqueness in achieving a GMPP for more than three local peaks [79].

d) Power increment algorithm (PI)

By using voltage line, load line and power line altogether, the tracking direction and step size are determined in PI (Power Increment Algorithm) [80]. This algorithm directly regulates the duty cycle of PPU (Power Processing Unit) instead of usage of output power command.

The stated algorithm realizes a successful convergence towards a GMPP (Global Maximum Power Point) under any pattern of PSC (Partial Shading Condition) with a simpler circuit design. It showed greater effectiveness in catching a GMPP versus conventional power increment algorithms [80].

e) Two stage using searching technique and bisection method (TS-ST-BM)

In the first stage of this algorithm the operating point is brought as closely as possible to the global maximum by means of a simple searching technique and bisection method [81]. In this part the possibility of a global peak occurrence is checked in decomposed zones of P–V (Power-Voltage) characteristic curve.

The second stage corresponds to the application of HC (Hill Climbing) method to maintain the operating point at GMPP (Global Maximum Power Point). The algorithm showed higher efficiency is locating a peak, rather than HC method [81].

f) Enhanced scanning based maximum power point tracking (ES-MPP)

The limitation of P–V (Power-Voltage) characteristic curve scanning, i.e. limiting the scanning interval of maximum and minimum values of duty ratio, is compensated via some analyses related to P–V curve in PSC (Partial Shading Condition) [82]. This way, the algorithm simplifies the tracking operation.

The simulation as well as the experimental results of the proposed algorithm stated that it traces GMPP (Global Maximum Power Point) effectively, with less components needs (uses only a single module rather than many in other PV power optimizers) [82].

3.2.4. Other GMPPT (global maximum power point tracking)

Recently developed and categorized as other GMPPT (Global Maximum Power Point Tracking) [48], Fig. 13 encapsulates these algorithms.

The GMPP (Global Maximum Power Point) is achieved under varying irradiations using a Bayesian fusion: an MLT (Machine Learning Technique) which segments or divides images into segments, detects curves and classifies tracked maximums with no direct supervisory control [83]. In order to keep operating at GMPP, a Bayesian network decides the correct path of $V_O(t)$ (instantaneous output voltage) of the PV array.

The network structure works on 2*N*nodes divided in half. The first N nodes $[A_1, \ldots, A_N]$ labels the maximum power voltages with multiples of V_{OC} (open circuit voltage) according to Eq. (41) [83]:

$$V_{MP} = n \times 0.8 \times V_{OC} \tag{41}$$

where V_{MP} denotes the maximum power voltage and n a constant of multiplication. This first node resembles in operation to the FOC (Fractional Open Circuit) voltage in determining V_{MP}.

The second N nodes $[A_{N+1}, \ldots, A_{2N}]$ correspond to MPP (Maximum Power Point) attained by conventional incremental conductance algorithm. All nodes within the two sets are compared mutually to check for any degree of resemblance. At this stage, the algorithm derives a feature vector, with Boolean elements of ones and zeroes to define the matching entries.

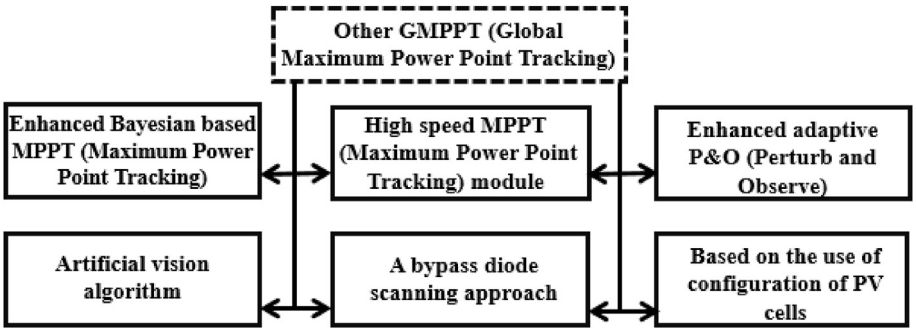

Fig. 13. Other GMPPT (Global Maximum Power Point Tracking) algorithms.

a) Enhanced Bayesian based MPPT (EB-MPPT)

The PID (Proportional Integral Derivative) accompanied along with the proposed algorithm showed an enhanced response time in front of achieving MPP with minimizing the steady-state oscillations and rise time of output power [83].

b) Artificial vision algorithm (AV)

Regardless of number of GMPPs (Global Maximum Power Points) appearing on the P–V (Power-Voltage) curve of a PV panel, the AV (Artificial Vision) algorithm is capable of detecting the highest GMPP with aid of artificial vision, that is implemented on a webcam. The webcam performs a real time identification of shadow irradiance hence provides the V_{ref} (reference voltage) that results in maximum power [84].

This algorithm showed high experimental efficiency (from 98.1% to 99.6%) in tracking procedures [84].

c) High speed MPPT module (HS-MPPT)

With the help of a high sampling rate ADC (Analog to Digital Converter) the P–V (Power-Voltage) curve scan is achieved, where the operating circuit functions under two modes to obtain the maximum power point [85]:

- Short circuit mode: a solid-state switch is closed to condemn the PV panel be confronted with an oscillate IC (Inductor Capacitor) circuit. At this level the I_{PV} (PV current) is sensed, with no oscillations due to existence of a freewheeling diode.
- Scanning mode: the same solid-state switch is open, allowing voltage sensor to measure V_{PV} (PV voltage).

After knowing voltage/current quantities from different modes working (at recorded amount of time) the P&O (Perturb and Observe) is initiated to track the MPP. The proposed algorithm quickly converges to GMPP under changing irradiation patterns. It is also suitable for online operation with any type of PV string [85].

d) A bypass diode scanning approach (BDS)

Assumed that the PV panel architecture contains internal bypass diodes (unidirectional electronic components that allow flow of current in only one path), this algorithm scans the voltage drops (if happening) across bypass diodes to estimate global peak power [86].

At each checking of bypass diodes state, a decision is held to identify if the operating point in the P–V (Power-Voltage) curve has reached the region of MPP (Maximum Power Point), where if not, the algorithm restarts from beginning by measuring different voltage/current quantities [86].

This method requires less components, and simpler algorithm implementation, where it showed lesser time in reaching MPP, compared to P&O (Perturb and Observe) and IC (Incremental Conductance) methods [86].

e) Enhanced adaptive P&O (EA-PO)

The limitations in conventional P&O (Perturb and Observe) are mitigated with an enhanced adaptive P&O where the updates of V_{OC} (open circuit voltage) and irradiance are done with no need for sensors [87].

This method requires less components, making it affordable to implement, and neglects unnecessary global peak scanning, hence fastening convergence speed [87].

f) Based on the use of configuration of PV cells (CPV)

By usage of PV cells serial/parallel configurations, this algorithm limits the blind search of GMPP (Global Maximum Power Point) through many local MPPs (Maximum Power Points) by reducing the search space [88].

In shading conditions, the maximum power is achieved by calculating the required combinations of serial/parallel PV cells. This method does not require any hardware modification and can easily be implemented by software modification of the controller [88].

Table 3 summarizes all available algorithms, corresponding to conventional, exploitative and others. Each set is categorized according to area of interest (uniform irradiance/partial shading), nature of the algorithm (metaheuristic, model based, soft computing), average efficiency (%) and input parameters (voltage V, current I, temperature T, irradiance G, and bypass diode BD). Similarly, the following Table 4 reveals algorithms corresponding to intelligent ones and some of the hybrid. The categorization is made in a perspective similar to that in Table 3, where P&O represents the most fundamental conventional maximum power point chasing algorithm [89], with HC [90] and FVI [92] as its derivatives, having HC method combining both meta-heuristic and model based topologies for MPPT under uniform irradiance.

4. Power processing units review

The PPUs (Power Processing Units) are DC-DC converters that modify the output voltage from the PV panel according to system's requirements, hence extracting its maximum power [93]. Such converters, labeled as power electronic conditioners, are under SMPS (Switched Mode Power Supply) circuit topology [94]. SMPS

Table 3
Conventional, exploitative and other GMPPT algorithm efficiency review.

		MPPT		GMPPT				
		Under uniform irradiance		Under partial shading condition			Efficiency (%)	Input Parameters
Type		Meta heuristic	Model Based	Meta heuristic	Model Based	Soft Computing		
Conventional	P&O	•					98.7% [89]	V, I
	HC	•	•				>95% [90]	V, I
	IC	•	•				>96% [91]	V, I
	FVI	•					93.5% [92]	V, I
Exploitative	A-IV			•	•		100% [77]	V, I
	CSR-IV			•	•		>99% [78]	V, I
	MPT			•	•		-	V, I
	PI			•	•		77.7% [80]	V, I
	TS-ST-BM			•	•		>99% [81]	V, I
	ES-MPPT			•	•		-	V, I
Others	EB-MPPT			•	•		98.9% [83]	V, I
	AV			•	•	•	98.1-99.6% [84]	V, I
	HS-MPPT			•	•		99.9% [85]	V, I
	BDS			•	•		100% [86]	V, I
	EA-PO			•	•		99% [87]	V, I
	CPV			•	•		-	V, I

includes a solid-state switching regulator, to transfer the power from DC supplies (PV panels) to other DC loads (batteries). The SSS (Solid State Switch) is governed by a duty cycle to continuously turn it ON/OFF according to MPPT algorithm state function. This transferring process involves converting V/I (Voltage/Current) characteristics.

All PPUs are categorized under two major groups [95]:

- Non-isolated DC-DC converters
- Isolated DC-DC converts

Each set can own three different circuit architecture:

- Buck converters: used to alleviate voltage values (low irradiance conditions).
- Boost converters: used to aggravate voltage values (high irradiance conditions).
- Buck-Boost converters: used to increment/decrement voltage values (fluctuating irradiance conditions).

4.1. Non-isolated DC-DC converters

A non-isolated DC-DC converter has no shield from the initial DC power supply (PV panel) [96]. Non-isolation refers to non-existence of an electrical barrier between its input and output [97]. Table 5 encapsulates different circuit architecture for this topological set of converters.

4.1.1. Buck converters

a. Standard

Fig. 14 shows the basic circuitry for a buck converter. When switch S_1 is closed, the inductor L is used as a current limiter component, to skip the instantaneous change in voltage of capacitor C that could cause considerable damage (since a large current will flow to charge the capacitor). Since the current passing through the inductor cannot change instantaneously, L will keep forcing the current to keep flowing even after opening S_1. This drawback is overcome by the addition of a diode D. The output voltage V_o is controlled by controlling the percentage of time S_1 is closed. This makes V_o of any value below V_g (input DC voltage).

The QIDO (Quad Input Dual Output) can achieve the maximum power point operation, for three different PV panels, for each panel aside [114]. In other terms, with the usage of this converter, a PV array (consisted of many PV modules) can be sub-divided for a total three major sets. It regulates each side on its own, by transferring excess voltage to battery bank. When radiation is insufficient to drive the load, this converter draws power from batteries in a reverse way. It has four different controllers to achieve its target [114]:

- PV input port controller
- Load/output port controller
- Battery input port controller

The last controller consists of a logic controller combining all

Table 4
Intelligent and hybrid GMPPT algorithm efficiency review.

		MPPT		GMPPT				
		Under uniform irradiance		Under partial shading condition			Efficiency (%)	Input Parameters
Type		Meta heuristic	Model Based	Meta heuristic	Model Based	Soft Computing		
Intelligent	ICSO					•	99.6% [49]	V,I
	MCSO					•	99.8% [50]	V,I
	IGS					•	99.9% [51]	T,G
	IDE					•	99% [52]	V,I
	MP-VB-PSO					•	99.6% [53]	V,I
	MF					•	99.9% [54]	V,I
	DCS					•	-	V,I
	MFO					•	99.9% [57]	V,I
	AMA					•	99.9% [58]	V,I
	MAKWO					•	99.9% [60]	-
Hybrid	OD-PSO					•	97.7% [68]	V,I
	HT					•	99.6% [72]	V,I
	SSHC-ABC					•	99.1% [66]	I
	GWO-GSO					•	99.9% [67]	V,I
	IVOC-PO					•	97.3% [70]	V,I
	HGWO-BM					•	99.9% [62]	V,I

Table 5
Different circuit configurations for non-isolated DC-DC converters.

DC-DC converter circuit topology		
Non-isolated DC-DC converters		
Buck converter	Boost converter	Buck-Boost converter
Standard	Standard	Standard
Quad-input dual-output	Modified high step-up	Ćuk
Variable inductor	Interleaved	
Fourth order	Double dual boost converter	SEPIC

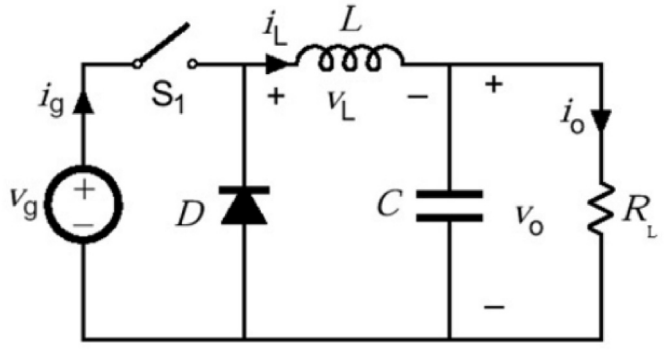

Fig. 14. Standard non-isolated buck DC-DC converter [98].

b. Quad-input dual-output

outputs of precedent controllers. This prototype was found reducing the component needs to regulate power coming from PV system by 56.25%, and that results in increasing the cost-efficiency of the system [114].

c. Variable inductor

The operation of a buck converter is stabilized by using a variable inductor in the place of the fixed one presented in Fig. 14. For the control algorithm, it enables the transition from CCM (Continuous Current Mode) to DCM (Discontinuous Conduction Mode) and vice-versa [115]. Since CCM can only be achieved for specific inductances, the minimum inductor value is given by Eq. (42) [115]:

$$L_{min} = \frac{D^2(1-D)V_P}{2f_S I_P} \tag{42}$$

with D the duty cycle, f_S the switching frequency, V_P and I_P the array

voltage and current respectively.

With the addition of the variable inductor to the standard buck converter, a decrease in the overall DC-DC converter type was seen by 75%. This also increases the operating range of the tracker, enabling MPP under lower solar radiations cases [115].

d. Fourth-order

The design of this circuit involves the addition of an inductor, mutual with the initial inductor found in standard buck converter [116]. The modified converter unit replaces the constant load by an equivalent load to maximum power transfer [116]. The gain of this converter is shown in Eq. (43):

$$\frac{V_o}{V_{in}} = kD \tag{43}$$

where k is a constant with respect to resistances/capacitances of resistors/capacitors and duty cycle D in the reference circuit design.

A fourth-order buck converter seemed to be able to track MPP (Maximum Power Point) at all solar irradiations, with reduced oscillations and, operation at most optimal power points for fluctuating radiations, reduced sampling time by 55% in accordance with a standard buck converter [116].

4.1.2. Boost converters

a. Standard

Fig. 15 displays the basic circuitry for a boost converter. When switch S_1 is closed, a DC voltage is created across the inductor L, where as long as the switch is closed, the current passing through the inductor keeps increasing. This current cannot change instantaneously, therefore the moment we open the switch, the inductor creates a force, causing the current to continue flowing. When S_1 is continuously turned on and off, the DC voltage created across the capacitor C increases (by charging through the resultant current from the inductor), hence the resultant output voltage V_o becomes larger than the input voltage V_g(coming from PV output voltage). This is to say that if S_1 remains off all the time, V_o will become equal to V_g. The on/off turning process of S_1 (that is a transistor) is judged by the duty ratio D launched by the MPPT algorithm.

This converter is inspired from the SEPIC (which is essentially a boost converter followed by a buck-boost converter). Fig. 16 reveals its connection diagram, where it utilizes the low voltage for switching in the converter what results in high voltage conversion. Its gain is presented in Eq. (44) [91]:

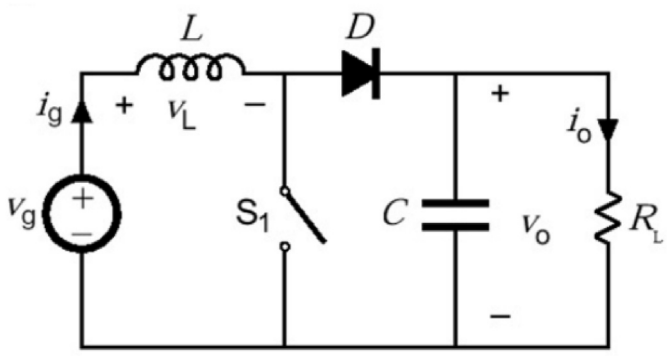

Fig. 15. Standard non-isolated boost DC-DC converter [98].

b. Modified high step-up

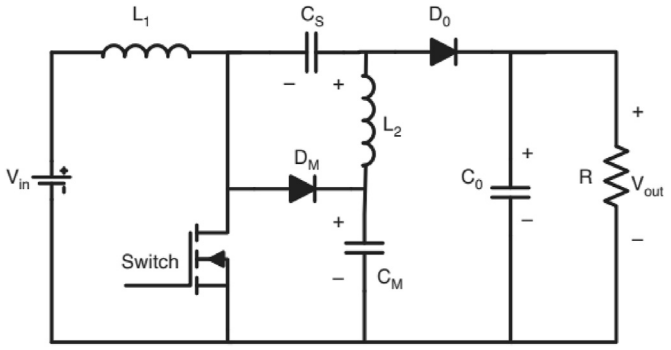

Fig. 16. Modified step-up boost converter [99].

c. Interleaved

$$\frac{V_o}{V_{in}} = \frac{D(V_o + V_{in}) - V_{in}}{V_{in}} \tag{44}$$

with D is the duty cycle condemning the on/off procedures of the switch.

A boost converter integrated with multiple capacitors series connected result in the interleaved converter. The added capacitors allow to obtain high static gain [100]. Fig. 17 shows the circuit diagram for the modified interleaved boost converter.

This converter can be extended to multiple number of parallel stages and different number of multiplier stages. For each of the two stages with one multiplier, two inductors L_1 and L_2 are connected at the input. The capacitors C_{M1} and C_{M2} are charged by diodes D_{M1} and D_{M2} respectively. The static gain is represented in Eq. (45) [100]:

$$\frac{V_o}{V_{in}} = \frac{(M+1)}{(1-D)} \tag{45}$$

where M is the number of multiplier stages and D the duty cycle. This interleaved converter presents high input current ripples. To bypass this consequence, a modification would help and extend the voltage gain by the following steps [101]:

- Alleviating voltage
- Replacement on conventional inductors by coupled inductors (CIs)
- Connecting a voltage multiplier cell across terminals with secondary windings of CIs

The corresponding gain of the modified converter is presented in Eq. (46):

$$\frac{V_o}{V_{in}} = \frac{2 + 2Nk}{(1-D)} \tag{46}$$

with D duty ratio for switches S_1 and S_2, k coupling factor and N the turns ratios of CIs. This modification resulted in lowering the input current ripple up to 20% with highest voltage conversion ratio (15.83) [101].

d. Double dual boost converter

Composed of two conventional boost converters with inversely coupled inputs, the circuit of a dual boost converter is shown in Fig. 18.

The gain of this converter is given in Eq. (47):

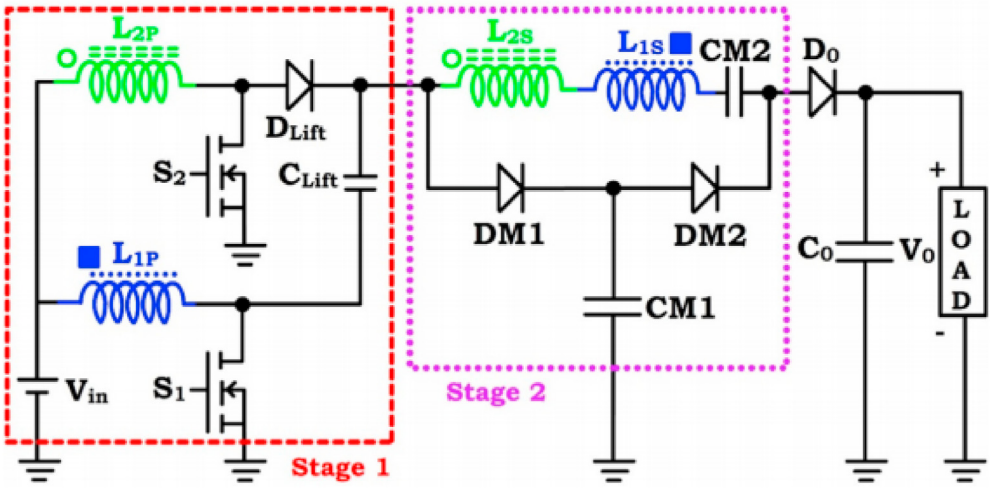

Fig. 17. Modified interleaved boost non-isolated DC-DC converter [101].

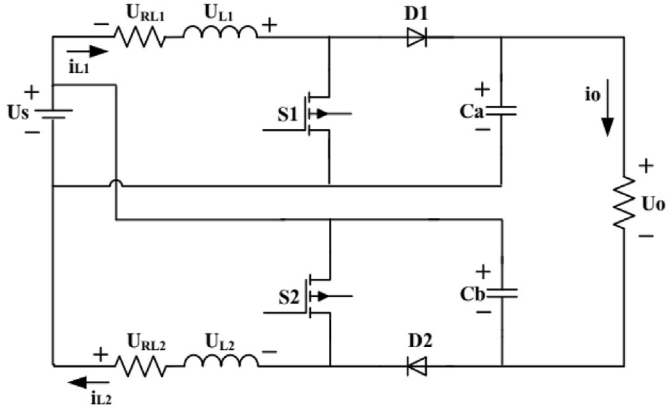

Fig. 18. Double dual boost converter circuit configuration [102].

$$\frac{U_o}{U_s} = \frac{(1+D)}{(1-D)} \tag{47}$$

with D representing the duty cycle for switches S_1 and S_2. This converter has an inversely proportional relation with D versus gain, the lower D the higher the efficiency. Compared to conventional boost converters, this inverse relation is advantageous [102].

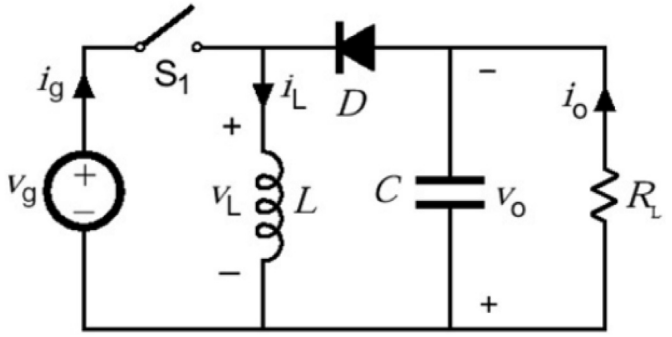

Fig. 19. Standard non-isolated buck-boost DC-DC converter [98].

b. Ćuk

4.1.3. Buck-boost converters

a. Standard

The functioning of this circuit is a combination between the previously stated buck and boost converters altogether. Fig. 19 presents the basic circuitry for a buck-boost converter. The notable modification in the circuitry is the flipped terminals connection of capacitor C where it permits current fed by the charged inductor L to pass through it when the switch is off.

The output voltage of a Ćuk converter can be either lower or bigger than the input voltage with reversed polarity. Its circuit arrangement is presented in Fig. 20. The inductor L_1 acts as a DC supply filter to prevent larger harmonics. The amount of energy transferred to L_2 depends on the value of C_1 [103]. This converter gain is presented in Eq. (48):

$$\frac{V_O}{V_{in}} = \frac{D}{1-D} \tag{48}$$

with D the duty ratio, generated by the MPPT algorithm.

A SEPIC (Single Ended Primary Inductor Converter) is identical to a Ćuk converter, except that the output voltage is in the same polarity with the input voltage. Its circuit can be constructed by swapping the positions of L_2 and D from Ćuk converter circuit. This converter gain is also same of Ćuk converter. Fig. 21 shows a SEPIC circuit configuration.

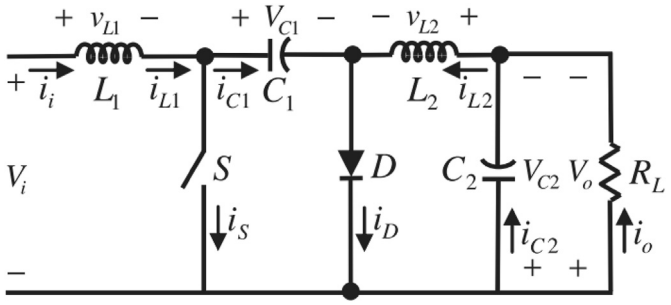

Fig. 20. Arrangement of a Ćuk converter [103].

c. SEPIC

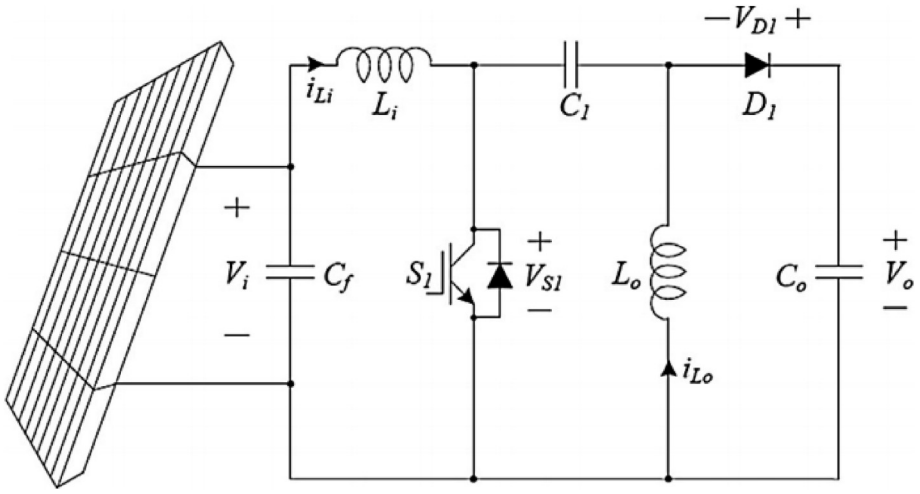

Fig. 21. Circuit configuration for SEPIC [104].

Table 6
Various circuit arrangement for isolated DC-DC converters.

DC-DC converter circuit topology	
Isolated DC-DC converters	
Buck converter	Boost converter
Single ended forward converter	Single ended fly-back
Half-bridge	Half-bridge
Full-bridge	Full-bridge
Push-pull	Switched capacitor

4.2. Isolated DC-DC converters

An isolated DC-DC converter embodies a high frequency transformer providing an electrical barrier between the input and the output [105]. Table 6 encloses different circuit configurations for isolated DC-DC converters. Indeed, the Buck-Boost configuration for such set exists but with major complexity in installation, great turndowns in term of hysteresis and other losses, hence reduction in efficiency. Moreover, a Buck-Boost isolated DC-DC converter permits the output of different voltage level, where it is found not suitable for PV system applications.

4.2.1. Buck converters

a. Single ended forward converter

The simplest forms of isolated DC-DC converter, utilizing one switch S and two diodes, D_R(Rectifier diode) and D_{FW} (Free-Wheeling diode), is presented in Fig. 22.

The voltage gain of this converter is shown in Eq. (49) [106]:

$$\frac{v_o}{V_{DC}} = \frac{n_2}{n_1} \cdot D \tag{49}$$

where v_o and V_{DC} represent the output and input voltages respectively, n_2 and n_1 the secondary and primary turns of the transformer, and D the duty ratio (generated by MPPT algorithm). This model seemed to suffer from transformer saturation problems [106].

b. Half-bridge

The half-bridge converter topology uses two switches in order to generate symmetrical AC waveforms at the primary side of the transformer. The gain of a half-bridge isolated DC-DC converter is shown in Eq. (50) [107]:

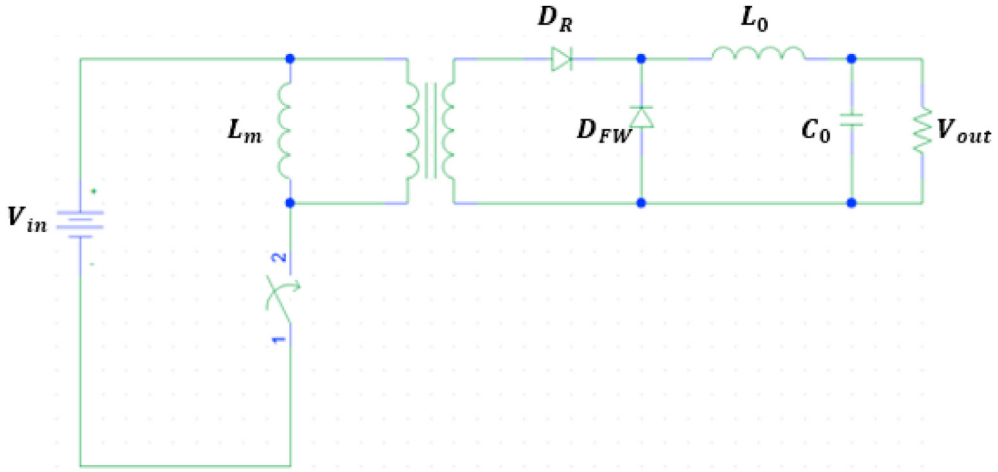

Fig. 22. Isolated single ended forward converter.

$$\frac{V_o}{V_{in}} = \frac{n_2}{2n_1} \cdot D \tag{50}$$

where V_o and V_{in} represent the output and input voltages respectively, n_2 and n_1 the secondary and primary turns of the transformer, and D the duty ratio (initializing the ON/OFF frequency for the two switches). This model avoids the saturation problem of the transformer and excites the core flux bi-directionally, which results in an increased power rating [107].

c. Full-bridge

The full-bridge converter maintains the same advantages that the half-bridge does (avoid saturation problem with increased power rating). In addition, a full-bridge converter enables any application for high voltage at the input of the transformer [108]. Its gain is shown in Eq. (51):

$$\frac{v_o}{V_{DC}} = D \Big/ \frac{n_1}{n_2} \tag{51}$$

d. Push-pull

A push-pull converter uses the transformer for voltage scaling and electrical isolation, and from the other part, an output inductor is used for energy storage. The gain of this converter is the same as Single Ended Forward Converter (SEFC). The push-pull is used for higher power applications than SEFC [109].

4.2.2. Boost converters

a. Single ended fly-back

This converter is the most commonly used in this set (boost converters). Its transformer has three major roles [110]:

- Steps-up/down the input voltage
- Provides an electrical isolation
- Provides energy storage during the operation

The voltage gain for this converter is given in Eq. (52):

$$\frac{V_o}{V_{in}} = \frac{D}{n(1-D)} \tag{52}$$

with n equals to the ratio of first winding over the second (n_1/n_2).

b. Half-bridge

Due to the presence of an input inductance in series with the DC source (from the PV panel), the circuit design of the isolated boost half-bridge converter requires the implementation of a center-tapped transformer [111]. The gain is shown in Eq. (53):

$$\frac{V_o}{V_{in}} = \frac{1}{2}\left(\frac{n_2}{n_1}\right)\frac{1}{1-D} \tag{53}$$

c. Full-bridge

Known as double-ended converter, where its core material is better utilized compared to single-ended converter [112]. The gain is given in Eq. (54):

$$\frac{V_o}{V_{in}} = \frac{n_2}{n_1}\left(\frac{1}{2(1-D)}\right) \tag{54}$$

d. Switched capacitor

Compared to other converters in isolated boost converters, this one produces the least stress on the transformer, requires small transformer turns ratio and offers a bi-directional power flow. Fig. 23 presents the circuitry arrangement of this converter.

The input/output voltage relation is shown in Eq. (55) [113]:

$$V_o = \left(V_{in} + 2\overline{V_c}\right) \cdot \frac{N_2}{N_1} D_2 + \frac{N_3}{N_1} D_2 \sqrt{\frac{R_L}{2L_t f_{tr}}} \Bigg) \tag{55}$$

with V_o , V_{in} representing output and input voltage respectively and $\overline{V_c}$ denoting capacitor voltages of C_1 or C_2. From another part, N_1 represents the number of turns for primary winding of the transformer, while N_2 and N_3 denotes the number of turns at the secondary center-tapped side. On the other hand, D_2 represents the duty cycle for switches S_3 and S_4. At last, R_L is the load resistor, L_t is the secondary side inductor and f_{tr} the switching frequency [113].

Ultimately, Table 7 summarizes major advantages and disadvantages between isolated and non-isolated DC-DC converters.

5. Discussion

With the varieties of MPPT (Maximum Power Point Tracking) algorithms and power electronic conditioners (isolated/non-isolated DC-DC converters), it becomes more confusing to design a case-specified optimum full MPPT solution. In order to come up with the most efficient tracking scheme, the following steps must be taken into consideration:

1. Fully acknowledge the atmospheric conditions in which the PV system would be installed in terms of irradiance, temperature and other climatic conditions (how abundant is solar irradiance and how often it rains).
2. Derive a reliable MPP (Maximum Power Point) tracking algorithm to be implemented in a central processor unit (decision maker, outputting relevant duty ratios): the design must take into consideration if the algorithm can go for single maximum peak, global peak between multiple locals or both.
3. Design a suitable SMPS (Switched Mode Power Supply) compatible with the derived algorithm to perform voltage regulation based on efficiency, reliability and complexity of construction: to choose whether it is an isolated or a non-isolated converter and of which circuit topology.
4. Choose a central processor for code execution (algorithm) based on I/O (Input/Output) ports configuration, operational speed, robustness against different perturbations: to know what would be the type of the decision-maker (Arduino, Raspberry Pi, Node MCU, etc.) and its corresponding programming language (C++, C#, BASIC, etc.).
5. Gather up the entire MPPT circuitry, as processor with SMPS and digitally simulate it to identify bugs in programming (if any) and instability of analog electronics (if existed), as a prior step before composing the system into a real world prototype.
6. Physical implementation of the simulated system, and its exposure to different real life scenarios while continuously

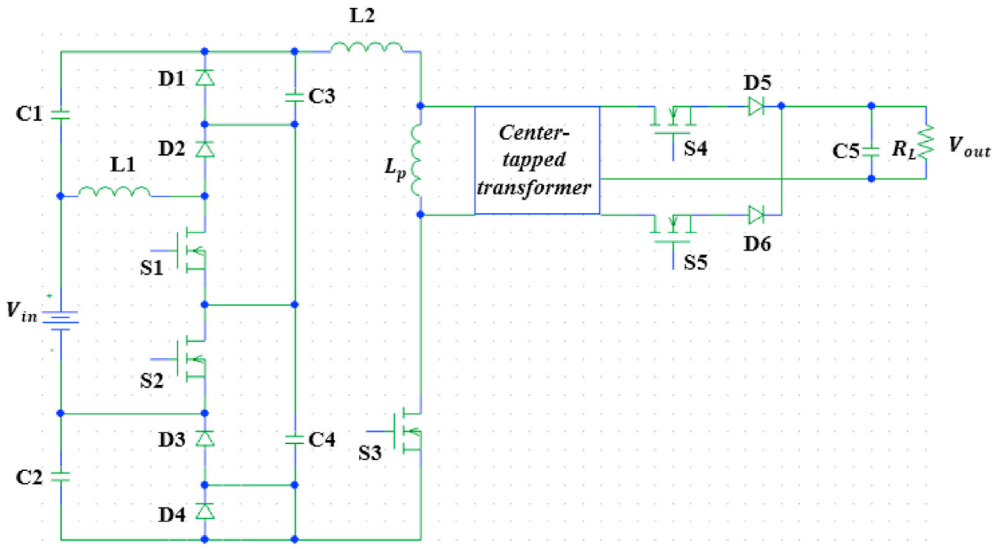

Fig. 23. Topology of switched-capacitor converter.

Table 7
Comparison between isolated and non-isolated DC-DC converters.

Converter scheme	Isolated	Non-isolated
Advantages	Safety to personnel: isolation prevents input voltage from being transmitted to the output in case of internal failure. Can be configured to provide positive/negative outputs from plus/minus rails. Voltage transients on the input are not transmitted to the output.	Simpler. Cheaper. Requires less space.
Disadvantages	Require more space. Existence of transformer losses (superimpose of hysteresis and eddy currents) what reduces overall efficiency.	Risk of electrocution (due to the existence of electrical connection between the input and the output).

monitoring its performance: seek the level of its real efficiency, compare the real performance values with simulated ones: this final step is to judge whether the fabricated MPPT solution is robust enough to be installed in real PV applications or not.

The set of algorithms which work under uniform irradiance conditions (whether metaheuristic or model based) such as perturb and observe, incremental conductance, hill climb and fractional open-circuit voltage/short-circuit current can only operate when a single peak exist in the P–V curve.

Therefore, the existence of any physical barrier (clouds, trees, etc.) in front the panels, would block such algorithms from attaining their required function, after the activation of bypass diodes. Locating the highest occurring peak process will definitely fail. For instance, P&O algorithm gives only a control signal to the DC-DC converter, to either increase/decrease the voltage level if the current power being investigated is bigger than precedent one ($P(n) > P(n-1)$). When the same characteristic curve has multiple peaks as shown in Fig. 24, the P&O as well as HC, IC and FVI would set a single decision, for the DC-DC converter to operate, after the first finding of calculated power at $P \cong 1000\ W$. In other words, the maximum power of $P \cong 2500\ W$ would not be seen by such primitive algorithms. Therefore, under fluctuating climatic conditions, the conventional algorithms of P&O, IC, HC and FVI would not succeed in extracting the maximum available power from the array.

Since partial shading are practically unavoidable [118], regardless of PV cell raw materials used [119] and no matter how careful the study of PV allocation is, the inability of conventional algorithms (P&O, HC, IC and FVI) to locate the greater maximum is a big

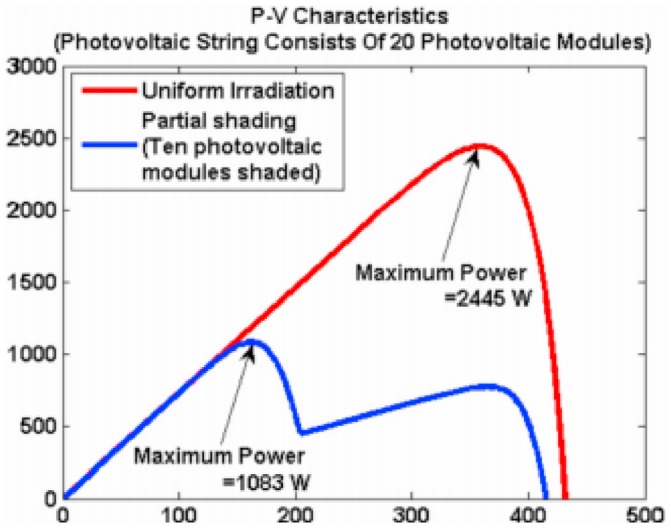

Fig. 24. P–V curve of an array subsequent to a partial shading scenario [117].

turndown. Therefore, the application of such algorithms versus different shading patterns, as seen in Fig. 25, would have no contribution in reducing power generation losses for the PV system [121]. The mismatching would still exist, accelerating the aging process of PV panels, increasing the occurrence of hotspots, hence decreasing the cost efficiency of the PV system [122,123].

On the other hand, maximum power trackers under partial

Fig. 25. Partial shading patterns on the PV array [120].

shading topologies, would overcome this problem, by differently analyzing the P–V characteristic curve of the PV array [124,125]. Beginning with intelligent and metaheuristic search algorithms, such techniques would help achieving the maximum peak, by adapting a nature behavior based search to locate the GMPP. By mimicking the attitude of chickens, cats, mountain apes, killer whales and other animals, employed to find food, based on the quantity and the time spent by the top fit individual, the global maximum is targeted. In other terms, the GMPP is found by such algorithms, as it was compared to finding largest amounts of food. The top fit individual is in turn compared to the algorithm process.

Though these algorithms overcome the obstacles held by conventional algorithms while detecting the greatest power peak, they require a complex level of programming, generally involved with artificial intelligence strategies and fuzzy logic.

The hybrid strategies from the other side, show more complexities in employing an efficient algorithm to track the global peak, as they are composed of two and more algorithms. This means that the effort in producing the software code of the algorithm is at least of twice of difficulty.

Among different algorithms sets, ones relying under the exploitation of characteristic curves, are the most recommended, since they dissect the V–I range into smaller sub-regions. In each region the peak is found, then compared to the other in the succeeding region. The global peak is hence reached by simple mathematical calculations, using a simple if-else conditioning in a high level programming language (C++, Java, etc.). Adapting these algorithms would reduce time and complexities, to outreach the GMPP, compared to the other sets.

Concerning the design of a suitable PPU, to be operated by the tracking algorithm, a non-isolated DC-DC converter is recommended to be installed in an MPPT prototype, against an isolated one. As non-isolated converters do not have any transformer existence in their design, the problems of hysteresis losses, eddy currents, and all sorts of current leakages are eradicated. Though that isolated DC-DC converters offer a galvanic isolation between the input and the output terminals, but they suffer from circulating power, higher current stress with reduced light-load efficiencies [126]. The design of non-isolated PPUs is much more simple, requiring less space (have higher reliability in physical realizations), is cost-effective, possess higher efficiency in voltage conversion and show more robustness versus different forms of disturbances and non-linear aspects [127,128].

6. Conclusion

Throughout this paper, it can be concluded that for a full maximum power point tracking solution, an MPPT tracks the optimum voltage/current ratio from an array compared to other trackers prototypes (PWM/Shunt). It can provide up to 30% increase in performance and allows input/output voltages to be of different quantities.

The MPPT has multiple value input/output voltage, causing it to be less expensive than PWM/Shunt as it requires smaller gauge wires, due to inverse relation between voltage and current according to Ohm's law (when voltage increases at the input, the current decreases correspondingly). It also works best in the case when the PV array is located far from the controller (reduced voltage drops).

Unlike other topologies, an MPPT works on conservation theorem (input power equals output power) where any scale up/down in voltage ratio signifies a reciprocal scale down/up in current ratio, therefore any excess in voltage is structured to be acquired from.

By diving into a maximum tracker scheme, it was made clear in this paper that it consists of two main functions: the maximum chasing algorithm (that is the logic behind the entire maximum chasing operation) and the power processing units (electronic circuits outputting a desired power levels).

The tracking algorithms are either derived to look after a single maximum (local, under homogeneous irradiation) or multiple (when many local peaks are existing in P–V curve of a PV array due to partial shading conditions). For the local peak trackers, different algorithms showed an efficiency range between 93.5% and 99% of peak detection, but all of them derived an oscillated behavior around the MPP (Maximum Power Point), resulting in achieving sometimes a false peak. These algorithms were not able to stabilize in front of rapidly changing weather conditions (fluctuating temperature and irradiance) hence, providing accumulated power losses.

In addition, the GMPP (Global Maximum Power Point) were found suitable for both local and global peaks detection, where they reduce damped oscillations and lower the operational time of the controller when detecting the peak under rapidly changing climatic conditions. Such algorithms also showed accelerating the convergence speed, by neglecting any unnecessary scanning. Their detection efficiency begins by 97.36%–99.99% for some algorithms.

Due to their generic working methodology, and accommodation to work for different climatic conditions, a GMPP algorithm is recommended to be implemented in any future MPPT prototype design. The choice of algorithm family is mainly conducted by the designers programming skills, as the AI (Artificial Intelligence) techniques require heavy software skills, since MLL (Machine Learning Languages) are complex and require specific code writing languages (mainly Python). Also, the implementation of GMPP algorithms takes additive inputs compared to conventional ones, which increases the design complexity in terms of adding temperature and irradiance sensors.

Alternatively, in term of power conversion efficiency, it can be

concluded that a linear voltage regulator (LM78xx family) cannot supersede the DC-DC converters reviewed in this paper. This is because any other converter than isolated/non-isolated will dissipate much heat while interfered with a PV system, causing a reduction up to 50% in conversion efficiency. Besides, all linear regulators would require a gargantuan heat sink to dissipate elevated heat, the fact that can be surpassed with the usage of isolated/non-isolated converters.

For the isolated converters, their construction is more complex than non-isolated, where the implementation of a transformer increases hysteresis and eddy current losses, the fact that reduces the overall conversion efficiency (91.2%) with respect to non-isolated converters (>95%).

Finally, a non-isolated buck-boost DC-DC converter is recommended to be implemented with a GMPP tracking algorithm as a final solution to detect peak power for different PV systems, due to the ability of elevating/decreasing output voltage under non-uniform irradiance conditions.

Credit author statement

Khaled Osmani: Writing – original draft, Investigation, Writing – review & editing, Visualization. Ahmad Haddad: Writing – review & editing, Visualization, Supervision. Thierry Lemenand: Writing – review & editing, Visualization, Supervision. Bruno Castanier: Writing – review & editing, Visualization, Supervision. Mohamad Ramadan: Conceptualization, Writing – review & editing, Visualization, Supervision, Project administration.

Declaration of competing interest

The authors declare that they have no known competing financial interests or personal relationships that could have appeared to influence the work reported in this paper.

References

[1] Bertrand C, Housmans C, Leloux J, Journée M. Solar irradiation from the energy production of residential PV systems. Renew Energy 2018;125:306–18.

[2] Ramadan Mohamad, Murr Rabih, Khaled Mahmoud, Abdul Ghani Olabi. Mixed numerical - experimental approach to enhance the heat pump performance by drain water heat recovery. Energy 2018;149:1010–21. https://doi.org/10.1016/j.energy.2018.01.086.

[3] Olabi AG, Onumaegbu C, Wilberforce Tabbi, Ramadan Mohamad, Ali Abdelkareem Mohammad, Abdul Hai Al – Alami. Critical review of energy storage systems. Energy 2021;214. https://doi.org/10.1016/j.energy.2020.118987.

[4] Ramadan Mohamad. A review on coupling Green sources to Green storage (G2G): case study on solar-hydrogen coupling. Int J Hydrogen Energy 2021. https://doi.org/10.1016/j.ijhydene.2020.12.165.

[5] Haddad A, Ramadan M, Khaled M, Ramadan H, Becherif M. Study of hybrid energy system coupling fuel cell, solar thermal system and photovoltaic cell. Int J Hydrogen Energy 2020;45(25):13564–74.

[6] Singh GK. Solar power generation by PV (photovoltaic) technology: a review. Energy 2013;53:1–13.

[7] Yang B, Wang J, Zhang X, Yu T, Yao W, Shu H, Zeng F, Sun L. Comprehensive overview of meta-heuristic algorithm applications on PV cell parameter identification. Renew Energy 2020;208:2–4.

[8] Tanesab J, Parlevliet D, Whale J, Urmee T. Energy and economic losses caused by dust on residential photovoltaic (PV) systems deployed in different climate areas. Renew Energy 2018;120:401–12.

[9] Fathabadi H. Novel fast dynamic MPPT (maximum power point tracking) technique with the capability of very high accurate power tracking. Energy 2016;94:466–75.

[10] Gayathri Devi B, Keshavan BK. A novel hybrid phase shifted-modified synchronous optimal pulse width modulation based 27-level inverter for grid-connected PV system. Energy 2019;178:309–17.

[11] Jately V, Arora S. Development of a dual-tracking technique for extracting maximum power from PV systems under rapidly changing environmental conditions. Energy 2017;133:557–71.

[12] Chen W, Shen H, Shu B, Qin H, Deng T. Evaluation of performance of MPPT devices in PV systems with storage batteries. Renew Energy 2007;32:1611–22.

[13] Qi J, Zhang Y, Chen Y. Modeling and maximum power point tracking (MPPT) method for PV array under partial shade conditions. Renew Energy 2014;66:337–45.

[14] Zhang X, Li S, He T, Yang B, Yu T, Li H, Jiang L, Sun L. Memetic reinforcement learning based maximum power point tracking design for PV systems under partial shading condition. Energy 2019;174:1079–90.

[15] Dolara A, Lazaroiu GC, Leva S, Manzolini G. Experimental investigation of partial shading scenarios on PV (photovoltaic) modules. Energy 2013;55:466–75.

[16] Wang F, Xuan Z, Zhen Z, Li Y, Li K, Zhao L, Shafie-khah M, S Catalão JP. A minutely solar irradiance forecasting method based on real-time sky image-irradiance mapping model. Energy Convers Manag 2020;220. Article ID: 113075.

[17] Wang F, Xuan Z, Zhen Z, Li K, Wang T, Shi M. A day-ahead PV power forecasting method based on LSTM-RNN model and time correlation modification under partial daily pattern prediction framework. Energy Convers Manag 2020;212. Article ID: 112766.

[18] Hernandez JC, Sanchez-Sutil F, Munoz-Rodriguez FJ. Design criteria for the optimal sizing of a hybrid energy storage system in PV household-prosumers to maximize self-consumption and self-sufficiency. Energy 2019;186:1–3.

[19] Jiang L, Li Y, Huang Y, Yu J, Qiao X, Wang Y, Huang C, Cao Y. Optimization of multi-stage constant current charging pattern based on Taguchi method for Li-Ion battery. Appl Energy 2020;259:1–9.

[20] Sivavara Prasad J, Obulesh YP, Sai Babu Ch. FPGA (Field Programmable Gate Array) controlled solar based zero voltage and zero current switching DC-DC converter for battery storage applications. Energy 2016;106:728–42.

[21] Xuan Z, Gao X, Li K, Wang F, Ge X, Hou Y. PV-load decoupling based demand response baseline load estimation approach for residential customer with distributed PV system. IEEE Transactions on Industry Applications. Early Access 2020. https://doi.org/10.1109/TIA.2020.3014575.

[22] Li K, Wang F, Mi Z, Fotuhi-Firuzabad M, Duić N, Wang T. Capacity and output power estimation approach of individual behind-the-meter distributed photovoltaic system for demand response baseline estimation. Appl Energy 2019;253. Article ID: 113595.

[23] Soudan B, Darya A. Autonomous smart switching control for off-grid hybrid PV/battery/diesel power system. Energy 2020;211. Article ID: 118567.

[24] Al-Addous M, Dalala Z, Class CB, Alawneh F, Al-Taani H. Performance analysis of off-grid PV systems in the Jordan Valley. Renew Energy 2017;113:930–41.

[25] Ebrahim MA, Osama A, Kotb KM, Bendary F. Whale inspired algorithm based MPPT controllers for grid-connected solar photovoltaic system. Energy Procedia 2019;162:77–86.

[26] Dileep G, Singh SN. Application of soft computing techniques for maximum power point tracking of SPV system. Sol Energy 2017;141:182–202.

[27] Ahmad R, Murtaza AF, Sher HA, Shami UT, Olalekan S. An analytical approach to study partial shading effects on PV array supported by literature. Renew Sustain Energy Rev 2017;74:721–32.

[28] Zaihidee FM, Mekhlief S, Seyedmahmoudian M, Horan B. Dust as an unalterable deteriorative factor affecting PV panel's efficiency: why and how. Renew Sustain Energy Rev 2016;65:1267–78.

[29] Deshkar SN, Dhale SB, Mukherjee JS, Babu TS, Rajasekar N. Solar PV array reconfiguration under partial shading conditions for maximum power extraction using genetic algorithm. Renew Sustain Energy Rev 2015;43:102–10.

[30] Omer AM. Renewable energy resources for electricity generation in Sudan. Renew Sustain Energy Rev 2007;11:1481–97.

[31] Abdalla O, Rezk H, Ahmed EM. Wind driven optimization algorithm based global MPPT for PV system under non-uniform solar irradiance. Sol Energy 2019;180:429–44.

[32] Ibrahim H, Anani N. Variations of PV module parameters with irradiance and temperature. Procedia Engineering 2017;134:276–85.

[33] Aouchiche N, Aitcheikh MS, Becherif M, Ebrahim MA. AI-based global MPPT for partial shaded grid connected PV plant via MFO approach. Sol Energy 2018;171:593–603.

[34] Babaa SE, Armstrong M, Pickert V. Overview of maximum power point tracking control methods for PV systems. J Power Energy Eng 2014;2:59.

[35] Putri RI, Wibowo S, Rifa'i M. Maximum power point tracking for photovoltaic using incremental conductance method. Energy Procedia 2015;68:22–30.

[36] A Ali AN, Saied MH, Mostafa MZ, Abdel-Moneim TM. A survey of Maximum PPT techniques of PV Systems. IEEE Energytech; 2012. p. 3–10.

[37] Liu L, Meng X, Liu C. A review of maximum power point tracking methods of PV power system at uniform and partial shading. Renew Sustain Energy Rev 2016;53:1500–7.

[38] Ishaque K, Salam Z. A review of maximum power point tracking techniques of PV system for uniform isolation and partial shading condition. Renew Sustain Energy Rev 2013;19:475–88.

[39] Bendib B, Belmili H, Krim F. A survey of the most used MPPT methods: conventional and advanced algorithms applied for photovoltaic systems. Renew Sustain Energy Rev 2015;45:637–48.

[40] Prasanth Ram J, Rajasekar N, Miyatake M. Design and overview of maximum power point tracking techniques in wind and solar photovoltaic systems: a review. Renew Sustain Energy Rev 2017;73:1138–59.

[41] Sivakumar P, Kader AA, Kaliavaradhan Y, Arutchelvi M. Analysis and enhancement of PV efficiency with incremental conductance MPPT technique under non-linear loading conditions. Renew Energy 2015;81:543–50.

[42] Das P. Maximum power tracking based open circuit voltage method for PV system. Energy Procedia 2016;90:2–13.
[43] Esram T, Chapman PL. Comparison of photovoltaic array maximum power point tracking techniques. IEEE Trans Energy Convers 2007;22:439–49.
[44] Tariq A, Asghar MSJ. Development of analog maximum power point tracker for photovoltaic panel. Proceedings of IEEE International Conference on Power Electronic Drive Systems 2005:251–5.
[45] Noguchi T, et al. Short-current pulse based adaptive maximum-power-point tracking for photovoltaic power generation system. Proc. 2000 IEEE Int. Symp. Ind. Electron. 2000:157–62.
[46] Feng Y, Hao W, Li H, Cui N, Gong D, Gao L. Machine learning models to qualify and map daily global solar radiation and photovoltaic power. Renew Sustain Energy Rev 2020;118:109–393.
[47] Belhachat F, Larbes C. A review of global maximum power point tracking techniques of photovoltaic system under partial shading conditions. Renew Sustain Energy Rev 2018;92:513–53.
[48] Belhachat F, Larbes C. Comprehensive review on global maximum power point tracking techniques for PV systems subjected to partial shading conditions. Sol Energy 2019;183:476–500.
[49] Wu Z, Yu D, Kang X. Application of improved chicken swarm optimization for MPPT in photovoltaic system. Optim Contr Appl Methods 2018;39:1–14.
[50] Guo L, Meng Z, Sun Y, Wang L. A modified cat swarm optimization based maximum power point tracking method for photovoltaic system under partially shaded condition. Energy 2018;144:501–14.
[51] Li L, Lin GQ, Tseng ML, Tan K, Lim MK. A maximum power point tracking method for PV system with improved gravitational search algorithm. Appl Soft Comput 2018;65:333–48.
[52] Tey KS, Mekhlief S, Seyedmahmoudian M, Horan B, Oo AT, Stojcevski A. Improved differential evolution-based MPPT algorithm using SEPIC for PV systems under partial shading conditions and load variation. IEEE Transactions on Industrial Informatics 2018;14:4322–33.
[53] Sen T, Pragallapati N, Agarwal V, Kumar R. Global maximum power point tracking of PV arrays under partial shading conditions using a modified particle velocity-based PSO technique. IET Renew Power Gener 2018;12:555–64.
[54] Yang XS. Firefly algorithms for multimodal optimization. Lecture Notes in Computer Science (including Subser Lect Notes Artif Intell Lect Notes Bioinformatics) 5792 LNCS 2010;5792:169–78.
[55] Peng BR, Ho KC, Liu YH. A novel and fast MPPT method suitable for both fast changing and partially shaded conditions. IEEE Transactions on Industrial Informatics 2017;65:3240–51.
[56] Li Z, Zhou Y, Zhang S, Song J. Lévy-flight moth-flame algorithm for function optimization and engineering design problems. Math Probl Eng 2016:1–22.
[57] Mirjalili S. Moth-flame optimization algorithm: a novel nature-inspired heuristic paradigm. Knowl Base Syst 2015;89:228–49.
[58] Gupta S, Saurabh K. Artificial mountain ape optimization algorithm for maximum power point tracking under partial shading condition. ICECDS: International Conference on Energy, Communication, Data Analytics and Soft Computing; 2017. p. 1–6.
[59] Gharehchopog FS, Gholizaadeh H. A comprehensive survey: whale Optimization Algorithm and its applications. Swarm and Evolutionary Computation 2019;48:1–24.
[60] Gupta S, Saurabh K. Modified artificial killer whale optimization algorithm for maximum power point tracking under partial shading condition. International Conference on Recent Trends in Electrical, Electronics and Computer Technologies; 2017. p. 89–91.
[61] Ramli MAM, Twaha S, Ishaque K, Al-Turki YA. A review on maximum power point tracking for photovoltaic systems with and without shading conditions. Renew Sustain Energy Rev 2017;67:144–59.
[62] Rocha MV, Sampaio LP, Oliveira da Silva SA. Maximum power point extraction in PV array under partial shading conditions using GWO-assisted Beta method. In: Proceedings of the international conference on renewable energies and power quality (ICREPQ'18), vol. 16; 2018. p. 450–5. Salamanca, Spain, 21–23 March.
[63] Daraban S, Petreus D, Morel C. A novel MPPT (maximum power point tracking) algorithm based on a modified genetic algorithm specialized on tracking the global maximum power point in photovoltaic systems affected by partial shading. Energy 2014;74:374–88.
[64] Shaeik Y, Smida MB, Sakly A, Mimouni MF. Comparison between conventional methods and GA approach for maximum power point tracking of shaded solar PV generators. Sol Energy 2013;90:107–22.
[65] Huang YP, Chen X, Ye CE. A hybrid maximum power point tracking approach for photovoltaic systems under partial shading conditions using a modified genetic algorithm and the firefly algorithm. Int J Photoenergy 2018:1–13.
[66] Goud JS, Kalpana R, Singh B. A hybrid global maximum power point tracking technique with fast convergence speed for partial-shaded PV systems. IEEE Trans Ind Appl 2018;54:5367–76.
[67] Shi JY, Zhang DY, Ling LT, Xue F. Dual-algorithm maximum power point tracking control method for photovoltaic systems based on grey wolf optimization and golden-section optimization. Journal of power electronics 2018;3:841–52.
[68] Li H, Yang D, Su W, Lu J, Yu X. An overall distribution particle swarm optimization MPPT algorithm for photovoltaic system under partial shading. IEEE Trans Ind Electron 2018;66:265–75.
[69] Anoop K, Nandakumar M. A novel maximum power point tracking method based on particle swarm optimization combined with one cycle control. International Conference on Power, Instrumentation, Control and Computing (PICC) 2018:1–6.
[70] Başoğlu ME, Cakir B. Hybrid global maximum power point tracking approach for photovoltaic power optimizers. IET Renew Power Gener 2018;12:875–82.
[71] Chen L, Wang X. Enhanced MPPT method based on ANN-assisted sequential Monte-Carlo and quickest change detection. IET Smart Grid 2019;2:635–44.
[72] Lee CT, Tsou HI, Chou TH, Weng KW. Application of the hybrid Taguchi genetic algorithm to maximum power point tracking of photovoltaic system. Proceedings of the IEEE International Conference on Applied System Innovation (ICASI) 2018:231–4.
[73] Said SZ. Maximum power point tracking of photovoltaic generators partially shaded using a hybrid artificial neural network and particle swarm optimization algorithm. Int J Energy Power Eng 2017;66:91–9.
[74] Jiang S, Ji Z, Shen Y. A novel hybrid particle swarm optimization and gravitational search algorithm for solving economic emission load dispatch problems with various practical constraints. Int J Electr Power Energy Syst 2014;55:628–44.
[75] Eltamaly AM, Farh HMH. Dynamic global maximum power point tracking of the PV systems under variant partial shading using hybrid GWO-FLC. Sol Energy 2019;177:306–16.
[76] Huang C, Wang L, Long H, Luo X, Wang JH. A hybrid global maximum power point tracking method for photovoltaic arrays under partial shading conditions. Optik 2019;180:665–74.
[77] Ghasemi MA, Ramyar A, Iman-Eini H. MPPT method for PV systems under partially shaded conditions by approximating I-V curve. IEEE Trans Ind Electron 2017;65:3966–75.
[78] Aquib M, Jain S. A global maximum power point tracking technique based on current source region detection of I-V curve. IEEE, Proceedings of the IEEMA Engineer Infinite Conference (eTechNxT) 2018:1–5.
[79] S Furtado AM, Bradaschia F, Cavalcanti MC, Limongi LR. A reduced voltage range global maximum power point tracking algorithm for photovoltaic systems under partial shading conditions. IEEE Trans Ind Electron 2017;65:3252–62.
[80] Li X, Wen H, Chu G, Hu Y, Jiang L. A novel power-incremented based GMPPT algorithm for PV arrays under partial shading conditions. Sol Energy 2018;169:353–61.
[81] Ramana VV, Mudlapur A, Damodaran RV, Venkatesaperumal B, Mishra S. Efficient global peak tracking of PV system under mismatching conditions using searching technique and bisection method. IEEMA Engineer Infinite Conference (eTechNxT) 2018:1–6.
[82] Başoğlu ME. An enhanced scanning based MPPT approach for DMPPT systems. Int J Electron 2018;105:6–10.
[83] Keyrouz F. Enhanced bayesian based MPPT controller for PV systems. IEEE Power and Energy Technology Systems Journal 2018;5:11–7.
[84] Martin AD, Vasquez JR, Cano JM. MPPT in PV systems under partial shading conditions using artificial vision. Elec Power Syst Res 2018;162:89–98.
[85] Selvakumar S, Madhusmita M, Koodalsamy C, Simon SP, Sood YR. High-speed maximum power point tracking module for PV systems. IEEE Trans Ind Electron 2018;66:1119–29.
[86] Winston DP, Kumar BP, Christabel SC, Chamkha AJ, Sathyamurthy R. Maximum power extraction in solar renewable power system- a bypass diode scanning approach. Comput Electr Eng 2018;70:122–36.
[87] Ahmed J, Salam Z. An enhanced adaptive P&O MPPT for Fast and efficient tracking under varying environmental conditions. IEEE Transactions on Sustainable Energy 2018;9:1487–96.
[88] Ashouri-Zadeh A, Toulabi M, Dobakhshari AS, Taghipour-Broujeni S, Ranjbar AM. A novel technique to extract the maximum power of photovoltaic array in partial shading conditions. Int J Electr Power Energy Syst 2018;101:500–12.
[89] Ahmed J, Salam Z. An improved perturb and observe (P&O) maximum power point tracking (MPPT) algorithm for higher efficiency. Appl Energy 2015;150:97–108.
[90] Dandoussou A, Kamta M, Bitjoka L, Wira P, Kuitché A. Comparative study of the reliability of MPPT algorithms for the crystalline silicon photovoltaic modules in variable weather conditions. Journal of Electrical Systems and Information Technology 2017;4:213–24.
[91] Elgendy MA. Comparative investigation on hill climbing MPPT algorithms at high perturbation rates. In: 2016 7th international renewable energy congress (IREC). IEEE; 2016. p. 1–6.
[92] Gupta A, Chauhan YK, Pachauri RK. A comparative investigation of maximum power point tracking methods for solar PV systems. Sol Energy 2016;136:236–53.
[93] Başoğlu ME, Cakir B. Comparisons of MPPT performances of isolated and non-isolated DC-DC converters by using a new approach. Renew Sustain Energy Rev 2016;60:1100–13.
[94] Parayandeh A, Prodic A. Programmable analog-to-digital converter for low power DC-DC SMPS. IEEE, IEEE Transactions on Power Electronics 2008;23:500–5.
[95] Hossain MZ, Rahim NA, Selvaraj J. Recent progress and development on power DC-DC converter topology, control, design and applications: a review. Renew Sustain Energy Rev 2018;81:205–30.
[96] Amir As, Amir A, Che HS, Elkhateb A, Abd Rahim N. Comparative analysis of high gain DC-DC converter topologies for photovoltaic systems. Renew

Energy 2019;136:1147–63.
[97] Taghvaee MH, Radzi MAM, Moosavain SM, Hizam H, Marhaban MH. A current and future study on non-isolated DC-DC converters for photovoltaic applications. Renew Sustain Energy Rev 2013;17:216–27.
[98] Enrique JM, Duran E, Sidrach-de-Cardona M, Andujar JM. Theoretical assessment of the maximum power point tracking efficiency of photovoltaic facilities with different converter topologies. Sol Energy 2007;81:31–8.
[99] Saravan S, Babu NR. A modified high step-up non isolated DC-DC converter for PV application. J Appl Res Technol 2017;15:242–9.
[100] Gules R, Pfitscher LL, Franco LC. An interleaved boost DC-DC converter with large conversion ratio. IEEE, 2013 IEEE International Symposium on Industrial Electronics. 2003. p. 411–5.
[101] Sri Revathi B, Mahalingam P, Gonzalez-Longatt F. Interleaved high gain DC-DC converter for integrating solar PV source to DC bus. Sol Energy 2019;188:924–34.
[102] Khadmun W, Subsingha W. High voltage gain interleaved DC boost converter application for photovoltaic generation system. Energy Procedia 2013;34:390–8.
[103] Babaei E, Mahmoodieh MES. Systematical method of designing the elements of the Ćuk converter. Electrical Power and Energy Systems 2014;55:351–61.
[104] Choi WY. Three-level single-ended primary-inductor converter for photovoltaic power conditioning. Sol Energy 2016;125:43–50.
[105] Gorji SA, Ektesabi M, Nguyen TN, Zheng J. Galvanically isolated switched-boost-based DC-DC converter. IEEE, 2016 IEEE Energy Conversion Congress and Exploitation (ECCE); 2016. p. 1–8.
[106] Waltrich G, Barbi I. Modelling, control and realization of the single-ended forward converter with resonant reset at the secondary side. IET Power Electron 2015;8:2097–106.
[107] Sharifian A, Sasansara SF, Balgori AA. A new control method based on type-2 fuzzy neural PI controller to improve dynamic performance of a half-bridge DC-DC converter. Neurocomputing 2016;214:718–28.
[108] Ramachandran R, Nymand M. A 98.8% efficient bidirectional full-bridge isolated dc-dc GaN converter. IEEE. 2016 IEEE Applied Power Electronics Conference and Exposition (APEC); 2016. p. 1–8.
[109] Liang TJ, Chen RY, Chen JF, Tzeng WJ. Buck-type current-fed push-pull converter with ZCS for high voltage applications. IEEE, TENCON 2007 – 2007 IEEE Region 10 Conference; 2007.
[110] Lopez del Moral D, Barrado A, Sanz M, Lazaro A, Fernandez C, Zumel P. Autotransformer Forward-Flyback converter applied to photovoltaic systems. Sol Energy 2019;194:995–1012.
[111] Lee HS, Kang B, Kim WS, Yoon SJ. Reduction of input voltage/current ripples of boost half-bridge DC-DC converter for photovoltaic micro-inverter. Sol Energy 2019;188:1084–101.
[112] Ikeda S, Kurokawa F. Isolated and wide input ranged boost full bridge DC-DC converter with low loss active snubber. 2017 IEEE Energy Conversion and Exposition (ECCE); 2017.
[113] Yang L, Zhang J, Yu W, Tong X, Wu X. Analysis of isolated high boost quasi-two switch boosting switched-capacitor converter. 2018 13th IEEE Conference on Industrial Electronics and Applications (ICIEA); 2018.
[114] Chew KWR, Siek L. Single inductor quad-input-dual-output buck converter for photovoltaic systems. IEEE, IECON 2012 – 36TH Annual Conference on IEEE Industrial Electronics Society; 2010.
[115] Zhang L, Hurley WG, Wolfle W. A new approach to achieve maximum power point tracking for PV system with a variable inductor. IEEE, IEEE Transactions on Power Electronics 2010;26:948–52.
[116] Veerachary M. Fourth-order buck converter for maximum power point tracking applications. IEEE, IEEE Transactions on Aerospace and Electronic Systems 2011;47:896–911.
[117] Teo JC, Tan RHG, Mok VH, Ramachandaramurthy VK, Tan C. Impact of bypass diode forward voltage on maximum power of a photovoltaic system under partial shading conditions. Energy 2020;191. Article ID: 116491.
[118] Osmani K, Haddad A, Lemenand T, Castanier B, Ramadan M. A review on maintenance strategies for PV systems. Sci Total Environ 2020;746. Article ID: 141753.
[119] Osmani K, Haddad A, Lemenand T, Castanier B, Ramadan M. Material based fault detection methods for PV systems. Key Eng Mater 2020;865:111–5.
[120] Meerimatha G, Rao BL. Novel reconfiguration approach to reduce line losses of the photovoltaic array under various shading conditions. Energy 2020;196. Article ID: 117120.
[121] Reddy SS, Yammani C. Odd-Even-Prime pattern for PV array to increase power output under partial shading conditions. Energy 2020;213. Article ID: 118780.
[122] Refaat A, Osman MH, Korovkin NV. Current collector optimizer topology to extract maximum power from non-uniform aged PV array. Energy 2020;195. Article ID: 116995.
[123] Gallardo-Saavedra S, Hernandez-Callejo L, Alonso-Garcia MdC, Santos JD, Morales-Aragones JI, Alonso-Gomez V, Monreton-Fernandez A, Gonzalez-Rebollo MA, Martinez-Sacristan O. Nondestructive characterization of solar PV cells defects by means of electroluminescence, infrared thermography, I-V curves and visual tests: experimental study and comparison. Energy 2020;205. Article ID: 117930.
[124] Başoğlu ME, Cakir B. A novel voltage-current characteristic based global maximum power point tracking algorithm in photovoltaic systems. Energy 2016;112:153–63.
[125] Bouilouta A, Mellit A, Kalogirou SA. New MPPT method for stand-alone photovoltaic systems operating under partially shaded conditions. Energy 2013;55:1172–85.
[126] Karthikeyan V, Gupta R. Light-load efficiency improvement by extending ZVS range in DAB-bidirectional DC-DC converter for energy storage applications. Energy 2017;130:15–51.
[127] Abdelmalek S, Dali A, Bakdi A, Bettayeb M. Design and experimental implementation of a new robust observer-based nonlinear controller for DC-DC buck converters. Energy 2020;213. Article ID: 118816.
[128] Mirzaei A, Jusoh A, Salam Z. Design and implementation of high efficiency non-isolated bidirectional zero voltage transition pulse width modulated DC-DC converters. Energy 2012;47(1):358–69. 2012.

Annexe 1.6

Atténuation des effets de l'ombrage partiel sur la performance du système PV grâce à la reconfiguration du réseau PV

New Journal and we have not received input yet 31 (2022) 101280

Contents lists available at ScienceDirect

Thermal Science and Engineering Progress

journal homepage: www.sciencedirect.com/journal/thermal-science-and-engineering-progress

Mitigating the effects of partial shading on PV system's performance through PV array reconfiguration: A review

Khaled Osmani [a], Ahmad Haddad [b,c], Hadi Jaber [d], Thierry Lemenand [a], Bruno Castanier [a], Mohamad Ramadan [b,c,*]

[a] LARIS EA 7315, Polytech Angers, UNIV Angers, France
[b] School of Engineering, International University of Beirut BIU, Beirut, Lebanon
[c] School of Engineering, Lebanese International University LIU, Bekaa, Lebanon
[d] Mechanical Engineering Department, Abu Dhabi University, United Arab Emirates

ARTICLE INFO

Keywords:
Physical
Electrical
Shading
Reconfiguration
Patterns
Dispersion

ABSTRACT

This paper aims at exploring different PhotoVoltaic (PV) array Reconfiguration (PVR) methods, used to reduce the negative impacts of Partial Shading Conditions (PSCs), that could affect the performance of a PV system (i.e. hotspots, electrical mismatch, etc.). The classification of different PVR techniques is formed under three main categories: physical, electrical, and physical-electrical combination. Physical PVR alters the actual locations of the panels within the array. Referred to as static reconfiguration methods, this set includes puzzle based, number based, symmetry based, distance maximizing based, and nature inspired methods. On the other hand, electrical PVR reorders the electrical interconnections between PV panels, and is composed of algorithm based, artificial intelligence based, hybrid, and basic/improved electrical configurations. A combined PVR method hybridizes the two precedent categories. Each method from the three main sets, is critically compared to the relevant others, according to a mathematical model, which includes many performance indices: Fill Factor (FF), Mismatch Power Loss (P_{ML}), Percentage Power Loss (%P_{Loss}), Performance Ratio (PR), Execution Ratio (ER), Efficiency (η), Percentage of Power Enhancement (%PE) and DC output power (P_{DC}). The thorough investigation of different PVR techniques, resulted that a Total Cross Tied (TCT) configured PV panels, physically relocated by means of Static Shade Dispersion Physical Array Relocation (SD-PAR) algorithm, while interfered with a switching matrix controlled by Modified Harris Hawks Optimizer (MHHO) algorithm, could be an optimum and effective solution to passively mitigate PSCs' effects.

Introduction

In compliance with immense modern energy demands, a substantial need for a cheaper and reliable energy supply is globally evolving [1]. On the other hand, intercontinental collaborative projects have been established in order to reduce the effects of climate change provoked by greenhouse gas emissions, by considering renewable energy generation [2]. Among different forms of renewable energy resources, solar energy, correlated with PV systems, is a great option, due to its abundancy and the non-detrimental nature of such systems [3]. In terms of achieving the sustainable development goals, solar energy is found one of the most efficient solutions [4]. Solar power hence possesses many derived field applications to produce an environment-friendly energy, such as the utilization of solar chimney power plants [5]. A PV based energy supply possesses a high power generation capability with a zero-noise and an emission-less performance, as well as a great flexibility for an efficient usage in many applications [6].

In terms of reliability, PV systems can be integrated with thermal collectors, to produce a hybrid solar photovoltaic-thermal system, yielding in better electrical power output as well as a facility to supply hot water demands for households [7]. For instance, the energy efficiency of buildings is improved, by using photovoltaic and thermal collectors [8]: thermal panels absorb the heat from PV panels what is regarded as a bonus cooling technique [9], thus lowering the operating temperature of PV panels [10] by utilizing the waste heat of the panels [11]. The cooling effect on PV panels in turn, results in better electrical power productivity, and more energy distribution to buildings [12]. The incorporation of different types of solar panels, such as PV, thermal collectors, and concentrating solar panels, offers a combined heat-

* Corresponding author.
E-mail address: mohamad.ramadan@liu.edu.lb (M. Ramadan).

https://doi.org/10.1016/j.tsep.2022.101280
Received 3 December 2021; Received in revised form 16 March 2022; Accepted 16 March 2022
Available online 19 March 2022

Nomenclature

AAR	Adaptive Array Reconfiguration
ACMS	Ancient Chinese Magic Square
AR	Automatic Reconfiguration
ARS	Automatic Reconfiguration System
ASP	Arithmetic Sequence Pattern
BCC	Bidirectional Cuk Converter
BL	Bridge Linked
BOA	Butterfly Optimization Algorithm
BPD	Bypass Diode
CS	Competence Square
D	Diagonal
DAS	Data Acquisition System
DDM	Double Diode Model
DPP	Differential Power Processing
DS	Dominance Square
DSP	Digital Signal Processor
EAR	Electrical Array Reconfiguration
ER	Execution Ratio
FF	Fill Factor
FPGA	Field Programmable Gate Array
FRA	Flow Regime Algorithm
FRPVA	Full Reconfigurable PV Array
FS	FutoShiki
GA	Genetic Algorithm
GMPP	Global Maximum Power Point
GMPPTs	Global Maximum Power Point Trackers
GOA	Grasshopper Optimization Algorithm
HC	Honey Comb
HHO	Harris Hawks Optimizer
HRPVA	Half Reconfigurable PV Array
HSV	Hue Saturation Value
IE	Irradiance Equalization
IGBT	Insulated Gate Bipolar Transistor
IMI	Irradiance Mismatch Index
IPT	Image Processing Technique
IS	Information System
KCL	Kirchoff`s Current Law
KK	KenKen
KVL	Kirchoff`s Voltage Law
LMPPs	Local Maximum Power Points
LN	Long Narrow
LP	Linear Programming
LS	Latin Square
LW	Long Wide
MAA	Munkres' Assignment Algorithm
MHHO	Modified Harris Hawks Optimizer
MIQP	Mixed Integer Quadratic Programming
MPP	Maximum Power Point
MPPTs	Maximum Power Point Trackers
$\%P_{Loss}$	Percentage power loss
$\%PE$	Percentage power enhancement
$[u_i]$	Equivalent class for index i
$[u_j]$	Equivalent class for index j
C_{ij}	Cell in ith row and jth column
E_0	Random variable
E_{act}	Actual produced energy
E_e	Error of currents summation
G_{F_0}	Irradiance on non-shaded submodule
G_{F_i}	Irradiance on each submodule
$GMPP_{CS}$	Case specified global power peak
$GMPP_{PSC}$	Global maximum peak at PSC
$GMPP_{STC}$	Global maximum peak at STC
$GMPP_{conv}$	Conventional global power peak
G_O	Irradiance at STCs
G_{ij}	Irradiance received by the module at the ith row and jth column
$I_{M_{ij}}$	Generated current at STCs
I_0	Diode saturation current
I_D	Diode current
I_M	Maximum output current
I_{MP}	Maximum peak current
I_{Ph}	Light generated current
I_{PV}	Cell current
I_{SC}	Short circuit current
I_{SH}	Shunt branch current
I_{Si}	String current at the ith row
I_{ij}	Module current
I_k	The current at k^{th} row of the array
K_{IJ}	Irradiance factor
K_i	Current temperature
M_{ij}	PV module at ith row and jth column
N_{P_A}	Number of parallel strings
N_{S_A}	Number of series panels in a string
N_p	Number of modules connected in parallel
N_s	Number of modules connected in series
$P_{GMPP_{PSC}}$	Maximum power at PSC
$P_{MAX_{unshaded}}$	Maximum power without any shading pattern
P_{DC}	DC Power
P_{GMPP}	Global maximum peak power
P_{Loss}	Power Losses
P_{ML}	Power Mismatch Losses
P_{PSC}	Maximum generated power at PSC
P_{STC}	Maximum generated power at STC
PV_{rated}	Rated output power
P_a	PV panel's output voltage without bypass diodes
P_{in}	Input power
P_k	The maximum output power for each code of shadow
R_{SH}	Parallel resistance
R_S	Series resistance
T_0	Temperature at STCs
T_{max}	Maximum number of iterations
α	Diode ideality factor
MS	Magic Square
MS-EC	Magic Square – Enhanced Configuration
NS	Non Symmetrical
NSCs	Non Shaded Cells
O-E	Odd-Even
O-E-P	Odd-Even-Prime
O-SDK	Optimized SuDoKu
PBA	Population Based Algorithms
P-CI	Parity-Column Index
PCM	Phase Change Material
PE	Power Enhancement
P-EC	Physical-Electrical Combined
PGI	Power Generation Index
PR	Performance Ratio
PSCs	Partial Shading Conditions
PV	Photo Voltaic
P-V	Power-Voltage
PVR	PV Reconfiguration
R	Random
RBFA	Rule Based Fuzzy Approach
RBL-HC	Rearranged Bridge Linked – Honey Comb
RBL-TCT	Rearranged Bridge Linked – Total Cross Tied
RCI	Row/Column Index
ROA	Rao Optimization Algorithm

RSP-TCT	Rearranged Series Parallel – Total Cross Tied
RST	Rough Set Theory
RTCT	Rearranged Total Cross Tied
SCs	Shaded Cells
SDK	SuDoKu
SDM	Single Diode Model
SDP	Static Shade Dispersion Positioning
SD-PAR	Static Shade Dispersion Physical Array Relocation
SIR	Sum of Irradiance
SM	Switching Matrix
SMOA	Social Mimic Optimization Algorithm
SN	Short Narrow
SP	Series Parallel
SPBC	Series Parallel with Binary Coding
SS	Sky Scraper
STCs	Standard Test Conditions
STF	Search Type Factor
SW	Short Wide
TCT	Total Cross Tied
TDM	Triple Diode Model
UC	Uneven Column
UI	Uniform Irradiance
UR	Uneven Row
ZZ	ZigZag

Symbols

$U_{rand_j}(t)$	Randomly selected position j for hawks from the population at iteration t
$U_{rand_k}(t)$	Randomly selected position k for hawks from the population at iteration t
$U_{rand_l}(t)$	Randomly selected position l for hawks from the population at iteration t
U_m	The mean position
U_{prey}	The position of the prey
V_M	Maximum output voltage
V_{MP}	Maximum peak voltage
V_{OC}	Open circuit voltage
V_T	Thermal voltage
V_k	The voltage at k^{th} row of the array
$Z_{i_{nt}}$	Solution vector of the i^{th} particle at iteration n_t
Z_i	Particle with number i
Z_j	Particle with number j
Z_k	Particle with number k
f_i	The fragrance of the i^{th} butterfly
$g^*_{n_t}$	Global best solution
g^*	Current best global solution
l^*_{nt}	Worst solution at n_t
n_t	Present iteration number
t_i	Current iteration
w_e	The weighting factor of E_e
w_f	The weighting factor of P_a
x^t_i	The i^{th} butterfly in iteration t
x^t_j	The j^{th} butterfly from the search space
x^t_k	The k^{th} butterfly from the search space
y_{iq}	Existence variable
C	Conditions set
A	Attributes set
CF	Capacity Factor
D	Decision set
E	Escape energy of the rabbit
EA	Total generated energy
ER	Execution Ratio
FF	Fill Factor
G	Actual irradiance
I	Stimulus intensity
M	Magic constant
P	Output DC power
PR	Performance Ratio
R	Relation rule
T	Actual system's temperature
U	Universe set
$U(t_i)$	Location vector in iteration t_i
V	Single diode model output voltage
a	Power exponent
c	Sensory fragrance
k	Boltzmann constant
n	Number of modules within the array
q	Electron charge
r	Random number

Greek letters

η	Efficiency

electricity production, resulting in better systems' efficiencies and faster return on investment [13].

However, a single PV module is incapable of generating a significant consumable power quantity, hence the need for interconnecting between many modules to meet higher load demands [14]. Inaccurate interconnections between PV modules, could decrease the life expectancy of the PV array, where the performance and cost efficiency of the system get diminished [15].

From the same perspective, the output of such systems is mainly dependent on radiation, environmental conditions, and ambient temperature [16]. As solar irradiance is irregularly available [17], and weather conditions are unpredictable [18], such etiologies manipulate the efficiency of a solar system, by affecting the values of series and parallel resistances (R_S and R_{SH} respectively) of the Single Diode Model (SDM) of solar cells [19]. This resultant dynamical change within inbuilt resistances becomes a challenge to be faced with [20].

Generally, irradiance conditions are subject to two distinct scenarios: either homogeneous (uniform) or non-homogeneous (partial shading). A uniform distribution of sunrays over the entire PV array, results in a single peak in the P-V (Power-Voltage) characteristic curve. On the other hand, the Partial Shading Conditions (PSCs) are met, when solar radiations are blocked by buildings, trees, poles, dust accumulation, passage of clouds and different forms of physical light obstacles. Also, shading can occur due to PV cell cracking and ageing [21]. In this case, many local peaks appear in the P-V curve [22]. There are also non-climatic triggers for PSCs, such as non-computational manufacturing designs, bad soldering bonds, and entropy of PV modules [23]. Under most circumstances, PSCs are unavoidable, due to space limitations and shadowing of adjacent PV modules [24].

PSCs have hazardous implications on the PV system's components (modules, array, etc.) and on its performance as well. For instance, hotspots are created when a portion of the PV module receives less irradiance than the unshaded portion of the same module [25]. Similarly, excessive thermal stresses play a significant role in the process of hotspots formation [26]. Shaded PV cells behave as a load while draining current from non-shaded cells, what elevates their temperature [7], and cause futuristic burnout scenes within the PV system.

PV modules are damaged due to hotspots creation, with inability to collect maximum available energy [27]. Shaded PV cells may operate in the negative voltage region causing power absorption from non-shaded cells, due to their transformation into a resistive load [28]. In other words, partial shading attenuates the PV power generation while leaving

a permanent damage in PV cells [29], with a notable voltage drop on the shaded panel's terminals [30] and a reduced conversion efficiency [31]. From a different perspective, electrical mismatch for a PV array is another consequence of PSCs, where electrical differences would exist between solar cells, leading eventually to a reduction in the overall PV output power [32]. This can be noted as the power difference between faulty and non-faulty PV modules [33]. For an accurate investigation of PV output power loss, the comparison of shading pattern with the shading area is a primary factor [34]. Power output reduction in PV systems is not only proportional to the shaded area, but also dependent on different other factors, such as shade intensity and physical locations of shaded modules within the PV array [35].

As a primary solution, the usage of Bypass Diodes (BPDs), connected in shunt across each PV module, reduces the probabilities of hotspots formation by enabling a bypass route for the generated current to follow, when an open-circuit of a module is established due to shading [36].

However, the usage of bypass diodes is not an optimum solution for PSCs, due to having many limitations [37], while inducing multiple peaks in the P-V curve [38]. Aside from BPDs, Maximum Power Points Trackers (MPPTs) are considered as an effective solution for uniform shading, whereas they fail in locating a global maximum between different locals. Consequently, unbalanced PV string currents will also exist [39].

Unlike MPPTs' chase for the local maximum, GMPPTs (Global Maximum Power Point Trackers) algorithms succeed in locating the highest maximum among different locals, thus, reducing the effects of PSCs and ensuring a maximum energy harvest [40]. However, GMPPTs are regarded as costly solution, demanding extra circuitry and complex algorithms implementation (artificial intelligence, machine learning, etc.) [41].

Aside from tracking maximums in P-V curves, and in order to compress the different undesirable effects of PSCs, the micro-inverters' employment on the level of each PV module, may alleviate the energy production of the entire PV system, by mitigating the electrical mismatch issue [42]. However, this solution adds additional financial burden on the PV system's operational cost [43].

Upgraded research is moving toward PV panel reconfiguration, as a way to distribute the shading effects over the entire PV modules in the system, rather than being centered over partial fragments [44]. As a result, this helps in equalizing the produced string currents [45] after an equal shade dispersion [46]. Array Reconfiguration (AR) adjusts the P-V characteristic curve, leaving space for a single maximum peak [47]. Compared to other PSCs' mitigation techniques, AR is effective on both operational as well as economical aspects of a PV system [48]. It can be applied to compensate the effects of stationary shadows (caused by fixed objects) as well as moving shadows (caused by passage of clouds) [49].

Three major classifications are established within this paper for PV array reconfiguration strategies, as either electrical (dynamic, by means of switches/matrices), physical (static, by actual physical relocation of the PV array) [50], or the combination of the two precedents. Dynamic reconfigurations are powerful in reducing the effects of passing clouds, instantaneously. The failing events of solar modules are limited by their automatic disconnection from the array, initiated by a Switching Matrix (SM) [51]. This in turn compensates the sudden changes in irradiance profiles, sparing away the problems of reduced PV system's efficiency and lowered energy generation [52]. Due to the fact that parallel interconnections within a PV module are more resilient to shading than serially connected ones, rules are set for SM accordingly. The grouping of newly created sub-modules is based on the insulation levels of different modules [53].

On the other hand, physical reconfiguration is a single time relocation arrangement. This configuration does not change according to the instantaneous shading patterns [54], where the combinatorial techniques, utilize the characteristics of both electrical and physical configurations. In this paper, the evaluation of different techniques for PV array reconfiguration will take place, according to the stated classifications. Each general method individually contains a set of sub-methods, which will be critically compared to the corresponding others within the same set. The remainder of this paper consists as follows: Section 2 models the electrical output of a PV system, where Section 3, reveals different effects of PSCs over PV systems' performance. Section 4 represents the complete surveyed reconfiguration schemes for PV arrays, Section 5 discusses the results of investigated reconfiguration methods, where finally, conclusions and related future work are conducted in Section 6.

Electrical modelling of a PV system's output

The output of a single PV cell is too small to be considered as consumable [55]. Different serial/parallel connections are required to increase the power output of PV cells [56]. A PV module is therefore established by a number of serial/parallel connected cells [57]. PV modules in turn are allied either in parallel, series, or in series–parallel combinations to build a PV string [58]. A parallel arrangement of strings forms finally a PV array [59]. This entire process can be graphically interpreted as shown in Fig. 1.

The PV cell shown in Fig. 1 can either be emulated by a Single Diode Model (SDM), Double Diode Model (DDM) or Triple Diode Model (TDM) [60].

The procedure of extracting larger power values from PV arrays, starts from the SDM shown in Fig. 1: the output current of a PV cell is calculated after applying Kirchoff's Current Law (KCL) at node A. The resulting cell current is represented in Eq. (1) [61,62].

$$I_{PV} = I_{Ph} - I_D - I_{SH} \tag{1}$$

where I_{Ph} corresponds to the light generated current, I_D the diode current and I_{SH} the shunt branch current. To have a more precise formulation of the cell current, all of the right sided quantities in Eq. (1) must be elaborated as follows in Eq. (2), (3), and (4) [61,62].

$$I_{Ph} = \frac{G}{G_O} \bullet [I_{SC} + K_i(T - T_0)] \tag{2}$$

$$I_D = I_0 \left[exp\left(\frac{q(V + R_s I_{PV})}{\alpha k T} \right) - 1 \right] \tag{3}$$

$$I_{SH} = \frac{V + R_s I_{PV}}{R_{SH}} \tag{4}$$

with G representing the actual system's irradiance, G_O the irradiance at the Standard Test Conditions (STCs: $G_O = 1000 W/m^2$), I_{SC} the short circuit current, K_i the current temperature coefficient, T the actual system's temperature, T_0 the temperature at the STCs ($T_O = 25^{\circ} C$) [63], I_0 the diode saturation current, V the single diode model output voltage, R_s the series resistance, α the diode's ideality factor, k the Boltzmann constant, q the charge of an electron, and R_{SH} the shunt resistance [61,62].

The substitution of Eqs. (2), (3), and (4) in Eq. (1), represents the expanded PV cell current shown in Eq. (5).

$$I_{PV} = \frac{G}{G_O} \bullet [I_{SC} + K_i(T - T_0)] - I_0 \left[exp\left(\frac{q(V + R_s I_{PV})}{\alpha k T} \right) - 1 \right] - \frac{V + R_s I_{PV}}{R_{SH}} \tag{5}$$

By referring to Fig. 1, a clear formulation for the PV module current, can be achieved by taking into consideration the amount of irradiance striking on the correspondent module with respect to G_O. Hence, Eq. (6) represents the module current I_{ij}.

$$I_{ij} = \frac{G_{ij}}{G_O} \bullet I_{M_{ij}} \tag{6}$$

where $I_{M_{ij}}$ represents the generated current at STCs [64], by the module

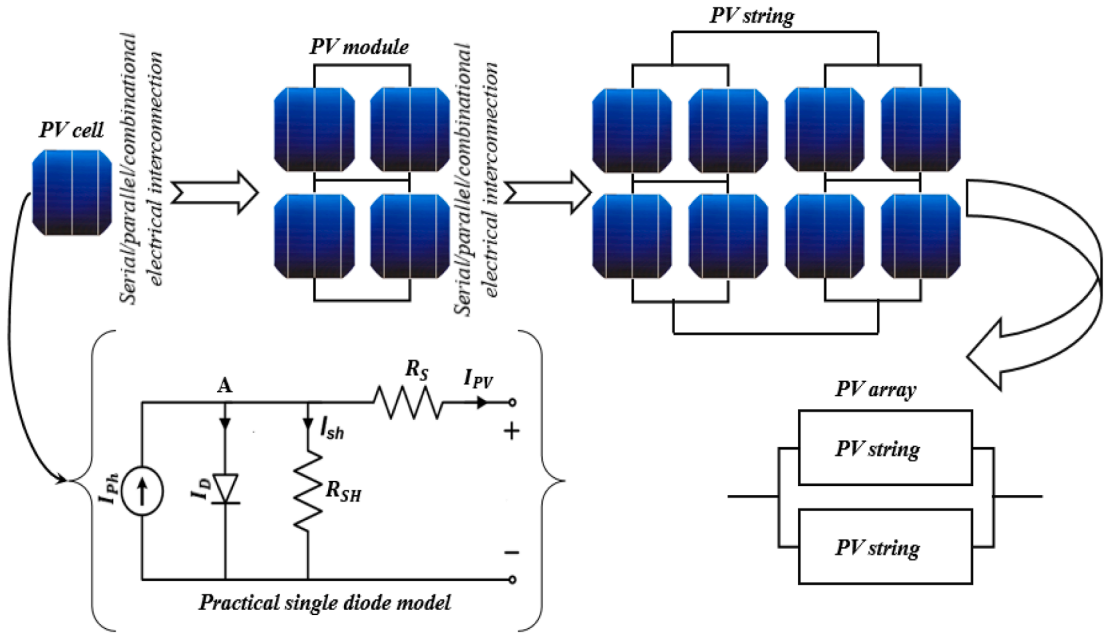

Fig. 1. The composition of a PV array from PV cells.

located at i^{th} row and j^{th} column in a PV array, with G_{ij} the irradiance received by the same module.

Additionally, the string currents depend on the PV modules' electrical interconnections, such as TCT (Total Cross Tied), SP (Serial Parallel), HC (Honey Comb) etc. However, a generic row current (delivered by a PV string) can be calculated with respect to the module's current as represented in Eq. (7), when the string is formed by successive PV modules connections in series [65].

$$I_{Si} = \sum_{i=1}^{i_{max}} K_{IJ} \bullet I_{M_{ij}} \tag{7}$$

where I_{Si} indicates the string current at i^{th} row and K_{IJ} the irradiance factor which equals to G_{ij}/G_O.

Successively, the PV array current depends on the values of resulting string currents, which in turn are dependent on how the strings are connected. For the generic case of serial/parallel electrical interconnections between different PV strings, the PV array current can be calculated according to Eq. (8) [66].

$$I_{Array} = N_p \left\{ I_{Ph} - I_0 \left[exp\left(\frac{V + R_s I_{PV}}{\alpha N_s V_T} \right) - 1 \right] \right\} - \frac{V + R_s I_{PV}}{R_{SH}} \tag{8}$$

where N_p and N_s denote the number of modules connected in parallel and series respectively, and V_T the thermal voltage [61].

The stated current calculations are the first indicators that judge the performance of the PV system [67]. For instance, partial shading can be detected from the PV cell to PV array levels. In other words, when a PV cell gets shaded, its produced current would be much smaller than the other receiving complete solar radiations [68].

The distinction between these two currents classifies PV cells as healthy or faulty. Similar perspective can be executed on the levels of PV modules, strings, and arrays. Non-shaded PV arrays would have zero string currents differences, thereby generating more power [69]. When partial shading exists, the differences between various string currents, indicate the creation of several LMPPs (Local Maximum Power Points) and a GMPP (Global Maximum Power Point) in the characteristic P-V curve [70]. By taking this into acknowledgment, a case-specified PV array reconfiguration would ensure that the PV system is delivering the highest available power [71].

Effects of partial shading on PV system's performance

With various reasons triggering partial shading scenarios over a PV system, hazardous effects can be seen affecting its operational behavior [72] as represented in Fig. 2. In PSCs, the PV array's composers (modules, strings) receive inhomogeneous solar irradiance [73]. The PV output energy is aggravated due to the mismatch in the electrical characteristics [74]. Resultant consequences can be summed up as follows [75]:

- Hotspots
- Multiple peaks
- Electrical mismatch losses

Hotspots

When the operating current of a PV module exceeds its short circuit current I_{SC}, hotspot heating occurs [76]. Hence, shaded PV cells generate less current [77] as exposed in Fig. 3. Shaded Cells (SCs) are obliged to carry a higher current originated from Non-Shaded Cells (NSCs) [78]. Accordingly, SCs operate as a load, and consume power from NSCs. This behavior compels an elevated temperature inside the cells. Consequently, PV modules get permanently damaged [79].

Multiple peaks

When the PV array examines a reduced power output due to PSCs, after activation of bypass diodes, a new problem arises, such as the apparition of multiple peaks in the P-V characteristic curve [80], as shown in Fig. 4. This fact acts as an obstacle in front of MPPTs, where such trackers are forced to locate a global peak among many locals [81]. This, in turn, adds hardware/software complexities in MPPT's design, the fact that would be reflected as an economical burden on the PV system design.

Electrical mismatch losses

Mismatch losses in a PV module occur when SCs act upon non-standard parameters [82], with increased values of series resistance R_S

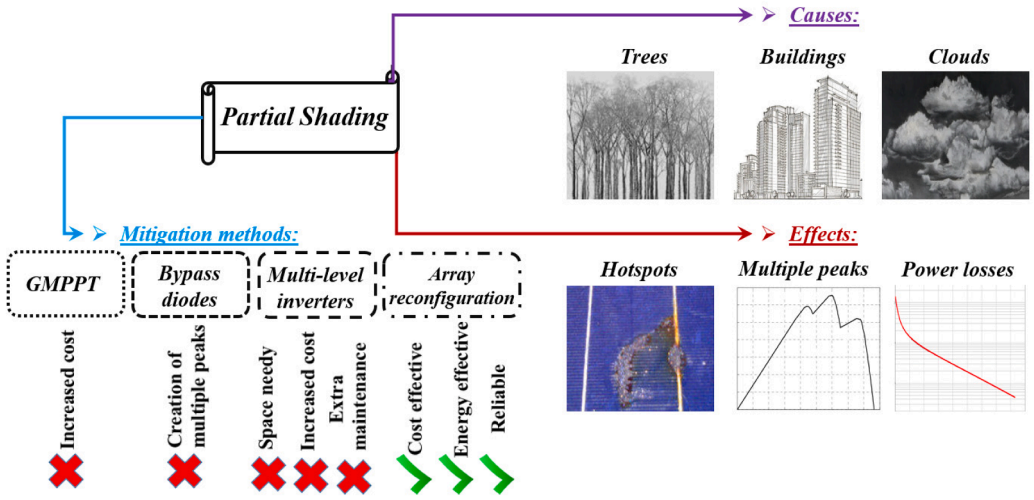

Fig. 2. Causes, effects and mitigation methods of partial shading.

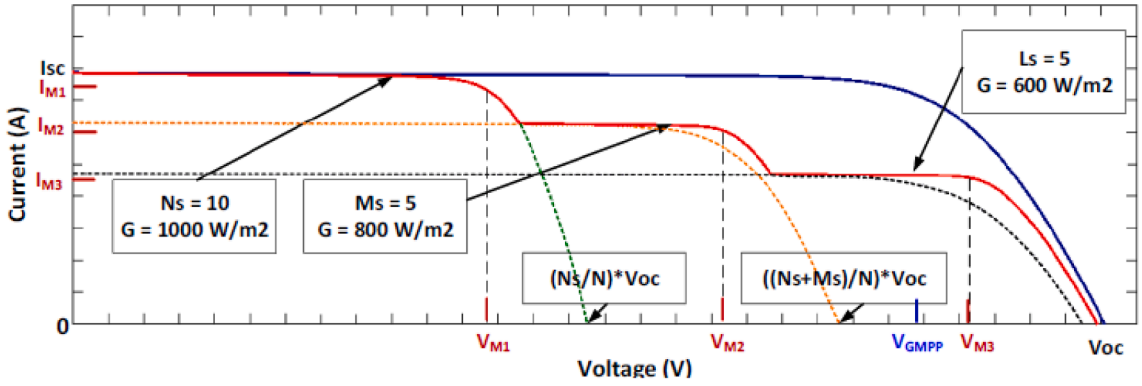

Fig. 3. Fluctuations in generated currents between shaded and non-shaded PV cells [81].

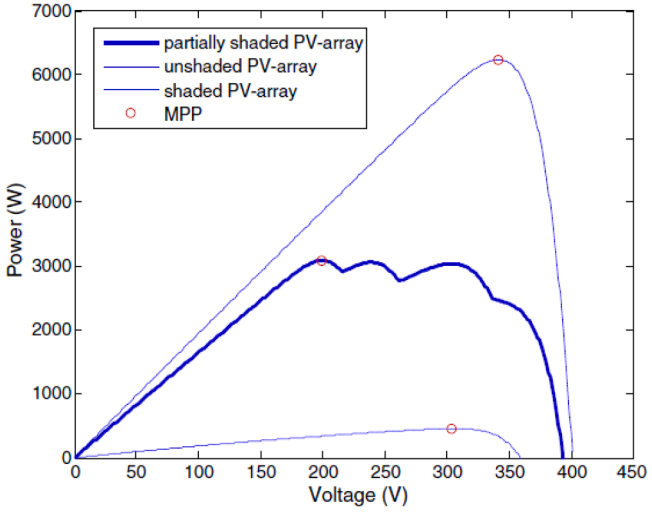

Fig. 4. Multiple peaks apparition in the P-V characteristic curve due to PSCs [78].

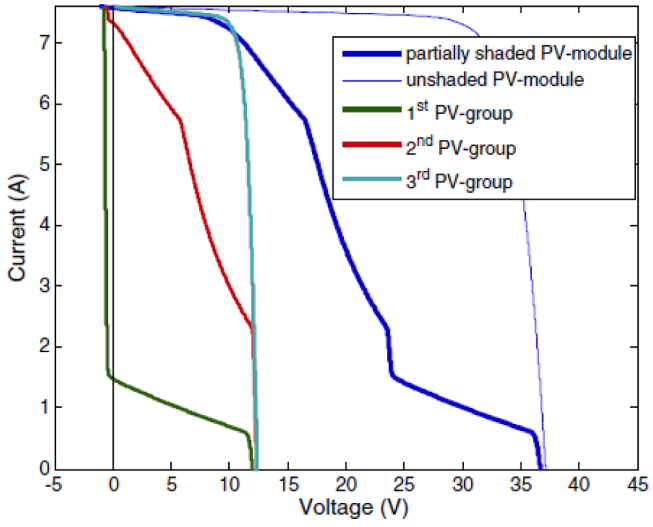

Fig. 5. Abnormalities in P-V characteristic curve due to PSCs [78].

and shunt resistance R_{SH} [83]. The resulting generated current I_{PV} becomes abnormal in both quantity and waveform [84], as indicated in Fig. 5. In other words, the output current from parallel connected blocks is hence lower than the one resulting from non-shaded blocks. A blackout can be noticed on the output power level of shaded blocks (complete open-circuit) [85].

Different negative impacts of PSCs do not depend only on the

intensity of shading, but also on the shading pattern [86], as encapsulated in Table 1. Regardless of their types (hotspot, mismatch, etc.), they all share in common a heat generation ignition phenomenon on the level of PV cells, reflected as elevated operating temperatures over exceeding limits. The heat-efficiency relation of PV cells is inversely proportional, where the higher their operating temperature is, the lower the power productivity [87]. This damaging consequence affect the PV characteristic curves, by lowering the open-circuit voltage quantities, hence disturbing the overall efficiency of PV power plants [88].

Accordingly, modern research focuses on the thermal management of PV systems, as a way to mitigate the heat generation aspect produced by PSCs, such as usage of nanofluid [89], finned heat sinks based cooling [90], water based cooling systems [91], Phase Change Materials (PCM) [92], and other techniques [93].

Alternatively, and despite the effectiveness of these PV thermal regulation methods, the PVR techniques can help in mitigating excess temperatures' effects and restoring the cells' operating temperatures as nearest to STCs, with less needs of additives over the PV system's components.

Accordingly, for an effective shading dispersion from a PV array, regardless of its configuration, and PV cells raw materials used [102], an optimum PV shading mitigation predictability system must take into consideration the different patterns stated in Table 1. As a graphical interpretation, Fig. 6 lists the eight different shading patterns.

Reconfiguration schemes for PV arrays

Since PV systems are considered as lifetime investments [103], with elevated capital costs [104], the supposed payback period is averaged of 25 years [105]. During their lifecycle, a stable efficiency [106], and solid performance [107] are presumed. However, such systems often interact with unfavorable climatic conditions, such as weather fluctuations, and mainly partial shading conditions [108]. The stated problematic scenarios cannot be avoided since PV systems are of outdoor nature.

Consequently, power losses are significant due to PSCs, which would decrease the popularity of such systems, by lowering their suitability as a robust alternative power supply [109]. To overcome these drawbacks, PV reconfiguration methods can adapt the arrays to produce higher power quantities, thus increasing the overall PV systems' efficiencies [110]. Three major classification for PV Reconfiguration (PVR) methods can be addressed as [111]:

- Physical (or static)
- Electrical (or dynamic)
- Physical-Electrical Combined (P-EC)

Table 1
Different shading patterns.

Shading pattern	Description	Ref.
Uneven row shading	Happens when physical barriers shadow more rows within the array than the others	[94]
Uneven column shading	Happens when physical barriers shadow more columns within the array than the others. This can also take place when the composers (modules) of the same column are unevenly shaded	[95]
Diagonal shading	Similar to uneven row/column shading, but the physical barrier is confronted in front of the array with an inclination angle	[96]
Random shading	Does not follow any uniform shading pattern	[97]
Short and narrow shading	Caused by nearby objects, where it can be the result of adjacent PV panels shading. It covers up 25% of the total PV array space	[98]
Short and wide shading	Similar to short and narrow shading, but covers more from the total PV array space, up to 70%	[99]
Long and narrow shading	Similar to uneven row shading, but with larger shading area of 50%	[100]
Long and wide shading	Similar to long and narrow shading, but with larger shading area of 75%	[101]

Physical reconfiguration methods

Without altering the electrical connections between the PV modules, their physical locations are statically rearranged only once [112]. Based on the reconfiguration's execution on the level of PV modules, the physical reconfiguration methods help in dispersing the shade uniformly within the PV array [113]. Consequently, the mismatch loss is greatly reduced, in the same time as the power generation is increased. Table 2 encloses different classification criteria for different static PV reconfiguration methods.

Puzzle based

SuDoKu (SDK). SuDoKu is a logic-based number placement puzzle [114]. Its aim is to maintain the digits from one to nine in each block (3 $\times$ 3 sub-matrices) of the puzzle without repetition [115]. Also, each row and column should follow the same procedure by withstanding same digits under the same law [115].

When adapting a SuDoKu approach to physically rearrange PV modules, the column number remains unchanged, but the row is altered [116]. As an example in reference [117], the PV panel corresponding to the 3rd row, 3rd column is physically relocated to the 9th row, while keeping the same electrical connections as within the 3rd row. This process can be graphically interpreted in Fig. 7.

For a 9 $\times$ 9 PV array, the corresponding output voltage is denoted in Eq. (9).

$$V_a = \sum_{m=1}^{9} V_m \tag{9}$$

with V_a indicating the PV array voltage and V_m the voltage of the panel at the m^{th} row [118].

On the other hand, and for the same PV array's architecture, its current at each node can be formulated as in Eq. (10).

$$I_a = \sum_{n=1}^{9} I_{mn} - I_{(m+1)n} = 0 \tag{10}$$

with I_a as the PV array current, I_{mn} the current at m^{th} row, n^{th} column [118].

In other terms, the electrically adjacent panels, which belong to a particular row, are physically separated, and then relocated in different positions in other rows.

For a good shade dispersion, the SuDoKu method needs additional wiring, and can be only effective for a symmetrical ($m \times m$) matrix. Consequently, this method presents high line losses (due to the extended wire lengths) with a poor dispersion factor [119]. Such drawback can be surpassed by an optimized SuDoKu physical rearranging method [120].

Optimized SuDoKu (O-SDK). Line losses seen in basic SuDoKu arrangement, are directly related to wire lengths (increased lengths signifies increased resistances) [121]. Accordingly, the Optimized SuDoKu (O-SDK) arrangement mainly focuses on shortening the interconnection wires as much as possible. The puzzle construction is established according to the following logic sequence [122]:

1. The first column of the puzzle is filled by digits from one to nine in ascending order.
2. The subsequent columns are shifted by three, concerning the maximum sub-array size from previous columns.
3. In order to avoid the arrangement of the first column in the fourth, an offset is added to the shifting process. Consequently, the second element starts from one, and the subsequent two columns are shifted by three, correspondingly to the previous column.
4. By incrementing the offset, the seventh column is filled.

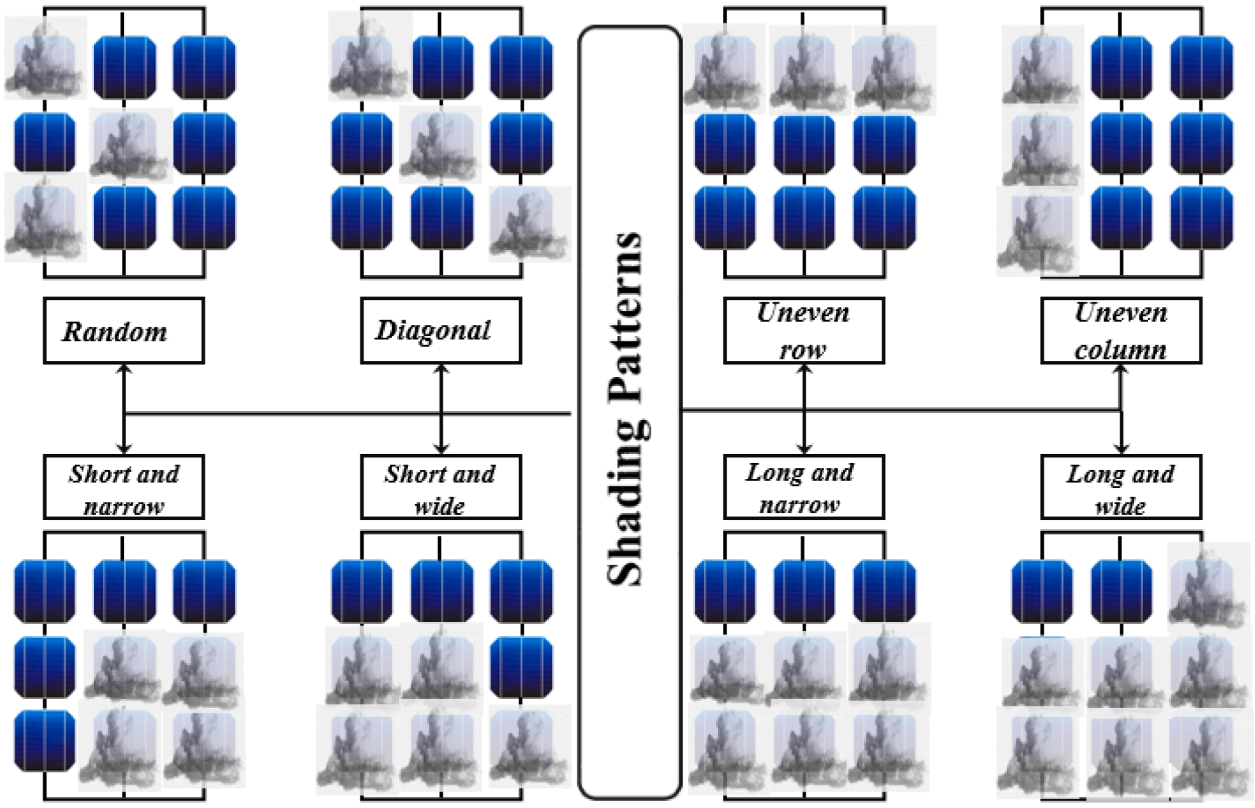

Fig. 6. Graphical representation of shading patterns.

Table 2
Major classification of physical PVR.

Physical PVR methods	Description
Puzzle based	The arrangements of PV arrays are done by mimicking the puzzle solving strategies. This set of methods include SuDoKu, optimized SuDoKu, Skyscraper, Futoshiki, Kenken and other puzzle patterns.
Number based	PV modules are arranged concerning their row/column indexes such as odd, even, etc.
Nature inspired	PV modules are arranged by imitating natural river flow behavior, which is believed to bring prosperity in life, including Lo Shu concept.
Symmetry based	Considering equal proportioning and balancing, PV modules are rearranged in a harmonious strategy, facing each other symmetrically around a defined axis.
Distance maximizing	In order to avoid mutual shading of adjacent PV modules, while taking into consideration the limited available installation area, the modules are rearranged with maximum available distances between them.
Algorithm based	The search for an optimum PV modules arrangement is conducted by means of an algorithm, including Static Dispersion Positioning algorithm, etc.

The optimized SuDoKu algorithm can be mathematically justified in Eq. (11) [122].

$$Shiftfornthcolumn = \left[\frac{n-1}{3}\right] + 3 \times ((n-1) mod 3) \quad (11)$$

with $\left[\frac{n-1}{3}\right]$ denoting the greatest integer function and n the correspondent column's number.

This method succeeds in eliminating the drawbacks of a conventional SuDoKu arrangement, but still have a problem in developing number repetition for non-symmetrical $(n \times m)$ sub-arrays [122].

Competence square (CS). The position of a PV panel is represented by an alphabet/number representation of the form X_{mn}, where X is the alphabetical row order, m is the row's number and n the column's number. The logical flowchart of the Competence Square (CS) method can be described according to the following four rules [123]:

The a_{11} panel is randomly repositioned within the puzzle. The alphabetically successive panel is displaced according to 'L' shape.
While 'L-shaping' successive panels, if > 9, the series is resumed from next row with second column.
Following the same process, when > 9, the series is resumed from the second column with next row position.
In the last stage of puzzle construction, if an alphabet occupies a previous place, then it should be moved to the nearest forward position in the same row.

Figure 8 reveals the final positioning of PV panels according to CS method, in an 9×9 array configuration.

The proposed CS reconfiguration method has showed an effectiveness in power enhancement by a maximum of 24.4% for short and wide shade patterns, and a minimum of 6.6% for short and narrow shade patterns. From another side, CS have lowered the power loss resulting in a PV system by 49% under long and narrow shade patterns and 30% under short and narrow shade patterns [123].

SkyScraper (SS). The Skyscraper formulation is based on the height of buildings (which represent the adjacent sides of rows/columns), that can be seen through a single sight [124]. The visibility of buildings must be evaluated from four adjacent sides, what would in turn increase the method's success probability. Its flowchart operates according to the following six steps [124]:

1. Selection of $(m \times n)$ matrix size.
2. Identification of visible buildings blocks.

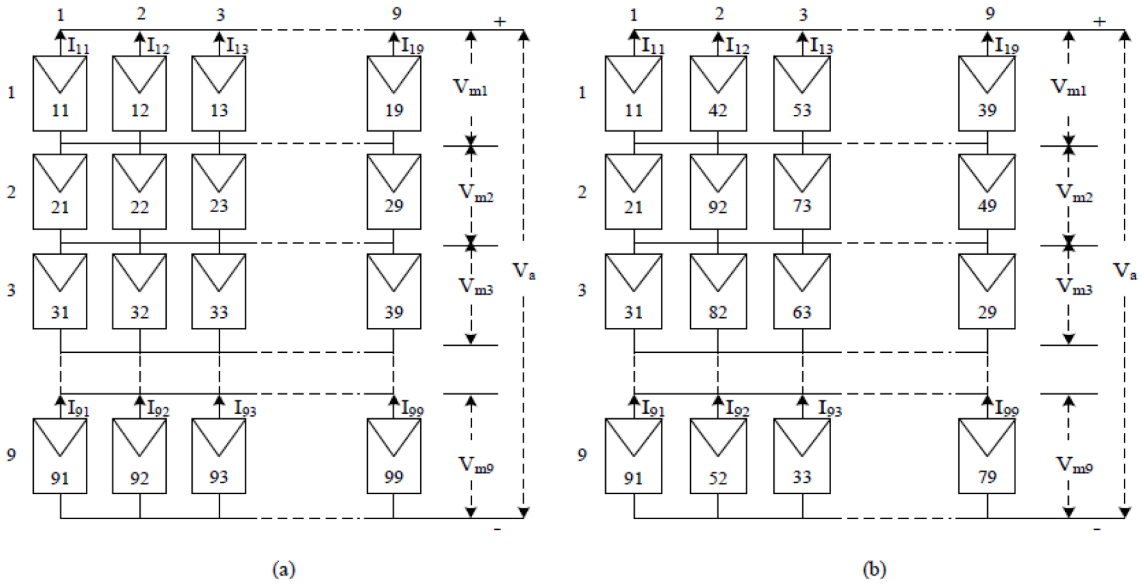

Fig. 7. PV array reconfiguration (a) before SuDoKu; (b) after SuDoKu [117].

56	66	76	86	76	16	26	36	46
37	47	57	67	77	87	97	17	27
18	28	38	48	58	68	78	88	98
89	99	19	29	39	49	59	69	79
61	71	81	91	11	21	31	41	51
42	52	62	72	82	92	12	22	32
23	33	43	53	63	73	83	93	13
94	14	24	34	44	54	64	74	84
75	85	95	15	25	35	45	55	65

Fig. 8. PV panels allocation using CS method [123].

3. Identification of total number of sub-blocks.
4. Reconfiguration of PV array based on maximum height possible in the building.
5. The PV array is another time reconfigured based on the first intermediate building height.
6. A total reconfiguration for PV array is done according to each individual sub-array reconfiguration.

The resultant final SS rearrangement is shown in Fig. 9.

The proposed physical PVR method reduces high computational burden seen in other puzzle-based reconfiguration methods (such as SuDoKu, optimized SuDoKu, etc.), with a greater dispersion factor [124].

Magic square (MS). Magic Square (MS) method is a logic based number placement puzzle, utilized to spread the shading effect, in which square grids have a special number arrangement [125]. The specialty in the number arrangement reflects in obtaining the same number after adding n digits in all rows, columns, and diagonal patterns, labelled as the magic constant M. The first number is stored at location $(n/2; n-1)$. In order to locate the succeeding number, a decrement/increment by 1 is held for

41	92	63	24	35	86	17	78	59
21	72	53	44	15	96	87	68	39
81	32	13	64	75	56	47	28	99
61	42	83	34	95	16	27	58	79
11	22	73	54	65	46	97	38	89
31	52	93	74	85	26	67	48	19
71	12	43	84	55	66	37	98	29
51	82	23	94	45	36	77	18	69
91	62	33	14	25	76	57	88	49

Fig. 9. Skyscraper PV rearrangement [124].

the previous row/column numbers respectively. If number repetition exists, the row's position is instead incremented by 1, where the column's position is decremented by 2. If the calculated row number is negative, and the calculated column position is n, the new position is held at $(0; n-2)$. This can be graphically interpreted as shown in Fig. 10 [126].

The 'n' order of a magic square is an arrangement of n^2 distinct integers, in which the rules for setting a 4×4 magic square are set according to the n^{th} element concerning the i^{th} row and j^{th} column of a pattern n_{ij} as shown in Eq. (12) [126].

$$n_{ij} where \begin{cases} i = numberofrow(i = 1, 2, \cdots) \\ j = numberofcolumn(j = 1, 2, \cdots) \end{cases} \quad (12)$$

The rules of row/column-wise additions are shown in Eqs. (13) and (14) respectively [126].

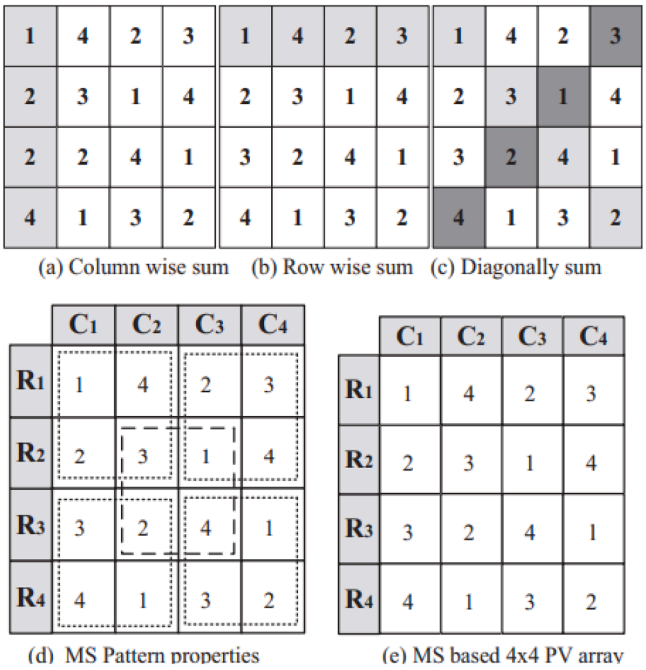

Fig. 10. Magic Square PV array arrangement [126].

$$\sum_{i=1}^{i=4} n_{ij} = MagicSum for i^{th} row (i = 1, 2, 3, 4) \tag{13}$$

$$\sum_{j=1}^{j=4} n_{ij} = MagicSum for j^{th} column (j = 1, 2, 3, 4) \tag{14}$$

The rules for diagonal-wise additions are shown in Eqs. (15) and (16) [126].

$$\sum_{j=1}^{j=4} n_{ij} = MagicSum for (i = j) \tag{15}$$

$$\sum_{i=1}^{i=4} n_{ij} = MagicSum for (j = i^{max} - (i - 1)) \tag{16}$$

Following the Eqs. (13) to (16) the MS configuration is obtained, where power loss is minimized, and fill factor is increased in the proposed PV system under investigation [126]. When using a GA (Genetic Algorithm) to obtain the optimal MS configuration, the maximum power output can be improved under different PSCs [127].

Dominance square (DS). The Dominance Square (DS) method has a similar approach of the CS based PV arrangement. The difference lies in the procedure while reshaping the PV panels, where instead of placing the successive modules in 'L' shape, they are diagonally rearranged. Other than that, the same four rules seen in CS method apply as well to DS method [128]. The difference can be noted when comparing Fig. 8 to the DS arrangement shown in Fig. 11.

FutoShiki (FS). The pattern arrangement is done using a Linear Programming (LP) approach in a FutoShiki (FS) based puzzle pattern [129]. The numbers from 1 to 'n' are arranged to make each row/column of a square grid, only include unique numbers, without any repetition [130]. Within the square grid, each number must obey the rule of inequality constraint between the two adjacent numbers. Ensuring a unique solution for the equidimensional square grid (i.e., FS puzzle reflected as the PV array), LP generates a proper combinatorial logic, to avoid any number repetition in each row/column. The application of the

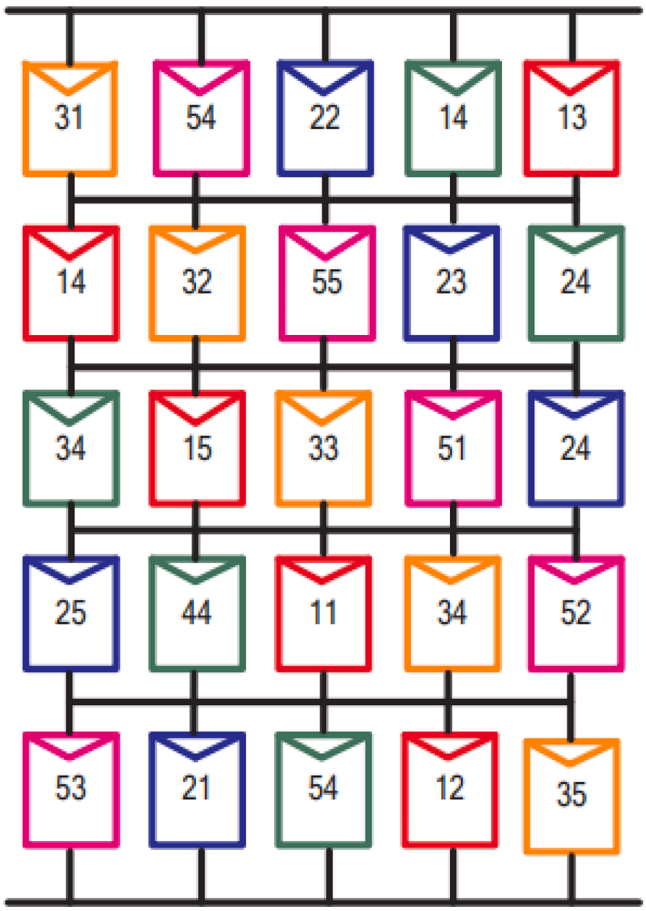

Fig. 11. Dominance square PV array reconfiguration [128].

formalized logic of numbers in FS puzzle (no repetition, etc.), is translated as the equalization of the produced output power between shaded and non-shaded PV modules. The proper FS arrangement can hence modify currents/voltages quantities in each row, to homogenize the produced power, thus dispersing the shade. Fig. 12 represents the

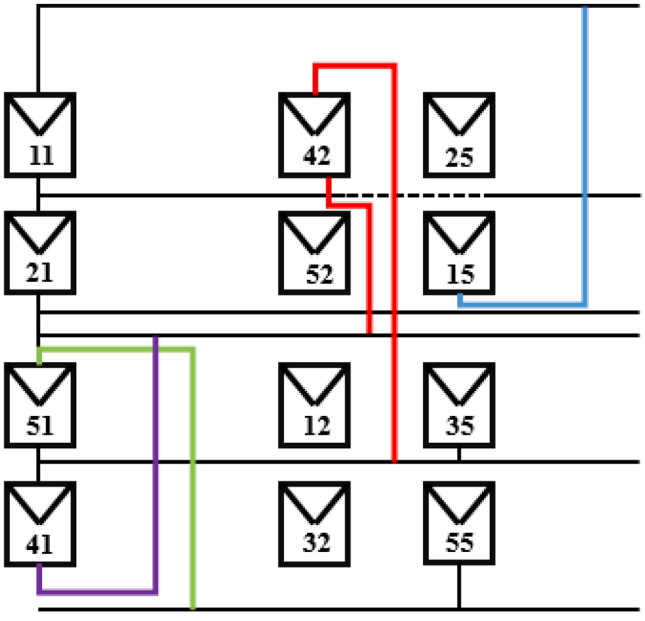

Fig. 12. Futoshiki based PV array arrangement.

Futoshiki puzzle arrangement for a PV array.

The proposed Futoshiki method disperses the shade affecting the modules in a single row, to other rows [130].

Latin square (LS). A Latin Square (LS) puzzle composes of square grids, in which the first column contains digits from one to six in ascending order [131]. Consequently, the second column's digits are shifted downward, row-wise, by 1 successively. The cell in this method is represented by C_{ij} with i,j denoting the row and column indexes respectively. The arrangement follows the basic properties shown in Eqs. ((17)-(18)) [131].

$$for\, i = j : \left\{ C_{ij} = C_{(i+1)(j+1)} = C_{(i+2)(j+2)} = C_{(i+n)(j+n)} \right\} \tag{17}$$

$$for\, i \neq j \; : \begin{cases} C_{ij} = C_{(i+1)(j+1)} = C_{(i+2)(j+2)} = C_{(i+n)(j+n)}, when(i+n<p, j+n<q) \\ C_{(i+n)(j+n)} = C_{(i+n-N-1)(j+n+1)}, when i+n=p \\ C_{(i+n)(j+n)} = C_{(i+n+1)(j+n-k+1)}, when j+n=q \end{cases} \tag{18}$$

with p, q representing the panel's row and column numbers respectively. The LSP method has a power enhancement of 6.81% compared to SuDoKu, with a reduced power loss of 13.78% [131].

KenKen square (KK). KenKen puzzle is formed by a grid surrounded by bold lines, which contains $m \times n$ square blocks. The procedure of number filling inside each block ensures the avoidance of number repetition is each row/column pattern. Each sub-grid is in turn decomposed into blocks, where according to an additive mathematical feature, the numbering (reflecting the arrangement) can be achieved [132]. Using this type of PVR, shade is dispersed across the entire PV array.

ZigZag (ZZ). By relocating the PV panels in their original columns, but in different row positions, with modules in the first row reconnected as the diagonal element, the novel ZigZag (ZZ) scheme in reference [142], can straighten the array P-V characteristics, thus decreasing the number of local maxima. Each column's elements (which represent a PV module) are kept within the same column: no horizontal shifting is made between alternate columns. From another part, rows' elements are interchanged (vertically shifted), such that the row's index of the first element is kept all along the diagonal path $(11, 12, 13, \cdots, (finalrowindex-1)(lastcolumnindex))$. In other terms, first row's modules for instance are each shifted to the diagonal path, where the remaining modules are reconnected in row-wise manner. The ZZ strategy is flexible in applications, as it can be employed to PV arrays of any dimensions, especially for large PV farms.

AdDoKu. As an improvement for the SuDoKu method, the novel AdDoKu has achieved better results, in PV power productivity, under many PSCs. The targeted PV array consists of nine 3×3 sub-array

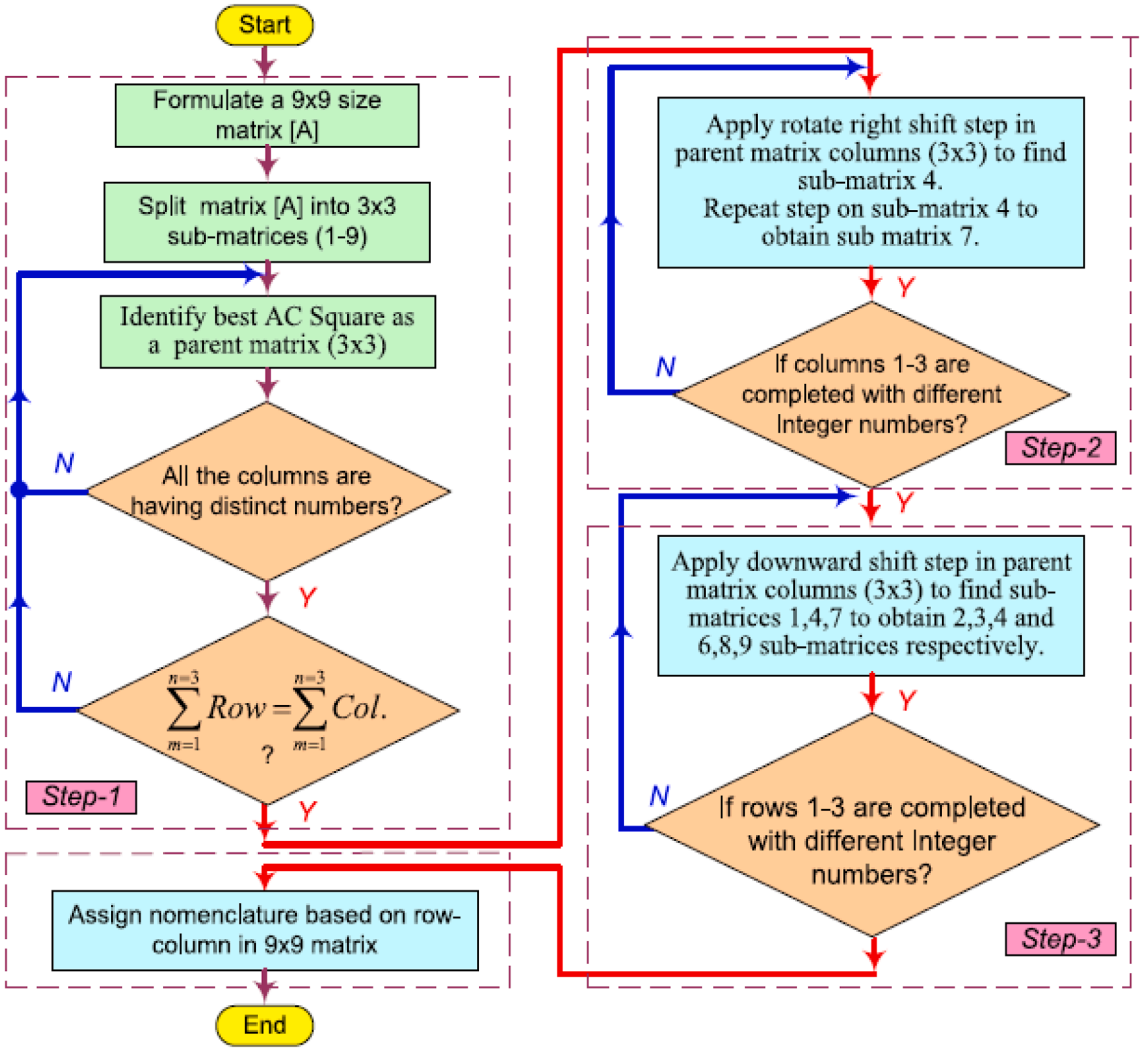

Fig. 13. The proposed ACMS based PVR method flowchart [134].

matrices, such that each row/column contains digits from 1 to 9 for only once. Each 3 × 3 sub-grid must in turn have digits from 1 to 9 only once. Eventually, the small number in the corner of a cells' group equals to the summation of the numbers in this group. Such logic based puzzle is formed using backtracking method [133]. The AdDoKu arrangement surpasses the performance of SuDoKu under all PSCs test, however it lacks experimental approval.

Ancient Chinese Magic square (ACMS). The Ancient Chinese Magic Square (ACMS) can effectively disperse shades over the entire PV array, where the parent ACM matrix is derived following the row/column/diagonal summations equality properties. As similar to SuDoKu method, to solve a 9 ×9 PV matrix, the ACMS technique's flowchart is presented in Fig. 13, with general rules as follows [134]:

i. Re-arrangements are done according to the best observed ACM matrix
ii. Columns are right shifted
iii. Rows are downward shifted

Despite the fact that ACMS have surpassed many other puzzle-based PVR methods, still its tested shading patterns conditions were narrow.

Arithmetic Sequence pattern (ASP). The Arithmetic Sequence Pattern (ASP) technique is proposed to reduce wire losses, and shading dispersion over sub-arrays, as in the case of other puzzle-based PVR methods, such as SuDoKu, FS, MS, etc. The reconfigured modules arrangements do not imply any radical change in the initial wires lengths. The ASP method's flowchart is presented in Fig. 14, and developed according to the two following procedures [135]:

i. The first column of the ASP's puzzle is shifted by 2. Succeeding columns are kept unique by shifting their corresponding previous columns by 2. Rows on the other hand are shifted by 1, until the stopping criteria is met.
ii. The established patterns in ASP puzzle must ensure that no sub-arrays would have the same numbering.

The drawback of ASP method is its need for skilled physical labors when selected for a real implementation in PV systems and impose additional wiring losses when compared to EAR technique [135].

Concerning different puzzle-based PV array reconfigurations, Table 3 records a comparative assessment of various techniques used in static PVR.

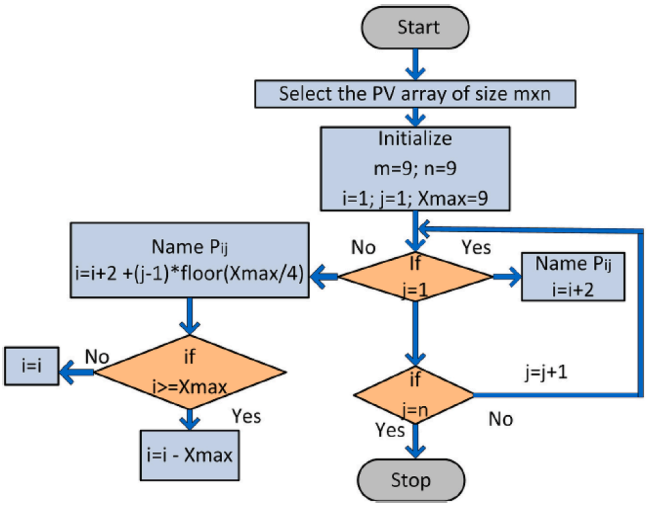

Fig. 14. Arithmetic Sequence Pattern method's flowchart [135].

Table 3
Comparison between different puzzle-based PVR methods.

Method	Advantages	Disadvantages
SuDoKu	• Ensures shade dispersion all over the array • Reduces mismatch losses	• Efficiency is related to the initial choice of SuDoKu pattern • Improper choice of the pattern could result in a reduced power output
Improved SuDoKu	• Reduces line losses • Increases dispersion factor	• Number repetition is seen in some of the sub-arrays • Can work optimally only for a 9 × 9 puzzle
Competence square	• Enhances power generation by up to 24.4% • Lowers power losses by up to 49%	The method was not investigated for various shading patterns such as random, diagonal, etc.
Skyscraper	• Applicable to any PV array size • Able to disperse all shading patterns	Presents difficulty in identifying accurate initial guesses
Magic square	• Decreases power losses • Develops a high fill factor	The method can withstand errors while adapting a higher than 4 × 4 PV array size
Dominance square	Similar to the advantages of CS	The diagonal reshaping gets harder with increasing PV array size
Futoshiki	Enables row shading dispersion into many rows	May include many inequality signs such as empty cells, number repetition, etc.
Latin square	• Power is enhanced by 6.81% compared to SuDoKu • Wiring loss is decreased by 18.86% compared to SuDoKu	In some shading patterns, the SuDoKu method achieves better fill factor than this method
KenKen	Increases output power while decreasing wire losses	A difficult mathematical model is behind the square's numeration
ZigZag	General improvement of PV operations under PSCs	Applicable to only small PV arrays.
AdDoKu	Superior performance compared to SuDoKu	Lacks real experimentation, and actual results' measurements
ACMS	Better than most other puzzle-based methods	Shading tests' conditions are very narrow
ASP	Possess a high power gain	Impose additional wire losses

Number based

Odd-Even (O-E). Each PV module of the array is labeled as M_{ij} with $i.j$ denoting the number of row and column respectively [136]. Considering a 4 × 4 array, the arrangement starts by placing the modules with odd numbered row and odd numbered column in the first row. In succession, modules with even numbered row and even numbered column, are placed in the second row. Consecutively, the modules with odd numbered row and even numbered column are placed in the third row. Finally, the modules with even numbered row and odd numbered column are placed in the fourth row. This rearrangement process can be

M_{11}	M_{13}	M_{31}	M_{33}
M_{42}	M_{22}	M_{44}	M_{24}
M_{12}	M_{32}	M_{14}	M_{34}
M_{41}	M_{21}	M_{43}	M_{23}

Fig. 15. Odd-Even PVR [136].

visualized in Fig. 15.

The usage of this method has resulted in an increased power output by bypassing row currents, while reducing the existence of multiple peaks in P-V characteristic curve [136].

Odd-Even-Prime (O-E-P). As a way to increase PV power generation from the Odd-Even method in [136], the Odd-Even-Prime method decreases the mismatch losses and power losses due to hotspots formation, by decreasing the difference between maximum and minimum Sum of Irradiance (SIR) [137]. With the ability of application to any array size, the PV modules are relocated within the PV array according to the following steps [137]:

1. Placement of odd numbered row/column modules
2. Placement of even numbered row/column modules
3. Placement of prime numbered row/column modules
4. Placement of even numbered row and odd numbered column modules
5. Placement of odd numbered row and even numbered column modules
6. Placement of prime numbered row and odd numbered column modules
7. Placement of odd numbered row and prime numbered column modules
8. Placement of even numbered row and prime numbered column modules
9. Placement of prime numbered row and even numbered column modules

Row/Column index (RCI). The initial 9 × 9 matrix is decomposed into nine 3 × 3 matrices, and the relocation process is held for each sub-array by adding the row/column indices of panels [138].

Each obtained number represents the shifting place for the correspondent panel accordingly. For example, the panel P_{11} which is located at first row, first column, results in an index of two. Consequently, this panel is shifted two places downward. Different sub-arrays will follow the same procedure, ending up with total PV reconfiguration [138]. Among different number-based PVR, this method adapts the simplest mathematical form.

Nature inspired

Symbolizing the scroll of a river as an essential part of the ancient spiritual life, by means of old nine hall diagram, the Lo Shu (oldest matrix originated from ancient China) technique can be linked to enhanced PV power outputs [139]. The scrolling river indicates the PV panels' movement for a better shade dispersion. The correspondent sequential flowchart of Lo Shu method is described in the following three steps [139]:

1. Identification of Lo Shu mother matrix: the resulting first 3 × 3 sub-matrix of the total 9 × 9 matrix is rearranged as mother Lo Shu matrix
2. Column shift: in which the matrix' forward column shift is executed
3. Row shift: done for the previously shifted first three columns

Lo Shu technique minimizes row current differences, thus enhancing PV power output. Its procedural steps are simple, yielding in shade scattering with few panel movements [139].

Symmetry based

For a 5 × 4 PV array, PV panels are relocated according to Non Symmetrical (NS) patterns denoted as NS1 and NS2 [140]. The configurations NS1 and NS2 are only possible for patterns with odd-numbered rows. In case of repositioning only even-numbered rows, there would be a single NS pattern. The modelled 5 × 4 PV array has its first column filled in digits from 1 to 5 in ascending order. The first three rows of the second column add 2 to the digits in the same previous row/column, except for the last two rows, corresponding to numbers 1 and 2 respectively. Third column adds two to the previous column's numbers, except for rows 2 and 3. The final fourth column adds 2 to the number of the previous column, except for first and last rows. The determination process of the row and column (i,j) for NS1 and NS2 configurations are interpreted in Eqs. (19) and (20) respectively.

$$i = \begin{cases} iifj = 1 \\ i + (j-1) \times floor\left(\frac{i_{max}}{2}\right) ifj > 1 \\ ifi < i_{max}, i = i \\ elsei = i - i_{max} end \end{cases} \tag{19}$$

$$i = \begin{cases} iifj = 1 \\ i + (j-1) \times ceil\left(\frac{i_{max}}{2}\right) ifj > 1 \\ ifi < i_{max}, i = i \\ elsei = i - i_{max} end \end{cases} \tag{20}$$

The NS PV array reconfiguration enhances the PV output power, and better reduce losses due to shading, compared with other static PVR methods [140], but is less efficient for large arrays, and its wiring mode is complicated. This method's performance is ameliorated using Parity-Column Index (P-CI) strategy [141], where Eqs. (19) and (20) are improved in order to reconstruct the first row's position, as well as to define other row arrangements with different constraints. Entire rows are parity-grouped, along with specific vertical and transverse parity shifts, P-CI seemed effective in reducing wiring complexities seen in [140], with higher fill factor than other PVR techniques [141].

Distance maximizing

By physically relocating the PV panels within an array as far as possible from each others, while modifying their corresponding row/column positioning, the shadow pattern affecting the PV system can be distributed all over the array, thus increasing its energy outcomes [143].

After the panels' row/column rearrangement, a shifting process is introduced to reduce the concurrence between shading inducers and PV modules as seen in Fig. 16.

Although this technique minimizes the need for protection diodes and eliminate the occurrence of multiple local peaks in the P-V characteristic curve, it does not take into consideration the area restriction complexity, which PV systems generally suffer from.

Algorithm based

Static Shade Dispersion Physical Array Relocation (SD-PAR).

The SD-PAR algorithm proposes a 3 × 3 PV array repositioning according to the five steps summarized in Table 4 [144].

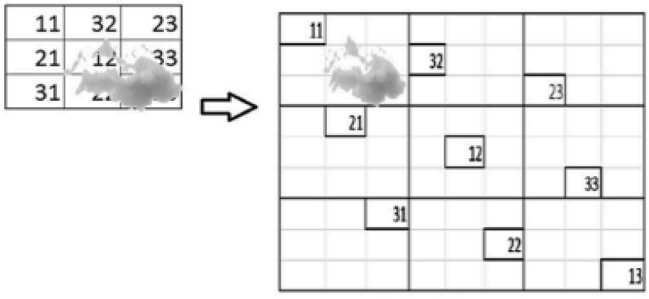

Fig. 16. Physical repositioning of PV panels based on distance maximizing [143].

Table 4
Executive steps for SD-PAR algorithm.

Step	Procedure
1	The matrix A is inputted having $m \times n$ as numbers of rows and columns respectively
2	Reset the value of the counter variable c to zero
3	While decreasing the value of the row variable i from n to one, increment c by 1, where the i^{th} column of the PV array is circularly shifted by c. Upon each increment, the value stored inside the variable d is horizontally concatenated then stored in the third column of the new PV array matrix B
4	Re-execution of the second iteration of the proposed algorithm
5	The value in matrix d is horizontally concatenated and stored in B

The resulting reconfiguration for the 3 × 3 PV array is exposed in Fig. 17.

This relatively simple, one time PVR, is found able to consequentially improve the output power under all shading conditions [144].

Static Shade Dispersion Positioning (SDP). The partial shading effect on a row, is dispersed over the entire PV array, where physical relocation of PV panels is condemned according to the following four steps [145]:

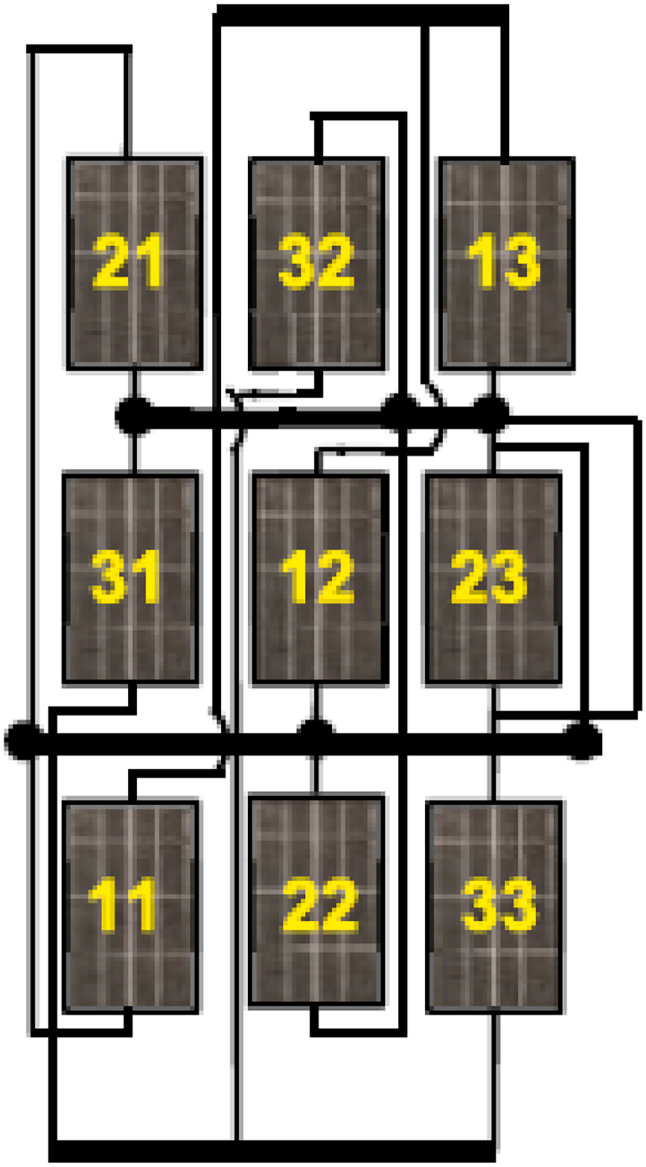

Fig. 17. SD-PAR reconfigured PV array [144].

Calculate the total number S of modules connected to the PV array.
Calculate the value of the real number $Z = \lfloor \sqrt{S} \rfloor$.
Check conditions when number of rows equals or not to the number of columns and rearrange the PV array accordingly.
When number of rows is different than number of columns, several increments/decrements by one, take place for numbers of rows/columns in order to create the modified PV array configuration.

When applied, this method better enhances the power production in a PV array, under various shading conditions, as compared to SuDoKu [145].

Electrical reconfiguration methods

The electrical (dynamic) PV array reconfiguration methods, are processes which continuously investigate the occurring shading patterns, and re-adapt the array accordingly, by means of switches and moveable electrical interconnections [146]. Different classifications for the surveyed electrical PVR techniques are recapitulated in Table 5.

Basic electrical interconnections

A single PV module's output power is limited due to its high dependence on environmental conditions, and its non-linear performance. Furthermore, parallel connected PV modules are more resilient as compared to series branches in front of PSCs (according to KCL). In contrast, series connected PV modules, offer bigger output voltage (according to KVL). Hence, panels are combined in series, parallel, and combination of Series/Parallel (SP) [147] for an optimized output power, as seen in Fig. 18.

The expansion of precedent interconnection schemes can be seen in Total Cross Tied (TCT), Honey Comb (HC) and Bridge Link (BL) circuit configurations [148]. Fig. 19 groups different expanded electrical interconnection for PV modules.

The Series-Parallel (SP) configuration shown in Fig. 18, takes advantage of current summation (from different branch currents in parallel connections), and voltage summation (from different series voltages). The TCT connection reduces the mismatch under uniform irradiance conditions when compared to SP. The BL scheme in turn, reduces cable losses and wiring's costs, since about half of the wires in TCT are avoided [149]. For most PV systems' configurations, TCT is more commonly used, due to its simplicity of execution and energy effectiveness [150].

Such electrical reconfiguration methods alter only the

Table 5
Major classification of electrical PVR.

Electrical PVR method	Description
Basic electrical interconnections	Involve basic wiring configurations for PV panels, such as series, parallel, honey comb, etc.
Improved electrical interconnections	The basic electrical interconnections are mutually hybridized with each others, to grant advantages from each. This involves series parallel mixed with bridge link, bridge link with honey comb, etc.
Algorithm based with/without embedded systems	The rules of reconfiguring electrical wirings are dictated by instructions' sets. Including full systems with algorithms executing on the actuators level, by switching on/off PV panels banks according to pre-defined conditions. This involves switching matrix, etc.
Artificial intelligence	Includes self-learning programming techniques which improve the PVR method's operational behaviors according to previous experiments
Hybrid	Includes two or more differently categorized methods within a single approach, such as electrical array reconfiguration mixed with a fuzzy logic controller operated under artificial neural network, etc.

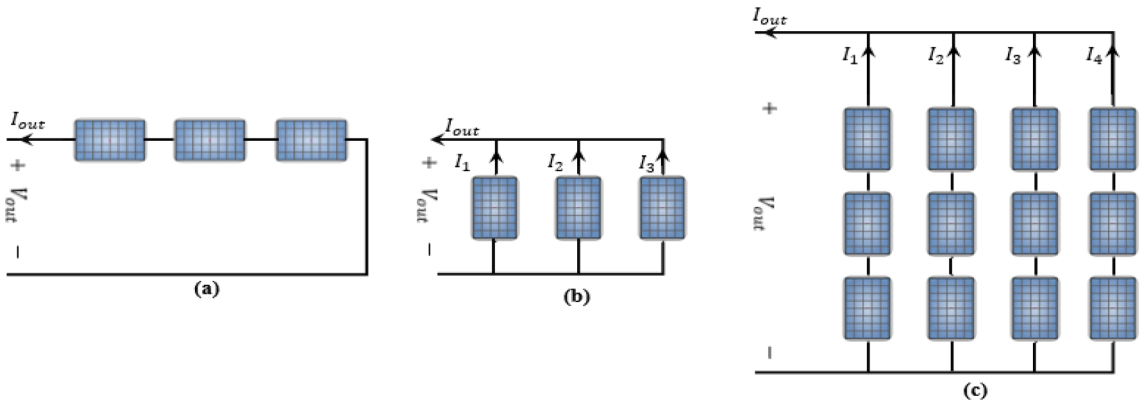

Fig. 18. Electrical interconnections (a) series (b) parallel (c) series–parallel.

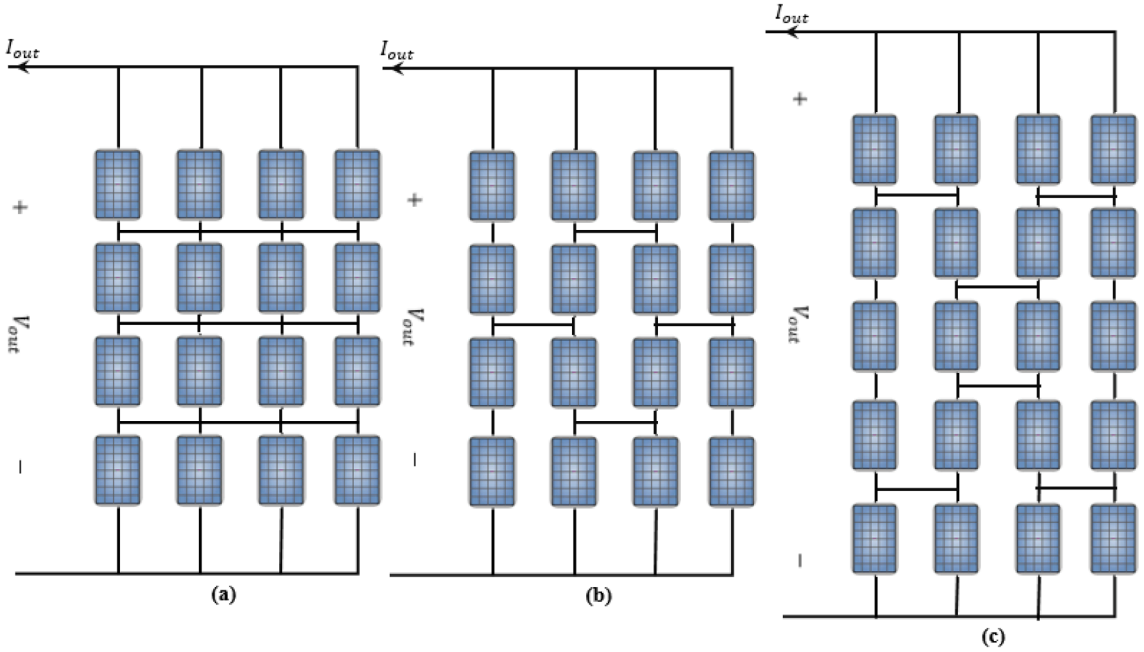

Fig. 19. Expanded electrical interconnections (a) Total-Cross-Tied (b) Honey Comb (c) Bridge Linked.

interconnections between the modules, without any dynamical switching in/off any part of the PV array.

Improved electrical interconnections

As a way to overcome the disabilities of conventional electrical interconnections, such as SP, TCT, BL, and HC, their modified rearrangements, such as Rearranged TCT (RTCT), Rearranged SP mixed with TCT (RSP-TCT), Rearranged BL mixed with TCT (RBL-TCT) and Rearranged BL mixed with HC (RBL-HC) yield in minor power losses. These configurations are presented in Fig. 20 [118].

Algorithm based with/without embedded systems

Mixed Integer Quadratic Programming (MIQP). Centered on branch and bound algorithm, the Mixed Integer Quadratic Programming (MIQP) improves a PV system's operational behavior under PSCs, by minimizing the Irradiance Mismatch Index (IMI). In other words, this dynamical reconfiguration of PV modules, reduces the sum of the differences' squares between normalized rows' irradiances. Such a process can take place after the formalization of the existence variable y_{iq} which is used in minimizing the objective function. This algorithm yields in defining a relocation process for shaded modules in both a Half Reconfigurable PV Array (HRPVA) and a Full Reconfigurable PV Array (FRPVA). The modules' repositioning process, in turns, is executed by means of 'm' number of switches, categorized as double-poled, multi-throws [151].

Population-Based algorithms (PBA). The set of Population Based Algorithms (PBA) includes the Flow Regime Algorithm (FRA), the Social Mimic Optimization Algorithm (SMOA) and Rao Optimization Algorithm (ROA) [152]. First and foremost, the FRA process relies on laminar and turbulent profiles of flowing fluids, where the exploitation and exploration phases are described by laminar and turbulent flows respectively. A Search Type Factor (STF) is used to achieve a balance between these two phases, as indicated in Eq. (21) [152].

$$STF_i = 3.2 \times 10^6 \times \frac{T_{max}}{n_t} \times \frac{||g^*_{n_t} - Z_i||}{||Z_j - Z_k||} \tag{21}$$

with $g^*_{n_t}$ denoting the global best solution, n_t the present iteration number, T_{max} the maximum number of iterations and Z_i, Z_j and Z_k the particles with the numbers i, j and k respectively. The STF comparison with the scalar 3.2×10^6 orientates the succeeding stage movement towards diversification or intensification.

Secondly, the SMOA bases on human expressions and body signals,

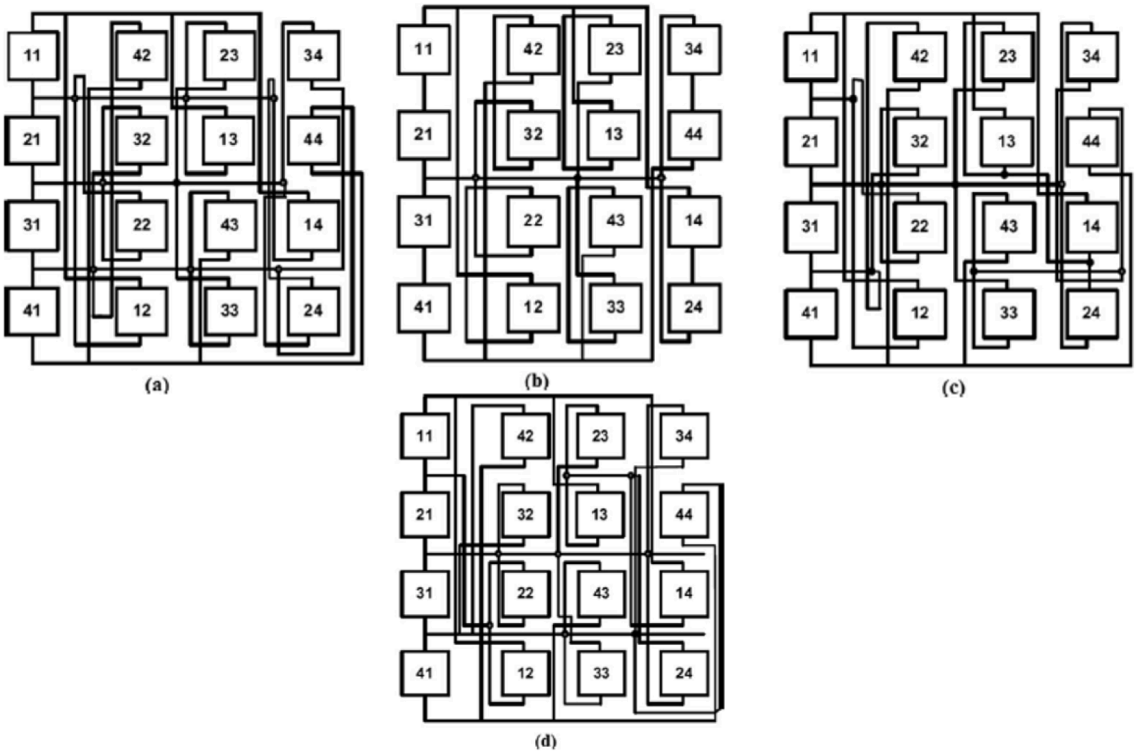

Fig. 20. Rearranged basic electrical interconnections (a) RTCT (b) RSP-TCT (c) RBL-TCT (d) RBL-HC [118].

in which the solution vector is updated according to the difference function between the individual and last iteration optimum solutions, as can be seen in Eq. (22) [152].

$$f_{Diff_{nt+1}} = \frac{\left(g^*_{n_t} - objectivefunction(Z_{i_{nt}})\right)}{objectivefunction(Z_{i_{nt}})} \tag{22}$$

where $g^*_{n_t}$ represents the global best solution, $Z_{i_{nt}}$ the solution vector of the i^{th} particle at iteration n_t and *objectivefunction* denoting the implemented fitness function.

Finally, the ROA, inspired from a new trend in population-size based optimization algorithm, depends on best/worst solutions resultant during the optimization process, in addition to random functions for solutions interconnections as explored in Eq. (23) [152].

$$Z_{i_{nt+1}} = Z_{i_{nt}} + rand_1\left(g^*_{nt} - |l^*_{nt}|\right) + rand_2\left(|Z_{i_{nt}}| - Z_{j_{nt}}\right) \tag{23}$$

with $Z_{i_{nt}}$ and $Z_{j_{nt}}$ representing the solutions of i^{th} and j^{th} candidates solutions respectively, $rand_1$ and $rand_2$ indicating randomly selected numbers from the interval [0;1] and g^*_{nt}, l^*_{nt} corresponding to best and worst solutions respectively at n_t iteration.

These three algorithms under the population based set, succeed over other PVR methods such as TCT and CS. The FRA algorithm has achieved the most superior performance and highest power enhancement among all, with 13% higher power generation than TCT [152].

Grasshopper Optimization algorithm (GOA). The Grasshopper Optimization Algorithm (GOA), with its simplicity and fewer requirements of controlling parameters, is able to reconfigure PV arrays according to the following six steps [153]:

1. Initialization of the controlling parameters of the algorithm with the correspondent PV array size
2. Construction of swarm matrix, where its number of rows/columns represent the number of search agents, and the dimension of the problem respectively
3. Application of the swarm matrix onto the PV array
4. Fitness function calculation, which represents the summed powers extracted from each given row as stated in Eq. (24)

$$\max(J) = \sum_{k=1}^{i}(V_k \times I_k) + (w_e/E_e) + (w_f \times P_a) \tag{24}$$

with i representing the rows' number, V_k, I_k the voltage and current at k^{th} row of the array respectively, P_a the panel's output voltage without bypass diodes, E_e the error of currents summation and w_e, w_f the weighting factors of E_e and P_a accordingly.

5. Removal of non-achieving constraint agents from the swarm
6. Finishing the algorithm if the difference error between the final fitness function and the precedent one is acceptable

The proposed GOA has enhanced the PV power output from 3.361% to 6.748% as compared to other PVR techniques such as TCT, SuDoKu and Genetic Algorithm (GA) [153].

Butterfly Optimization algorithm (BOA). Inspired by the food searching and mating processes followed by butterflies, the Butterfly Optimization Algorithm (BOA) exhibits a three staged mechanism, that would be later on employed for an optimal PVR solution, as follows [154]:

Initialization: in which the initial objective function is calculated, after a random formulation of butterflies' positions.
Iteration: here the fitness function f is calculated, after updating the butterflies' positions, as shown in Eq. (25).

$$f = cI^a \tag{25}$$

with c as the sensory fragrance, I as the stimulus' intensity and a a power

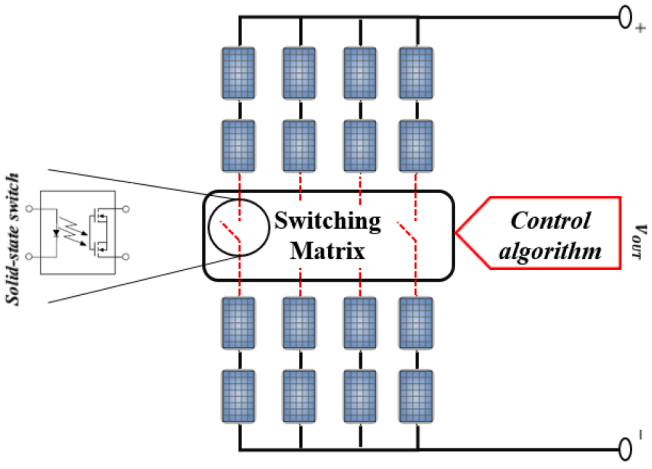

Fig. 21. PV switching matrix used in EAR.

exponent. Afterwards, during the first (global) search phase, the butterfly's position is updated towards the best global solution as shown in Eq. (26).

$$x_i^{t+1} = x_i^t + f_i(r^2 g^* - x_i^t) \tag{26}$$

with x_i^t representing the i^{th} butterfly at iteration t, f_i the fragrance of the i^{th} butterfly, r a random number within the interval [0;1] and g^* the current best global solution. On the other hand, the remaining local search can be expressed as in Eq. (27).

$$x_i^{t+1} = x_i^t + f_i(r^2 x_j^t - x_k^t) \tag{27}$$

with x_j^t and x_k^t denoting the j^{th} and k^{th} butterflies from the search space respectively.

Final stages: The stopping conditions are met, and the optimal solution is obtained.

The proposed BOA enhances the PV power productivity by 27.43% when compared to an SP-TCT arrangement. This algorithm, however, may suffer from delayed operations when implemented in hardware [154].

Munkres' Assignment algorithm (MAA). The usage of Munkres' Assignment Algorithm (MAA) allows a PVR with a minimum number of switching modules, thus increasing the lifetime of the Switching Matrix (SM) of a dynamic reconfiguration system [155].

The MAA sequential flowchart can be investigated according to the following steps:

Calculation of row irradiances' sum.(avg)
In the new matrix B, rows contain elements whose irradiances' sum is equal (or close) to.avg
Use MAA to find the minimum number of switching modules.
The matrix B is suitably re-arranged.

The MAA produces an optimum dynamic PVR, with delayed switches ageing processes [155].

Electrical array reconfiguration (EAR). By utilizing the irradiation data from Data Acquisition System (DAS), the Electrical Array Reconfiguration (EAR) allows a suitable modules repositioning based on irradiation levels and row currents [156]. The switching matrix shown in Fig. 21, is configured by means of computerized control systems (FPGA, DSP, etc.) where it would generate the switching states between PV modules [157].

With repetitive on/off switching mechanisms, governed by the present shading conditions, the connections between the PV modules are dynamically changed. This would offer a continuous monitoring of the shading patterns, thus enhancing a case-specified power production under different PSCs.

This method requires a fully reconfigurable array, with intensive need of sensors and switches, the fact that would decreases the PV system's cost efficiency [158].

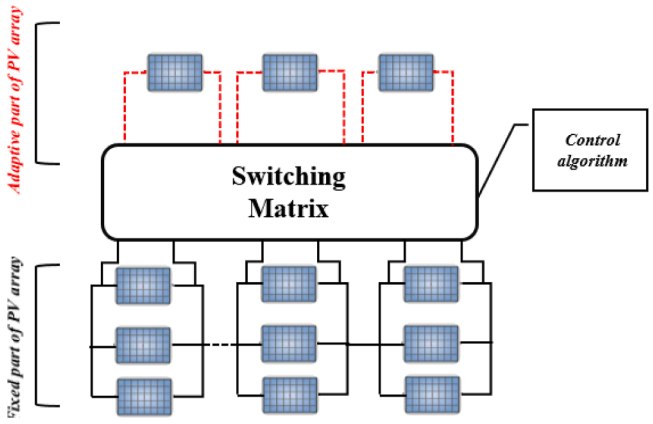

Fig. 22. Adaptive array reconfiguration method circuitry.

Adaptive array reconfiguration (AAR). With a similar approach to mitigate the effects of PSCs over PV arrays as seen in EAR, the Adaptive Array Reconfiguration (AAR) categorizes the panels into either fixed or adaptive. Consequently, the switching matrix, shown in Fig. 22, is installed between fixed and adaptive parts, thus reducing rows' irradiance differences with a controller [159].

The AAR overcomes the drawbacks of EAR, by requiring less number of switching devices and sensors.

Modified Harris hawks Optimizer (MHHO). To avoid premature converging to local solutions in Harris Hawks Optimizer (HHO) [160], the Modified Harris Hawks Optimizer (MHHO), presented in reference [161] improves the exploration strategies, while reducing the escaping distribution over the number of iterations. The MHHO functions under two modified stages.

In the first stage, the global search is boosted during the modified exploration phase: the misleading zigzag motion of the prey is eliminated, by hawk's detection via Lé'vy flight (a probability distribution), as indicated in Eq. (28).

$$U(t+1)_i = U_m(t) + Le\vec{}vy(D)\left(U_{prey}(t) - U(t_i)\right), P < 0.5 \tag{28}$$

with U_m denoting the mean position, U_{prey} the position of the prey, $U(t_i)$ the location vector in current iteration t_i and P a switching factor.

In the second step, the hawk's position is upgraded with reference to the average distance between three other random hawks, as shown in Eq. (29).

$$U(t+1)_i = \frac{\left(\left|U(t_i) - U_{rand_j}(t)\right| + \left|U(t_i) - U_{rand_k}(t)\right| + \left|U(t_i| - U_{rand_l}(t)\right)\right)}{3} + U(t_i), P \geq 0.5 \quad (29)$$

with $U_{rand_j}(t), U_{rand_k}(t), U_{rand_l}(t)$ representing the randomly selected positions j, k, l for hawks from the population at iteration t.

The final stage of MHHO corresponds to evaluating the modified prey's energy equation, induced from the prey's fear of the predator, where it is noticed that a randomly shrinking exponential function is the most accurate in defining the rabbit energy, as expressed in Eq. (30).

$$E = 2E_0\left(2 \times rand \times exp^{-\left(\frac{g \times t}{2 \times T}\right)}\right) \quad (30)$$

with E representing the escape energy of the rabbit and E_0 a random variable inside the interval $[-1;1]$.

Under short/long-wide/narrows shading patterns, the MHHO showed a superior performance in determining the optimum interconnection for PV modules, when compared to other PVR methods such as HHO, TCT and CS [161].

Insulated Gate Bipolar Transistor model (IGBT model). A reconfiguration algorithm condemns the status of solid-state switches (Insulated Gate Bipolar Transistor (IGBT)), with a smart switching technique [162]. Each string within the PV array is set to be regrouped into two parallel strings: half of series-connected panels correspond to the modules in each string. Such process transforms the PV array dimensions into $(N_{S\_A}/2 \times 2N_{P\_A})$ where N_{S_A} and N_{P_A} represent the number of series panels in a string and the number of parallel strings respectively. Hence, conductors and converters' sizes can be reduced.

The MPPT algorithm, exposed in Fig. 23, tracks the GMPP simultaneously while calculating the optimum PV array reconfiguration. As a result, the reverse currents across shaded cells are reduced, where the entire model reflects a high reliability index. Still, this algorithm did not succeed in reducing reverse currents under all studied shading patterns [162].

Artificial intelligence

Rough Set Theory (RST). This artificial intelligence based technique, the Rough Set Theory (RST), has the ability to represent the conceptual similarities between the data of a given set, by grouping the corresponding similar values, and managing the relation between data, based on their intrinsic meaning [163].

Upon each submitted situation, the RST possesses a strong ability in decision making, according to the following logical flow chart, described in three steps:

Equivalence relation: The division of a given set of data into smaller subsets (equivalence classes), takes place as described in Eq. (31).

$$[u_i]R \bigcap_{\substack{i=1 \\ j \neq i}}^{n} [u_j]R = \varnothing \quad (31)$$

with $[u_i]R, [u_j]R$ representing the equivalence classes for indexes i and j and R a relation rule defining the relation between all elements of a given equivalence class. The intersection of all equivalent classes belonging to R is adapted as an equivalence relation.

Reduction of knowledge: This step ensures that the knowledge about a universe of objects is neither too insufficient nor too excessive.

3. Knowledge representation: by means of an Information System (IS), consisted of a tabulated data, the information is manipulated, to form a decision table as expressed in Eq. (32).

$$T = (U, A, C, D) where C \subseteq A and D \subseteq A \quad (32)$$

with U, A, representing universe and attributes sets respectively, and C, D representing conditions and decisions attributes respectively.

With simple logic circuits, an Automatic Reconfiguration System (ARS) is obtained after RST, through computer simulation, where the energy produced by shaded PV modules is better utilized [163]. However, this method is complex and requires heavy measurements.

Rule Based Fuzzy Approach (RBFA)

In order to reconfigure modules within a PV array, a Rule Based Fuzzy Approach (RBFA) is formulated by utilizing shading degree and irradiance derivative as control variables for designing fuzzy rules [164]. The approach starts by checking for partial shading by noticing the difference in the output voltage of each row.

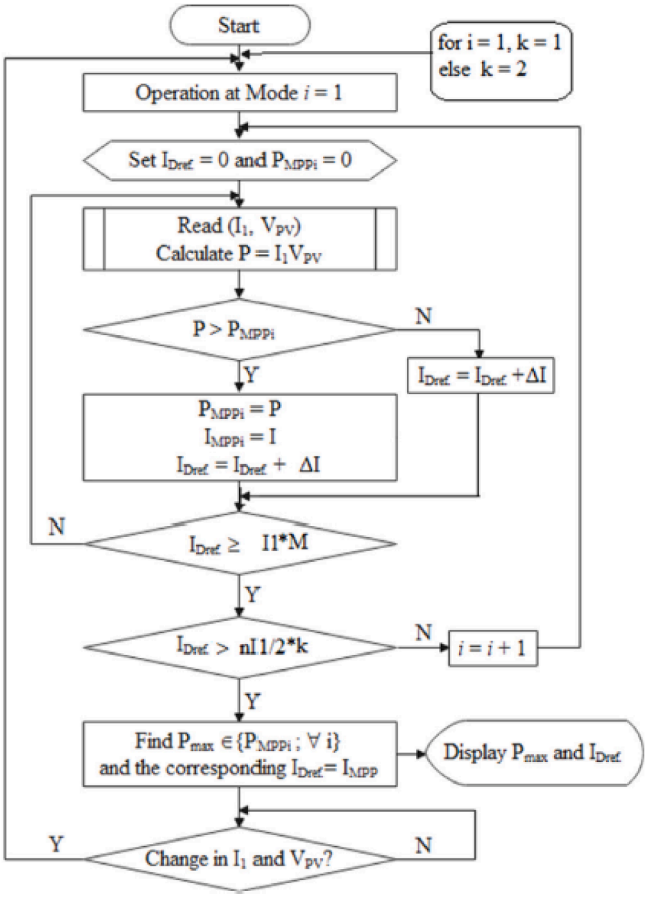

Fig. 23. Proposed MPPT and switching algorithm [162].

After the occurrence of a PSC, the shading degree is calculated according to Eq. (33).

$$\Delta G_{F_i} = G_{F_0} - G_{F_i} \tag{33}$$

with G_{F_0} and G_{F_i} denoting the irradiance on the non-shaded and other submodule respectively.

The obtained shading degree of each submodule and the derivative of irradiance are the input to the fuzzy controller, where after the fuzzification process, the output control is obtained. The PV array is finally rearranged after the fuzzy controller closes some switches of the matrix [164]. This method can be judged as non-reliable, since threshold based switching by a fuzzy controller does not accurately generate the switching matrix at dynamic irradiation conditions.

Hybrid

Series-parallel with binary coding (SPBC)

A binary coding has shown the potential of detecting PSCs. The

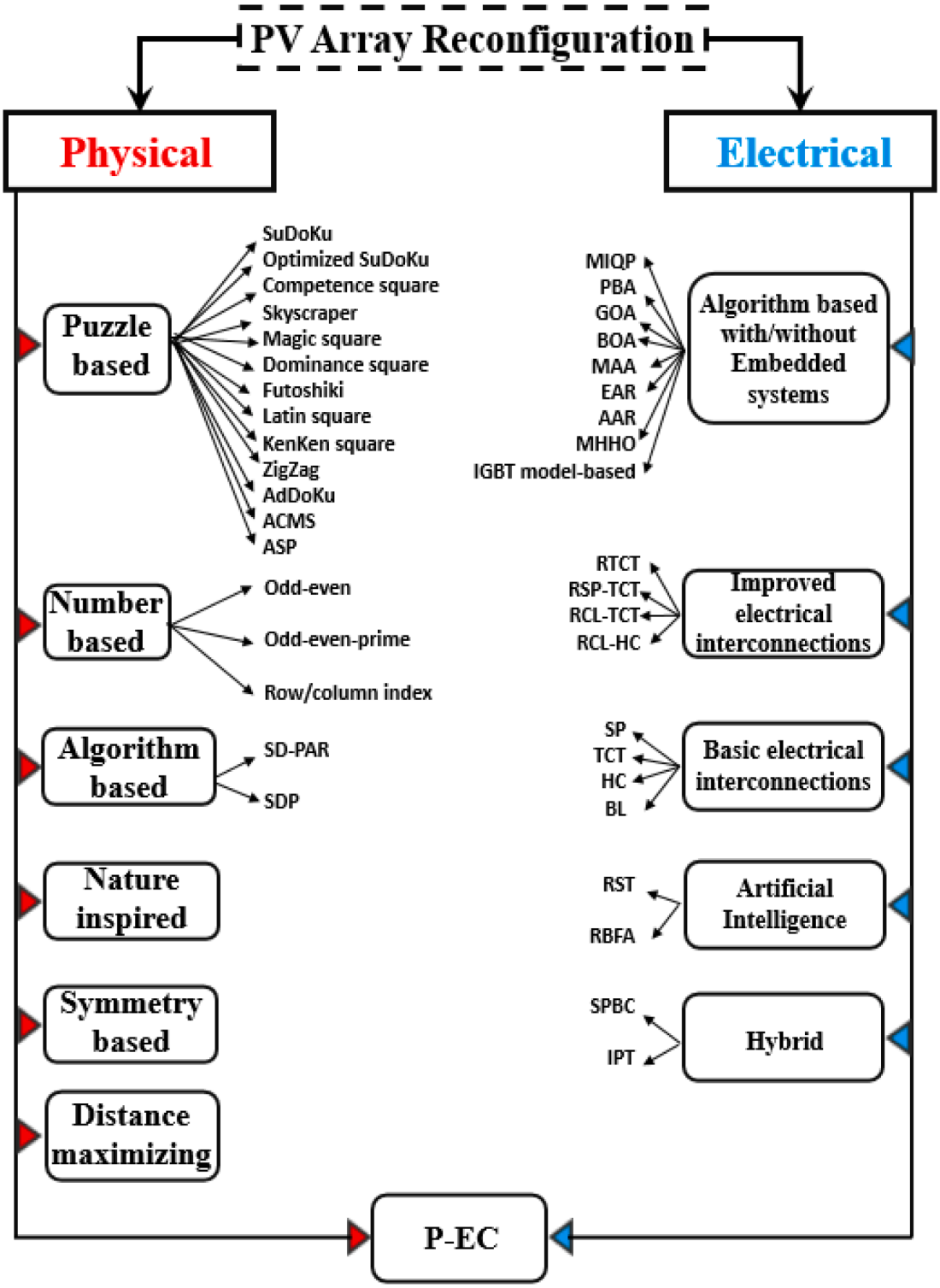

Fig. 24. Summary of all physical/electrical based PV array rearrangement methods.

combination of binary coding with conventional electrical reconfiguration methods (series, parallel, etc.), results in a PVR with superior efficiency as compared to standalone basic electrical interconnections [165]. A 3 × 3 PV array has its modules connected with a 9-bit binary up-counter, which produces a five hundreds twelve different states reflecting the shading scenarios from full shadow to full sun.

The choice of the best PVR is done after analyzing each reconfiguration according to its Power Generation Index (PGI) shown in Eq. (34).

$$PGI = \sum_{k=0}^{k=2^n-1} \left(\frac{1}{n}\right)\left(\frac{1}{2^n}P_k\right) \tag{34}$$

with n denoting the number of modules in the array, and P_k the maximum output power for each code of shadow (binary representation from 000000000 to 111111111).

The Series-Parallel Binary Coding (SPBC) can detect abnormalities in the produced currents, after adaptation of different reconfiguration patterns and definition of an average overcurrent value, for all codes of shadows. This would lead to an optimum choice for PVR pattern [165].

Image processing technique (IPT)

The AAR technique is hybridized with Image Processing Techniques (IPT) [166,167] which include a camera-centered system [168,169] that continuously monitors the shadow patterns on PV arrays [170]. The resulting image is afterwards submitted to an image processing unit. By means of a moving shadow detection algorithm, the control decision unit selects optimum panel layout according to image findings.

The process from image capture to algorithm output, passes through an image conversion to HSV (Hue Saturation Value) color space. The HSV in turn is filtered, undergoing through morphological process from erosion, dilation to blur. The shading rate is hence calculated according to the findings of black pixels. After comparison between the total frame and threshold times, the correspondent information is sent to the control unit, to finally dictate the on/off switching processes of the switching matrix. The application of IPT on a PV array, increases the MPP by up to 15% [170] but adds extra financial burden on the PV system's total cost.

Physical-electrical combined (P-EC). The P-EC (Physical-Electrical Combined) PVR strategy utilizes an enhanced configuration of the MS method, incorporated with an IE (Irradiance Equalization) strategy, applied for TCT arrays [171]. The dynamics of electrical interconnections are conducted via BCC-DPP (Bidirectional Cuk Converter-Differential Power Processing) unit, which in turn is controlled by MS-EC (Magic Square-Enhanced Configuration) algorithm.

Applied on a 6 × 6 TCT array, P-EC enhances the configuration of the conventional MS puzzle, by mixing 36 modules into 4 sub-TCT groups, each consisting of 9 modules, arranged into 3 ×3 TCT arrays. The IE algorithm in turn reduces the number of LMPP, thus directly targeting at GMPP. This is achievable by re-building the I-V characteristics for each PV module, where when added together, and overall I-V characteristics is obtained and stored within the best found maximum power, after several iterations [171].

The final destination of the proposed P-EC method takes place at the level of BCC-DPP unit, which is controlled by the developed IE algorithm. As output, P-EC offers a cross-connection function between PV chains, and the DC bus, resulting in power enhancements. The P-EC method is found flexible versus any shading pattern, however seemed extremely complex to construct [171].

After the expansion of each electrical-based PVR, it is clear that not all techniques involve a dynamical array rearranging. For instance, all basic and improved electrical interconnections are statically made, between electric terminals, rather in the geographical positioning of the entire module within the array. Dynamic reconfiguration methods are ones that involve a switching mechanism (switching matrix, etc.) to continuously reconnect/disconnect external PV modules to the array. To locate different found PVR methods, under physical, electrical, and combined categorizations, Fig. 24 points out all sub-methods corresponding to each set.

Discussion

The varieties of PVR methods, with different approaches, make it a hard choice for designers to adapt a standalone method, considered as the most optimum. In fact, the majority of the reviewed methods consider a cross connection between electrical and physical classifications: for example in reference [120], the SuDoKu based reconfiguration is applied for a TCT array. From another part, even within same PVR classification, the MIQP [151] and MAA [155] for example, are applied for TCT connected PV arrays.

The performance evaluation hence must be based upon a formulated scalar model, which underlies all techniques under the same mathematical aspects. The obtained results from different formulas give the chance to compare different rearranging methods, based on numbered evaluation criteria. Performance indices can be enumerated as Fill Factor (FF), Percentage Power Loss ($\%P_{Loss}$), Mismatch Power Loss (P_{ML}), Performance Ratio (PR), Execution Ratio (ER), Capacity Factor (CF), Efficiency (η), Percentage of Power Enhancement ($\%PE$) and outputted DC Power (P) [172,173].

The performance evaluation indices should also include a complexity index, to check how difficult the method is when implemented, and how many LMPPs exist in the characteristic P-V (Power-Voltage) curve after the implementation. Below are the mathematical expressions for different performance evaluation indices [172,173].

Fill factor: The ratio of the actual maximum power to the product of voltage and current in open-circuit, short-circuit respectively, represents the FF:

$$FF = \frac{V_{MP} \times I_{MP}}{V_{OC} \times I_{SC}} \tag{35}$$

such that V_{MP}, I_{MP} represent the maximum peak voltage and current respectively, and V_{OC}, I_{SC} the open-circuit voltage and short-circuit current respectively.

Mismatch power loss: The difference between power at unshaded condition and power at PSCs represents the $P_{MismatchLoss}$ as expanded in Eq. (36).

$$P_{ML} = P_{MAX_{unshaded}} - P_{GMPP_{PSC}} \tag{36}$$

with $P_{MAX_{unshaded}}$ and $P_{GMPP_{PSC}}$ representing the maximum power while no occurrence of any shading pattern and maximum power at PSCs respectively.

iii. Percentage power loss: the ratio of the global maximum peak at STC (Standard Test Conditions) subtracted from the global maximum peak at PSCs over the first denotes $\%P_{Loss}$ as indicated in Eq. (37).

$$\%P_{Loss} = \frac{GMPP_{STC} - GMPP_{PSC}}{GMPP_{STC}} \tag{37}$$

where $GMPP_{STC}$ and $GMPP_{PSC}$ represent global maximum peak at STC and global maximum peak at PSCs respectively.

iv. Performance ratio: a quality factor representing the amount of consumable solar energy as the ratio of the total energy generated by the array to the absolute power corresponds to PR as indicated in Eq. (38).

$$PR = \frac{EA}{P_{DC}} \tag{38}$$

with EA denoting the total energy generated by the array and P_{DC} the absolute power.

Execution ratio: The ratio of the maximum power generated at PSCs over the maximum power achieved at STC, represent the *ER* as expanded in Eq. (39).

$$ER = \frac{P_{PSC}}{P_{STC}} \tag{39}$$

where P_{PSC} and P_{STC} represent maximum power generated at PSCs and the maximum power achieved at STC respectively.

Capacity factor: It is the ratio of the actual energy produced E_{act} over the rated output power PV_{rated}, as indicated in Eq. (40).

$$CF = \frac{E_{act}}{PV_{rated}} \tag{40}$$

Efficiency: Corresponds to the ratio of global maximum peak power P_{GMPP} over input power P_{in} as indicated in Eq. (41).

$$\eta = \frac{P_{GMPP}}{P_{in}} \tag{41}$$

viii. Percentage of power enhancement: the ratio of the total power difference between conventional global power peak $GMPP_{conv}$ and case-specified global power peak $GMPP_{CS}$ over the power at conventional power peak is termed as $\%PE$, expanded in Eq. (42).

$$\%PE = \frac{GMPP_{conv} - GMPP_{CS}}{GMPP_{conv}} \tag{42}$$

ix. Outputted DC power: the output power P_{OUT} obtained at the PV array's terminals is shown in Eq. (43), with$k$ denoting a scalar smaller than one and V_M and I_M the maximum output voltage and current respectively.

$$P_{OUT} = k \times V_M \times I_M \tag{43}$$

In addition to Eqs. (35)–(43), the assessment of different PVR methods must take into consideration, their supportable shading patterns. From Table 1, the shading patterns are labeled as Random (R), Uneven Row shading (UR), Uneven Column shading (UC), Diagonal shading (D), Short and Narrow shading (SN), Short and Wide shading (SW), Long and Narrow shading (LN) and Long and Wide shading (LW).

Concerning all of these properties, Tables 6–9 present tabulated data for evaluating the performances of each of the PVR methods: the higher values of FF, PR, ER, η, %PE and P_{OUT} indicate a superior performance of the mentioned technique, as compared to others having lower values of the mentioned indexes. The ability of adapting different shading patterns within a method is a bonus. On the other hand, the high values of P_{ML} and $\%P_{Loss}$ reflect a foible for the method in use [176]. The most recent PVR techniques are encapsulated in Table 10 and are mutually compared to relevant older techniques. It is found that newer PVR methods are mainly centered over puzzle-based static category, where only a single research [171] hybridizes between electrical (initial circuit interconnections, with a dynamic computer-controlled re-arrangements) and physical schemes.

From another part the percentage of power enhancement in RST method is up to 84% [163] and 10% in IPT [170], where both RBFA [164] and SPBC [165] methods were seen easy to implement. Not all the methods presented in Tables 6–10, adapt the same shading patterns case studies, and concern the same PV array size: to standardize the comparison, the averaged values for each performance index were taken into consideration. Results shown in Table 10 clearly imply the need to concentrate on combined PVR strategies in future PVR research.

Conclusions and future work

The inescapable PSCs' traits accelerate the PV systems' aging process, while reducing their consumable output power, thus continuously decelerating the overall PV power generation's efficiency. As a solution, PVR methods show a good reliability when applied on PV systems, in terms of increasing their energy efficiency: by dispersing the shading pattern over the entire PV array, hence eliminating as much as possible

Table 6
Comparative assessment of physical puzzle based PVR methods.

Physical:	PVR	Shading	Electrical properties								Complexity	Number	Refs.
Puzzle based	**methods**	**patterns**	FF	P_{ML}	$\%P_{Loss}$	PR	ER	η	%PE	P_{OUT}		**of LMPP**	
	SDK	SW, LW, SN, LN	≤62.8	≈11%	–	–	–	≤20%	Up to 26.1%	Up to 63 $V_M I_M$	High	2	[115119]
	O-SDK	SW, LW, SN, LN	–	≈3%	–	–	–	≤20.6%	26.88%	–	High	–	[122]
	CS	SW, LW, SN, LN	≤53	≥3.08%	≥30%	–	–	–	Up to 24.4%	Up to 65.7 $V_M I_M$	High	1	[123]
	SS	LW, SN, SW	≤70.7	≈3.4%	≥30.5%	–	–	–	Up to 43.7%	Up to 64.8 $V_M I_M$	Medium	3	[124]
	MS	LW	90.9	–	≥14%	–	–	–	25.40%	Up to 48.6 $V_M I_M$	High	1	[125126]
	DS	All	≤65.4	≥2.5%	≥34.5%	–	–	≤90%	–	Up to 19 $V_M I_M$	High	3	[128]
	SS	SW, LW, SN, LN	–	–	–	–	–	≤88.5%	Up to 24.24%	Up to 21.6 $V_M I_M$	High	1	[129]
	FS	SW, LW, SN, LN	≤22.94	–	≥16.1%	–	Up to 84.50%	–	–	Up to 31.2 $V_M I_M$	High	2	[131]
	LS	SW, LW, SN, LN	≤64.7	–	–	–	–	≤10.9%	–	Up to 13.6 $V_M I_M$	High	1	[132]
	ZZ	LN, SN, LW, UR	≤70.5	≥0.44%	≥15%	≤0.92%	–	–	Up to 22%	Up to 10 $V_M I_M$	High	2	[142]

Table 7
Comparative assessment of Physical PVR: number based, algorithm based, nature inspired, symmetry based and distance maximizing based methods.

	PVR methods	Shading patterns	Electrical properties								Complexity	Number of LMPP	Refs.
			FF	P_{ML}	$\%P_{Loss}$	PR	ER	CF	η	%PE	P_{OUT}			
Physical: ***Number based***	O-E	SW, LW, SN, LN	–	≥1.03%	–	–	–	–		Up to 30.88%	Up to 13.2 $V_M I_M$	Medium	2	[136]
	O-E-P	SN	≤63.18	≥14.5%	–	–	–	–	≤11.3%	–	Up to 64.81 $V_M I_M$	Low	2	[137]
	RCI	SW, LW, SN, LN	≤81	≥24.1%	≥19%	–	–	–	–	–	Up to 63.9 $V_M I_M$	High	3	[138]
Physical: ***Algorithm based***	SD-PAR	All	–	–	–	–	–	–	≈ 99.4%	Up to 70%	–	Low	2	[145]
	SDP	SW, LW, SN, LN	–	–	–	–	–	–	≈ 98%	Up to 23.65%	Up to 6.6 $V_M I_M$	Medium	3	[145]
Physical: ***Nature inspired***		SW, LW, SN, LN	≤52.63	≥3%	≥31%	100%	≤91%	≤0.69	–	–	Up to 63 $V_M I_M$	Low	2	[139]
Physical: ***Symmetry based***		All	≤22	–	≥12.2%	–	–	–	–	–	Up to 16.75 $V_M I_M$	Medium	2	[140]
Physical: ***Distance maximizing***		SW, LW, SN, LN	–	–	–	–	–	–	≤90%	–	–	Low	1	[143]

Table 8
Comparative assessment of Electrical PVR: algorithm based methods.

Electrical:	**PVR**	**Shading**	**Electrical properties**							**Complexity**	**Number of**	**Refs.**
Algorithm based	**methods**	**patterns**	FF	P_{ML}	$\%P_{Loss}$	PR	η	%PE	P_{OUT}		**LMPP**	
	MIQP	SN, LN, UR	–	–	–	Up to 1	–	Up to 41.6%	–	Medium	3	[151]
	PBA	LW, SN, LN	≤78.6	≥21.2%	≥18.6%	–	≈ 81.37%	Up to 28%	Up to 63.91 $V_M I_M$	High	2	[152]
	GOA	SN, SW, LN, LW	–	–	–	–	–	3.36%	Up to 65.71 $V_M I_M$	Medium	1	[153]
	BOA	UC, R, LW, LW	≤16.38	–	≥69.9%		–		Up to 20 $V_M I_M$	High	4	[154]
	MAA	All	–	–	–	–	–	–	–	High	1	[155]
	EAR	All	–	–	–	–	Up to 43%	Up to 31%	–	High	2	[156]
	AAR	All	–	–	≥0.06%	0.8675	–	–	–	Medium	4	[159]
	MHHO	SN, SW, LN, LW	≤75.9	≥18.7%	≥15.7%	–	Up to 78.37%	Up to 33.2%	Up to 82.2 $V_M I_M$	High	2	[161]

Table 9
Comparative assessment of Electrical PVR: improved and basic electrical interconnections based methods.

	PVR methods	Shading patterns	Electrical properties					Complexity	Number of LMPP	Refs.
			FF	P_{ML}	$\%P_{Loss}$	η	%PE			
Electrical:	RTCT	All	≤75.2	≥7%	≥6.54%	Up to 13.9%	–	High	2	[174]
Improved	RSP-TCT	All	≤70.44	≥11.7%	≥4.04%	–	Up to 6.59%	High	3	[175]
electrical	RBL-TCT	All	≤70.77	≥11.2%	≥3.07%	–	Up to 7.55%	High	3	[175]
interconnections	RBL-HC	All	≤70.87	≥10.9%	≥2.49%	–	Up to 10.02%	High	2	[175]
Electrical:	SP	All	≤68.30	≥14.3%	≥12.9%	–	–	Low	3	[175]
Basic	TCT	All	≤71.48	≥10.6%	≥2.42%	–	Up to 19.58%	High	1	[175]
electrical	HC	All	≤70.19	≥11.9%	≥3.73%	–	Up to 18.08%	High	2	[175]
interconnections	BL	All	≤68.76	≥12.7%	≥5.33%	–	Up to 8.04%	High	2	[175]

Table 10
Recent PVR methods.

Recent PVR method	Classification			Results	Refs.
	Physical	Electrical	Combined		
AdDoKu	✓ (puzzle-based)			• Better output power when compared to TCT by up to 30.15% • Power improvement by 1.94% when compared to SuDoKu • Lower line losses when compared to both SuDoKu (12.2%-36.8%) and TCT (19.5%-51.5%) • FF is the same as in SuDoKu	[133]
ACMS	✓ (puzzle-based)			• $\%P_{Loss}$ is decreased by 1.93% when compared to SuDoKu • FF has improved by 0.51% when compared to SuDoKu • 1.93 increment in PR when compared to SuDoKu • 7.15% power gain as compared to TCT	[134]
ASP	✓ (puzzle-based)			• Provides a maximum reduction of 37.98% in needed wires as compared to SS • FF is up to 71.5% • Up to 33.78% reduction in P_{ML} as compared to TCT	[135]

P-CI	✓ (symmetry-based)			• Recorded experimental power gain was up to 42.91%
				• Almost same efficiency as SuDoKu, FS, O-SDK, SS, and MS
				• P_{OUT} is up to $71.1V_MI_M$
				  • FF is up to 69.3%
				  • Largest $\%P_{Loss}$ is 29.1% smaller than one in O-E
					[141]

IGBT model-based		✓ (algorithm-based)		• Highest $\%P_{Loss}$ was beneath 2.48% • Switching losses of IGBTs were at maximum of 2.34% as compared to ideal switch circuits	[162]
P-EC			✓	• Average power gain is up to 48% • Efficiency is up to 98.95%	[171]

any rows' currents differences. When compared to other PSCs mitigation techniques (i.e., MPPT, micro-inverters, etc.) PVR methods require less complexity/space for installation while still relatively ensuring a homogeneous power production across the PV array. This in turn reduces the hotspots creation probability and its consequences (i.e., burnouts, fire hazards, etc.).

Through this paper, PVR methods were characterized as either physical, electrical, or physical-electrical combined. Physical PVR techniques are based on PV modules' positioning adjustments within the array. This major set contains puzzle-based techniques (difficult to construct), number-based and symmetry-based methods (require complex circuit designs). Additionally, distance maximizing based techniques require extra spaces to be implemented, where Lo Shu based method imposes hard computational skills. Among various physical PVRs, the SD-PAR algorithm is resilient in front of all possible shading patterns, with an almost 100% efficiency and 70% power enhancement (Table 7).

On the other hand, electrical PVR techniques reshape the electrical interconnections between circuits' nodes, rather than dislocating the entire PV module from its place. As revealed from Table 9, the TCT circuit architecture is the most suitable configuration for PV arrays as it requires less wire demand when compared to HC and BL, RSP and other connections' arrangements. Minor power improvements were noticed upon the application of hybrid based electrical PVR, where artificial intelligence methods require difficult programming specialties. Among algorithm-based electrical PVR strategies, the MHHO algorithm produced the highest output DC power (82.2 V_MI_M), with a high fill factor (around 75%) and minimum power losses and power mismatch losses (around 16% and 19% respectively). The majority of the surveyed PVR methods, hybridize between electrical (with no SM) and physical sets, such as TCT-SuDoKu, TCT-KenKen, etc., where only a single method (P-EC) combines physical and electrical PVR (including switching devices) with a decision making algorithm for a dynamical PV modules' switching.

For a future PVR scope, the PV panels are first recommended to be TCT-configured, as a tradeoff between complexity and efficiency when compared to other electrical interconnections (i.e., RSP-TCT, RBL-TCT, R-TCT, etc.). Successively, the SD-PAR algorithm after different iterations, relocates (for only once) the TCT configured modules. At this level, the static reconfiguration process is done. After so, configured PV modules are to be interfered with an SM which in turn is controlled by the MHHO algorithm. Theoretically, this crossed configuration planning would have an efficiency near 100%, more than 75% power enhancement, with reduced mismatch and power losses to around 10% and 3% respectively, and a high fill factor around 80%. Such PVR scheme is encouraged to be experimentally investigated in real PV systems, in order to have discrete and quantitative results, which evaluates its effectiveness versus PSCs mitigation, and better PV power productivity.

Declaration of Competing Interest

The authors declare that they have no known competing financial interests or personal relationships that could have appeared to influence the work reported in this paper.

References

[1] A.G. Olabi, The 3rd international conference on sustainable energy and environmental protection SEEP 2009 – Guest Editor's Introduction, Energy 35 (12) (2010) 4508–4509.
[2] B.R. David, S. Spencer, J. Miller, S. Almahmoud, H. Jouhara, Comparative environmental life cycle assessment of conventional energy storage system and innovative thermal energy storage system, Int. J. Thermofluids 12 (2021), 100116.
[3] S. Abdo, H. Saidani-Scott, M.A. Abdelrahman, Numerical study with eco-exergy analysis and sustainability assessment for a stand-alone nanofluit PVT/T, Therm. Sci. Eng. Progress 24 (2021), 100931.
[4] K. Obaideen, M.N. AlMallahi, A.H. Alami, M. Ramadan, M.A. Abdelkareem, N. Shehata, A.G. Olabi, On the contribution of solar energy to sustainable developments goals: case study on Mohammed bin Rashid Al Makhtoum Solar Park, Int. J. Thermofluids 12 (2021), 100123.
[5] S. Mehranfar, A. Gharehghani, A. Azizi, A.M. Andwari, A. Pesyridis, H. Jouhara, Comparative assessment of innovative methods to improve solar chimney power plant efficiency, Sustain. Energy Technol. Assess. 49 (2022), 101807.
[6] A.H. Alami, M. Ramadan, M.A. Abdelkareem, J.J. Alghawi, N.T. Alhattawi, H. A. Mohamad, A.-G. Olabi, Novel and practical photovoltaic applications, Therm. Sci. Eng. Progress 29 (2022), 101208.
[7] N. Khordehgah, V. Guichet, S.P. Lester, H. Jouhara, Computational study and experimental validation of a solar photovoltaics and thermal technology, Renewable Energy. 143 (2019) 1348–1356.
[8] M. Venturelli, D. Brough, M. Milani, L. Montorsi, H. Jouhara, Comprehensive numerical model for the analysis of potential heat recovery solutions in a ceramic industry, Int. J. Thermofluids 10 (2021), 100080.
[9] V. Guichet, N. Khordehgah, H. Jouhara, Experimental investigation and analytical prediction of a multi-channel flat heat pipe thermal performance, Int. J. Thermofluids 5-6 (2020), 100038.
[10] H. Jouhara, A. Zabnienska-Gora, N. Khordehgah, D. Ahmad, T. Lipinski, Latent thermal energy storage technologies and applications: a review, Int. J. Thermofluids 5-6 (2020), 100039.
[11] F. Hengel, C. Heschl, F. Inschlag, P. Klanatsky, System efficiency of pvt collector-driven heat pumps, Int. J. Thermofluids 5-6 (2020), 100034.
[12] M. Rashad, N. Khordehgah, A. Zabnienska-Gora, L. Ahmad, H. Jouhara, The utilisation of useful ambient energy in residential dwellings to improve thermal comfort and reduce energy consumption, Int. J. Thermofluids 9 (2021), 100059.

[13] L. Ahmad, N. Khordergah, J. Malinauskaite, H. Jouhara, Recent advances and applications of solar photovoltaics and thermal technologies, Energy 207 (2020), 118254.
[14] K. Osmani, M. Ramadan, T. Lemenand, B. Castanier, A. Haddad, Optimization of PV array tilt angle for minimum levelized cost of energy, Comput. Electr. Eng. 96 (2021), 107474.
[15] K. Osmani, A. Haddad, T. Lemenand, B. Castanier, M. Ramadan, A review on maintenance strategies for PV systems, Sci. Total Environ. 746 (2020), 141753.
[16] O.K. Ahmed, Z.A. Mohammed, Dust effect on the performance of the hybrid PV/Thermal collector, Therm. Sci. Eng. Progress 3 (2017) 114–122.
[17] H. Wang, R. Cai, B. Zhou, S. Aziz, B. Qin, N. Voropai, L. Gan, E. Barakhtenko, Solar irradiance forecasting based on direct explainable neural network, Energy Convers. Manage. 226 (2020), 113487.
[18] A.H. Alami, M.K.H. Rabaia, E.T. Sayed, M. Ramadan, M.A. Abdelkareem, S. Alasad, A.-G. Olabi, Management of potential challenges of PV technology proliferation, Sustain. Energy Technol. Assess. 51 (2022), 101942.
[19] H.M. Ridha, Parameters extraction of single and double diodes photovoltaic models using Marine Predators Algorithm and Lambert W function, Solar Energy. 209 (2020) 674–693.
[20] H. Mohammed, M. Kumar, R. Gupta, Bypass diode effect on temperature distribution in crystalline silicon photovoltaic module under partial shading, Solar Energy. 208 (2020) 182–194.
[21] L. Papargyri, M. Theristis, B. Kubicek, T. Krametz, C. Mayr, P. Papanastasiou, G. E. Georghiou, Modelling and experimental investigations of microcracks in crystalline silicon photovoltaics: a review, Renewable Energy 145 (2020) 2387–2408.
[22] H.-D. Liu, C.-H. Lin, K.-J. Pai, C.-M. Wang, A GMPPT algorithm for preventing the LMPP problems based on trend line transformation technique, Solar Energy 198 (2020) 53–67.
[23] M.P. Bonkile, V. Ramadesigan, Physics-based models in PV-battery hybrid power systems: thermal management and degradation analysis, J. Energy Storage 31 (2020), 101458.
[24] C. Tubniyom, W. Jaideaw, R. Chatthaworn, A. Suksri, T. Wongwuttanasatian, Effect of partial shading patterns and degrees of shading on Total-Cross-Tied (TCT) photovoltaic array configuration, Energy Procedia. 153 (2018) 35–41.
[25] C.E. Clement, J.P. Singh, E. Birgersson, Y. Wang, Y.S. Khoo, Hotspot development and shading response of shingled PV modules, Solar Energy 207 (2020) 729–735.
[26] J. Zaraket, M. Aillerie, C. Salame, E. Losson, Output voltage changes in PV solar modules after electrical and thermal stresses. Experimental analysis, Energy Procedia 157 (2019) 1404–1411.
[27] S. Deng, Z. Zhang, C. Ju, J. Dong, Z. Xia, X. Yan, T. Xu, G. Xing, Research on hot spot risk for high-efficiency solar module, Energy Procedia 130 (2017) 77–86.
[28] M.L. Orozco-Gutierrez, J.M. Ramirez-Scarpetta, G. Spagnuolo, C.A. Ramos-Paja, A method for simulating large PV arrays that include reverse biased cells, Appl. Energy 123 (2014) 157–167.
[29] T. Ghanbari, Permanent partial shading detection for protection of photovoltaic panels against hot spotting, IET Renewable Power Generation 11 (1) (2016) 1–9.
[30] K. Mahmoud, M. Lehtonen, Three-level control strategy for minimizing voltage deviation and flicker in PV-rich distribution systems, Int. J. Electr. Power Energy Syst. 120 (2020), 105997.
[31] L. Ahmad, N. Khordehgah, J. Malinauskaite, H. Jouhara, Recent advances and applications of solar photovoltaics and thermal technologies, Energy 207 (2020), 118254.
[32] Z. Wang, N. Zhou, L. Gong, M. Jiang, Quantitative estimation of mismatch losses in photovoltaic arrays under partial shading conditions, Optik 203 (2020), 163950.
[33] M. Dhimish, V. Holmes, B. Mehrdadi, M. Dales, B. Chong, L. Zhang, Seven indicators variations for multiple PV array configurations under partial shading and faulty PV conditions, Renewable Energy 113 (2017) 438–460.
[34] D.P. Winston, S. Kumaravel, B.P. Kumar, S. Devakirubakaran, Performance improvement of solar PV array topologies during various partial shading conditions, Solar Energy 196 (2020) 228–242.
[35] I.H. Mahammed, A.H. Arab, S. Berrah, Y. Bakelli, M. Khennene, S.H. Oudjana, A. Fezzani, L. Zaghba, Outdoor study of partial shading effects on different PV modules technologies, Energy Procedia 141 (2017) 81–85.
[36] J.C. Teo, R.H.G. Tan, V.H. Mok, V.K. Ramachandaramurthy, C.K. Tan, Impact of bypass diode forward voltage on maximum power of a photovoltaic system under partial shading conditions, Energy 191 (2020), 116491.
[37] P. Bauwens, J. Doutreloigne, Reducing partial shading power loss with an integrated Smart Bypass, Solar Energy 103 (2014) 134–142.
[38] K. Lappalainen, S. Valkealahti, Number of maximum power points in photovoltaic arrays during partial shading events by clouds, Renewable Energy 152 (2020) 812–822.
[39] M.V. da Rocha, L.P. Sampaio, S.A.O. da Silva, Comparative analysis of MPPT algorithms based on Bat algorithm for PV systems under partial shading conditions, Sustain. Energy Technol. Assess. 40 (2020), 100761.
[40] K. Osmani, A. Haddad, T. Lemenand, B. Castanier, M. Ramadan, An investigation on maximum power extraction algorithms from PV systems with corresponding DC-DC converters, Energy 224 (2021), 120092.
[41] M. Mao, L. Cui, Q. Zhang, K. Guo, L. Zhou, H. Huang, Classification and summarization of solar photovoltaic MPPT techniques: a review based on traditional and intelligent control strategies, Energy Rep. 6 (2020) 1312–1327.
[42] O. Celik, A. Teke, A. Tan, Overview of micro-inverters as a challenging technology in photovoltaic applications, Renew. Sustain. Energy Rev. 82 (3) (2018) 3191–3206.
[43] Z.E.T. Ternifi, P. Petit, G. Bachir, M. Aillerie, New Topology of Photovoltaic Microinverter based on Boost converter, Energy Procedia 119 (2017) 938–944.
[44] R. Pachauri, R. Singh, A. Gehlot, R. Samakaria, S. Choudhury, Experimental analysis to extract maximum power from PV array reconfiguration under partial shading conditions, Eng. Sci. Technol. Int. J. 22 (1) (2019) 109–130.
[45] A. Hazra, S. Das, M. Basu, An efficient fault diagnosis method for PV systems following string current, J. Clean. Prod. 154 (2017) 220–232.
[46] H.N. Manjunath, S.R. Suresh, Reduction of mislead power and mismatch power loss under partial shading conditions using novel square matrix shade dispersion technique, Solar Energy. 207 (2020) 1364–1383.
[47] M. Matam, V.R. Barry, Improved performance of dynamic photovoltaic array under repeating shade conditions, Energy Convers. Manage. 168 (2018) 639–650.
[48] M. Horoufiany, R. Ghandehari, Optimization of the Sudoku based reconfiguration technique for PV arrays power enhancement under mutual shading conditions, Solar Energy 159 (2018) 1037–1046.
[49] X. Chen, Y. Du, E. Lim, H. Wen, K. Yan, J. Kirtley, Power ramp-rates of utility-scale PV systems under passing clouds: Module-level emulation with cloud shadow modeling, Appl. Energy 268 (2020) 114980.
[50] B. Mukhopadhyay, D. Das, Multi-objective dynamic and static reconfiguration with optimized allocation of PV-DG and battery energy storage system, Renew. Sustain. Energy Rev. 124 (2020), 109777.
[51] S. Xue, Q. Jia, S. Tian, Y. Su, H. Yu, Performance improvement strategy for photovoltaic generation through dynamic reconfiguration of cell strings, Int. J. Electric. Power Energy Syst. 125 (2021), 106456.
[52] P.R. Satpathy, R. Sharma, Reliability and losses investigation of photovoltaic power generators during partial shading, Energy Convers. Manage. 223 (2020), 113480.
[53] C. Dechthummarong, B. Wiengmoon, D. Chenvidhya, C. Jivacate, K. Kirtikara, Physical deterioration of encapsulation and electrical insulation properties of PV modules after long-term operation in Thailand, Solar Energy Mater. Solar Cells 94 (9) (2010) 1437–1440.
[54] M. Horoufiany, R. Ghandehari, An optimal fixed reconfiguration scheme for PV arrays power enhancement under mutual shading conditions, IET Renewable Power Generation 11 (11) (2017) 1456–1463.
[55] L. Idoko, O. Anaya-Lara, A. McDonald, Enhancing PV modules efficiency and power output using multi-concept cooling technique, Energy Rep. 4 (2018) 357–369.
[56] H. Hanifi, M.Z. Khan, B. Jaeckel, C. Hagendorf, J. Schneider, A. Abdallah, K. Ilse, Optimum PV module interconnection layout and mounting orientation to reduce inhomogeneous soiling losses in desert environments, Solar Energy 203 (2020) 267–274.
[57] O.W. Yen, B.C. Babu, Simple and easy approach for mathematical analysis of photovoltaic (PV) module under normal and partial shading conditions, Optik 169 (2018) 48–61.
[58] Y. Yang, K.A. Kim, T. Ding. 2018. Chapter 9 – Modeling and Control of PV Systems. Control of Power Electronic Converters and Systems. Academic Press. pp. 243-68.
[59] S.R. Pendem, S. Mikkili, Modeling, simulation and performance analysis of solar PV array configurations (Series, Series-Parallel and Honey-Comb) to extract maximum power under Partial Shading Conditions, Energy Rep. 4 (2018) 274–287.
[60] D. Yousri, S.B. Thanikanti, D. Allam, V.K. Ramachandaramurthy, M.B. Eteiba, Fractional chaotic ensemble particle swarm optimizer for identifying the single, double, and three diode photovoltaic models' parameters, Energy 195 (2020), 116979.
[61] D. Yousri, T.S. Babu, D. Allam, V.K. Ramachandaramurthy, M.B. Etiba, A novel chaotic flower pollination algorithm for global maximum power point tracking for photovoltaic system under partial shading conditions, IEEE Access 7 (2019) 121432–121445.
[62] D.P. Winston, B.P. Kumar, S.C. Christabel, A.J. Chamkha, R. Sathyamurthy, Maximum power extraction in solar renewable power system – a bypass diode scanning approach, Comput. Electr. Eng. 70 (2018) 122–136.
[63] A. Ndiaye, C.M.F. Kébé, A. Charki, V. Sambou, P.A. Ndiaye, Photovoltaic platform for investigating PV module degradation, Energy Procedia 74 (2015) 1370–1380.
[64] E.I. Batzelis, Simple PV performance equations theoretically well founded on the single-diode model, IEEE J. Photovoltaics 7 (5) (2017) 1400–1409.
[65] T.S. Babu, J.P. Ram, T. Dragicevic, M. Miyatake, F. Blaabjerg, N. Rajasekar, Particle swarm optimization based solar PV array reconfiguration of the maximum power extraction under partial shading conditions, IEEE Trans. Sustain. Energy 9 (1) (2017) 74–85.
[66] M.A. Awadallah, Variations of the bacterial foraging algorithm for the extraction of PV module parameters from nameplate data, Energy Convers. Manage. 113 (2016) 312–320.
[67] W. Charfi, M. Chaabane, H. Mhiri, P. Bournot, Performance evaluation of a solar photovoltaic system, Energy Rep. 4 (2018) 400–406.
[68] L.A.A. Bunthof, S. Veelenturf, E.J. Haverkamp, W.H.M. Corbeek, D. van der Woude, G.J. Bauhuis, P. Mulder, E. Vlieg, J.J. Schermer, Partially shaded III-V concentrator solar cell performance, Solar Energy Mater. Solar Cells 179 (2018) 231–240.
[69] S. Pareek, R. Dahiya, Enhanced power generation of partial shaded photovoltaic fields by forecasting the interconnection of modules, Energy 95 (2016) 561–572.
[70] M.N. Bhukya, V.R. Kota, A quick and effective MPPT scheme for solar power generation during dynamic weather and partial shaded conditions, Eng. Sci. Technol. Int. J. 22 (3) (2019) 869–884.

[71] E. Kandemir, N.S. Cetin, S. Borekci, A comprehensive overview of maximum power extraction methods for PV systems, Renew. Sustain. Energy Rev. 78 (2017) 93–112.
[72] K. Chandrasekaran, S. Sankar, K. Banumalar, Partial shading detection for PV arrays in a maximum power tracking system using the sine-cosine algorithm, Energy Sustain. Dev. 55 (2020) 105–121.
[73] M.B. Ogaard, H.N. Riise, H. Haug, S. Sartori, J.H. Selj, Photovoltaic system monitoring for high latitude locations, Solar Energy 207 (2020) 1045–1054.
[74] E. Piccoli, A. Dama, A. Dolara, S. Leva, Experimental validation of a model for PV systems under partial shading for building integrated applications, Solar Energy 183 (2019) 356–370.
[75] D. Wang, T. Qi, Y. Liu, Y. Wang, J. Fan, Y. Wang, H. Du, A method for evaluating both shading and power generation effects of rooftop solar PV panels for different climate zones of China, Solar Energy 205 (2020) 432–445.
[76] A. Wang, Y. Xuan, Multiscale prediction of localized hot-spot phenomena in solar cells, Renewable Energy 146 (2020) 1292–1300.
[77] N. Agrawal, B. Bora, A. Kapoor, Experimental investigations of fault tolerance due to shading in photovoltaic modules with different interconnected solar cell networks, Solar Energy 211 (2020) 1239–1254.
[78] E. Diaz-Dorado, J. Cidras, C. Carrillo, Discrete I-V model for partially shaded PV-arrays, Solar Energy 103 (2014) 96–107.
[79] P. Rajput, M. Malvoni, N.M. Kumar, O.S. Sastry, G.N. Tiwari, Risk priority number for understanding the severity of photovoltaic failure modes and their impacts on performance degradation, Case Stud. Therm. Eng. 16 (2019), 100563.
[80] G. Li, Y. Jin, M.W. Akram, X. Chen, J. Ji, Application of bio-inspired algorithms in maximum power point tracking for PV systems under partial shading conditions – A review, Renew. Sustain. Energy Rev. 81 (1) (2018) 840–873.
[81] R. Kumar, S. Khandelwal, P. Upadhyay, S. Pulipaka, Global maximum power point tracking using variable time and p-v curve region shifting technique along with incremental conductance for partially shaded photovoltaic systems, Solar Energy 189 (2019) 151–178.
[82] C. Han, H. Lee, Investigation and modeling of long-term mismatch loss of photovoltaic array, Renewable Energy 121 (2018) 521–527.
[83] M.C. Lopez-Escalante, F.M. Jiménez, M.G. Pérez, D. Leinen, J.R.R. Barrado, Shunt resistance criterion: design and implementation for industrial silicon solar cell production, Solar Energy 206 (2020) 269–278.
[84] M.H. Ali, A. Rabhi, A. El hajjaji, G.M. Tina, Real time fault detection in photovoltaic systems, Energy Procedia 111 (2017) 914–923.
[85] Y.-K. Wu, S.M. Chang, Y.-L. Hu, Literature review of power system blackouts, Energy Procedia 141 (2017) 428–431.
[86] S. Pareek, N. Chaturvedi, R. Dahiya, Optimal interconnections to address partial shading losses in solar photovoltaic arrays, Solar Energy 155 (2017) 537–551.
[87] A. Boccalatte, M. Fossa, R. Sacile, Modeling, design and construction of a zero-energy PV greenhouse for applications in mediterranean climates, Therm. Sci. Eng. Progress 25 (2021), 101046.
[88] A.S. Vaka, P. Talukdar, Novel inverse heat transfer technique for estimation of properties and location-specific process parameters of roof-mounted solar PV plants, Therm. Sci. Eng. Progress 19 (2020), 100657.
[89] S.R. Abdallah, I.M.M. Elsemary, A.A. Altohamy, M.A. Abdelrahman, A.A.A. Attia, O.E. Abdellatif, Experimental investigation on the effect of using nano fluid (Al2O3-Water) on the performance of PV/T system, Therm. Sci. Eng. Progress 7 (2018) 1–7.
[90] E. Johnston, P.S.B. Szabo, N.S. Bennett, Cooling silicon photovoltaic cells using finned heat sinks and the effect of inclination angle, Therm. Sci. Eng. Progress 23 (2021), 100902.
[91] A.N. Shmroukh, Thermal regulation of photovoltaic panel installed in Upper Egyptian conditions in Qena, Therm. Sci. Eng. Progress 14 (2019), 100438.
[92] S.R.M. Baygi, S.M. Sadrameli, Thermal management of photovoltaic solar cells using polyethylene glycol 1000 (PEG1000) as a phase change material, Therm. Sci. Eng. Progress 5 (2018) 405–411.
[93] A.H.A. Al-Waeli, H.A. Kazem, M.T. Chaichan, K. Sopian, Experimental investigation of using nano-PCM/nanofluid on a photovoltaic thermal system (PVT): technical and economic study, Therm. Sci. Eng. Progress 11 (2019) 213–230.
[94] S.R. Pendem, S. Mikkili, Modelling and performance assessment of PV array topologies under partial shading conditions to mitigate the mismatching power losses, Solar Energy 160 (2018) 303–321.
[95] T. Ramesh, K. Rajani, A.K. Panda, A novel triple-tied-cross-linked PV array configuration with reduced number of cross-ties to extract maximum power under partial shading conditions, CSEE J. Power Energy Syst. 7 (3) (2020) 567–581.
[96] F. Bayrak, H.K. Oztop, Effects of static and dynamic shading on thermodynamic and electrical performance for photovoltaic panels, Appl. Therm. Eng. 169 (2020), 114900.
[97] G. Shankar, V. Mukherjee, MPP detection of a partially shaded PV array by continuous GA and hybrid PSO, Ain Shams Eng. J. 6 (2) (2015) 471–479.
[98] J. Ma, X. Pan, K.L. Man, X. Li, H. Wen, T.O. Ting, Detection and assessment of partial shading scenarios on photovoltaic strings, IEEE Trans. Ind. Appl. IEEE 54 (6) (2018) 6279–6289.
[99] J.R. Louis, S. Shanmugham, K. Gunasekar, N.R. Atla, K. Murugesan, Effective utilisation and efficient maximum power extraction in partially shaded photovoltaic systems using minimum-distance-average-based clustering algorithm, IET Renewable Power Generation 10 (3) (2016) 319–326.
[100] A.A. Desai, S. Mikkili, Modelling and analysis of PV configurations (alternate TCT-BL, total cross tied, series, series parallel, bridge linked and honey comb) to extract maximum power under partial shading conditions, CSEE J. Power Energy Syst. (2020) 1–16.
[101] K. Lappalainen, S. Valkealahti, Effects of irradiance transition characteristics on the mismatch losses of different electrical PV array configurations, IET Renewable Power Generation 11 (2) (2017) 248–254.
[102] K. Osmani, A. Haddad, T. Lemenand, B. Castanier, M. Ramadan, Material based fault detection methods for PV systems, Key Eng. Mater. 856 (2020) 111–115.
[103] J.L. Prol, Regulation, profitability and diffusion of photovoltaic grid-connected systems: a comparative analysis of Germany and Spain, Renew. Sustain. Energy Rev. 91 (2018) 1170–1181.
[104] B. Steffen, Estimating the cost of capital for renewable energy projects, Energy Econ. 88 (2020), 104783.
[105] Md.S. Chowdhury, K.S. Rahman, T. Chowdhury, N. Nuthammachot, K. Techato, Md Akhtaruzzaman, S.K. Tiong, K. Sopian, N. Amin, An overview of solar photovoltaic panels' end-of-life material recycling, Energy Strategy Rev. 27 (2020), 100431.
[106] F.H. Alharbi, S. Kais, Theoretical limits of photovoltaics efficiency and possible improvements by intuitive approaches learned from photosynthesis and quantum coherence, Renew. Sustain. Energy Rev. 43 (2015) 1073–1089.
[107] A. Elamim, B. Hartiti, A. Haibaoui, A. Lfakir, P. Thevenin, Performance evaluation and economical analysis of three photovoltaic systems installed in an institutional building in Errachidia, Morocco, Energy Procedia 147 (2018) 121–129.
[108] T. AlSkaif, S. Dev, L. Visser, M. Hossari, W. van Sark, A systematic analysis of meteorological variables for PV output power estimation, Renewable Energy. 153 (2020) 12–22.
[109] V. Matulaitis, G. Straukaite, B. Azzopardi, E.A. Martinez-Cesena, Multi-criteria decision making for PV deployment on a multinational level, Solar Energy Mater. Solar Cells 156 (2016) 122–127.
[110] M. Balato, L. Costanzo, M. Vitelli, Reconfiguration of PV modules: a tool to get the best compromise between maximization of the extracted power and minimization of localized heating phenomena, Solar Energy 138 (2016) 105–118.
[111] R.K. Pachauri, O.P. Mahela, A. Sharma, J. Bai, Y.K. Chauhan, B. Khan, H. H. Alhelou, Impact of partial shading on various PV array configurations and different modeling approaches: a comprehensive review, IEEE Access 8 (2020) 181375–181403.
[112] S.G. Krishna, T. Moger. 2020. Static Reconfiguration approach for Photovoltaic Array to Improve Maximum power. 2020 International Conference on Electrical and Electronics Engineering (ICE3). IEEE. ISBN: 978-1-7281-5847-1.
[113] Y. Hu, J. Zhang, P. Li, D. Yu, L. Jiang, Non-uniform aged modules reconfiguration for large-scale PV array, IEEE Trans. Device Mater. Reliab. 17 (3) (2017) 560–569.
[114] G.S. Krishna, T. Moger. 2018. SuDoKu and Optimal SuDoKu Reconfiguration for TCT PV array Under Non-Uniform Irradiance Condition. 2018 IEEE 8th Power India International Conference (PIICON). IEEE. ISBN: 978-1-5386-7339-3.
[115] B.I. Rani, G.S. Ilango, C. Nagamani, Enhanced power generation from PV array under partial shading conditions by shade dispersion using Su Do Ku configuration, IEEE Trans. Sustain. Energy 4 (3) (2013) 594–601.
[116] N.D. Tuyen, L.V. Thinh, V.X.S. Huu. 2020. On the Sudoku-based Arrangement in Reconfiguring a Large-scale Photovoltaic Array. 2020 59th Annual Conference of the Society of Instrument and Control Engineers of Japan (SICE). IEEE. ISBN: 978-1-7281-1089-9.
[117] N.A. Rajan, K.D. Shrikant, B. Dhanalakshmi, N. Rajasekar, Solar PV array reconfiguration using the concept of Standard deviation and Genetic algorithm, Energy Procedia 117 (2017) 1062–1069.
[118] G.S. Krishna, T. Moger, Reconfiguration strategies for reducing partial shading effects in photovoltaic arrays: state of the art, Solar Energy 182 (2019) 429–452.
[119] S.G. Krishna, T. Moger, Optimal SuDoKu reconfiguration technique for total-cross-tied PV array to increase power output under non-uniform irradiance, IEEE Trans. Energy Convers. 34 (4) (2019) 1973–1984.
[120] G.S. Krishna, T. Moger, Improved SuDoKu reconfiguration technique for total-cross-tied PV array to enhance maximum power under partial shading conditions, Renew. Sustain. Energy Rev. 109 (2019) 333–348.
[121] S.V. Lokanath, B. Skarbek, E.J. Schindelholz. 2019. Chapter 9 – Degradation Processes and Mechanisms of PV Wires and Connectors. Durability and Reliability of Polymers and Other Materials in Photovoltaic Modules, Plastics Design Library. William Andrew. pp. 217-33.
[122] S.R. Potnuru, D. Pattabiraman, S.I. Ganesan, N. Chilakapati, Positioning of PV panels for reduction in line losses and mismatch losses in PV array, Renewable Energy 78 (2015) 264–275.
[123] B. Dhanalakshmi, N. Rajasekar, A novel Competence Square based PV array reconfiguration technique for solar PV maximum power extraction, Energy Convers. Manage. 174 (2018) 897–912.
[124] M.S.S. Nihanth, J.P. Ram, D.S. Pillai, A.M.Y.M. Ghias, A. Garg, N. Rajasekar, Enhanced power production in PV arrays using a new skyscraper puzzle based one-time reconfiguration procedure under partial shade conditions (PSCs), Solar Energy 194 (2019) 209–224.
[125] L. El Iysaouy, M. Lahbabi, A. Oumnad, A novel magic square view topology of a PV system under partial shading condition, Energy Procedia 157 (2019) 1182–1190.
[126] A.S. Yadav, R.K. Pachauri, Y.K. Chauhan, S. Choudhury, R. Singh, Performance enhancement of partially shaded PV array using novel shade dispersion effect on magic-square puzzle configuration, Solar Energy 144 (2017) 780–797.
[127] S.S. Reddy, C. Yammani, A Novel Magic-Square puzzle based one-time PV reconfiguration technique to mitigate mismatch power loss under various partial shading conditions, Optik 222 (2020), 165289.

[128] B. Dhanalakshmi, N. Rajasekar, Dominance square based array reconfiguration scheme for power loss reduction in solar PhotoVoltaic (PV) systems, Energy Convers. Manage. 156 (2018) 84–102.
[129] H.S. Sahu, S.K. Nayak, S. Mishra, Maximizing the power generation of a partially shaded PV array, IEEE J. Emerg. Selected Top. Power Electron. 4 (2) (2015) 626–637.
[130] H.S. Sahu, S.K. Nayak. 2014. Power enhancement of partially shaded PV array by using a novel approach for shade dispersion. 2014 IEEE Innovative Smart Grid Technologies – Asia (ISGT ASIA). IEEE. ISBN: 978-1-4799-1300-8.
[131] A.S. Yadav, V. Mukherjee, Lines losses reduction techniques in puzzled PV array configuration under different shading conditions, Solar Energy 171 (2018) 774–783.
[132] S.G. Krishna, T. Moger. 2020. A Novel Fixed Interconnection Topology for Photovoltaic Array to Gain Maximum Energy Yields. 2020 International Conference on Electrical and Electronics Engineering (ICE3). IEEE. ISBN: 978-1-7281-5846-4.
[133] S. Anjum, V. Mukherjee, G. Mehta, Modelling and simulation of AdDoKu based reconfiguration technique to harvest maximum power from photovoltaic array under partial shading conditions, Simul. Model. Pract. Theory 115 (2022), 102447.
[134] R.K. Pachauri, S.B. Thanikanti, J. Bai, V.K. Yadav, B. Aljafari, S. Gosh, H. H. Alhelou, Ancient Chinese magic square-based PV array reconfiguration methodology to reduce power loss under partial shading conditions, Energy Convers. Manage. 253 (2022), 115148.
[135] S. Anjum, V. Mukherjee, A novel arithmetic sequence pattern reconfiguration technique for line loss reduction of photovoltaic array under non-uniform irradiance, J. Clean. Prod. 331 (2022), 129822.
[136] I. Nasiruddin, S. Khatoon, M.F. Jalil, R.C. Bansal, Shade diffusion of partial shaded PV array by using odd-even structure, Solar Energy 181 (2019) 519–529.
[137] S.S. Reddy, C. Yammani, Odd-Even-Prime pattern for PV array to increase power output under partial shading conditions, Energy 213 (2020), 118780.
[138] D.S. Pillai, N. Rajasekar, J.P. Ram, V.K. Chinnaiyan, Design and testing of two phase array reconfiguration procedure for maximizing power in solar PV systems under partial shade conditions (PSC), Energy Convers. Manage. 178 (2018) 92–110.
[139] R. Venkateswari, N. Rajasekar, Power enhancement of PV system via physical array reconfiguration based Lo Shu technique, Energy Convers. Manage. 215 (2020), 112885.
[140] A.S. Yadav, R.K. Pachauri, Y.K. Chauhan, Comprehensive investigation of PV arrays with puzzle shade dispersion for improved performance, Solar Energy 129 (2016) 256–285.
[141] Z. Yang, N. Zhang, J. Wang, Y. Liu, L. Fu, Improved non-symmetrical puzzle reconfiguration scheme for power loss reduction in photovoltaic systems under partial shading conditions, Sustain. Energy Technol. Assess. 51 (2022), 101934.
[142] S. Vijayalekshmy, G.R. Bindu, S.R. Iyer, A novel Zig-Zag scheme for power enhancement of partially shaded solar arrays, Solar Energy 135 (2016) 92–102.
[143] N. Belhaouas, M.-S.-A. Cheikh, P. Agathoklis, M.-R. Oularbi, B. Amrouche, K. Sedraoui, N. Djilali, PV array power output maximization under partial shading using new shifted PV array arrangements, Appl. Energy 187 (2017) 326–337.
[144] P.R. Satpathy, R. Sharma, S. Dash, An efficient SD-PAR technique for maximum power generation from modules of partially shaded PV arrays, Energy 175 (2019) 182–194.
[145] P.R. Satpathy, R. Sharma, Power loss reduction in partially shaded PV arrays by a static SDP technique, Energy 156 (2018) 569–585.
[146] J. Storey, P.R. Wilson, D. Bagnall, The optimized-string dynamic photovoltaic array, IEEE Trans. Power Electron. 29 (4) (2013) 1768–1776.
[147] M. Balato, L. Costanzo, M. Vitelli, Series-Parallel PV array re-configuration: maximization of the extraction of energy and much more, Appl. Energy 159 (2015) 145–160.
[148] O. Bingol, B. Ozkaya, Analysis and comparison of different PV array configurations under partial shading conditions, Solar Energy 160 (2018) 336–343.
[149] D. Picault, B. Raison, S. Bacha, J. de la Casa, J. Aguilera, Forecasting photovoltaic array power production subject to mismatch losses, Solar Energy 84 (7) (2010) 1301–1309.
[150] S. Mohammadnejad, A. Khalafi, S.M. Ahmadi, Mathematical analysis of total-cross-tied photovoltaic array under partial shading condition and its comparison with other configurations, Solar Energy 133 (2016) 501–511.
[151] M.Z. Shams El-Dein, M. Kazerani, M.M.A. Salama, Optimal photovoltaic array reconfiguration to reduce partial shading losses, IEEE Trans. Sustain. Energy 4 (1) (2013) 145–153.
[152] T.S. Babu, D. Yousri, K. Balasubramanian, Photovoltaic array reconfiguration system for maximizing the harvested power using population-based algorithms, IEEE Access 8 (2020) 109608–109624.
[153] A. Fathy, Recent meta-heuristic grasshopper optimization algorithm for optimal reconfiguration of partially shaded PV array, Solar Energy 171 (2018) 638–651.
[154] A. Fathy, Butterfly optimization algorithm based methodology for enhancing the shaded photovoltaic array extracted power via reconfiguration process, Energy Convers. Manage. 220 (2020), 113115.
[155] E.R. Sanseverino, T.N. Ngoc, M. Cardinale, V.L. Vigni, D. Musso, P. Romano, F. Viola, Dynamic programming and Munkres algorithm for optimal photovoltaic arrays reconfiguration, Solar Energy 122 (2015) 347–358.
[156] H. Tian, F. Mancilla-David, K. Ellis, E. Muljadi, P. Jenkins, Determination of the optimal configuration for a photovoltaic array depending on the shading condition, Solar Energy 95 (2013) 1–12.
[157] M. Alahmad, M.A. Chaaban, S.K. Lau, J. Shi, J. Neal, An adaptive utility interactive photovoltaic system based on a flexible switch matrix to optimize performance in real-time, Solar Energy 86 (3) (2012) 951–963.
[158] L.F.L. Villa, T.-P. Ho, J.-C. Crebier, B. Raison, A power electronics equalizer application for partially shaded photovoltaic modules, IEEE Trans. Ind. Electron. 60 (3) (2012) 1179–1190.
[159] P.S. Rao, G.S. Ilango, C. Nagamani, Maximum power from PV arrays using a fixed configuration under different shading conditions, IEEE J. Photovoltaics 4 (2) (2014) 679–686.
[160] A.A. Heidari, S. Mirjalili, H. Faris, I. Aljarah, M. Mafarja, H. Chen, Harris hawks optimization: algorithm and applications, Fut. Gener. Comput. Syst. 97 (2019) 849–872.
[161] D. Yousri, D. Allam, M.B. Eteiba, Optimal photovoltaic array reconfiguration for alleviating the partial shading influence based on a modified harris hawks optimizer, Energy Convers. Manage. 206 (2020), 112470.
[162] V.K. Yadav, A. Yadav, R. Yadav, A. Mittal, N.H. Wazir, S. Gupta, R.K. Pachauri, S. Ghosh, A novel reconfiguration technique for improvement of PV reliability, Renewable Energy 182 (2022) 508–520.
[163] P. dos Santos, E.M. Vicente, E.R. Ribeiro. 2011. Reconfiguration methodology of shaded photovoltaic panels to maximize the produced energy. XI Brazilian Power Electronics Conference. IEEE. ISBN: 978-1-4577-1646-1.
[164] Z. Cheng, Z. Pang, Y. Liu, P. Xue. 2010. An adaptive solar photovoltaic array reconfiguration method based on fuzzy control. 2010 8th World Congress on Intelligent Control and Automation. IEEE. ISBN: 978-1-4244-6712-9.
[165] H. Ziar, E. Afjei, A. Siadatan, A. Arjhangmehr. 2011. Different diode configurations evaluation in photovoltaic arrays using binary coding method. International Aegean Conference on Electrical Machines and Power Electronics and Electromotion, Joint Conference. IEEE. ISBN: 978-1-4673-5003-7.
[166] R. Cavieres, R. Barraza, D. Estay, J. Bilbao, P. Valdivia-Lefort, Automatic soiling and partial shading assessment on PV modules through RGB images analysis, Appl. Energy 306 (2022), 117964.
[167] M. Waqar Akram, G. Li, Y. Jin, X. Chen, C. Zhu, X. Zhao, M. Aleem, A. Ahmad, Improved outdoor thermography and processing of infrared images for defect detection in PV modules, Solar Energy 190 (2019) 549–560.
[168] L. Pratt, D. Govender, R. Klein, Defect detection and quantification in electroluminescence images of solar PV modules using U-net semantic segmentation, Renewable Energy 178 (2021) 1211–1222.
[169] A.M. Moradi Sizkouhi, S.M. Esmailifar, M. Aghaei, M. Karimkhani, RoboPV: an integrated software package for autonomous aerial monitoring of large scale PV plants, Energy Convers. Manage. 254 (2022), 115217.
[170] M. Karakose, M. Baygin. 2014. Image processing based analysis of moving shadow effect for reconfiguration in PV arrays. 2014 IEEE International Energy Conference (ENERGYCON). IEEE. ISBN: 978-1-4799-2449-3.
[171] M. Etarhouni, B. Chong, L. Zhang, A combined scheme for maximising the output power of a Photovoltaic array under partial shading conditions, Sustain. Energy Technol. Assess. 50 (2022), 101878.
[172] G.M. Masters, Chapter 5 – Photovoltaic materials and electrical characteristics, in: Renewable and Efficient Electric Power Systems, 2nd Edition., Wiley-IEEE Press, 2013, pp. 253–301.
[173] G.M. Masters, Chapter 6 – Photovoltaic systems, in: Renewable and Efficient Electric Power Systems, 2nd Edition., Wiley-IEEE Press, 2013, pp. 316–387.
[174] V.B. Raju, C.h. Chengaiah, A comprehensive study on re-arrangement of modules based TCT configurations of partial shaded PV array with shade dispersion method, Trends Renew. Energy 6 (2020) 37–60.
[175] M. Premkumar, U. Subramaniam, T.S. Babu, R.M. Elavarasan, L. Mihet-Popa, Evaluation of mathematical model to characterize the performance of conventional and hybrid PV array topologies under static and dynamic shading patterns, Energies 13 (12) (2020) 24–37.
[176] A.M. Ajmal, V.K. Ramachandaramurthy, A. Naderipour, J.B. Ekanayake, Comparative analysis of two-step GA-based PV array reconfiguration technique and other reconfiguration techniques, Energy Convers. Manage. 230 (2021), 113806.

Annexe 1.7

Aperçu de l'utilisation des matériaux à changement de phase (PCM) pour le refroidissement des systèmes photovoltaïques

Key Engineering Materials
ISSN: 1662-9795, Vol. 922, pp 3-9
doi:10.4028/p-t2m41c

Submitted: 2021-09-09
Revised: 2022-01-10
Accepted: 2022-01-13
Online: 2022-06-08

An Overview on the Use of Phase Change Material (PCM) for PV Cooling

Khaled Osmani[1,a], Mohamad Ramadan[2,3,b*], Ahmad Haddad[2,3,c], Thierry Lemenand[1,d] and Bruno Castanier[1,e]

[1]LARIS EA 7315, Polytech Angers, UNIV Angers, France

[2]School of Engineering, International University of Beirut BIU, Beirut, Lebanon

[3]School of Engineering, Lebanese International University LIU, Bekaa, Lebanon

[a]khaled.alosmani@etud.univ-angers.fr, [b]mohamad.ramadan@liu.edu.lb, [c]ahmad.haddad@liu.edu.lb, [d]thierry.lemenand@univ-angers.fr, [e]bruno.castanier@univ-angers.fr

Keywords: Heat absorption, temperature effect, thermal management, phase change, PV cooling.

Abstract. The thermal management processes for PhotoVoltaic (PV) cooling applications, increase PV systems' overall efficiency and yield to a maximized power generation. Accordingly, this paper investigates recent PV thermal management methods, which involve the use of Phase Change Material (PCM) under the back of PV modules. Compared to other cooling methods (such as air and water based methods) PCM based techniques show less need for maintenance, are environment-friendly, and have a longer life cycle. Since PCM are diverse in nature, and many methods exist to guide their selection procedure, this paper begins by revealing different types of PCM, which are found to be as Organic, Inorganic, Eutectic and Commercial PCM, with the characteristics of each. After acknowledging different PCM natures, a selection process is established based on either the melting temperature, latent heat, or thermal conductivity of PCM. Results have shown that Commercial PCM are the best option followed by Organic PCM, due to their improved chemical aspects when compared with Inorganic and Eutectic PCM. Concerning PCM selection criteria, the easiest yet sufficient process is based on the melting temperature method, due to the simplified calculations when compared to other thermic quantities. At the end, future work recommendations are declared, related to PCM lifecycle assessment and cooling/heating cycles effects on PV entropy.

Introduction

Among various types of renewable energy supplies, PhotoVoltaic (PV) systems are top ranked, with most optimum efficiency and power generation capabilities. While possessing performance robustness, and ability to meet different load demands, PVs have a high future scope in power production [1]. The emission-less static operational mechanisms, omnipresent characteristics, and low maintenance costs [2], have popularized the adaption of such systems, with an elevated power productivity during a long life cycle.

In addition, solar irradiations are abundant where $1.2 \cdot 10^5$ TW of energy is continuously attaining earth's surface [3]. This fact has elevated the status of PV systems as a reliable and clean green energy supply. Accordingly, the usage of such systems would definitely contribute in reduction of global emissions, hence stabilizing climate change and global warming. Such granted advantages have globally evolved the market share of PV industry and increased different research topics of PV systems.

The PV power output can be maximized upon adaptation of certain optimization methods, since PV systems rely on unstable climatic conditions (i.e., irradiance, etc.) to produce power. This represents the new concern in PV research area. In other words, PV's outcomes are better exploited after installation of auxiliary sub-systems, such as Solar Trackers (ST) for example. An ST ensures that the maximum quantity of solar radiations hit the PV modules' surfaces in a perpendicular matter [4], hence producing more electrical power. From the same perspective, the monthly modification of

PV modules' tilt angle, have shown an increase in produced power, and a decrease in the levelized cost of energy [5].

From another part, PV Array Reconfiguration (PVAR) methods would equalize the generated PV string currents, hence compensating the negative effects of Partial Shading Conditions (PSC), which are caused by unavoidable physical (moving or static) light barriers [6].

When PV faults are accurately categorized and detected via PV Fault Diagnostic Tools (PV-FDT), further complications are prevented, such as partial/complete blackouts. This in turn would ensure a maximum power productivity with an increased PV system's lifecycle [7].

Apart of the importance of applying ST, PVAR, and PV-FDT as additional systems on a PV network, a proper PV modules' thermal management scheme is a key factor in elevating the overall system's efficiency, referred to as PV cooling methods [8]. Since the reduction of PV module's temperature (T_{PV}) would greatly enhance the generated power output of PV systems, cooling processes began by water and air based thermal removers [9]. The water-based cooling methods include water spraying, and usage of water nozzles on PV modules surfaces, but such methods deplete ground water which is considered the most vital human need. Instead, immersing the modules into water would reduce such losses, but in turn is not applicable in arid regions.

On the other hand, air-based cooling techniques also play a critical role in T_{PV} reduction, while not adding any additional equipment weights onto the PV system, as in the case of water-based methods. From another side, such cooling methods impose the need of ducts and other installations to conduct a proper airflow, which increases the overall cost of the system [10]. Aside from the previous PV thermal management strategies, heat sink coolers reduce T_{PV} effectively [11], with less maintenance costs, but would only properly operate when the wind speed is high.

Apart from the mentioned cooling methods, the usage of Phase Change Material (PCM) is the best remedial alternative. In this paper, an in-depth overview of various PCM types is conducted after a graphical representation of temperature effect over PV power output. Progressively, an investigation of the selection procedure of a PCM takes place, followed by a descriptive section revealing the effects of PCM application in PV systems. Finally, conclusions and future recommendations are exposed.

Temperature effect on PV output

PV systems' operations are highly affected by irradiation and ambient temperature. An inverse relation condemns the behavior of these systems, where any increase in temperature decreases a PV module's power generation, as seen in Fig. 1, based on the PV's mathematical model [12]. They also suffer from a low light-to-electricity conversion efficiency and dissipate large quantities of potential energy in form of heat.

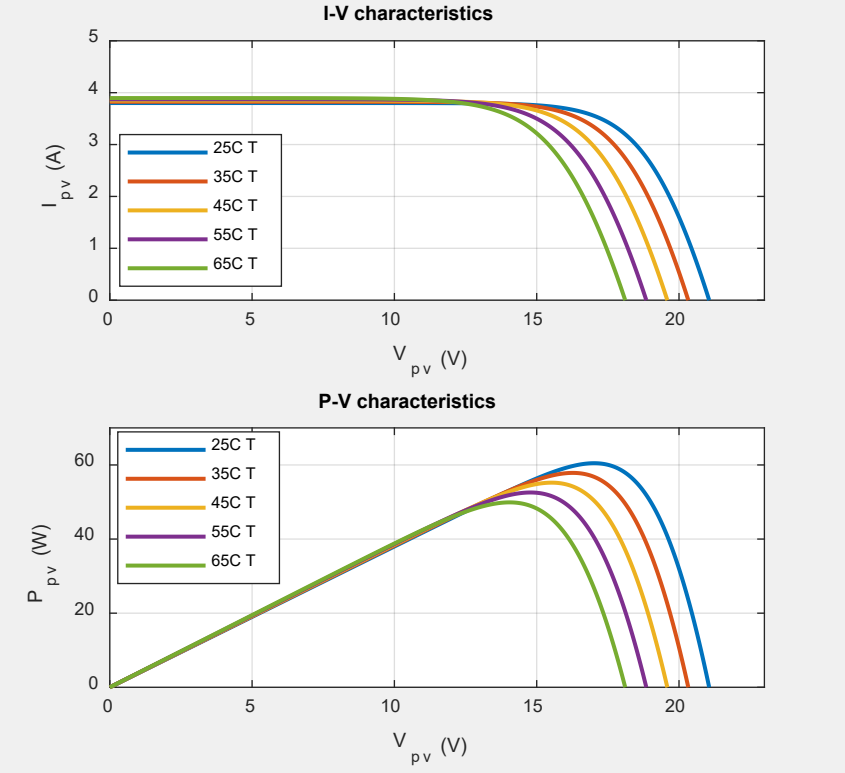

Fig. 1. Temperature effect over PV characteristic curves

It can be clearly deduced from Fig. 1 that an increase of 10℃ in temperature would decrease the output power by 2 W. Accordingly, a temperature of 65℃ would reflect an output power of 50 W, decreased by 10 W from the Standard Test Conditions (STC) temperature of 25℃ [12]. Therefore, cooling down T_{PV} has a direct positive effect on PV's output power, in parallel with other optimization techniques, such as Maximum Power Point Tracking (MPPT) [12], and PV cell raw materials designs [13].

Overview of different Phase Change Material (PCM)

A PCM is a physical entity that is able to absorb and release large amount of latent heat, during its phase transition (from solid-solid, solid-liquid, solid-gas, etc.). Between various physical properties transformations, solid-liquid transition type is the center of interest for PV module cooling process [14]. The PCM attains three distinct phases during the charging/discharging cycle. It first stores energy in form of sensible heat, of the solid phase PCM ($C_{P,s}$) until the material attains its melting temperature (T_{melt}). Afterwards, the PCM melts, consuming a thermal energy equivalent to the latent heat of fusion (H_m). In the last stage, the molten PCM absorbs the sensible heat in liquid phase PCM ($C_{p,l}$) [15]. The different types of PCM are shown in Fig. 2.

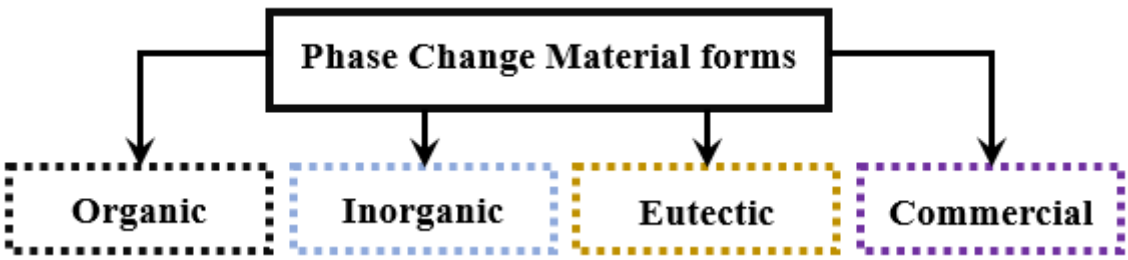

Fig. 2. Different types of PCM

Organic PCM are either Paraffin wax or fatty acids type (Capric acid, Lauric acid, coconut oil, petroleum jelly, etc.). Paraffin compounds can in turn have various natures, but they all share in

common the saturated hydrocarbon (C_nH_{2n+2}) in essence, combined with other hydrocarbon chains. Such compounds offer an acceptable thermal stability, favorably to work for low-temperature applications [16]. Fatty acids PCM on the other hand, are still limited in PV cooling applications, mainly due to their low T_{melt} and low H_m.

Inorganic PCM are salt hydrate based, which contain higher H_m, density, and thermal conductivity when compared to Organic PCM. But still, the salt content, and its chemical instability pose a problem over a sustained PV module functioning [17], that is why Organic PCM are more preferred for PV cooling applications. The combination and hybridization between Organic and Inorganic PCM would result in a Eutectic PCM which overcome the issue of chemical degradation of individual Organic/Inorganic PCM. Eutectic PCM offer better flexibility in tuning T_{melt} but are more expensive than Organic PCM [18]. Hereafter, Eutectic mixtures result in Commercial PCM, which have longer thermally stable operations, possess a sharp T_{melt} as well as a high H_m, and present no super-cooling effects on PV modules. Although Commercial PCM reduce T_{PV} significantly, they are considered too expensive to install [19]. Table 1 encapsulates the differences between various PCM.

Table 1. Major differences between PCM types

PCM type	T_{melt}	Supercooling effect	Thermal conductivity	Cost
Organic	25℃ *to* 60℃	Low	Low	Very low
Inorganic	30℃ *to* 40℃	Moderate	High	Low
Eutectic	22℃ *to* 23℃	Low	Moderate	Moderate
Commercial	10℃ *to* 60℃	Low	Low	Very high

Selection criteria for different PCM

Concerning the various types of PCM, their selection process can be challenging. The PCM diversity, in terms of thermodynamic, kinetic, chemical, and financial standards, offer different selection processes intended for PV cooling, as summarized in Fig. 3.

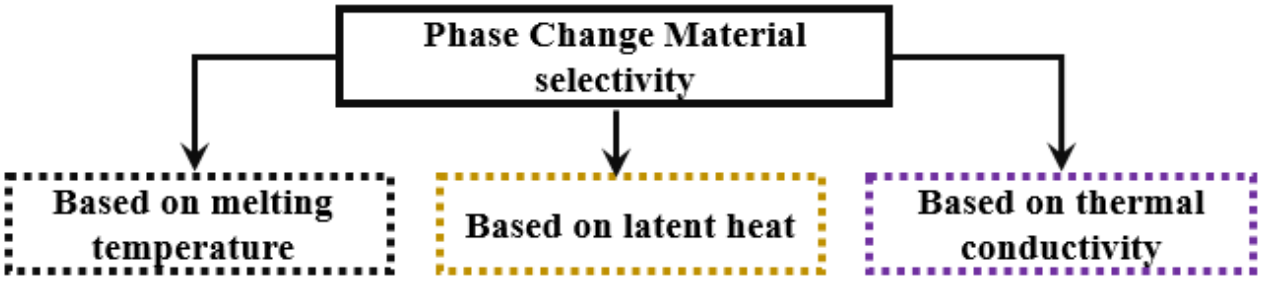

Fig. 3. Selection criteria of PCM

For isothermal heat removal, the selection of PCM based on T_{melt} is of crucial importance. In this case, the climatic conditions in the geographical region, at which the PV system is installed, governs the selectivity, as shown in Eq. (1) [20].

$$T_{PV} = T_a + \left(\frac{\tau\alpha}{U_{L0} + U_{L1}v}\right) G \tag{1}$$

with T_{PV}, T_a , $\tau\alpha$ representing the PV panel temperature, ambient temperature, and transmittance respectively, U_{L0}, U_{L1}, denoting the heat loss coefficients and v, G indicating the wind speed and irradiance respectively.

As a result from Eq. (1), the acknowledgment of T_{PV} would give a discrete option upon selecting an optimum T_{melt}. From another side, and since the latent heat is another characteristic of a PCM, the selection process can be based upon. The thermal regulation of an elevated T_{PV} depends on the PCM volume and its latent heat value. In other words, higher latent heat, provides longer thermal regulation. This process is mainly dependent on solar irradiance patterns, rather than ambient temperature conditions as in the previous criteria [21].

Lastly, the choice of PCM can be based upon material heat transfer. As indicated in Table 1, the majority of PCM have a low thermal conductivity, but for PV cooling aim, a high thermal conductivity is needed. Accordingly, this conductivity can be enhanced and thus the choice of a PCM can be based upon enhancement techniques. Some of these techniques include the addition of fins [22], and nanoparticles [23] to the heat sinks, what reflects as better energy storage of PCM. The choice in this case is based on the technique involved to enhance the thermal conductivity by auxiliary procedures.

Discussion

Aside from acknowledging different structures of PCM, as well as their selection processes, more data should be extracted from real world applications of PCM-cooled PV systems and investigated in order to truly determine what PCM type is most suitable for which PV application.

In other words, it is never sufficient to choose a PCM based on its most optimum thermal characteristics only. Despite the linear drop of PV cell efficiency by 0.45% for each temperature rise of 1℃ from PV's manufacturers datasheets [24], all of kinetic, chemical, technical, and economical criteria must be also taken into consideration in the selection process. This must take place in parallel with historical data information of actual PV networks, cooled via PCM. For this purpose, and as an example, Table 2 encloses different PV module temperature profiles, with/without usage of certain PCM.

Table 2. Thermal regulation effects for different PCM [24]

PCM type		T_{PV} before usage	T_{PV} after usage	T_{PV} reduction
Organic	Paraffin 46	55℃	45℃	10℃
	Octadecane	55℃	32℃	23℃
Inorganic	$Na_2SO_4.10H_2O$	45℃	35℃	10℃
	$Na_2HPO_4.12H_2O$	45℃	38℃	7℃
Eutectic	$CaCl_2.6H_2O$	60℃	38℃	22℃
	Capric:palmitic	60℃	50℃	10℃
Commercial	RT50HC	78℃	65℃	13℃
	RT54HC	78℃	62℃	16℃

As shown in Table 2, the varieties of PCM within the same set, could contribute differently to PV thermal management. For instance, concerning the Inorganic PCM set, the non-Paraffin compound (Octadecane) has better reduced T_{PV} in comparison with Paraffin 46, by 13℃. In some cases the T_{PV} reduction between mutual varieties is less, such as by 3℃, like in the case of using two different Inorganic PCM.

The important to notice is that not necessarily a set of PCM could better replace another, just because it had scored better temperature reduction for a PV module. Being said, since the T_{PV} tested with Organic PCM is higher than T_{PV} under Inorganic PCM study, that does not mean that Organic PCM would contribute better in lowering T_{PV} when subjected to the same environmental conditions, as in Inorganic PCM test scenario.

Instead, a major study of the geographical location of the PV system in action is recommended, to acknowledge other factors related to thermal management (such as wind speed, etc.). That refers to the climatic zone variations, expressed in climate, air pressure, and average temperature. Accordingly, a PCM set might better be suitable for a tropical zone, instead of sub-tropical zone.

Conclusion

For a sustainable and maximum power extraction from PV systems, PV modules must be thermally managed, due to the inverse relation between T_{PV} and power output. The thermal effect over PV power generation is influential, such that for each increase of 1℃, the PV cell efficiency is reduced by 0.45%. The usage of PCM for PV cooling processes, have shown better performance, regarding older cooling strategies, such as air-forced and water-forced cooling methods. A PCM needs less maintenance than other techniques, deplete less water, and show dynamic performance for day-fluctuating temperatures. In order to optimally choose a PCM for a case specified PV system installation, designers must be exposed to different types of PCMs, with corresponding advantages/disadvantages of each.

In this work, four main classifications for PCM have taken place, where Commercial PCM offered largest range for T_{melt}, offering a global suitability for different climatic zones. When there are no economic constraints, Commercial PCMs are the best option, followed by Organic PCMs, mainly Paraffin compounds, for their non-toxicity and better chemical aspects compared to Inorganic and Eutectic PCM. In other terms, Paraffin wax and commercial PCM are better and more widely used than others, in tropical and sub-tropical areas. For dry and temperate climatic zones, single PCM is not sufficient to cool PV modules due to high ambient temperatures, where a cascaded structuring of multi-PCM is needed. The direct approach PCM selection process on the other hand, is greatly advised by the choice based on T_{melt}, since ambient temperature calculations are simpler than dealing with other thermic quantities such as latent heat and thermal conductivity. Melting temperature of a PCM should be as close as possible to T_{PV} under STC. In general, PCMs are environment-friendly, and considered as non-hazardous energy storing materials. The future work recommendations, begin with the life cycle assessment of different PCM types versus cost efficiency, and studies of relation between continuous cooling/heating cycles and PV modules entropy.

References

[1] C. Prons-Seres de Brauwer, J.J. Cohen, Analyzing the potential of citizen-financed community renewable energy to drive Europe's low-carbon energy transition, Renewable and Sustainable Energy Reviews. 133 (2020) Article ID: 110300.

[2] K. Osmani, A. Haddad, T. Lemenand, B. Castanier, M. Ramadan, A review on maintenance strategies for PV systems, Science of the Total Environment. 746 (2020) Article ID: 141753.

[3] G. Li, S. Shittu, T.M.O. Diallo, M. Yu, X. Zhao, J. Ji, A review of solar photovoltaic-thermoelectric hybrid system for electricity generation, Energy. 158 (2018) 41-58.

[4] A. Awasthi, A.K. Shukla, M. Manohar S.R., C. Dondariya, K.N. Shukla, D. Porwal, G. Richhariya, Review on sun tracking technology in solar PV system, Energy Reports. 6 (2020) 392-405.

[5] K. Osmani, M. Ramadan, T. Lemenand, B. Castanier, A. Haddad, Optimization of PV array tilt angle for minimum levelized cost of energy, Computers & Electrical Engineering. 96 (2021) Article ID: 107474.

[6] F. Belhachat, C. Larbes, PV array reconfiguration techniques for maximum power optimization under partial shading conditions: A review, Solar Energy. 230 (2021) 558-582.

[7] Z. Zhang, M. Ma, H. Wang, Ha. Wang, W. Ma, X. Zhang, A fault diagnosis method for photovoltaic module current mismatch based on numerical analysis and statistics, Solar Energy. 225 (2021) 221-236.

[8] A. Sethiya, Cooling material for solar PV module to improve the generation efficiency, materialstoday: PROCEEDINGS. 47 (2021) 7064-7066.
[9] A. Maleki, A. Haghighi, M.E.H. Assad, I. Mahariq, M.A. Nazari, A review on the approaches employed for cooling PV cells, Solar Energy. 209 (2020) 170-185.
[10] N.A.S. Elminshawy, A.M.I. Mohamed, K. Morad, Y. Elhenawy, A.A. Alrobaian, Performance of PV panel coupled with geothermal air cooling system subjected to hot climatic, Applied Thermal Engineering. 148 (2019) 1-9.
[11] U.J. Rajput, J. Yang, Comparison of heat sink and water type PV/T collector for polycrystalline photovoltaic panel cooling, Renewable Energy. 116 (2018) 479-491.
[12] K. Osmani, A. Haddad, T. Lemenand, B. Castanier, M. Ramadan, An investigation on maximum power extraction algorithms from PV systems with corresponding DC-DC converters, Energy. 224 (2021) Article ID: 120092.
[13] K. Osmani, A. Haddad, T. Lemenand, B. Castanier, M. Ramadan, Material Based Fault Detection Methods for PV Systems, Key Engineering Materials. 856 (2020) 111-115.
[14] T. Ma, Z. Li, J. Zhao, Photovoltaic panel integrated with phase change materials (PV-PCM): technology overview and materials selection, Renewable and Sustainable Energy Reviews. 116 (2019) Article ID: 109406.
[15] K. Velmurugan, C. Sirisamphanwong, S. Sukchai, Thermal Investigation of Paraffin Wax for Low-Temperature Application, Journal of Advanced Research in Dynamical and Control Systems. 11 (2019) 1437-1443.
[16] V. Karthikeyan, C. Sirisamphanwong, S. Sukchai, S.K. Sahoo, T. Wongwuttanasatian, Reducing PV module temperature with radiation based PV module incorporating composite phase change material, Journal of Energy Storage. 29 (2020) Article ID: 101346.
[17] M.F. Junaid, Z. ur Rahman, M. Cekon, J. Curpek, R. Farooq, H. Cui, I. Khan, Inorganic phase change materials in thermal energy storage: A review on perpesctives and technological advances in building applications, Energy and Buildings. 252 (2021) Article ID: 111443.
[18] A.K. Hamzat, A.Z. Sahin, M.I. Omisanya, L.M. Alhems, Advances in PV and PVT cooling technologies: A review, Sustainable Energy Technologies and Assessments. 47 (2021) Article ID: 101360.
[19] A. Wahab, M.A.Z. Khan, A. Hassan, Impact of graphene nanofluid and phase change material on hybrid photovoltaic thermal system: Exergy analysis, Journal of Cleaner Production. 277 (2020) Article ID: 123370.
[20] M. Zouine, M. Akhsassi, N. Erraissi, N. Aarich, A. Bennouna, R. Mustapha, A. Outzourhit, Mathematical Models Calculating PV Module Temperature Using Weather Data: Experimental Study, Lecture Notes in Electrical Engineering. 519 (2018) 630-639.
[21] R. Kumar, P. Praveen, S. Gupta, J. Saikiran, R.S. Bharj, Performance evaluation of photovoltaic module integrated with phase change material-filled container with external fins for extremely hot climates, Journal of Energy Storage. 32 (2020) Article ID: 101876.
[22] M. Khodadadi, M. Sheikholeslami, Numerical simulation on the efficiency of PVT system integrated with PCM under the influence of using fins, Solar Energy Materials and Solar Cells. 233 (2021) Article ID: 111402.
[23] M. Sivashankar, C. Selvam, S. Manikandan, S. Harish, Performance improvement in concentrated photovoltaics using nano-enhanced phase change material with graphete nanoplatelets, Energy. 208 (2020) Article ID: 118408.
[24] K. Velmurugan, S. Kumarasamy, T. Wongwuttanasatian, V. Seithtanabutara, Review of PCM types and suggestions for an applicable cascaded PCM for passive PV module cooling under tropical climate conditions, Journal of Cleaner Production. 293 (2021) Article ID: 126065.

Annexe 1.8

Évaluation comparative de différents suiveurs solaires : Vers une conception rentable, facile à mettre en œuvre et à haut rendement

Comparative assessment of different solar trackers: Towards a cost effective, easily implemented and high efficiency design

Khaled Osmani[3], Ahmad Haddad[1,2], Thierry Lemenand[3], Bruno Castanier[3] and Mohamad Ramadan[1,2,*]

[1]School of Engineering, International University of Beirut BIU, Beirut, Lebanon

[2]School of Engineering, Lebanese International University LIU, Bekaa, Lebanon

[3]LARIS EA 7315, Polytech Angers, UNIV Angers, France

mohamad.ramadan@liu.edu.lb

Abstract: For an efficient operation of PV systems with maximum power extraction, carried out by minimizing the capture losses of radiations, and by ensuring that PV panels are exposed in a perpendicular way under sunrays, this paper aims first at exploring different classification standards for solar trackers (STs). Control systems are at first, founded as either open or close looped structuring. The driving mechanisms, as either active or passive are the second label in STs classification. Moreover, the number of moving axis is the third trackers' characterization, based as either a single-axis or double-axis platforms. The final destination for classifying a solar tracker is its tracking strategies encapsulated as either processor based, date and time based or a combinational scheme between date/time and sensors. A critical comparison between different methodologies in each criteria is established to conclude an efficient ST design based on advantages and disadvantages of various models. An economical statement is conducted as well, to see how worthy it is to install an ST within a PV system. This work would serve as an informative background for researchers in field to help in designing an accurate case-specified solar tracker. A future model of an ST at the end is proposed, granting from most advantageous classification of each term.

Keywords*:* Closed-loop, dual-axis, passive, irradiance, PV panel, solar tracker.

Nomenclature

AC	Alternating Current
AI	Artificial Intelligence
ANN	Artificial Neural Network
BTU	British Thermal Unit
CGF	Compressed Gas Fluid
CPC	Compound Parabolic Concentrator
DAT	Double Axis Tracker
DC	Direct Current
FL	Fuzzy Logic
FLC	Fuzzy Logic Controller
HOMER	Hybrid Optimization Model for Electric Renewable
LCD	Liquid Crystal Display
LDR	Light Dependent Resistor
MPPT	Maximum Power Point Tracking
MW	Mega Watts
NiTi	Nickel-Titanium
Op-Amps	Operational Amplifier
PID	Proportional Integral Derivative
PLC	Programmable Logic Controller
PLD	Programmable Logic Device
PV	Photo Voltaic
RS232	Serial Communication Standard Protocol
RSM	Reluctance Stepper Motor
SAT	Single Axis Tracker
SMA	Shape Memory Alloy
ST	Solar Tracker
Greek letters	
δ	Declination, º
ω	Hour, º
φ	Latitude, º
α	Altitude, º
Φ	Zenith, º
γ_S	Azimuth, º

1. Introduction

Increased energy demands, as a result of civilization progress, yields to tyrannical exploitation of conventional (non-renewable) energy supplies [1]. Power consumption from non-renewable stocks, get inflated in a way, leaving fossil fuels, natural gas, diesel and other forms of classical energy residuals in shortage [2]. The necessity of finding green renewable energy supplies, become societies' recent fatiguing challenges [3-6], since non-renewable energy forms led to high emissions of greenhouse gases, and much environmental damages [7-10].

Global emissions which contribute in climate changing and global warming [11-12], are directly linked to heavily populated countries. India for instance, produces alone 7% of total global emissions, while doubling the primary consumption to 32 quadrillion BTU (British Thermal Unit) [13].

On the other hand, renewable energy supplies (solar, wind, hydro, etc.) show a solid potential, for meeting bulky load demands [14]. In particular, solar power gained most popularity among different forms of renewable energies for its omnipresent characteristics and low maintenance costs [15]. Due to the abundancy of solar radiations, where $1.2 \cdot 10^5$ TW of energy hit the earth's surface continuously [16], PV systems gained huge popularity, as an interface of recommended green energy supply [17].

Accordingly, evolution in renewable energy is globally witnessed, where in China, the market share of Chinese PV has increased from 1% to 35% from 2002 to 2010, and the yield of PV power output increased from 2.6 MW in year 2000 to 2000 MW in year 2008 [18].

Due to the increase in PV systems usage, ample researches took place for designing optimized techniques to extract as maximum as available energy from solar radiations [19-24]. The output generated by such systems is dependent on quantity of radiations collected [25]. Part of incident sunrays are scattered or absorbed by air molecules [26]. From another part, the environmental surrounding conditions, day/night variations and PV faults interference can reduce the expected power output of such systems [27-29]. Due to all precedent reasons, and for the sake of maintaining an efficient, reliable and durable PV output, solar trackers along with MPPT (Maximum Power Point Tracking) are the most common procedures to ensure maximum energy harvesting from PV systems [30-33].

In other words, in order to increase both output and efficiency of the overall PV system, various applications, deploying sun tracking can accomplish this target [34]. Solar trackers are noticed elevating the efficiency, while maintaining a solid output of a PV system, when tracking the position of the sun according to seasonal/day-time attributes [35]. Such devices put down PV panels, according to certain angular positions [36], in the most exposable way to solar radiations, while precisely locating the position of the sun. This happens by compensating changes in daily altitude angles, seasonal latitude offset and changes in azimuth angle of the sun [37].

Solar trackers implemented within PV systems, have 0 to 100% energy gains, compared to static PV systems [38]. The design of such devices, is of crucial importance, since the same solar tracker can have different energy gains under different climatic environments [39]. For instance,

the usage of same solar tracker in two environmentally opposite areas (cold: Berlin, hot: Aswan) showed a 39% increase in energy gain for the first area, and 8% for the second area respectively [39]. Whereas the cumbersome movement of the sun, and shading caused by clouds, requires a non-oscillatory control system for an optimum operation of the tracker [40].

Put to say, a solar tracker in turns needs a cooperative control technique and optimization methods [41]. Its design must take into consideration the number of tracking axes [42-44], the control system [45-48], the driving mechanisms [49-52] and the tracking proposals [53-54]. Each of the design criteria, presents different modes of operation, advantages, and disadvantages [55].

In this paper, the classification of different solar trackers will take place according to the pre-mentioned design standards. The control strategies for instance are found as either closed-loop or open-loop controls. The driving mechanisms are classified as either passive or active techniques. For the number of axis of rotation, solar trackers are either single-axis or dual-axis based. As for the tracking strategies, they can either rely on date and time, a decision making processor inputted by electro-optical sensors, or by combination of sensors and date/time perspective. Within each set of categorization, different sub-methods will be mutually compared, and linked to foreign sets, conducting a cost-effective, reliable and efficient solar tracker design.

2. Solar radiation angular study

A proper ST design must take into consideration, the site related, different incident/reflection angles of solar radiations. Since earth is in continuous movements, around the sun and around itself, this reflects as instantaneous difference in incident angles, throughout different times of the day, season and year. Designing attributes of the ST must be carefully studied to accommodate this truth, in a way that, input parameters to the design, must cover all differences in incident angles, solar beam, etc. throughout the entire year, for the uniqueness of ST's site of implementation.

The motion of the earth towards the sun is characterized by an elliptic plane, resultant of the elliptical orbit of earth's trajectory [56], where the position of the sun with respect to earth is defined by the celestial sphere around the earth [57]. The line joining both centers of earth and sun, and its corresponding projection on the equatorial plane results in the solar declination angle δ [58]. When earth rotates around its polar axis, the celestial sphere in parallel rotates around same polar axis. Accordingly, the instantaneous position of the sun is defined by the hour angle ω [59].

The angle resulting from the radial line joining the location of earth's center with the projection of same radial line on the equatorial plane, denotes the latitude φ of a point [60]. Consequently, any location (of PV panels, arrays, etc.) on the earth's surface can be defined by the intersection of both latitude and longitude angles [61].

For the case of ST implementation, an accurate latitude/longitude angles acknowledgment, gives a boost for its proper design, since knowing such angles will give a clear idea about the status of solar irradiation, as well as number of hours of radiance. The three angles of solar declination, hour angle and latitude are shown in Fig. 1.

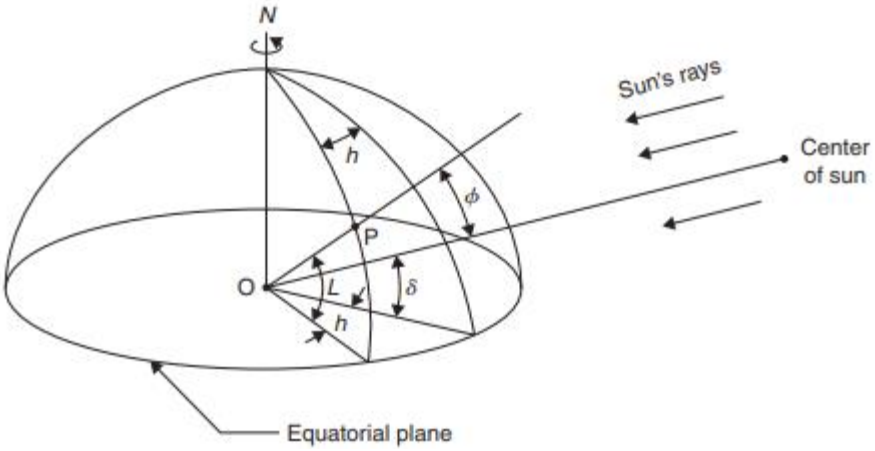

Fig. 1: Graphical representation of solar declination angle (δ), hour angle (h), latitude (L) [62]

The vertical angle between the projection of sunrays on the horizontal plane and the direction of sunrays passing through a point is defined as solar altitude α [63] shown in Fig. 2.

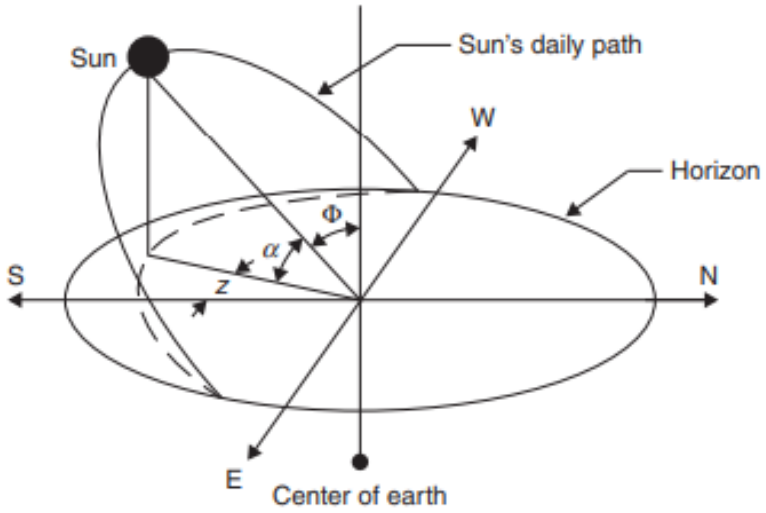

Fig. 2: Solar altitude angle [62]

A complementary angle to solar altitude α, indicated as solar zenith angle Φ, is the angle between the sun's disc and the zenith [64]. The zenith angle can be an alternative to solar altitude, since its cosine equals the sine of the other.

The horizontal angle measured in the northern hemisphere to the horizontal projection of sunrays is designated by solar azimuth angle γ_S [65]. Table 1 groups different solar angles, necessary to be taken into consideration when designing a solar tracker.

Angle	Description
δ	Solar declination angle: between the equator, and a line joining both centers of sun and earth
ω	Hour angle: is the angle between two planes, one containing the earth's axis and meridian plane, the other including the earth's axis and destination point
φ	Latitude: angle that ranges between 0° and 90° created by the radial line joining earth's center with its projection on the equatorial plane
α	Solar altitude angle: between the horizontal and the line to the sun
Φ	Solar zenith angle: between the zenith and the center of the sun's disc
γ_S	Solar azimuth angle: angular displacement resulting in east, west or south positioning

Table 1: Description of different solar angles

After recognizing different angular measurements resultant from motion/positioning of earth and sun respectively, recorded as references for an optimum solar tracker design, turn comes for calculating the energy input to PV systems.

The geographical data of the site in process (where the installation of ST is assumed to be) are needed to determine direct-beam and diffuse radiations [66-68], such as:

- Direct-beam radiation: passes a straight line through the atmosphere to the receiver (PV panels)
- Diffuse radiation: scattered in the atmosphere or absorbed by air molecules.

The direct beam radiation calculation, places the capture area in specific conditions [69], in which the power received on it is given by Eq. (1):

$$I_{DIR} = A \cdot e^{(-k \cdot m)} \quad (1)$$

where A is the apparent terrestrial flux, k is the optical depth and m the relative path's length traveled by solar radiations through the atmosphere [69].

On the other hand, the diffused radiations, caused by shading contributors (clouds, aerosols, etc.), permits the diffused power calculation received on capture area (after losses) as shown in Eq. (2):

$$I_{DIf} = C \cdot I_{DIR} \cdot R_{Dif} \quad (2)$$

where C is a constant, I_{DIR} is the direct received power and R_{Dif} the correction factor on the diffused radiation [69].

Calculating both I_{DIR} and I_{DIf} allows the calculation of the total daily irradiation, whose value will be used as a reference value for estimated daily radiation (according to geographical site attributes) within ST design. Any value that is more/less than the calculated total daily irradiation (with a permissible range of error) resets the solar tracker to correct its work by changing its movement.

3. Classification of solar trackers

Solar trackers are systems that aim to position PV panels towards the sun to achieve as maximum radiations as possible. Their orientation is continuously modified throughout the day, to follow the sun's maximum radiation path. Such trackers help in minimizing the incidence angle between incoming radiation beam and PV panels. The dedicated function for STs can be achieved using different structures [70-71].

On the first hand, STs' control systems judge the overall performance and data acquisition for various physical quantities (current, irradiance, etc.) [72]. On the other hand, driving mechanisms indicate how the motion is commanded [73]. From another part, rotation axis defines how the motion is directed [74], and finally tracking mechanisms enfold the set of reference values, algorithms and methods of identifying where the radiation's peak is taking place at [75]. Table 2 encapsulates different classifications of STs, which are deeply described in the following sections.

Classification criteria	Identification
Control systems	Open-loop
	Closed-loop
Driving mechanisms	Passive trackers: by means of Freon, shape memory alloy, bimetallic strips, thermal actuator, thermo-hydraulic actuator
	Active trackers: based on motors (AC, DC, universal, stepper, etc.) which displace the panels by means of mechanical shafts, operated by computerized systems
Number of moving axis	Single-axis
	Dual-axis
Tracking scheme	Algorithm based via processor
	Date and time
	Sensors and date/time based
	Bifacial solar cell based

Table 2: Classification of solar trackers

3.1. Classification of ST based on control systems

3.1.1 Open-loop

The command is driven to motor/moving actuators based on implementation algorithm and present-state data input (temperature, irradiance, etc.). Open-loop control systems do not present any analysis of output data [76]. Feedback signals between output and input are absent, in a way that, no comparison is ever held between actual and desired outputs [77]. Compared to closed-loop control systems, such strategy is cheaper and simpler to implement but with less efficiency [78]. Fig. 3 reveals the general block diagram structure for an open-loop control system.

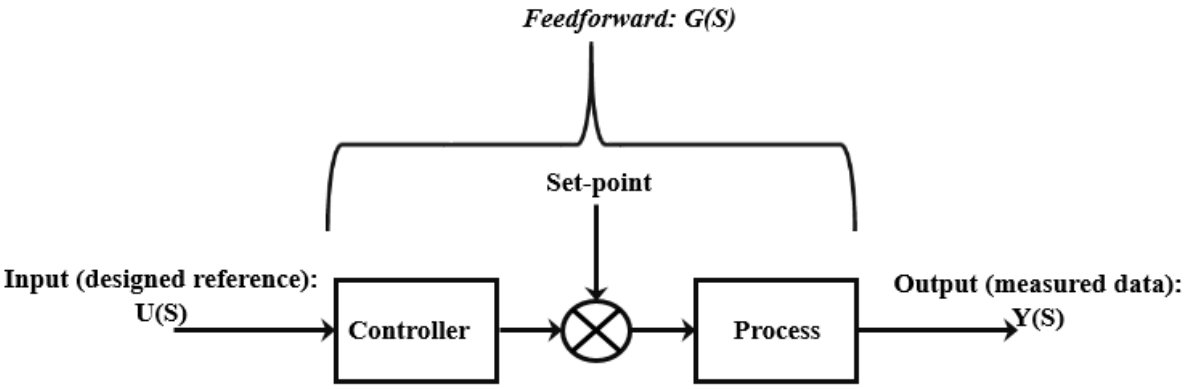

Fig. 3: General block diagram structure for an open-loop control system

In Fig. 3, $S = j \cdot \omega$ is the Laplace transform, the transfer function $H(S)$ for an open-loop control system is shown in Eq. (3).

$$H(S) = \frac{Y(S)}{U(S)} = G(S) \tag{3}$$

3.1.2 Closed-loop

Such control scheme deploys sensors in order to detect the sun's position. Once this position is acknowledged, it passes through feedback to the comparative node of the system, where accordingly the deviation error is calculated [79-80]. By compensating the resultant error, all required actuating signals are fed to the driving mechanisms, in a way, to modify the position of solar panels to minimize the error. Fig. 4 shows the general block diagram structure used in closed-loop systems.

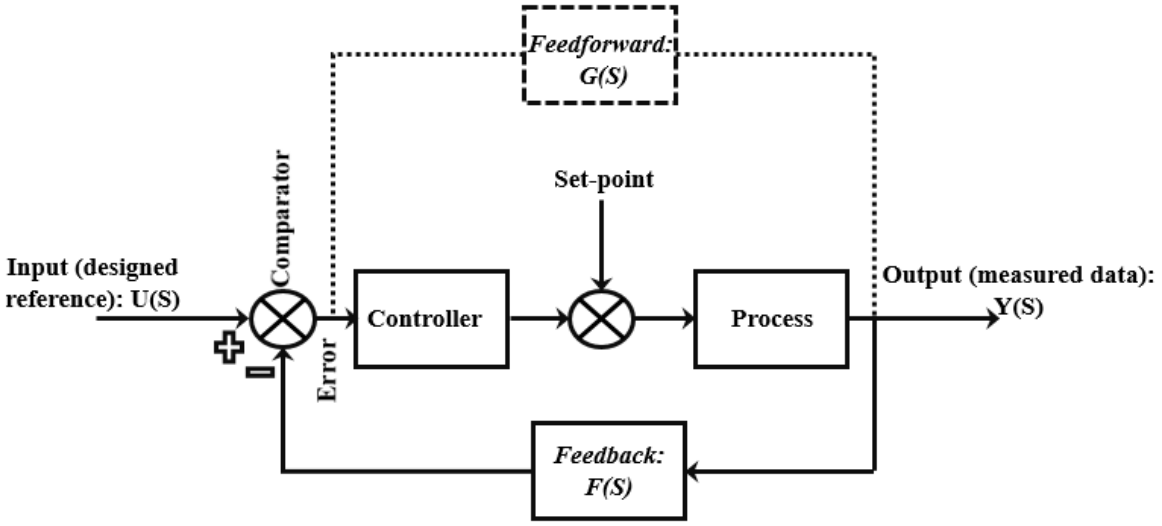

Fig. 4: General block diagram structure for a closed-loop control system

By means of Laplace transform, the transfer function $H(S)$ of a closed-loop control system is shown in Eq. (4).

$$H(S) = \frac{Feedforward}{1 + Feedforward \cdot Feedback} = \frac{G(S)}{1 + G(S) \cdot F(S)} \tag{4}$$

The process block in both Fig. 3 and 4 corresponds to the driving mechanisms, whether they are active or passive. For the controller, in both control manners, various natures exist, where it can be a microprocessor, a proportional P, integral I, derivative D, or mixture in between, such as PI, PD and PID controllers [81]. With K_p, K_i and K_d representing the gains for a proportional, integral and derivate controller respectively, different block diagram structures of PI, PD and PID controllers, that can be used in solar trackers are shown in Fig. 5.

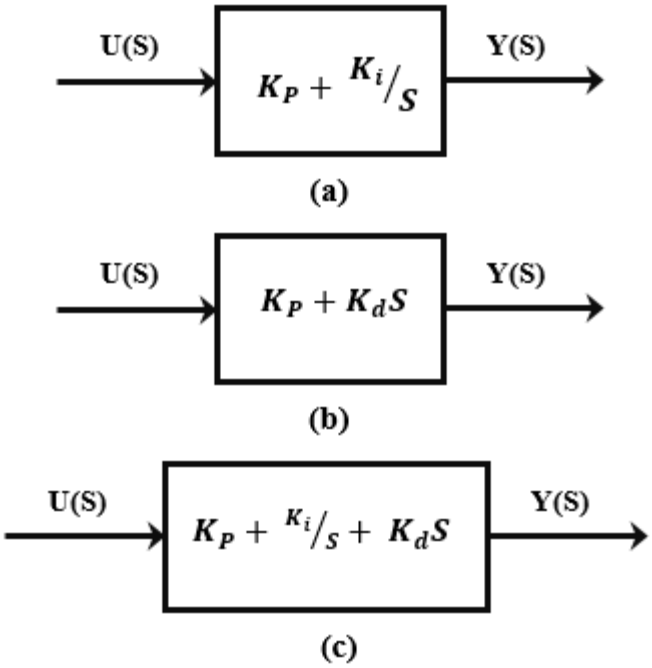

Fig. 5: Gain function for (a) PI controller, (b) PD controller and (c) PID controller

With dissimilarity between the different control schemes, Table 3 encapsulates comparative criteria between both open and closed loop control systems.

Design	Open-loop control	Closed-loop control
Measurement of output		●
Comparison with input		●
Error based control		●
Simplicity	●	
Cost effectiveness	●	
Faster operation	●	

Table 3: Comparison between open and closed loop control topologies

3.2. Classification of ST based on driving mechanisms

3.2.1 Passive STs

Without any intervention of mechanical drives (stepper motors, induction motors, etc.) and in order to adjust PV panels' orientation, passive driving scheme uses the following attributes as actuators [82-84]:

- Compressed gas fluid
- Shape memory alloys / memory foam

When unbalanced illumination is received on any of the two actuators, PV panel is forced to undergo angular movements in a way, to re-compensate equilibrium of irradiance. This can be done after thermal expansion of the compressed gas, or by re-structuring of the shape memory alloy [85-86]. Fig. 6 explores a passive ST with a pair of identical cylindrical tubes, filled with a compressed gas fluid.

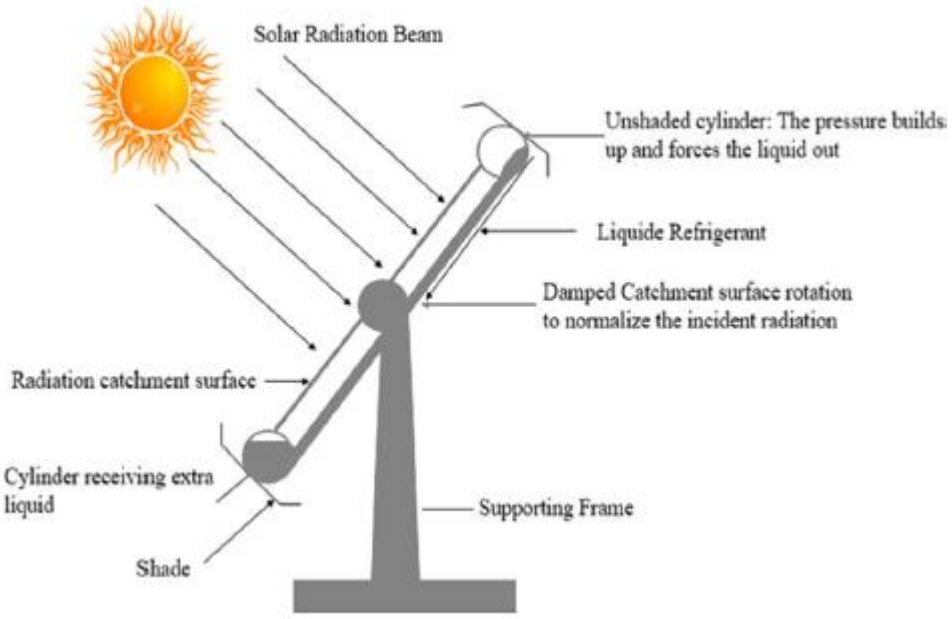

Fig. 6: Example of a passive ST driven by thermal expansion of compressed gas [87]

When one side (either top or bottom) of gas containers shown in Fig. 6 receives more sunlight than the other, the gas expands and move towards the opposite direction. This process is kept continuous until a point of equal illumination is reached [88]. In other words, a weight difference is created by liquid gas to displace the entire PV module into new coordinates that match as possible as homogenous illumination across the entire surface of the module.

For the case of passive STs operated by SMAs (Shape Memory Alloys), the orientation of PV panels is driven through their sizing modification when subjected to temperature/magnetic field effects [89-90]. A mechanical push re-positions the coordinates of the panel during SMAs

expansion/abridgment [91]. According to shape change, three different categories can be classified for SMAs as follows:

1. One-way shape memory effect: The SMA returns into its original form after heating (by ambient temperature), where in absence of external force (heating) it develops into a deformed state [92].
2. Two-way shape memory effect: a two-way SMA can recognize its shape, under both high and low temperatures [93].
3. Pseudo-elasticity or Super-elasticity: For such SMA, there is no need for any thermal activation, to return to its original shape. Instead, the reshaping process happens upon application of mechanical loading under borderline temperature values [94].

The design of an SMA is a chemical process that can include Nickel-Titanium (NiTi) and other intrinsic materials for its fabrication [95]. A stable passive ST design for a PV system must be carefully implemented with a relevant type of SMAs. Table 4 explores a comparison for different actuator types for SMAs.

Actuator type	Stress (MPa)	Strain (%)	Efficiency (%)	Bandwidth (Hz)	Work per volume (J/cm^3)	Power per volume (W/cm^3)
NiTi SMA	200	10	3	3	10	30
Piezoceramic	35	0.2	50	5000	0.035	175
Single crystal piezoelectric	300	1.7	90	5800	2.55	15000
Human muscle	0.007-8	1-100	35	2-173	0.035	0.35
Hydraulic	20	50	80	4	5	20
Pneumatic	0.7	50	90	20	0.175	3.5

Table 4: Comparison of different SMAs compositions [96]

A passive ST design is more dependent for solar angular data shown in Table 1 than active STs. Since their performance is not automated, designers must bear in mind, upon site installation, seasonal north/south orientation adjustment, which is in turn relevant to α, δ, φ and other solar incidence related angles.

Passive STs can operate for a prolonged amount of time, where no induced high torque will be present across PV frames. The tight welding between PV panels and containers (of gas or alloys) make them resistant to degradation and tear.

Compared to active driving mechanisms, this technique is less complex and cheaper with decreased maintenance costs, since their design require less equipment. In terms of reliability, passive STs are suitable, as they don't need any extra power consumption. This fact increases the overall power production efficiency of the PV system.

From another perspective, passive STs suffer from reduced efficiency under cold temperature environment, where in some cases, were seen non-functional.

3.2.2 Active STs

Centered on using electrical drives and mechanical actuators (i.e. motors), helping in achieving a better power output [97-103], active STs orient PV panels normal to sun's radiation (in a perpendicular way) by means of:

- Sensors / Bifacial solar cells: as input
- Microprocessors / comparators: as decision making blocks

Unlike thermal expansion used in passive solar trackers, active STs command motors to re-orientate PV modules according to illumination captured by LDR (Light Dependent Resistor) and other photo-electric sensors. A differential signal is created after non-homogeneous illumination is received by input modules, which is later on fed to the microprocessor or comparator [104-105]. The appropriate movement (towards left or right) in the convenient direction (vertically or horizontally) is hence conducted by the differential signal. Fig. 7 exposes a representation for an active solar tracker.

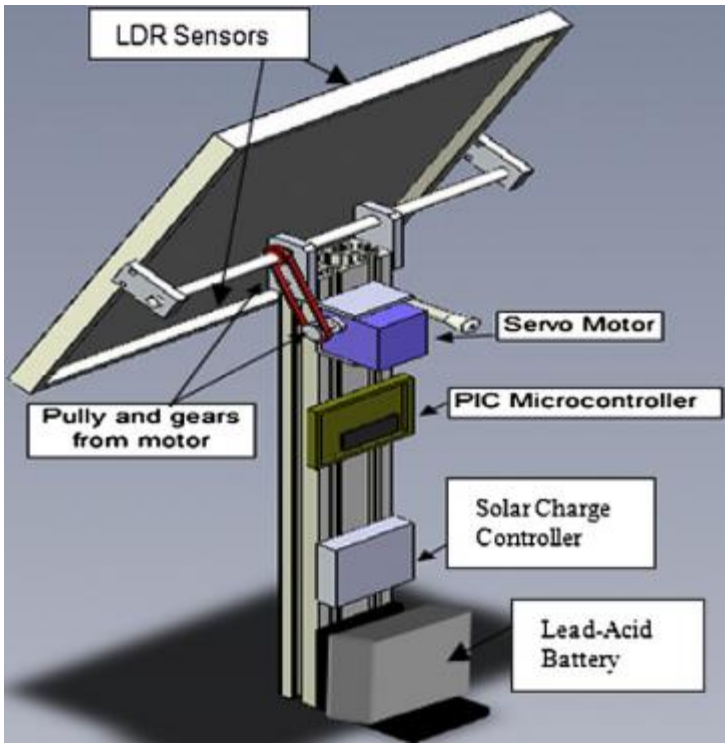

Fig. 7: Design of an active ST [106]

The orientation process halts when all sensors receive equal illumination while continuously monitoring the states of ADC (Analog to Digital Conversion) captured by the sensors. A fast and adaptive compensation of the positioning error is hence held.

The central making order block can be a PLC (Programmable Logic Controller), employed to control and monitor the mechanical movements of hydraulic drives. The tracking error of the system was found less than 0.6 degrees [107]. When automated with a Siemens S7-300 PLC, a supervisory control is implemented in active STs with function modules consisting the bridge of communication between the PLC and step motors actuating blocks. For users' communication a multi-option exists (either local or remote), where radiation quantity is measured using an auxiliary PV cell. Fig. 8 reveals the electro-mechanical structure of the proposed model [108].

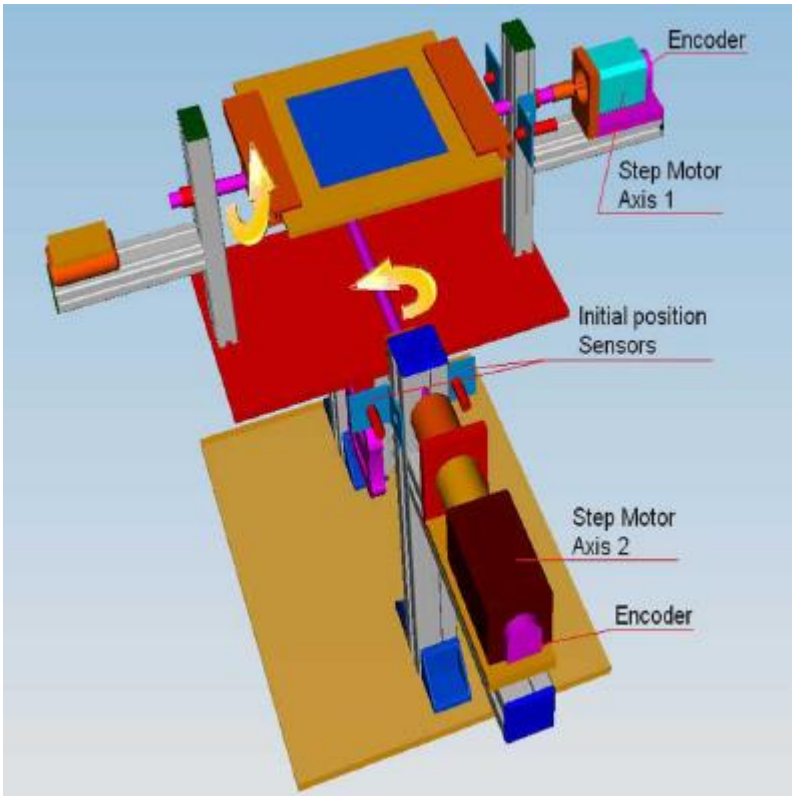

Fig. 8: General overview of proposed solar tracker structure [108]

For the cases of angular tracking error, occurring within active STs performance, it can be reduced to be fit in the interval of $[-0.4°; +0.4°]$ by adapting a testing procedure technique from the international standard IEC 62817 [109].

Various coding languages can be implemented inside the processor label. By usage of FLC (Fuzzy Logic Control), an FPGA (Field Programmable Gate Array) the processor can be programmed in a way overcoming drawbacks of conventional PID controllers. System's non-linearity were seen better compensated. The FPGA drives the DC motor to keep the PV panel aligned with sun's direct incidence, with the help of an optimum tilt angle determination and optimum orientation [110].

In a similar fashion of employing FPGA in a central decision making unit, a PLA (Programmable Logic Array) can control a four-phase RSM (Reluctance Stepper Motor). The

angular position resolution is of 7.5° of accuracy, stable at this value due to locking of RSM at each stop by means of a power converter [111]. Fig. 9 reveals the tracking system with RSM control.

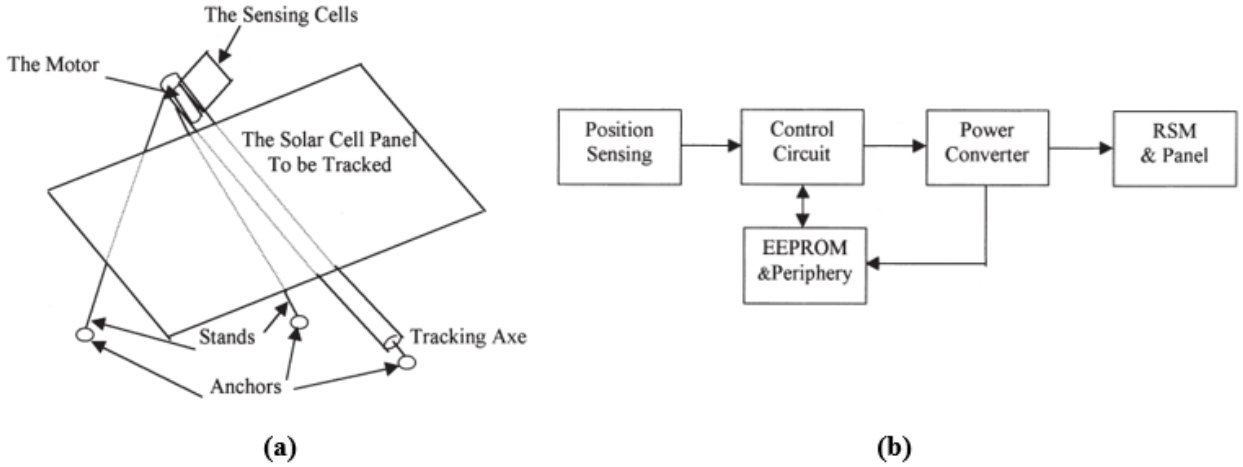

Fig. 9: (a) the tracking system of the proposed model, (b) RSM control attributes [111]

During sun tracking process, unnecessary scans are often employed within circuitry design, referred to as haunting. The process of haunting can be eliminated (to increase positioning operational time) with a convenient design of microprocessor controlled motor drive circuit [112].

As a miniature of the microprocessor control design in reference [112], an active solar tracker design based on a microcontroller instead, with four LDRs (Light Dependent Resistors) as input and two servomotors as switching gear, employed at the backside of PV panel, can increase up to 19.73% in output power. Considering other active STs' designs, this model possesses a considerably higher than 15% average efficiencies [113]. A wide varieties of microcontrollers as central decisive unit for an active solar tracker exist [114-116], where the recruitment of a new solar sensor can be used to produce an 18% gain of output power [117].

Using a tri-positional control strategy as shown in Fig. 10, the corresponding algorithm when implemented on a solar-tracking experimental platform, allows a fast deployment for STs' implementation. Radiation quantities are obtained from appropriate sensors, where two positioning motors at the actuating stage, ensure that the PV panel is in optimum orientation [118].

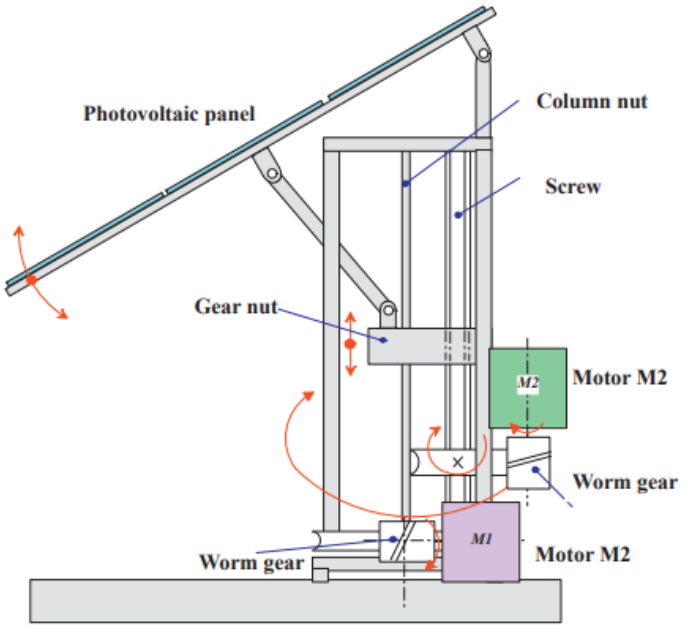

Fig. 10: Mechanical control strategy for an active ST [118]

The sun's apparent motion during an entire year can be followed by means of a parallel kinematic machine of U-2PUS type. The synthesized mechanism is able to operate at latitudes between (0°; 50°) [119]. Fig. 11 shows the corresponding optimized mechanism flowchart, where it would only be satisfied, if the sun workspace W_S is included in the mechanism workspace W, and the i^{th} joint torque τ_i does not reach a limit value $\tau_{i,max}$ with no joints collided.

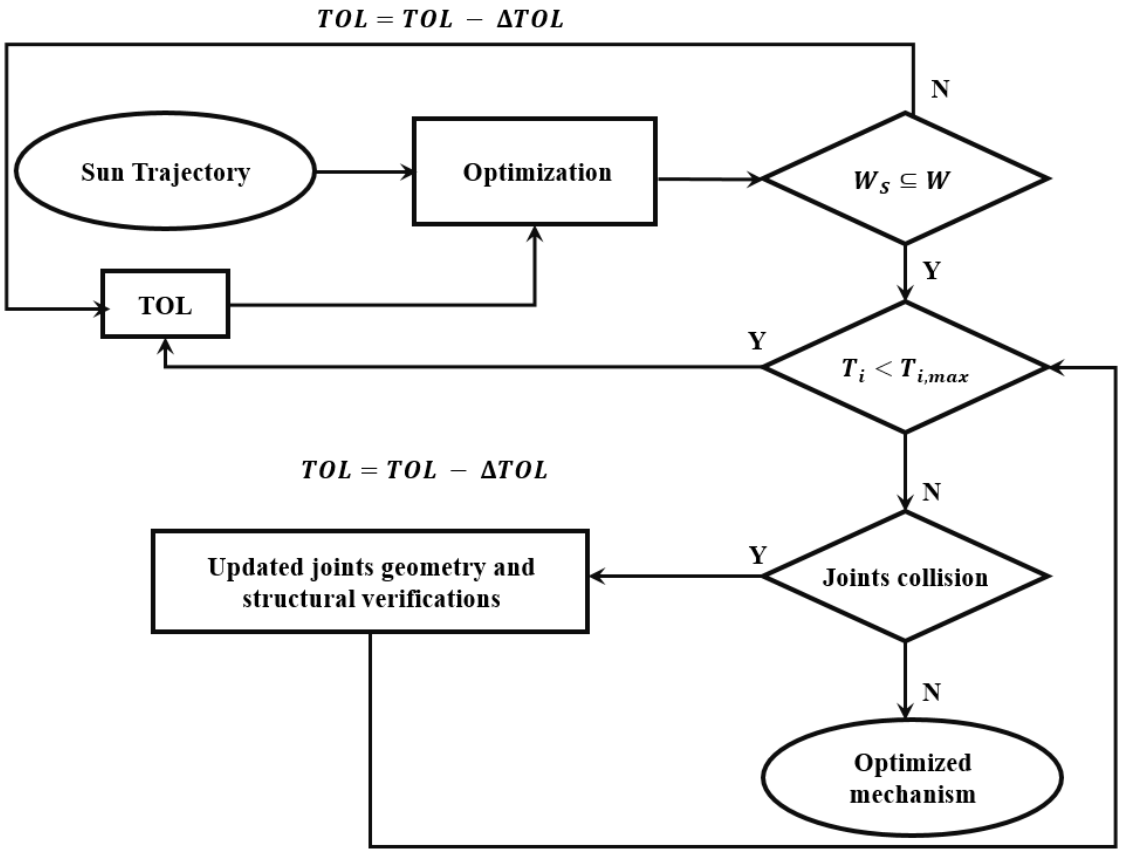

Fig. 11: Optimization flowchart [119]

In terms of popularity, reliability and system's robustness, active STs succeed over passive ones, due to better dynamic monitoring and accurate adjustments of PV modules positioning. On the other hand, active trackers are found to encounter more complexities in design, with the need of extra equipment. Accordingly, both maintenance costs and time are increased in turn.

3.3. Classification of ST based on number of moving axis

3.3.1 Single axis

Single Axis Trackers (SATs) are one type solar trackers, involving a single axis that round which, the motion of a PV panel can be adjusted to align the panel's normal to sun's horizontal [120-135]. In other words, the sun is tracked from one point to another by means of single rotating pivot point, providing only one degree of freedom [136-143].

Some of these trackers (HSAT, i.e. Horizontal SAT) have their axis of rotation in horizontal position with respect to the ground, where the system's frontal lobe is oriented in parallel to its axis of rotation. Other trackers (i.e. VSAT for Vertical SAT), have their axis of rotation in vertical with respect to the ground, where the system's front side is oriented through an angle with respect to its axis of rotation [144]. Including several architectures, SATs include different structures encapsulated in Table 5.

Refs.	SATs	Definition	Description
[145]	HSAT	Horizontal SAT	Aligned with North and South, these trackers follow sun's direction from rise until set
[144]	HTSAT	Horizontal with Tilted module SAT	Operate same as HSAT, but are mounted with a certain tilt
[146]	VSAT	Vertical SAT	Follow sun's motion path around a vertical axis
[147]	TSAT	Tilted SAT	Have a rotational axis centered between both horizontal and vertical axes
[148]	PSAT	Polar aligned SAT	Mounted with same manner as telescopes

Table 5: Characterization of different SATs

With a direct connection of an auxiliary bifacial solar panels to a DC motor, a coordination is established between sun's tracking and the motor [149], where an increased yearly energy gain by 17.5% is obtained after fixing a PV cell on a SAT [150]. Fig. 12 displays hardware topology of a terrestrial tracker with a single-axis motion.

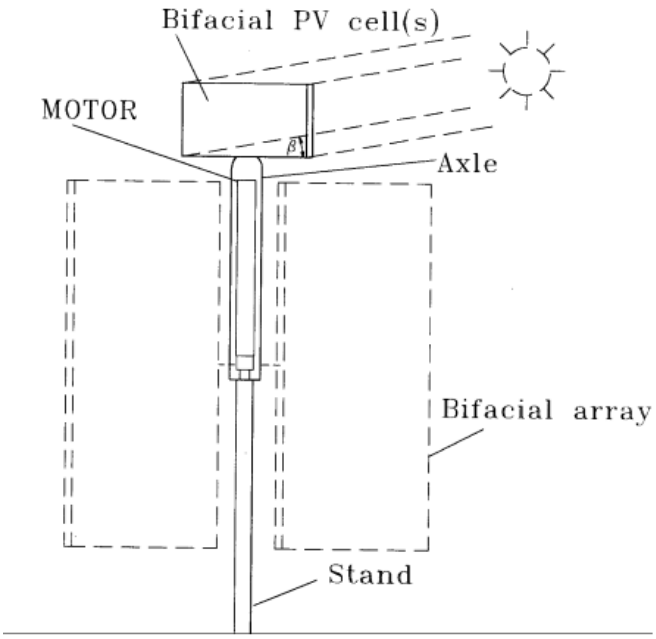

Fig. 12: Single axis terrestrial tracker topology [149]

Similarly, within a 15º/hour rotational speed, following the polar axis, a SAT based solar collector has shown ability in tracking the sun's motive path accordingly, with ability to predict

the thermal efficiency. An increased thermal efficiency of 14.9% higher than fixed CPC (Compound Parabolic Concentrator) were shown [151].

A bi-directional movement by means of a special support fixture as shown in Fig. 13 is enabled for a SAT azimuthal-tracker, where (1) indicates the collector plane, (3) the main rotational axis and (8) the oblique slot [152].

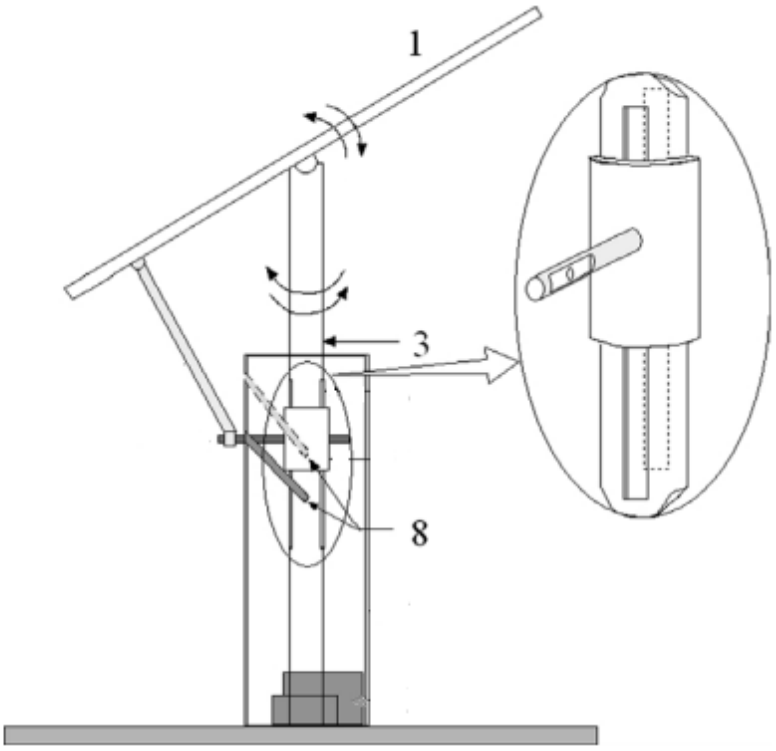

Fig. 13: Azimuthal heliotrope schematic that can be used in PV tracking [152]

With positioning manipulations on a single axis tracker, a three different angles orientation (3-positions) can be obtained using a SAT with a DC motor as rotating actuator. The algorithm is implemented on PIC18F452 as a central decision unit. A triggering signal for the motor is established using a timer IC (Integrated Circuit). The study [153] has shown that if the single axis three positioned solar tracker is used in an area of high solar energy resource, the long term generation of PV power can increase to more than 37.5% with respect to static PV systems. Fig. 14 reveals the design of the 3-positioned SAT.

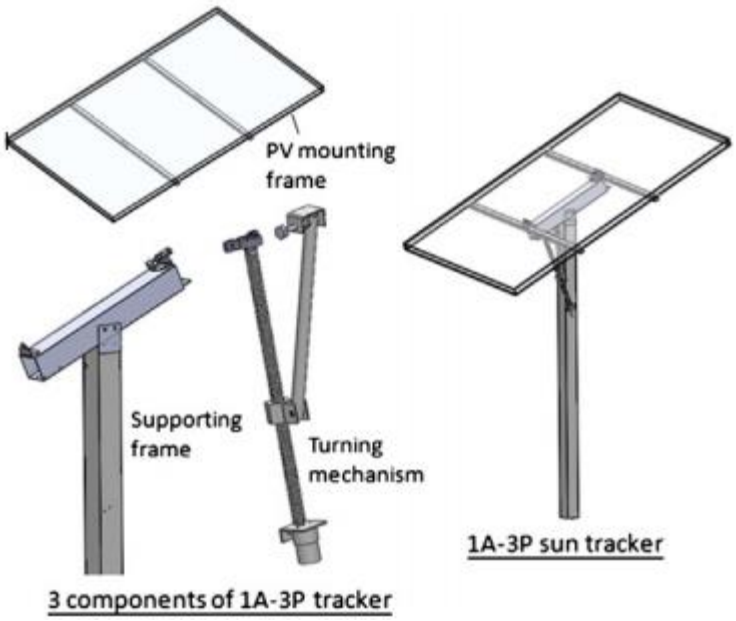

Fig. 14: Single-axis three-position ST [153]

While not being affected by geographical attributes of ST's installation site, the maximum solar irradiance in the entire azimuth angle of 360º, can be reached when using an automated SAT. From one side, the PV panel is optimally tilted. Concerning the secondary side of the same panel, its positioning is controlled by the tracker [154].

Comparing both a static and a passive-tracked PV system versus a SAT based one, results show better power generation efficiency when using SATs. The maximum power extraction is better achieved, where irradiance losses, due to continuous earth's movement and barriers shading (clouds, trees, etc.) are better compensated. The comparative studies between fixed and SAT based PV systems show better energy gain for solar tracked PVs. In terms of cost of installation, and with a better power outcome, the cost of return might be accelerated upon using SATs [155-158]. In terms of popularity and real systematic installations within PV systems, SATs based PV systems succeed over static PVs. However, such equipment are considered as extra installations on PV systems, what could increase system's overall costs. On the other hand, these devices can break, interfere with different faulty scenarios and cause further external damages to PV panels. This in turn elevate from maintenance costs of the system. Compared with other multi-tracking axes based solar trackers, SATs are seen less efficient than double-axis STs [159-161].

3.3.2 Dual axis

With dual axis of rotation, DATs (Double Axes Trackers) are given two degrees of freedom (north-south and east-west) where accordingly sun ray's facing throughout the daily is better achieved [162]. Although SATs are cheaper and less complex in designs than DATs, numerous researchers were conducted to promote the usage of double axes trackers due to their elevated efficiencies [163-165]. According to maximum solar radiation absorption capabilities and consistent production of maximum energy, DATs were found top trackers based on degree of freedom [166]. Fig. 15 reveals general double-sided movements of DATs.

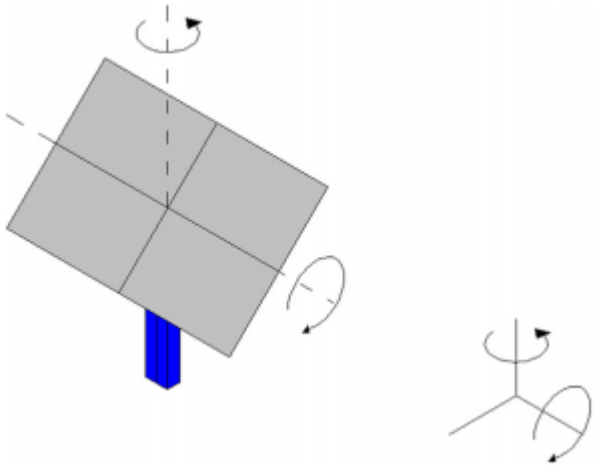

Fig. 15: DAT characteristics movements [167]

To keep the sun's image centered into the four-quadrant photo-detectors (which are used to sense the sun's position) plane, two DC motors move the PV module accordingly. For scenarios of partial shading, an algorithm estimates the sun's position by calculation, until the sun is visible again. Fig. 16 shows the mechanism control for the double-axis tracker, having φ_s (solar angle) and φ_m (moving mechanism direction) as inputs and h, e as indexes for HH axis (east-west motion axis) and EE axis (elevation axis) respectively [168].

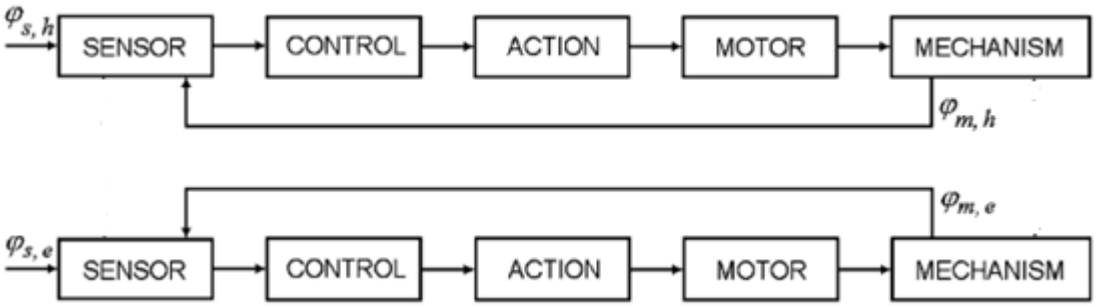

Fig. 16: Transfer function for double axis [168]

Based on the processing images of a bar shadow using a webcam, a DAT is proposed [169], composing of electronic circuits, computer controls and stepper motors. With an accuracy of $\pm 2°$, the system kept the PV panel perpendicular to irradiations' direction, thus generating as highest as possible of power at the output. Fig. 17 clarifies the rotation orienting steps for the PV panel, according to processed object's size.

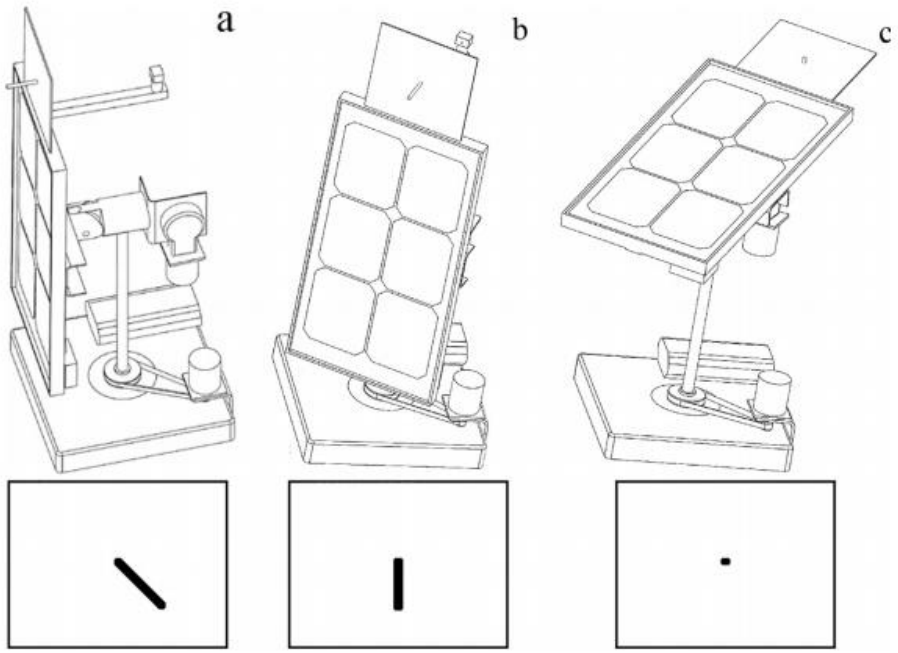

Fig. 17: Different orientations scenes (a, b and c) according to different processed images [169]

An open-loop controlled DAT, based on input captured by photo-sensors, has shown an acceptable degree of accuracy between referenced (calculated) and measured (actual), both azimuth and zenith angles [170]. Fig. 18 encapsulates the flowchart of the algorithm used in the DAT's solar tracking process.

The tracking process shown in Fig. 18 is decomposed into two parts: the first corresponds to on/off switching processes of the azimuth DC motor (aDCm), the other for zenith DC motor (zDCm). Both stages' flowcharts only starts if unequal illumination is received by Light Dependent Resistors (LDRs). As a results, aDCm and zDCm motors are power cut off, if each of their correspondent Limit Switches (LS) is conducting.

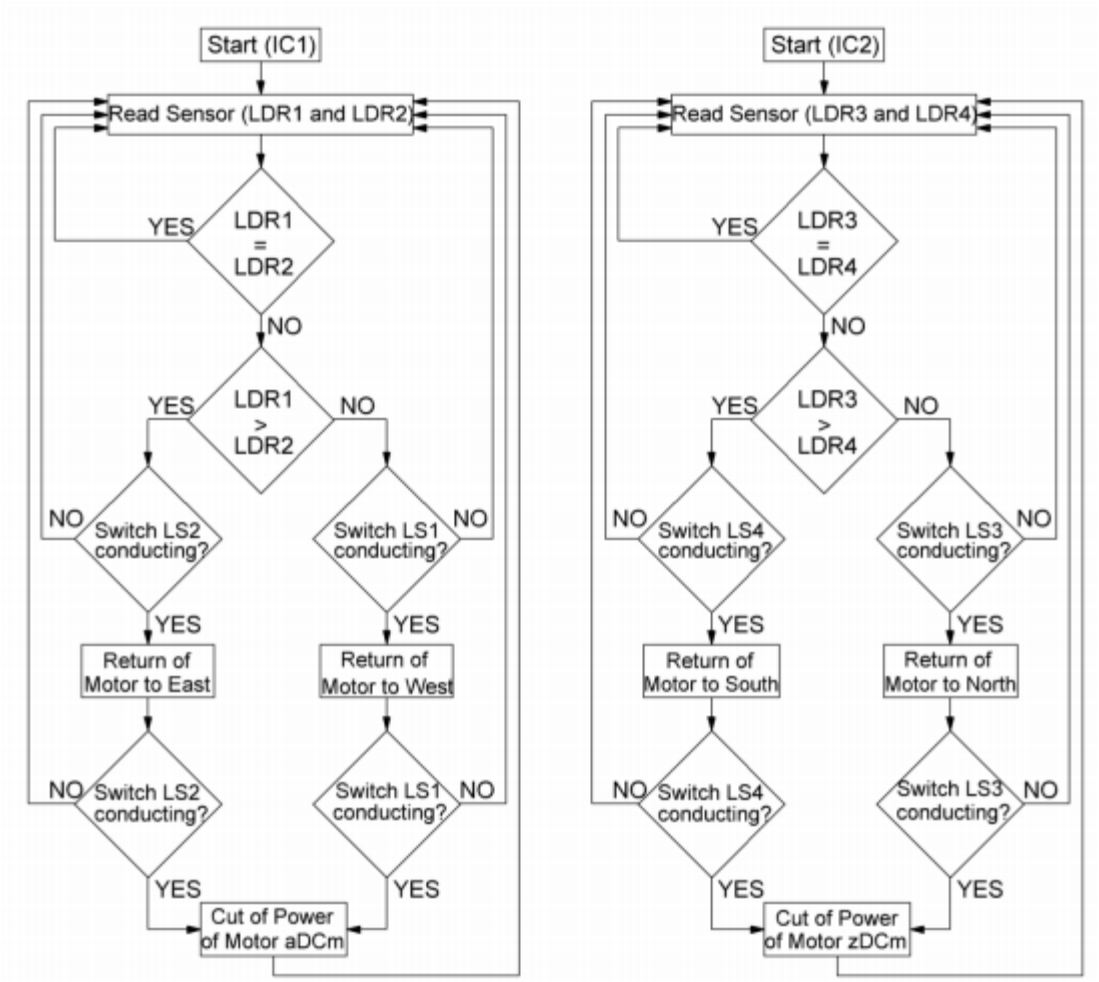

Fig. 18: DAT's flowchart [170]

For a dual-axis solar tracker, based on four-quadrant LDRs input, the motion command of vertical/horizontal axes is established by the resultant signals of Op-Amps (Operational Amplifier) used in differentiator mode [171], such that the slope of the surface β and the surface azimuth angle γ were calculated according to Eq. (5) and (6) respectively.

$$\beta = \theta_z \tag{5}$$

$$\gamma = \gamma_s \tag{6}$$

where θ_z corresponds to zenith angle, and γ_s to solar azimuth angle, both shown in Eq. (7) and (8) respectively.

$$\theta_z = 90 - \alpha_s \tag{7}$$

$$\gamma_s = \cos^{-1}\left(\frac{[\sin(\alpha_s)\cdot sin(\emptyset) - \sin(\delta)]}{cos(\alpha_s)\cdot cos(\emptyset)}\right) \tag{8}$$

where α_s is the solar elevation angle, δ the declination angle and $\emptyset$ the latitude angle [171]. Theoretical calculations of different solar angles were experimentally verified by a real prototype. The triggering movements of DC motors (from 0º to 180º on the horizontal axis, and from 0º to 90º on the vertical axis) are due to higher/lower light intensities captured by LDRs [171]. The flowchart of comparators logic for DC motor driving circuits is shown in Fig. 19.

The process shown in Fig. 19 does not start unless different illumination is received by sensors A and B. When this condition is satisfied, east-west motion is conducted according to the states of limit switches A and B. The motor is turned off, when both limit switches are opened.

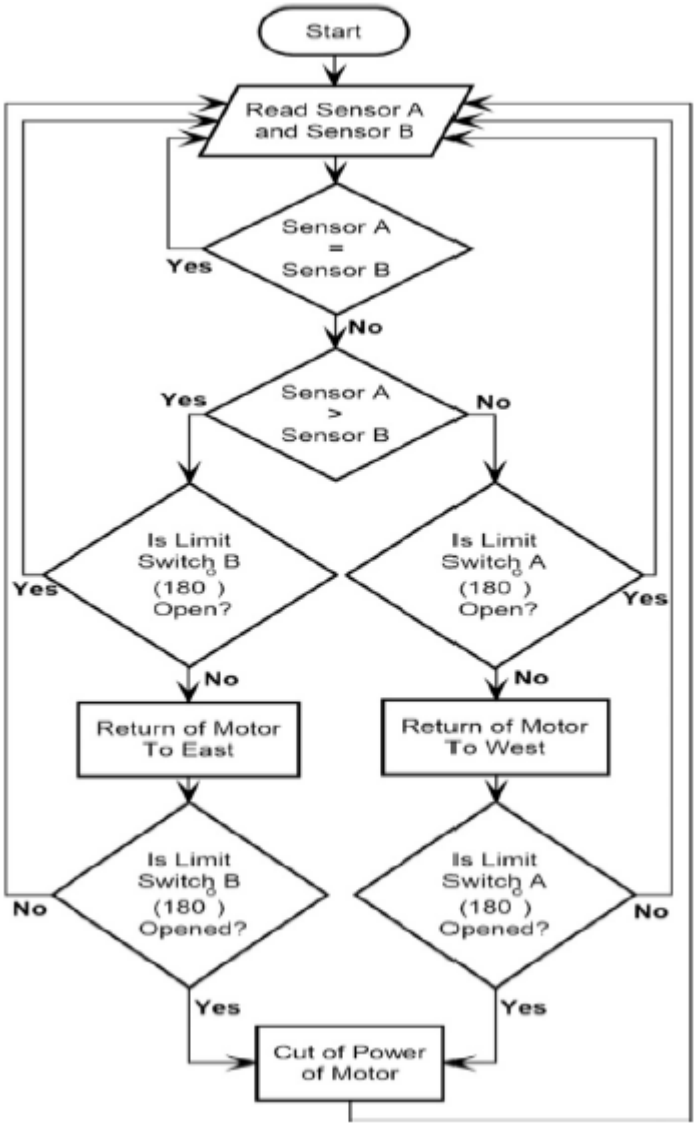

Fig. 19: Flowchart for DAT's governed PV panel movement [171]

When relying on HOMER (Hybrid Optimization Model for Electric Renewable) inputs, the global radiation incident as well as PV output power are calculated. By using recursive

calculations, the diffuse radiations are calculated at the same time that the beam radiation is calculated. When all inputs are ready, the flowchart presented in Fig. 20 identifies if maximum solar radiations are reached or not [172].

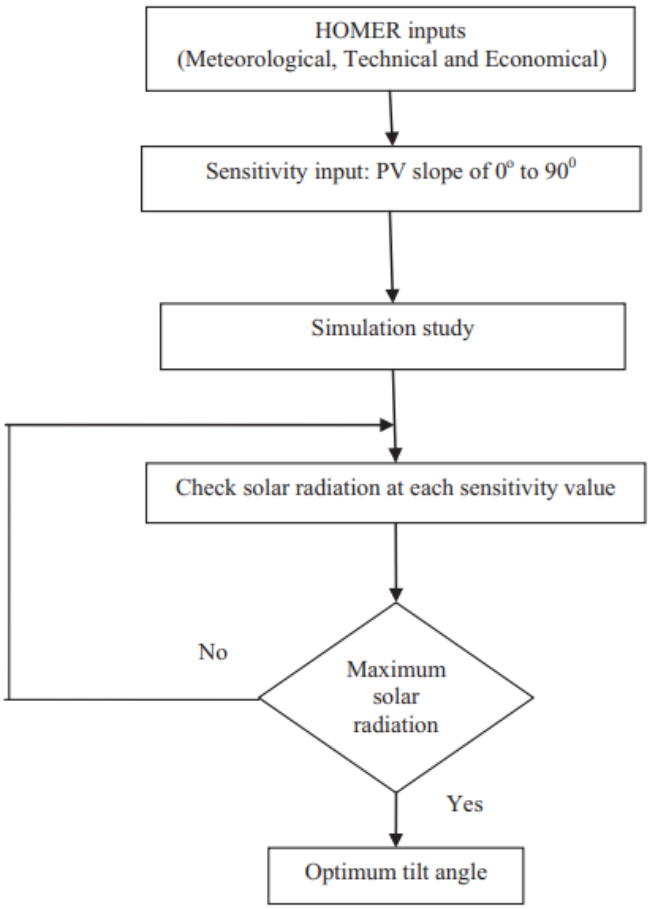

Fig. 20: Optimum tilt angle calculation using HOMER [172]

Without the need of any input sensors (to solar radiations, temperature, etc.) an offline sensor-less, dual-axis based solar tracker is found efficient in elevating the PV output power by an average of ~25%, while relying only on mathematical calculations for different solar angles. The mechanical gearbox for both axes are driven through opto-triacs. A very simple structure and cost effective model is yet verified [173].

Based on the mathematical calculations of azimuth and solar angles, a PLC (Programmable Logic Controller) drive the actuator terminals for moving both horizontal/vertical axes accordingly as shown in Fig. 21. The tracking system was guided by slope angles calculated by the PLC over a period of one year, at every hour daily. Compared with the same PV system in static mode, the tracker reached 42.6% more energy outcome [174]. Table 6 encapsulates a comparison for different DATs performances.

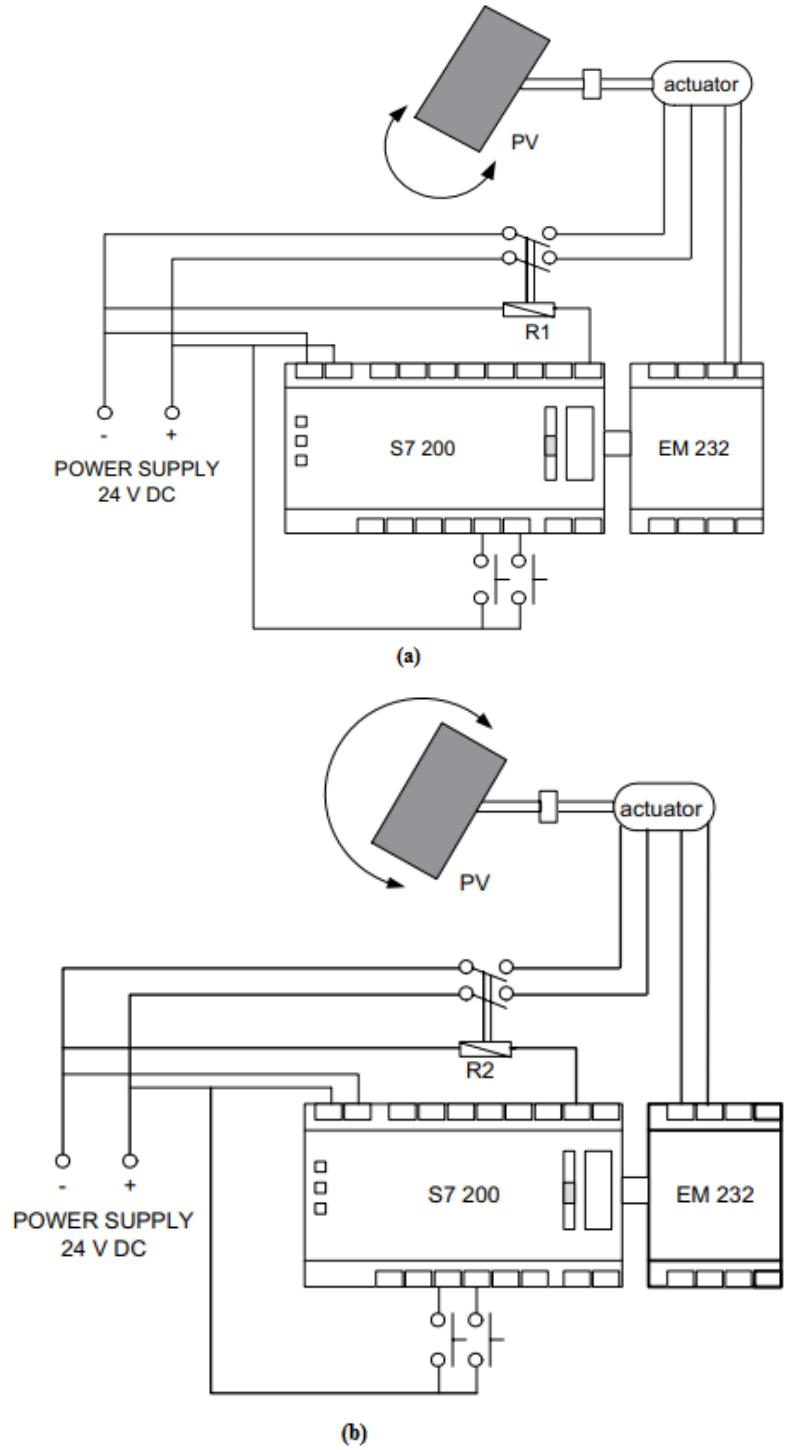

Fig. 21: PLC to actuator connection for movement of (a) vertical axis, (b) horizontal axis [174]

Ref.	Control parameters	Input	Velocity of moving axes	Motor type	Accuracy	Advantages	Disadvantages
[168]	φ_s, φ_m	Photo-detector Pyrhelio-meter	Low: Axis HH: 15°/h Axis EE: 40°-120°/h	DC motors		Low-cost Automatic Reduced maintenance costs	System does not function for irradiation below 140 W/m^2
[169]	α_s, γ_s	Webcam		Stepper motors	±2°	Economically efficient	Low efficiency in overcast weather conditions
[170]	R_Φ, R_{γ_s}	Light dependent resistors		DC motors		27% more electric energy was produced compared to static PV	The LM1458 can interfere with noise/offset
[171]	β, γ	Light dependent resistors		DC motors		Adaptation in installation in multi-PV systems' sizes	Used Op-Amp does not allow inputs to get closer to positive rail voltage
[172]	G_T	Estimated mathematical calculations				Increase in power generation	The tracking system needs bigger spacing
[173]		Estimated mathematical calculations		Stepper motors	0.43°	19.1%-30.2% increase in power	Gearboxes need continuous lubricating
[174]	α_s, α	Estimated mathematical calculations				42.6% increase in power generation	Low-bit analog modules

Table 6: Comparison between different DATs performances

3.4. Classification of ST based on tracking scheme

3.4.1 Algorithm based via processor

Moving actuators (i.e. motors) are driven by a differential signal resulting from differential illumination captured by electro-optical sensors (photodiodes, LDRs, etc.) [175-177]. PV panel is then moved until equal illumination falls on the sensors. The addition of photodiodes can increase the photocurrent sensitivity [178].

The resulting differential signal is evaluated by an algorithm written on the microprocessor/microcontroller. As long as the signal is different than zero (i.e. un-homogeneous irradiance still occurs) the re-orientation of the panel is continuously processed, by means of a set of instructions being fed to the motors [179-180].

Involvement of a PC (Personal Computer) via RS232 for sun's position monitoring can take place within algorithm based solar tracking methods. The decision making microcontroller fed with 4 MHz crystal acquaint input from LDR sensors, and reactively send commands for the stepper motor to move the PV panel in pre-defined steps (of around 5.2º). After thermal investigation between a static PV and a rotary one, it was concluded that rotary panels have taken more light density [181]. With four-axes based open-loop solar tracking, one as two-axis, one as vertical, and the remaining two are one for east-west, the other for north-south respectively, a PLC algorithm to calculate the required position of the four electromechanical axes, increases power gain up to 43.87% [182]. The PLC takes as input different solar angles. Fig. 22 reveals the block diagrams for the proposed sun tracking system.

For the east-west axis in Fig. 22 (a), the motion of the 36V DC motor is controlled after investigation of the slope angle β by the instruction set inside the PLC controller. For the two axis motion control in (b), same process is executed as in (a) except for the an additional input, the surface azimuth angle γ , investigated by another set of instructions located in PLC2

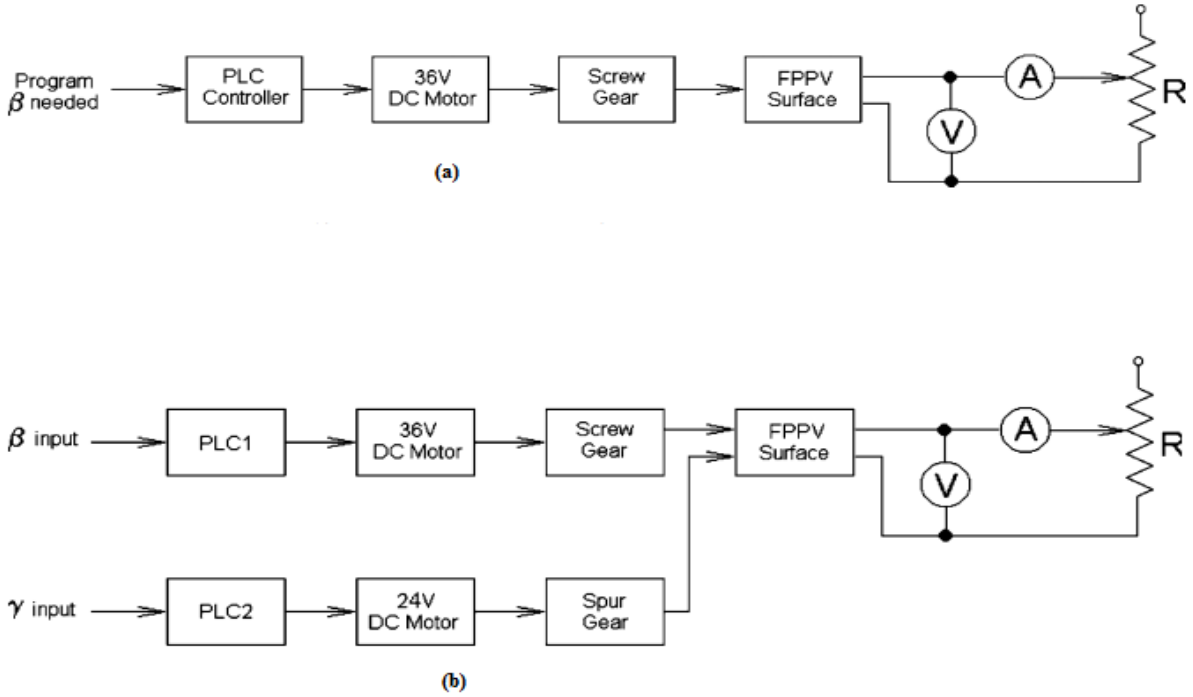

Fig. 22: Block diagram for positioning of (a) east-west axis, (b) two axes [182]

Likewise, the central decision unit in reference [182], a PLC algorithm is driven to compute the sun's position, where consequently two DC linear actuators modify PV's position. Solar cells are 11.1 times illuminated more than the solar irradiance incident, due to focal band light reflection with mirrors. Compared to a static PV surface, with a static tilt angle, the energy increase was elevated by 50% [183].

Apart from having a PLC as a central decisive unit, a PLD (Programmable Logic Device) can track sun's position according to azimuth and solar direction. The controller is Xilinx XC95108, where its code can be adjusted and transferred in C++ language to PC to monitor the power generation. This tracker was found cost-effective and flexible [184,185].

3.4.2 Date and time

With formulas based on time/date attributes and geographical information about PV installation site, sun's trajectory can be calculated. Accordingly such grouped data are fed from a processor to a control system. Consequently, signals are generated to give orders (rotate left, rotate right, etc.) to the motors to ensure perpendicularity of sunrays towards PV panel's surface.

With no feedback loops or sensory data acquisition, predefined mathematical calculations can determine the sun's position at particular periods of time. Equivalent to chronologically controlled trackers, moving actuators displace within a fixed rate and a fixed angle throughout the day. As for seasonal changes, the rate/angle are changed within calculations. Considered as open-loop controlled tracker, energy losses are diminished (almost null) due to low tracking error.

Using parabolic PV collectors, a PC is used to control the tracking movement of actuators by speed change at constant intervals of time [186]. For the case of already existing tracking

algorithms, they get re-learned and advised to better achieve greater performance. The software operational diagram is shown in Fig. 23 [187].

The communication between the PC and Licor Li-1800 solar tracker in Fig. 23 is done through a management block, where its output consist the control block of the generator. The state of the solar tracker (i.e. angular position, displacement rate, etc.) are fed into a data storage processor, in order to evaluate the effectiveness of PC calculations and tracking performance from one side, and from the other, to compose a learning environment for preexisting algorithms.

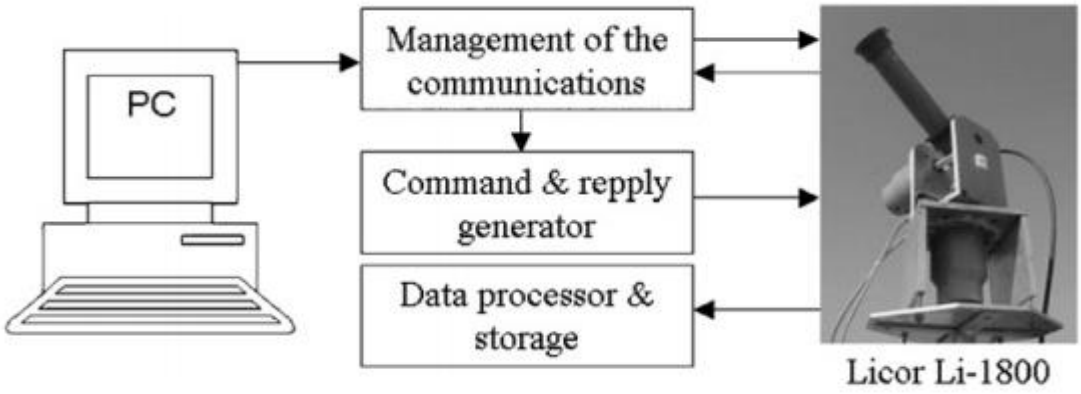

Fig. 23: Date and time software to actuator operation [187]

The implementation of fuzzy logic in time based trackers control, gives encouraging results in motion enhancement [188]. From another part, sun prediction can be achieved using solar azimuth and altitude angles. The tracking process takes place on double axes, where each axis is actuated by a DC motor [189].

Sometimes, date and time based algorithms are not as accurate as they seem. In the study [190], Michalsky algorithms (considered as most complete algorithms in sun tracking processes) were not as perfect as they are known about. A true zenith and azimuth angles of 22.14º and 28º respectively, were achieved via novel open-loop added to a date and time algorithm based on the error of previous ones.

Solar radiation energy is converted to voltage, where a decoder and a counter are used to receive signals from an optical encoder. Signals are then transformed into current signal for axis positioning. An increase of 7.084% in the output voltage is noticed with $\pm 10°$ tracking error [191].

When using a chronological method with 15º as rotation angle per hour, solar irradiance was precisely tracked from 8:00 AM to 03:00 PM. A noticeable increase of power output was witnessed [192].

3.4.3 Sensors and date/time

As addition on derived detection formulas for sun's tracking, sensors are involved to identify specific positions and to obtain more accurate results, by taking into consideration the acceptable marginal error, which can be present after excessive mathematical calculations of date and time. Through precise positioning of PV panels, bigger energy harvesting can be done. Sensors in this

category of solar tracking, continuously monitor the entire operation of tracking under predefined references (related to date, time and geographical data).

Output power is measured by sensors and feeds back an equivalent signal to the closed-loop control. On the other hand, open-loop control on its turn relates to solar movement model. The term hybrid control in the study, signifies a mixture between different control schemes [193]. Fig. 24 shows the operation in tracking mode.

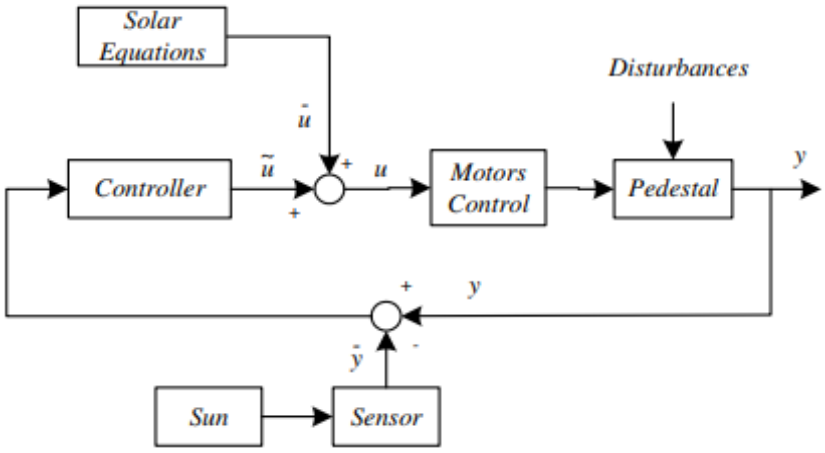

Fig. 24: Control block diagram of sun's tracking [193]

By mixing the inquiries of photo-resistors with the programmed control method, a solar tracker can be created by means of four relays, two electronic circuits, two series-connected sensors and two AC motors. The model can track the sun in both directions (east-west, north-east), thus elevating the PV system efficiency by 46.66% compared to a static one [194]. Fig. 25 reveals the corresponding comparative circuit used for sensing different solar intensities.

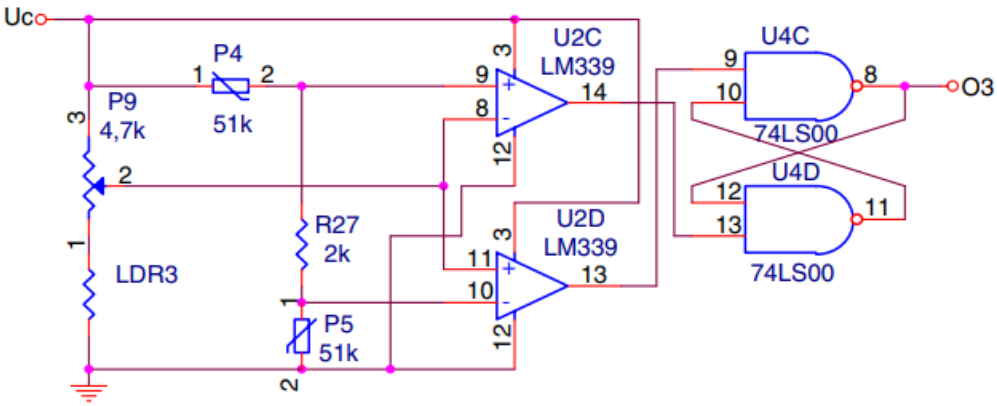

Fig. 25: Solar intensity comparative circuit based on Op-Amps and logic gates [194]

A combinational manner of three distinct solar tracking modes, where the first starts with clock mode (date and time), the second with sun's positioning (according to photo-electric sensors) and the last in remote mode (algorithm based), a solar tracker is constructed. A PC controls over a

brushless DC motor on each of the two axes and a wormlike transducer activates the movement. The vertical axis tracks the sun with a resolution angle of 0.05º. Measurements were taken through pyrheliometers where a 60 W/m^2 of excess power was detected for tracked PV systems compared to static ones [195].

3.4.4 Using bifacial solar cell

By direct connection to a permanent magnet DC motor, the auxiliary PV cell, senses the optimum positioning of rotary axes while sufficiently supplying enough energy for tracking.

With four solar modules installed on a rotor, forming two giant bifacial cells, the tracker is formed [196]. Different modules were divided into two groups (including two modules in each) and the angle between the modules of a pair was 170º, each pair of PV modules consisted a bifacial cell with the ability to sense solar radiations from morning (using upper modules) until afternoon (using lower modules). Modules connection shown in Fig. 26 resembles to the Wheatstone bridge. The motor starts turning as long as the output voltage of PV modules is not zero. Such tracker collected 30% more energy compared to a fixed system [196].

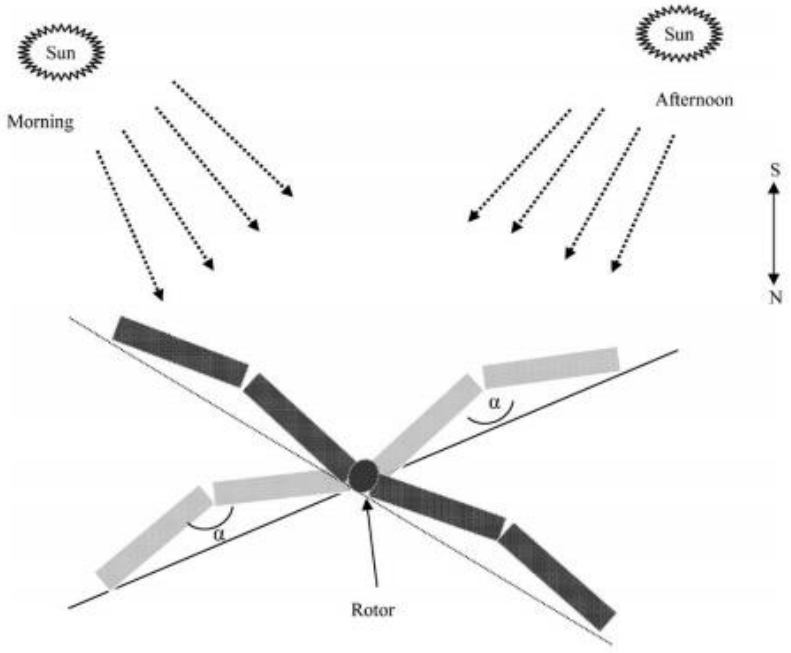

Fig. 26: Four PV modules arrangement forming two big bifacial cells [196]

The classification of an ST is overlapped between four major categorization schemes of control systems, driving mechanisms, number of moving axes and strategy of tracking. For instance, the tracker can correspond to an open-loop control, with active driving mechanism of double axis processed by a microprocessor, as in reference [182]. Various combinations can take

place between the major classification structures, to obtain a single ST with four distinctly varied categorization manners. Fig. 27 encapsulates different paths for an ST full classification.

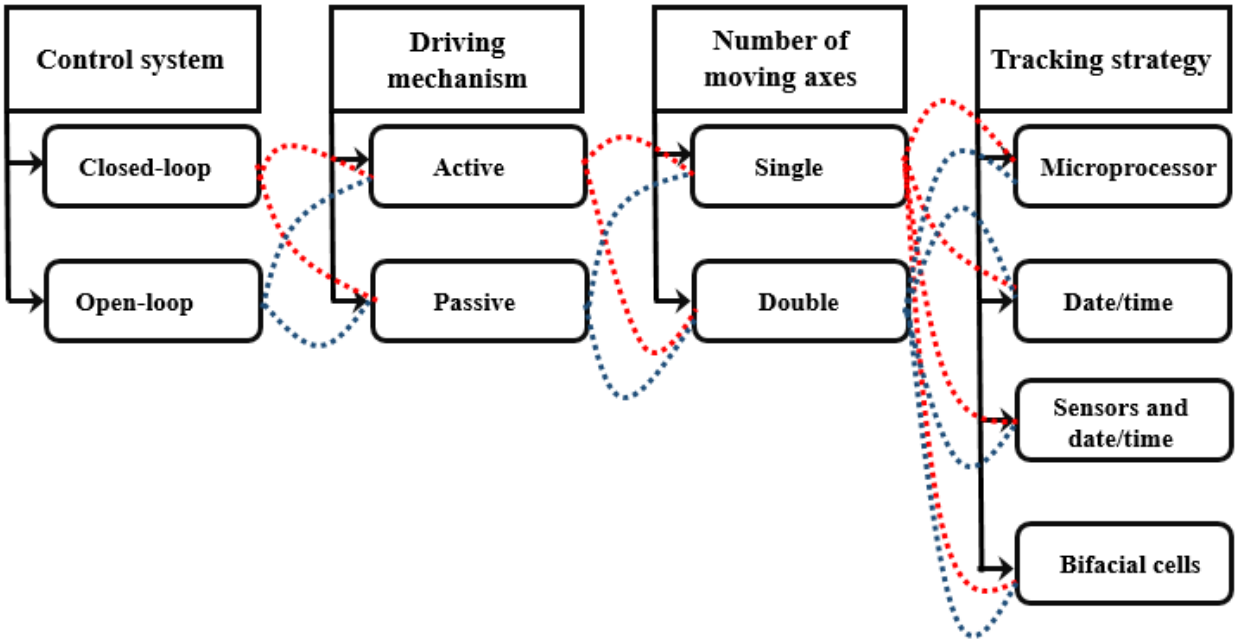

Fig. 27: Possibilities for ST nature according to the four categories of classification

4. Discussion

4.1 Advantages of using solar trackers

Solar trackers coincide as much as possible the angle that a ray of light makes with the perpendicular (normal) line to the surface of PV panel. By this phenomenon, panels are projected to maximum beam of radiations, hence collecting more energy. From another perspective, reflected/lost radiations are minimized proportionally.

Another desirable aspect of implementing a solar tracker within a PV system is the nocturnal repositioning of the panels, hence anticipating sunrise, compensating date/time changes due to seasonal fluctuations, thus panels are repositioned with time-changeable altitude, latitude and azimuth angles of the sun [197].

Cleaning brushes can be installed in conjunction with an ST. A double bonus hence occurs where the generated power is first elevated due to maximum radiations incidence over the PV panels, and the last, all physical barriers (i.e. soil, dust, leaves, etc.) are removed from the top of the surfaces. This in turns elevates the light absorption efficiency [198-199]. Table 7 encapsulates different cases of increase in produced outputs of recent STs implemented in PV systems. The increase is referred to a comparison between studies in process (with ST) and same PV systems in static mode.

Solar trackers classification												
	Control system		Driving mechanism		Number of axis		Tracking strategy				Energy gain (%)
Ref.	Open -loop	Closed -loop	Active	Passive	Single	Double	Electronic (Processor , etc.)	Date/time	Sensors and date/time	Bifacial solar cell	
[200]		●	●			●	●				≈50%
[201]		●	●			●	●				35%
[202]	●			●	●					●	25-31%
[203]	●			●	●			●			34%
[204]		●	●			●	●				>10%
[205]		●	●		●		●				32.12%
[206]		●	●			●		●			28.8-43.6%
[207]		●	●			●	●				22%
[208]		●	●			●	●				60%
[209]		●	●			●			●		35.78-89.14%

Table 7: Energy gain for PV systems installed with recent STs

Energy gains from Table 7 ranged from 10% to 89%. For the case of [200], where the energy gain ranked at 50%, this means that by using a solar tracker, within same PV system's characteristics (cell voltage, panel rated power, total output power, etc.) the system will have its output outcome multiplied by 1.5. Table 1 in reference [200] shows the daily power output without the usage of the tracker, recorded from 7:30 AM (sunrise) until 5:30 PM (sunset), it was of 4.5 W at 03:30 PM. Table 2 in the same study [200] recorded daily power output, at same time intervals than in Table 1 for the same system when accompanied with a solar tracker, the output power was 8.31 W at 03:30 PM.

Accordingly, the usage of a solar tracker boost the generated power by the percentage of energy gain. In other terms, when producing a doubled power of PV system ST based versus a static one, it means as if the dynamic system functioned like two static PV systems in parallel.

In terms of cost, reliability and efficiency of the PV systems, usage of solar trackers accelerate the cost of return, and grant advantage from systems at most, as if two of the original one are connected instead of one (the higher the gain, the bigger the ratio). This in turns reduces the cost per watt generated by the PV system.

4.2 Future scope

Programmable embedded systems (by means of processors) are invading the control systems domain. From low programming languages (assembly, etc.) to high ones (C++, Java, etc.), control systems show higher levels of accuracy than other control techniques [210]. For instance, ANN (Artificial Neural Network) is making PV outcomes more efficient with shorter computational time. ANN with FL (Fuzzy Logic) have dominated modern technologies, including PV systems [211].

Sun tracking processes with cascaded control algorithms have lower errors compared to other control structures (open-loop, primitive electronic based, etc.) [212]. Deep learning for instance, is getting heavily popular and well accepted in supportive PV systems (trackers, maximum pointers, etc.) where it is seen to have elevated energy extracting efficiencies [213]. Consequently, any new design for an ST must include a processor, coded in closed-loop, to help extract maximum available power from PV arrays. The input to the controlling system is held by means of optical sensors (LDRs, photo-diodes, etc.). An ADC (Analog to Digital Conversion) process is made within the processor to furtherly make mathematical calculations, in order to know the percentage of illumination/temperature received by the PV panels. A good positioning of sensors across PV modules is hence needed.

The number of moving axes in a solar tracker (sometimes referred as degree of freedom) is the second designing task after programming a processor to track sunrays [214]. Dual-axis based solar tracker helps better compensate both geographical and climate conditions effects on PV systems. Compared to single-axis based STs, more energy can be withdrawn from PV panels when using a two degree of freedom system [215]. Both single and double axis based solar trackers, belong to the set of active trackers, where an actuator (i.e. motor) is the tool that physically controls the positioning of PV panels [216]. Compared with passive trackers (based on shape memory alloys, foams, etc.), also bigger energy is harvested from solar modules [217].

Some modern design for sun tracking, employs a structural positioning, inspired by natural tree positioning. In other words, and in order to avoid any losses while capturing sunrays, PV modules can be arranged in a tree-branches architectural prospect, minimizing the need for extra spaces to install the PV modules, and at the same time, ensuring that all radiations incident from different angles are captivated by the modules [218].

Accordingly, to overcome the disadvantages of old topologies of sun trackers, modem designs must involve a closed-loop programmed controller (processor), inputted by optical sensors, to actively re-position the location of PV panels by means of motors/mechanical drives, according to X-Y axes corresponding to Cartesian plane. By following guidelines of STs classification shown in Fig. 27, a future scoped solar tracker, classified based on Table 2, would have the characteristics shown in Fig. 28.

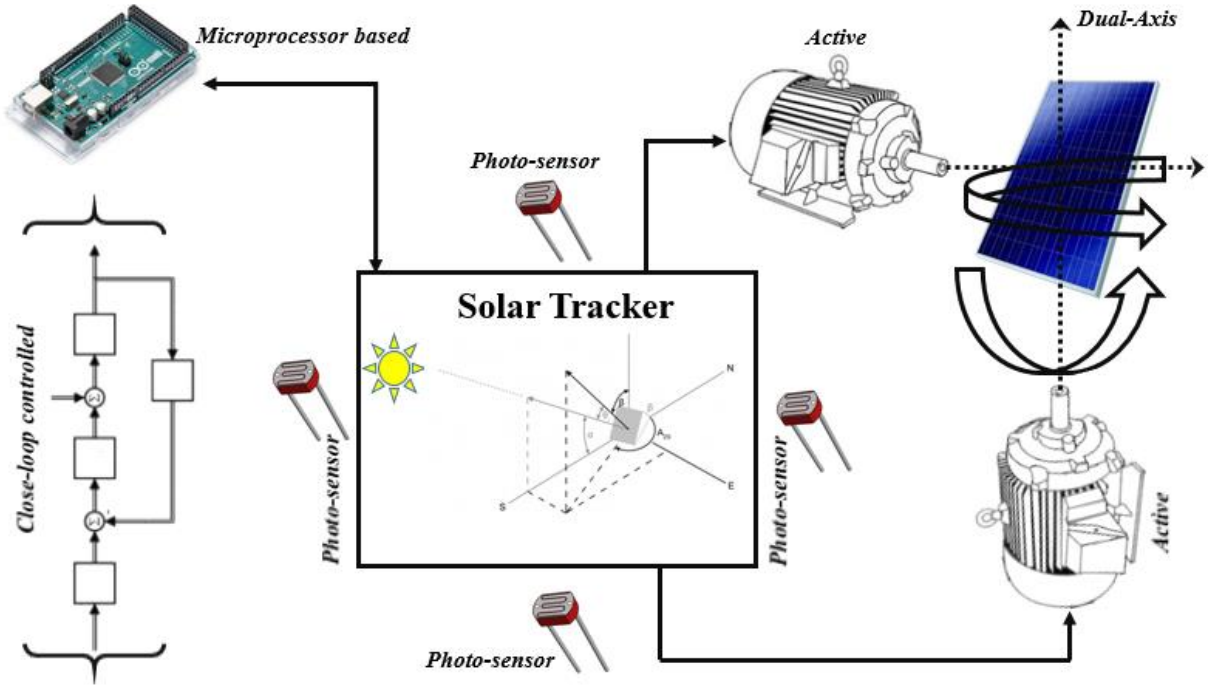

Fig. 28: Future scope solar tracker

A bifacial solar cell can be added to the ST proposed in Fig. 28, allowing a back-tracking in a complete 360º angle of rotation. This in turns would elevate the time tracking ability of the model. A convenient mechanical gear can be installed in the tracker in a way, reducing the need of double actuators to perform the double-sided orientations. In other terms, the actuator rotation is executed on a crankshaft, where horizontal or vertical movement is judged via gearbox.

For an accurate acknowledgment of current illumination status, many time-sampled ADC processes can be done (in the processor code), divided by number of conversion, to give a real idea about radiations quantities.

The close-loop control can be software-implied within a continuous loop (of irradiance checking, motion of the panel, resultant output power, etc.). The different degrees of rotation in both horizontal and vertical axes can be tabulated as cases in the software, where a group of if-else conditioners (according to C++ programming language) defines various states for degree/hour motion of the actuators.

5. Conclusion

Modern civilizations dictums produced a bulky energy need, mainly of electrical power. On the controversy, conventional power supplies (gas, diesel, etc.) are getting heavily shrank due to excessive usage. Biggest challenges of societies are to find alternative power resources, to be tuned with current and future life's requirements.

Since solar radiations are clean, abundant and common to almost every region of the globe, PV systems were found very reliable as a renewable form of energy. The conversion of solar rays, to electricity, is a safe, silent and effective power supply, but often encountered with climatic fluctuations (as shading, hot temperature, low irradiance, etc.). Therefore to be recorded as solid supplies, PV systems need optimization techniques, which ensure that maximum available power is being withdrawn from their panels. Not to forget about their huge cost of installation, such techniques became a must for a reasonable cost of return time, and to add attractiveness on PV systems as a solution of sustainable power supply, for residential, industrial and different customers ranking.

Solar trackers are one way to ensure maximum power productivity and energy harvesting from PV panels. By subjecting the panels to the maximum beam of radiations available in a particular zone, thus minimizing lost sunrays due to earth's constant moving trajectory across the sun.

The diversity of solar trackers types makes it a hard choice for adapting a system-specific tracker. In order to design an accurate tracker, one must well identify their different characterizations. Solar trackers through this paper were classified based on control strategies, driving mechanisms, number of moving axes and tracking strategies.

Under control strategies, close-loop control were found more competitive versus open-loop one. Feed-back signals help in lowering the differential errors (if existed) thus achieving more precise outputs. Mixing between open and close loop control, referred to as hybrid strategies, take advantages of both natures of control schemes, but on the other hand consume more operational time.

Unlike passive driving methods, based on shape memory alloys and memory foams, which operate according to thermal implications of STs' surrounding environments, active trackers are found to be more effective, reliable and users' approved. By directly controlling mechanical actuators (motors), preciseness is better achieved, rather than deviated by thermal dissipation in passive techniques. The choice of stepper motors to rotate the orientation of PV panels are better recommended than using permanent magnet DC motors, AC induction motors or any other form of mechanical actuators. This is because stepper motors consume less energy, while moving at specified angular positions, rather than continuous movement in other types of motors, what in turns increase the power efficiency of the system.

Double-axes trackers minimize lost radiations (due to earth's rotation around the sun, unavailable spaces to install PV modules at different solar angles, etc.) more than single-axis trackers. Consequently, more beams of radiations are captured due to higher degree of freedom in positioning, thus more energy can get harvested.

For the fact of higher energy gains by means of processor-based tracking strategies, with sensors as input, seen in tabulated data within this paper, these techniques were found the most optimum compared to date/time (that are somehow not flexible, relies mainly on pre-calculated mathematical formulas that could suddenly not well operate due to chaotic environmental conditions, or after changing the region of installed solar tracker). It is true that bifacial solar cells allow back-tracking of solar radiations, but still, processor based methods have more reliability and better dynamics in tracking solar positions, with the help of sensors (LDRs, photo-diodes, etc.). A mixing scheme between processor-based ST, inputted by LDRs, and bifacial solar cells would be a bonus.

Artificial intelligence based programming methods to make the solar tracker self-learn and grants from previous tracking experiences refers to designer's skill in this field and how to employ it in an ST's design. Such programming routines require complex coding algorithm, that can be classified in turn as time/money consuming. A trade-off between AI (Artificial Intelligence) complex programming and low-leveled programming languages (Assembly, etc.) could offer an intermediate solution, as to program a closed-loop controlled algorithm, using a high-leveled language (such as C++) with an Arduino platform.

The designer can interact with the program, troubleshoot and debug easily and in shorter amount of time, any bug within the software. The performance of the tracker can be manually upgraded (by adding more loops, reducing variables, etc.). This can easily be done via the processor simulator/platform.

With a good positioning of sensors across a test PV panel (by taking into consideration its length, width and overall size), ADC (Analog to Digital Conversion) process can swiftly present amount of solar radiations on a graphical interface board (such as LCD), informing the user about current situation facing the panel, and how the system will interact accordingly. Stepper motors can be controlled with PWM (Pulse Width Modulation) output pins, via solid-state or electro-mechanical relays.

Movements towards right, left, up and down will be code written according to sensory data acquisition. A continuous monitoring and orientation would take place to carefully compensate any differences in angles presented in Table 1. Offering a constant supervisory control, the recommended processor-based, closed-loop controlled, double-axis active solar tracker will guarantee a maximum power extraction from a PV system, what in turns increases its cost efficiency and robustness against any erroneous behavior.

6. References

[1] X. Yang, S. Liu, L. Zhang, J. Su, T. Ye. 2020. Design and analysis of a renewable energy power system for shale oil exploitation using hierarchical optimization. Energy. 206, Article ID: 118078.

[2] A. Garcia-Olivares, J. Solé, O. Osychenko. 2018. Transportation in a 100% renewable energy system. Energy Conversion and Management. 158, 266-85.

[3] M.Z. Jacobson, M.A. Delucchi. 2011. Providing all global energy with wind, water, and solar power, Part I: Technologies, energy resources, quantities and areas of infrastructure, and materials. Energy Policy. 39, 1154-69.

[4] A. Garcia-Olivares, J. Ballabrera, E. Garcia-Ladona, A. Turiel. 2012. A global renewable mix with proven technologies and common materials. Energy Policy. 41, 561-74.

[5] H. Lehmann, M. Nowakowski. 2014. Archetypes of a 100% renewable energies power supply. Energy Procedia. 57, 1077-85.

[6] F. Creutzig, J.C. Goldschmidt, P. Lehmann, E. Schmid, F.V. Blucher, C. Breyer, B. Fernandez, M. Jakob, B. Kopf, S. Lohrey, T. Susca, K. Wiegandt. 2014. Catching two European birds with one renewable stone: Mitigating climate change and Eurozone crisis by an energy transition. Renewable and Sustainable Energy Reviews. 38, 1015-28.

[7] W.N.W. Mansor, S. Abdullah, C.W.M.N.C.W. Othman, M.N.K. Jarkoni, H.R. Chao, S.L. Lin. 2020. Data on greenhouse gases emission of fuels in power plants in Malaysia during the year of 1990-2017. Data in Brief. 30, 1-9.

[8] J. Chen, Y. Ma, Z. Pang. 2020. A mathematical model of global solar radiation to select the optimal shape and orientation of the greenhouses in southern China. Solar Energy. 205, 380-9.

[9] T.F. Kristjansdottir, C.S. Good, M.R. Inman, R.D. Schlanbusch, I. Andersen. 2016. Embodied greenhouse gas emissions from PV systems in Norwegian residential Zero Emission Pilot Buildings. Solar Energy. 133, 155-71.

[10] H. te Heesen, V. Herbort, M. Rumpler. 2019. Performance of roof-top PV systems in Germany from 2012 to 2018. Solar Energy. 194, 128-35.

[11] B.H. Gebreslassie, G. Gullién-Gosalbez, L. Jimenéz, D. Boer. 2012. Solar assisted absorption cooling cycles for reduction of global warming: A multi-objective optimization approach. Solar Energy. 86(7), 2083-94.

[12] S. Abdul-Wahab, Y. Charabi, A.M. Al-Mahruqi, I. Osman, S. Osman. 2019. Selection of the best solar photovoltaic (PV) for Oman. Solar Energy. 188, 1156-68.

[13] S.Manju, N. Sagar. 2017. Progressing towards the development of sustainable energy: A critical review on the current status, applications, developmental barriers and prospects of solar photovoltaic systems in India. Renewable and Sustainable Energy Reviews. 70, 298-313.

[14] C. Prons-Seres de Brauwer, J.J. Cohen. 2020. Analyzing the potential of citizen-financed community renewable energy to drive Europe's low-carbon energy transition. Renewable and Sustainable Energy Reviews. 133, Article ID: 110300.

[15] K. Osmani, A. Haddad, T. Lemenand, B. Castanier, M. Ramadan. 2020. A review on maintenance strategies for PV systems. Science of the Total Environment. 746, Article ID: 141753.

[16] G. Li, S. Shittu, T.M.O. Diallo, M. Yu, X. Zhao, J. Ji. 2018. A review of solar photovoltaic-thermoelectric hybrid system for electricity generation. Energy. 158, 41-58.
[17] K.N. Nwaigwe, P. Mutabilwa, E. Dintwa. 2019. An overview of solar power (PV systems) integration into electricity grids. Materials Science for Energy Technologies. 2(3), 629-33.
[18] L.Q. Liu, Z.X. Wang, H.Q. Zhang, Y.C. Xue. 2010. Solar energy development in China-A review. Renewable and Sustainable Energy Reviews. 14, 301-11.
[19] A. Allouhi. 2020. Solar PV integration in commercial buildings for self-consumption based on life-cycle economic/environmental multi-objective optimization. Journal of Cleaner Production. 270, Article ID: 122375.
[20] L. Liu, Q. Sun, Y. Wang, Y. Liu, R. Wennersten. 2018. Research on Short-term Optimization for Integrated Hydro-PV Power System Based on Genetic Algorithm. Energy Procedia. 152, 1097-102.
[21] R.O. Bawazir, N.S. Cetin. 2020. Comprehensive overview of optimizing PV-DG allocation in power system and solar energy resource potential assessments. Energy Reports. 6, 173-208.
[22] K. Alboaouh, S. Mohagheghi. 2020. Voltage, var and watt optimization for a distribution system with high PV penetration: A probabilistic study. Electric Power Systems Research. 180, Article ID: 106159.
[23] U.G.K. Mulleriyawage, W.X. Shen. 2020. Optimally sizing of battery energy storage capacity by operational optimization of residential PV-Battery systems: An Australian household case study. Renewable Energy. 160, 852-64.
[24] H. Li, M. Mao, K. Guo, G. Hao, L. Zhou. 2021. A decentralized optimization method based two-layer Volt-var control strategy for the integrated system of centralized PV plant and external power grid. Journal of Cleaner Production. 278, Article ID: 123625.
[25] S.O. Fadlallah, D.E.D. Serradj. 2020. Determination of the optimal solar photovoltaic (PV) system for Sudan. Solar Energy. 208, 800-13.
[26] Z. Xu, H. Qu, X. Li, Y. Zhao, Y. Li, Z. Han. 2020. Theoretical model of optical transmission and reflection characteristics of dusty PV modules. Solar Energy Materials and Solar Cells. 213, Article ID: 110554.
[27] D.S. Pillai, N. Rajasekar. 2018. A comprehensive review on protection challenges and fault diagnosis in PV systems. Renewable and Sustainable Energy Reviews. 91, 18-40.
[28] S.R. Madeti, S.N. Singh. 2017. A comprehensive study on different types of faults and detection techniques for solar photovoltaic system. Solar Energy. 158, 161-85.
[29] A. Mellit, G.M. Tina, S.A. Kalogirou. 2018. Fault detection and diagnosis methods for photovoltaic systems: A review. Renewable and Sustainable Energy Reviews. 91, 1-17.
[30] A. Bahrami, C.O. Okoye. 2018. The performance and ranking pattern of PV systems incorporated with solar trackers in the northern hemisphere. Renewable and Sustainable Energy Reviews. 97, 138-51.
[31] B.J. Huang, Y.C. Huang, G.Y. Chen, P.C. Hsu, K. Li. 2013. Improving Solar PV System Efficiency Using One-Axis 3-Position Sun Tracking. Energy Procedia. 33, 280-87.
[32] B. Yang, T. Zhu, J. Wang, H. Shu, T. Yu, X. Zhang, W. Yao, L. Sun. 2020. Comprehensive overview of maximum power point tracking algorithms of PV systems under partial shading conditions. Journal of Cleaner Production. 268, Article ID: 121983.

[33] F. Belhachat, C. Larbes. 2019. Comprehensive review on global maximum power point tracking techniques for PV systems subjected to partial shading conditions. Solar Energy. 183, 476-500.
[34] Y. Zhu, J. Liu, X. Yang. 2020. Design and performance analysis of a solar tracking system with a novel single-axis tracking structure to maximize energy collection. Applied Energy. 264, Article ID: 114647.
[35] J. Lu, S. Hajimirza. 2017. Optimizing sun-tracking angle for higher irradiance collection of PV panels using a particle-based dust accumulation model with gravity effect. Solar Energy. 158, 71-82.
[36] N. AL-Rousan, N.A.M. Isa, M.K.M. Desa. 2018. Advances in solar photovoltaic tracking systems: A review. Renewable and Sustainable Energy Reviews. 82, part 3, 2548-69.
[37] S. Yadav, S.K. Panda, C. Hachem-Vermette. 2020. Optimum azimuth and inclination angle of BIPV panel owing to different factors influencing the shadow of adjacent building. Renewable Energy. 162, 381-96.
[38] G. Quesada, L. Guillon, D.R. Rousse, M. Mehrtash, Y. Dutil, P.L. Paradis. 2015. Tracking strategy for photovoltaic solar systems in high latitudes. Energy Conversion and Management. 103, 147-56.
[39] S.A. Sharaf Eldin, M.S. Abd-Elhady, H.A. Kandil. 2016. Feasibility of solar tracking systems for PV panels in hot and cold regions. Renewable Energy. 85, 228-33.
[40] J. Antonanzas, R. Urraca, F.J. Martinez-de-Pison, F. Antonazas. 2018. Optimal solar tracking strategy to increase irradiance in the plane of array under cloudy conditions: A study across Europe. Solar Energy. 163, 122-30.
[41] L.M. Fernandez-Ahumada, J. Ramirez-Faz, R. Lopez-Luque, M. Varo-Martinez, I.M. Moreno-Garcia, F. Casares de la Torre. 2020. Influence of the design variables of photovoltaic plants with two-axis solar tracking on the optimization of the tracking and backtracking trajectory. Solar Energy. 208, 89-100.
[42] P. Munanga, S. Chinguwa, W.R. Nyemba. 2020. Design for manufacture and assembly of an intelligent single axis solar tracking system. Procedia CIRP. 91, 571-76.
[43] E.K. Mpodi, Z. Tjiparuro, O. Matsebe. 2019. Review of dual axis solar tracking and development of its functional model. Procedia Manufacturing. 35, 580-88.
[44] B.H. Lim, C.S. Lim, H. Li, X.L. Hu, K.K. Chong, J.L. Zong, K. Kang, W.C. Tan. 2020. Industrial design and implementation of a large-scale dual-axis sun tracker with a vertical-axis-rotating-platform and multiple-row-elevation structures. Solar Energy. 199, 596-616.
[45] Z. Mi, J. Chen, N. Chen, Y. Bai, R. Fu, H. Liu. 2016. Open-loop solar tracking strategy for high concentrating photovoltaic systems using variable tracking frequency. Energy Conversion and Management. 117, 142-49.
[46] Y.M. Safan, S. Shaaban, M.I.A. El-Sebah. 2018. Performance evaluation of a multi-degree of freedom hybrid controlled dual axis solar tracking system. Solar Energy. 170, 576-85.
[47] R. Garrido, A. Diaz. 2016. Cascade closed-loop control of solar trackers applied to HCPV systems. Renewable Energy. 97, 689-96.
[48] M.H.M. Sidek, N. Azis, W.Z.W. Hasan, M.Z.A. Ab Kadir, S. Shafie, M.A.M. Radzi. 2017. Automated positioning dual-axis solar tracking system with precision elevation and azimuth angle control. Energy. 124, 160-70.

[49] M. Natarajan, T. Srinivas. 2017. Experimental and simulation studies on a novel gravity based passive tracking system for a linear solar concentrating collector. Renewable Energy. 105, 312-23.
[50] S. Obara, K. Matsumura, S. Aizawa, H. Kobayashi, Y. Hamada, T. Suda. 2017. Development of a solar tracking system of a nonelectric power source by using a metal hydride actuator. Solar Energy. 158, 1016-25.
[51] S. Tu, L. Xu, J.K. El-Demellawi, H. Liang, X. Xu, S. Lopatin, S. De Wolf, X. Zhang, H.N. Alshareef. 2020. Autonomous MXene-PVDF actuator for flexible solar trackers. Nano Energy. 77, Article ID: 105277.
[52] W. Batayneh, A. Bataineh, I. Soliman, S.A. Hafees. 2019. Investigation of a single-axis discrete solar tracking system for reduced actuations and maximum energy collection. Automation in Construction. 98, 102-9.
[53] H. Kang, T. Hong, M. Lee. 2020. A new approach for developing a hybrid sun-tracking method of the intelligent photovoltaic blinds considering the weather condition using data mining technique. Energy and Buildings. 209, Article ID: 109708.
[54] Y. Away, M. Ikhsan. 2017. Dual-axis sun tracker sensor based on tetrahedron geometry. Automation in Construction. 73, 175-83.
[55] M.A.V. Rad, A. Toopshekan, P. Radhan, A. Kasaeian, O. Mahian. 2020. A comprehensive study of techno-economic and environmental features of different solar tracking systems for residential photovoltaic installations. Renewable and Sustainable Energy Reviews. 129, Article ID: 109923.
[56] L.J. Lourens. 2016. Climate Change (Second Edition):. Observed Impacts on Planet Earth. Chapter 25: The Variation of the Earth's Movements (Orbital, Tilt and Precession). pp. 401-02.
[57] J.R.S. Brownson. 2014. Solar Energy Conversion Systems. Chapter 06: Sun-Earth Geometry. Academic Press. pp. 140-2.
[58] I. Sarbu, C. Sebarchievici. 2017. Solar Heating and Cooling Systems: Fundamentals, Experiments and Applications. Chapter 2 – Solar Radiation. Academic Press. pp. 16-8.
[59] I. Yahyaoui. 2017. Specifications of Photovoltaic Pumping Systems in Agriculture: Sizing, Fuzzy Energy Management and Economic Sensitivity Analysis. Chapter 2 – Modeling of the Photovoltaic Irrigation Plant Components. ELSEVIER. pp. 17-8.
[60] H. Darhmaoui, D. Lahjouji. 2013. Latitude Based Model for Tilt Angle Optimization for Solar Collectors in the Mediterranean Region. Energy Procedia. 42, 426-35.
[61] W. Zhang, X. Xu, Y. Wu. 2016. A new method of single celestial-body sun positioning based on theory of mechanisms. Chinese Journal of Aeronautics. 29,(1), 248-56.
[62] S.A. Kalogirou. 2014. Solar Energy Engineering (Second Edition): Processes and Systems. Chapter 2 - Environmental Characteristics. Academic Press. pp. 56-60.
[63] A. Martinez-Garcia, I. Arauzo, J. Uche. 2019. Solar Hydrogen Production: Processes, Systems and Technologies. Chapter 5 – Solar energy availability. Academic Press. pp. 119-20
[64] R.A. Pielke Sr. 2013. International Geophysics. Chapter 7 – Traditional Parameterizations. 98, 157-80.
[65] M. Rosa-Clot, G.M. Tina. 2018. Submerged and Floating Photovoltaic Systems: Modelling, Design and Case Studies. Chapter 2 – Photovoltaic Electricity. Academic Press. pp. 16-7.

[66] J.L. Chen, L. He, Q. Chen, M.Q. Lv, H.L. Zu, Z.F. Wen, S.J. Wu. 2019. Study of monthly mean daily diffuse and direct beam radiation estimation with MODIS atmospheric product. Renewable Energy. 132, 221-32
[67] L. Benali, G. Notton, A. Fouilly, C. Voyant, R. Dizene. 2019. Solar radiation forecasting using artificial neural network and random forest methods: Application to normal beam, horizontal diffuse and global components. Renewable Energy. 132, 871-84.
[68] A. Barbon, P.F. Ayuso, L. Bayon, J.A. Fernandez-Rubiera. 2020. Predicting beam and diffuse horizontal irradiance using Fourier expansions. Renewable Energy. 154, 46-57.
[69] N. Nfaoui, K. El-Hami. 2018. Extracting the maximum energy from solar panels. Energy Reports. 4, 563-45.
[70] H. Kang, T. Hong, M. Lee. 2019. Technical performance analysis of the smart solar photovoltaic blinds based on the solar tracking methods considering the climate factors. Energy and Buildings. 190, 34-48.
[71] A. Herez, H. El Hage, T. Lemenand, M. Ramadan, M. Khaled. 2020. Review on photovoltaic/thermal hybrid solar collectors: Classifications, applications and new systems. Solar Energy. 207, 1321-47.
[72] C.K. Yang, T.C. Cheng, C.H. Cheng, C.C. Wang, C.C. Lee. 2017. Open-loop altitude-azimuth concentrated solar tracking system for solar-thermal applications. Solar Energy. 147, 52-60.
[73] R. Wang, J. Sun, H. Hong. 2019. Proposal of solar-aided coal-fired power generation system with direct steam generation and active composite sun-tracking. Renewable Energy. 141, 596-612.
[74] C. Jamroen, P. Komkum, S. Kohsri, W. Himananto, S. Panupintu, S. Unkat. 2020. A low-cost dual-axis solar tracking system based on digital logic design: Design and implementation. Sustainable Energy Technologies and Assessments. 37, Article ID: 100618.
[75] J.A. Carballo, J. Bonilla, M. Berenguel, J. Fernandez-Reche, G. Garcia. 2019. New approach for solar tracking systems based on computer vision, low cost hardware and deep learning. Renewable Energy. 133, 1158-66.
[76] K. Ogata. 2010. Modern Control Engineering (5th Edition). Chapter 1: Introduction to Control Systems. ISBN: 978-0-13-615673-4. Prentice Hall. pp. 1-10.
[77] F. Golnaraghi, B. Kuo. 2010. Automatic Control Systems (9th Edition). Chapter 1: Introduction. ISBN: 978-0470-04896-2. Wiley. pp. 2-5.
[78] R.C. Dorf, R.H. Bishop. 2011. Modern Control Systems (12th Edition). Chapter 1: Introduction to Control Systems. Prentice Hall. ISBN: 978-0-13-602458-3. pp. 24-39.
[79] J.J. Distefano, A.R. Stubberud, I.J. Williams. 1990. Feedback and Control Systems (2nd Edition), Continuous (Analog) and Discrete (Digital). Chapter 2: Control Systems Terminology. ISBN: 0-07-017052-5. McGraw-Hill. pp. 15-7.
[80] K.J. Astrom, R.M. Murray. 2020. Feedback Systems: An Introduction for Scientists and Engineers (2nd Edition). Chapter 1: Introduction. Princeton University Press. pp. 1-6.
[81] F. Asadi, R.E. Bolanos, J. Rodriguez. 2019. Feedback Control Systems: The MATLAB/Simulink Approach. Chapter 4: Controller design in MATLAB. ISBN: 9781681735405. Morgan & Claypool Publishers. pp. 163-6.
[82] J. Parmar, N. Parmar, S. Gutam. 2015. Passive solar tracking system. International Journal of Emerging Technologies and Advanced Engineering. 5, 138-45.

[83] M. Neagoe, I. Visa, B.G. Burduhos, M.C. Moldovan. 2014. Thermal Load Based Adaptive Tracking for Flat Plate Solar Collectors. Energy Procedia. 48, 1401-11.
[84] S.Z. Farooqui. 2013. A gravity based tracking system for box type solar cookers. Solar Energy. 92, 62-8.
[85] A.J. Grede, G.S. Brulo, A.J. Ren, M.D. Lenko, C.D. Rahn, N.C. Giebink. 2018. Motorless Microtracking for Rooftop CPV. 2018 IEEE 7th World Conference on Photovoltaic Energy Conversion. IEEE. pp. 1-4
[86] I. Mihalcz. 2001. Fundamental characteristics and design method for Nickel-Titanium shape memory alloy. Periodica Polytechnica Mechanical Engineering.45, 75-86.
[87] M.J. Clifford, D. Eastwood. 2004. Design of a novel passive solar tracker. Solar Energy. 77(3), 269-80.
[88] P.R. Holambe, D.B. Talange, V.B. Hole. 2015. Motorless solar tracking system. 2015 International Conference on Energy Systems and Applications. IEEE. pp. 1-4.
[89] J.M. Jani, M. Leary, A. Subic, M.A. Gibson. 2014. A review of shape memory alloy research, applications and opportunities. Materials and Design. 56, 1078-113.
[90] S. Thomas, P. Peralta, R. Mottet, M. Lehmann, Y. Civet, Y. Perriard. 2018. Analysis and Reduction of Time Response in Thermally Activated Shape Memory Alloys. 2018 21st International Conference on Electric Machines and Systems (ICEMS). IEEE. pp. 1-4.
[91] M. Raslan, R. Balog. 2019. Bi-stable Shape Memory Alloy Actuated Switch for Smart PV Skin. 2019 2nd International Conference on Smart Grid and Renewable Energy (SGRE). IEEE. pp. 1-3.
[92] P.K. Kumar, D.C. Lagoudas. 2008. Shape Memory Alloys: Modeling and Engineering Applications (1st Edition). Chapter 1: Introduction to Shape Memory Alloys. Springer. pp. 1-10.
[93] W. Huang, W. Toh. 2000. Training two-way shape memory alloy by reheat treatment. Journal of Materials Science Letters. 19, 1540-50.
[94] W.M. Huang, Z. Ding, C.C. Wang, J. Wei, Y. Zhao, H. Purnawali. 2010. Shape memory materials. Materials today. 13,(8), 54-61.
[95] S. Angioni, M. Meo. 2010. Impact damage resistance and damage suppression properties of shape memory alloy in hybrid composites – A review. Smart Materials and Structures. 20, 2-4.
[96] L. Sun, W.M. Huang. 2009. Nature of the multistage transformation in shape memory alloys upon heating. Material Science and Heat Treatment. 51, 573-8.
[97] G.C. Lazaroiu, M. Longo, M. Roscia, M. Pagano. 2015. Comparative analysis of fixed and sun tracking low power PV systems considering energy consumption. Energy Conversion Management. 92, 143-48.
[98] L.M. Gutierrez-Castro, P. Quinto-Diez, J.G. Barbosa-Saldana, L.R. Tovar-Galvez, A. Reyes-Leon. 2014. Comparison between a Fixed and a Tracking Solar Heating System for a Thermophilic Anaerobic Digester. Energy Procedia. 57, 2937-45.
[99] M. Mahendran, H.L. Ong, G.C. Lee. 2013. An experimental comparison study between single-axis tracking and fixed photovoltaic solar panel efficiency and power output: Case study in east coast Malaysia. Sustainable Development Conference. Bangkok, Thailand.
[100] P. Battacharya, S. Mukhopadhay, B.B. Gosh, P.K. Bose. 2012. Optimized Use of Solar Tracking System and Wind Energy. Procedia Technology. 4, 834-39.

[101] S. Abdallah, O.O. Badran. 2008. Sun tracking system for productivity enhancement of solar still. Desalination. 220(3), 669-76.
[102] J.F. Lee, N. Abd Rahim, Y.A. Al-Turki. 2013. Performance of dual-axis solar tracker versus static solar system by segmented clearness index in Malaysia. International Journal of Photoenergy. pp. 1-13.
[103] F. Cruz-Peragon, P.J. Casanova-Pelaez, F.A. Diaz, R. Lopez-Garcia, J.M. Palomar. 2011. An approach to evaluate the energy advantage of two axes solar tracking systems in Spain. Applied Energy. 88(12), 5131-42.
[104] N.A. Kelly, T.L. Gibson. 2009. Improved photovoltaic energy output for cloudy conditions with a solar tracking system. Solar Energy. 83(11), 2092-102.
[105] J. Wu, H. Hou, Y. Yang. 2016. Annual economic performance of a solar-aided 600 MW coal-fired power generation system under different tracking modes, aperture areas, and storage capacities. Applied Thermal Engineering. 104, 319-32.
[106] C.S. Chin, A. Babu, W. McBride. 2011. Design, modeling and testing of a standalone single axis active solar tracker using MATLAB/Simulink. Renewable Energy. 36(11), 3075-90.
[107] J. Wang, J. Zhang, Y. Cui, X. Bi. 2016. Design and implementation of PLC-based automatic sun tracking system for parabolic trough solar concentrator. 2016 3rd International Conference on Mechanics and Mechatronics Research (ICMRR 2016). MATEC Web Conf. 77, 1-4.
[108] B.M.B. Robalo, J.M.G. Figueiredo. 2010. Supervisory Control developed for a Solar Tracking Prototype based on PV-Technology. IFAC Proceedings Volumes. 43(1), 291-96.
[109] F. Sallaberry, R. Pujol-Nadal, M. Larcher, M.H. Rittmann-Frank. 2015. Direct tracking error characterization on a single-axis solar tracker. Energy Conversion and Management. 105, 1281-90.
[110] R.R. Patel, A.J. Patil, A.N. Shewale. 2015. Intelligent sun tracking system using FLC implemented on FPGA. International Journal of Advanced Research in Computer. 2, 33-41.
[111] M. Abouzeid. 2001. Use of a reluctance stepper motor for solar tracking based on a programmable logic array (PLA) controller. Renewable Energy. 23(4), 551-60.
[112] R.I. Salawu, T.A. Oduyemi. 1987. A microprocessor controlled solar tracking system. Journal of Microcomputer Applications. 10(1), 55-62.
[113] S. Das, S. Chakraborty, P.K. Sadhu, O.S. Sastry. 2015. Design and experimental execution of a microcontroller (μC)-based smart dual-axis automatic solar tracking system. Energy Science & Engineering. 3, 558-64.
[114] S. Gosh, N. Haldar. 2014. Solar tracking system using AT89C51 microcontroller and LDR. International Journal of Emerging Technology and Advanced Engineering. 4, 403-7.
[115] M.M. Lwin, N.N. Win. 2014. Microcontroller based smart solar tracking system. International Journal of Scientific & Technology Research. 3, 1845-50.
[116] A. Bose, S. Sarkar, H.S. Das. 2012. A low cost high efficient solar tracking system using AVR microcontroller. International Journal of Scientific and Engineering Research. 3, 1-6.

[117] N. Mohammed, T. Karim. 2012. The design and implementation of hybrid automatic solar tracking system. International Journal of Electrical and Power Engineering. 6, 111-7.
[118] I. Stamatescu, I. Fagarasan, G. Stamatescu, N. Arghira, S.S. Illiescu. 2014. Design and Implementation of a Solar-tracking Algorithm. Procedia Engineering. 69, 500-7.
[119] A. Cammarata. 2015. Optimized design of a large-workspace 2-DOF parallel robot for solar tracking systems. Mechanism and Machine Theory. 83, 175-86.
[120] D. Zhao, E. Xu, Z. Wang, Q. Yu, L. Xu, L. Zhu. 2016. Influences of installation and tracking errors on the optical performance of a solar parabolic trough collector. Renewable Energy. 94, 197-212.
[121] A.S.C. Roong, S.H. Chong. 2016. Laboratory-scale single axis solar tracking system: Design and Implementation. International Journal of Power Electronics and Drive Systems. 7, 254-64.
[122] L. Li, H. Li, Q. Xu, W. Huang. 2015. Performance analysis of Azimuth Tracking Fixed Mirror Solar Concentrator. Renewable Energy. 75, 722-32.
[123] Y.K. Choi, I.S. Kim, S.T. Hong, H. Lee. 2014. A study on development of azimuth angle tracking algorithm for tracking-type floating photovoltaic system. Advanced Science and Technology Letters. 51, 197-202.
[124] I. Abadi, A. Soeprijanto, A. Musyafa. 2014. Design of a single axis solar tracking system at photovoltaic panel using fuzzy logic controller. Proceedings of the 5th Brunei International Conference on Engineering and Technology. IET. pp. 1-6.
[125] D. Bawa, C.Y. Patil. 2013. Fuzzy control based solar tracker using Arduino uno. International Journal of Engineering and Innovative Technology. 2(12), 179-87.
[126] A. Gama, C. Larbes, A. Malek, F. Yettou, B. Adouane. 2013. Design and realization of a novel sun tracking system with absorber displacement for parabolic trough collectors. Journal of Renewable and Sustainable Energy. 5, 1-18.
[127] E.L. Peterson, S.R. Gray. 2012. Effectiveness of desalination powered by a tracking solar array to treat saline bore water. Desalination. 293, 94-103.
[128] A. Ghazali M, A.M. Abdul Rahman. 2012. The performance of three different solar panels for solar electricity applying solar tracking device under the Malaysian climate condition. Energy and Environment Research. 2, 235-43.
[129] G. Ferretti, G. Gruosso, G. Mangani, M. Redaelli, P. Rocco, G. Guardabassi. 2010. Mechatronic Design of the Sun Tracking System of a Linear Fresnel Reflector Solar Plant. IFAC Proceedings Volumes. 43(18), 248-54.
[130] H. Tanaka, Y. Nakatake. 2009. One step azimuth tracking tilted-wick solar still with a vertical flat plate reflector. Desalination. 235, 1-8.
[131] T. Tomson. 2008. Discrete two-positional tracking of solar collectors. Renewable Energy. 33(3), 400-5.
[132] B.J. Huang, F.S. Sun. 2007. Feasibility study of one axis three positions tracking solar PV with low concentration ratio reflector. Energy Conversion and Management. 48(4), 1273-80.
[133] C. Grass, W. Schoelkopf, L. Staudacher, Z. Hacker. 2004. Comparison of the optics of non-tracking and novel types of tracking solar thermal collectors for process heat applications up to 300ºC. Solar Energy. 76(3), 207-15.
[134] G. Mwithiga, S.N. Kigo. 2006. Performance of a solar dryer with limited sun tracking capability. Journal of Food Engineering. 74(2), 247-52.

[135] I.M. Michaelides, S.A. Kalogirou, I. Chrysis, G. Roditis, A. Hadjiyianni, H.D. Kambezidis, M. Petrakis, S. Lykoudis, A.D. Adampoulos. 1999. Comparison of performance and cost effectiveness of solar water heaters at different collector tracking modes in Cyprus and Greece. Energy Conversion and Management. 40(12), 1287-303.
[136] Z. Li, X. Liu, R. Tang. 2011. Optical performance of vertical single-axis tracked solar panels. Renewable Energy. 36(1), 64-8.
[137] Z. Li, X. Liu, R. Tang. 2010. Optical performance of inclined south-north single-axis tracked solar panels. Energy. 35(6), 2511-6.
[138] N. AL-Rousan, N.A.M. Isa, M.K.M. Desa. 2020. Efficient single and dual axis solar tracking system controllers based on adaptive neural fuzzy inference system. Journal of King Saud University – Engineering Sciences. In Press, Corrected Proof. pp. 7-8.
[139] M.K. Sharma, J. Bhattacharya. 2020. A novel stationary concentrator to enhance solar intensity with absorber-only single axis tracking. Renewable Energy. 154, 976-85.
[140] G. Li, R. Tang, H. Zhong. 2012. Optical Performance of Horizontal Single-Axis Tracked Solar Panels. Energy Procedia. 16, Part C, 1744-52.
[141] R.G. Vieira, F.K.O.M.V. Guerra, M.R.B.G. Vale, M.M. Araujo. 2016. Comparative performance analysis between static solar panels and single-axis tracking system on a hot climate region near to the equator. Renewable and Sustainable Energy Reviews. 64, 672-81.
[142] S.A. Pelaez, C. Deline, P. Greenberg, J.S. Stein, R.K. Kostuk. 2019. Model and Validation of Single-Axis Tracking with Bifacial PV. IEEE Journal of Photovoltaics. 9(3), 715-21.
[143] A. Colli, W.J. Zaaiman. 2012. Maximum-Power-Based PV Performance Validation Method: Application to Single-Axis Tracking and Fixed-Tilt c-Si Systems in the Italian Alpine Region. IEEE Journal of Photovoltaics. 2(4), 555-63.
[144] N.H. Helwa, A.B.G. Bahgat, A.M.R.E. Shafee, E.T.E. Shenawy. 2000. Maximum collectable solar energy by different solar tracking systems. Energy Sources. 22, 23-4.
[145] L. Ngan, C. Jepson, A. Blekicki, A. Panchula. 2013. Increased energy production of First solar horizontal single-axis PV systems without backtracking. 2013 IEEE 39th Photovoltaic Specialists Conference (PVSC). IEEE. pp. 1-5.
[146] M.H. Tania, Md. Samiul Alam. 2014. Sun tracking schemes for photovoltaic panels. 2014 3rd International Conference on the Development in Renewable Energy Technology (ICDRET). IEEE. pp. 1-5.
[147] B. Khadidja, K. Dris, A. Boubeker, S. Noureddine. 2014. Optimisation of a Solar Tracker System for Photovoltaic Power Plants in Saharian Region, Example of Ouargla. Energy Procedia. 50, 610-8.
[148] S.A. Kalogirou. 2004. Solar thermal collectors and applications. Progress in Energy and Combustion Science. 30(3), 231-95.
[149] V. Poulek, M. Libra. 2000. A very simple solar tracker for space and terrestrial applications. Solar Energy Materials and Solar Cells. 60(2), 99-103.
[150] T.P. Chang. 2009. Output energy of a photovoltaic module mounted on a single-axis tracking system. Applied Energy. 86(10), 2071-8.
[151] Y. Kim, G. Han, T. Seo. 2008. An evaluation on thermal performance of CPC solar collector. International Communications in Heat and Mass Transfer. 35(4), 446-57.
[152] F. Mavromatakis, Y. Franghiadakis. 2008. A highly efficient novel azimuthal heliotrope. Solar Energy. 82(4), 336-42.

[153] B.J. Huang, W.L. Ding, Y.C. Huang. 2011. Long-term field test of solar PV power generation using one-axis 3-position sun tracker. Solar Energy. 85(9), 1935-44.
[154] A. Konar, A.K. Mandal. 1991. Microprocessor based automatic Sun tracker. IEE Proceedings A - Science, Measurement and Technology. IET. 138(4), 237-41.
[155] R. Singh, S. Kumar, A. Gehlot, R. Pachauri. 2018. An imperative role of sun trackers in photovoltaic technology: A review. Renewable and Sustainable Energy Reviews. 82, Part 3, 3263-78.
[156] B. Hammad, A. Al-Sardeah, M. Al-Abed, S. Nijmeh, A. Al-Ghandoor. 2017. Performance and economic comparison of fixed and tracking photovoltaics systems in Jordan. Renewable and Sustainable Energy Reviews. 80, 827-39.
[157] H. Kang, T. Hong, S. Jung, M. Lee. 2019. Techno-economic performance analysis of the smart solar photovoltaic blinds considering the photovoltaic panel type and the solar tracking method. Energy and Building. 193, 1-14.
[158] H.J. Veermak. 2014. Techno-economic Analysis of Solar Tracking Systems in South Africa. Energy Procedia. 61, 2435-8.
[159] A.Z. Hafez, A.M. Yousef, N.M. Harag. 2018. Solar tracking systems: Technologies and trackers drive types - A review. Renewable and Sustainable Energy Reviews. 91, 754-82.
[160] T. Maatallah, S. El Alimi, S.B. Nasrallah. 2011. Performance modeling and investigation of fixed, single and dual-axis tracking photovoltaic panel in Monastir city, Tunisia. Renewable and Sustainable Energy Reviews. 15(8), 4053-66.
[161] C.D. Rodriguez-Gallegos, O. Gandhi, S.K. Panda, T. Reindl. 2020. On the PV Tracker Performance: Tracking the Sun Versus Tracking the Best Orientation. IEEE Journal of Photovoltaics. 10(5), 1474-80.
[162] M.M. Abu-Khader, O.O. Badran, S. Abdallah. 2008. Evaluating multi-axes sun-tracking system at different modes of operation in Jordan. Renewable and Sustainable Energy Reviews. 12(3), 864-73.
[163] S. Abdallah, S. Nijmeh. 2004. Two axes sun tracking system with PLC control. Energy Conversion and Management. 45(12), 1931-9.
[164] S. Kivrak, M. Gunduzalp, F. Dincer. 2012. Theoretical and experimental performance investigation of a two-axis solar tracker under the climatic condition of Denzili, Turkey. Prz Elektrotech. 88(2), 332-6.
[165] S. Kivrak. 2013. Design of a low cost sun tracking controller system for photovoltaic panels. Journal of Renewable and Sustainable Energy. 5(3), 2-10.
[166] D.V. Tekumalla, D. Pal, P. Bajpai. 2019. Comprehensive performance evaluation of various solar PV system configurations. IET Renewable Power Generation. 13(8), 1261-70.
[167] J. Reca-Cardena, R. Lopez-Luque. 2018. Advances in Renewable Energies and Power Technologies. Volume 1: Solar and Wind Energies. Chapter 9 – Design Principles of Photovoltaic Irrigation Systems. pp. 306-7.
[168] P. Roth, A. Georgiev, H. Boudinov. 2004. Design and construction of a system for sun-tracking. Renewable Energy. 29(3), 393-402.
[169] M. Abdollahpour, M.R. Golzarian, A. Rohani, H.A. Zarchi. 2018. Development of a machine vision dual-axis solar tracking system. Solar Energy. 169, 136-43.

[170] S. Seme, G. Srpcic, D. Kavsek, S. Bozicnick, T. Letnik, Z. Praunseis, B. Stumberger, M. Hadziselimovic. 2017. Dual-axis photovoltaic tracking system – Design and experimental investigation. Energy. 139, 1267-74.
[171] S. Yilmaz, H.R. Ozcalik, O. Dogmus, F. Dincer, O. Akgol, M. Karaaslan. 2015. Design of two axes sun tracking controller with analytically solar radiations calculations. Renewable and Sustainable Energy Reviews. 43, 997-1005.
[172] S. Sinha, S.S. Chandel. 2016. Analysis of fixed tilt and sun tracking photovoltaic-micro wind based hybrid power systems. Energy Conversion and Management. 115, 265-75.
[173] H. Fathabadi. 2016. Novel high efficient offline sensorless dual-axis solar tracker for using in photovoltaic systems and solar concentrators. Renewable Energy. 95, 485-94.
[174] C. Sungur. 2009. Multi-axes sun-tracking system with PLC control for photovoltaic panels in Turkey. Renewable Energy. 34(4), 1119-25.
[175] A.A. Rizvi, K. Addoweesh, A. El-Leathy, H. Al-Ansary. 2015. Sun position algorithm for sun tracking applications. IECON 2014 – 40th Annual Conference of the IEEE Industrial Electronics Society. IEEE. pp. 1-4.
[176] T. Yu, G. Wencheng. 2010. Study on Tracking Strategy of Automatic Sun-Tracking System Based on CPV. 2010 International Conference on Intelligent System Design and Engineering Application. IEEE. pp. 1-4.
[177] H. Tchakounté, C.B.N. Fapi, M. Kamta, H. Djalo, P. Woafo. 2020. Performance Comparison of an Automatic Smart Sun Tracking System Versus a Manual Sun Tracking. 2020 8th International Conference on Smart Grid (icSmartGrid). IEEE. pp. 1-6.
[178] I.L. Heredia, J.M. Moreno, P.H. Magalhaes, R. Cervantes, G. Quéméré, O. Laurent. 2007. Inspira's CPV sun tracking (concentrator photovoltaics). Springer. pp. 221-51.
[179] B. Koyuncu, K. Balasubramanian. 1991. A microprocessor controlled automatic sun tracker. IEEE Transactions on Consumer Electronics. 37(4), 913-7.
[180] T. Kaur, S. Mahajan, S. Verma, Priyanka, J. Gambhir. 2016. Arduino based low cost active and dual axis solar tracker. 2016 IEEE 1st International Conference on Power Electronics, Intelligent Control and Energy Systems (ICPEICES). IEEE. pp. 1-5.
[181] O. Bingol, A. Altintas, Y. Oner. 2006. Microcontroller based solar-tracking system and its implementation. Journal of Engineering Sciences. 12(2), 243-8.
[182] S. Abdallah. 2004. The effect of using sun tracking systems on the voltage-current characteristics and power generation of flat PV. Energy Conversion and Management. 45, 1671-9.
[183] J.I. Rosell, X. Vallverdu, M.A. Lechon, M. Ibanez. 2005. Design and simulation of a low concentrating photovoltaic/thermal system. Energy Conversion and Management. 46(19), 3034-46.
[184] S. Lakeou, E. Ososanya, B.O. Latigo, W. Mahmoud, G. Karanga, W. Oshumare. 2006. Design of a low-cost digital controller for a solar tracking photo-voltaic (PV) module and wind turbine combination system. 21st European PV solar energy conference.
[185] S. Lakeou, E. Ososanya, B.O. Latigo, W. Mahmoud. 2006. Design of a low-cost solar tracking photo-voltaic (PV) module and wind turbine combination system. 21st European Photovoltaic Solar Energy Conference, Dresden, Germany.
[186] B.P. Edwards. 1978. Computer based sun following system. Solar Energy. 21, 491-6.
[187] J. Canada, M.P. Utrillas, J.A. Martinez-Lozano, R. Pedros, J.L. Gomez-Amo, A. Maj. 2007. Design of a sun tracker for the automatic measurement of spectral irradiance and

construction of an irradiance database in the 330-1100 nm range. Renewable Energy. 32(12), 2053-68.
[188] M. Alata, M.A. Al-Nimr, Y. Qaroush. 2005. Developing multipurpose sun tracking system using fuzzy control. Energy Conversion and Management. 46(8), 1229-45.
[189] R.Y. Nuwayhid, F. Mrad, R. Abu-Said. 2001. The realization of a simple solar tracking concentrator for university research applications. Renewable Energy. 24(2), 207-22.
[190] M. Blanco-Muriel, D.C. Alarcon-Padilla, T. Lopez-Moratalla, M. Lara-Coira. 2001. Computing the solar vector. Solar Energy. 70(5), 431-41.
[191] P. Khlaichom, K. Sonthipermpoon. 2006. Optimization of solar tracking system based on genetic algorithms. Thai Sci Info. 3, 23-35.
[192] A.C.S. Roong, S.H. Chong. 2016. Laboratory-Scale Single Axis Solar Tracking System: Design and Implementation. International Journal of Power Electronics and Drive Systems. 7, 254-64.
[193] F.R. Rubio, M.G. Ortega, F. Gordillo, M. Lopez-Martinez. 2007. Application of new control strategy for sun tracking. Energy Conversion and Management. 48(7), 2174-84.
[194] G.C. Bakos. 2006. Design and construction of a two-axis Sun tracking system for parabolic trough collector (PTC) efficiency improvement. Renewable Energy. 31(15), 2411-21.
[195] A. Georgiev, P. Roth, A. Olivares. 2004. Sun following system adjustment at the UTFSM. Energy Conversion and Management. 45(12), 1795-806.
[196] Kh.S. Karimov, M.A. Saqib, P. Akhter, M.M. Ahmed, J.A. Chattha, S.A. Yousafzai. 2005. A simple photo-voltaic tracking system. Solar Energy Materials and Solar Cells. 87(4), 49-59.
[197] F. Schenkelberg. 2015. Reliability Characterization of Electrical and Electronic Systems. Chapter 11: Reliability modeling and accelerated life testing for solar power generation systems. WoodHead Publishing. p. 227.
[198] Y. Ajgaonkar, M. Bhirud, P. Rao. 2019. Design of Standalone Solar PV System using MPPT controller and Self-Cleaning Dual Axis Tracker. 2019 5th International Conference on Advanced Computing and Communication Systems (ICACCS). IEEE. India.
[199] R. Tejwani, C.S. Solanki. 2010. 360º sun tracking with automated cleaning system for solar PV panels. 2010 35th IEEE Photovoltaics Specialists Conference. IEEE. USA.
[200] A.R. Sagar, S. Al Saim, A.S.M. Ittehad, H.U. Zaman. 2017. A novel design of a Bi-level automatic solar tracker using rotations around orthogonal axes. 2017 8th International Conference on Computing, Communication and Networking Technologies (ICCCNT). IEEE. India.
[201] F.I. Mustafa, S. Shakir, F.F. Mustafa, A.T. Naiyf. 2018. Simple design and implementation of solar tracking system with two axis with four sensors for Baghdad city. 2018 9th International Renewable Energy Congress (IREC). IEEE. Tunisia.
[202] Z. Zengwei, Z. Zhen, J. Yongfeng, L. Haolin, Z. Shengcheng. 2019. Performance Analysis on Bifacial PV Panels With Inclined and Horizontal East-West Sun Trackers. IEEE Journal of Photovoltaics. 9(3), 636-42.
[203] K.E. Kanyarusoke, J. Gryzagoridis. 2016. The new hydro-mechanical solar tracker: Performance testing with a PV panel. 2016 International Conference on the Domestic Use of Energy (DUE). IEEE. South Africa.

[204] H. Allamehzadeh. 2019. An Update on Solar Energy and Sun Tracker Technology with a Dual Axis Sun Tracker Application. 2019 IEEE 46th Photovoltaic Specialists Conference (PVSC). IEEE. USA.
[205] P. Sharma, N. Malhotra. 2014. Solar tracking system using microcontroller. 2014 1st International Conference on Non Conventional Energy (ICONCE 2014). IEEE. India.
[206] H. Fathabadi. 2017. Novel Online Sensorless Dual-Axis Sun Tracker. IEEE/ASME Transactions on Mechatronics. 22(1), 321-8.
[207] I.H. Rosma, I.M. Putra, D.Y. Sukma, E. Safrianti, A.A. Zakri, A. Abdulkarim. 2018. Analysis of Single Axis Sun Tracker System to Increase Solar Photovoltaic Energy Production in the Tropics. 2018 2nd International Conference on Electrical Engineering and Informatics (Icon EEI). IEEE. Indonesia.
[208] I.H. Rosma, J. Asmawi, S. Darmawan, B. Anand, N.D. Ali, B. Anto. 2018. The implementation and Analysis of Dual Axis Sun Tracker System to Increase Energy Gain of Solar Photovoltaic. 2018 2nd International Conference on Electrical Engineering and Informatics (ICon EEI). IEEE. Indonesia.
[209] A. Masih, I. Odinaev. 2019. Performance Comparison of Dual Axis Solar Tracker with Static Solar System in Ural Region of Russia. 2019 Ural Symposium on Biomedical Engineering, Radioelectronics and Information Technology (USBEREIT). IEEE. Russia.
[210] S. Farajdadian, S.M.H. Hosseini. 2019. Design of an optimal fuzzy controller to obtain maximum power in solar power generation system. Solar Energy. 182, 161-78.
[211] C.O. Okeye, A. Bahrami, U. Atikol. 2018. Evaluating the solar resource potential on different tracking surfaces in Nigeria. Renewable and Sustainable Energy Reviews. 81, Part 1, 1569-81.
[212] A. Bahrami., C.O. Okeye, U. Atikol. 2016. The effect of latitude on the performance of different solar trackers in Europe and Africa. Applied Energy. 177, 896-906.
[213] Q. Lin, Y. Zhang, A.V. Mieghem, Y-C. Chen, N. Yu, Y. Yang, H. Yin. 2020. Design and experiment of a sun-powered smart building envelope with automatic control. Energy and Buildings. 223, Article ID: 110173.
[214] M. Abdollapour, M.R. Golzarian, A. Rohani, H.A. Zarchi. 2018. Development of a machine vision dual-axis solar tracking system. Solar Energy. 169, 136-43.
[215] F.M. Hoffmann, R.F. Molz, J.V. Kothe, E.O.B. Nara, L.P.C. Tedesco. 2018. Monthly profile analysis based on a two-axis solar tracker proposal for photovoltaic panels. Renewable Energy. 115, 750-9.
[216] A. Narendra, N.V. Naik, A.K. Panda, N. Tiwary. 2020. A Comprehensive Review of PV Driven Electrical Motors. Solar Energy. 195, 278-303.
[217] A. Zurita, A. Castillejo-Cuberos, M. Garcia, C. Mata-Torres, Y. Simsek, R. Garcia, F. Antonanzas-Torres, R.A. Escobar. 2018. State of the art and future prospects for solar PV development in Chile. Renewable and Sustainable Energy Reviews. 92, 701-27.
[218] F. Hyder, K. Sudhakar, R. Mamat. 2018. Solar PV tree design: A review. Renewable and Sustainable Energy Reviews. 82(1), 1079-96.

Titre : Optimisation des systèmes photovoltaïques : vers une meilleure efficacité et une performance sans défaut

Mots clés : Performance photovoltaïque, amélioration de l'efficacité, ombrage partiel, hotspots, maintenance préventive.

Résumé : Les systèmes photovoltaïques (PV) recèlent un potentiel important pour permettre la transition vers un avenir neutre en carbone dans la production d'électricité. En raison de l'abondance de l'irradiation solaire et du fonctionnement statique et silencieux des systèmes PV, ils peuvent constituer une puissante source d'énergie alternative. Cependant, les systèmes PV sont souvent confrontés à divers scénarios de défaillance, principalement dus à des conditions environnementales indésirables. Les conditions d'ombrage partiel en particulier ont de graves conséquences sur les modules PV. Dans ce contexte, l'objectif de cette étude est de présenter dans un premier temps une revue de littérature approfondie et récente qui clarifie concrètement les impacts négatifs liés à l'irradiation sur la performance des systèmes PV. Par conséquent, quatre études sont établies pour compenser ces effets, en commençant par une nouvelle approche d'optimisation dynamique de l'angle d'inclinaison des panneaux PV. De plus, un chargeur solaire complet est conçu pour les systèmes PV hors-réseau, ce qui optimise le processus de charge des systèmes de stockage d'énergie. En outre, une nouvelle modification de l'algorithme Particle Swarm Optimization (PSO) basé sur les mécanismes pathogènes du diabète de type 1 (T1D), est élaborée et vise à extraire la puissance maximale disponible d'un générateur PV dans des conditions sévères d'ombrage partiel. Enfin, une étude de faisabilité est menée pour tester l'applicabilité des traqueurs solaires en fonction des zones géographiques d'installation des systèmes PV.

Title : Optimizing PV systems : towards better efficiency and faultless performance

Keywords : PV performance, enhancing efficiency, partial shading, hotspots, preventive maintenance.

Abstract : Photovoltaic (PV) systems hold a significant potential for enabling the shift towards a carbon-neutral future in power production. Due to the abundance of solar irradiance, the static and silent operation of PV systems, they can constitute a powerful alternative power supply. However, PV systems are often confronted with various faulty scenarios, mainly due to undesired environmental conditions. Partial shading conditions specifically, have severe consequences over PV modules and are also hard to detect and identify. In this context, the aim of this study is to first present a thorough and recent literature review that concretely sheds light over the irradiance based negative impacts on the performance of PV systems. Consequently, four studies are established to compensate such effects, starting with a novel approach in dynamically optimizing the PV panels' tilt angle in order to increase the direct normal irradiance at their surfaces. Moreover, a complete solar charger is designed for off-grid PV systems which optimizes the charging process of energy storage systems. Additionally, the third study corresponds to a novel modification of the Particle Swarm Optimization (PSO) algorithm based on the pathogenic mechanisms of Type 1 Diabetes (T1D) disease, which aims to extract the maximum available power from a PV array under severe partial shading conditions. Finally, a feasibility study is conducted to test the applicability of solar trackers according to the geographical zones of PV systems' installation.